NASA
Technical Memorandum 104356

111-1
11706
P.340

AVSCOM
Technical Report 90-C-012

Effects of Inlet Distortion on the Development of Secondary Flows in a Subsonic Axial Inlet Compressor Rotor

Albert K. Owen
Propulsion Directorate
U.S. Army Aviation Systems Command
Lewis Research Center
Cleveland, Ohio

(NASA-TM-104356) EFFECTS OF INLET DISTORTION ON THE DEVELOPMENT OF SECONDARY FLOWS IN A SUBSONIC AXIAL INLET COMPRESSOR ROTOR Ph.D. Thesis - Toledo Univ., OH (NASA) 340 p CSCL 21F G3/07
N91-23179
Unclas
0011706

April 1991

NASA

US ARMY
AVIATION
SYSTEMS COMMAND
AVIATION R&T ACTIVITY

EFFECTS OF INLET DISTORTION ON THE DEVELOPMENT

OF SECONDARY FLOWS IN A SUBSONIC AXIAL INLET

COMPRESSOR ROTOR

Albert K. Owen

Propulsion Directorate
U. S. Army Aviation Systems Command
Lewis Research Center
Cleveland, Ohio 44135

Detailed flow measurements were taken inside an isolated axial compressor rotor operating subsonically near peak efficiency. Laser Anemometer measurements were made with two inlet velocity profiles. One profile consisted of an unmodified baseline flow, and the second profile was distorted by placing axisymmetric screens on the hub and shroud well upstream of the rotor. A primary flow is defined in the rotor and deviations from this primary flow for each inlet flow condition are identified. A comparison between the two flow deviations is made to assess the development of a passage vortex due to the distortion of the inlet flow. A comparison of experimental results with computational predictions from a Navier-Stokes solver showed good agreement between predicted and measured flows. Measured results indicate of a distorted inlet profile has a minimal effect on the development that the flow in the rotor passage and the resulting passage vortex.

TABLE OF CONTENTS

LIST OF TABLES

LIST OF FIGURES

NOMENCLATURE

ANGLE	Absolute Flow Angel (Figure 12)
C_v	Confidence Interval
c_v	Specific Heat
d	Buleev Length Scale
D	Jameson dissipative Term
DSPD	Design Speed
e	Total Energy
f_d	Probe Volume Interference Frequency
FA, a	Glow Angle, Absolute (Figure 27)
FAdf, a	Relative Flow Angle Differences (Figure 33)
k	Kinetic Energy
N	Number of Laser Measurements
N_b	Number of Blades
N_{wp}	Number of Windows per Passage
P,p	Pressure
Pr	Prandl Number
r,θ,z	Cylindrical Coordinate System
R,r	Radius
Re	Reynolds Number
s	Normal Distance from Wall, Buleev Length Scale
$\mathcal{R}$	Gas Constant
t	Time
T	Temperature

U, V, W Contravariant Velocity Components

u,v,w Velocity components from Squire and Winter

V_{ax} Axial Velocity (Figure 21)

$Vt_{,a}$ Tangential Velocity (Figure 23)

V_{to} Absolute Total Velocity (Figure 12)

$V_{to,r}$ Total Velocity, Relative (Figure 32)

V_θ Tangential Velocity

W Relative Velocity

x,y,z Cartesian Coordinate System

Z Desired Confidence Interval

γ Angle of Turning

δ Standard Second Difference Operators

ϵ Smoothing Parameters

κ Probe Volume Laser Beams Crossing Angle

λ Laser Beam Light Wavelength

λ_c Courant Number

μ Viscosity

ν Kinematic Viscosity

ξ,η,ζ Generalized Body Fitted Coordinates, from Chima

ξ Streamwise Vorticity

ρ Density

σ Standard Deviation

Ω Vorticity

ω Rotor Angular Rotation

Superscripts

'	Relative Reference Frame, from Chima
$\bar{}$	Vector

Subscripts

av	Average
bi	Biased
m	Meridional Direction (Figure 19)
o	Stagnation
pav	Passage Average
p	Primary Flow
r, θ, Z	Cylindrical Coordinate System (Figure 19)
s	Secondary Flow
1,2	Inlet, Outlet Conditions

I. INTRODUCTION

Current turbomachinery design techniques are based, to a large extent, on the very large body of empirical data accumulated over the past 50 years. In a normal design procedure these data are used in conjunction with a steady state, axisymmetric through-flow calculation to produce an initial design. This design is then analyzed using a Quasi-3D or full-3D Euler solver with or without a boundary layer approximation. After this process, the design is normally fabricated and then tested, first alone and then in its operating environment. Modifications are made as a result of the tests. This cycle is then repeated, as necessary, until the machine reaches its design specifications. While this process has provided a number of excellent designs, it tends to be difficult, lengthy, and expensive. Further, since it makes extensive use of previous designs and the empirical relations derived from these results, new machines tend to be similar to previous designs, regardless of possible improvements that might result in more radical design departures. A better understanding of the flow processes occurring inside a turbomachine would not only improve the reliability of the design process but would also improve the performance of the machine. Further, the rapid growth in computational capabilities over the past decade has allowed the development of a number of fully three-dimensional viscous flow solutions. These solutions promise greater understanding of the flow physics, improvements in performance, and increased design procedure efficiency.

Detailed data of benchmark quality is essential for a better understanding of flow physics and to provide experimental verification of the advanced codes currently becoming operational.

The present study was designed to explore in detail the flow inside a compressor rotor. Specifically, it endeavored to examine certain "secondary" flows generated in the rotor. The ultimate goals were two-fold: (1) to provide detailed quality data for an improved understanding of the flow physics and (2) to explore the effects of inlet distortion on the development of a compressor rotor flow field.

The term "Secondary Flows" encompasses many of the flow processes inside a compressor rotor that result in lowered efficiencies and range. These flows can be exceedingly complex and difficult to analyze. Secondary flow is usually defined as the difference between the actual flow and the idealized axisymmetric flow. Wood [1] includes cascade secondary flows, scraping effects, tip leakage flows, and radial flows in his definition of secondary flow. These flows are shown schematically in Fig. 1.

The primary focus of this research was the cascade secondary flow or the "Passage Vortex." This type of flow results when a nonuniform inlet velocity profile is turned by a row of blades. This can be visualized by considering the simple example of flow through the bend of a rectangular channel, as shown in Fig. 2. For this example, it has been assumed that the flow is incompressible and that viscous effects can be neglected. Further, consider an inlet velocity profile that varies in the spanwise direction. This variation ranges from some low velocity near the endwalls to freestream velocity near midspan. If the distance from an endwall to where the velocity approximates the freestream value is of the order of magnitude of the cross channel distance or less, the freestream static pressure will be nearly the same as the static pressure in the region of lower velocity. Simply put, the static pressure is nearly constant across the passage inlet. This type of velocity profile is common at the inlets of the middle stages of axial compressors. It results from the increasing thickness of the endwall boundary layers and the gradual convergence of the passage endwalls. However, it is not important here how this velocity deficit occurs. This profile will be influenced by the blade-to-blade pressure gradient that results from the turning of the flow as it moves through the passage. There will then be a pressure gradient that exists between the suction and pressure surfaces. This pressure gradient can closely be approximated by [2]:

$$\frac{\partial P}{\partial y} = \frac{\rho V}{R} \tag{1}$$

Equation 1 demonstrates that any reduction in the fluid velocity, V, must be matched by an equivalent reduction in the radius of curvature of the flow. This results in the generation of the cascade secondary flow shown in Figs. 1 and 2.

The passage vortex, then, is caused by an axisymmetric distortion of the inlet total pressure profile. It is most often caused by endwall boundary layers, which can be quite substantial in the middle and aft stages of an axial flow compressor. To date, this effect of inlet distortion on the middle stage compressor rotors has only been approximated by empirical relations.

This thesis presents the results of an experimental study of the flow phenomena resulting from the presence of these flow distortions on a transonic inlet compressor rotor operating subsonically at 60% of design speed.

Two operating conditions were observed. One was a "uniform" or baseline inlet velocity profile with no unusually thick boundary layers. The other flow condition was at the same operating point with artificially enhanced endwall boundary layers. These boundary layers were generated upstream of the rotor using screens that extended partially into the inlet flow passage. The differences in the generated velocity profiles are indicative of the size and structure of the passage vortex that was generated by the inlet flow distortion.

These two flow conditions were compared and their differences were calculated. These results were compared with a state-of-the-art three-dimensional Navier-Stokes solver. This solver includes endwall and blade boundary layer effects and has been used at the NASA Lewis Research Center to accurately model the velocity fields of several compressor designs. The LDV data acquired during this experiment and its follow on program should greatly aid in the validation of this and other codes for analyzing turbomachinery fluid flows.

II. LITERATURE SURVEY

A. INTRODUCTION

Research accomplished in the area of secondary flow or even just the "Passage Vortex" is quite extensive and it would be impractical, if not impossible, to adequately describe all of the previous work in this area. Therefore, the following section will merely highlight work in the specific area of this study.

The analytical/numerical modeling of the passage vortex will be reviewed first and then the experimental work done will be considered.

Literature on secondary flows dates back at least to 1877 when J. Thompson [3] published an article discussing the flow of water in a river bend. Fifty years later, W. R. Dean [4] published a study of the secondary flows generated in laminar pipe flows.

B. ANALYTICAL/NUMERICAL WORK

The first "modern" publication in the area was the now classic 1949 paper by Squire and Winter [5]. They analyzed the secondary flow generated in an inviscid fluid with a nonuniform inlet profile moving through a cascade channel. Fig. 3 shows the channel they analyzed.

This early effort was very narrow in scope and was certainly restricted by the lack of computational power. Accordingly, a number of simplifications were made which included:

(1) a nonrotating reference frame,

(2) a perfect fluid,

(3) steady flow,

(4) no body forces,

(5) deflection without expansion or contraction,

(6) passage width small compared to the radius of turn ($a \ll R_{bo}$, Fig. 3),

(7) small approach-flow velocity non-uniformity, and

(8) two-dimensional approach flow, i.e., the approach velocity varies only in the direction of the blade span (b).

The equations of motion:

$$\nabla \times (\mathbf{V} \times \mathbf{\Omega}) = 0 \tag{2}$$

along with the conservation of vorticity:

$$\nabla \cdot \mathbf{\Omega} = 0 \tag{3}$$

were used to develop a simplified description of the downstream streamwise vorticity:

$$\xi_2 = \frac{\partial w_2}{\partial \beta_2} - \frac{\partial v_2}{\partial z_2} = -2\gamma \frac{\partial U_1}{\partial z_1} \tag{4}$$

W. R. Hawthorne has published numerous papers on the subject of secondary flow. He derived a general equation for inviscid, incompressible flow in a cascade [6]. Beginning with Eqs. (2) and (3), and continuity, Hawthorne showed that:

$$(\xi/V)_2 - (\xi/V)_1 = 2\int_1^2 |\nabla P_o| \sin\gamma \, \frac{d\delta}{\rho V^2} \tag{5}$$

This equation does not, as written, require the Bernoulli surface distortion to be small or a uniform spanwise pressure distribution. Further, it allows velocity variations in other than the spanwise direction.

Both of these papers approached the problem of the passage vortex by considering it as a phenomenon developing in a fluid flowing in a closed channel. This "Channel Theory" is not, however, the only way to look at this phenomenon. It can be viewed as the result of flow over an airfoil. In 1951, Lieblien and Ackley [2] took this approach when they analyzed the secondary flows in cascades and inlet guide vanes in this manner.

L. H. Smith must also be mentioned in this section for the seminal work he did using the airfoil approach to the problem. In 1955, he published two papers [7, 8] which recommended a definite method for accounting for the secondary velocities generated by the passage vortex.

These early publications set the direction for analytical work for the next twenty five years. Secondary flows were assumed small and then were "decoupled" from the main through-flow. Much was done in this direction.

These concepts were broadened and generalized in the 1960's and 1970's and culminated in several numerical algorithms for accounting for secondary flow effects [9-11]. During this same time frame, another more general approach to describing flows in a compressor rotor passage was developing. This approach was based on the solution of the equations of motion on the digital computer.

The ultimate goal for any analytical formulation is, of course, the solution of the complete Navier-Stokes Equations. However, even with the current capabilities available, the solution of these equations can be extremely time consuming for even relatively simple geometries such as turning ducts. Thus, the initial use of digital computers was to solve simple models of flow through compressors.

Although two-dimensional blade-to-blade solutions were being published in the late 1940's [12], perhaps the major event paving the way for the analysis of turbomachinery flow consisted of the publishing of a series of papers by Wu [13-17]. In these papers, Wu developed a "General Theory" where the stream function equations are solved on two intersecting families of stream surfaces; a blade-to-blade stream surface and a hub-to-shroud stream surface (Fig. 4). He postulated a procedure where the stream functions are solved iteratively on each series of surfaces until a converged solution is obtained. A detailed derivation of the stream function equations used in Wu's analysis may be found in Ref. [15].

There have been numerous attempts to use Wu's stream function surfaces to solve for the flow in turbomachines. They are, however, two-dimensional solutions and cannot, directly, provide information on the various secondary flow phenomena that occur in turbomachinery.

To begin to effectively explore the development of secondary flows computationally, a three-dimensional solution is required. In 1969, MacCormack [18] published a three-dimensional Euler solution that provided second order accuracy in both time and space. Thomkins [19] used the MacCormack algorithm in a full three-dimensional code. This method can be applied to any general compressor blade shape.

Denton [20-22] has written Euler codes using the control volume approach with quadrilateral elements in two dimensions and six sided elements in three-dimensions. This approach results in simpler expressions for surface fluxes. He has improved convergence by using "multigridding" techniques where the flux balances are applied over large grids concurrently with the finer mesh. Denton uses upwind differencing in the streamwise direction for the mass and momentum flux with downwind differencing for pressure. Central differencing is used for all quantities in the pitchwise and spanwise directions.

Recently, Denton and Wood [23] have added a simple one-dimensional boundary layer calculation to the original code.

A great deal of effort is currently being directed towards the development of fully three-dimensional solutions to the Navier-Stokes equations.

An operational code developed by Hah [24-26] is currently being used at the Lewis Research Center to analyze the flow field inside turbomachinery.

Just becoming available at the center is a Navier-Stokes solver developed by Chima [27] for use in the analysis of turbomachinery flow fields. This code represents an operational 3-D Navier-Stokes solver for use in turbomachinery and has been used in the current effort to evaluated the data acquired and to aid in accurately describing the flow phenomena observed. This code will be discussed in more detail in a later section (Section III, part F).

C. EXPERIMENTAL WORK

There are two broad types of turbomachines: compressors and turbines. The differing purposes of each, of course, result in greatly differing designs. Both of these broad classifications can be further divided, for experimental purposes, into three subdivisions of increasing complexity and difficulty: (1) two-dimensional cascades, (2) annular cascades, stators, and inlet guide vanes, and (3) rotors. While all three areas have contributed to the understanding of secondary flows, the great extent of the published work requires this survey to be largely restricted to the last of these subcategories.

Smith [8] examined the secondary flows that were generated inside an axial compressor stage consisting of inlet guide vanes, a rotor and a stator. While he did not specifically look at the effects of a variable boundary layer thickness, he did make detailed full span measurements through both the hub and shroud boundary layers and, for the inlet guide vanes and stator, across the pitch. Unfortunately, since only "conventional" instrumentation was available, he obtained only pitchwise average information behind the rotor. No information was gathered between the blades of either the stator or the inlet guide vanes. Smith unsuccessfully attempted to obtain secondary flow information on the rotor by attaching tufts of wool to the trailing edge of the blades and observing them with a stroboscopic light. Regrettably, centrifugal effects nullified this attempt. Commenting on the data obtained, he reflects that "in view of the experimental difficulties involved, the coarseness of the data, and the sensitivity of the method to small changes, we can only say there appears to be no conflict between the calculated and measured values. Thus, no clear-cut experimental verification of the secondary flow theories has been made."

In the 1950's, turbomachinery development efforts began in earnest at several research organizations. Most notably, the engine companies such as General Electric at Evandale and Pratt and Whitney at Hartford (UTRC) and research institutes such as Vrije Universiteit Brussel, VKI, Pennsylvania State University, and Escole Centrale de Lyon began to obtain detailed measurements of the flow fields generated in axial rotors.

One set of extensive data on the development of secondary flow was published by McKensie [28] at Rolls Royce in England. Dixon and Horlock [29] used the experimental data generated by McKensie to test the accuracy of their method of predicting secondary flow development. McKensie's compressor consisted of four axial stages. Dixon and Horlock show boundary layers which occupy roughly one-half the passage. The information presented consists entirely of pitch averaged axial velocities and flow angles at the exits of the inlet guide vanes and the first stage rotor exit. They concluded that while their technique for calculating secondary flow development works well behind the inlet guide vanes, the accuracy of the technique is greatly impaired by the boundary layer growth through the rotor. They do propose, however, that their calculations would be useful for predictions in an "ultimate steady flow" occurring downstream of a number of compressor stages.

De Ruyck, Hirsch, and Kool [30-32] published several papers in the late 1970's showing the three-dimensional flow behind a relatively low speed compressor rotor and comparing it to A. G. Smith's [33] theoretical treatment of secondary flow development. As such, they assume the correctness of Smith's assumptions. Their data were obtained with a hot wire probe placed behind the rotor. In their analysis, they assume a primary flow in the direction of the blade angles and ignore the tip leakage. The agreement between their hot wire measurements and Smith's predictions was, at best, not very good. However, when they included trailing shed and trailing filament vortices, they were able to obtain "qualitive agreement." They concluded that the trailing shed and trailing filament vortices must be included in the analysis and that tip leakage effects must also be considered.

The General Electric Company has supported an extensive experimental program at their Low Speed Research Compressor Facility (LSRC) in Evandale, Ohio. This low speed compressor has a 1.52M tip diameter, a 1.07M hub diameter and can operate at a tip speed of over 60 m/s.

Smith's 1970 presentation [34] at a symposium on blading research contributed extensive pitchwise-average data on 10 separate compressor configurations tested in the LSRC facility. These different "builds" each consisted of four identical stages. The program varied spacing, clearance height, gap, and pitch. Smith concluded that there was an "ultimate steady flow" profile that developed in a multistage machine and that this pitchwise-average flow could be analyzed in a manner similar to that suggested by Mellor and Strong [35], among numerous other authors.

Smith, along with Adkins [36] and Koch [37] continued to publish results from the General Electric LSRC at Evandale, Ohio. Smith and Adkins paper represents a rather extensive effort to analyze all of the secondary flows occurring in rotors. They present only pitch-averaged spanwise data taken for two different configurations at General Electric They also analyze data taken by Larguier [38] at ONERA, consisting of spanwise averaged pitchwise exit flow angles. These analyses are based on Smith's early work at Johns Hopkins.

The LSRC data showed relatively small secondary flow fields primarily because of the high blade aspect ratios (2.8) and it should be noted that the data was acquired primarily to study tip clearance flows.

Smith and Adkins concluded:

(1) that secondary flows are important to the design of axial flow compressors,

(2) that for compressors operating at the design point, secondary flows can be adequately calculated using inviscid analysis, and

(3) that downstream mixing processes are quite complex and current modeling techniques are quite crude and empirical.

Work at General Electric has continued in the 1980's on the "ultimate steady flow" concept with Wisler et al. [39] publishing an important paper attempting to clarify the relative importance of classic secondary flow with respect to turbulent diffusion in the spanwise mixing in axial compressors.

This problem was considered in earlier papers by Gallimore [40] and Gallimore and Cumpsty [41]. This work, done at the Whittle Lab in England indicated that turbulent diffusion was the dominant mixing mechanism in axial flow compressors. These results were based on observations of two four stage axial flow compressors. A tracer gas technique [42] was used where ethylene was injected upstream of the first stage rotor and its density was sampled downstream of the fourth stage stator.

Wisler et al.'s work made use of the same gas tracing technique, in conjunction with hot wire anemometry, in the LSRC at Evandale. These extensive measurements included ethylene injection in front of the third stage stator and through static taps on both the suction and pressure surface of the third stage stator. The trace gas was sampled downstream of the third stage stator and the fourth stage rotor. Cross channel plots were presented showing the spread of the trace gas with respect to the third stage stator that indicate that "in addition to being mixed by turbulent diffusion, the low momentum fluid in the endwall is transported radially along the stator vane edges by secondary flow. The passing rotor then chops, turns and transports this low momentum fluid, spreading it circumferentially across the stator passage" [41].

Note that both of these programs looked at "ultimate steady flow" in compressor stages. Here both rotor and stator effects were considered and information was gathered between compressor components.

Lebeouf and Papailiou et al. [43-45] have published a number of reports on the secondary flows in cascades and compressor rotors. This work was performed on a transonic axial compressor rotor and was conducted at the high speed compressor test facility at the Ecole Centrale de Lyon. Their 1977 and 1978 papers describe the results of tests conducted using a SNECMA compressor. In these studies, the flow angles, static and total pressures and temperatures upstream and downstream of the rotor were measured. A 1977 report describes extensive pitchwise average data at these axial locations for two operating conditions: "nominal" and near surge. In this report the experimental results were compared with a simple radial equilibrium analysis and the following conclusions were reached:

(1) that data reduction using radial equilibrium will require the use of curvature terms, and

(2) that difficulties exist when an analytical representation of the velocity profiles is sought in both the absolute and the relative systems of reference.

It was determined in the report that these conclusions favor a differential formulation of the endwall boundary layers.

In a later 1982 work, Lebeouf and Papailiou et al. [45] dealt with a single stage axial transonic compressor consisting of inlet guide vanes, a rotor, and a stator. The theoretical analysis used was based on a Quasi-3D-inviscid computation using a method described by Katsanis [46] for the blade-to-blade solution and a meridional solution by Lebeouf combined with a viscous endwall solution based on the work of Mellor and Wood [47].

Data was taken for this report using conventional instrumentation. Circumferential radial surveys at two axial locations between the inlet guide vanes and the rotors and pitch averaged radial surveys at two axial locations behind the rotor were all acquired.

In comparing the results behind the rotor with theoretical computations, the report notes that, between 20% and 85% of the blade height, the prediction of average total pressure losses and outlet flow angles are "well reproduced." The secondary flow (endwall boundary layer) model presented in the report reproduces the hub β angles well. The theoretical reproduction of the flow in the tip area is less exact because the model fails to account for tip clearance and moving wall effects. Small discrepancies in total temperature near the hub were also highlighted in the paper.

The conclusion section states that "in spite of the usefulness of global methods for the computation of secondary flows, (such as the one developed by Mellor and Wood), it is believed that the use of detailed flow computation, ---, may result to improvements in the efficiency of modern machines through the gain obtained in better understanding the flow behaviour."

Under the guidance of Lakshiminarayana, an extensive program exploring, both experimentally and computationally, turbomachinery flows is being conducted at the Pennsylvania State University. The experimental work is being done in a low speed axial flow compressor [48] to include work in both rotors and stators. The work in rotors has examined not only general internal flows [49] but has also studied wake structures [46-49], annulus boundary layers [54] and tip clearance effects.

Lakshiminarayana and his associates have published well over one hundred papers on internal turbomachinery flows. A number of articles, however, are particularly pertinent to the current research. For example, the team at Pennsylvania State University placed conventional pressure probes and hot wire anemometers on the hub of a compressor rotor. As a result, they were able to measure the velocities and turbulence levels of the wake behind [51-53] and the pressures [55] inside this lightly loaded, low speed compressor. The results were compared with the predictions on Katsanis and McNally [56-57], obtaining "very good" agreement with the exception of the region near the tip of the rotor. The report theorizes that this may be the result of tip clearance effects. This data, taken for one inlet velocity profile at one operating condition covers the region from 10 to 90% pitch at six axial locations and five radial locations.

Some of the conclusions that resulted from these tests are:

(1) in the inviscid regions of the rotor passage, the radial velocity is small;

(2) relative velocity develops from a linear variation from blade-to-blade at the inlet to nearly uniform at the exit;

(3) "metal blockage" from the blades has an appreciable effect on the axial velocity;

(4) passage averaged relative total pressure remains constant with respect to the axial distance in the inviscid regions of the blade passage;

(5) static pressure varies appreciably in the blade wake;

(6) with the exception of the wake region, all properties are uniform at the exit; and

(7) the quasi - 3D predictions of Katsanis and McNally [56-58] are very good except near the blade leading edges and blade tip regions.

The United Technologies Research Center, a Division of Pratt and Whitney, has maintained a strong experimental program studying the flows within axial compressors.

Their test facility, the "Large Scale Rotating Rig" (LSRR) is 1.52 m in diameter. The rotating gear speed is roughly 500 RPM which gives an operating Reynolds number of approximately $5x10^5$.

In two separate papers, Dring, Josyln, and Hardin [59, 60] detailed what they considered a "benchmark" study of the nonstrip theory (secondary flow) effects in a compressor rotor. Data were obtained inside the rotor using flow visualization techniques and static pressure taps. Also acquired were detailed three-dimensional pressure and angle distributions behind almost two full passages of a single stage rotor. The inlet conditions in this study were uniform with the exception of the thin inlet endwall boundary layers.

All velocity components, C_{ps}, C_{pt} and angle distribution plots at four axial positions aft of the blade are presented. Data is provided at four flow settings:

axial velocity/mean tip speed = 0.65,0.75,0.85,0.95.

The overall conclusion from these reports was that "radial flow effects (on the blade surface) can have a major impact on the nature of the wake of a compressor rotor." It was noted that the accumulation of low energy fluid in the suction surface corner is inhibited by radial flow effects. Thus, corner stall can be inhibited. Further, mid-span performance closely models that of a two-dimensional cascade [61].

Later, Wagner et al. [62] specifically studied the effects of a nonuniform inlet profile on the performance of a rotor identical to the machine described in the previous report. A mechanical device was able to generate a thickened boundary layer on both the hub and the shroud of about 37% of the span. Then the rotor was surveyed at the same operating points that were studied in the previous work, i.e., the same four flow coefficients.

In the summary of results the following observations were noted:

(1) increased loss in the midspan region and decreased loss near the hub and tip regions relative to previous results,

(2) a general increase in radial displacement of the flow with increased loading,

(3) a rise of static pressure compared with the previous flow,

(4) only a very small rotation of the flow due to the relative eddy,

(5) increased tip losses and increased hub and tip blockage occurring with increased loading, and

(6) exit relative flow angles were only "weakly" affected by the inlet profile.

These, then, are the major experimental programs in the area of secondary flows in compressors. The important features of each can be summarized as follows:

(1) Researchers at General Electric, have attempted to create a comprehensive system to account for secondary flow effects. This work has been greatly concerned with tip clearance effects. They have developed an "ultimate steady state" model to help describe the flow in axial compressors. They consider secondary flows important media for spanwise fluid transport in compressors.

(2) LeBeouf et al. have worked primarily with a transonic compressor. The data is pitch averaged and taken behind the rotor.

(3) Lakshiminarayana et al. have used hot wires and conventional pitot static instrumentation in a low speed compressor. Their work includes secondary flow measurements inside the rotor passage. The overall program has looked at all potential secondary flow effects.

(4) Dring et al. have specifically examined the effects of a nonuniform inlet profile and the effects it has on the generation of the passage vortex and other flow effects. Their work was performed on a low speed compressor rotor. They obtained tangential surveys by means of a rotating pitot static instrumentation system positioned behind the rotor.

A summary of the performance parameters and measurement capabilities of the various facilities previously discussed is presented in Table I.

III. APPARATUS AND FACILITIES

A. INTRODUCTION

There are five broad areas that will be presented in this section:

(A) the Laser Anemometer system which includes the optics, flow seeding, and probe volume positioning system.

(B) the data Acquisition/Reduction system which includes the conventional pitot static instrumentation.

(C) the test facility.

(D) the compressor rotor, its' design and specifications.

(E) and the Computational Development for the Navier-Stokes Solver.

Previous publications have discussed, to some extent, all of the areas listed above and these previous publications will be noted where necessary.

B. THE LASER ANEMOMETER SYSTEM

1. Optical System

The Laser Anemometer measures the velocity of a fluid by measuring the velocities of particles immersed in that fluid, the assumption being that the particles observed are moving at a velocity near that of the fluid. The Laser Anemometer makes use of the coherence, monochromicity, and nondivergence characteristics of the typical laser beam. It makes its measurements nonintrusively and has become, in the last decade, one of the preferred methods of studying turbomachinery flows.

There are several types of laser anemometer systems. The system used at the Lewis Research Center's single stage axial flow compressor facility is a "fringe type" system and was developed in-house.

There are a number of excellent publications [63-65] describing the optical operation of the laser-fringe anemometer (laser doppler velocimeter). Simply put, the system operates by measuring the heterodyne frequency of light reflected (or emitted) from a particle illuminated simultaneously by two incident laser beams.

The fringe type system splits a single laser beam into two beams. These two beams are focused and cross at a desired point in the flow - called the "Probe Volume." Using the fringe model for explanation, it is said that in the region of beam intersection, a pattern of constructive and destructive interference is created (Fig. 5). A particle in the flow traversing the probe volume will alternately be illuminated or not, depending on the region of the probe volume it is in. This intermittent illumination of the particle can be observed using a photomultiplier tube (PMT). This explanation of the operation of a laser anemometer is the "fringe model."

The PMT signal takes the form of a sine wave of varying amplitude. The frequency of this sine wave can be related to the measured velocity of the particle using the relation [65]:

$$V = \frac{f_D \lambda}{2 \times \sin\kappa} \tag{6}$$

If the particle is small, generally less than a micron in diameter, the particle velocity and the fluid velocity can be assumed to be the same.

Particles observed in this investigation were measured and were virtually all less than one half micron in diameter. This size is considered small enough to accurately reflect the velocities of the fluid [64, 66].

Of critical importance here is the obvious fact that the intersection of these two beams results in the measurement of only one component of velocity (Fig. 5). This component lies along a line formed by the intersection of two planes. One of these is the plane in which the two incoming laser beams lie. The other plane is perpendicular to the line bisecting these two beams and is in the probe volume. Figure 5 illustrates the probe volume and the measured velocity component.

During the normal operation of the laser system the incoming laser beams are oriented in two directions about the bisecting line. This allows the resolution of two of the three orthogonal velocity components. In turbomachnes, these two components are usually the axial (through-flow) and the tangential components. Normally the radial components are considered small and are not resolved.

The laser anemometer system used currently at the Lewis Research Center has been highly modified from the system described in Refs. [66-68]. It remains a fringe type, on axis, backscatter system using light at a frequency of 5145Å. The velocity components measured are in or near the axial/tangential planes and the components resolved are the tangential and the axial velocity components.

The modifications to the original Lewis Research Center fringe system that are detailed below were initiated principally to allow the inclusion of a frequency shifter to the system.

The optical system used can be characterized as a two component, one color, three beam system. Table II and the schematic in Fig. 6 provide detailed information concerning the order in which the system was assembled, and Refs. [65, 66, 69] provide specific information on each commercially purchased system part.

This three beam system was designed to create two separate probe volumes. The beam pairs were perpendicular resulting in measurements of velocity components that were perpendicular to each other. During the current program, the frequency shifted beam (Fig. 5d) was common to both probe volumes. A mechanical shutter blocked one of the two unshifted beams, allowing only one probe volume in the target volume at any given moment. Therefore, only one component of velocity was measured at any given time.

Although the complete system originally was designed to measure two velocity components simultaneously, the velocity and turbulence intensities of the flow inside the test rotor precluded this mode of operation. For example, at the -5% chord location in the passage, the axial velocity and the absolute tangential velocities were of the same order of magnitude at a significant number of radial/tangential locations. These locations are near the leading edge of the rotor blades and reflect the approaching blade. The similarity of velocity magnitudes precludes the effective separation of velocity component information taken simultaneously.

This region near the blade leading edge was not the only region where the two orthogonal measured velocity components were nearly equal. Regions in the vicinity of the trailing edge also showed similar velocity magnitudes.

The argon-ion laser was operated in the tem_{oo} mode (the lowest Transverse Electric Magnetic mode) at a power level varying between 1.5 and 2.5 W to generate a beam at a frequency of 514.5 nm. The variation in output power of the laser over the test period was the result of variations in input cooling water temperature and input electric power. The tem_{oo} mode of operation provides the highest available power output for the laser used during this investigation. Even so, losses in the optical system reduced the actual power delivered to the probe volume to less than 0.8 W. These losses result from the unavoidable imperfect transmission of light through the various components of the optical train, both passive and active. This resulted in marginal operation in a number of regions. Specifically, areas near the hub where blade blockage reduced the light collected by the collection optics. Also, near the trailing edge where flow conditions have spread the seed and reduced the seed particle density. And finally, where the rear lip of the observation window reduced the viewing solid angle.

A brief discussion of the components used in this Laser Anemometer system has been included here to help clarify its assembly and operation. More detailed information on the purposes and specifications are included in Ref. [65].

The laser is positioned below the optical package (Fig. 6) and its beam is directed through a vertical 180° turn up to the optics level of the Table. The beam then passes through a collimator which allows the laser beam waist to be positioned at the probe volume. This insures that the wave fronts are flat and, therefore, the resulting interference pattern is constant throughout the probe volume. This is important since the calculated particle velocity is a function of the heterodyne frequency which remains constant only if the wave fronts remain planar. Following the collimator are a series of beam splitters and polarization rotators.

The polarization rotators insure that the beams are properly polarized. It is important, to achieve a strong interference pattern, that the polarization of all three beams is the same. This was achieved within ±4°. It is also important to achieve an equal power split among all three beams. Unfortunately, the available equipment precluded achieving both the proper power split and the same polarization simultaneously. Therefore, since the proper polarization has proved more important than an equal power split in achieving high contrast fringes, polarization was optimized in lieu of power split. This resulted in a Bragg shifted beam with approximately 0.1 W less power (0.25 versus 0.35 W.). This number varied somewhat with the available laser power output and with adjustment of the Bragg cell.

The frequency shifter changes the middle beam frequency by 40 mHz, causing the interference pattern to "move" in the probe volume and thereby adding a velocity offset to the emitted signal. For example, if a particle were stationary in the probe volume, the movement of the pattern over the particle would create an apparent velocity that is associated with the 40 mHz signal. There are several advantages to this technique. The bias eliminates the problem of directional ambiguity. Laser Anemometry provides only a line along which the velocity is observed and a velocity magnitude is measured. In flows with low or zero velocities, the direction of particle motion, even if observed, may be uncertain. This problem is circumvented by using frequency shifting.

The use of the frequency shifting technique also eliminates the problem of angle biasing. Angle biasing is a bias in the measurements that result from a variation in the actual flow angle. The signal processor used in this present work requires that a seed particle cross at least 8 fringes as it passes through the probe volume. Therefore, more valid measurements per unit time occur when the flow is parallel to the fringe normal. In an unshifted probe volume, the error is proportional to the angle between the fringe normal and the velocity vector. In a Bragg shifted system, virtually any particle entering the probe volume will cross 8 fringes since the fringes are moving at relatively high speed.

Another advantage to frequency shifting is that, since the fringe pattern moves through the probe volume with a frequency of 40 mHz, it allows the probe volume to be focused to its minimum size and still retains the required minimum number of fringes (8) for signal processing. This maximizes power density and minimizes position uncertainties.

The beam stop blocks out extraneous laser beams generated by the frequency shifter and the beam steering module allows the two separate probe volumes to be accurately superimposed.

The beam pair selector consists of a high speed shutter that selects two of three laser beams generated in the system. They are orientated as if at the corners of a right angle isosceles triangle (Fig. 5e). The triangle is orientated so that one of the right angle sides is parallel to the axial direction and one is parallel to the tangential direction. The beam at the right angle corner (the vertex of the triangle) is frequency shifted and is the common beam to both of the two sets of beams. The beam selector blocks one of the nonfrequency shifted beams. These two sets of beams create two orthogonal probe volumes that measure the axial and the tangential velocities.

The 2.27X beam expander is used to effectively reduce the size of the probe volume. Since the probe volume linear dimensions are a function of $(1/D_{e^{-2}})$, an increase in the beam diameter $(D_{e^{-2}})$ by 2.27 results in a corresponding reduction in the probe volume length and width. The principle advantages in using a beam expander are the reduction in the depth of the measuring volume and the increase in the power density in this volume.

As discussed in section 3 below, the light fluoresced by the particles in the probe volume is orange in color. The orange band-pass filter stops light of frequencies other than orange from entering the photomultiplier tube. This can improve the signal-to- noise ratio by eliminating extraneous reflected light. However, during the current investigation, the orange pass filter was used only near the rotor endwalls, since the fluoresced light intensity is only approximately 10% that of the light scattered in the direct backscatter mode. Since signal strength was marginal in the direct reflection mode in most regions, operation in the fluorescent mode was normally not feasible.

The final optical element in the beam's path is a 3.2 mm thick window made of chemically strengthened glass and extends from 1.5 blade chord lengths upstream to 1 chord length downstream of the rotor blades. The window covers a circumferential width of 20° or two rotor pitches. It conforms with the outer flow path in both the axial (streamwise) and tangential directions.

An inhouse code [70] was used to verify that refraction errors created by observing the flow through this window would not seriously degrade the signal acquired.

Further, during the daily operation, the probe volume position was accurately determined prior to the start of the days data acquisition phase.

All optical elements were either bolted to the optical table with clamps or attached with permanent magnets.

The probe volume is an ellipsoidal shaped region approximately 125 μm wide and 2 mm long.

To obtain data the light emitted or reflected from the probe volume is collected by a focusing lens. It is then directed through an orange pass filter and another focusing lens that focuses it through a 125 μm diameter pinhole onto the face of a photomultiplier tube.

The combination of the 160 mm and the 200 mm focal lengths of the transmitting and receiving lenses actually results in a pinhole image diameter of 125 μm at the probe volume. The beam waist diameter at the probe volume dictates the selection of the image diameter and, hence, the pin-hole diameter.

The lenses are cemented doublet, commercially available, corrected to obtain "negligible" spherical aberration.

Table III provides the design probe volume specifications and the calculated probe volume specifications from the measured crossing angles.

2. Positioning System

The entire optical system is mounted on top of a mobil metal cart. This cart can be rolled away from the compressor facility for easy access and maintenance. When rolled into position, the cart is bolted to the floor to insure a firm base for the laser anemometer.

Mounted on the cart are three commercially available translating stages. These stages provide more than 45 cm of movement in three orthogonal directions. This movement insures complete coverage of a rotor passage.

3. Flow Seeding

Liquid seed particles, nominally 0.5 μm in diameter, are injected into the flow through a 6 mm diameter tube located 35 cm upstream of the rotor.

In order to minimize the problem of a noisy signal produced from light scattering off solid surfaces, the fluorescent dye technique [67] was used near rotor endwalls. Here, fluorescent seed particles absorb the incident laser light and emit light at a different wavelength. An optical filter in the receiving optics blocks the unwanted reflected light scattered from surfaces near the probe volume. The selected seed material was a 0.02 molar solution of Rhodamine 6G in a 50-50 mixture by volume of ethylene glycol and benzyl alcohol. This material fluoresces orange when it absorbs green laser light. As was mentioned earlier, beam power limitations restricted operations in the fluorescent mode to regions immediately adjacent to the endwalls. As will become apparent from a review of the provided output, the data obtained in this mode of operation is of far poorer quality.

In the passage areas away from the endwall regions, direct light scattering from the seed was observed. In these regions of low background light levels, the greater intensity of the scattered light greatly enhanced the data acquisition rates.

C. DATA ACQUISITION AND REDUCTION

The data acquisition system consisted of the optical system to acquire the signal, a signal processor to do preliminary processing and validation of the data, a shaft angle encoder to provide information on the circumferential (or tangential) position of the compressor rotor and a minicomputer to control the data acquisition and do preliminary post processing. A laser buffer interface received the signal from the signal processor and the shaft angle encoder, combined them and sent them to the minicomputer. The signal processor, shaft angle encoder, and minicomputer are described in greater detail below.

1. The Minicomputer

The data acquisition and online data reduction was greatly enhanced by the addition of a larger, more capable minicomputer and the implementation of additional software.

The current minicomputer, a VAX-11/750 using the VMS operating system is described in some detail in Ref. [72]. The machine contains sixteen 32-bit general purpose registers. The computer has hardware floating point multiply-divide capability. It also has dual cartridge magnetic disk storage with a total capacity of 360 million 16-bit words.

The minicomputer terminal has a CRT display for presentation of both alphanumeric and graphic information.

Typical data acquisition sessions required the use of the machine simultaneously in at least three ways: (1) data acquisition, (2) probe volume positioning, and (3) preliminary data screening and observation.

2. The Signal Processor

PMT signal bursts were processed by a commercially available counter type processor [73]. This processor contains a 250 mHz clock accurate to within ±1 nanosecond.

Invalid measurements will result from any of the following conditions:

(1) amplifier saturation,

(2) amplitude limit exceeded,

(3) an end of burst condition before eight cycles are detected,

(4) more than 254 cycles per burst,

(5) failure to meet the comparison criteria:

$$t_8 \cdot \frac{8}{5} - 2 \cdot 10^{-9} \text{ sec} \le t_5 \le t_8 \cdot \frac{8}{5} + 2 \cdot 10^{-9} \text{ sec} \tag{7}$$

where t_8 = time measured for 8 cycles and

t_5 = time measured for 5 cycles,

(f) time measured exceeds 2^{24}-2 counts.

A validated signal representative of the time to cross eight fringes and, thus, the appropriate velocity component, is sent to the minicomputer along with a signal from the electronic shaft angle encoder. This latter signal defines the tangential position of the rotor when the PMT signal burst was processed.

Previously provided to the minicomputer is information concerning the velocity component measured, probe volume axial position, and fluid temperature.

3. Electronic Shaft Angle Encoder

This device, developed in part at the Lewis Research Center, provides the current angular position independent of the rotor speed with the only required input being an accurate once-per-rev pulse (OPR). The encoded angular position of the rotor is produced by a counter that is clocked by a frequency synthesizer. The synthesizer frequency is adjusted as necessary each revolution so that the number of counts per revolution remains constant.

An operational requirement of the shaft angle encoder is that the fractional change in the angular velocity of the rotor for each revolution be small compared to the desired resolution in the angular position expressed as a fractional change in the angular position expressed as a fractional part of one revolution.

During the current project, the rotor had 36 blades and a design operating speed of 17189 RPM. It was operated at 60% design speed or approximately 10313 RPM (then corrected to standard day conditions). For a desired count of 200 per blade passage, the counts per revolution are 7200. The long term (1 sec) speed drift in the facility is about 0.3% (22 counts per 7200). However, the rev-to-rev speed changes are less than one count.

For the data taken during this study, the encoder was divided by four to yield a resolution of 50 angular positions per blade passage (suction surface to suction surface).

Note that the velocity measurements do not occur at discrete shaft positions, but rather are made anywhere within an interval between adjacent shaft positions marked by the shaft angle encoder. This interval is along an arc in the flow passage at a given region radial/axial location. For the data taken in this experiment, this arc length varies between 0.621 mm at the hub and 0.896 mm at the rotor tip.

At each radial and axial position surveyed, data are recorded at 1100 different shaft positions. These shaft positions are distributed as 50 positions per passage across 22 consecutive passages. The velocity and flow angle are calculated at each position from runs made at the two different beam orientations. The velocity distribution across the measured 22 passages is considered to be 22 separate observations of the flow in an average blade passage.

Velocities and flow angles at corresponding points relative to the blade in each individual blade passage are averaged together to yield a spatially-ensemble averaged blade-to-blade velocity and flow angle distribution; i.e. an "average passage" velocity field.

A typical run for the laser data acquisition system consists of collecting approximately 5000 measurements at a given axial/radial position, yielding an average of about 5 measurements at each of the 1100 measured shaft angle positions. Run times varied from 1 to 30 min for each position. Generally, the closer to the endwalls and the farther downstream in the rotor, the longer the data acquisition time needed and the poorer the quality of the data.

4. Conventional Instrumentation

The conventional pitot-static instrumentation available in the facility was used to set and monitor the rotor operating conditions. It was also used to provide information for the analytical solution that was subsequently used for comparison and analysis of the experimental data.

This conventional data and the rig operating conditions were monitored and recorded using the center-wide "Escort" data acquisition system [74]. This system is an interactive, real time data acquisition, display, and recording system which is used for steady state measurements. The system consists of a remote acquisition microprocessor (RAMP), data input and output peripherals, and a minicomputer. The minicomputer coordinates and executes all real time processing. The RAMP acquires the data from the facility instruments, sends the data to the minicomputer, and distributes the processed data from the minicomputer to the display device.

Surveys of flow conditions upstream and downstream were made on a regular basis to insure the stability of the flow conditions.

The rotor casing was modified for this test to include substantial additional instrumentation. This instrumentation includes static taps on the casing and hub, and surveys upstream and downstream of the rotor. Table IV shows the locations of the surveys. Table V provides the positions of the static taps.

The survey instrumentation consisted of total pressure, static pressure, total temperature, and flow angle. Survey data was taken at 9 radial locations and two axial locations.

Total pressure, total temperature, and flow angle were measured with a combination cobra probe similar to the one shown in Fig. 7a. The static pressure was measured with an 8° "C-shaped" wedge probe similar to that shown in Fig. 7b. Each probe was positioned with a null-balancing, stream-directional-sensitive control system that automatically aligned the probe to the direction of flow. The material used for the thermocouples was iron-constantan. The wedge probes were calibrated in a low speed air tunnel. The total pressure and thermocouple probes were calibrated to a freestream Mach number of 0.9 in a high speed wind tunnel. Two combination and two static wedge probes were used both upstream and downstream of the rotor.

A calibrated flat-plate orifice was used to determine the flow rate and an electronic speed counter, in conjunction with a magnetic pickup, was used to measure rotative speed (RPM).

Data uncertainties due to the inherent errors of the instrumentation and recording systems are given in Table VI.

D. TEST FACILITY

The entire investigation was carried out at the Lewis Research Center single stage compressor test facility. A schematic of this research facility is shown in Fig. 8. It is described in detail in Refs. [75, 76].

The drive motor for the system consists of a 3000 HP electric motor with a variable-frequency power supply. Motor speed can vary from 400 to 3600 RPM. The motor is coupled to the compressor rotor through a 5.52 ratio gear box that increases the compressor rotor speed to an approximate maximum of 19850 RPM (the program rotor design speed was 17189 RPM). Ambient, unconditioned air was the working fluid and was drawn in from the roof of the building and exhausted through the basement of the building. The amount of airflow was measured across a thin plate orifice and was controlled using the downstream collector valve.

E. RESEARCH COMPRESSOR

The aerodynamic and mechanical design of the compressor used for this experiment is presented in detail in Ref. [75]. Aerodynamic performance is presented in Ref. [77]. The design parameters are summarized in Table VII. This rotor was designed as the first stage rotor for an eight stage compressor. The first stage design pressure ratio was 1.82. The blades were designed to be multiple circular arc blade profiles. Figure 9 shows a meridional plane view of the compressor flow path and Fig. 10 shows the rotor blade sections at three radial locations: near the hub, midspan, and near the tip. Table VIII provides axial and radial geometry for both the endwalls and the blade leading and trailing edges. Rotor design tip clearance was 0.5mm.

F. COMPUTATIONAL DEVELOPMENT

1. Introduction

Recently a fully three-dimensional Navier-Stokes code has become available at the Lewis Research Center. This program, developed in-house by Dr. R. V. Chima, was developed for the analysis of turbomachinery blade rows and other internal flows [27].

It was used for the analysis of both the baseline and the enhanced endwall test configurations of this investigation. The information presented below was taken from Refs. [27] and [78]. A more detailed presentation is available in these publications.

2. Computational Grid

This Navier-Stokes solver requires the generation of a number of computational grids spanning various portions of the solution space.

Initially, a coarse, equally spaced, meridional grid, Fig. 9, is generated between the supplied hub and shroud contours. The blade geometry is interpolated onto this coarse grid.

Next a series of two dimensional blade-to-blade grids are generated along the meridional grid lines using a code developed by Sorenson [79]. This series of two-dimensional C-type grids are reclustered spanwise to form a fully three-dimensional grid. The two-dimensional grids are arranged along the radial stacking line and stretched so that the blade shape remains constant and the angular pitch of the outer periodic boundary remains constant. This grid is shown in Fig. 11. Once the grid is generated, the coordinates are transformed from cylindrical to cartesian coordinates for the solution.

Finally, because the C-type grid generated does not extend far enough upstream, the grid generation program also generated an H-type grid for the upstream solution space.

3. Governing Equations

The Navier-Stokes equations were written in a Cartesian coordinate system rotating with an angular velocity, ω, about the x-axis. This rotation introduces source terms into the y- and z- momentum equations. These governing equations are mapped onto a general body-fitted (ξ,η,ζ) coordinate system; the ξ-coordinate direction is assumed to follow the flow direction. The thin-layer approximation is used to eliminate all viscous terms in the flow direction while retaining all viscous terms in the cross channel plane. The resulting equations are:

$$\partial_t q + J[\partial_\xi \hat{E} + \partial_\eta \hat{F} + \partial_\zeta \hat{G} - \frac{1}{Re}\,(\partial_\eta \hat{F}_V + \partial_\zeta \hat{G}_V)] = H \tag{8}$$

where:

$$\begin{aligned}
\hat{Q} &= J^{-1}[\rho,\ \ \rho u,\ \ \rho v,\ \ \rho w,\ \ e]^T \\
H &= \quad [0,\ \ 0,\ \ -\omega\rho w,\ \ \omega\rho v,\ \ 0]^T \\
\hat{E} &= J^{-1}[\rho U',\ \rho u U' + \xi_x p,\ \rho v U' + \xi_y p,\ \rho w U' + \xi_z p,\ e U' + pU]^T \\
\hat{F} &= J^{-1}[\rho V',\ \rho u V' + \eta_x p,\ \rho v V' + \eta_y p,\ \rho w V' + \eta_z p,\ e V' + pV]^T \\
\hat{G} &= J^{-1}[\rho W',\ r u W' + \zeta_x p,\ \rho v W' + \zeta_y p,\ \rho w W' + \zeta_z p,\ e W' + pW]^T
\end{aligned} \tag{9}$$

It should be noted that the velocities in Eq. (9) are absolute with respect to a coordinate system that is fixed to the blade. Relative velocities (denoted by prime) are given by:

$$\begin{aligned}
u' &= u \\
v' &= v - \omega z \\
w' &= w + \omega y
\end{aligned} \tag{10}$$

Further, the relative contravariant velocity components are given by:

$$\begin{aligned}
U' &= \xi_x u' + \xi_y v' + \xi_z w' \\
V' &= \eta_x u' + \eta_y v' + \eta_z w' \\
W' &= \zeta_x u' + \zeta_y v' + \zeta_z w'
\end{aligned} \tag{11}$$

where it should be observed that u'=u but U'≠U.

The energy and static pressure are given respectively by:

$$e = \rho[c_v T + (u^2+v^2+w^2)/2] \tag{12}$$

$$p = (\gamma-1)[e-\rho(u^2+v^2+w^2)/2] \tag{13}$$

Using the Stokes' hypothesis, $\lambda = -\frac{2}{3}\mu$, the viscous flux can be written:

$$\hat{F} = J^{-1}\mu[0, F_2, F_3, F_4, F_5]^T \tag{14}$$

where

$$\begin{aligned} F_2 &= C_1\partial_\eta u + C_2\eta_x + C_3\partial_\zeta u - C_4\eta_x + C_5\zeta_x \\ F_3 &= C_1\partial_\eta v + C_2\eta_y + C_3\partial_\zeta v - C_4\eta_y + C_5\zeta_y \\ F_4 &= C_1\partial_\eta w + C_2\eta_z + C_3\partial_\zeta w - C_4\eta_z + C_5\zeta_z \\ F_5 &= \frac{\mu\gamma}{Pr}[C_1\partial_\eta(C_v T) + C_3\partial_\zeta(C_v T)] + uF_2 + vF_3 + wF_4 \end{aligned} \tag{15}$$

and

$$\begin{aligned} C_1 &= \eta_x^2+\eta_y{}^2+\eta_z{}^2 \\ C_2 &= \frac{1}{3}(\eta_x\partial_\eta u+\eta_y\partial_\eta v+\eta_z\partial_\eta w) \\ C_3 &= \eta_x\zeta_x+\eta_y\zeta_y+\eta_z\zeta_z \\ C_4 &= \frac{2}{3}(\zeta_x\partial_\zeta u+\zeta_y\partial_\zeta v+\zeta_z\partial_\zeta w) \\ C_5 &= \eta_x\partial_\zeta u+\eta_y\partial_\zeta v+\eta_z\partial_\zeta w \end{aligned} \tag{16}$$

Terms multiplied by C_1 and C_2 lead to nonmixed second derivative viscous terms, e.g., $u_{\eta\eta}$. On the other hand, terms multiplied by C_3, C_4, and C_5 lead to mixed derivative terms such as $u_{\eta\zeta}$. The viscous flux vector G can be written similarly, with directions η and ζ everywhere interchanged.

Metric terms are defined using the following relations.

$$\begin{bmatrix} \xi_x & \eta_x & \zeta_x \\ \xi_y & \eta_y & \zeta_y \\ \xi_z & \eta_z & \zeta_z \end{bmatrix} = J \begin{bmatrix} y_\eta z_\zeta - y_\zeta z_\eta & y_\zeta z_\xi - y_\xi z_\zeta & y_\xi z_\eta - y_\eta z_\xi \\ x_\zeta z_\eta - x_\eta z_\zeta & x_\xi z_\zeta - x_\zeta z_\xi & x_\eta z_\xi - x_\xi z_\eta \\ x_\eta y_\zeta - x_\zeta y_\eta & x_\zeta y_\xi - x_\xi y_\zeta & x_\xi y_\eta - x_\eta y_\xi \end{bmatrix} \tag{17}$$

where

$$J = (x_\xi y_\eta z_\zeta + x_\zeta y_\xi z_\eta + x_\eta y_\zeta z_\xi - x_\xi y_\zeta z_\eta - x_\eta y_\xi z_\zeta - x_\zeta y_\eta z_\xi)^{-1} \tag{18}$$

The equations are nondimensionalized by arbitrary reference quantities. The Reynolds number, Re, and the Prandtl number, Pr, are defined in terms of these quantities. It is assumed that the specific heats C_p and C_v and the Prandtl number are constant, that Stokes' hypothesis is valid, and that the effective viscosity for turbulent flows may be written as:

$$\mu_{eff} = \mu_{lam} + \mu_{turb} \tag{19}$$

where the laminar viscosity is calculated using a power law function of temperature:

$$\frac{\mu_{lam}}{\mu_{ref}} = \left(\frac{T}{T_{ref}}\right)^n \tag{20}$$

with n=⅔ for air.

4. Turbulence Model

The Baldwin-Lomax algebraic two-layer eddy viscosity model [80] is applied on cross-channel (η,ζ) planes. Two modifications to the standard model are made to account for the endwall boundary layer, the blade boundary layer and wake, and their interactions at the corners.

First, the distance from the wall is calculated using the Buleev [81] length scaled:

$$d = \frac{2s_\eta s_\zeta}{s_\eta + s_\zeta + (s_\eta^2+s_\zeta^2)^{\frac{1}{2}}} \tag{21}$$

where s_η and s_ζ are normal distances from the walls in the η- and ζ-directions, respectively. This length scale has the desirable property that d approaches the normal distance from one wall at large distances from the other wall.

Secondly, the turbulent viscosities are calculated across each boundary layer or wake separately and then the total turbulent viscosity is taken as the vector sum of the components. This assumption has the following desirable properties: (1) that outside of one viscous layer, μ_{turb} takes on values calculated for the other layer, (2) that it goes to zero in the core flow, and (3) that near the corners it accounts for both walls.

5. Boundary Conditions

At the inlet, total temperature $T_{0,ref}$ is specified as a constant. A ζ-distribution of total pressure $(P_0/P_{0,ref})$ is specified, as a constant or as appropriate for an inlet boundary layer with a given thickness and a power-law profile. The inlet whirl distribution, rv_θ, is specified.

For both test cases, measured survey data as shown in Fig. 12 was input to the solver.

The hub exit static pressure is specified and (ρ, ρu, ρv, ρw) are extrapolated. The exit radial pressure distribution is found by integrating the axisymmetric radial momentum equation:

$$\frac{dp}{dr} = \frac{\rho v_\theta^2}{r} = \frac{\rho}{r^3}(vz-wy)^2 \tag{22}$$

Sidewalls and the trailing edge are treated as periodic boundaries.

On the blade surface V'= U'= W'= 0 for viscous flows such as the current test cases. Blade surface pressures are found from the normal momentum equation. On the hub ζ=1 and on the tip ζ=ζ_{max}:

$$\begin{aligned}(\zeta_x\xi_x+\zeta_y\xi_y+\zeta_z\xi_z)\partial_\xi p + (\zeta_x\eta_x+\zeta_y\eta_y+\zeta_z\eta_z)\partial_\eta p \\ + (\zeta_x^2+\zeta_y^2+\zeta_z^2)\partial_\zeta p = -\rho\,[\omega(\zeta_y w-\zeta_z v) + U'(\zeta_x\partial_\xi u \\ + \zeta_y\partial_\xi v+\zeta_z\partial_\xi w) + V'(\zeta_x\partial_\eta u+\zeta_y\partial_\eta v+\zeta_z\partial_\eta w)]\end{aligned} \tag{23}$$

On the blades (η=1) the normal momentum equation can be found from Eq. 23 by replacing ζ everywhere by η and V' by W'.

6. Multistage Runge-Kutta Algorithm

The governing equations are discretized using a node-centered finite difference scheme. Second order central differences are used throughout.

The multistage Runge-Kutta scheme developed by Jameson, Schmidt, and Turkel [82] is used to advance the flow equations in time from an initial guess to steady state. If Eq. (8) is rewritten as

$$\partial_t q = -J[R_I - (R_v + D)] \tag{24}$$

where R_I is the inviscid residual including the source term, R_V is the viscous residual, and D is an artificial dissipation term described in the next section, then the multistage Runge-Kutta algorithm can be written as follows:

$$\begin{aligned} q_0 &= q_n \\ q_1 &= q_0 - \alpha_1 J\Delta t[R_I q_0 - (R_v + D)q_0] \\ . &= . \\ . &= . \\ q_k &= q_0 - \alpha_k J\Delta t[R_I q_{k-1} - (R_v + \ )q_0] \\ q_{n+1} &= q_k \end{aligned} \tag{25}$$

For efficiency both the physical and artificial dissipation terms are calculated only at the first stage, then held constant for subsequent stages.

7. Artificial Dissipation

The dissipative term D in Eq. (24) is a nonconservative version of that used by Jameson et al. [75]. It is given by:

$$D_q = (D_\xi + D_\eta + D_\zeta)q \tag{26}$$

where the ξ-direction operator is given by:

$$D_\xi q = C(V_2 q_{\xi\xi} - V_4 q_{\xi\xi\xi\xi}) \tag{27}$$

where

$$C = \frac{1}{J\Delta t} \tag{28}$$

is a coefficient that cancels similar terms in Eq. (25). To minimize the artificial dissipation in viscous regions, C is reduced linearly across several grid points to zero at the walls. The terms V_2 and V_4 in Eq. (27) are given by:

$$\begin{aligned} V_2 &= \mu_2 \max(v_{i+1}, v_i, v_{i-1}) \\ V_4 &= \max(0, \mu_4, V_2) \end{aligned} \tag{29}$$

where

$$v_{i,j} = \frac{|P_{i+1,j} - 2P_{i,j} + P_{i-1,j}|}{|P_{i+1,j} + 2P_{i,j} + P_{i-1,j}|} \tag{30}$$

and

$$\begin{aligned} \mu_2 &= O(1) \\ \mu_4 &= O(\frac{1}{16}) \end{aligned} \tag{31}$$

In smooth regions of the flow the dissipative terms are of third order and do not detract from the formal second-order accuracy of the scheme.

8. Three-Dimensional Stability Limit

Applying a linear stability analysis to the inviscid form of the governing equation gives the following expression for the time step:

where

$$\Delta t \leq \frac{CFL}{l_x|u|+l_y|v|+l_z|w|+c\sqrt{l_x^2+l_y^2+l_z^2+\omega^2}} \tag{32}$$

$$\begin{aligned} l_x &= |\xi_x| + |\eta_x| + |\zeta_x| \\ l_y &= |\xi_y| + |\eta_y| + |\zeta_y| \\ l_z &= |\xi_z| + |\eta_z| + |\zeta_z| \end{aligned} \tag{33}$$

The Courant limit for a particular multistage scheme depends on the number of stages and the choice of coefficients, α_i, of Eq. (25).

To accelerate convergence to the steady state, the maximum permissible time step at each point is used so that the Courant number is constant everywhere. The time step is calculated once based on the initial conditions. It is stored and not updated during the calculations.

9. Implicit Residual Smoothing

Residual smoothing was introduced by Lerat [83] for use with the Lax-Wendroff scheme and was later applied to Runge-Kutta schemes by Jameson [84]. The technique involves replacing the residual calculated in Eq. (24) with a value that has been smoothed by an implicit filter such as:

$$(1-\epsilon_\xi\delta_{\xi\xi})(1-\epsilon_\eta\delta_{\eta\eta})(1-\epsilon_\zeta\delta_{\zeta\zeta})\bar{R} = R \tag{34}$$

where $\delta_{\xi\xi}$, $\delta_{\eta\eta}$, and $\delta_{\zeta\zeta}$ are standard second difference operators and ϵ_ξ, ϵ_η, and ϵ_ζ are smoothing parameters.

Linear stability analysis has shown that the Runge-Kutta scheme with implicit residual smoothing may be made unconditionally stable if the ϵ smoothing parameters are made sufficiently large. In one dimension:

$$\epsilon \geq \frac{1}{4}\left[\left(\frac{\lambda_c}{\lambda_c^*}\right)^2 - 1\right] \tag{35}$$

gives unconditional stability if λ^* is the Courant limit of the unsmoothed scheme, and λ is a larger operating Courant number. In three dimensions different ϵ's may be used in each direction, and their magnitudes may be often reduced below the value given by Eq. (35).

10. Application of the Solver

Experimental information of the inlet flow conditions was used as inputs to the solver. These initial experimental conditions are density, the velocity vector, and the internal energy at the measured inlet radial locations. All input conditions were nondimensionalized by the inlet stagnation speed of sound and stagnation density. The inlet endwall boundary layers were assumed fully turbulent.

The code was then solved for a number of mass flows to generate an operating map for the compressor for both test configurations. Flow points on the computed maps were matched to the test operating conditions and results at the same relative position on the flow map were compared. Mass flows for the baseline test case, 10.727 Kg/sec and the enhanced endwall, 10.545 Kg/sec compared favorably with the mass flows calculated using the Chima solver, 10.661 Kg/sec for the baseline and 10.904 Kg/sec for the enhanced endwall.

Mass was conserved to within 0.1% between inlet and exit conditions for all calculations for both inlet test cases. Both test cases were carried through at least 2040 iterations, during which maximum residuals decreased by approximately two orders of magnitude. Both maximum and average residual values had reached minimum values by 1700 iterations and solutions were considered final by 2040 iterations.

Next, the ASCII files containing the two computed solutions were downloaded to the MicroVax from the Cray YMP for additional post processing. The information in these files was interpolated from the solution "C" grid to the locations where data was acquired using a spline fitting routine. The information was then ploted using the same plotting routine that was used to plot the acquired experimental results.

Since the computed mass flows do not match exactly, slight differences in velocity magnitudes and flow angles can be expected.

Finally, it should be noted that the solver, in it's current form, contains no provisions for tip clearance. Therefore, differences between computed flow solutions and measured flow conditions can be expected in regions near the shroud where clearance effects might be observed. However, since data was not successfully acquired beyond 90% span, this discrepancy is not expected to adversely affect the comparisons between experimental and predicted results.

IV. EXPERIMENTAL PROCEDURE

A. INTRODUCTION

The primary goal of the current research was to explore the effects of axisymmetric inlet flow radial distortion on the performance of a typical compressor rotor. To accomplish this, it was necessary to minimize the possibility of extraneous flow features developing in the passage due to facility instabilities which could be produced by small variations in rotor speed. Operation at a flow rate slightly lower than the peak efficiency point would tend to stabilize the flow and still minimize off-design flow abnormalities. Therefore, the flow condition analyzed was specified to be near the 60% design RPM peak efficiency point (60% DSPD). Operation at 60% eliminated shock induced secondary flows. As an additional benefit, data acquisition rates were greatly improved and noise levels were correspondingly reduced.

To further isolate the secondary flow effects caused by the inlet distortion, the data was acquired for two different inlet conditions. The first, or nominal, flow condition was specified to be at the near peak efficiency, "smooth" inlet velocity profile, 60% DSPD flow condition. Then, for the second flow configuration, axisymmetric screens were placed on the hub and shroud, approximately 25 cm upstream of the rotor. These screens had the effect of generating a nonuniform inlet profile, thereby developing the thicker inlet endwall boundary layers that enhance the passage vortex. These blocking screens consisted of a coarse mesh (four wires per 2.54 cm mesh) extending 3.05 cm from each endwall into the flow. A finer mesh (eight wires per

2.54 cm) screen was laid on top of the coarse screens and these extended from the endwalls approximately 0.76 cm into the flow.

The mesh design used was based on previous work done at the Lewis Research Center. The design has been shown to produce a smoothly varying inlet velocity profile. The selected screen coarseness was chosen to provide an inlet profile severe enough to provide substantial difference between the two test cases and mild enough to allow stable operation of the rotor. Further, the velocity profiles needed to be mild enough to allow a computational solution to be obtained.

Figure 12 shows both profiles of the absolute total velocity, V_{to}, and absolute flow angle, angle, as surveyed at the upstream aerodynamic survey location. The profiles were selected to be different enough to generate a measurable passage vortex but moderate enough to allow smooth operation of the rotor and successful modeling on the available analysis codes. Flow conditions were matched by adjusting the flow coefficients, as discussed by Wagner et al. [64]. Here, the area average inlet axial velocity was used to define the flow coefficient.

Aerodynamic data consisting of total pressures, static pressures, and temperatures were acquired at two locations; one upstream and one downstream of the rotor. The upstream location was 2.54 cm upstream of the hub/rotor leading edge intersection and the downstream location was at 10.668 cm downstream of the hub/rotor leading edge intersection. Data acquired at the aerodynamic survey location was used for several purposes. First, this data provided the inlet pressure profile and exit static pressure required as inputs for the flow solver used in the analysis portion of this project. Second, these profiles were used to adjust the calculated flow coefficients and, lastly, regular surveys during the data acquisition period were used to help maintain constant rig flow conditions.

The inlet surveys show the average total velocity, V_{to}, and absolute flow angle at a position well upstream of the rotor. A comparison between the two velocity profiles shows a difference of over 5 m/sec at the midspan of the passage with the thickened or artificially enhanced boundary layer (AEBL) velocities higher. The situation is reversed closer to the endwalls with the baseline profile over 6 m/sec larger near the hub endwall and over 4 m/sec higher on the shroud side of the passage. This difference in the inlet velocity profile is the desired difference to generate the passage vortex that is the object of this thesis. The differences here are of the order of 10% of the freestream velocities.

Differences in the inlet flow angle measurements between the two velocity profiles is small except near the shroud. There is some indication that the enhanced boundary layer is turned more at the midspan than the baseline with the converse being true at the endwalls. However, with the exception of the two measurements nearest the shroud, the differences are very small; less than 0.3°. More interesting is the fact that there seems to be, for both profiles, a turning of the inlet flow from axial near the hub to about 2° near the tip. The cause of this is unclear. There is nothing upstream of the rotor to cause any turning of the flow. Further, while laser anemometer measurements indicate some turning of the flow upstream of the rotor, the profile is of a more constant magnitude from hub to shroud rather than one of increasing magnitude. It seems unlikely that the rotor would affect the flow this far upstream. Therefore, the most likely cause of this profile is a small, systematic error in the measurement of the flow.

Overall results of the surveys at the aerodynamic exit are shown in Fig. 12b. These results show the enhanced boundary layer case with only slightly higher exit velocities, less than 3 m/sec, over most of the flow passage. They also show slightly higher turning of less than 2° over most of the passage.

It is difficult to see any great differences between the two test flow conditions. However, the enhanced boundary layer case seems to be slightly more turned near the endwalls than at the midspan than the baseline case. Maximum differences are of the order of 2°. This increased turning would be consistent with the generation of the passage vortex.

Laser Anemometer data was acquired at eight different chord locations, the farthest upstream was at the upstream aero-survey location and the farthest downstream was at the 105% chord location. At each of these locations, data was taken at ten spanwise locations varying from 5% span (from the hub) to 90% span. No usable data was obtained at any chord location at 95% span. Figure 13 shows a schematic of the locations and Table IX gives the chord, span, axial, and radial position of each location.

Little usable data was acquired at the 105% chord line due to extremely high noise levels. Table X lists the points where the data acquired was, at best, marginal. Data acquisition was attempted at the 95% span location but was unsuccessful due to high noise levels and to a rapid buildup of particle seed on the surface of the observation window.

The test program began with rig "shakedown" runs in September of 1987. Aerodynamic surveys of the rotor were accomplished in October of 1987. Laser Anemometer shakedown runs began in February of 1988 and data acquisition began in mid-September of that year. A facility wide shutdown forced the termination of data acquisition on November 1 of 1988. It is important to note that data was acquired over a six week period from mid-September to the end of October. During this time frame, stagnation temperatures at the inlet varied from approximately 25° C to below freezing and relative humidities from 20% to saturation conditions. A typical data acquisition period would start at 9:00 AM and would terminate near midnight.

To minimize the effect of varying atmospheric conditions, every effort was made to acquire the data for one chord location during one test period. Further, rig operating conditions were continuously monitored and the operating point of the rig was regularly corrected to standard day conditions.

The installation and removal of the screens for generating the enhanced endwall boundary layers required an extensive disassembly of the test compressor. For this reason, all "baseline" data was obtained first and then the screens were installed. After the screen installation, all the thickened endwall boundary layer data was secured. This strategy reduced the number of compressor assemblies to two.

The "growth" of the rotor, due to rotational forces and blade aerodynamic loading, was measured to insure the proper positioning of the probe volume. Due to the relative shortness of the blade, little growth occurred between 1% and 60% speed. This radial growth was less than 0.3 mm. Growth between 60% and design speed was about 0.3 mm. No measurable blade "untwist" occurred between 1% and 60% design speed.

B. RUN PERIOD SETUP AND DATA ACQUISITION PROCEDURES

Prior to each daily data acquisition period, the laser anemometer and the probe volume position with respect to the rotor were checked. Laser Anemometer alignment was checked by attempting to acquire signal at an upstream location at low flow conditions. Approximately 25% of the time a system realignment was required. To realign, a small wire was placed in the probe volume and the pinhole positioned to optimize PMT output signal. The wire simulated the presence of particles in the flow and provided a reflected image or signal. This image was superimposed on the pinhole and the PMT signal optimized. On these occasions, beam trueness (parallelness with respect to the other beams), laser power, beam polarization, and probe volume coincidence (both probe volumes occupy the same space) were all checked. Of these variables, pinhole position and laser output power were most likely to require optimization.

After the laser anemometer alignment was optimized, the probe volume position with respect to the rotor was determined. This was done by positioning the probe volume on the front lip of the rotor disk. This position was accurately known with respect to the blade surfaces. Once the probe volume was accurately positioned on the rotor, software offsets in the laser anemometer positioning code were corrected to insure accurate positioning of the probe volume.

Aerodynamic surveys were taken upstream and downstream of the rotor at the start, finish, and at regular intervals of each data taking session. Flow conditions were continuously monitored during the run period to minimize run point drift. Estimates in the run point drift have been previously given in the facilities section of this thesis.

Prior to each day of testing, an inhouse computer program was run to determine the axial and radial positions for each point in the flow field to be surveyed. The passage was generally surveyed at one chord location during each data acquisition period. The data acquisition began at the closest to hub location to be surveyed (5% span) and moved radially outward towards the tip. This program also generated an optimum offset from radial that would minimize the blade blockage for runs inside the blade.

The aerodynamic design of the rotor blades resulted in a blade shape that "leaned" off a radial line. Figure 14a shows a schematic of a typical area blocked by the blade shadowing. This lean leads to a shadowing of portions of the blade passage. This blockage was minimized by moving the line of sight off radial while remaining in a plane perpendicular to the axis of machine rotation (Fig. 14b). This was accomplished by mounting turning mirror 18, shown in Fig. 6, on a goniometer cradle. It must be noted that when this was done, it caused a rotation of the beam planes equal in magnitude to the size of the radial offset.

The goniometer offset was increased and decreased for a number of runs in an unsuccessful attempt to obtain data nearer the blade surfaces (Fig. 14c). The maximum off-radial goniometer setting used was 6°. This off-radial positioning of the goniometer was calculated using the inhouse computer code mentioned above. The calculation yielded the setting that would minimize the effects of blade shadowing. The size of the off-radial movement of the optical package was determined using an inhouse computer code that geometrically traced the optical paths of the incoming laser beams and calculated an off radial line-of-sight that would minimize the effects of blade blockage. This leads to a maximum velocity error of less than 0.6% for the tangential component. This maximum offset was used in only two locations. All velocities were corrected for goniometer offsets used. Table IX lists the various goniometer offsets used.

All laser anemometer data acquisition was done through the test cell minicomputer. Each radial/axial data point was manually entered into the software on the computer. This software then directed the proper positioning of the laser table.

Additional software acquired and processed the raw PMT signal to present a real time velocity or frequency histogram and ensemble averaged blade-to-blade velocity information to the operator. Example output is shown is Figs. 15 and 16.

The information in these two figures, and in Fig. 18, needs some clarification. The data acquisition software was designed to operate not only in turbomachinery but also in wind tunnels. Therefore, position is displayed in terms of cartesian coordinates. For this experiment, X and Xpos refer to axial location while Y and Ypos refer to the radial location. Z and Zpos were not used and the position measurements were provided in inches. Zt or "beam rotation" refer to the measured velocity component where 0° indicates the axial throughflow component and 90° indicates the tangential velocity component. The term RT or "beam deflection" indicates the deviation from zero of the observation angle of the laser anemometer package, i.e., the off-radial goniometer angle. The total temperature of the flow is presented in degrees Rankine and "nmeas" presented in Fig. 16 refers to the total number of processed measurements acquired at that axial/radial location. "Run" of "Run nos" indicates which data runs are being presented. These numbers are the first or original run numbers given in Table XI.

In Fig. 15, nplot is the number of plotted measurements. Lclip and hclip indicate the number of measurements not plotted because they exist beyond the plotted range. Vmean is the mean measured frequency and stdev is the standard deviation. In Fig. 15, the abscissa is the frequency in mHz. The data acquired has been artificially shifted by forty mHz. This offset has been removed for this figure. The negative frequencies reflect measurements of particles with negative tangential velocities. These velocities result in frequencies less than forty mHz.

In Figs. 16 and 18, the abscissa represents the ensemble average window in which a velocity measurement was acquired.

The laser anemometer data acquisition technique is presented in more detail in Ref. [68].

At each axial/radial location, an attempt was made to acquire at least 5000 data measurements. A reduced number of measurements were obtained at 75%, 95%, and 105% chords due to excessively low data acquisition rates in these regions.

Two orthogonal velocity components were obtained at each radial/axial location.

One of the input laser beams was frequency shifted by 40 mHz, thereby effectively eliminating the flow angle biasing problem and the directional uncertainty problem.

The laser anemometer survey locations in Fig. 12 represent, in actuality, arcs in space at these locations. During a data acquisition sequence, data began to be recorded on reception of a specific once-per-rev signal transmitted by the shaft angle encoder. Data was then accepted over a period of time during which the rotor accomplished 0.6111 revolutions (22 of 36 rotor passages). During this time interval, 22 passages of the rotor passed through the stationary position of the probe volume. Whenever a valid signal was acquired, it was stored, along with the specific time interval that started after the arrival of the once-per-rev signal. Each velocity signal was then assigned a position in one of 1100 "windows" or bins that together made up the arc that spanned the 22 passages of the rotor over which data was acquired. This is 50 windows per passage. In the post processing phase of the project, these 22 passages were further combined into one "average" passage. At each axial/radial location in this average passage, an arc spanning the passage from suction surface to suction surface was divided into 50 windows. Each contained an average velocity of data acquired in that average arc segment from data acquired in each of the 22 passages at the geometrically equivalent arc segment.

This consolidation of data acquired over these 22 passages was justified because there were no appreciable differences in the data acquired in any of the passages. This indicated that, aerodynamically, the passages were equivalent and could be viewed as identical.

The time required to complete a revolution (the remaining 14 of 36 blade passages) was used by the software to store and perform preliminary processing of the acquired data.

PMT voltage was normally set at 1800 V for florescence and 1400 V when the seed particles were observed from direct scattering. This voltage was varied to optimize data rate with a minimum of adverse noise effects.

The laser was operated at maximum power at all times. This varied from 1.6 to 2.4 W. Losses in the optical system typically reduced the power delivered to the probe volume for two beams by 75%, i.e., for the 2.4 W case only 0.6 Watts was delivered to the probe volume. Data acquisition with laser power levels less than 2.0 W was marginal or impossible in some locations and power levels of less than 1.6 W made data acquisition impossible at all locations. The variation in power output from the laser was the result of variations in the input power from the commercial power system. Since the laser power supply was closely tuned to the voltage level of the input power, small variations resulting from load variations on the commercial power grid caused substantial variations in the laser output power. The laser output power also depended upon the fine orientation of the laser reflector mirrors. These were hand adjusted, if necessary, prior to the days run and it was not always possible to achieve a perfect orientation.

C. DATA REDUCTION

At the end of the data acquisition phase, there were 960 sets of ensemble averaged velocity measurements. A set of measurements consisted of all the measurements of a single velocity component taken in each of the 1100 shaft positions at one axial/radial position. To obtain the complete measured velocity vector at an axial/radial location, two sets of velocity measurements must be combined: one axial velocity and one tangential measurement. At each location, at least two sets of data, one for each velocity component, were taken for each flow configuration. The flow configurations were the baseline or uniform inlet configuration and the enhanced endwall boundary layer (AEBL) configuration. At many locations, more than two sets of data were acquired. At a minimum, 320 sets of laser anemometer data are required to complete the test (80 locations times 2 configurations times 2 velocity components).

The initial step in the data reduction process involved visually comparing all data sets at each location to determine the most noise free data at each location for additional processing. Acceptable runs with the same spatial location, goniometer setting, velocity orientation, and inlet configuration were combined into single sets. At least one set for each velocity component, regardless of data quality, was retained at each spatial location, for each inlet flow condition for additional processing. There were 486 sets of data selected for further processing and combining into the 320 final sets of measurements. Table XI shows the initial combined runs and indicates how many runs were combined for each of the initial 486 selected runs. These runs are paired with their sister run at that spatial location.

To this point, no attempt had been made to improve the quality of the data acquired by removing "outlier" noise that had been included in the online data processing. To accomplish this, each of the 486 runs was processed to provide three plots. These were similar to the two plots shown in Figs. 15 and 16 and as well as a frequency histogram output similar to that shown in Fig. 17.

Some explanation of Fig. 17 is required. For each run or set of data, all data in each rotor passage spatial location (radial/axial) was combined into an ensemble averaged rotor passage equal to one pitch (10°). This passage was further divided into 50 windows, each of which was 12 minutes wide. Spaced along the abscissa of Fig. 15 are histograms of each of these 50 windows. The ordinate of Fig. 17 represents velocity ranges. The second row from the top is the first velocity range that contains the lowest velocity measurement. The second row from the bottom contains the range with the highest velocity measurement. Each range is approximately 5 m/sec wide.

The number displayed in each of these bins or velocity ranges represents the number of successfully processed velocity measurements in that applicable velocity range. This number, however, has been non-dimensionalized with respect to the velocity range in that window containing the greatest number of measurements. For example, range 50 in window 10 (circled) displays a 4. Range 45 (circled) in the same window contains a 9 and represents the velocity range with the highest number of successfully acquired velocity measurements. The displayed 4 indicates this velocity range contains 30% to 40% of the number of measurements in range 45. Thus the figure gives a feel for the distribution of velocities in each of the passage averaged windows at an axial/radial location.

To reduce the "outlier noise," the number of measurements in each velocity bin of a data acquisition run was reduced by a constant number of measurements. This number was calculated to be 20% of the number of measurements of the bin that contained the maximum number of velocity measurements. This procedure can be considered roughly equivalent to adjusting the triggering level in the signal processor to minimize noise. The 20% figure was arrived at by individually reviewing each of the 486 runs to insure that the 20% reduction would not adversely affect the accuracy of the result.

Following this processing, the two orthogonal velocity vectors for each inlet flow condition, spatial (axial/radial/circumferential) position, and goniometer orientation were combined to create a combined axial/tangential velocity vector. Figure 18 shows a typical output. Goniometer orientation was taken into account here to insure that the correct axial/tangential velocity components were calculated.

Finally, the 243 remaining runs were combined to generate 158 separate datasets; one for each axial/radial location at each of two inlet flow conditions. There were two locations where no data were acquired due to time constraints during a run period. Each spatial location was divided into 50 circumferential bins (arcs in space) that were 12 min wide.

D. ERROR ANALYSIS

Schenk [86] divides the possible errors inherent in a given experiment into three general classes: (1) accuracy errors, (2) precision errors, and (3) uncertainty errors. Accuracy errors are repeatable deviations from correct values that are the result of inherent errors in the system of the experiment. For example, a positioning device that consistently reads "x" cm lower than its actual position. Errors such as these have been accounted for in the data acquisition and reduction phases of this investigation whenever they have been found or suspected. For example, frequency shifting stability and laser table positioning and leveling with respect to the compressor facility were established prior to the data acquisition phase.

Precision errors and uncertainty errors are random errors occurring during the acquisition of data.

Precision errors are errors, for example, in the stability and repeatability of the equipment used in the study. The stability of the compressor rotor speed during the acquisition of the laser data is an example of this type of error. Information is provided concerning the compressor test facility and the system positioning table and represents the "best" measured information concerning the maximum possible inaccuracies in these variables.

Uncertainty errors are errors in the data acquisition for which a maximum imprecision cannot be measured. The uncertainties of these errors must be estimated statistically. Errors such as the velocity uncertainties are provided below.

Various errors discussed below can be divided into errors resulting (1) in the operation of the test compressor, (2) in the position of the probe volume, and (3) in the act of measuring the fluid velocities and processing those measurements.

1. Compressor Test Facility

The compressor test facility has been in operation for a number of years and the inaccuracies associated with its operation are well documented [76]. Table VI presents a synopsis of the inaccuracies associated with the measurement of test facility operational parameters and conventional instrumentation used at the facility.

2. Laser Anemometer system positioning error

The accuracy of the optical system positioning table is 0.05 mm over a range of 25 cm in either direction. This figure is applicable to all three axes of movement. The direction of the input beams bisecting line can be determined to within ±0.01° using the goniometer over the goniometer operational range of ±3° from the compressor rig horizontal.

The measured precision error from the vertical and horizontal of the input laser beams is less than 1.4°. This results in a maximum measured velocity error of less than 1.5%.

The translating table was measured to be square with respect to the compressor facility to within less than 0.1°, resulting in a maximum positioning error of less than 0.38 mm over the distance of movement.

3. Discussion of Laser Anemometer system measurement error

There have been a number of excellent publications dealing with the assessment of errors in the data acquired using Laser Anemometry. Information from three of these, Strazisar [87], Seasholtz [88], and Strazisar and Powell [89] was utilized extensively in assessing the errors present in the data acquired.

As has been previously mentioned, data was acquired over 22 of the 36 blade passages in the rotor at any of the desired radial/axial locations. At each of these locations an arc is described in space that traverses the 22 passages. Along this arc, each of these blade passages is divided into 50 windows or bins starting at the suction surface of the passage and extending to the next suction surface. This occurs 22 times. There are, then, 1100 windows (50 per passage). The passage to passage variations in the velocity fields have been minimal in previous investigations involving similar rotors. Therefore, to reduce the magnitude of the data processing problem, the measurements in the windows in each of the 22 measured passages have been combined into one of 50 equivalently positioned windows (with respect to the rotor blade suction surface) in an "average" passage. Then the velocity for any given window may be calculated as:

$$V_{pav}(k) = \frac{1}{nme(k)} \sum_{m=1}^{nme} V(m,k) \tag{36}$$

where $k=1,\ldots.N_{wp}$, and nme is the number of measurements. The standard deviation is given by:

$$\sigma_{pav}(k) = \left[\frac{1}{nme-1} \sum_{m=1}^{nme-1} [V_{pav}(k) - V(m,k)]^2 \right]^{\frac{1}{2}} \tag{37}$$

So, the average velocity in any of the 50 windows at an axial/radial location in the average passage is the average of all the velocity measurements in any of the windows at the same axial/radial location and the same circumferential location with respect to the suction surface of the rotor passage in which a particular velocity measurement was acquired.

Strazisar [87] states that the velocity probability density distribution is broadened by several factors which include:

(1) the random turbulent fluctuations in the flow,

(2) the flow unsteadiness that occurs at frequencies which are not integral multiples of the rotor rotational frequency,

(3) the average velocity gradients across the width of the measurement window (typically 1% or 2%),

(4) the flow variations caused by rotor speed drift during data acquisition (set to 0.4%), and

(5) the individual Laser Anemometer measurement errors (such as PMT noise).

There are a number of uncertainties and bias errors inherent in the laser anemometer method of velocity data acquisition. Reference [87] provides a detailed discussion of the various errors associated with the laser anemometer. Table XII is a listing of estimates of the size of the errors involved.

Two sources of measurement error are: statistical biasing error and angle biasing error.

Statistical biasing results from the fact that, in a uniformly seeded flow, more particles of higher velocity cross the field of view per unit time than for lower velocity flows. Therefore, the calculated mean velocity measurement over a given period of time yields a velocity higher than the true mean. This bias can be removed using the relation:

$$V_{av} = \frac{(V_{bi})_{av}}{\left[1+\left(\frac{V}{V_{av}}\right)^2_{bi}\right]} \qquad (38)$$

where "bi" denotes the biased measurements during the course of testing. Typical values of $(V/V_{av})_{bi}$ in the regions of usable data are of the order of 0.2%. Peak values in the leading edge region were as high as 10%. Since the vast majority of data included far smaller errors than the 10% near the leading edge region, this error was not taken into account in the data provided.

Angle biasing [87] is a result of variations in the flow direction with time. More measurements per unit time occur when the flow direction is parallel to the normal direction of the fringe pattern than when the flow direction fluctuates away from the fringe normal direction. This is because a particle entering the probe volume is more likely to cross the required minimum number of fringes to generate a signal that will be processed as valid. The error is proportional to the angle between the "fringe normals" and the mean flow direction. In the current experiment, the measured flow velocity measurements were frequency shifted. When frequency shifting is used, the frequency of one of the two beams that form the probe volume is slightly changed. In this experiment, the frequency shift was 40 mHz. The result is a change in the frequency of the signal emitted from a particle in the probe volume. Using the frequency model of the probe volume, it would appear that the fringes in the probe volume move. In such a probe volume, a stationary particle would emit a signal indicating a velocity as the fringes sweep across it. This signal, of the order of magnitude of the through-flow velocity, is optically added to all the measured velocity signals. This artificial velocity added to the optical signal insures that virtually any particle that enters the probe volume will cross the necessary fringes to generate a valid signal, thus eliminating the problem of angle biasing. Of course, this artificially added velocity is removed from the calculated velocity component during the post processing of the signal. More detailed discussion of these various statistical errors is presented in Refs. [87-89].

Another potential cause of error is particle lag. Particle lag is an inertial effect resulting from differences in density between the fluid being measured and the particles used to "seed" the flow that are actually being measured. There have been a number of analyses performed in the past to consider this problem [90-91]. It has been shown that particles less than 1 μm in diameter are required for accurate flow measurement. Measurements of the particles used in seeding the flow indicated that the mean particle size was near 0.5 μm. Less than 5% of the measured seed was greater than 1 μm in diameter. In this well behaved, steady state, subsonic environment, error due to particle lag should be very small.

Not all of the errors in the measurement of the average velocity, or more precisely, the error in a single Laser Anemometer measurement can be directly assessed. This error associated with a single L.A. measurement is a function of, among other things, flow turbulence intensity, optical noise from various components (photomultiplier tube, Bragg cell, blade flash, etc.), and electronic noise from various components (signal amplifiers, cabling, connections, etc.).

It is, therefore, standard procedure at the Lewis Research Center to determine the precision error by using:

$$C_v = \frac{Z \cdot \sigma}{\sqrt{N}} \tag{39}$$

where C_V is the confidence interval as a fraction of the calculated average velocity, σ is the calculated standard deviation, N is the number of measurements, Z is a measure of the confidence interval (nominally set to 1.97 for a Gaussian confidence interval of 95%). This calculation is used to determine the error margins presented in Tables A5 and A6 of Appendix A below.

V. RESULTS AND DISCUSSION

A. INTRODUCTION

A considerable amount of experimental data were acquired over the course of this investigation. It included "conventional" steady-state aerodynamic data that encompassed, among other measurements, surveys of total pressures, static pressures, and temperature at the inlet and exit of the rotor. The axial through-flow and the absolute tangential velocities were obtained via laser anemometer measurements. In order to contrast these data, computational predictions of the flow field were made as well.

All of this information was obtained for two different inlet velocity profiles: a baseline inlet flow condition and an enhanced (thickened) endwall boundary layer condition. The latter flow was created, as was explained earlier, by placing axisymmetric distortion screens on the hub and shroud of the rotor upstream of the inlet. Furthermore, all of the experimental data was acquired in a stationary reference frame. The computational predictions were made in a relative reference frame that was defined to be stationary with respect to the spinning rotor.

It must be understood that in a turbomachine, the flows into and out of a rotor are best analyzed in a stationary reference frame. This is because the component generating the rotor inlet flow conditions is stationary as is the downstream component that is affected by the rotor exit flow. On the other hand, the rotor is spinning and the effects of the flow-rotor interaction are best considered in a reference frame that is stationary with respect to the rotor: a relative reference frame. This reference frame is created by the addition of the rotor wheel speed to the fluid velocity.

Consideration of the various frames of reference were used to organize the presentation of the data. Accordingly, this chapter is divided into five main sections: (A) Introduction, (B) A Review of Data Acquired in the Stationary Reference Frame, (C) A Comparison of Results in the Stationary Reference Frame, (D) A Comparison of Results in the Rotating Reference Frame, and (E) Assessment of the Grid Velocity Deviations.

Section B is a station-by-station assessment of the acquired data. The section will provide a familiarization of the rotor flow, the type of data and its accuracy, and will briefly discuss some of the difficulties in interpreting the information gathered. Data from both inlet test configurations will be considered here because many of the difficulties in acquiring and interpreting the data are common to both cases. The computational results will also be reviewed when necessary to help clarify questionable data and to point out differences between the computational and experimental results.

The following section, section C, examines the inlet and exit flow features to assess what effects the different inlet profiles exert on the exit flow conditions.

Section D contains considerations of the differences between the two inlet profiles in the rotating reference frame, how these differences propagate downstream, and any unique flow features that occur in the rotor. The baseline flow condition will be considered first, and will be followed by the enhanced inlet boundary layer flow condition. Differences between the two will be noted. This section will also include comparisons between the computed predictions and the experimental data. Differences and similarities will be noted.

Section E provides a discussion of the Grid Velocity Deviations. The principal thrust of this experiment was to determine the effects of thickened endwall boundary layers on the development of the classic passage vortex. Since the radial velocity component was not measured, the actual passage vortex could not be measured. Nevertheless, some information on the development of the passage vortex can be obtained by comparing the measured velocity components with respect to each other and with respect to a calculated primary flow component. This section addresses this point.

Throughout the analysis of these flows, the computational results will be used as necessary to clarify the experimental results.

Before discussing the results obtained, some information which will help clarify the figures to be presented will be given herein.

In particular, Fig. 19 shows the coordinate system that is used in this analysis. When referring to a percent span, distance is measured from the hub, rather than as a percent immersion.

One way that the laser anemometry information is presented here is using cross channel plots. With one exception, these plots are of data at a constant chord location. The exceptions are the station 1 plots which are at a constant axial location upstream of the rotor. The view of these plots is downstream along the streamsurfaces seen in meridional view in Fig. 9.

All cross channel plots presenting both experimental results and computational predictions are viewed looking downstream into the rotor. Compressor rotation as viewed is clockwise. Therefore, the suction surface is at the bottom of each figure and the pressure surface on the top. The hub is at the left of the figure and the shroud is at the right.

Data presented in the figures containing line plots has been smoothed to improve the appearance and to clarify the flow features. To accomplish this, the separate measured velocities, axial and tangential, were individually reviewed and smoothed. As explained earlier, data was acquired at a number of axial/radial locations. At each location, velocities were measured along an arc spanning 22 passages. This data was combined into an arc spanning an average passage from one suction surface to the following blade suction surface. The data was smoothed by considering values along each of these arcs. A running average of the velocities in the nearest four windows along the arc to the window averaged was calculated. The velocity to be smoothed was not allowed to deviate more than 10% from that calculated average velocity.

A particularly difficult problem occurs in dealing with windows where no velocity measurements were acquired. These null velocity windows are not well handled by the spline curve fitting routine used and had to be eliminated from consideration. This was done by replacing all null velocity windows with values calculated by using linear interpolation between the velocities in the two windows bracketing the area of no measurements along the measurement arc considered.

With the exception of the -5% chord location, all tangential velocities were constrained to be within a range from 0.0 to 150.0 m/sec and axial velocities were constrained to be within 50.0 and 150.0 m/sec for this smoothing procedure. These limits were determined by reviewing the range of values in the calculated predictions for the regions where data was acquired and by reviewing the data itself to insure no regions existed that contained accurate velocity measurements outside of these ranges. The -5% chord location was not considered because it contained velocities outside of those ranges. Appendix A contains tables of all the measured test results obtained during the course of this investigation.

Two sets of cross channel plots that have not been smoothed are presented in Figs. 28 and 29. These are colorbar plots that are simple four corner averages.

Also presented in this Chapter are a number of mid-channel plots, specifically, Figs. 21, 23, 25, 27, and 32. They represent information from a window near mid-pitch, normally window 25, at each of the axial/radial locations. This mid-pitch location is not an "average" location. It does, however, represent a location approximately equidistant from either blade surface. Thus, it is likely to contain information that is freer from blade light reflection noise. While blade-to-blade effects are more obvious at the more downstream locations, these plots can be instructive, with reservations, when searching for spanwise variations in the flow. Since the inlet conditions are axisymmetric and vary only in the spanwise direction, it is worthwhile to consider the information in these figures.

Appendix A contains computer printouts listing the measured data and calculated results. The 'cp' is the window number. Window 1 starts on the suction surface and window 50 is the window that ends at the suction surface of the blade which is one counterclockwise passage away. In the first column of the tables are the 5% span from hub values, in the next column are the 10% span from hub values and the values in each column thereafter are 10% farther from the hub. The final column lists values from the 90% span measurements. No data was successfully acquired at 95% span.

B. REVIEW OF DATA ACQUIRED IN THE STATIONARY REFERENCE FRAME

The velocities measured by the laser anemometer were the axial and the absolute tangential velocity. The radial velocity vector could not be obtained using the current laser anemometer configuration. The other basic data obtained included the number of laser measurements at each axial/radial/circumferential location in each of the 22 blade passages surveyed. The information reviewed below has been combined into one "average" passage. This passage contains data obtained from all surveyed passages. Earlier experiments [67-69] have indicated that the differences between passages are extremely small and thus no important aerodynamic effects will be overlooked when combining all acquired data into one typical passage. The measured average passage axial and absolute tangential velocities, number of measurements, and calculated uncertainty ranges are presented in Appendix A.

The first part of this section contains a detailed review of the velocities measured at each location. This review should provide some strong indicators of which data obtained is accurate.

In areas near blade surfaces and passage endwalls, the quality of the acquired data is poorer due to increased optical noise. Data acquisition is further hampered by the difficulties in adequately seeding the flow in these regions. Seeding difficulties and metal blockage from the blades and rear window frame edge also reduced the quality of the measured data at locations further downstream.

We will look at the data one station at a time, starting with the inlet survey location and proceeding downstream. We will examine the baseline (uniform inlet) case and the AEBL (enhanced endwall boundary layer) case together but will consider the baseline case first at each station.

Please refer to Appendix A and Figs. 20 to 23, 41 and 42 for the following discussions in section A.

1. Station 1, Inlet Survey

In general, it can be said that the farther upstream and the farther from the endwalls that the data was acquired, the higher is the quality of the data obtained. The measurements made at the inlet survey location were the highest quality of any data at any of the test stations. The baseline case showed only one location where the information acquired was of questionable accuracy. This was at the 90% span location and is most likely the result of the accumulation of seed particles on the observation window. It should be noticed that in Table A1 in Appendix A the velocities varied from 50 m/sec to 100 m/sec within the space of only three windows. The only negative flow angles measured occur at this span location. The differences between the 80% span and the 90% span coupled with the rapid variations in velocity at this location, far upstream and steady state, indicate the data at this location is unreliable.

Data at 90% span for the enhanced endwall boundary layer case does not have the large velocity variations or the negative flow angles. Further, the number of measurements, error margins, and comparisons with the 80% span data suggest that this data is accurate.

The axial velocity profiles indicate a velocity bulge at the 10% span (Figs. 20 and 21) for the baseline configuration. This bulge does not seem to exist for the thickened endwall boundary layer test configuration. The aerodynamic measurements indicate a much smaller profile of this nature (Fig. 12) for both the baseline configuration and the enhanced endwall boundary layer configuration. However, the aerodynamic measurements show much weaker "bumps" in the velocity profiles. This may reflect actual flow conditions or it may be the result of a change in operating conditions between the two span locations. Figure 21 is a midpitch plot of the axial velocities. The midpitch plot is useful in that it is the most distant from each blade surface and, therefore, the signal is least likely to be corrupted by stray light. The data for one circumferential position is much easier to interpret.

The effects of the distortion screens are apparent in the enhanced endwall boundary layer test configuration with lower velocities extending farther from the endwalls and the velocity profile having a more distinctive parabolic shape.

There is a tangential velocity component that has been measured for both the baseline and the enhanced endwall boundary layer test configurations at the inlet. This velocity component is not apparent in the aerodynamic measurements and, given the inlet configuration, it is not indicative of the actual flow conditions and has been discussed earlier.

2. Station 2, -5% Chord

This location is immediately upstream of the rotor and the effects of the rotor bow wave are very apparent in the velocity and flow angles measured.

The velocities measured at 90% span appear to be invalid for the baseline flow case. The results shown in Appendix A are lower and more unsteady. Higher uncertainties have been calculated for the 90% span location.

A study of the number of measurements and the uncertainties (Appendix A) for the 5% and the 90% span readings highlights some of the difficulties in assessing the validity of these measurements. The 5% span data shows a large number of measurements and, as a result, very low uncertainties. Far more measurements have been processed for this radial location than for measurements at larger radial locations. The total number of measurements taken at any location was approximately 5000, but, for this location, approximately 10000 measurements were taken. However, the very large number of processed measurements at this location would indicate a spurious measurement, such as reflection from the hub or the blades, was processed as a valid velocity, since it reflects a much higher data rate.

In contrast, measurements at the 90% span location are more sparse, which indicates that a large number of measurements were found to be unusable and thus were not processed. The questions here are twofold. First, the validity of the unusually large number of measurements at 5% span and, second, the higher uncertainties at 90% span resulting from the fewer measurements at that location. Both of these argue against the usefulness of the data taken at these radial locations.

3. Station 3, 5% Chord

This chord location is immediately inside the rotor. It was very difficult to obtain data at this location, because of the blade blockage due to blade geometry.

No velocities were measured at the 5% span location for the baseline configuration and the information obtained at the 80% and 90% span locations was also not usable. The velocities measured at 10% span also reflect some deterioration with almost one out of five of the windows containing corrupted data.

The information from the enhanced endwall boundary layer configuration appears valid from 10% span to 80% span. Velocities measured at 5% and 90% are not indicative of actual flow conditions. Uncertainty measurements, large variations between neighboring windows, and the disparity between the magnitudes at 5% and 90% spans and of the 10% and 80% spans suggest that these measurements are not correct.

Since this chord location is inside the blade row, the effects of blade blockage are apparent. In the baseline configuration, the zero measurements in windows 1 through 8 and again in windows 47 through 50 reflect the presence of a blade in one or both of the incoming laser beams. The numbers in windows 1 through 4 probably reflect that the system is trying to process data from reflections from the blades or endwalls.

The enhanced endwall boundary layer test configuration also contains data affected by blade blockage with 15% to 20% of the windows being blocked by the presence of a rotor blade.

Figure 41 presents the computed axial velocities for stations 3 to 7.

Station 3 results for the baseline experimental results and the baseline computed prediction show good qualitative agreement. The axial velocity contour plots show axial velocities varying from 90 m/sec near the pressure surface to 120 m/sec near the suction surface.

The computed predictions for the enhanced endwall boundary layer configuration show that the axial velocities also appear very similar to the experimental results. The computed results reflect a region of high velocities that peak at about 140 m/sec near midspan on the suction surface side of the passage. There exists a much larger region of 130 m/sec velocities that exist around this area. The experimental results for the enhanced endwall boundary layer show no velocities of 140 m/sec or greater but these results do show a large region of 130 m/sec. Both the computed predictions and the measured experimental results for the enhanced endwall case also indicate a region of lower velocities (50 m/sec) in both of the pressure surface endwall regions.

The enhanced endwall boundary layer case axial velocity prediction shows a large region of low velocities near the shroud for the enhanced endwall boundary layer case. This might be the result of the lower total velocities near the endwall for this test configuration, due to the inlet profile.

Figure 42 presents the predicted absolute tangential velocities at stations 3 to 7 for both the baseline and the enhanced endwall boundary layer test cases. for both inlet configurations, regions of low tangential velocities exist near the suction surface. Computed predictions for both cases show blade pressure surface effects as the absolute tangential velocity field shows increasing velocities in the region near the pressure surface. Few differences exist between the predictions for the absolute tangential velocities for the two test cases. The exception is a slightly larger region of zero absolute tangential velocities for the enhanced endwall boundary layer test configuration.

The measured tangential velocities for both the baseline and the enhanced endwall boundary layer test cases reflect the same trends as the predicted computation results. A region of low or zero absolute tangential velocities exists from hub to shroud near the suction surface. Then, as the pitch increases towards the pressure surface, the tangential velocities increase. This region of increasing tangential velocities near the pressure surface is not prominent in the experimental results. This is the result of the poorer quality of the data that occurs in the regions near solid surfaces.

No regions of zero velocity are apparent for either set of experimental results. This would indicate that the spurious tangential velocity bias that was observed at the inlet station was also present in the downstream measurements.

4. Station 4, 25% Chord

Station 4 measurements highlight another of the difficulties in assessing the data acquired near the endwalls of the passage.

The baseline case velocities at 5% and 90% seem very reasonable but are lower in magnitude than the velocities nearer the center of the passage. In both locations, higher tangential velocities are obtained in conjunction with much lower axial velocities, indicating greater turning in these regions.

These trends are reflected, to some extent, in the computational predictions. However, when the quality of the data deteriorates, it is often accompanied by a gradual lowering of the magnitude of the measured velocity component. The first component to be lost using this laser anemometer system is normally the axial component. Therefore, the information presented at 5% and 90% span may indeed reflect accurate measurements of the velocities or it may reflect the gradual degradation of the axial velocity component. Probably both possibilities occur to some extent here; although the proportions of each is not known.

Blade blockage at this location is substantial. It is almost 20% at 10% span and decreases only to 10% at 80% span.

The data acquired at the 5%, 10%, and 90% span locations in the enhanced endwall boundary layer configuration is not usable.

5. Station 5, 50% Chord

The velocities measured at this chord location are much better than the measurements at the previous intrablade locations. This is the result of a more favorable blade geometry at this location and a narrowing of the passage due to the convergence of the endwalls.

Enhanced endwall boundary layer data for the 5% span can only be considered reasonable from windows 17 to 35. At this location, the number of measurements in these windows is very small, leading to large uncertainty errors. Notice the large number of measurements at other window locations, i.e., 37-39. The velocities here are very unreasonable, but uncertainties are low due to the large number of measurements. In general, the most reasonable velocity measurements are the ones with the lowest number of measurements. Data at 10% span can be considered reliable from windows 17 to 34. It generally indicates the same structure that is found at 5% span.

The data acquired at 90% span shows reasonable numbers of measurements and uncertainties. Still, the magnitudes of the measured absolute velocities are reduced by almost 50% from data at 80% span. Notice also the large variation in velocities between windows for both the axial and tangential velocities. Measurements at 90% span cannot be considered reliable.

The predicted computed axial velocity field has changed significantly between station 3 and station 5. Both sets of computational results show regions of lower axial velocities near the shroud suction surface corners and regions of higher velocities near the hub suction surface corners. For both test inlet configurations, the axial velocity gradients in the shroud side of the passage are generally in the radial direction. Both sets of experimental data also show flow gradients that are essentially radial in the outer or shroud side of the passage. Both sets of experimental results also reflect somewhat higher velocities in the hub suction surface corner.

The measured enhanced endwall boundary layer velocities show a small region of higher axial velocities (140 m/sec) near the shroud suction surface corner that is not reflected in the computational prediction.

Although the experimental data of axial velocities does show a great deal of scatter, it generally shows the same flat velocity profile as the predicted computed results with the tendency towards higher velocities in the hub suction surface corner.

The computational results show a larger region of decreasing axial velocities along the suction surface in both cases. This is indicative of the development of a more prominent boundary layer along this surface. This velocity gradient is only faintly apparent in the experimental data. The most likely explanation for this discrepancy is the poorer quality of the data near solid surfaces. It is possible that the blade has been slightly mis-positioned on this plot.

Overall differences in the axial velocity contour plots between the two computed predictions are small at this location.

Station 5, 50% chord, predicted results indicate a continued growth of the endwall effects in the shroud region. For both sets of predictions, the predicted results show a region of increasing absolute tangential velocities in the shroud suction surface corner. Both show a region of lower absolute tangential velocities roughly one third of the span from the shroud and one third of the pitch from the suction surface. Both predictions also show a region of higher absolute tangential velocities in the hub pressure surface region.

However, differences in the two predicted sets of absolute tangential velocities remain minimal at this station which is at 50% chord. Higher absolute tangential velocities are predicted by the baseline results. However, this may be partially the result of the higher wheel speed of the baseline operating condition, which resulted in approximately a 3 m/sec difference at the tip.

A comparison with the baseline experimental data indicates a region of lower velocities in the midpassage region with higher tangential velocities near the blade surface and near the endwalls. On the shroud side of the passage, there are indications of higher tangential velocities near the shroud suction surface corner, where velocities increase from 70 m/sec to 100 m/sec. There are also indications at the 90% span location of higher tangential velocities (approximately 10 m/sec). Also, there does appear to be a region of lower velocities in the tip pressure surface corner of the passage. It is not clear if this is the result of a lower quality of data or reflects the predicted results. the experimental results do indicate a larger region of relatively constant tangential velocities at approximately 70 m/sec than are indicated by the computed predictions.

The region of low velocities in the hub suction surface corner for both test inlet configurations is obviously the result of spurious measurements. Both sets of experimental results show some indications of higher absolute tangential velocities in the hub suction surface corner.

The measured absolute tangential velocity data at the 90% span for the enhanced endwall boundary layer configuration has been considered questionable. This data, which indicates much lower tangential velocities near the shroud appears to no be usable, since the predicted results clearly indicate much higher velocities in the shroud region.

6. Station 6, 75% Chord

Baseline data at this location appears valid across the passage with the exception of data at the 90% span location. At least 10% of the passage appears blocked by the presence of blades. Of course, this percentage increases nearer the hub.

The axial velocities at 90% span for the baseline case are somewhat lower but the tangential velocities are higher, resulting in much greater turning angles. Consider the large variations in velocity for both axial and tangential components as presented in Tables A1 and A2 of Appendix A and Figs. 20 and 22. Notice the reduction in tangential velocities at 80% span and then an increase at 90% span.

The velocities measured at 80% span appear more consistent with the velocities at other locations.

The baseline configuration axial velocities at 80% span show some interesting features. At 80% span the magnitude of these axial velocities is approximately that of the velocities at 70% span. A close inspection of these velocities reveals some large window-to-window variations. Calculated uncertainties are also much larger than those at 70%, due to the fewer measurements taken at this axial/radial location.

7. Station 7, 95% Chord

Baseline configuration velocities at this location provide data from 10% to 90% span. The measurements at 5% span are not self consistent or consistant with data gathered at more distant radial locations. The large calculated uncertainty values are the result of poorer axial measurements at this location.

The number of valid measurements for the axial 5% span are very low and the velocities are generally much lower. Window 25 shows, perhaps, the only valid velocity at 5% span and this velocity results from only 2 measurements.

Notice the reduced blade blockage at this location, varying from 20% at 10% span to less than 10% at 90% span.

The data at 5%, 10%, and 90% are not usable for the enhanced endwall boundary layer test configuration.

The experimental results show a gradually increasing axial throughflow velocity component from the pressure surface tip corner towards the suction surface corner region. The experimental data also shows lower axial velocities in the suction surface tip region. Overall, and consistent with the more upstream locations, the velocity gradients for the axial velocities in this location are flatter in both the pitchwise and spanwise directions.

The experimental tangential velocity results are flatter than the predicted results. Both the baseline and the enhanced endwall boundary layer case contain tangential velocities near the suction surface side.

The computed predictions indicate, for both cases, a region of higher axial velocities in the hub suction surface region, as do the experimental results. Measured baseline velocities peak at 140 m/sec, as do predicted maximum velocities. The peak enhanced endwall boundary layer velocities are greater than 130 m/sec but do not exceed 140 m/sec.

The baseline configuration, the 130 m/sec axial velocity contour moves generally from the suction surface tip region towards the hub pressure surface region for both the measured (contour line I) and the computed prediction (contour line N).

The measure enhanced endwall velocities continue to reflect somewhat lower axial velocity gradients over most of the passage than were predicted by the solver.

Both sets of experimental data show lower axial velocities near the suction surface that indicate the continued growth of the boundary layer. However, these gradients are somewhat less prominent in the case of the baseline data. Both sets of experimental data only hint at the lower axial velocities in the suction surface tip region. However, this is not a prominent feature in the experimental data.

The predicted station 7 absolute tangential velocity contour plots remain very similar. Overall, the most prominent difference between the two test cases is the somewhat higher absolute tangential velocity level of the baseline flow case.

Both sets of computed predicted results show an increasing absolute tangential velocity component from the midpassage toward the suction surface tip region. Both show a rather constant increase in the absolute tangential velocity toward the hub from the midspan location. Both show a large region of increasing absolute tangential velocity inside a significant suction surface boundary layer. Both predicted test cases show much thinner pressure surface boundary layers. Both sets of computed predictions are very similar in appearance.

Experimental measurements of the absolute tangential velocities at the station 7 location show good qualitative agreement with the calculated predictions. Experimental data shows a region of increasing absolute tangential velocities near the suction surface. Also apparent are regions of increasing absolute tangential velocities from mid span towards the hub surface.

8. Station 8, 105% Chord.

Data acquisition was extremely difficult at this location for a number of reasons. First, the presence of the rear edge of the window frame reduced optical signals reaching the PMT. Second, seeding was difficult since aerodynamic spreading of the seed was greatest at this location. Third, blade blockage, even at 105% chord, reduced the quality of data in those windows immediately downstream of the rotor blades. The existence of blade wakes greatly enhanced the spreading of seed particles.

Nevertheless, some data was acquired at this station. Baseline inlet configuration data was valid from 40% span to 80% span. The measurements at 50% span show a slight reduction in the axial velocity. This lower axial velocity is not apparent in the aerodynamic data measurements downstream of the rotor. The measured axial velocities at 5%, 10%, 20%, and 30% are much lower than the velocities measured at greater radial locations. These velocities are of the order of 50 m/sec or less. This trend is not shown in the aerodynamic data downstream of the rotor. The tangential velocity measurements show a fairly consistent variation in velocities from 10% span to 90% span. Uncertainty measurements for these velocities are also very low.

The baseline tangential velocities appear valid over most of the passage from 20% span to 90% span.

The extremely low axial velocities from 5% span to 30% span generate absolute flow angles of over 60°. These flow angles do not agree with the acquired aerodynamic data. Therefore, it appears likely that these axial velocities are in error.

The enhanced endwall boundary layer data at station 8 was of poorer quality than the data acquired at station 8 during the baseline configuration test. Extremely low axial velocities at 10%, 30%, 40%, and 90% span, coupled with large window to window variations and calculated uncertainties make axial velocity measurements at this locations highly suspect. The extremely high axial velocities at 20% span are not physically possible.

The absolute tangential measurements at 5%, 10%, 20%, 30%, 40%, and 90% span show large window-to-window variations, large negative velocities, and numerous windows containing no measurements. The signal was stronger for the tangential component and it was acquired to 20% span with the baseline configuration. The enhanced endwall boundary layer test case data was only valid for the 50%, 60%, and 70% span. It is most probable that for the enhanced endwall boundary layer test case that the only trustworthy data exists from 50% to 80% both for the axial and the absolute tangential velocities.

9. Summary

The quality of the measurements acquired during this experiment was strongly dependent upon the location at which they were acquired. Overall data quality deteriorates the farther downstream into the flow passage that the measurements were taken. Data acquired at station 8 is usable only in the outer half of the passage at best.

Data acquired near passage boundaries is also of lower quality than the data acquired at mid-passage. The data acquired at 5% and 90% span is generally marginal.

Blade metal blockage greatly increased the areas of the passage where velocities could be measured near blade surfaces. Since the beam crossing angle is only approximately 4°, increased areas of poor data near the blade surfaces must be the result of the blockage of signal reflected from the particles towards the collecting optics lens.

An overall summary, including those axial/radial locations at which data is not usable was presented earlier in Table X.

Qualitative agreement between the computed predicted results and the measured experimental data is good. However, quantitative agreement between the two sets of results can be improved.

Unfortunately, velocity measurements could not be obtained near the blade surfaces or in the endwall regions. As a result, the predicted velocity gradients off the suctions surface and in the endwall regions could not be observed.

C. COMPARISON OF RESULTS IN THE STATIONARY REFERENCE FRAME

In this section, the inlet and exit flow fields will be discussed in some detail. As was mentioned above, these flows are best considered in a stationary reference frame. This is because the components both upstream and downstream of the rotor are stationary and their interactions with the flow are in an absolute reference frame.

Figure 24 includes line plots of the absolute total velocities measured at the inlet (station 1), 95% chord (station 7), and exit (station 8) locations for both test flow conditions. The station 7 data is presented here since the station 8 information is of such poor quality. Station 7 is at 95% chord and is, therefore, very near the trailing edge of the blade. Therefore, it will be used when considering the exit station flow.

A comparison between the absolute flow velocities measured at the inlet shows that the baseline case is very flat between 20 and 80% span. Here the velocity variations of the axial velocities are of the order of 5 m/sec. The enhanced endwall boundary layer varies over 15 m/sec in this range of span. Thus, the baseline variation represents about 5.5% of the average inlet velocity vector while the thickened endwall boundary layer variation is of the order of 15.5%.

At Station 7, 95% chord, the baseline total velocities vary from 167 m/sec to 144 m/sec from 20 to 80% span while the enhanced configuration shows a change from 165 m/sec at 20% span to 147 m/sec at 80% span. These numbers are approximate and are taken from the window

25 readings. These profiles are more graphically displayed in Fig. 25. This figure includes plots of the mid-pitch window (window 25) absolute total velocity at stations 1, 5, 7, and 8. Here the baseline configuration changes in the spanwise direction 25 m/sec while the enhanced endwall boundary layer profile is somewhat shallower at 20 m/sec.

Differences in the shape of the inlet velocity profiles have become very similar by station 7, 95% chord.

Both the station 7 and station 8 line plots are difficult to interpret. The baseline case shows an obvious gradient increasing from the blade tip pressure surface corner to the hub suction surface corner. The change in total velocities is less than 25 m/sec. The enhanced boundary layer condition shows a similar gradient but it is much less apparent due to the quality of the data. It also shows a change in total velocities of about 20 m/sec. Both flow cases have very low blade to blade velocity gradients. This is indicative of the low blade loadings that result in the relatively low pressure rise across this rotor at 60% speed.

Overall, for both flow conditions, blade-to-blade variations seem to disappear in the blade tip region. Somewhat nearer the midspan, very shallow gradients from suction surface (high values) to pressure surface (low values) exist.

Only a small region between 60 and 80% span present any usable data at station 8. In this region, only small differences in velocity magnitudes and overall flow appearances between the two flow test cases can be seen. Station 8 data in this small region of the outer passage appears relatively flat from blade to blade. The only information that reliably extends beyond the 60% span location towards the hub are the baseline absolute tangential velocities. This data shows higher absolute tangential velocities in the hub suction surface corner.

Of course, total velocity is only part of the picture. The absolute flow angle must also be considered in comparing the differences between the two inlet flow conditions. Figure 26 shows the absolute flow angles at stations 1, 7 and 8. Figure 27 contains the midchannel window plots of the absolute flow angles at these stations.

The angle plots present essentially similar profiles at the inlet and exit with a slightly steeper angle gradient at station 7 for the baseline (approximately 0.6°).

Station 7 absolute flow angles, for both the baseline and the enhanced endwall boundary layer case contain large midpassage regions where the absolute flow angles are between 30° and 35°. Both have regions of slightly lower turning (less than 30°) at the 70% span location.

Notice that the region of slightly lower turning is somewhat larger for the enhanced configuration. Overall, the flow in the outer half of the enhanced passage is turned slightly less than that in the baseline configuration while the flow in the inner or hub half has very nearly the same turning as the baseline configuration.

Because the data acquired at station 8 is largely unusable, direct observation of much of the exit flow is not possible. The station 7 location is near the exit and the following statements can be made concerning the flow at this location. It is appears that the crosschannel variations both blade-to-blade and hub-to-shroud are small with absolute total velocities varying only 20 m/sec and flow angles varying only 5°. In general, the regions of highest measured turning and greatest velocity are in the hub suction surface corner. The regions of lowest measured total velocity and lowest measured turning are near the tip and in the tip pressure surface corner.

The overall design intent of this rotor is to provide a constant exit flow angle of about 50° and a gradually decreasing total velocity from hub to shroud. It should be noted that this is at design speed and mass flow. At the part speed operation of the present test, the rotor did maintain the decreasing velocity profile for both configurations. It did not, however, provide a constant exit flow angle for either test configuration.

It appears that the differences between the two inlet velocity profiles are reduced at the exit of this rotor and are primarily confined to the outer half of the passage. Overall, the enhanced endwall boundary layer configuration contains velocities that are slightly lower than the baseline configuration. The blade-to-blade velocity gradients appear smaller in the outer half of the passage. Lastly, the enhanced endwall boundary layer case turning is slightly smaller in the outer half of the passage by 2°.

D. COMPARISON OF RESULTS IN THE ROTATING REFERENCE FRAME

1. Introduction

While the absolute reference frame is the most useful for flows upstream of the rotor, where the inlet conditions are determined, and downstream of the rotor, where the stators and combustors are found, the most useful reference frame for designing and studying the rotor itself is the relative reference frame. In this reference frame, the rotational speed of the rotor is vectorially added to the fluid velocity.

This section will consider the flow in the relative reference frame. A comparison of the two test cases in this reference frame should help show why the differences between the two test cases becomes less prominent as the flow moves through the rotor.

The flows will also be reviewed to ascertain any other prominent flow features that have developed in the passage.

2. Inlet flow features.

Figure 28 shows the relative total velocities at each station and Fig. 29 shows the relative flow angles. These colorfill charts, which have not been smoothed, can give a better feel for the qualitive changes in flow features. However, color reproduction is somewhat limited and some of the more subtle flow features can be lost. Figures 30 and 31 provide the same information for the inlet station, station 1, presented as line plots.

When viewing these plots the most striking feature about the flow in the relative reference frame is the similarity of the flows at station 1. Moving from the absolute to the relative reference frame reduces the severity of the differences between the two test cases because the addition of the large tangential velocity component due to wheel speed reduces the effects of the differences in axial component on the total relative velocity. Still, these differences have not completely disappeared.

Relative total velocities for both inlet cases vary from about 210 m/sec to about 270 m/sec and a plot of the midpitch relative total velocities shows little effective difference between the two test cases (Fig. 32).

Relative flow angle plots show slightly more prominent differences at station 1. Here the baseline configuration shows a greater relative flow angle at the inlet along the outer or shroud half of the passage than the enhanced inlet. The midpitch (Fig. 33) plots of flow angle differences at station 1 reveal differences of less than 3°. The enhanced endwall boundary layer configuration showing larger relative flow angles near the endwalls and the baseline case contains greater relative flow angles at midspan. It would be more appropriate to examine the incidence angle shown in Fig. 34. This figure shows the relative flow angle differences from the input grid. This grid, an "H-Grid", was generated by dividing the blade passage into 11 constant span, axisymmetric surfaces. Each of these surfaces was further divided into a grid with equally spaced lines in the meridional direction and equally spaced lines between the passage boundaries. This input grid is shown in Fig. 35. These angle differences will be explored more completely in a later section that will deal with the secondary flows generated in these cases. However, upstream of the rotor, these differences are equivalent to the blade leading edge incidence angle. As would be expected, the baseline configuration shows a much smaller variation in incidence than the enhanced configuration. Variations in the baseline are from 15° at 5% span to 11° at 60% span. The enhanced endwall condition shows variations from 19° at 5% span to 9.5° at 60% span.

The measured design speed inlet incidence angles, Fig. 36a [75], are much lower at 6°. The design is with a uniform inlet flow and is at design speed and at design mass flow. Figure 36b, from Reid and Moore [77], shows the peak efficiency incidence angles measured at 60% design speed.

Overall, then, a much greater incidence angle occurs at all spans for both inlet flow test cases. Obviously, this requires a greater turning of the flow as it initially enters the passage.

The baseline case requires a more constant turning along the span than the enhanced case where the incidence is substantially larger at the endwalls than at midspan. In fact, the required turning at the blade inlet for both cases is of the same magnitude as that which occurs through the remainder of the passage.

Thus, at the inlet of the rotor, the velocity profiles are very similar due to the addition of the rotational component. If the flow successfully negotiates the initial turning, the differences between the two test cases have been greatly reduced. Further, the initial flow angles into the rotor passage would tend to oppose the development of the classical passage vortex with the endwall flows moving towards the blade pressure surfaces and the midspan flow more in the direction of the suction surface.

Station 3 is situated at the 5% chord location. This is downstream of the blade leading edge and is the farthest upstream location at which data was acquired inside the passage. The quality of the data acquired at this location is poorer than many of the results acquired farther downstream in the passage, particularly near the endwalls and the blade surfaces. Nevertheless, it does provide some information concerning the condition of the flow immediately downstream of the blade leading edge.

A review of the relative flow angles (Figs. 29 and 31) and the absolute flow angles (Fig. 26) at the 5% chord location shows that the flow near the midpitch of the channel has not yet been affected by the presence of the blades. This can be seen by the region of very low absolute turning angles near the midpitch location.

The negative flow angles near the suction surface indicate that the flow is being accelerated and turned by the presence of the blade leading edge. Conversely, the large positive flow angles reflect the deceleration of the flow along the pressure surface.

Direct comparison reveals that there are definite differences between the two test flow cases. The enhanced test case shows generally more positive flow angles on the hub side of the passage than the baseline case, while the reverse of this is the case in the mid passage region. The shroud side of the passage, specifically the 80 and 90% span locations, shows no clear difference between the two flows.

The relative flow angles reveal that, overall, in the midpitch region away from the blade surfaces, the enhanced boundary layer flow is somewhat less turned (>5°) than the baseline flow. This is a direct result of the lower incidence angle of the enhanced boundary layer case in the midspan region. The higher relative flow angles near the hub are the result of the lower axial velocity and, thus, the higher incidence angle of the enhanced boundary layer test case in this region. While the same effect may occur in the tip region, the differences are not clear cut. This may be the result of the quality of the data acquired here or the effects of the tip clearance.

In summary, the rotational effects of the rotor reduce the differences between the total velocity profiles at the rotor. Further, the rotational effects result in a difference in the incidence angles presented to the rotor by the two test cases. The differences are higher incidence angle region near the endwalls and lower incidence angles near midspan for the enhanced endwall boundary layer case. This incidence variation of the enhanced endwall case results a flow condition where the midspan flow of the enhanced case contains a less prominent movement towards the pressure surface of the passage than the baseline condition and, conversely, a more prominent movement of the flow towards the pressure surface by the flow near the hub and possibly near the shroud in the enhanced endwall flow case.

It should be noted here that in the classical development of the passage vortex, the flow situation is reversed. In that instance, the midspan flow has a more prominent movement towards the pressure surface than the endwall flow.

3. Exit Flow Features

Due to the poor quality of the data acquired at the exit station, station 8, most of the observations of the exit flow features must be made at the 95% chord location, station 7.

First, the effects of the rotor on the relative total velocities and flow angles will be considered.

Relative total velocities and relative flow angles at station 7, in those areas where the data is acceptable, are very similar. The two sets of data reflect no important differences. However, the enhanced endwall configuration shows a slightly more parabolic profile between the endwalls with the midspan velocities about 5 m/sec higher. Figure 32 shows the midspan relative velocity gradient from hub to shroud and Figure 30 shows the cross channel line plots. The flow reflects little variation in the relative total velocities blade-to-blade with the highest velocities in the midpitch region and slightly lower velocities near the blade surfaces.

Figure 33 presents the midpitch window relative flow angle differences for the two flow configurations. These represent the differences between the relative flow angle and the input computational grid shown in Fig. 35. This grid reflects what is considered the direction of the primary through flow in this investigation, i.e., the relative flow is assumed to be along the grid lines that run from inlet to exit. The grid is generated in an axisymmetric coordinate system.

As was mentioned in the previous section, the inlet profiles have lower incidence angles at midspan and higher incidence angles near the endwall for the enhanced endwall configuration as compared to the baseline configuration.

The differences at inlet were about 3.25° between 25 and 50% span and over 1.65° from 50 to 80% span. This demonstrates the large differences in inlet velocity profiles.

At 95% chord, in contrast, the midspan "bulge" appears to be largely gone with the change in difference between 20% span and 50% span only about 0.75° at window 25. Generally, the differences between the two sets of flow angles is smaller at 95% chord with the greatest differences near the hub. Overall, the enhanced endwall boundary layer shows somewhat less turning than the baseline case with the greatest discrepancies near the hub. Nonetheless, the overall character of the flow angles is similar.

To summarize these results, it can be said that the inlet velocity differences are minimized in the rotating reference frame by the vectorial addition of the wheel speed. The total velocity and flow angle differences are further reduced as the flow moves through the rotor.

The magnitude of the differences in the total relative velocity profile has been reduced for both inlet profiles because of the addition of the rotational component. The reduction has been most striking for the enhanced endwall case.

The enhanced inlet relative flow angles have lost the parabolic distribution that they entered the passage with. Instead, both test cases show a gradual and somewhat linear decrease in flow angle differences from hub to shroud. In any event, the magnitude of the spanwise differences in flow angles has been greatly reduced in both the baseline case (from 3.2° to 1.3°) and in the enhanced endwall boundary layer (from 6.3° to 3.0°).

The relative flow angle cross channel plots, Fig. 31, display indications of greater turning along the suction surface corner. This is only slightly apparent for the enhanced case but is more prominent in the baseline case. Overall, however, the blade-to-blade relative flow angle gradients are smaller across the entire passage.

4. Additional Flow Features

a. Introduction

A primary goal of this study was to enhance the understanding of the flow physics underlying the generation of the classic passage vortex inside a compressor rotor. Before turning to a more detailed review of the results concerning this goal, a few additional observations of the flow fields in question will be made.

b. Exit Flow Rotational Effects

A flow feature that is apparent in the plots is the addition of a rotational component to the exit flow for both inlet flow configurations. Figure 22 presents lineplots of the absolute tangential velocity. As was mentioned earlier, the small tangential component at inlet is an error caused by the data acquisition system. It was not measured by the aerodynamic probes and there is no physical reason for the existence of such a tangential velocity. The flow at the inlet is axisymmetric and has only an axial flow component.

As shown in Fig. 22, larger tangential velocities can be seen developing nearer the hub with the greatest velocities in the hub SS corner at station 6, 75% chord. This is also apparent at the 95% chord location. Tangential velocities were acquired for the baseline configuration at station 8 across most of the passage. This is the only velocity component successfully acquired over the inner half of the passage at this station and it also shows higher velocities near the hub.

The absolute flow angles at station 7 (midpitch values are shown in Fig. 27) and the aeroprobe measured flow angles display roughly the same trends in flow angle variation from hub to shroud. Both sets of data demonstrate a decreasing flow angle from the hub towards the midspan. The aerosurvey probes reveal a very gradual increase in absolute flow angle, while the laser anemometer survey data indicates a decrease until near the tip. The LA survey data is along a midpitch window while the aerosurvey data represents an average exit flow condition. The aerosurvey measurements contain values of the flow near the blade surfaces where turning is greater.

In summary, the exit velocity profiles include a clockwise rotation in both test conditions. This is shown by the higher flow angles near the hub that decrease towards the shroud. As was previously mentioned, both tangential and axial velocities decrease from hub to shroud.

Interestingly enough, in the rotational reference frame the added rotational component is counterclockwise. Figure 31 includes the line plots of the relative flow angles and Fig. 29 has the colorbar plots. Station 7, 95% chord, reveals increasing flow angles from the hub to the shroud. The baseline configuration indicates slightly lower relative flow angles in the suction surface corner. This feature is not quite so obvious in the enhanced endwall boundary layer configuration.

c. Radial Flow Migrations

Figure 37 shows the total relative velocities for the first 15 windows away from the suction surface towards the pressure surface. Data for five chord positions, both inlet configurations, and for five spanwise locations (10%, 30%, 50%, 70%, and 90%) is presented. These total relative velocities have been nondimensionalized by dividing them by the velocity in window 15.

The data shown at 5% chord at all of the spanwise locations only extends part of the distance to window 1 because the blade blockage is included in windows 1 through 7.

Baseline configuration data at 90% span indicates a great deal of scatter and therefore it is difficult to observe any trends at this span location except at the 95% chord location where a velocity gradient is apparent for both flow configurations.

Most noticeable here for the baseline configuration is that the effects of an adverse pressure gradient over the suction surface are not apparent until 95% chord near the hub.

As the span increases towards the rotor tip, the effects become noticeable earlier in the flow. At 30% span, the effects seem to begin by 75% chord. At 50% and 70% span the effects are apparent at 50% chord and possibly by 25% chord. At 70% span, the effects are very prominent by 75% chord.

The enhanced configuration at 10% span actually shows usable data only at 75% chord. At this location, it appears that there are no effects from an adverse pressure gradient.

However, as opposed to the baseline configuration, all remaining span locations of the enhanced flow configuration show the effects of the pressure gradient. It is apparent by 25% chord at all span locations and is very prominent by 75% and 95% chord. A likely cause of this is the migration of the blade boundary layer due to the enhanced endwall boundary layers.

E. GRID VELOCITY DEVIATIONS

The major objective of this investigation was the observation and analysis of the development of the passage vortex that is thought to be developed in a turning passage from the spanwise shear. The classic passage vortex is created in a turning passage such as a compressor rotor by the spanwise total pressure gradient (velocity gradient).

While this vortex is generated by the velocity gradients that exist in the endwalls of both test configurations, it should be more pronounced in the enhanced endwall boundary layer configuration because of the more prominent velocity gradients generated by the insertion of the distortion screens upstream of the rotor.

Since the total velocity vector could not be resolved because radial velocity information was not obtained, this section must be confined to an examination of the "velocity deviations" that can be calculated from the two velocity components that were measured.

The velocity deviations from the grid lines provide an indication of the development of this passage vortex.

There are a number of different specific definitions for the term "secondary flow." It is generally defined as the difference between the measured three dimensional flow and some "primary flow." For the purposes of the investigation, the primary flow field is considered the flow along the generated primary computational grid (Fig. 35). This has been used primarily because of the ease of generation of this field and the uncertainties in the definition of the term "primary flow" field. In fact, since the rotor is operating subsonically and it is far from the measured stall point, this velocity field should be near any actual potential flow field.

Therefore, the tangential velocity deviation was calculated for the two inlet flow configurations and compared instead to assess the development of the passage vortex.

Consider Fig. 38a. The relative velocity can be written as [92]:

$$W_\theta = W_{p\theta} + W_{s\theta} \tag{40}$$

where $()_p$ = primary flow,

$()_s$ = secondary flow, and

$$W = \sqrt{W_\theta^2 + W_z^2} \tag{41}$$

The grid slope is:

$$Tan\psi = r\frac{d\theta}{dz} \tag{42}$$

and the relative flow angle is:

$$\beta = \tan^{-1}(W_\theta / W_z) \tag{43}$$

The calculation develops as:

$$W_p = W\cos(\beta - \psi) \tag{44}$$

$$W_{p\theta} = W_p \sin\psi = W\sin\psi\cos(\beta - \psi) \tag{45}$$

$$W_{s\theta} = W_\theta - W_{p\theta} \tag{46}$$

and, finally,

$$W_{s\theta} = W_\theta - W\sin\psi\cos(\beta - \psi) \tag{47}$$

A second calculation can be made for the radial or meridional secondary velocity. Considering Fig. 38b it is seen that

$$W_r = W_{pr} + W_{sr} \tag{48}$$

$$W = \sqrt{W_r^2 + W_z^2} \tag{49}$$

$$Tan\phi = \frac{dr}{dz} \tag{50}$$

$$\alpha = \tan^{-1}(W_r/W_z) \tag{51}$$

$$W_p = W\cos(\alpha-\phi) \tag{52}$$

$$W_{pr} = W_p\sin\phi = W\sin\phi\cos(\alpha-\phi) \tag{53}$$

and

$$W_{sr} = W_r - W\sin\phi\cos(\alpha-\phi) \tag{54}$$

The grid used in these calculations is shown in Fig. 35.

Figure 39 presents line plots of the calculated flow deviation velocities, $W_{s\theta}$, at each of the axial locations where data was acquired.

Line plots of relative flow angle differences, which are the differences between the relative grid and the relative flow angles, are shown in Fig. 34. As may be seen at Station 1, the inlet station, relatively flat velocity deviations are obtained for both configurations. The positive velocities represent a fairly large positive incidence for both test configurations. This is consistent with the flow condition selected for this test. The positive deviation velocities indicate that the flow has not turned far enough to be parallel to the grid lines.

The inlet baseline deviation velocities are relatively constant across the passage. The spanwise variations tend to reflect variations in the grid extrapolations upstream of the rotor. These extrapolations reflect the three-dimensionality of the blades themselves.

A listing of the difference between the two inlet velocity deviations, $V_{sec,b}-V_{sec,a}$ is given in Appendix A, Table A9.

Figure 40 is a three-dimensional plot of the velocity deviation differences. When looking at the plots in Fig. 40, the rotor hub is on the left side and the compressor shroud will be on the right. The blade suction surface is towards the back of the plot and the pressure surface is towards the front.

For these plots, no differences in flow deviations that were greater than 25 m/sec were permitted. This was done to improve the scaling and readability of the plots. It was determined that differences larger than 25 m/sec were unrealistic.

The first plot shows the inlet survey location. The differences in the velocity deviations is very noticeable with the baseline configuration having the greatest deviations at midspan and the enhanced configuration having larger deviations at the endwalls. This is a manifestation of the thickened endwall boundary layers of the enhanced test configuration.

The differences in the deviation velocities at the inlet are very noticeable, but are small. The enhanced configuration is 6 m/sec larger near the hub and about 5 m/sec larger near the midspan. At the 90% span line, the differences are much smaller with the enhanced, about 1 m/sec larger at the 80% span location.

At station 7, the 95% span location, the character of the differences has changed with the enhanced velocity differences larger at all span locations. Rather than having the largest discrepancies between the enhanced and the baseline at the endwalls, now there is a gradual decrease in the differences from the hub to the shroud. The enhanced configuration shows a deviation velocity about 6 m/sec larger at 20% span and this decreases to near 0 at 90% span.

It was mentioned earlier that the character of the relative flow angle differences also changes from inlet to exit. At the inlet, the enhanced endwall configuration shows greater incidence than the baseline configuration and the enhanced mid-span region shows a lower incidence than the baseline. At station 7, the hub endwall shows this same difference with the enhanced configuration showing larger relative flow angles than the baseline. The enhanced endwall boundary layer is approximately 2° greater. This is nearly the same magnitude as the difference at the inlet of the rotor. However, by mid-span at the inlet, the baseline incidence is greater than the enhanced endwall by approximately 2°. At station 7, the enhanced configuration shows the greater deviation from the grid by about 2°.

The difference in the relative flow angles is much smaller near the tip region at the inlet of the flow with the enhanced configuration showing about 0.5° higher incidence at the 80% span than the baseline configuration. It is difficult to estimate such a small difference but it appears that this 0.5° difference has disappeared by 95% chord, station 7.

These results can be summarized as follows. In the rotating reference frame, the enhanced endwall boundary layer configuration flow contains a prominent clockwise rotational component in the inner half of the passage that is not apparent in the baseline configuration inlet flow. There is also a weaker counterclockwise flow in the outer third of the passage of the enhanced endwall flow that does not exist in the baseline configuration. It is, however, weaker due to the larger wheel speed in the outer half of the passage.

In both cases, due to the wheel speed, the relative total velocity increases from hub to shroud at inlet. This gradient is slightly larger for the enhanced case than for the baseline case along the inner half of the passage and slightly less for the outer half of the passage.

By the 95% chord location, the character of the flows has changed in the following way. In the inner half of the passage, the enhanced boundary layer configuration turns about 2° less than the baseline configuration with that number slightly higher at the hub. In the outer half of the passage, the difference in turning essentially goes to zero by the 80% span location.

The differences between the flow deviation velocities at the 95% chord location in the inner or hub side of the passage are essentially constant at 4 m/sec. In the outer half of the passage the differences decrease to essentially zero by the 80% span location.

Thus the differences at exit between the flows are constant along the inner half of the passage and tend towards zero in the outer half of the passage.

During the development of the classic passage vortex, larger velocity deviations and deviation angles exist in the mid-span region of the passage as the higher energy fluid in this region tends to move towards the pressure surface. Correspondingly, the endwall flows would tend to move towards the suction surface in the passage, resulting in lower velocity deviation angles.

In the test, the addition of the wheel speed has greatly reduced the magnitude of the differences in the inlet velocity profiles and, at least initially, have added rotational effects to the inlet flows that are opposite to the classic passage vortex. The result is that near the exit, the secondary velocities and relative flow angle differences are constant along the inner half of the passage. In the outer half or shroud side of the passage, the enhanced endwall boundary layer configuration develops slightly larger velocity deviations than the baseline configuration. This suggests that a weak passage vortex is developing in the outer half of the passage for the enhanced endwall boundary layer configuration. Note, however, that the differences in relative flow angles at this location are only 1° or so, indicating a very weak passage vortex at this location if any exists at all.

Figure 43 presents cross channel plots of the differences of the relative flow angles, β, for the computed predictions. For these plots, the enhanced endwall boundary layer relative flow angles were subtracted from the corresponding relative flow angles for the baseline configuration. These plots show the differences in the flow directions for the two sets of predictions.

Station 1 in Fig. 43 is immediately downstream of the rotor leading edge at approximately 2% chord. The remaining stations are at the equivalent locations that the experimental results were acquired at; these locations are 5, 50, 95, and 105% chord.

A classic passage vortex flow would appear as a flow containing a region of lower turning or greater relative flow angles in the center region of the passage and regions of greater turning near the endwall regions where low momentum fluid would be found. The station 1 figure indicates the opposite trends where the larger positive differences indicate the enhanced endwall boundary layer flows are moving more towards the suction surface than the baseline configuration. Further, the negative numbers in the endwall regions indicate the enhanced endwall boundary layer flow is moving more towards the pressure surface than the baseline configuration. These movements are opposite the movements that would be expected in the classic passage vortex.

Notice that the variations are most prominent on the hub side of the passage with the differences going from +1.5° near midspan to -1° near the hub. The variations are much less prominent on the shroud side of the passage with the differences only varying down to 0.5°. this may be due to the increasing radius which results in higher relative tangential velocities and correspondingly greater relative flow angles.

By station 5, 50% chord, the differences between the two flow predictions have been greatly reduced with the variations between 0° and -1° over most of the passage outside of the boundary layers.

At station 8, predicted relative flow angle differences are less than ±1° over the entire passage, with the exception of small regions near the endwalls and in the blade wakes. There is little indication of the development of a passage vortex anywhere in the predicted flow fields.

VI. SUMMARY AND CONCLUSIONS

The purpose of this investigation was to assess the development of the passage vortex inside a high speed compressor rotor. This was done by obtaining a detailed map of the flow field inside a high speed rotor operating subsonically for two different inlet flow field configurations. One flow field configuration consisted of an "undistorted" inlet velocity profile and the other configuration consisted of a parabolic inlet profile generated by placing an axisymmetric distortion screen on the hub and on the shroud well upstream of the rotor.

The two flow fields were evaluated and compared. The similarities and differences were noted and the following statements can be made:

(1) The differences between the two inlet velocity profiles tend to wash out as the flow moves through the rotor.

(2) There is a clockwise rotation added to the absolute flow as it moves through the rotor. This rotation is counterclockwise in the relative reference frame.

(3) The total velocity, axial velocity, and tangential velocity all are greatest near the hub and decrease as the flow is observed further towards the shroud.

(4) There are some indications of the development of a passage vortex at the 95% chord location when the differences between the calculated flow deviations are calculated. Computational predictions indicate little or no passage vortex development for the test conditions examined in this project.

This investigation marked the first time that a detailed evaluation of the effects of inlet flow field distortion on the internal flow field of an axial compressor rotor was made. The results provide significant information to aid the compressor designer by indicating that the generation of a passage vortex due to thickened endwall boundary layers of the type normally found at the middle stages of an axial compressor has only minor effects on compressor rotor performance.

VII. RECOMMENDATIONS

There are a number of continuations to the present research that could be pursued in order to obtain a better understanding of secondary flows and the passage vortex. The following is a list of suggested efforts:

(1) The laser anemometer system should be improved to allow the acquisition of velocity measurements nearer the endwalls and blade surfaces. It is in these regions that many secondary flow effects become most apparent.

(2) The laser anemometer system should be improved to allow the acquisition of velocity measurements at higher operating speeds. It was not possible to acquire measurements at design speed with this laser anemometer system. Yet, the effects of supersonic flows and the associated shocks can be significant causes of secondary flows.

(3) The measurement of the third, or radial velocity, component has been accomplished for this rotor in a follow-on effort. Unfortunately, scheduling conflicts allowed the measurement of only one inlet configuration, the baseline configuration. This information needs to be reduced and measurements for the AEBL configuration need to be acquired.

(4) Measurements, including radial velocities, need to be made at other flow conditions on the operating line. Certainly near the stall point the increased blade loading will encourage additional secondary flows.

(5) Stronger inlet velocity gradients need to be observed. These stronger gradients should enhance the development of the passage vortex and will allow easier observation and analysis of the resulting flows.

(6) Experimental data acquired during this project should be closely reviewed to assess the possibility of improving the experimental results with additional post processing of the data.

(7) Laser Anemometer measurements need to be made much closer to the blade leading edges to observe the flow physics occurring as the flow turns to enter the passage.

(8) Additional computational results must be done to more accurately map the predicted operating line and thus more closely match the computational operating point and the measured operating point.

(10) Inclusion of a tip clearance model is important. This model will be included in the solver in the first quarter of 1991 and should be used to assess the effects of tip clearance on the flow.

VIII. ACKNOWLEDGEMENTS

Over the course of this program a very large number of people have provided assistance in facility assembly and maintenance, data acquisition and reduction, computational predictions, and the publishing of this thesis. The author wishes to express his sincere gratitude to everyone involved. There are, however, a number of people who should be specifically recognized.

Mr. Rick Murphy, Mr. Tom Toddy, and Mr. Bob Gronski were crucial in maintaining and operating the facility and in the acquisition of the "conventional" aerodynamic data. In particular, Mr. Rick Murphy's willingness to work long days and evenings to accomplish the task are a fine example of dedication and professionalism.

Mr. Glenn Christman's efforts in maintaining the laser anemometer data acquisition computers and hardware interfaces were vital to the successful completion of this project. The author is deeply indebted to him for his willingness to give of his free time in the evenings and weekends to aid in correcting data reduction problems.

The author is deeply indebted to Dr. Rod Chima for providing the source code and information for operating it. Dr. Chima, however, went further by providing important insight to the code results and suggestions for the code operation. His review of input data and operating parameters was essential to the successful completion of the program.

Special thanks go to Mr. Lawrence Schumann, Mr. Ken Suder and Dr. Eric McFarland for their helpful insights into the flow physics and operational programs.

The author must express his profound gratitude to Dr. Ted Keith and Dr. Ken DeWitt. Their suggestions, observations, guidance, and recommendations throughout the course of this program were pivotal to its' successful completion. More than that, however, was their unwavering support. They continued to believe and that made it possible.

IX. REFERENCES

1. Wood, J. R., Jr.: "The Analytical Treatment of Secondary Flows and Associated Losses in Axial-Flow Turbomachines," Naval Postgraduate School, Monterey, Ca, Dec. 10, 1971.
2. Lieblien, S. and Ackley, R. H.: "Secondary Flows in Annular Cascades and Effects on Flow in Inlet Guide Vanes," NACA RM E51G27, Aug 21, 1951.
3. Thompson, J.: "Experimental Demonstration in Respect to the Origin of Windings of Rivers in Alluvial Plains and to the Mode of Flow of Water Round Bends of Pipes," Proceedings of the Royal Society of London, Vol 26, pp. 356-357, 1877.
4. Dean, W. R.: "Note on the Motion of Fluid in a Curved Pipe," Philosophical Magazine and Journal of Science, Vol 4, pp. 208-223, July 1927.
5. Squire, H. R. and Winter, K. G.: "The Secondary Flow in a Cascade of Aerofoils in a Nonuniform Stream," RAE Report Aero 2317, March 1949. Also in The Journal of the Aeronautical Sciences, pp. 271-277, April 1951.
6. Hawthorne, W. R.: "Secondary Circulation in Fluid Flow," Proceedings of the Royal Society, V. A206, pp. 374-387, 1951.
7. Smith, L. H.: "Secondary Flows in Axial-Flow Turbomachinery," Transactions of the ASME 77, pp. 1065-1076, October, 1955.
8. Smith, L. H.: "Three-Dimensional Flow in Axial-Flow Turbomachinery," Vols I and II, Aeronautical Research Laboratory contract No. AF 33(616)-152, John Hopkins University, August, 1955.

9. Dixon, S. L.: "Secondary Vorticity in Axial Compressor Blade Rows," Fluid Mechanics, Acoustics, and Design of Turbomachinery, Part I, NASA SP-304, pp. 173-191, 1974.

10. Adkins, G. E. and Smith, L. H.: "Spanwise Mixing in Axial-Flow Turbomachines," Transactions of the ASME, Journal of Engineering for Power, 1980.

11. Pouagare, M. and Lakshiminarayana, B.: "Development of Secondary Flow and Vorticity in Curved Ducts, Cascades, and Rotors, Including the Effects of Viscosity and Rotation," Three-Dimensional Turbulent Shear Flows, pp. 61-68, 1982.

12. Stanitz, J. D.: "Two-Dimensional Compressible Flow in Conical Mixed Flow Compressors," NACA TN 1744, 1948.

13. Wu, Chung-Hua; and Wolfenstein, L.: "Application of Radial Equilibrium Condition to Axial-Flow Compressor and Turbine Design," NACA RPT 955, 1950.

14. Wu, Chung-Hua: "A General Through Flow Theory of Fluid Flow with Subsonic or Supersonic Velocity in Turbomachines of Arbitrary Hub and Casing Shapes," NACA TN 2302, 1951.

15. Wu, Chung-Hua and Brown, C. A.: "Method of Analysis for Compressible Flow Past Arbitrary Turbomachine Blades on General Surface of Revolution," NACA TN 2407, 1951.

16. Wu, Chung-Hua: "A General Theory of Three-Dimensional Flow with Subsonic and Supersonic Velocity in Turbomachines having Arbitrary Hub and Casing Shapes" Part II, Paper NO 50-A-79, presented at the Annual Meeting of the ASME (New York), Nov. 27- Dec. 1, 1950.

17. Wu, Chung-Hua: "A General Theory of Three-Dimensional Flow in Subsonic and Supersonic Turbomachinery of Axial-, Radial-, and Mixed Flow types," NACA TN 2604, January, 1952.

18. MacCormack, R. W.: "The Effect of Viscosity in Hypervelocity Impact Cratering,"" AIAA Paper 69-345, 1969.

19. Thompkins, W. T.: "A Fortran Program for Calculating Three-Dimensional, Inviscid, Rotational Flows with Shock Waves in Axial Compressor Blade Rows I, User's Manual," NASA CR 1982.

20. Denton, J. D.: "A Time Marching Method for Two- and Three-Dimensional Blade-to-Blade Flow," Aeronautical Research Council R+M 3775, 1975.

21. Denton, J. D. and Singh, U. K.: "Time Marching Methods for Turbomachinery Flow Calculation; Part I Basic Principles and 2D Applications, and Part II Three-Dimensional Flows," VKI Lecture Series 1979-7, 1979.

22. Denton, J. D.: "An Improved Time Marching Method for Turbomachinery Flow Calculation," Presented at the ASME Gas Turbine Conference, London, 1982.

23. Denton, J. D.: "Extension of 3D Flow Calculations in Turbomachinery to Include Splitter Blades and Blade Boundary Layers," Internal NASA Publication, Circa 1987.

24. Hah, C.: "A Navier-Stokes Analysis of the Three-Dimensional Flows Inside Turbine Blade Rows at Design and Off-Design Conditions," ASME Paper No. 83-GT-40, 1983.

25. Hah, C.: "Calculation of Three-Dimensional Viscous Flows in Turbomachinery with an Implicit Relaxation Method," Journal of Propulsion, Vol 3, No 5, pp. 415-522, Sep-Oct, 1987.

26. Hah, C.: "Generation and Decay of Secondary Flows and Their Impact on Aerodynamic Performance of Modern Turbomachinery Components," Proceedings of AGARD 74th Specialists Meeting on Secondary Flow in Turbomachinery, 1989.

27. Chima, R. V. and Yokota, J. W.: "Numerical Analysis of Three-Dimensional Viscous Internal Flows," Prepared for the First National Fluid Dynamics Congress, Cincinnati, Oh., July 24-28 1988, NASA TM 100878.

28. McKensie, A. B.: Rolls Royce Internal Report No. 22081, 1959.

29. Dixon, S. L. and Hollock, J. H.: "Velocity Profile Development in an Axial Flow Compressor Stage," Gas Turbine Colla.

30. Kool, P.: "Experimental Investigation of the Three-Dimensional Flow Field Downstream of Axial Compressors," PhD Thesis, Vrije Universiteit Brussel, Jan 1977.

31. Hirsch, C. H. and Kool, P.: "Measurement of the Three-Dimensional Flow Field Behind an Axial Compressor Stage," ASME Paper No. 76-GT-18, 1976.

32. De Ruyck, J. and Hirsch, C.: "Investigation of an Axial Compressor End Wall Boundary Layer Prediction Method," ASME Paper 80-GT-53, 1980.

33. Smith, A. G.: "On the Formation of the Streamwise Component of Vorticity for Flows in Rotating Passages," The Aeronautical Quarterly, pp. 369-382, Nov, 1957.

34. Smith, L. H.: "Casing Boundary Layers in Multistage Axial Flow Compressors," Flow Blading on Research, Ed. L.S. Dzung, pp. 275-304, 1970.

35. Mellor, G. L. and Strong, R. E.: "End-Wall Effects in Axial Compressors," ASME Paper No. 67-FE-16, Presented at the ASME Fluids Engineering Conference May 8-11, 1967.

36. Adkins, G. G. and Smith, L. H.: "Spanwise Mixing in Axial-Flow Turbomachines," ASME Paper No. 81-GT-57, 1981.

37. Koch, C. C. and Smith, L. H.: "Loss Sources and Magnitudes in Axial Flow Compressors" ASME Paper No. 75-WA-GT-76, 1976.

38. Larguier, R.: "Experimental Analysis Methods for Unsteady Flows in Turbomachinery," Measurement Methods in Rotating Components of Turbomachinery, p. 71, Presented at the ASME Joint Fluids Engineering Gas Turbine Conference and Products Show, New Orleans, LA., Mar 10-13, 1980.

39. Wisler, D. C., Bauer, R. C., and Okiishi, T. H.: "Secondary Flow, Turbulent Diffusion and Mixing in Axial Flow Compressors," ASME Paper 87-GT-16, May, 1987.

40. Gallimore, S. J.: "Spanwise Mixing in Multi-stage Axial Compressors," Ph.D. Dissertation, Cambridge University, 1985.

41. Gallimore, S. J. and Cumpsty, N. A.: "Spanwise Mixing in Multistage Axial Flow Compressors: Part I-Experimental Investigation," ASME Paper No. 85-GT-20, 1986.

42. Denton, J. D. and Usui, S.: "Use of a Tracer Gas Technique to Study Mixing in a Low Speed Turbine," ASME Paper No. 81-GT-86.7.

43. Bario, F., Lebeouf F., and Papailoiu, K. D.: "Study of Secondary Flows in Blade Cascades of Turbomachines," ASME Paper No. 81-GR/GT-4, April, 1981.

44. Bois, G., Lebeouf, F., Comte, A., and Papailiou, K. D.: Experimental Study of the Behaviour of Secondary Flows in a Transonic Compressor," in AGARD Conference Proceedings No. 214, Secondary Flows in Turbomachines, pp. 3-1:3-20, Sept, 1977.

45. Lebeouf, F., Bario, F., Boris, G., and Papailiou, K. D.: "Experimental Study and Theoretical Prediction of Secondary Flows in a transonic Axial Flow Compressor," ASME Paper No. 82-GT-12, 1982.

46. Katsanis, T.: "Computer Program for Calculating Velocities and Streamlines on a Blade-to-Blade Streamsurface of a Turbomachine," NASA TN D-4525, 1968.

47. Mellor, G. and Wood, G.: "An Endwall Boundary Layer Theory," ASME Paper No. 70-GT-80.

48. Lakshiminarayana, B.: "An Axial Flow Research Compressor Facility Designed for Flow Measurement in Rotor Passages," ASME Journal of Fluids Engineering, Vol 102, No. 4., Dec 1980.

49. Pierzga, M. J.: "Experimental Verification of the Streamline Curvature Numerical Analysis Method Applied to the Flow Through an Axial Flow Fan," M.S. Thesis, Dept of Aerospace Engineering, Pennsylvania State University, 1981.

50. Lakshminarayana, B. and Davino, R.: "Mean Velocity and Decay Characteristics of the Guide Vane and Stator Blade Wake of an Axial Flow Compressor," Journal of Engineering for Power, Vol 102, No. 1, pp. 50-60, 1988.

51. Lakshminarayana, B. and Govindan, T. R.: "Analysis of Turbulent Boundary Layer on Cascade and Rotor Blades of Turbomachinery," AIAA Journal, Vol 19, No. 10, p. 1333, 1981.

52. Ravindranath, A. and Lakshminarayana, B.: "Mean Velocity and Decay Characteristics of the Near and Far Wake of a Moderately Loaded Compressor," Journal of Engineering for Power, Vol 102, No. 1, pp. 50-60, 1980.

53. Reynolds, B., Lakshminarayana, B., and Ravindranath, A.: "Characteristics of the Near Wake of a Compressor Rotor," AIAA Paper A78-1141, Presented at the 11th Fluid and Plasma Dynamics Conference, Seattle, Wa., July 10-12, 1978.

54. Lakshminarayana, B. and Ravindranath, A.: "Interaction of Compressor Rotor Blade Wake with Wall Boundary Layer/Vortex in the End-Wall Region," Journal of Engineering for Power, Vol 104, pp. 467-478, April, 1982.

55. Pouagare, M., Murthy, K. N. S., and Lakshminarayana, B.: "Three-Dimensional Flow Field Inside the Passage of a Low Speed Axial Flow Compressor Rotor," AIAA Paper No. 82-1006, Presented at the AIAA/ASME 3rd Joint Thermophysics, Fluids, Plasma, and Heat Transfer Conference, June 7-11, 1982.

56. Katsanis , T. and McNally, W. D.: "Fortran Program for Calculating Velocities and Streamlines on the Hub-Shroud Mid-Channel Flow Surface of an Axial- or Mixed Flow Turbomachine," Vol I User's Manual and Vol II Programmer's Manual, NASA TN's D-7343 and D-7344, 1973.

57. Katsanis, T. and McNally, W. D.: "Revised Fortran Program for Calculating Velocities and Streamlines on the Hub and Shroud Mid-Channel Stream Surface of an Axial-, Radial-, or Mixed-Flow Turbomachine or Annular Duct," Vol I User's Manual and Vol II Programmer's Manual, NASA TN's D-8430 and D-8431, 1977.

58. Katsanis, T. and McNally, W. D.: "Fortran Program for Calculating Velocities in a Magnified Region of a Blade-to-Blade Stream Surface of a Turbomachine," NASA TN D 5044, 1969.

59. Dring, R. P., Joslyn, H. D., and Hardin, L. N.: "Experimental Investigation of Compressor Rotor Wakes," Aeropropulsion Laboratory, AFAPL-TR-79-2107, Final Report, AFSC, Wright-Patterson AFB, Dayton, Ohio, Jan 1980.

60. Dring, R. P., Joslyn, H. D., and Hardin, L. N.: "An Investigation of Axial Compressor Rotor Aerodynamics," ASME Paper No 81-GT-56, Dec. 4, 1980.

61. Joslyn, H. D. and Dring, R. P., Briefing at Lewis Research Center, Apr. 15, 1983.

62. Wagner, J. H., Dring, R. P. and Joslyn, H. D.: "Axial Compressor Middle Stage Secondary Flow Study," NASA Contractor Report No 3701, July 1983.

63. Durst, F., Melling, A., and Whitlaw, J. H.: "Principles and Practice of Laser Doppler Anemometry," Academic Press, 1976.

64. "Lectures for the International Short Course on Laser Velocimetry," Purdue University, W. Lafayette, Indiana, March 25-29, 1974.

65. "Laser Velocimetry Systems," Catalogue from TSI Inc.

66. Powell, J. A., Strazisar, A. J., and Seasholtz, R. G.: "High-Speed Laser Anemometer System for Intra-Rotor Flow Mapping in turbomachinery," NASA TP-1663, Feb, 1982.

67. Powell, J. A., Strazisar, A. J., and Seasholtz, R. G.: "Efficient Laser Anemometer for Intra-Rotor Flow Mapping in Turbomachinery," Measurement Methods in Rotating Components of Turbomachinery, Ed. B. Lakshiminarayana and P. Rundstadler, Jr. ASME, pp. 157-164, 1980.

68. Strazisar, A. J., and Powell, J. A.: "Laser Anemometer Measurements in a Transonic Axial Flow Compressor Rotor," in Measurement Methods in Rotating Components of Turbomachinery, Ed. B. Lakshiminarayana and P. Rundstadler, Jr. ASME, pp. 165-176, 1980.

69. RCA Electronics components manual, RCA-4526 Photomutiplier Tube.

70. Owen, A. K.: "A Fortran Code for the Calculation of Probe Volume Geometry Changes in a Laser Anemometry System Caused by Window Refraction," NASA TM-100210, Nov 1987.

71. Stevenson, W. H., Dos Santos, R., and Mettler, S. C.: "Fringe Mode FLourescence Velocimetry," AGARD CP-193, pp. 20-1, 20-9, 1976.

72. "VAX, Technical Summary," Digital Equipment Corporation, 1982.

73. "Model 1990B Signal Processor Counter Type Instruction Manual," Revision A, TSI P/N 1990147, TSI Incorporated.

74. Escort User's Manual, Data Systems and Analysis Branch, Computer Services Division, Lewis Research Center, April 1982.

75. Reid, L. and Moore, R. D.: "Design and Overall Performance of Four Highly Loaded, High Speed Inlet Stages for an Advanced High-Pressure-Ratio Core Compressor," NASA TP-1337, Oct. 1978.

76. Hathaway, M. D., "Unsteady Flows in a Single-Stage Transonic Axial Flow Fan Stator Row," NASA TM-88929, 1986.

77. Reid, L. and Moore, R. D.: "Performance of Single Stage Axial Flow Transonic Compressor with Rotor and Stator Aspect Ratios of 1.19 and 1.26, Respectively, and with Design Pressure Ratio of 1.82," NASA TP-1338, Nov., 1978.

78. Chima, R.V.: "Tcgrid," Internal Publication, Lewis Research Center, Nov., 1988.

79. Sorenson, R. L.: "A Computer Program to Generate Two-Dimensional Grids About Airfoils and Other Shapes by the Use of Poisson's Equation," NASA TM 81198, 1980.

80. Baldwin, B. S., and Lomax, H.: "Thin-Layer Approximation and Algebraic Model for Separated Turbulent Flows," AIAA pp. 78-257, Jan 1978.

81. Gessner, F. B. and Po, J. K.: "A Reynolds Stress Model for Turbulent Corner Flows - Part II: Comparisons Between Theory and Experiment," J. Fluids Eng., pp. 269-277 June, 1976.

82. Jameson, A., Schmidt, W., and Turkel, E.: "Numerical Solutions of the Euler Equations by Finite Volume Methods using Runge-Kutta Time-Stepping Schemes," AIAA pp. 81-1259, June 1981.

83. Hollanders, H., Lerat, A., and Peyret, R.: "Three-Dimensional Calculation of Transonic Viscous Flows by an Implicit Method," AIAA Journal, Vol 23, No. 11, pp. 1670-1678 Nov., 1985.

84. Jameson, A., and Baker, T. J.: "Solutions of the Euler Equations for Complex Configurations," AIAA pp. 83-1929, July, 1983.

85. Leonard, B. P.: "A Stable and Accurate Convective Modeling Procedure Based on Quadratic Upstream Interpolation," Computer Methods in Applied Mechanics and Engineering, Vol 19, pp. 59-98, 1979.

86. Schenk, H.: "Theories of Engineering Experimentation," 2nd Ed., McGraw Hill, pp. 12-67, 1965.

87. Strazisar, A. J.: "Laser Fringe Anemometry for Aero Engine Components," NASA TM-88798, May, 1986.

88. Seasholtz, R. G.: "Laser Doppler Velocimeter Systems for Turbine Stator Cascade Studies and Analysis of Statistical Biasing Errors," NASA TN D-8297, 1977.

89. Strazisar, A. J. and Powell, J. A.: "Laser Anemometer Measurements in a Transonic Axial Compressor Rotor," reprinted from Measurement Methods in Rotating Components of Turbomachinery, Ed. B. Lakshiminarayana and P. Rundstadler.

90. Maxwell, B. R.: "Tracer Particle Flow in a Compressor Rotor Passage with Application to LDV," American Institute of Aeronautics and Astronautics, Journal, Vol 13, No. 9, pp. 1141-1142, Sept., 1975.

91. Melling, A.: "Scattering Particles I - Specification," Lectures for International Short Course on Laser Velocimetry, Purdue University, March 25-29, 1974.

92. Chima, R. V.: Internal Publication on Plotting Procedures in the Internal Fluid Mechanics Branch, Feb,1981.

TABLE I. - PERFORMANCE PARAMETERS OF SEVERAL COMPRESSOR RESEARCH FACILITIES

Organization	Type of compressor	Inlet tip diameter, m	Hub/ tip ratio	Approximate inlet velocity, m/s	Approximate maximum, rpm	Number of blades			Maximum tip speed, m/s	Maximum pressure rise	Types of rotor measurements
The Pennsylvania State University	Low speed stage	0.9398	0.5	30	1700	45	21	25	61	≃0	Various conventional - hot wire, temperature total and static pressures inside and downstream or rotor
L.H. Smith (1955); John Hopkins University	Low speed stage	0.9398	0.5	30	1250	45	21	25	61	≃0	Pitchwise average downstream of rotor, total pressure
LeBoeuf Ecolg CC-WTRAL De Lyon; France	Transonic stage	0.55	0.78	--	12000	*	*	*	345	1.38	Pitchwise average downstream of rotor using conventional pressure and temperature
United Technologies Research Center	Low speed rotor	1.52	0.8	35	510	--	28	--	40	≃0	Rotating pressure probe provides circumferential surveys of wake. Static pressure readings on blade surfaces
General Electric, Cincinnati	Four low speed stages	1.524	0.7	--	750	*	38 to 96	37 to 94	61	≃0	Pitchwise average surveys behind rotor wake
Lewis Research Center	Transonic stage	0.505	0.7	75	17200	*	36	*	450	1865	Conventional pressure and temperature upstream and downstream, conventional and secondary flow LDV
Hunter Compaty	Low speed rotor	1.524	0.4	--	525	*	22	*	42	≃0	Hot wire tip clearance measurements in the wake region

TABLE II COMPONENT LIST FOR LASER ANEMOMETER SYSTEM		
NUMBER	COMPONENT	FUNCTION OR SPECIFICATION
(1)	Lexel Laser	Green line:514.5 NM Argon Ion
(2)	90° Turning Mirror	Turns beams from horizontal to vertical
(3)	90° Turning Mirror	Turns beams from vertical to horizontal
(4)	Collimator	Collimates Beam
(5)	Polarization Rotator	Two Quarter Wave Plates. Optimum beam polarization.
(6)	Offset Beam Splitter	Splits Beam into two. One at centerline, one at 135°. Optimum split not achieved.
(7)	Polarization Rotator	Half wave plate orients center beam polarization for beam splitter.
(8)	Beam Splitter	Center beam split into beams at 225° and 45°, 50mm apart. Optimum power split not achieved
(9)	Bragg cell w/ compensation wedge	135° beam shifted by 40 Mhz. Path length compensation required for remaining beams.
(10)	Polarization Rotator	Half wave plate to properly orientate the shifted beam.
(11)	Beam Stop	Blocks Extraneous beams created by Bragg shifting
(13)	Beam Pair Selector	Remotely actuated beam stop selects either horizontal or vertical beam pair.
(14)	22 mm beam spacer	Spaces beams to a separation of 22 mm.
(15)	Beam Expander	Expands beams by 2.27X
(16)	13 mm Beam Spacer	Spaces beams to a separation of 13 mm.
(17)	90° Turning Mirror	2.54 cm mirror turns transmitted beams 90° into goniometer mirror.
(18)	90° Turning Mirror Goniometer Cradle	10.16 cm mirror turns transmitted beams and collected light 90° into probe volume. Directs transmitted beams off radial to minimize blade shadowing.
(19)	Focusing Lens	122 mm focal length, 7.62 cm diameter (Transmitting and Collecting).
(20)	90° Turning Mirror	7.62 cm diameter (Collecting Optics).
(21)	Orange Pass Filter	Blocks all light except in the fluorescent range.
(22)	Focusing Lens	160 mm focal length, 7.62 cm diameter (Collecting Optics).
(23)	Pinhole and Photomultiplier Tube	Mounted on a remotely adjustable base.

TABLE III
LASER ANEMOMETER PROBE VOLUME SPECIFICATIONS

	DESIGN CRITERIA*	MEASURED THROUGH FLOW**	MEASURED TANGENTIAL FLOW**
LENS FOCAL LENGTH (f)	122 mm	122 mm	122 mm
BEAM SPACING	9. mm	8.832 mm	8.295 mm
PROBE VOLUME HALF CROSSING ANGLE (κ)	2.156°	2.073°	1.947°
FRINGE SPACING (d_f)	6.838×10^{-3} mm	7.112×10^{-3} mm	7.572×10^{-3} mm
BEAM WAIST DIAMETER ($d_{e\text{-}2}$)	2.713×10^{-2} mm	2.713×10^{-2} mm	2.713×10^{-2} mm
PROBE VOLUME DIAMETER (d_m)	2.715×10^{-2} mm	2.7148×10^{-2} mm	2.7146×10^{-2} mm
PROBE VOLUME LENGTH (l_m)	0.721 mm	0.75 mm	0.799 mm
FRINGE VOLUME (V_{FR})	2.782×10^{-4} mm^3	2.892×10^{-4} mm^3	3.079×10^{-4} mm^3
NUMBER OF FRINGES (N_{FR}) UNSHIFTED	9	11	11

* All values are calculated using the measured crossing angles and a separation between the two parallel incoming beams of 9mm.

**All values are calculated using the measured crossing angles and assume a focal length of 122mm with parallel incoming beams

TABLE IV LOCATION OF CONVENTIONAL SURVEY PROBE INSTRUMENTATION				
SURVEY STATION NUMBER	AXIAL LOCATION* (cm)	NUMBER OF PROBES	NUMBER OF INNER WALL STATICS	NUMBER OF OUTER WALL STATICS
-1	-30.48	2	2	2
0	-15.24	2	2	2
1	-2.568	2	2	2
2	4.859	2	2	2
3	10.64	1 circum-ferential 1 radial	2	2
4	15.24	4	4	4
*Measured from the hub blade leading edge intersection				

TABLE V SHROUD STATIC TAP LOCATIONS						
POSITION NUMBER	% TIP CHORD	AXIAL POSITION (cm)*		POSITION NUMBER	% TIP CHORD	AXIAL POSITION (cm)
1	-200	-5.295		12	50	1.325
2	-173	-4.583		13	60	1.59
3	-120	-3.179		14	70	1.854
4	-60	-1.590		15	80	2.119
5	-20	-.530		16	90	2.384
6	-10	-.265		17	100	2.649
7	0	0.		18	140	3.709
8	10	0.265		19	160	4.239
9	20	0.530		20	200	5.296
10	30	0.795		21	223	5.906
11	40	1.060				

*Measured from the hub leading edge intersection

TABLE VI. - ESTIMATED INACCURACIES IN CONVENTIONAL INSTRUMENTATION AND RECORDING SYSTEMS	
Flow (Kg/sec)	±0.3
Rotative Speed (RPM)	±30.
Survey Flow Angles (Deg)	±1.0
Temperatures (Deg K)	±0.6
Total Pressures (N/cm^2)	±0.17
Static Pressures (N/cm^2)	±0.10

TABLE VII OVERALL DESIGN PERFORMANCE PARAMETERS FOR ROTOR 35	
ROTOR TOTAL PRESSURE RATIO	1.865
ROTOR TOTAL TEMPERATURE RATIO	1.225
ROTOR ADIABATIC EFFICIENCY	0.865
ROTOR POLYTROPIC EFFICIENCY	0.877
ROTOR HEAD RISE COEFFICIENT	0.273
FLOW COEFFICIENT	0.451
WEIGHT FLOW PER UNIT FRONTAL AREA (Kg/sec)	100.808
WEIGHT FLOW PER UNIT ANNULUS AREA (Kg/sec)	199.989
WEIGHT FLOW (Kg/sec)	20.188
RPM	17188.7
TIP SPEED (m/sec)	454.456
HUB/TIP RADIUS RATIO	0.70
ROTOR ASPECT RATIO	1.19
NUMBER OF ROTOR BLADES	36

TABLE VIII
MERIDIONAL AND RADIAL COORDINATES OF THE ENDWALLS AND ROTOR BLADES
a) ENDWALL COORDINATES

HUB AXIAL POSITION (CM)	HUB RADIAL POSITION (CM)		SHROUD AXIAL POSITION (CM)	SHROUD RADIAL POSITION (CM)
-22.86	17.526		-22.860	25.654
-15.40	17.526		-15.400	25.654
-7.62	17.526		-7.62	25.645
-2.588	17.539		-2.588	25.643
0.0	17.780		0.0	25.4
1.854	18.255		1.854	24.925
4.137	18.714		3.282	24.511
4.859	18.821		4.859	24.232
6.566	19.035		6.538	24.145
8.89	19.279		8.89	23.993
10.640	19.380		10.64	23.851
12.7	19.431		12.7	23.749
15.4	19.431		15.4	23.749

b) Blade Leading and Trailing Edge Coordinates

LEADING EDGE			TRAILING EDGE	
AXIAL POSITION (CM)	RADIAL POSITION (CM)		AXIAL POSITION (CM)	RADIAL POSITION (CM)
0.	17.969		4.096	18.88
.039	18.849		4.017	19.466
.088	19.662		3.935	20.044
.140	20.428		3.852	20.616
.212	21.157		3.752	21.168
.286	21.856		3.675	21.719
.346	22.533		3.579	22.262
.410	23.197		3.533	22.796
.476	23.841		3.47	23.324
.544	24.480		3.404	23.849
.611	25.11		3.312	24.375

TABLE IX LASER ANEMOMETER SURVEY LOCATIONS				
SPAN (PERCENT)	CHORD (PERCENT)	AXIAL POSITION (CM)	RADIAL POSITION (CM)	GONIOMETER OFFSETS (DEGREES)
5	UPSTREAM SURVEY LOCATION	-2.54	17.856	0.
10		-2.54	18.273	0.
20		-2.54	19.098	0.
30		-2.54	20.752	0.
40		-2.54	21.58	0.
50		-2.54	22.329	0.
60		-2.54	22.804	0.
70		-2.54	23.233	0.
80		-2.54	24.061	0.
90		-2.54	24.881	0.
5	-5% CHORD	-.175	18.151	0.
10		-.157	18.542	0.
20		-.102	19.319	0.
30		-.064	20.063	0.
40		0.018	20.825	0.
50		0.104	21.577	0.
60		0.183	22.329	0.
70		0.262	23.066	0.
80		0.348	23.807	0.
90		0.439	24.541	0.

TABLE IX
continued

5	5% CHORD	0.231	18.202	0.
10		0.244	18.588	-5.,0.,5.
20		0.290	19.352	-5.,2.,5.
30		0.318	20.081	-5.,2.,5.
40		0.378	20.833	-5.,2.,5.
50		0.450	21.575	-5.,0.,2., 4.,5.
60		0.513	22.316	-5.,2.,5.
70		0.562	23.066	-5.,2.,5.
80		0.648	25.238	-5.,2.,5.
90		0.724	26.501	0.,2.
5	25% CHORD	1.046	18.354	0.
10		1.049	18.677	-5.,-1.,5.
20		1.069	19.434	-5.,-1.,5.
30		1.074	20.137	-5.,-1., 4.,5.
40		1.102	20.851	-5.,-1., 0.,4.,5.
50		1.140	21.562	-5.,0,.5.
60		1.168	22.273	-5.,-2.16, 2.16,5.
70		1.204	22.974	-5.,4.,5.
80		1.247	23.683	-5.,4.,5.
90		1.290	24.381	2.

TABLE IX continued				
5	50% CHORD	2.065	18.545	-3.,-2.5, 2.5,3.
10		2.057	18.877	-3.,-2.5, 2.5,3.
20		2.045	19.545	-3.,-2.5, -2.5,3.
30		2.022	20.206	-3.,-2.5, -1.,1.,3.
40		2.007	20.876	-3.,-2.5, 2.5,3.
50		2.002	21.547	-3.,-1., 1.,3.
60		1.989	22.217	-3.,3.
70		1.989	22.885	-3.,3.
80		1.994	23.566	-3.,3.
90		2.002	24.229	0.
5	75% CHORD	3.086	18.733	-3.5,-.5
10		3.063	19.040	-5.,-3.5, 0.5
20		3.018	19.655	-5.5,0.
30		2.967	20.272	-6.,-0.6, 0.
40		2.911	20.899	-6.,0., 1.,6.
50		2.865	21.529	-5.5,0.
60		2.860	22.164	-2.5, -2.469
70		2.774	22.799	-3.03
80		2.741	23.449	-4.
90		2.710	24.077	-2.,-4.

TABLE IX continued				
5	95% CHORD	3.901	18.885	-5.,-3.
10		3.868	19.169	-2.
20		3.797	19.741	-2.
30		3.724	20.328	-2.
40		3.635	20.917	-2.
50		3.553	21.518	-2.
60		3.465	22.121	-2.
70		3.401	22.728	-4.
80		3.340	23.355	-4.
90		3.277	23.957	-4.,0.
5	105% CHORD	4.308	18.933	0.
10		4.270	19.213	0.
20		4.188	19.769	0.
30		4.105	20.345	0.
40		3.995	20.925	0.
50		3.899	21.516	0.
60		3.795	22.111	0.
70		3.716	22.708	0.
80		3.640	23.327	0.
90		3.561	23.922	0.

TABLE X. - SCHEMATIC OF MARGINAL OR UNACCEPTABLE DATA POINTS.

(1) Axial velocity component.

Radial position	Station							
	1	2	3	4	5	6	7	8
Chord	I	-5%	5%	25%	50%	15%	95%	105%
1 (5%)			•	•	+	?+	•	•
2 (10%)				+			+	•
3 (20%)								•
4 (30%)								•
5 (40%)								+
6 (50%)								
7 (60%)								
8 (70%)								
9 (80%)			X					+
10 (90%)	X?	•	•	•	•	?•	?•	?•
11 (95%)	•	•	•	•	•	•	•	•

• Unacceptable data, both configurations.
X Unacceptable data, base line.
+ Unacceptable data, enhanced.
? Indicates questionable data.

(2) Tangential velocity component.

Radial position	Station							
	1	2	3	4	5	6	7	8
Chord	I	-5%	5%	25%	50%	15%	95%	105%
1 (5%)			X		?+	+	?*	*
2 (10%)							+	+
3 (20%)								+
4 (30%)								+
5 (40%)								+
6 (50%)								
7 (60%)								
8 (70%)								
9 (80%)								+
10 (90%)		X	+	?+	?*	?*	?*	?*
11 (95%)	*	*	*	*	*	*	*	*

* Unacceptable data, both configurations.
X Unacceptable data, base line.
+ Unacceptable data, enhanced.
? Indicates questionable data.

(3) Total velocity component.

Radial position	Station							
	1	2	3	4	5	6	7	8
Chord	0	-5%	5%	25%	50%	75%	95%	105%
1 (5%)			•	•	?+	+	•	•
2 (10%)				+	?+		+	•
3 (20%)								•
4 (30%)								•
5 (40%)								+
6 (50%)								
7 (60%)								
8 (70%)								
9 (80%)			•					+
10 (90%)	X	?•	•	•	•	?•	•	•
11 (95%)	•	•	•	•	•	•	•	•

• Unacceptable data, both configurations.
X Unacceptable data, base line.
+ Unacceptable data, enhanced
? Indicates questionable data.

TABLE XI. - DATA RUN COMBINATION SCHEDULE

Final run	Combined	Reduced	Original				
1	1	1 2	1 3	2			
2	2	3 4	4 5	365 366			
3	3	5 6	6 7				
4	4	7 8	8 9	451 452			
5	5	9 10	10 11				
6	6	11 12	12 13	403 404			
7	7	13 14	14 15				
8	8	15 16	16 17				
9	9	17 18	18 19	454 453			
10	10	19 20	20 21				
11	11	21 22	37 38	75 76			
	12	23 24	39 78	41	77		
12	13	25 26	368 367				
	14	27 28	369 370				
13	15	29 30	79 80				
	16	31 32	45 44				
14	17	33 34	81 82				
	18	35 36	68 67	 456	 457		
15	19	37 38	69 71	70			
	20	39 40	72 73				
16	21	41 42	406 405	467 469	468 470		

17	22	43 44	89 90				
18	23	45 46	91 92				
19	24	47 48	93 95	94 96			
20	25	49 50	97 98				
	26	51 52	102 103	107 104			
	27	53 54	373 372	374			
	28	55 56	101 371				
21	29	57 58	106 105				
	30	59 60	108 111				
22	31	61 62	109 110				
	32	63 64	112 115				
23	33	65 66	113 114				
	34	67 68	116 119				
24	35	69 70	117 118				
	36	71 72	120 123	126 127			
25	37	73 74	407 408	575 578	577 579		
	38	75 76	410 409				
	39	77 78	121 122	125 128			
	40	79 80	131 132				
26	41	81 82	129 130				
	42	83 84	133 134				
27	43	85 86	135 136				
	44	87 88	139 141	142			

28	45	89 90	137 138				
29	46	91 92	143 144	145			
30	47	93 94	146 149	147 150	148 151		
	48	95 96	155 157	156 158	159		
31	49	97 98	152 153	154			
	50	99 100	160 161				
32	51	101 102	162 163				
	52	103 104	166 167				
33	53	105 106	164 165				
	54	107 108	174 175	178 176			
	55	109 110	62 63				
34	56	111 112	172 170	173 171			
	57	113 114	179 180	182 181			
	58	115 116	423 424				
35	59	117 118	183 184	422 421			
	60	119 120	187 188				
36	61	121 122	186 185				
	62	123 124	190 189	191			
37	63	125 126	192 193				
	64	127 128	200 199				
38	65	129 130	197 198	196 195	194		
39	66	131 132	201 202	204 203			

	67	133 134	212 210	213 211			
40	68	135 136	205 208	206 209	207		
	69	137 138	214 215				
	70	139 140	378 377				
41	71	141 142	375 376				
	72	143 144	216 217				
	73	145 146	218 219				
	74	147 148	220 221				
42	75	149 150	222 223				
	76	151 152	226 227				
43	77	153 154	224 225				
	78	155 156	228 230	229			
44	79	157 158	232 231				
	80	159 160	234 235				
	81	161 162	427 428				
45	82	163 164	426 425				
	83	165 166	237 236				
46	84	167 168	238 239				
	85	169 170	242 243				
47	86	171 172	241 240				
	87	173 174	245 244	246			
48	88	175 176	247 248				
49	89	177 178	473 472	474			

50	90	179 180	251 252				
	91	181 182	250 249				
	92	183 184	385 384				
51	93	185 186	255 253	 254			
	94	187 188	256 257	382 383			
52	95	189 190	259 258	 260			
	96	191 192	262 263				
53	97	193 194	265 264				
	98	195 196	269 268				
54	99	197 198	266 267				
55	100	199 200	270 271				
	101	201 202	273 271				
56	102	203 204	274 275				
57	103	205 206	277 276				
58	104	207 208	278 279	 280	 281		
59	105	209 210	282 284	283 287	286		
60	106	211 212	290 288	291 289	312 310	313 311	
61	107	213 214	307 308	309 387	389 388		
	108	215 216	297 299	298 300	 301	 302	
62	109	217 218	314 315				
	110	219 220	306 305				
63	111	221 222	320 316	 317			
64	112	223 224	319 318				

ORIGINAL PAGE IS
OF POOR QUALITY

65	113	225 226	321 322				
66	114	227 228	324 323				
67	115	229 230	325 326				
68	116	231 232	332 329	330			
69	117	233 234	333 334				
70	118	235 236	337 335	338 336			
72	119	237 238	346 345	347			
71	120	239 240	390 392	391 393			
	121	241 242	342 343				
73	122	243 244	348 350	349			
74	123	245 246	352 351				
75	124	247 248	353 354				
76	125	249 250	356 355				
77	126	251 252	357 358				
78	127	253 254	360 359				
79	128	255 256	361 362	363 364			
80	129	257 258	480 475	481 476	477	478	479
81	130	259 260	482 484	483 485			
82	131	261 262	488 486	487			
83	132	263 264	489 491	490 492			
84	133	265 266	494 493				
85	134	267 268	495 496				
86	135	269 270	499 497	500 498			

87	136	271 272	501 503	502 504			
88	137	273 274	507 505	508 506			
89	138	275 276	509 510				
90	139	277 278	513 511	566 512	 565		
91a	140	279 280	515 516	523 517	524 518	 526	 527
91b	141	281 282	563 564				
92a	142	283 284	533 528	534 529	 530		
92b	143	285 286	562 560				
	144	287 188	539 543	540 544	541		
93	145	289 290	558 559				
94	146	291 292	554 555				
96	147	293 294	547 549	548 550			
97	148	295 296	553 551				
98	149	297 298	567 568				
99	150	299 300	570 569				
100	151	301 302	571 572				
101	152	303 304	586 580	587 581	 582		
102	153	305 306	593 596	595 597	 598		
103	154	307 308	602 599	603 600	 601		
104	155	309 310	604 608	607 609			
105	156	311 312	612 611	613	614		
106	157	313 314	615 616				
107	158	315 316	620 625	621	622		

108	159	317 318	623 624				
109	160	319 320	628 626	629 627	630		
	161	321 322	632 635	636			
110	162	323 324	643 638	644 639	641	642	
	163	325 326	645 646				
111	164	327 328	669 647	670 651			
112	165	329 330	653 652	654 655	657 656		
	166	331 332	658 662	660 663	661	664	
113	167	333 334	665 667	666			
	168	336 336	671 672				
114	169	337 338	669 668	670			
	170	339 340	673 674				
	171	341 342	675 677	676			
115	172	343 344	683 682				
	173	345 346	684 685				
116	174	347 348	687 686				
117	175	349 350	688 689				
118	176	351 352	691 690				
119	177	353 354	692 693				
	178	355 356	695 694				
120	179	357 358	712 711				
	180	359 360	705 708	706 709	707 710		
121	181	361 362	713 719	714 720	715	717	718

	182	363 364	725 726				
122	183	365 366	731 732	 733			
	184	367 368	729 727	730 728			
123	185	369 370	736 734	737 735	738		
	186	371 372	699 698				
	187	373 374	696 697				
	188	375 376	743 742				
	189	377 378	739 741	740			
124	190	379 380	749 748				
	191	381 382	746 747				
125	192	383 384	750 751				
	193	385 386	700 702	701			
	194	387 388	704 703				
	195	389 390	753 752				
126	196	391 392	757 756				
	197	393 394	754 755				
127	198	395 396	758 759				
128	199	397 398	761 760				
	200	399 400	766 765				
129	201	401 402	762 763				
130	202	403 404	768 770	769 773	771		
	203	405 406	782 784	783 785	 786		
	204	407 408	780 777	781 779			

ORIGINAL PAGE IS
OF POOR QUALITY

	205	409 410	789 787	788			
131	206	411 412	790 792	791 793			
	207	413 414	795 794				
132	208	415 416	798 799	800			
	209	417 418	797 796				
133	210	419 420	805 806				
134	211	421 422	803 801	804 802			
	212	423 424	809 810	811			
	213	425 426	808 807				
135	214	427 428	814 815				
136	215	429 430	813 812				
137	216	431 432	817 816	818 819			
138	217	433 434	822 820	823 821			
139	218	435 436	824 825				
140	219	437 438	830 826	831 827	828	829	
141	220	439 440	834 840	835 841	836	837	
142	221	441 442	844 842	845 843	846	847	848
143	222	443 444	851 854	852 855	856		
144	223	445 446	859 857	860 858			
145	224	447 448	861 862				
146	225	449 450	864 863				
147	226	451 452	865 866				
148	227	453 454	868 867				

	228	455 456	931 932				
149	229	457 458	935 933	934			
150	230	459 460	874 869	875 870	942 871	872	873
	231	461 462	877 881	943 882	951 944	950	
151	232	463 464	876 879	878 880	947 945	952 946	948
152	233	465 466	885 883	953 884	954 887	955	956
153a	234	467 468	890 888	891 889	958 957	960	
153b	235	469 470	895 897	896			
154	236	471 472	918 898	919 899	920 922	921	
	237	473 474	901 902				
155	238	475 476	915 916	917			
156	239	477 478	904 903	914 913			
157	240	479 480	905 906	911 912			
158	241	281 482	910 909				
	242	483 484	928 924	929			
95	243	485 486	927 923	925	926		

TABLE XII
ESTIMATED INACCURACIES IN LASER ANEMOMETRY INSTRUMENTATION

Probe Volume Position (mm)	±0.05
Beam Director Setting Angle (Deg)	±0.01
Statistical biasing Error (maximum)	1.0%
Window Width Velocity Gradient Error	2.0%
Particle Velocity Lag (Leading edge region)	10%
Particle Angle Lag (Deg)(blade trailing edge)	6%

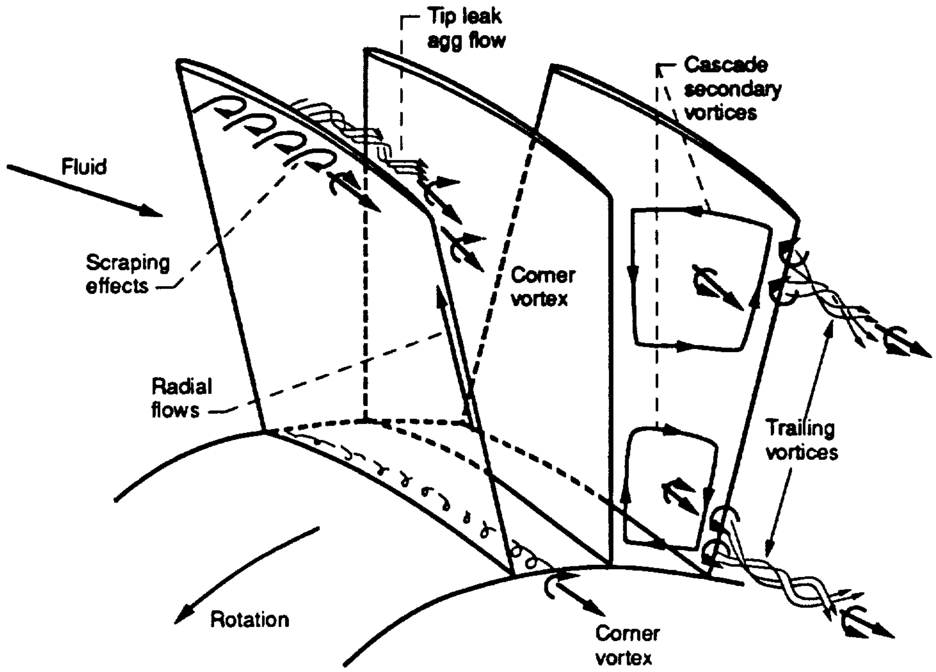

Figure 1.—Secondary flow and vortices in an axial flow compressor rotor.

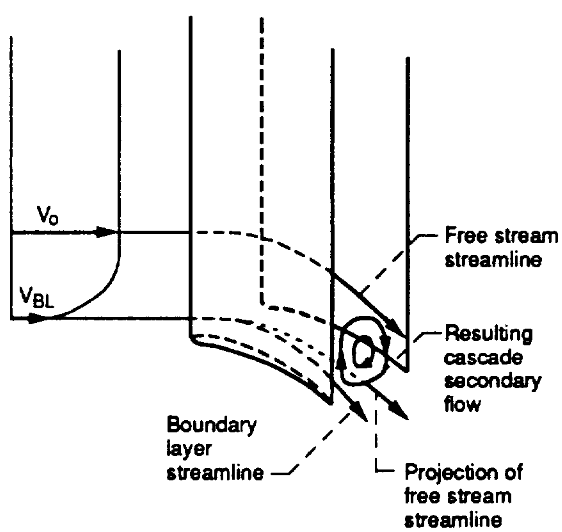

Figure 2.—Generation of secondary flows in a channel bend due to a nonuniform inlet velocity.

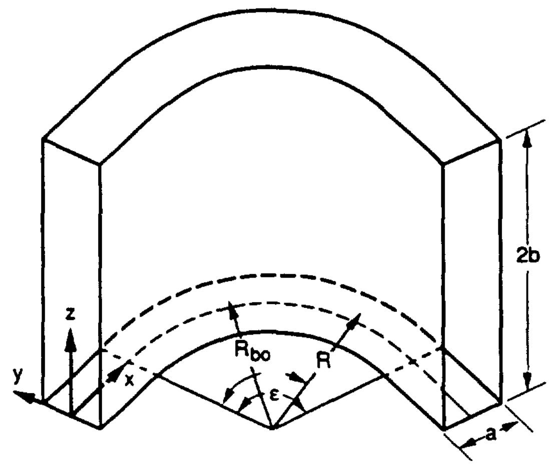

Figure 3.—Channel used for Squire and Winter analysis.

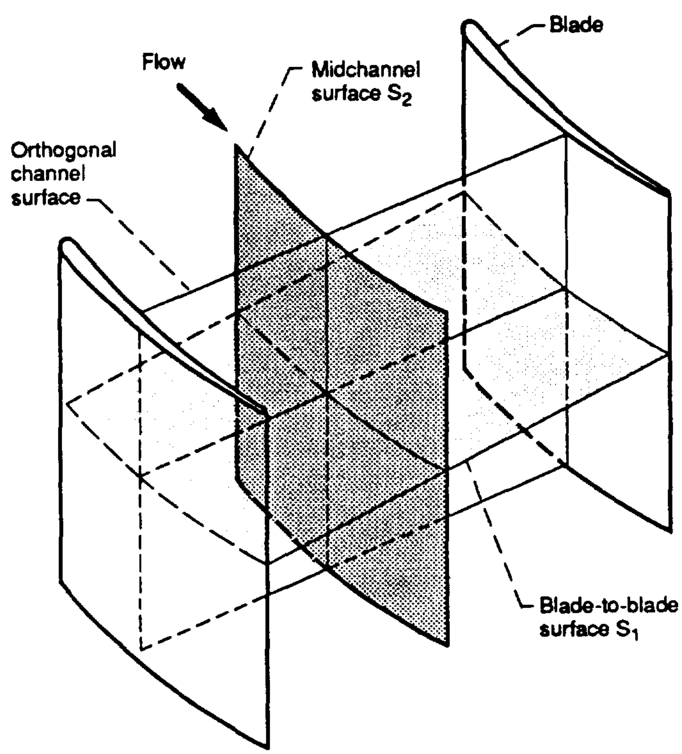

Figure 4.—Two-dimensional analysis surfaces in a turbomachine.

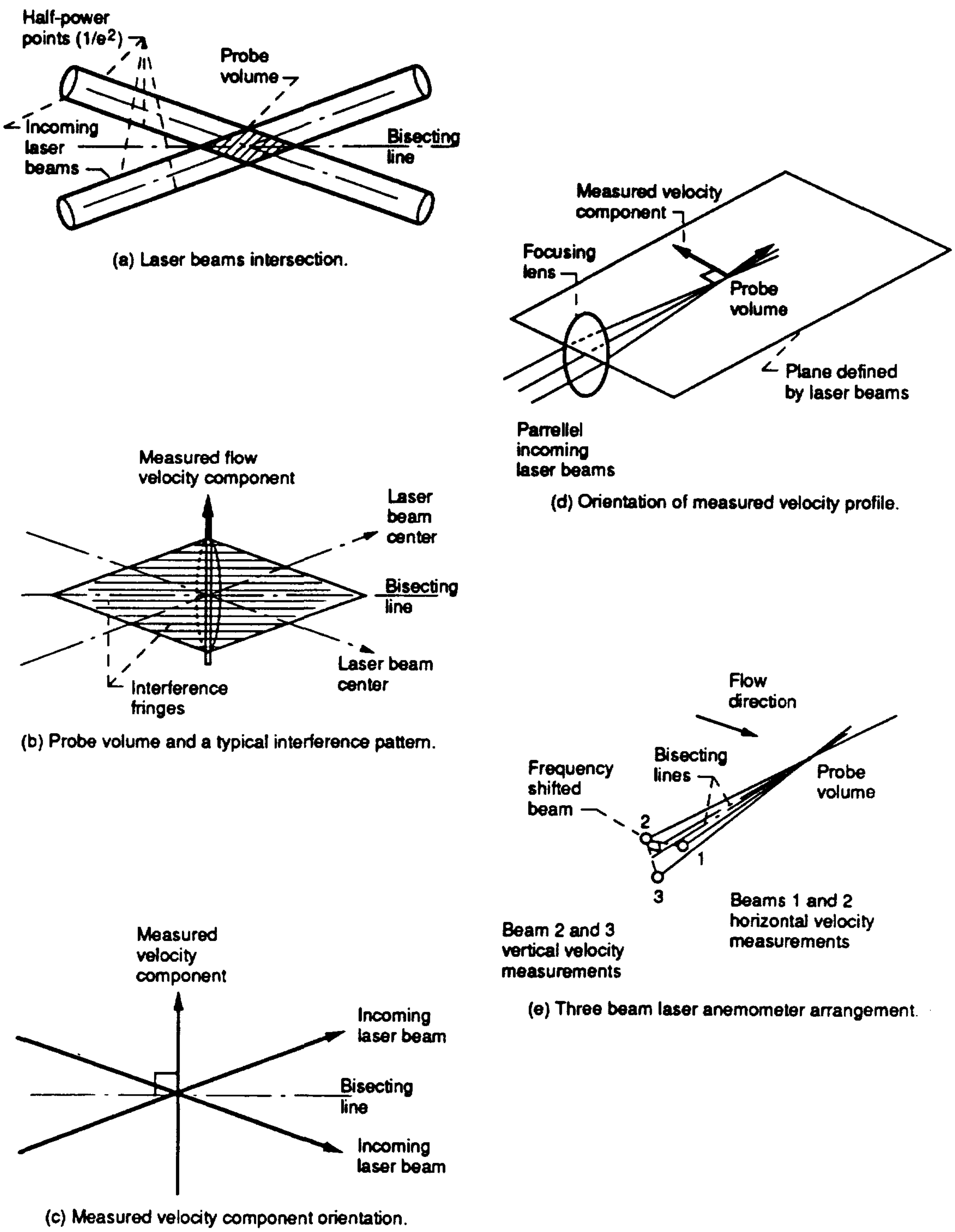

Figure 5.—Typical laser anemometer probe volume.

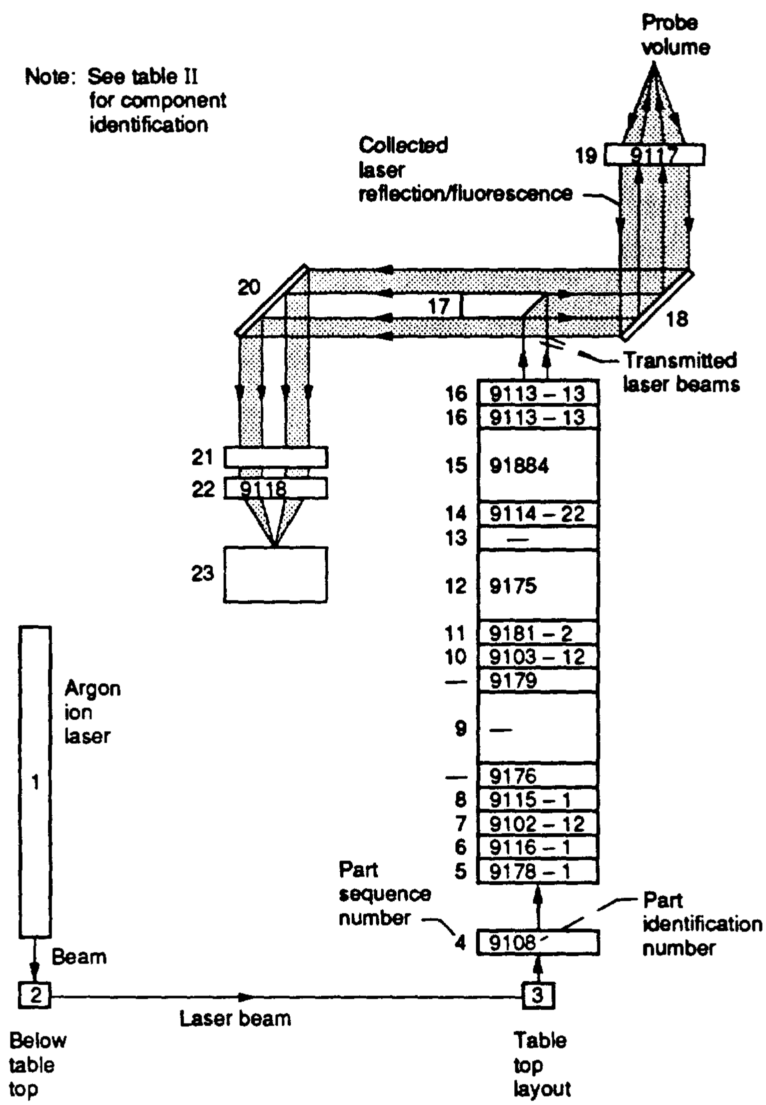

Figure 6.—Schematic of laser optical system.

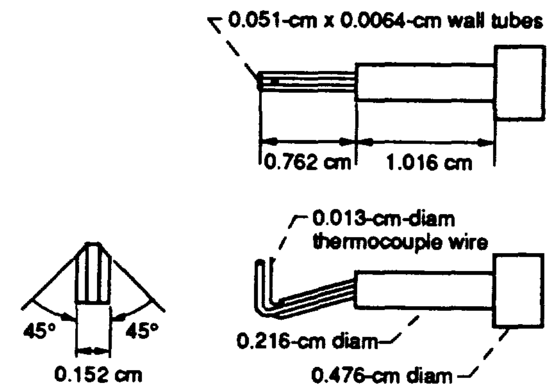

(a) Cobra probe for total pressure, total temperature, and andle measurements.

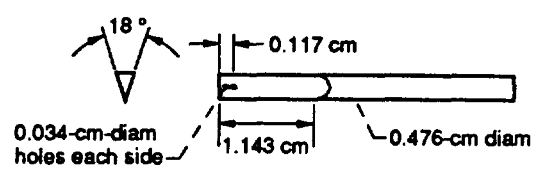

(b) Wedge probe for static pressure measurements.

Figure 7.—Aerodynamic survey probes.

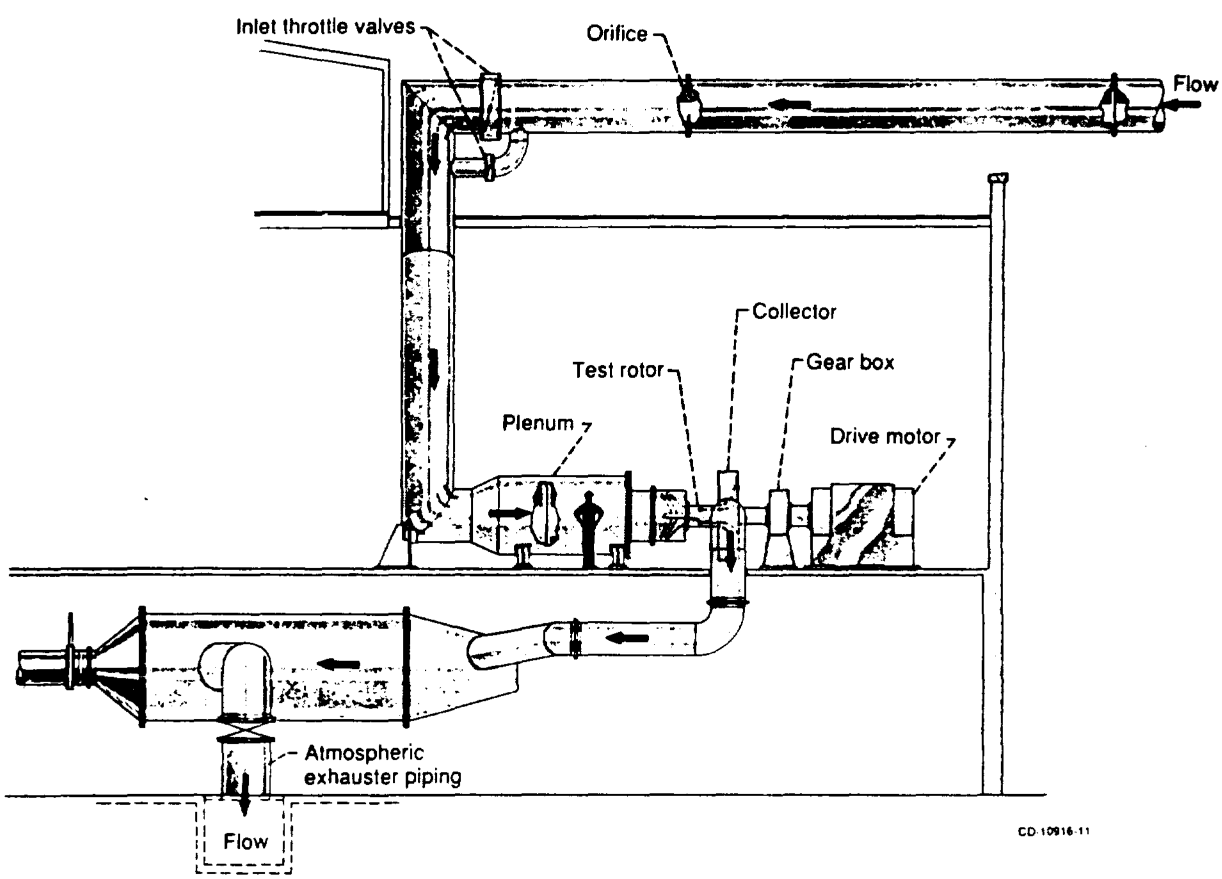

Figure 8.—Test facility.

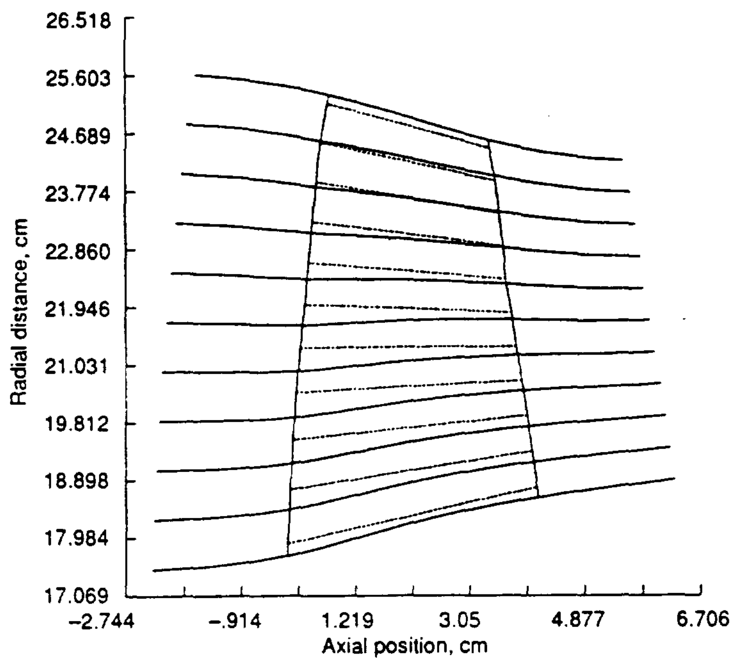

Figure 9.—Compressor rotor meridional view.

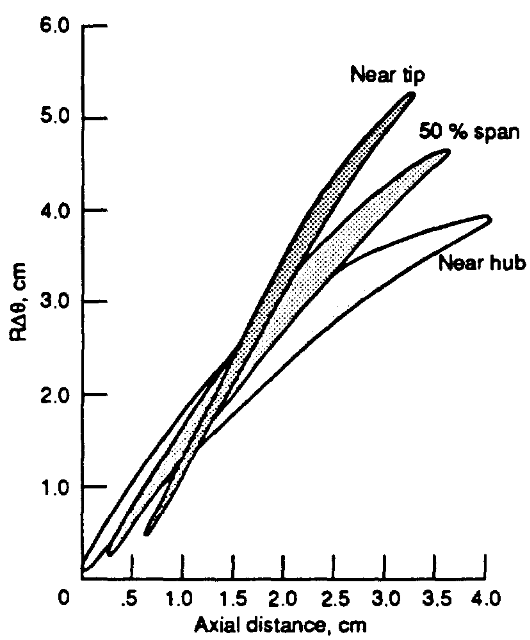

Figure 10.—Compressor rotor blade sections at three radial locations.

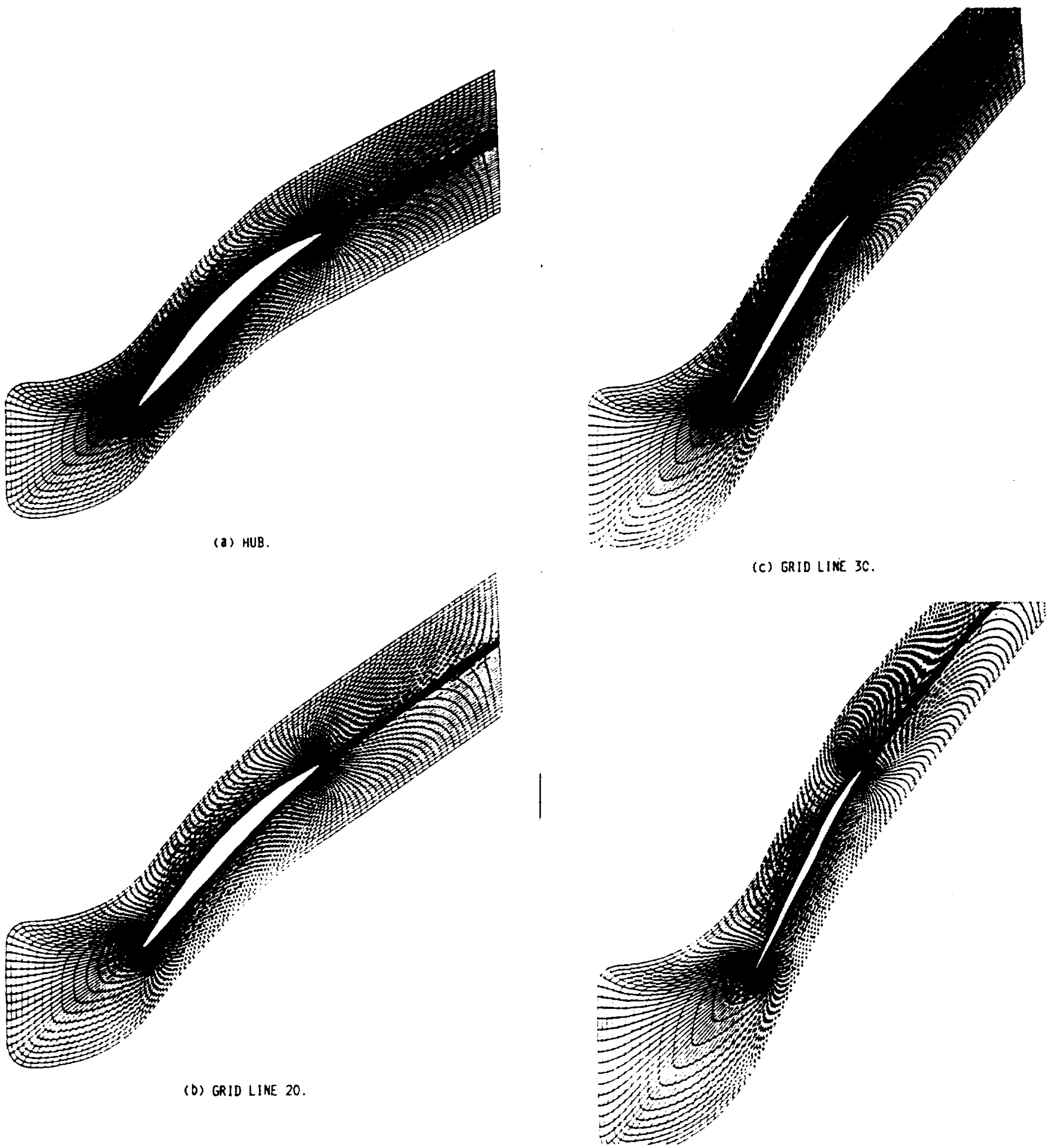

(a) HUB.

(c) GRID LINE 30.

(b) GRID LINE 20.

(d) SHROUD.

FIGURE 11. - TYPICAL BLADE-TO-BLADE COMPUTATIONAL PLANE.

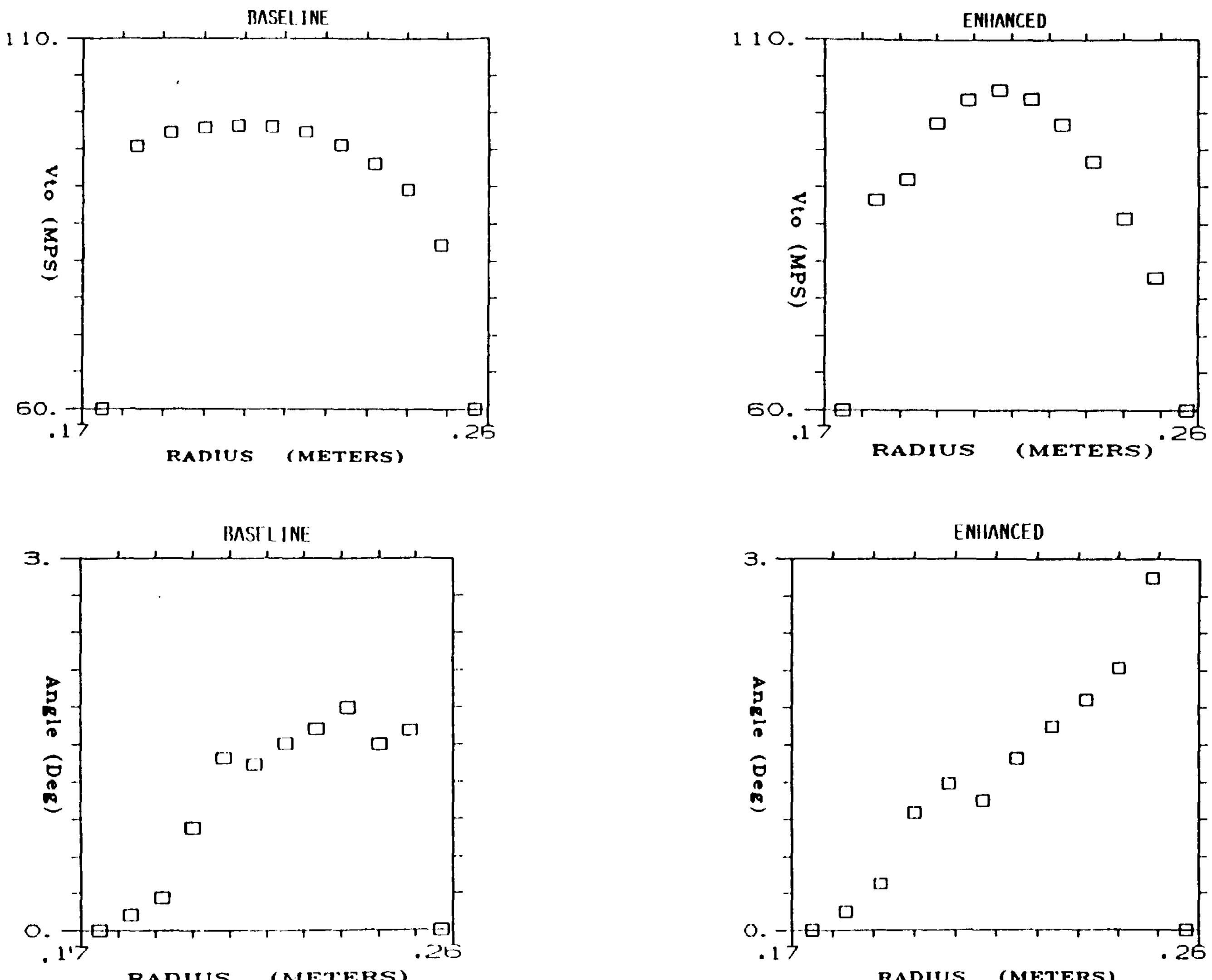

INLET AERO-SURVEYS

FIGURE 12a.

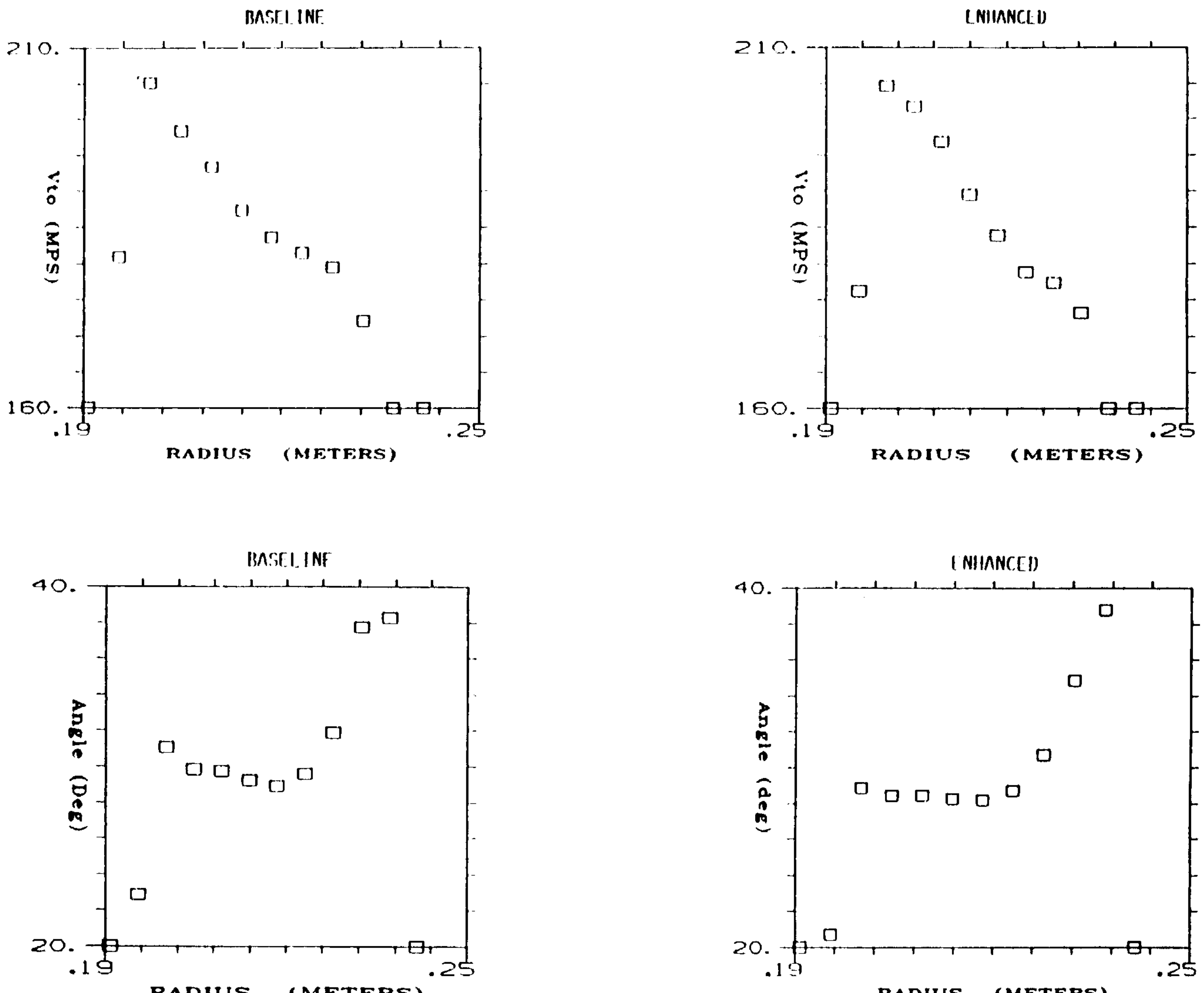

EXIT AEROSURVEY

FIGURE 12b.

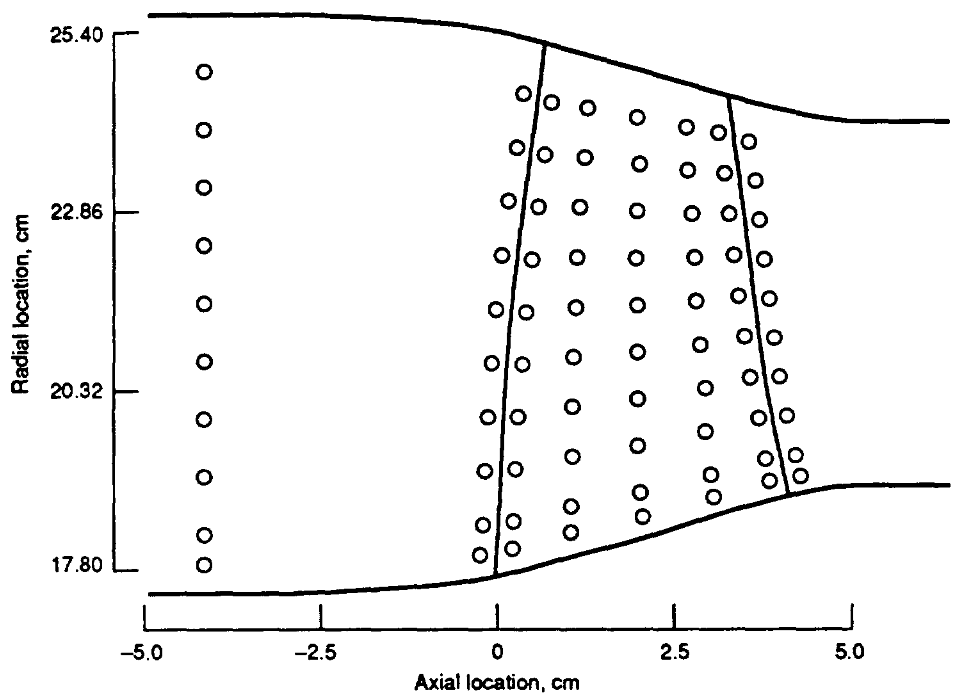

Figure 13.—Laser anemometer survey locations.

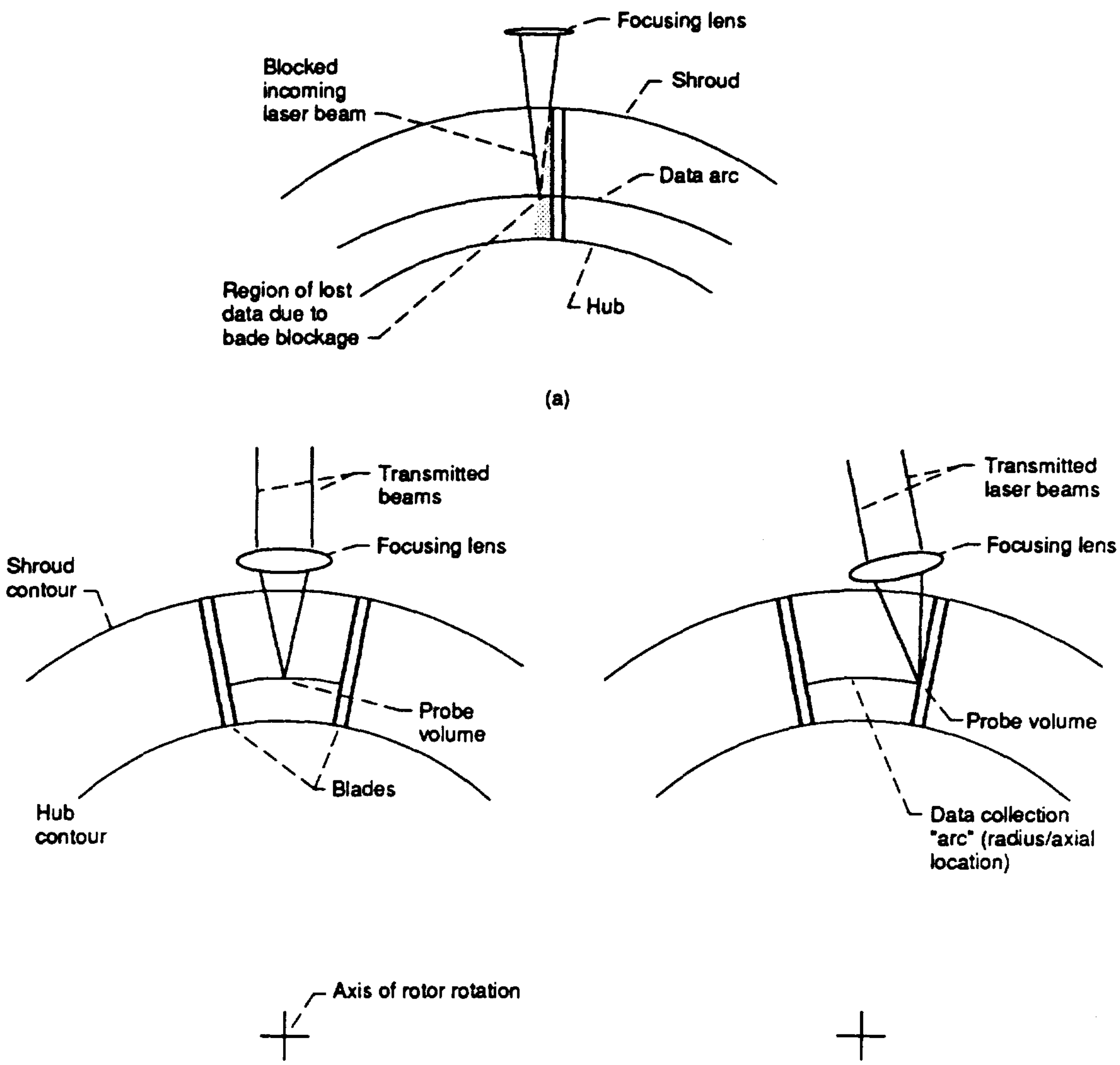

(b) Normal goniometer position.

(c) Offset goniometer positions.

Figure 14.—Goniometer movement to minimize blade blockage.

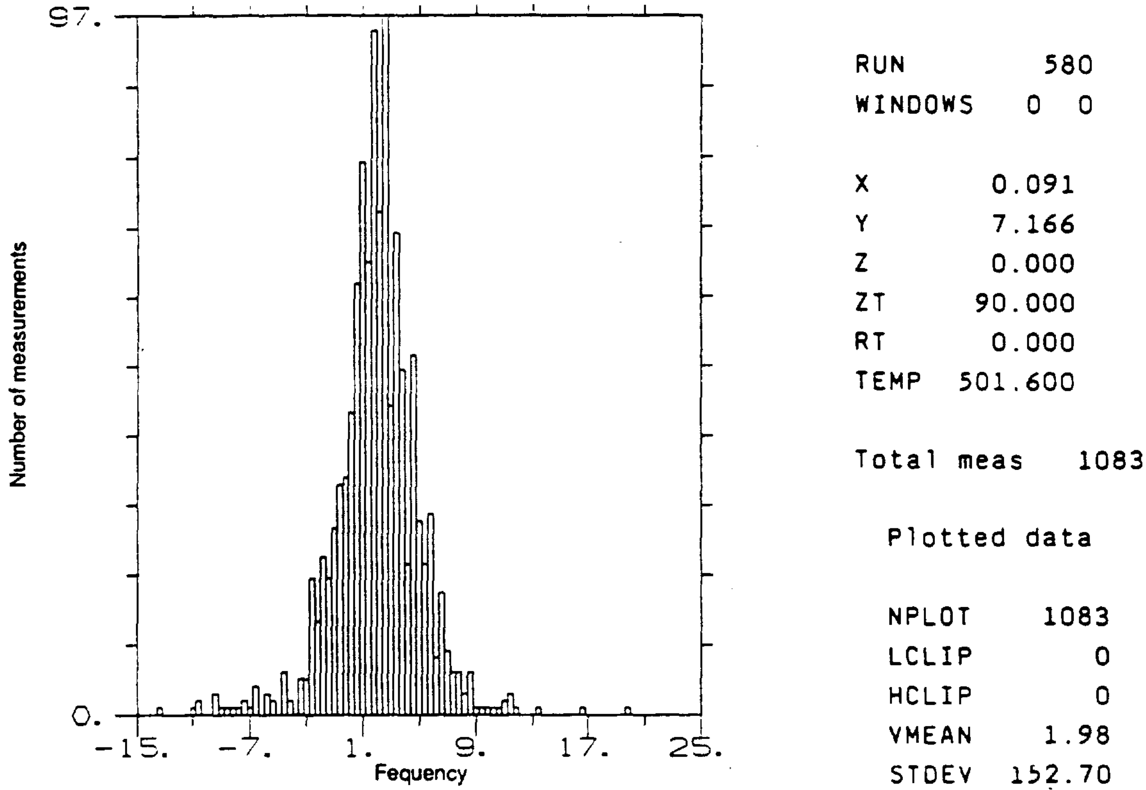

Figure 15.—Typical frequency histogram.

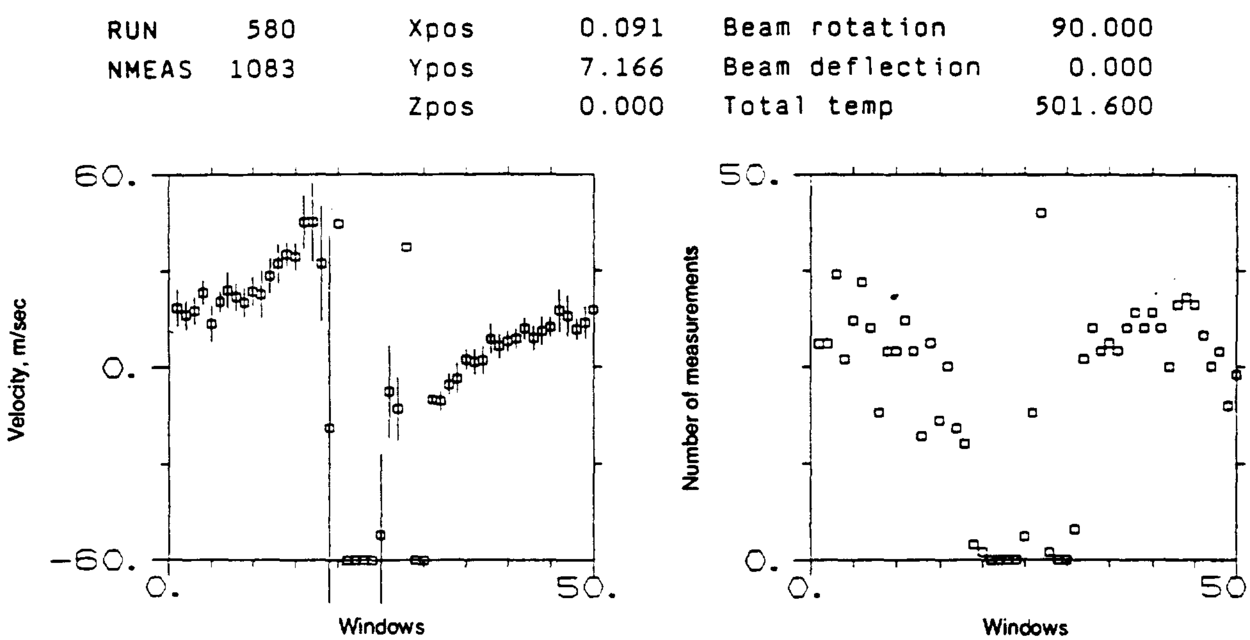

Figure 16.—Typical blade-to-blade velocity plot.

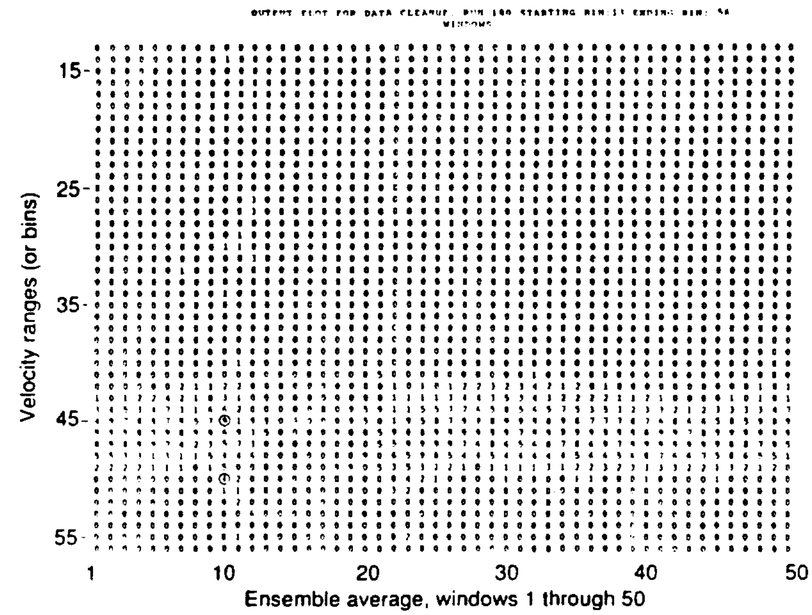

Figure 17.—Nondimensionalized frequency histogram for a typical data run.

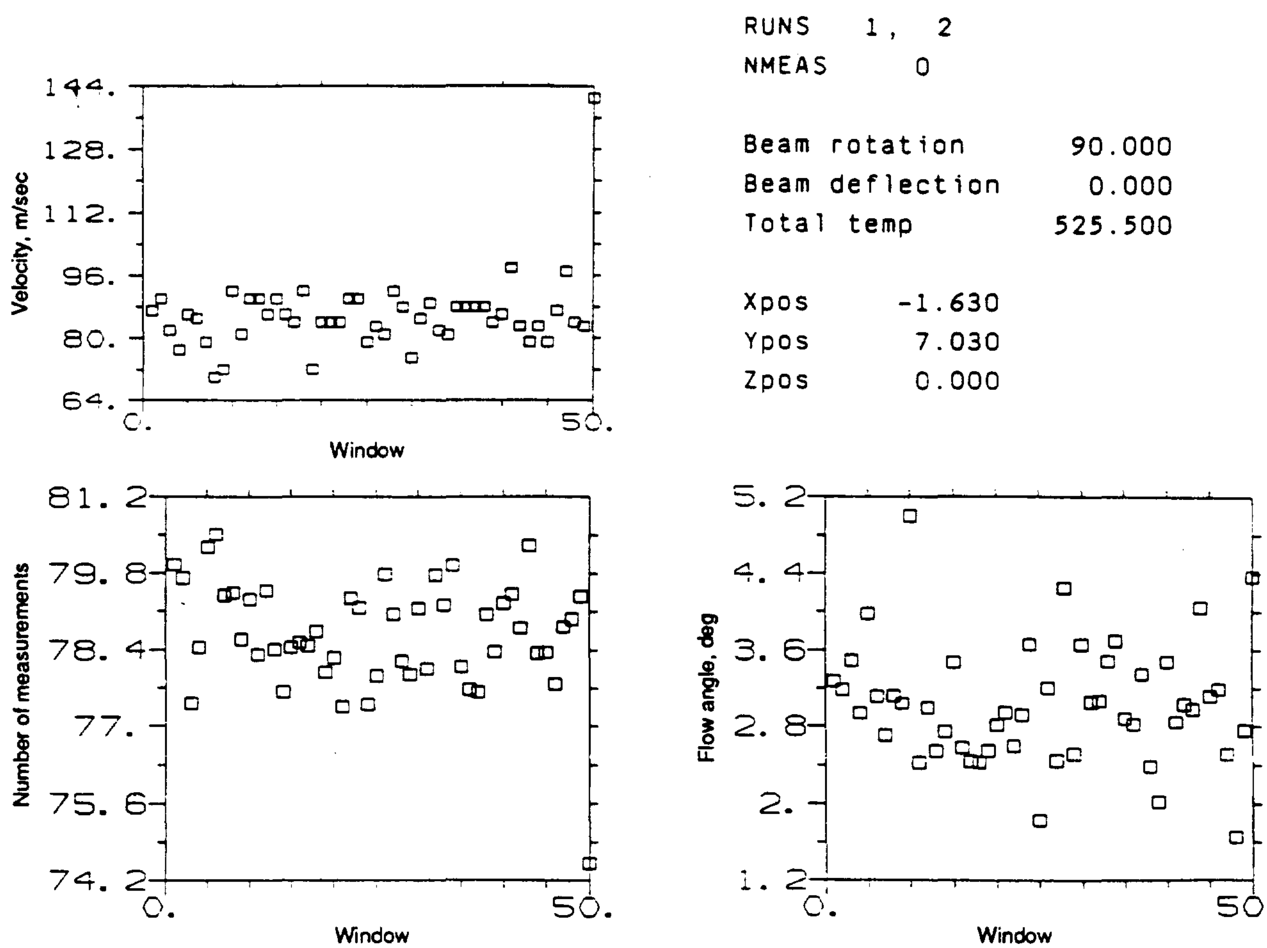

Figure 18.—Typical combined component velocity output, showing axial/tangential velocity, flow angle and measurements per bin.

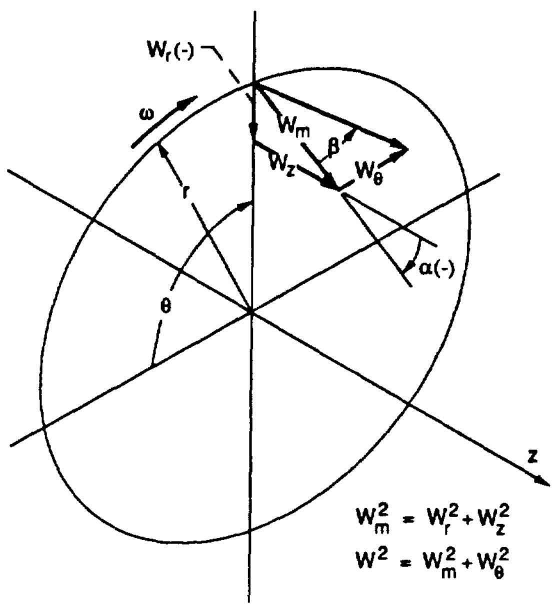

Figure 19.—Cylindrical coordinate system and velocity components.

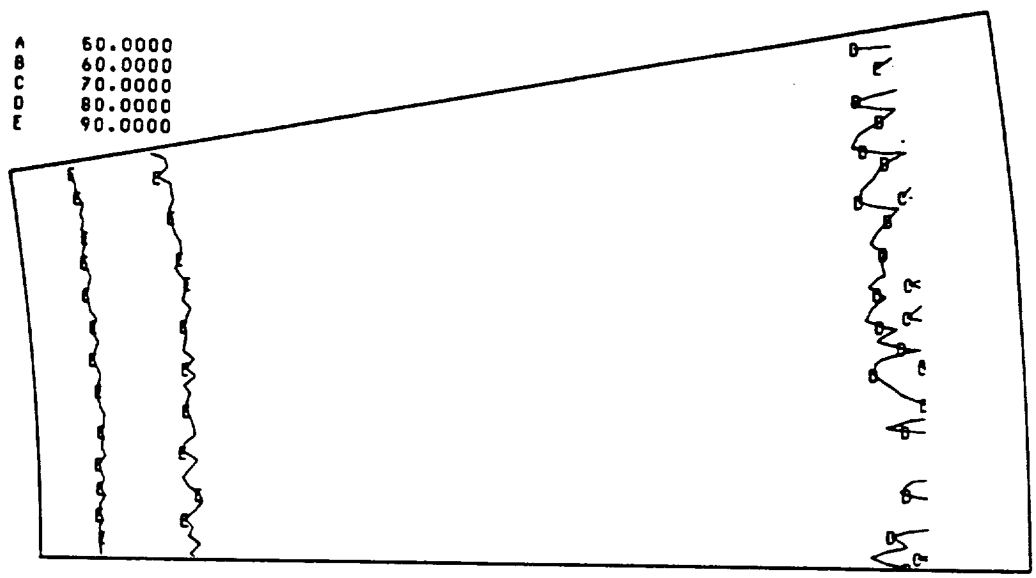

BASELINE

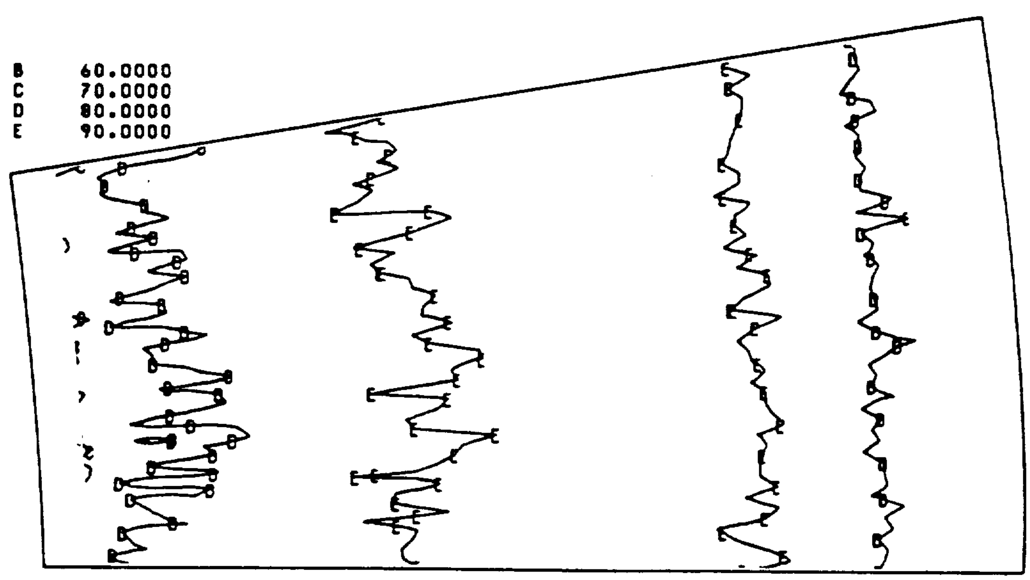

ENHANCED

(a) STATION 1.

FIGURE 20. - AXIAL VELOCITY, CROSS CHANNEL.

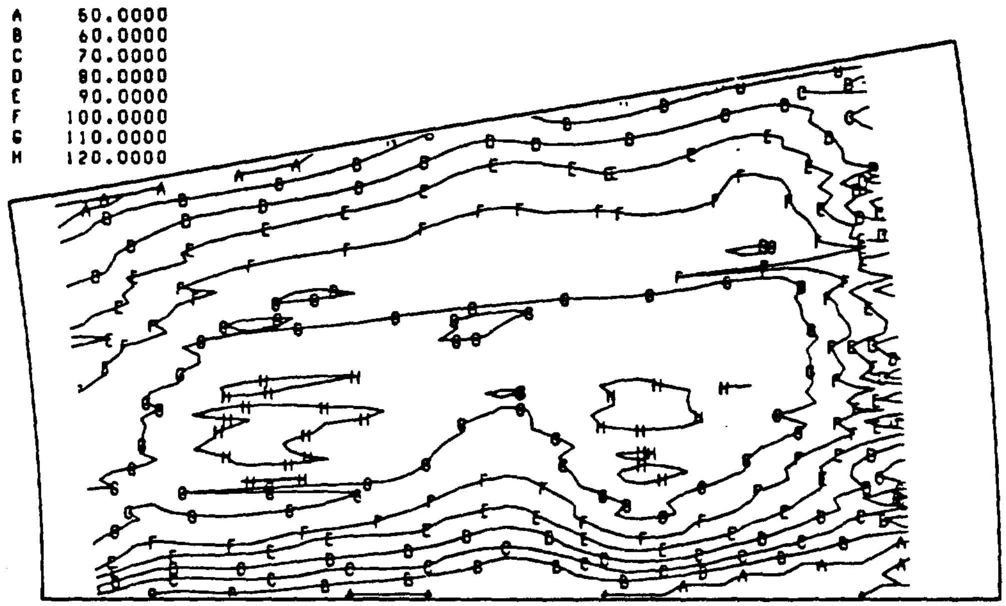

BASELINE

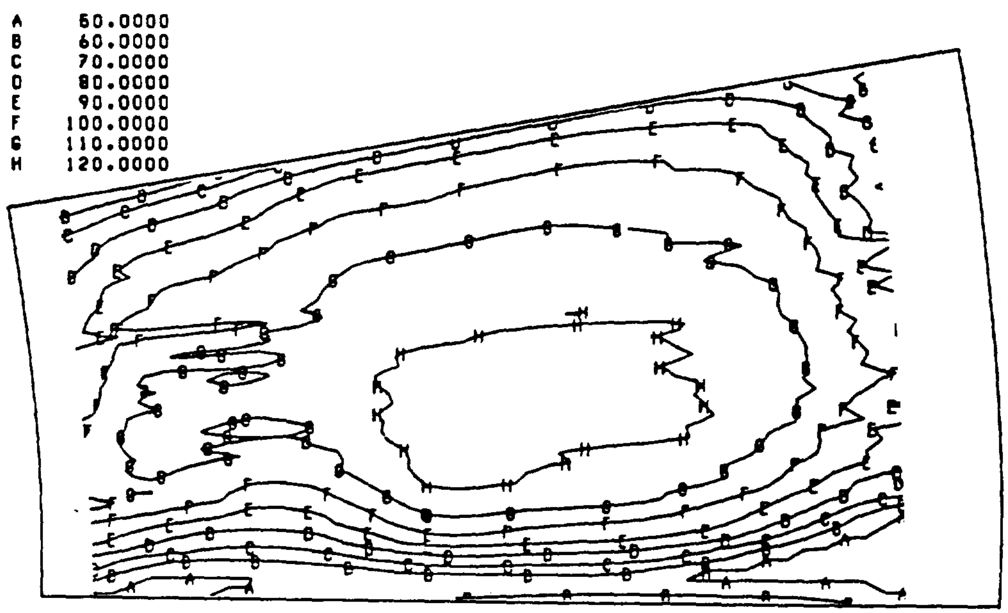

ENHANCED

(b) STATION 2.

FIGURE 20. - CONTINUED.

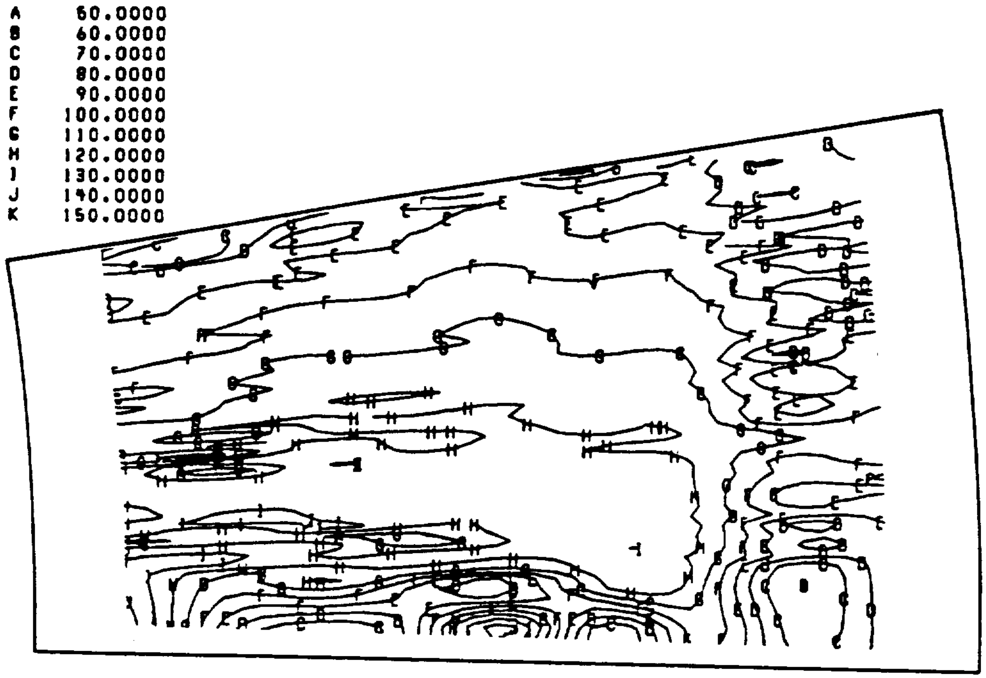

BASELINE

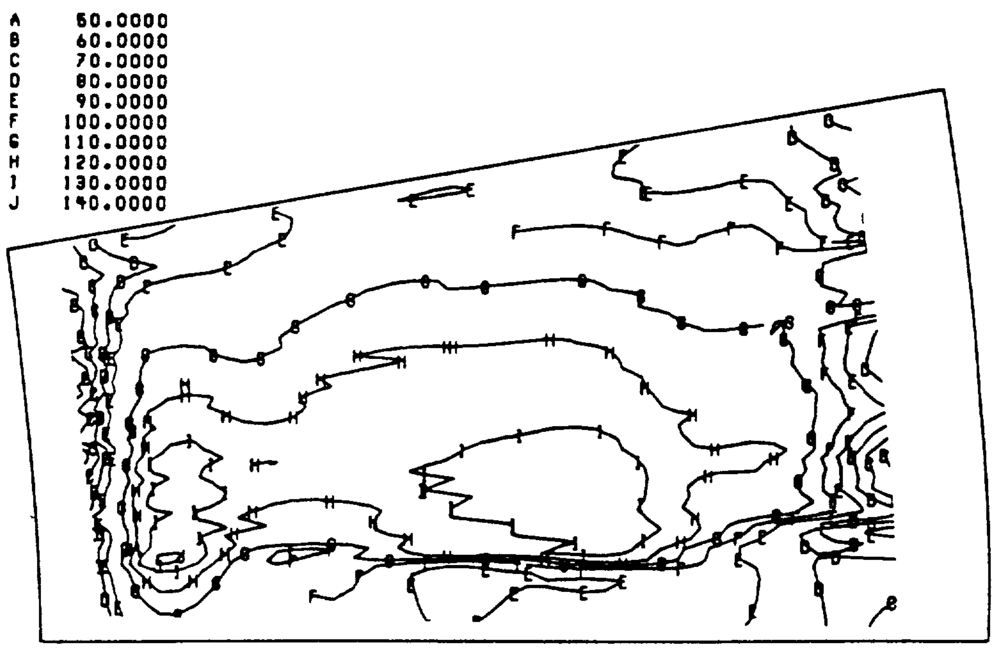

ENHANCED

(c) STATION 3.

FIGURE 20. - CONTINUED.

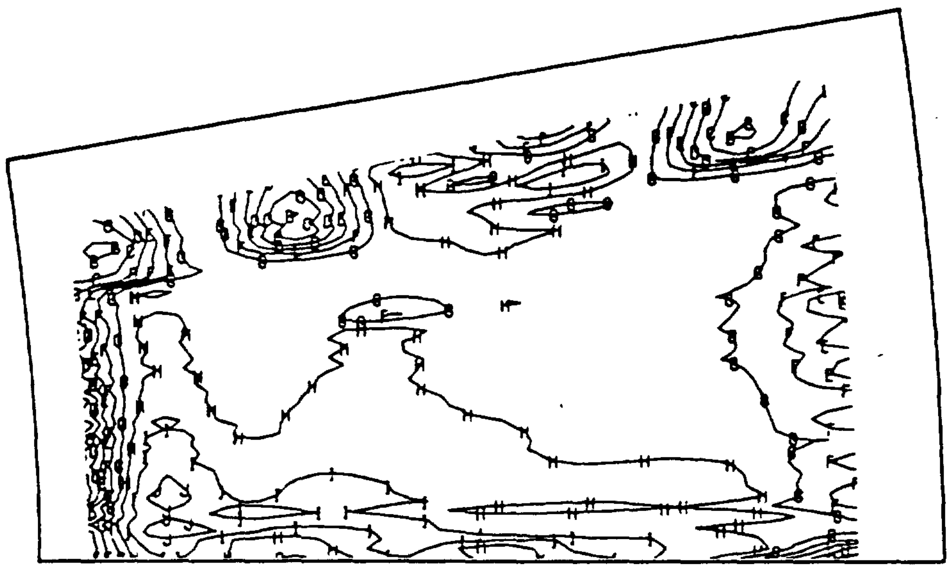

BASELINE

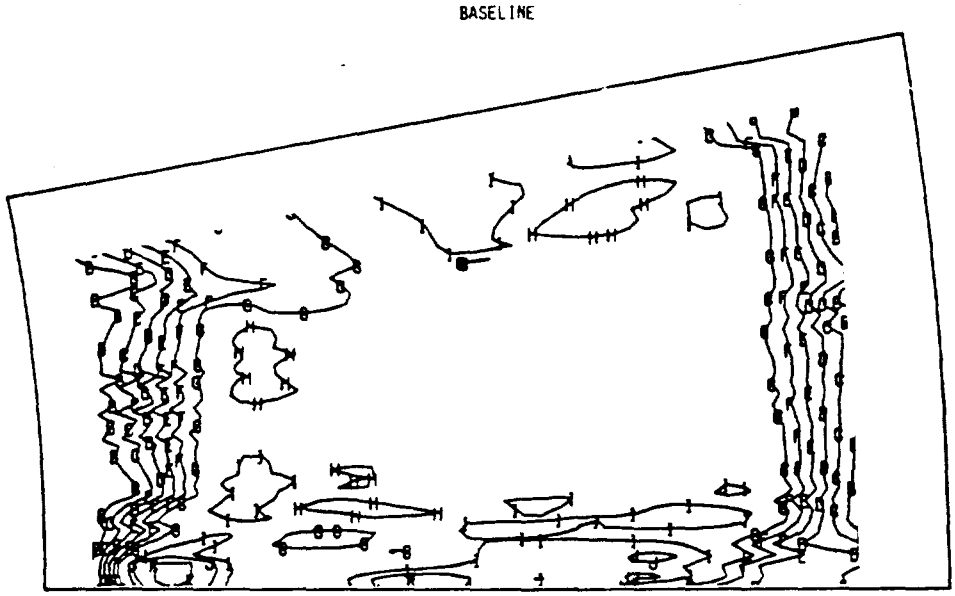

ENHANCED

(d) STATION 4.

FIGURE 20. - CONTINUED.

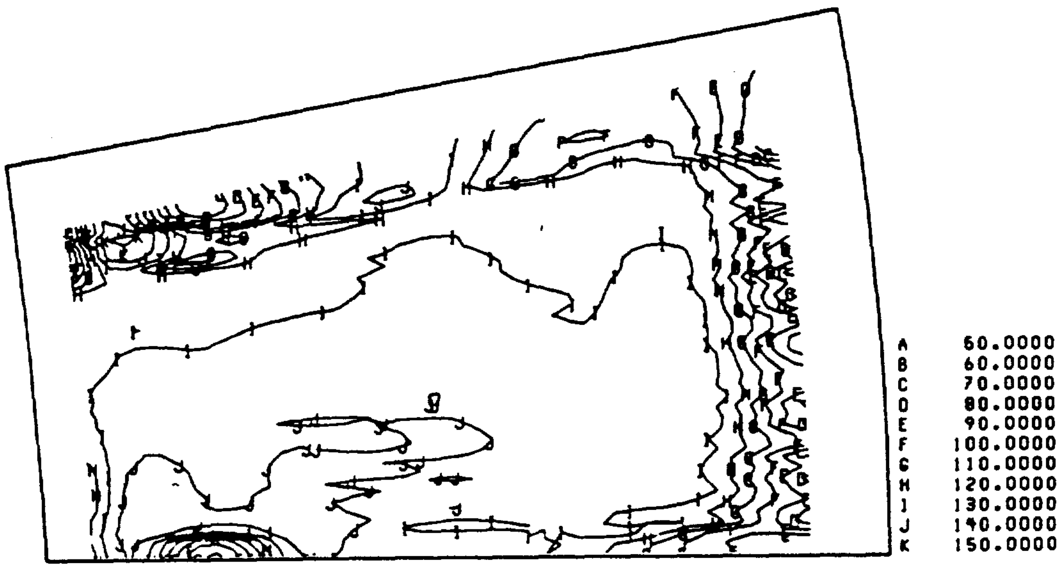

BASELINE

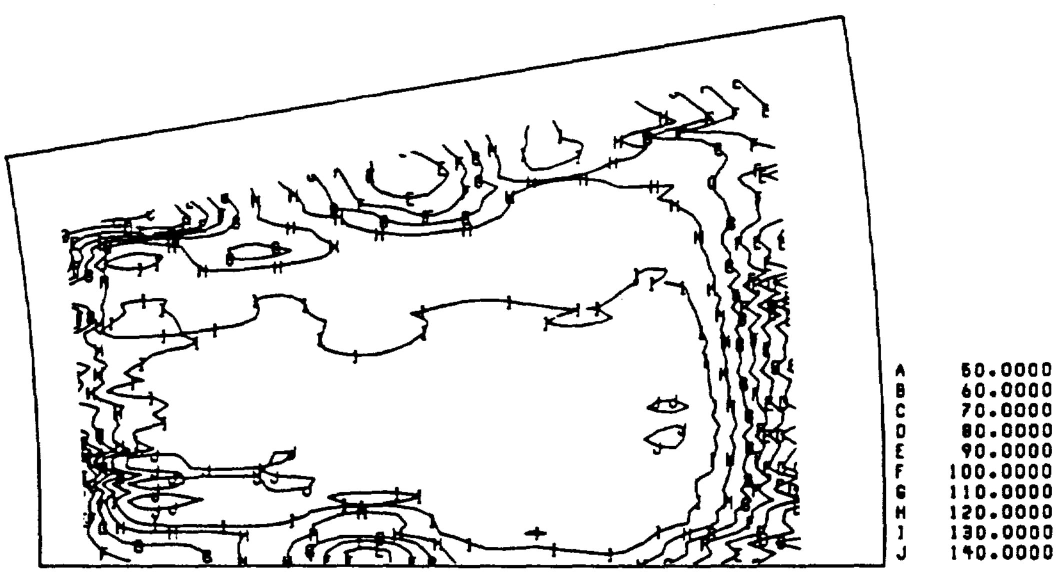

ENHANCED

(e) STATION 5.

FIGURE 20. - CONTINUED.

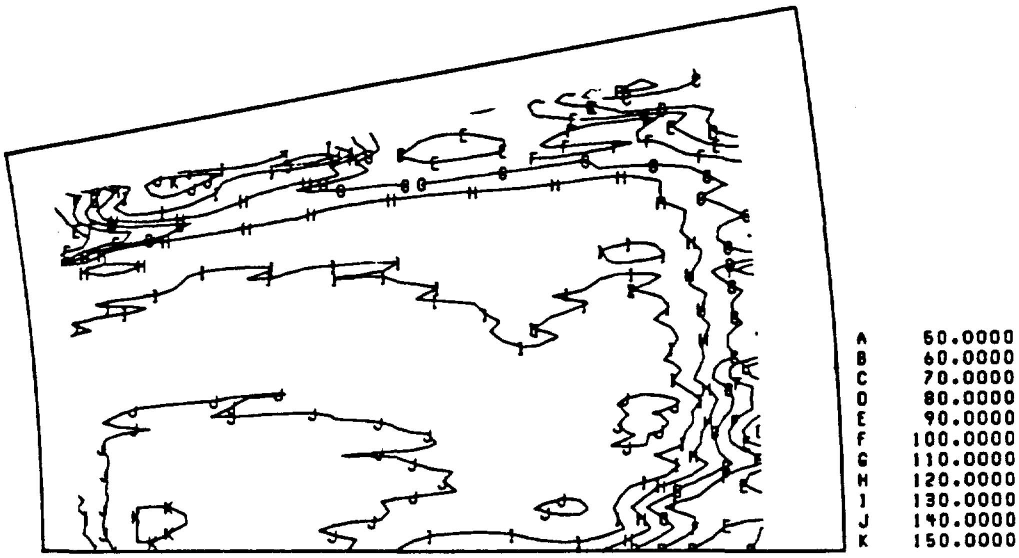

BASELINE

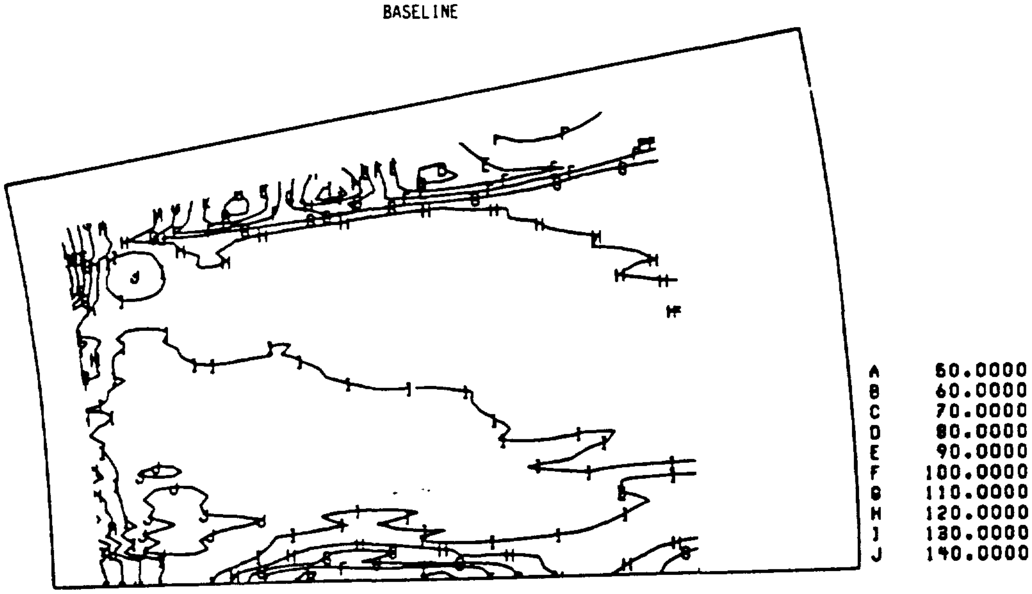

ENHANCED

(f) STATION 6.

FIGURE 20. - CONTINUED.

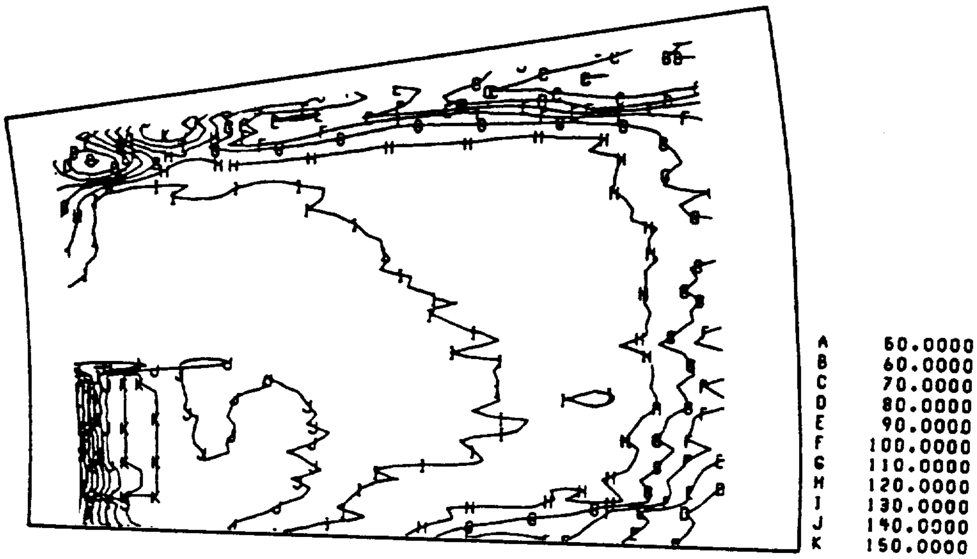

BASELINE

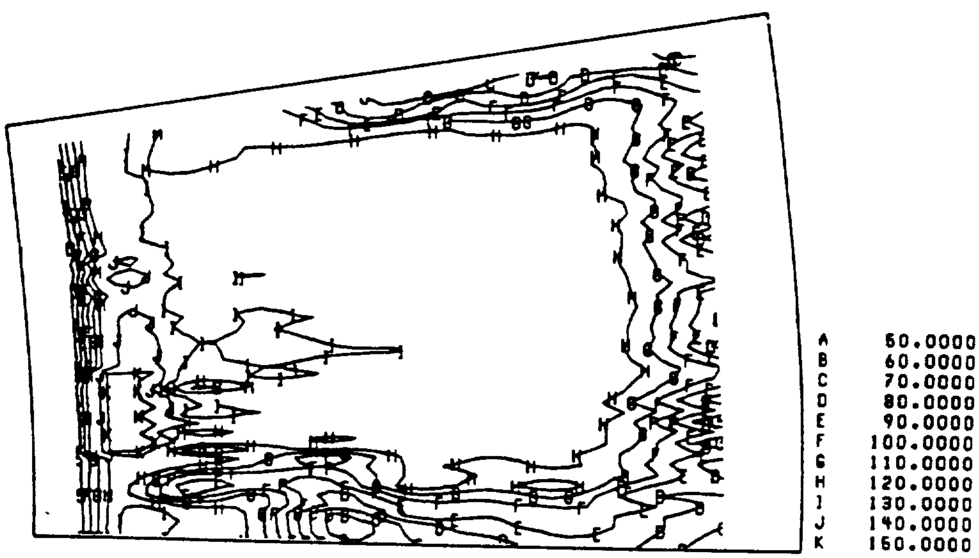

ENHANCED

(g) STATION 7.

FIGURE 20. - CONTINUED.

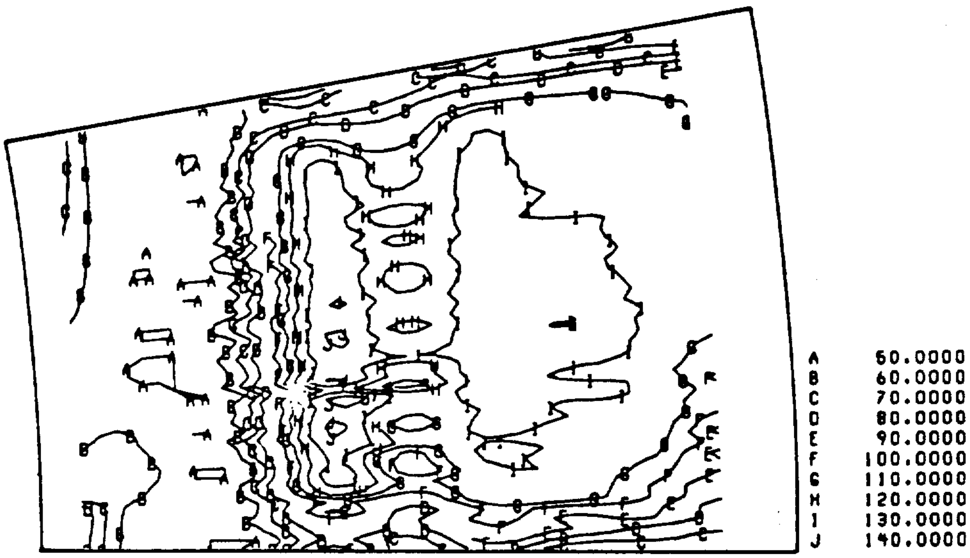

BASELINE

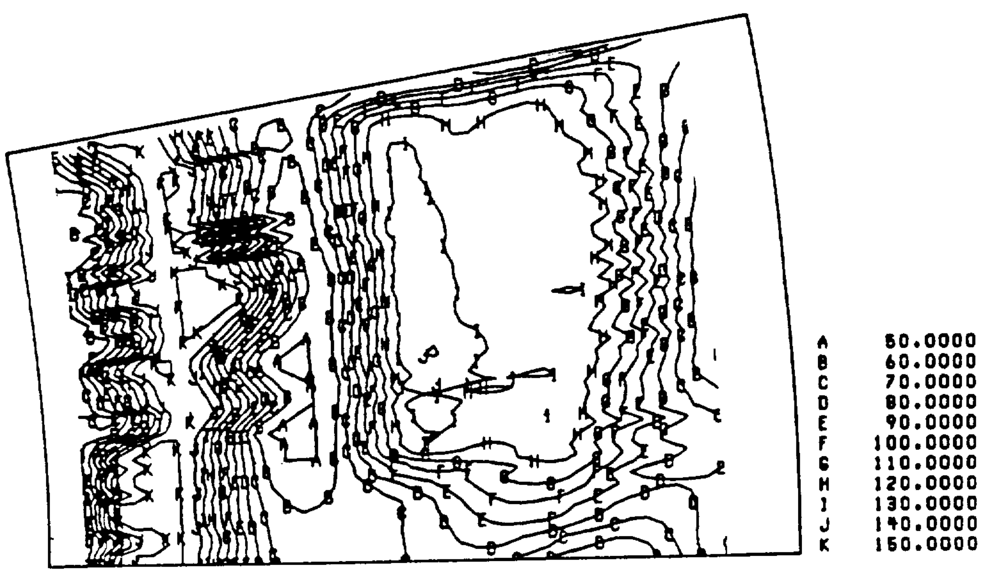

ENHANCED

(h) STATION 8.

FIGURE 20. - CONCLUDED.

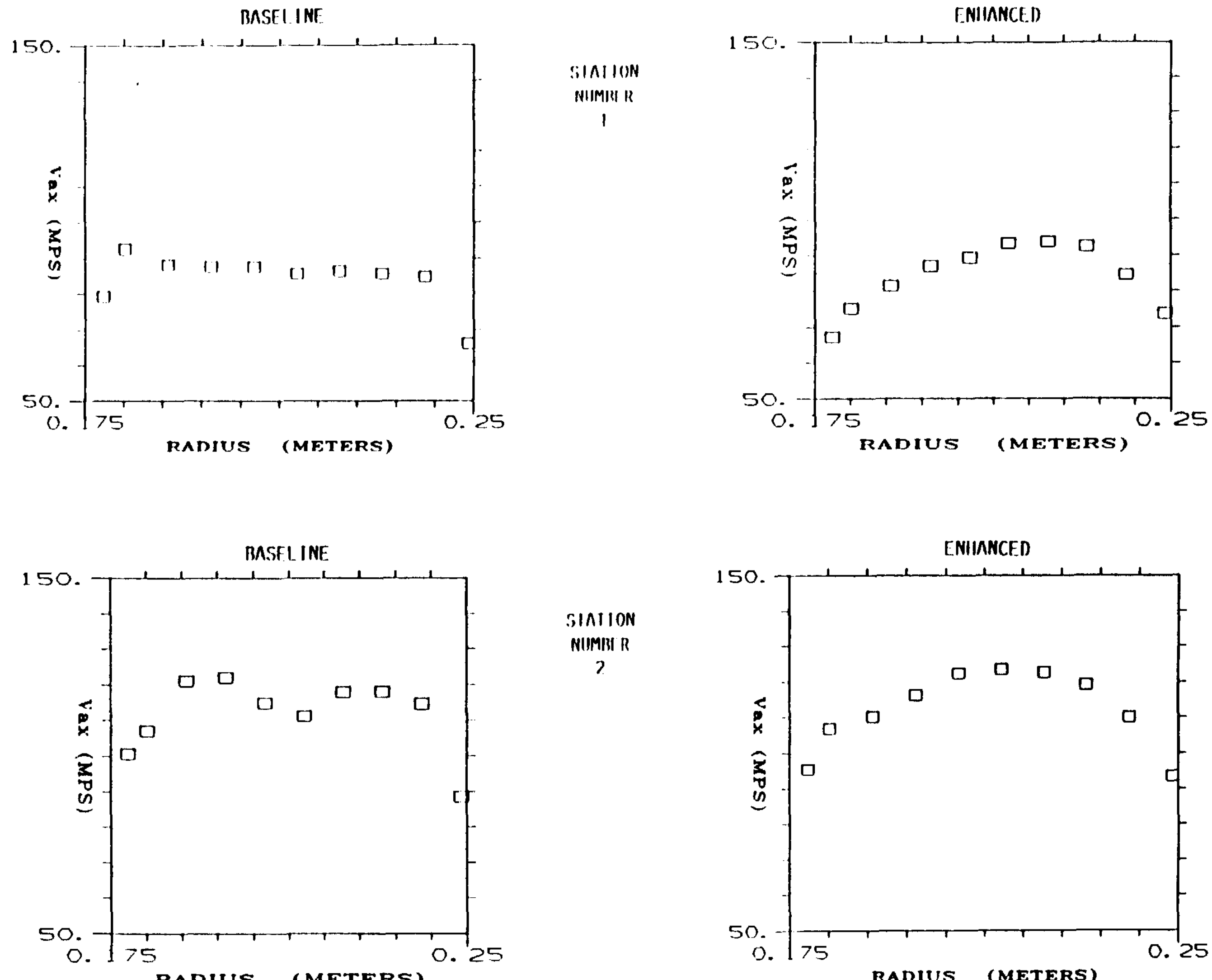

AXIAL VELOCITY, ST 1,2

FIGURE 21a.

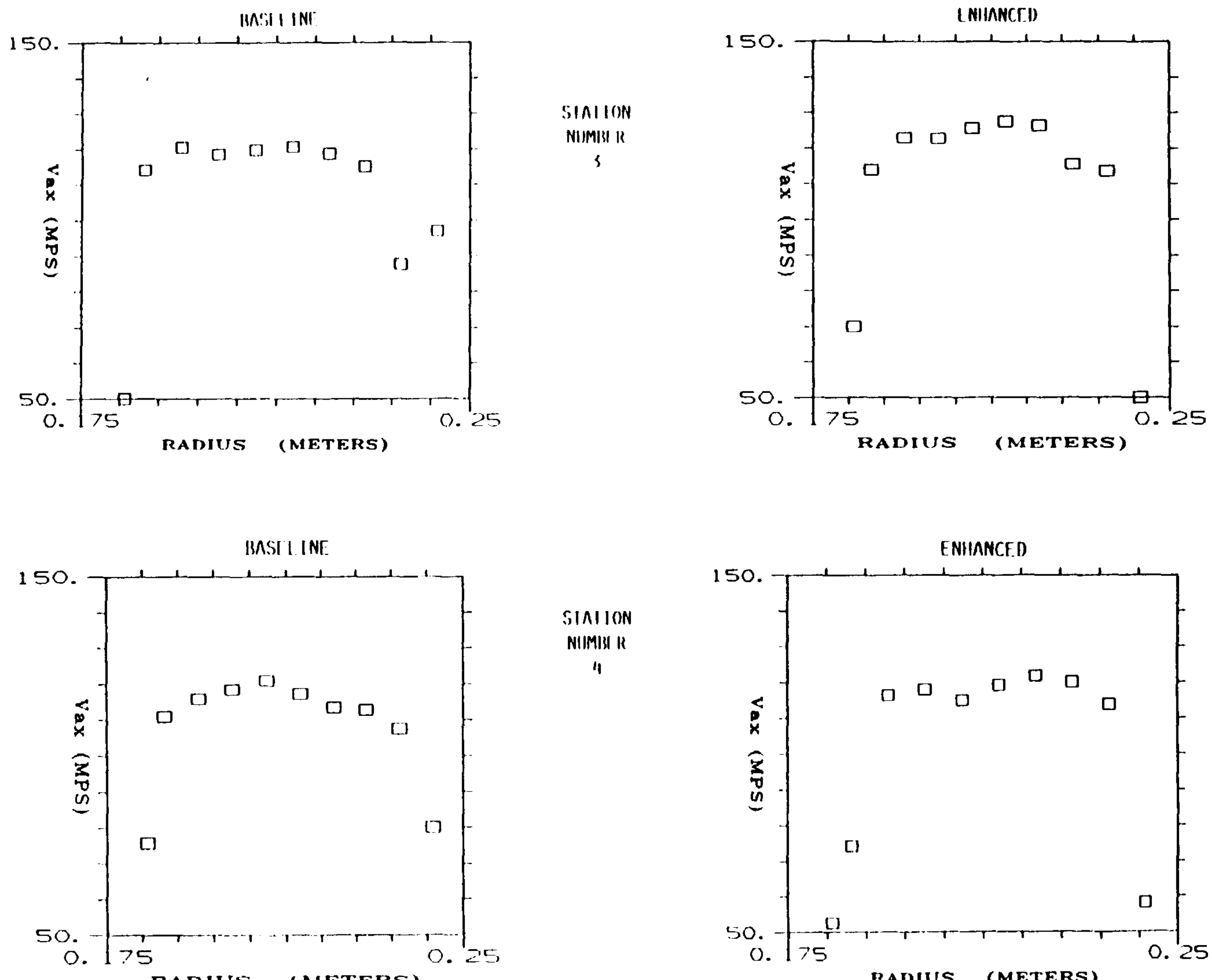

AXIAL VELOCITY, ST 3,4

FIGURE 21b.

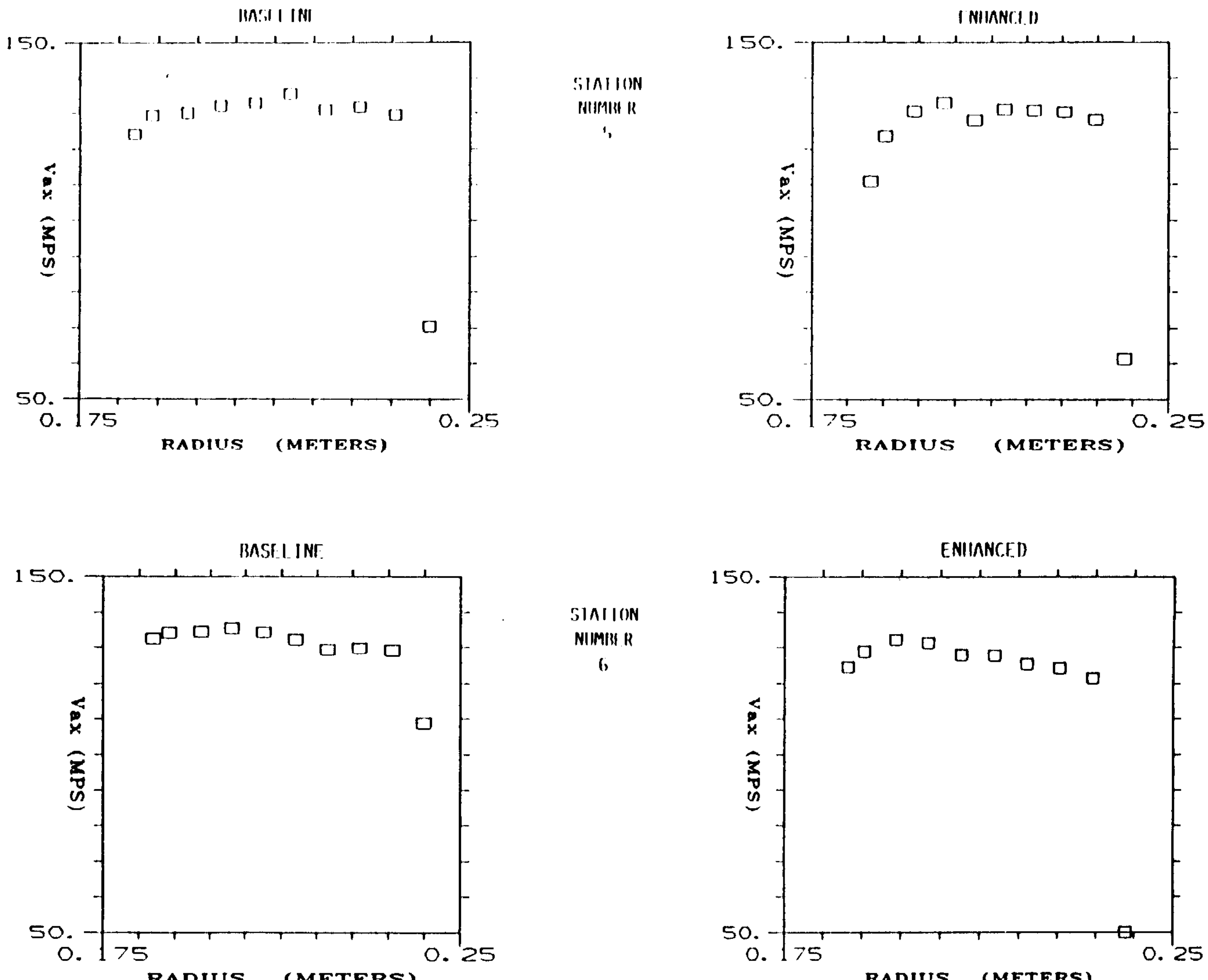

AXIAL VELOCITY ST 5,6

FIGURE 21c.

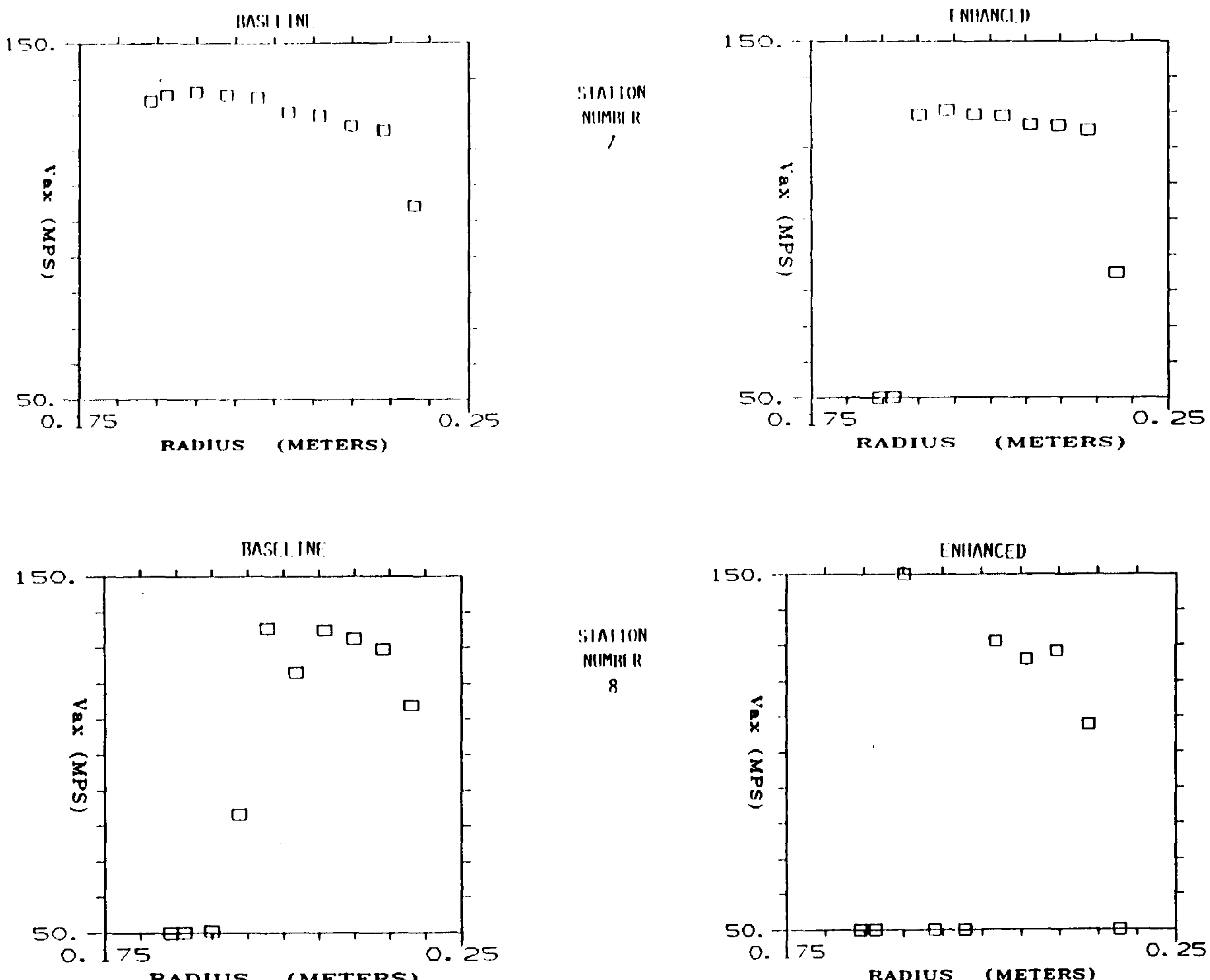

AXIAL VELOCITY ST 7,8

FIGURE 21d.

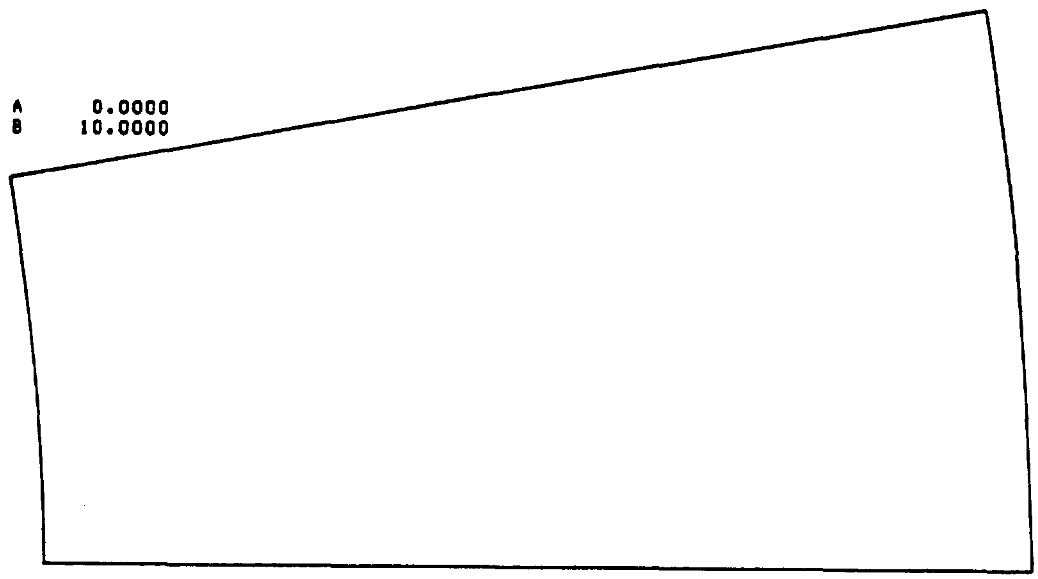

BASELINE

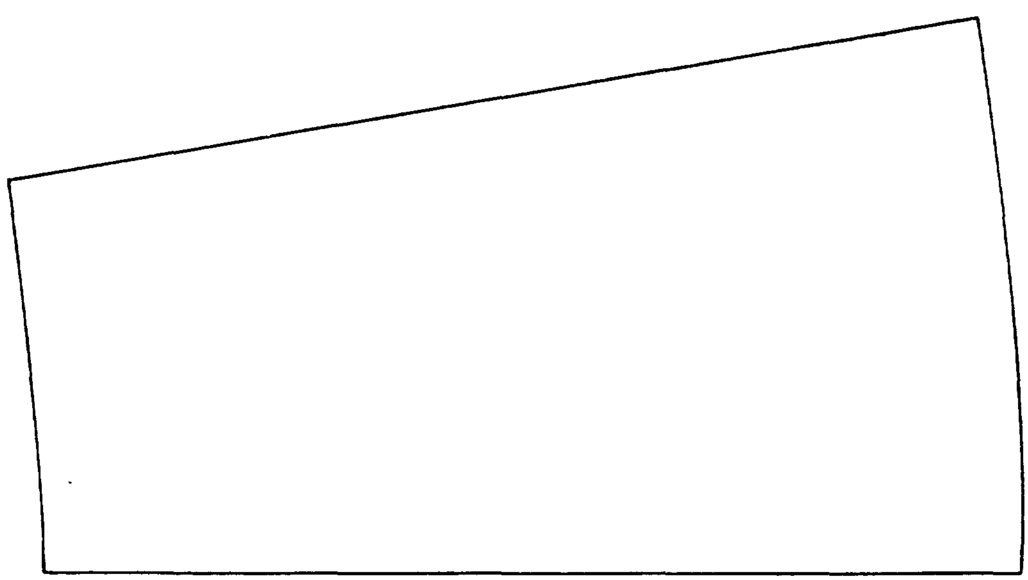

ENHANCED

(a) STATION 1.

FIGURE 22. - ABSOLUTE TANGENTIAL VELOCITY.

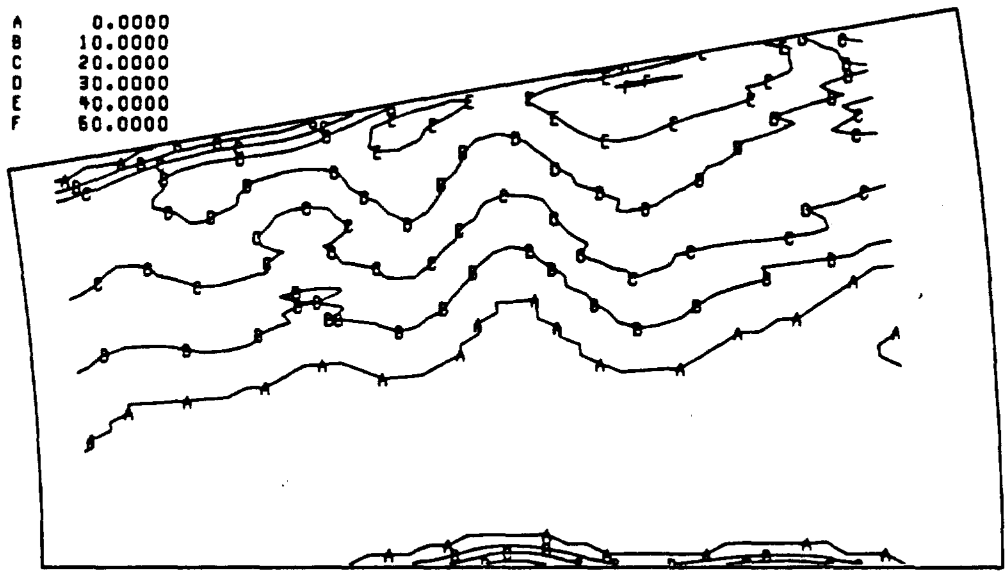

BASELINE

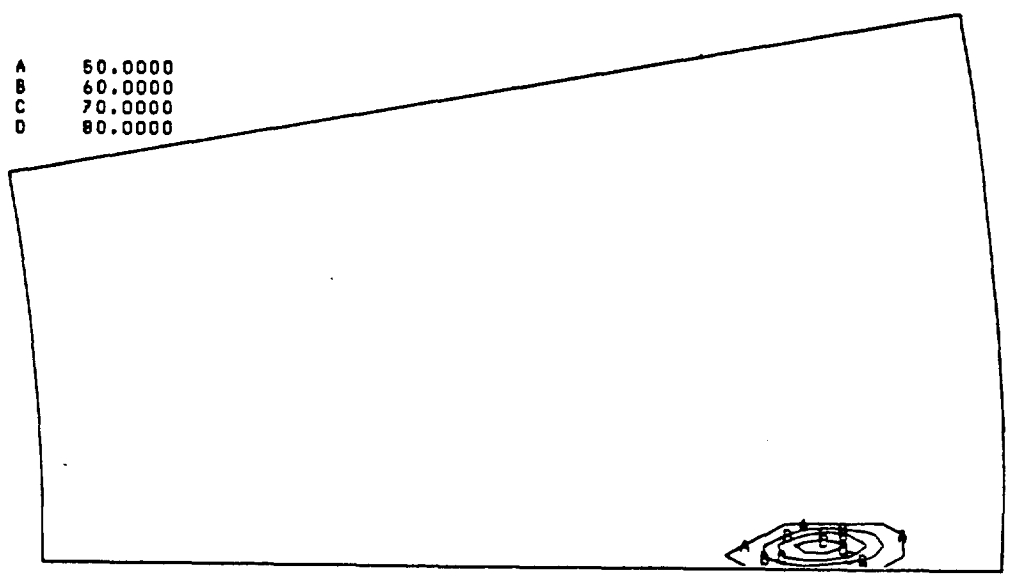

ENHANCED

(b) STATION 2.

FIGURE 22. - CONTINUED.

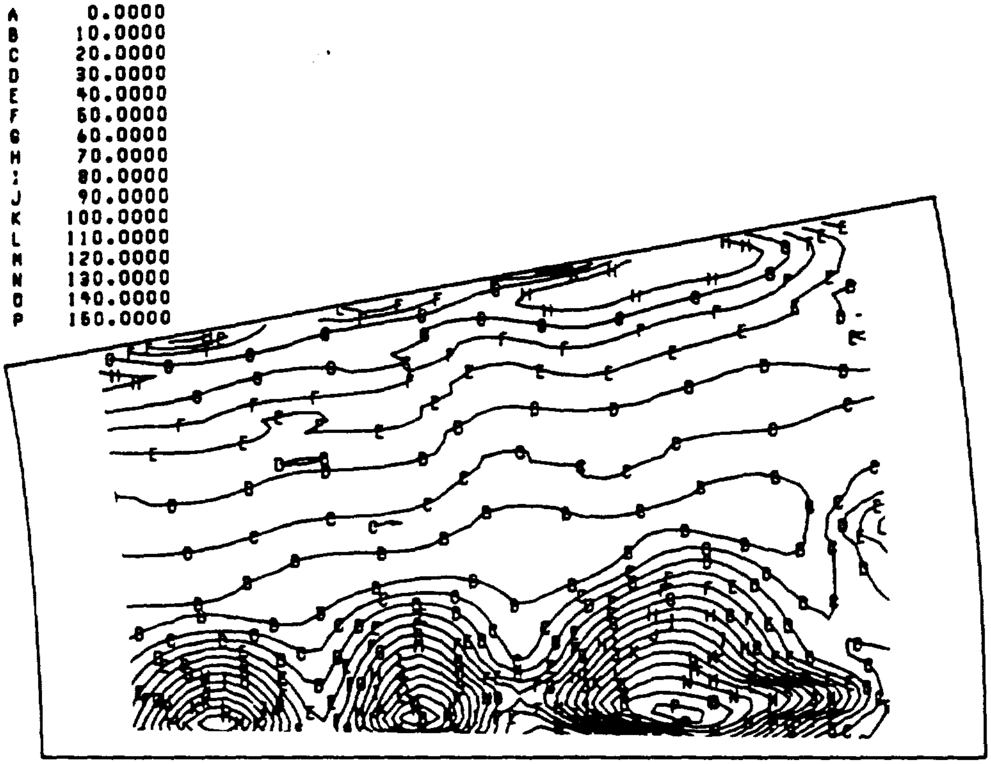

BASELINE

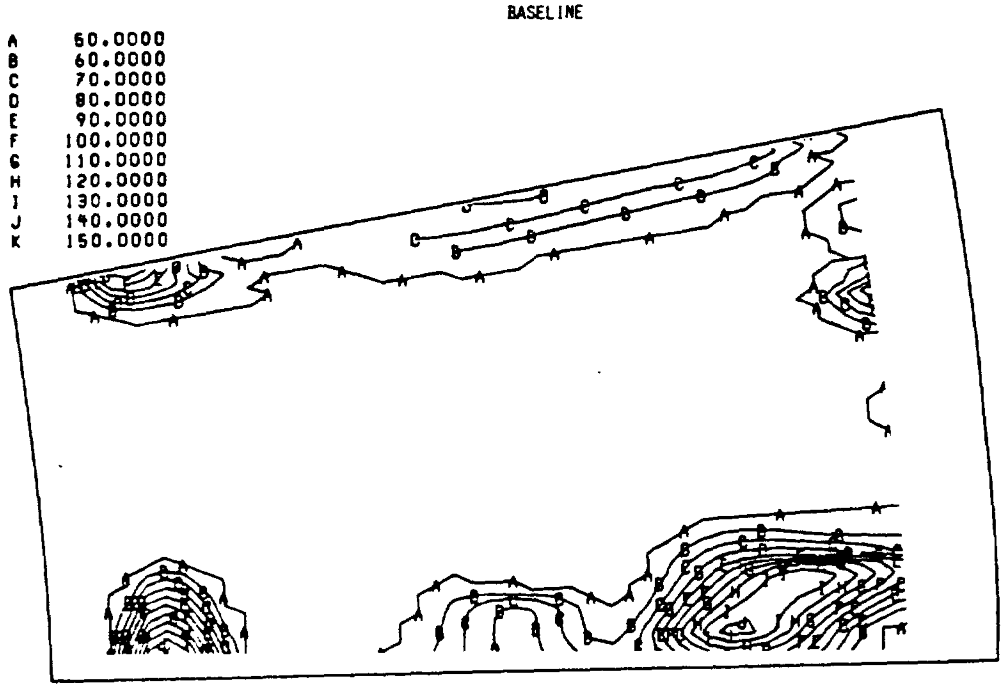

ENHANCED

(c) STATION 3.

FIGURE 22. - CONTINUED.

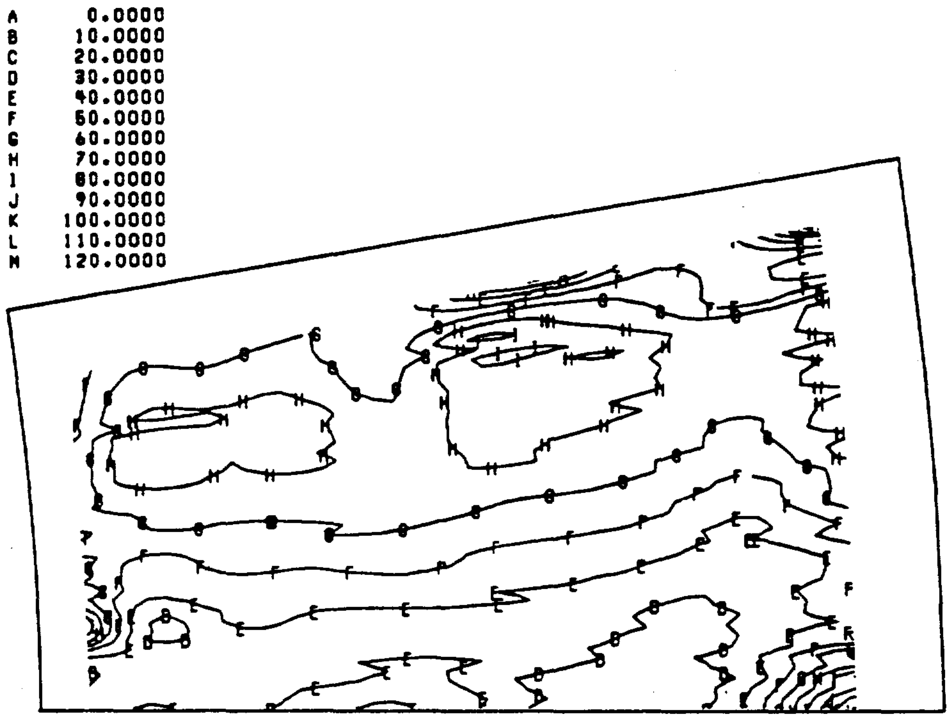

BASELINE

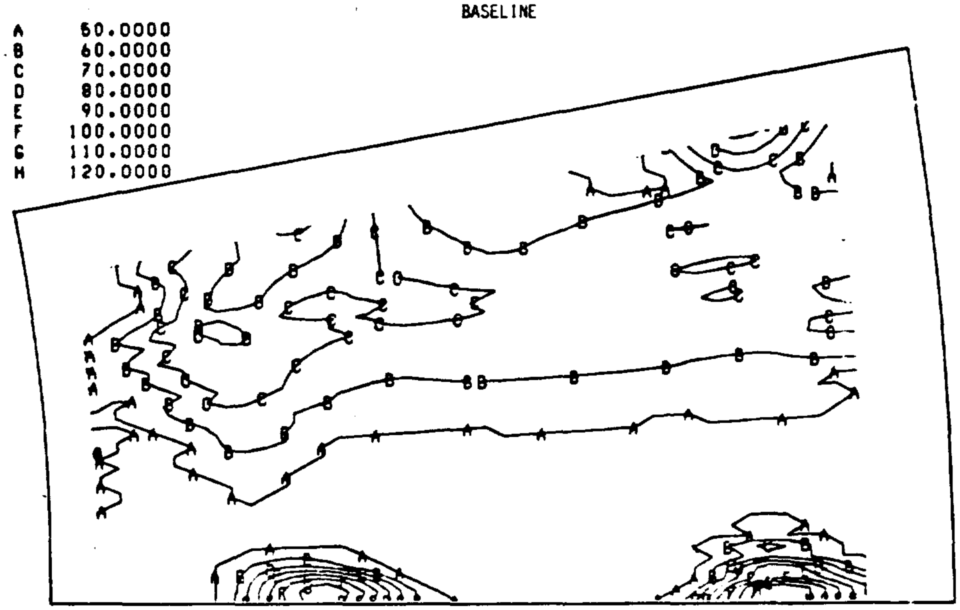

ENHANCED

(d) STATION 4.

FIGURE 22. - CONTINUED.

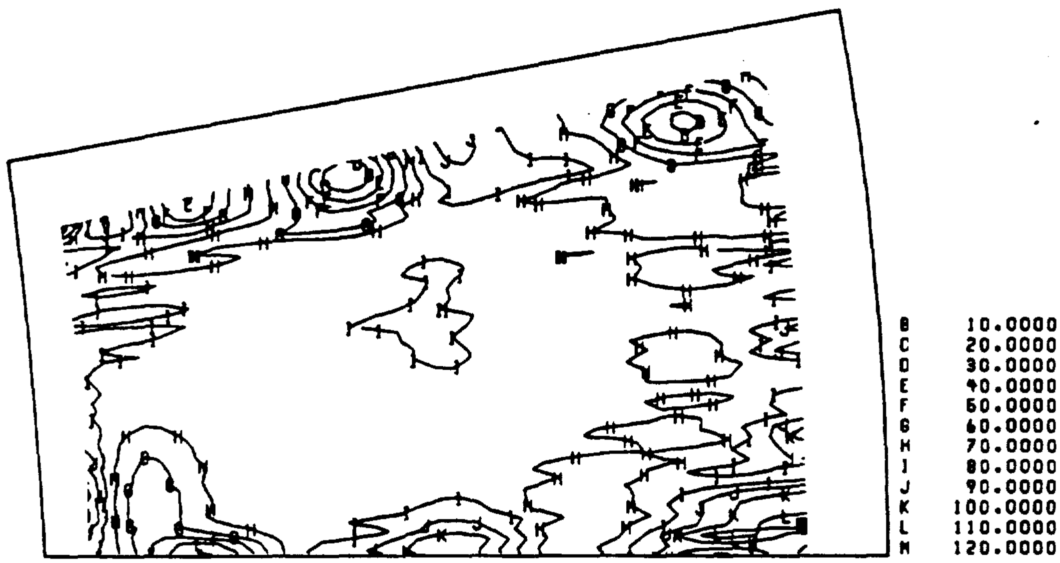

BASELINE

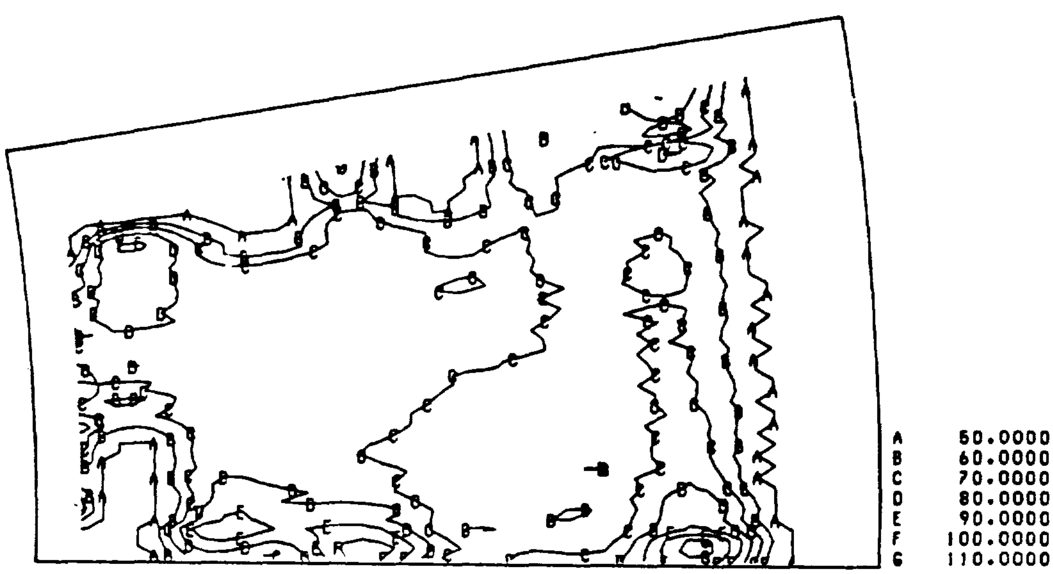

ENHANCED

(e) STATION 5.

FIGURE 22. - CONTINUED.

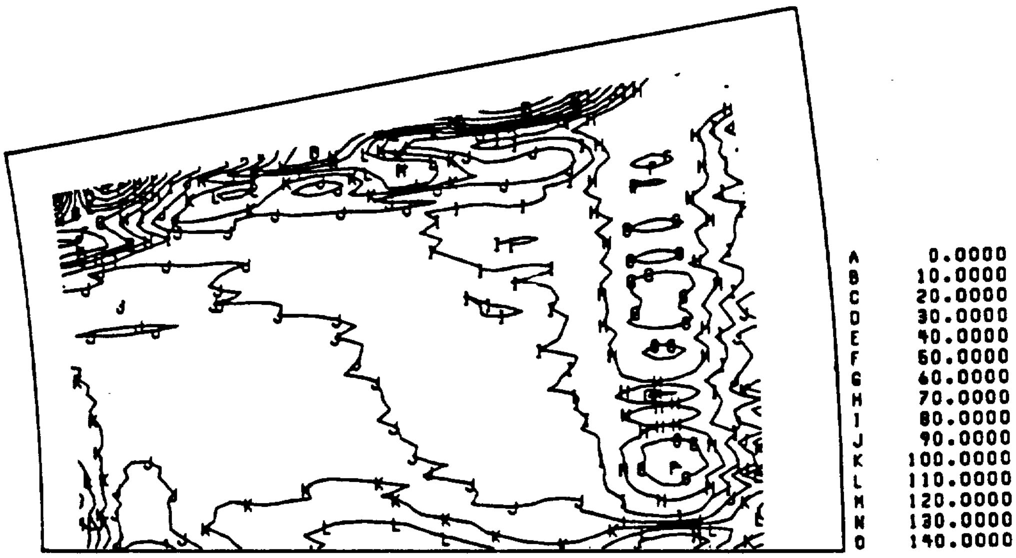

BASELINE

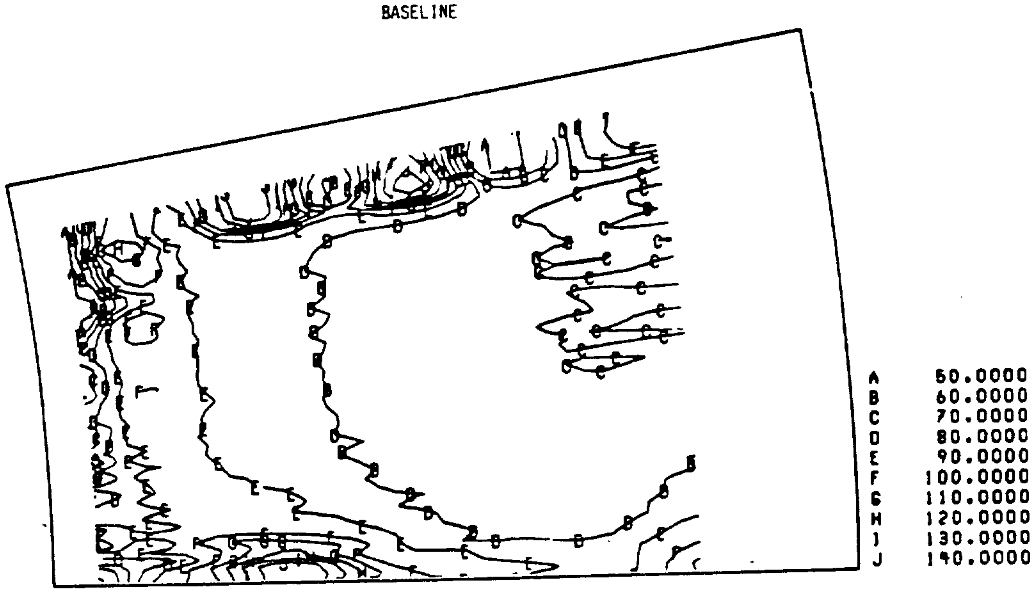

ENHANCED

(f) STATION 6.

FIGURE 22. - CONTINUED.

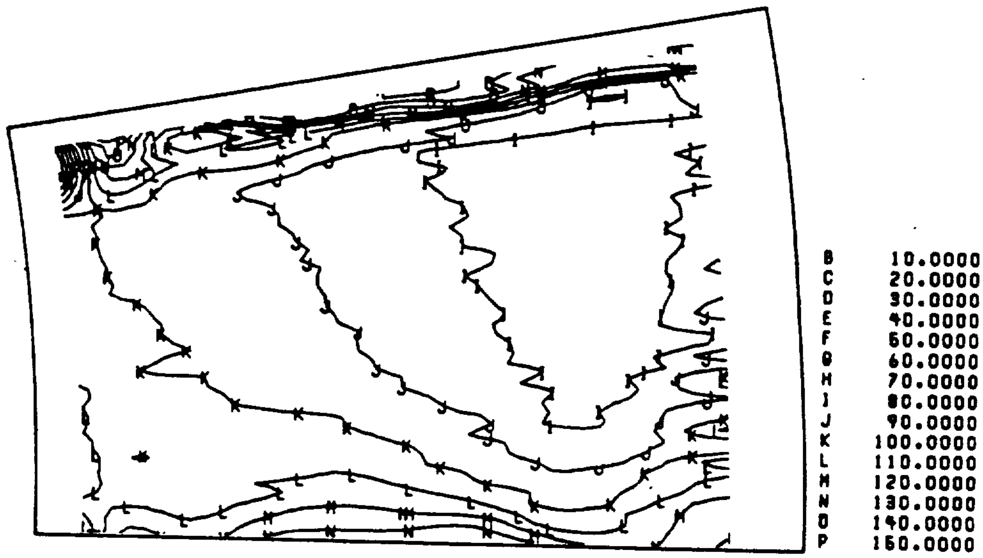

BASELINE

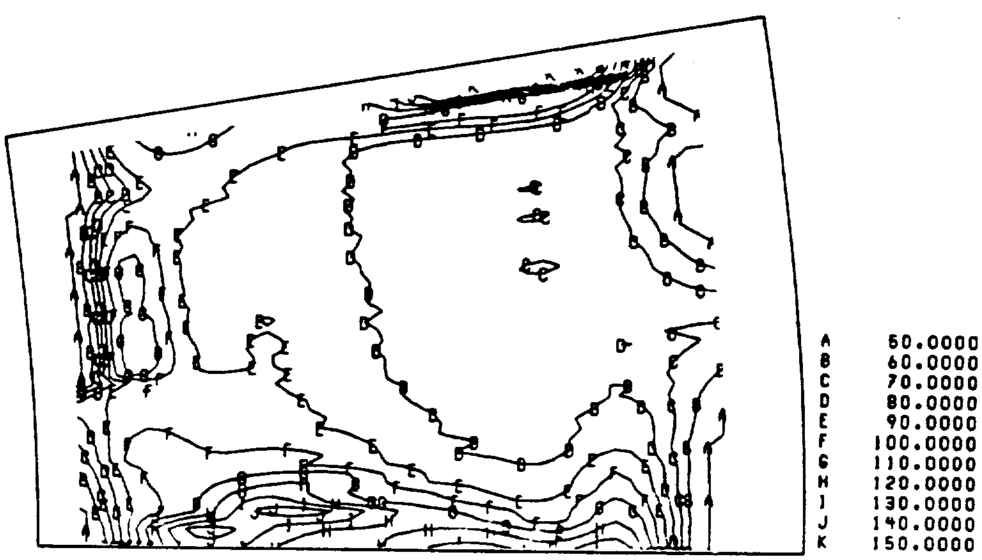

ENHANCED

(g) STATION 7.

FIGURE 22. - CONTINUED.

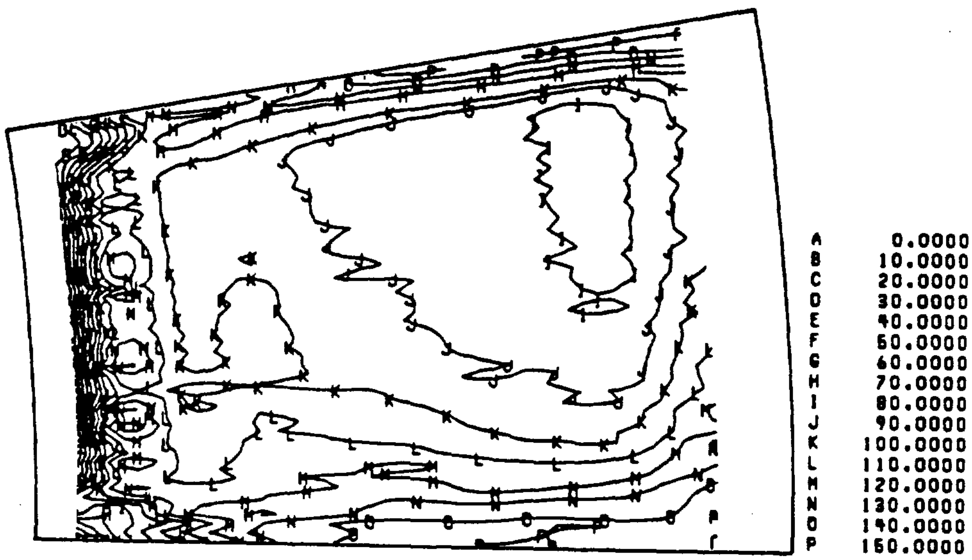

BASELINE

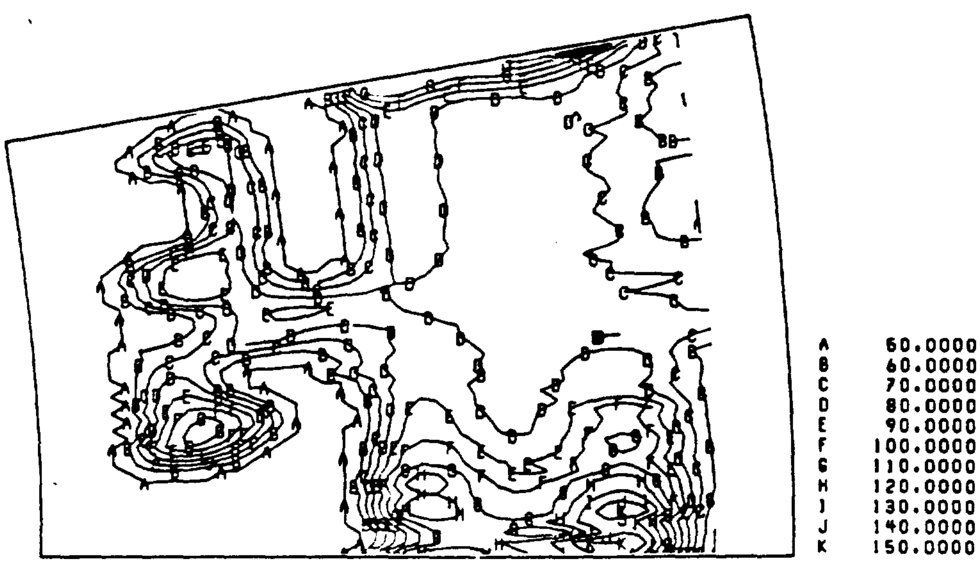

ENHANCED

(h) STATION 8.

FIGURE 22. - CONCLUDED.

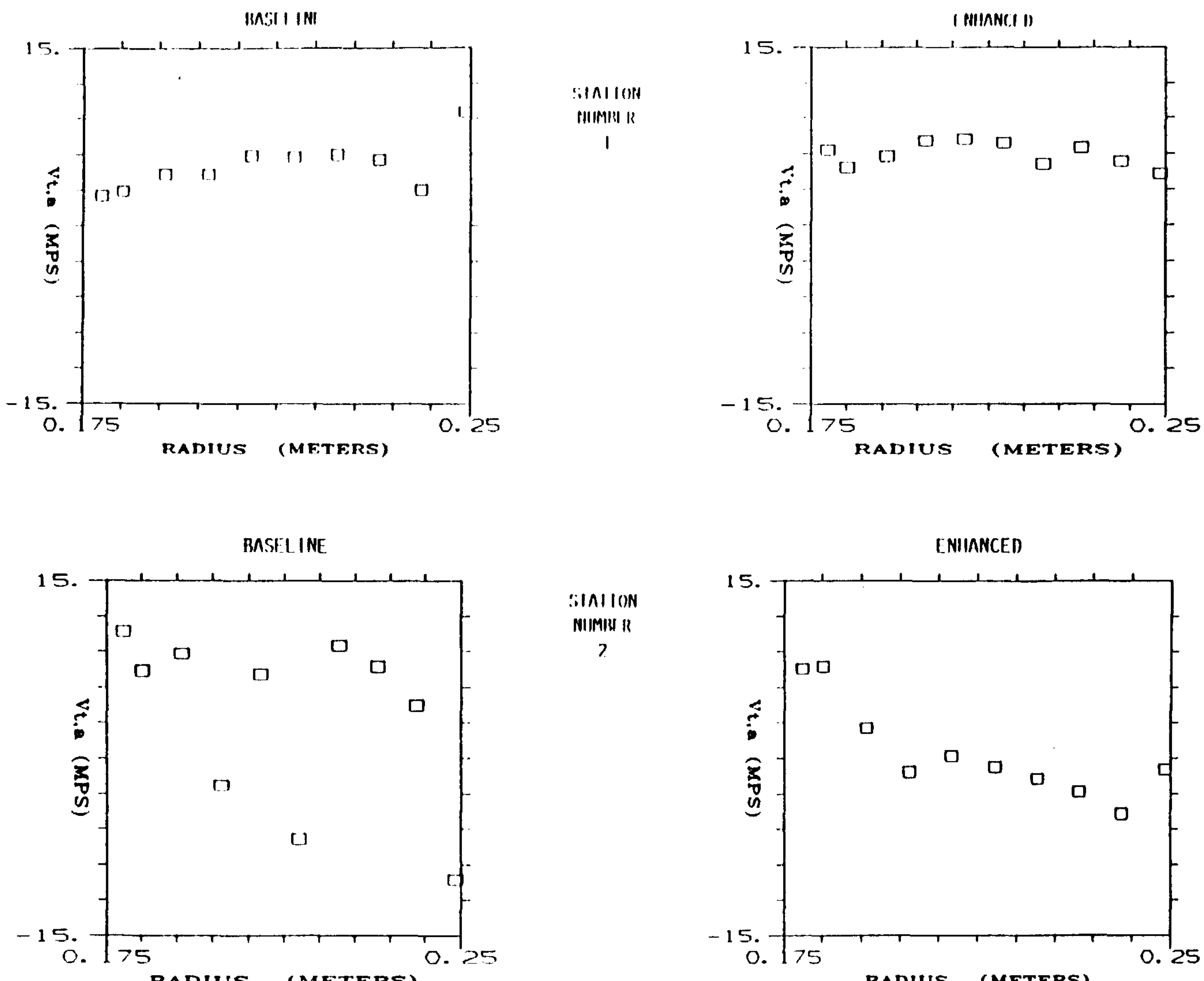

ABS TANG VELOCITY ST 1,2

FIGURE 23a.

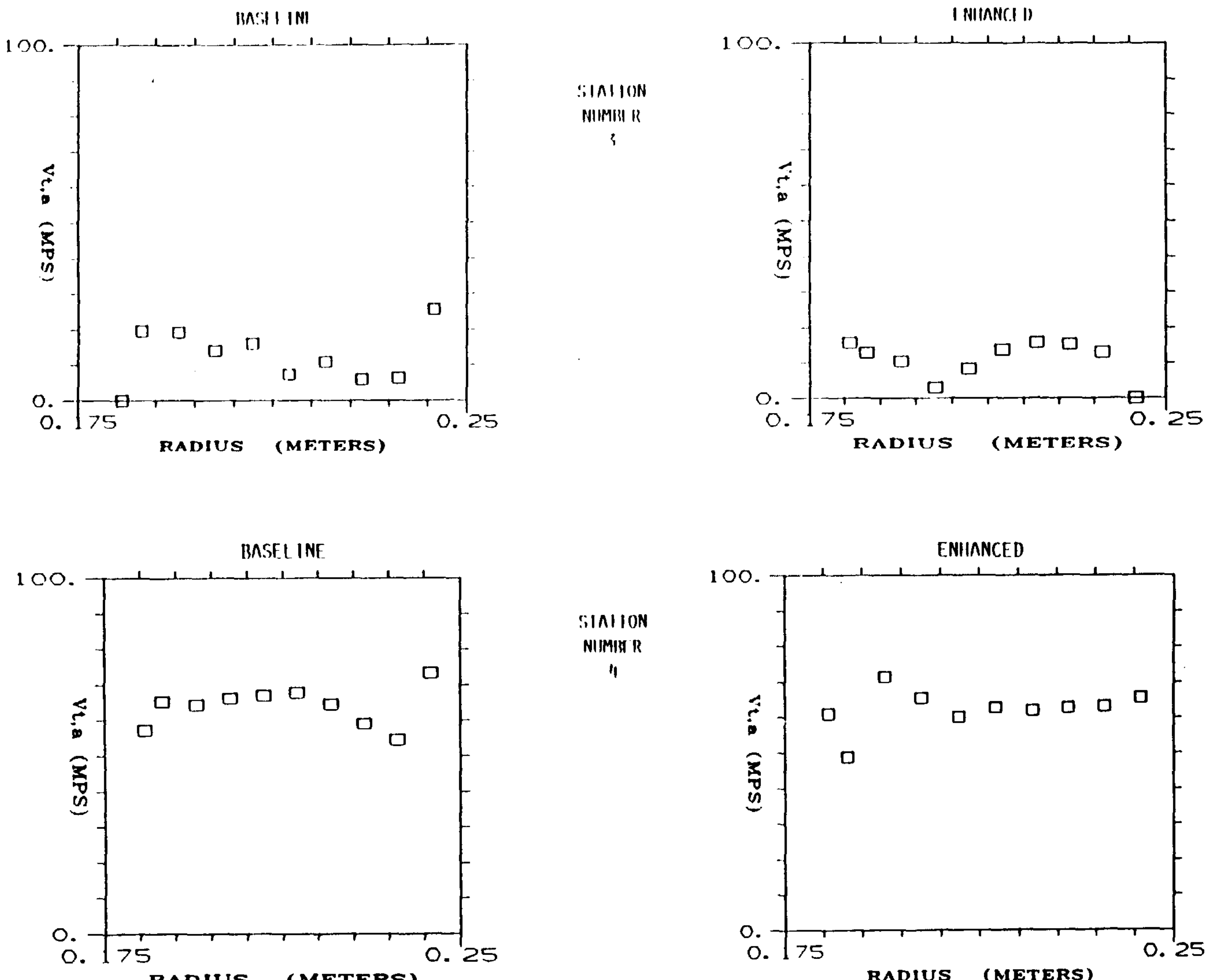

ABS TANG VELOCITY ST 3,4

FIGURE 23b.

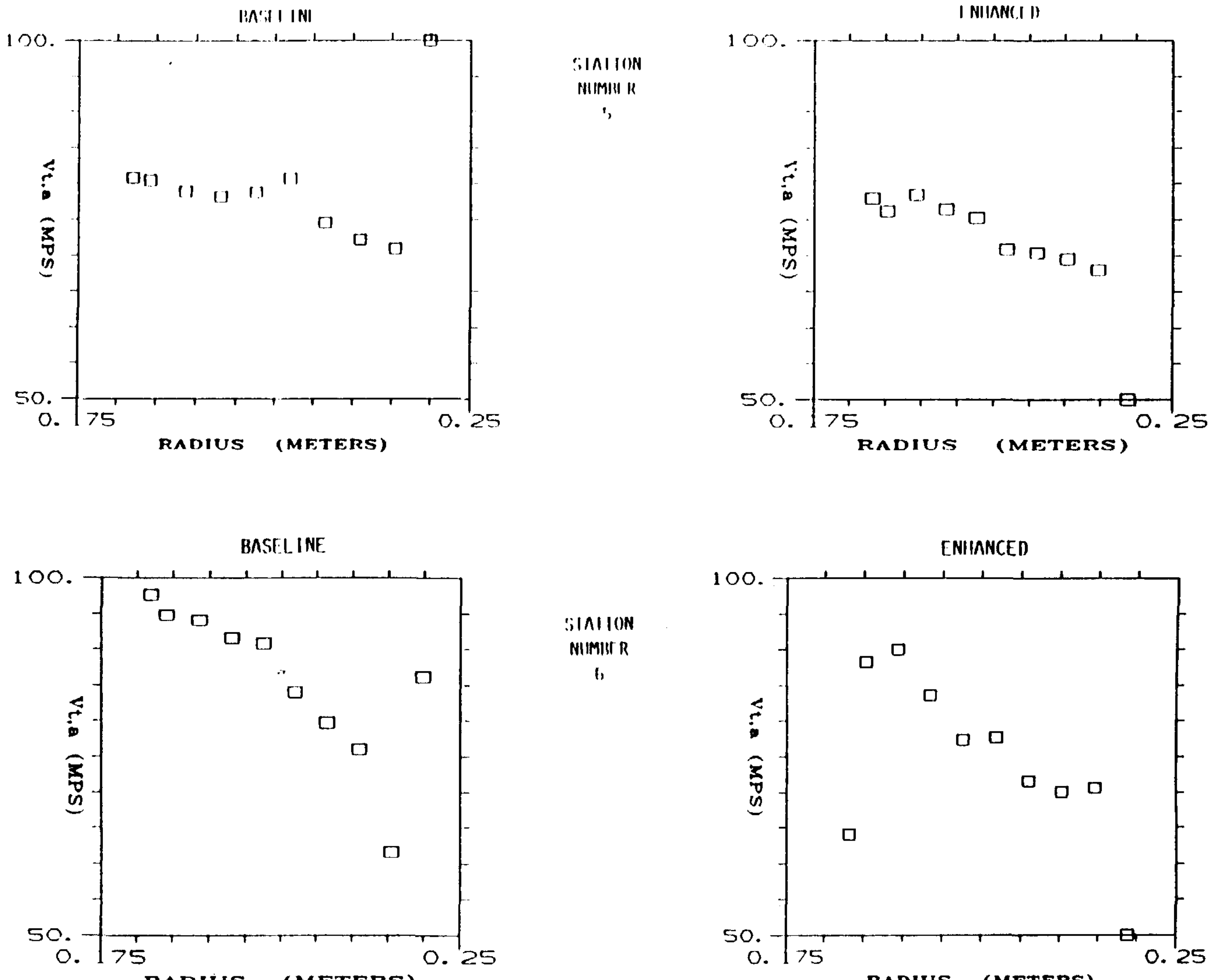

ABS TANG VELOCITY ST 5,6

FIGURE 23c.

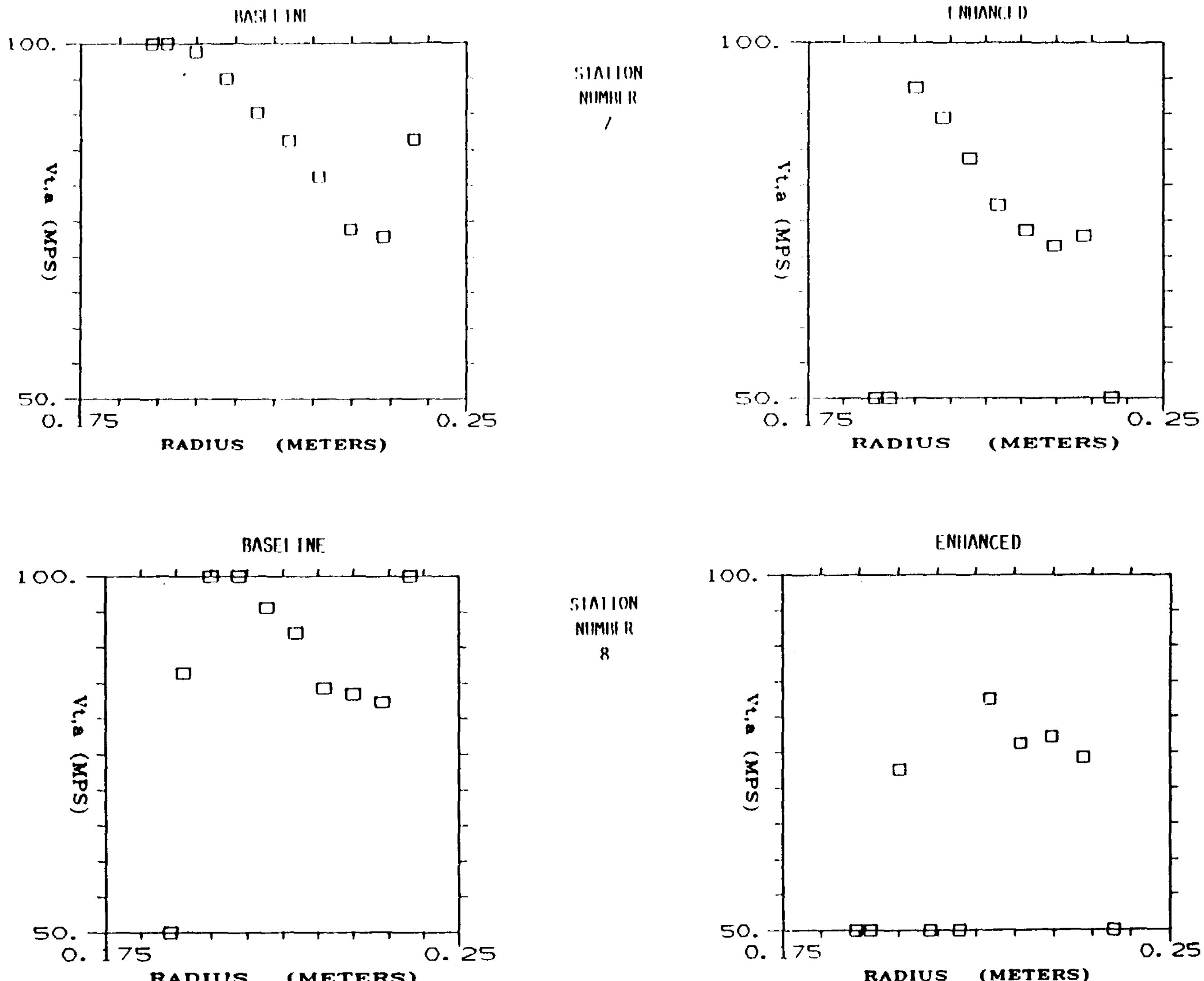

ABS TANG VELOCITY ST 7,8

FIGURE 23d.

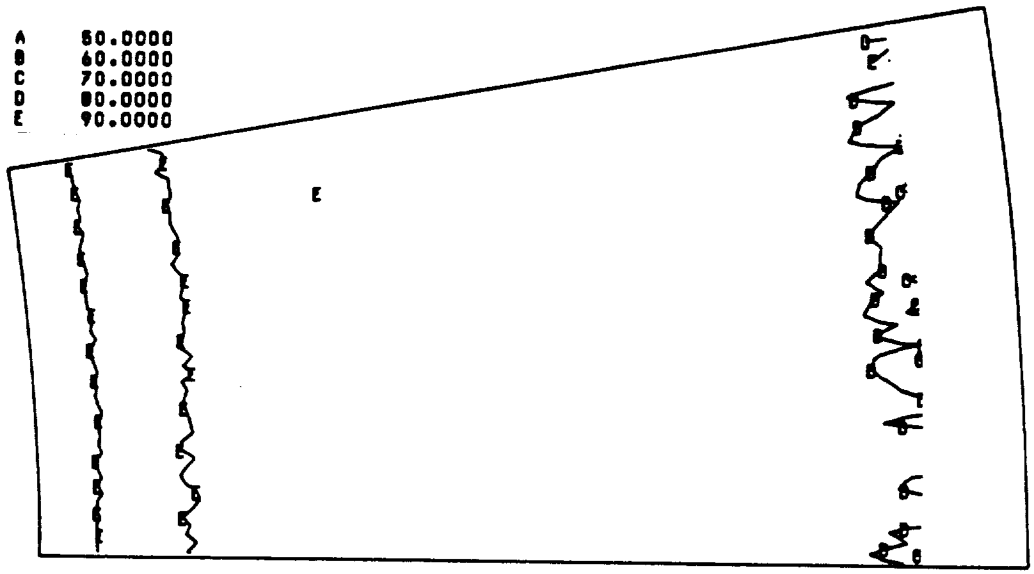

BASELINE

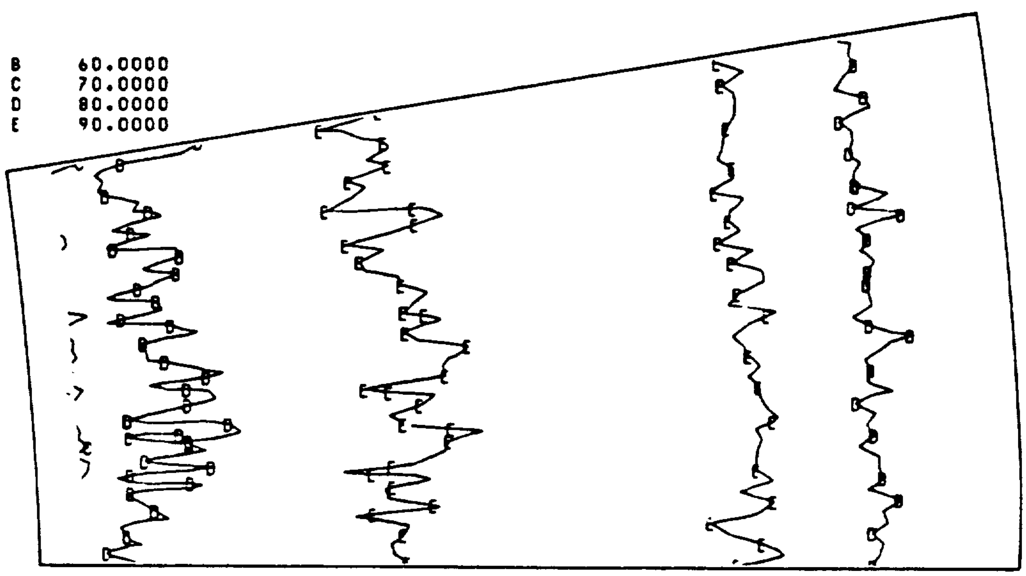

ENHANCED

(a) STATION 1.

FIGURE 24. - ABSOLUTE TOTAL VELOCITY, CROSS CHANNEL.

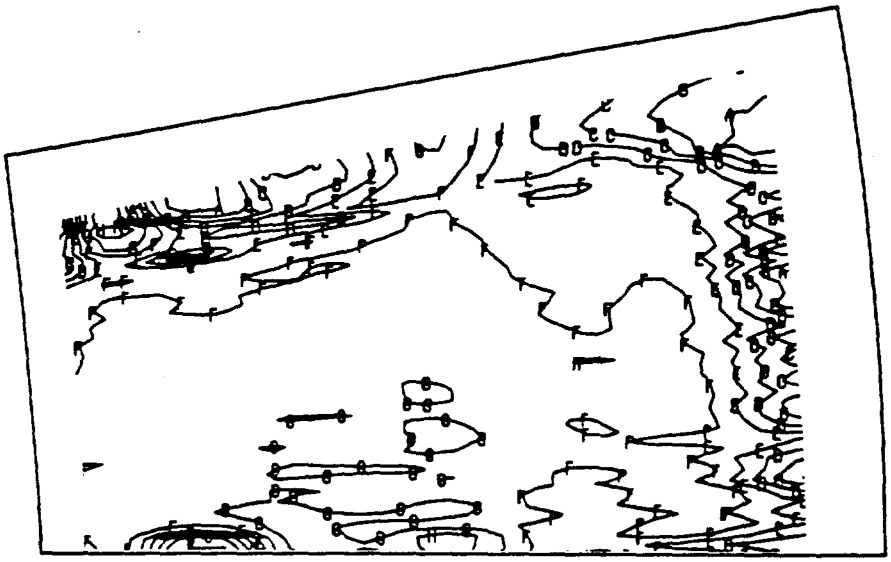

A	100.0000
B	110.0000
C	120.0000
D	130.0000
E	140.0000
F	150.0000
G	160.0000
H	170.0000

BASELINE

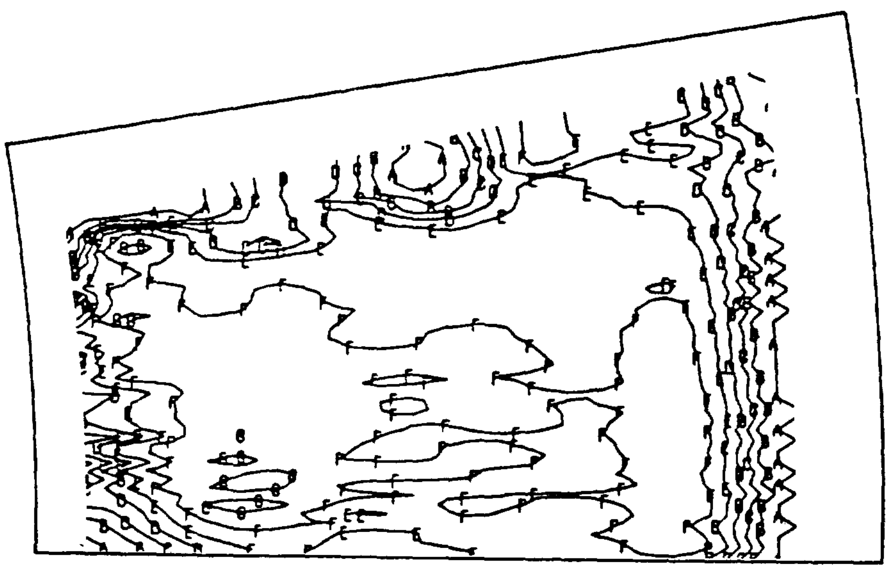

A	100.0000
B	110.0000
C	120.0000
D	130.0000
E	140.0000
F	150.0000
G	160.0000

ENHANCED

(b) STATION 5.

FIGURE 24. - CONTINUED.

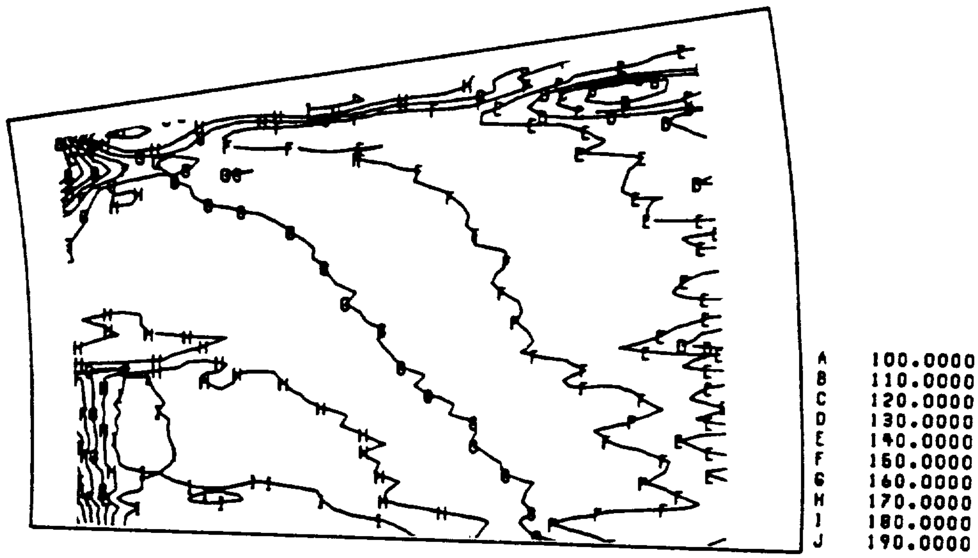

BASELINE

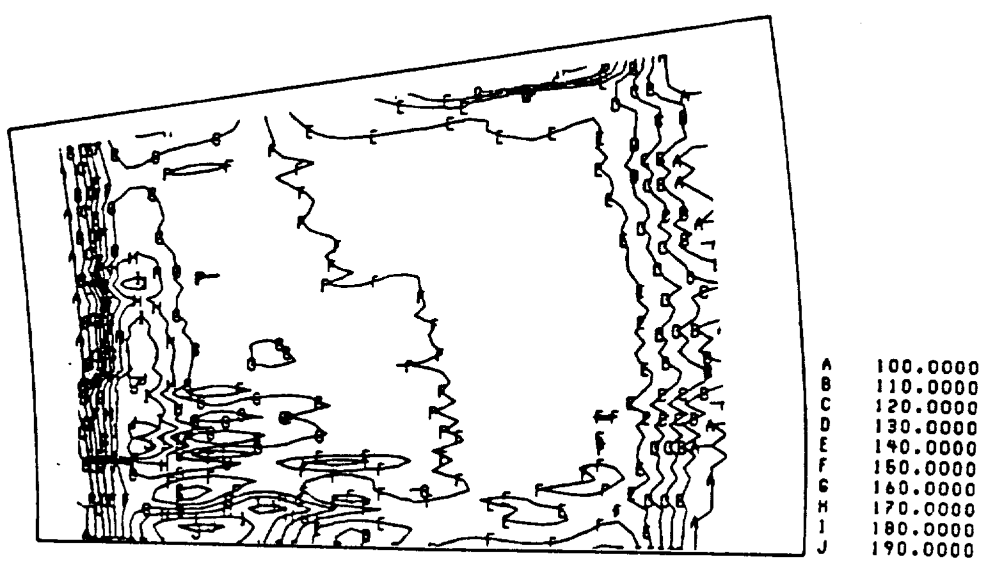

ENHANCED

(c) STATION 7.

FIGURE 24. - CONTINUED.

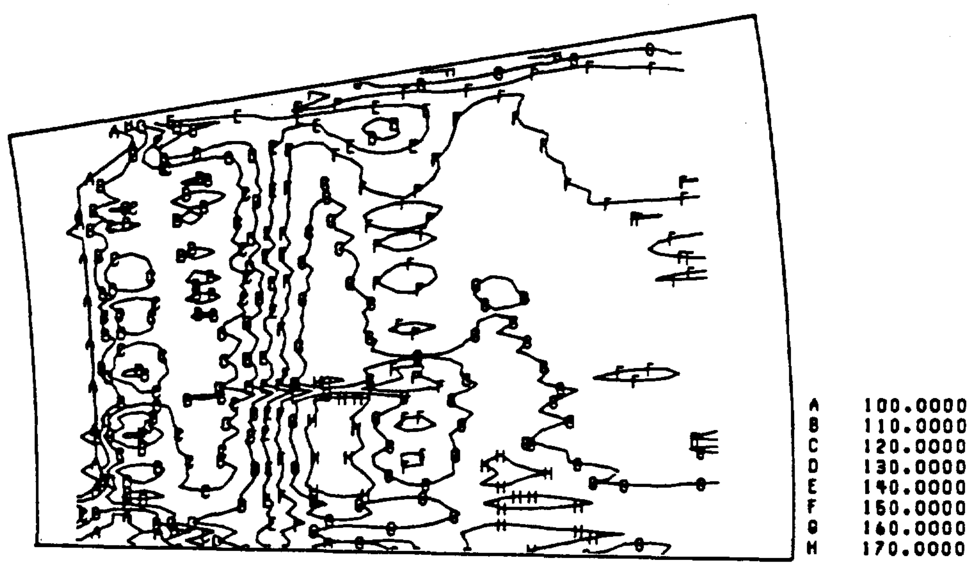

BASELINE

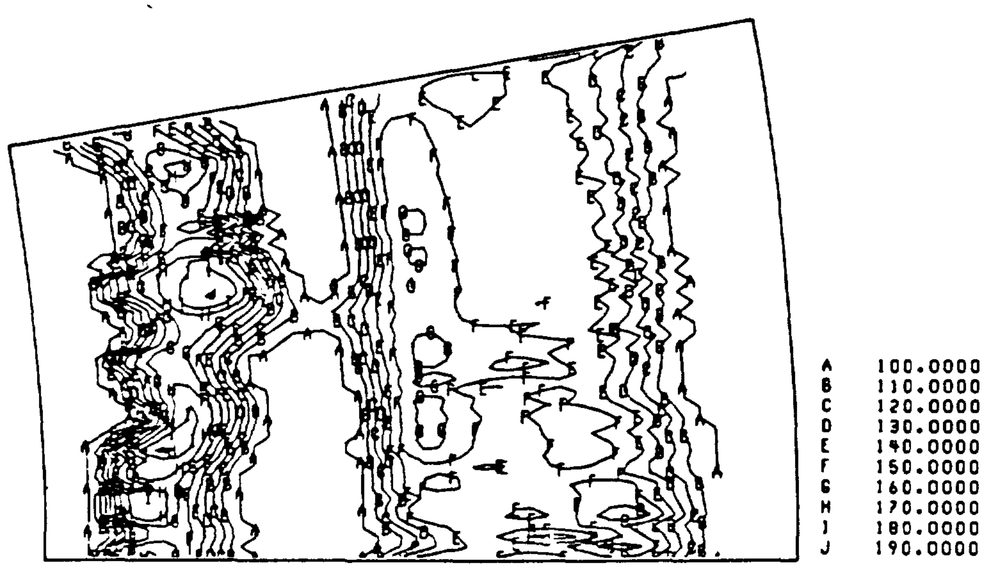

ENHANCED

(d) STATION 8.

FIGURE 24. - CONCLUDED.

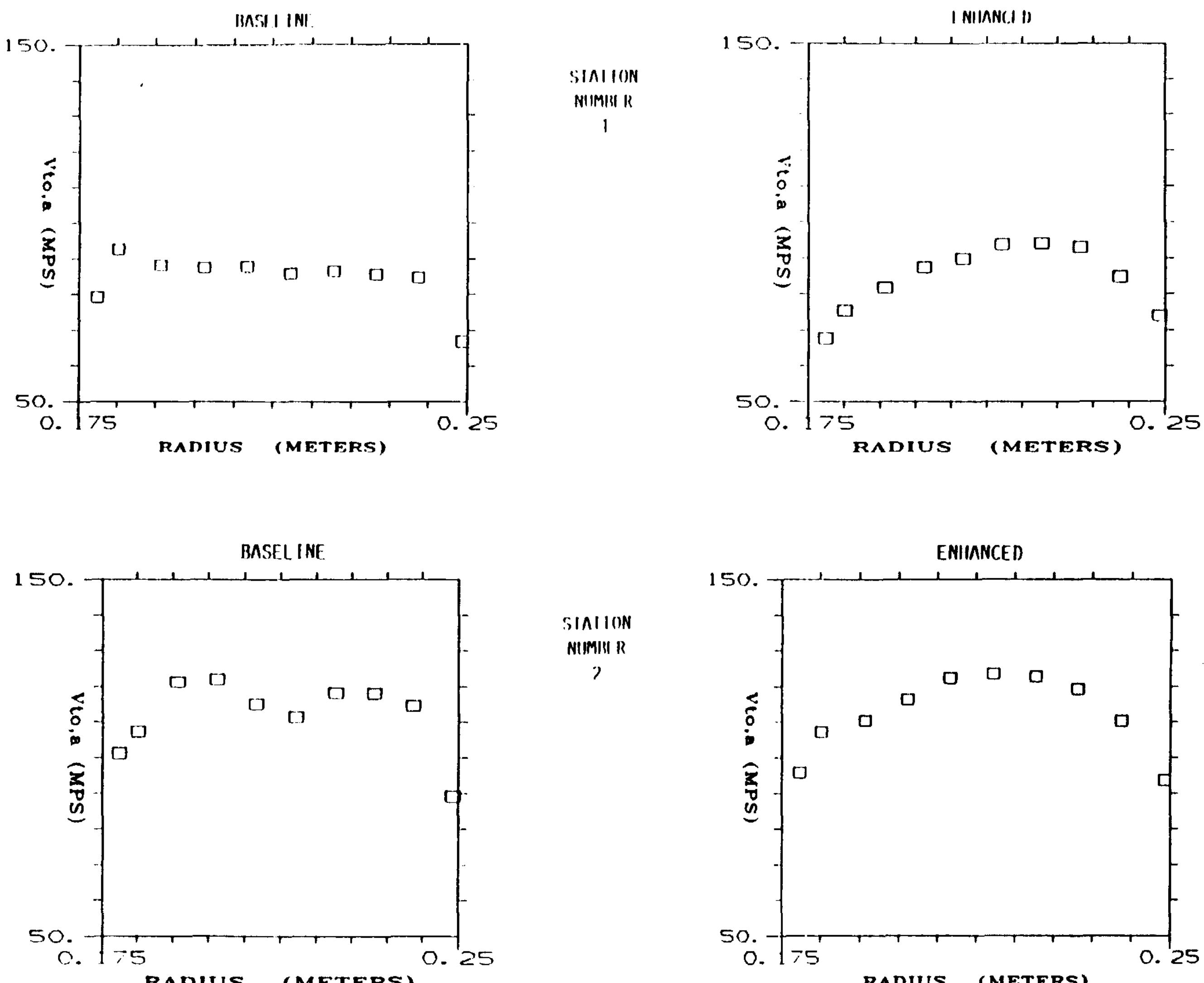

ABS TOTAL VELOCITY ST 1,2

FIGURE 25a.

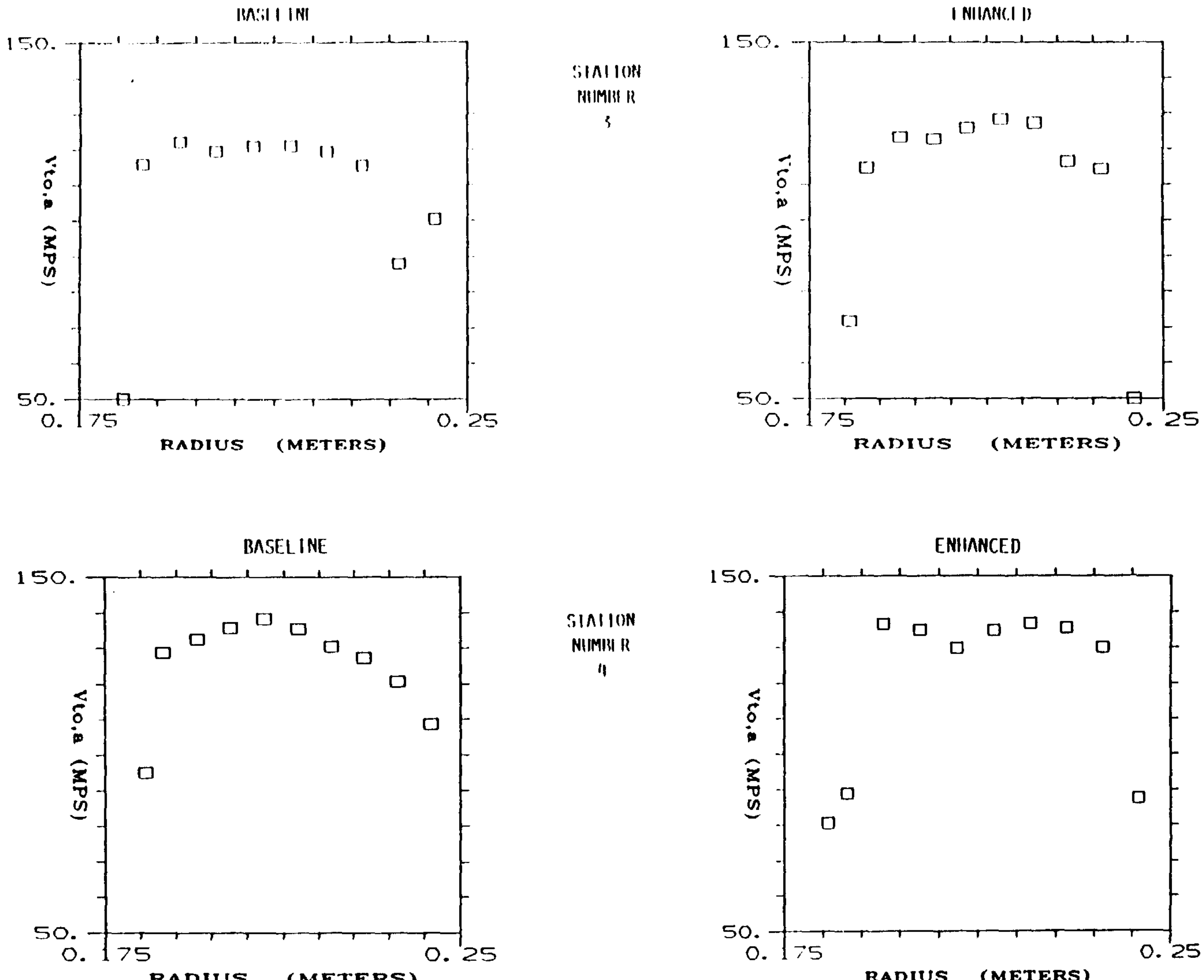

ABS TOTAL VELOCITY ST 3,4

FIGURE 25b.

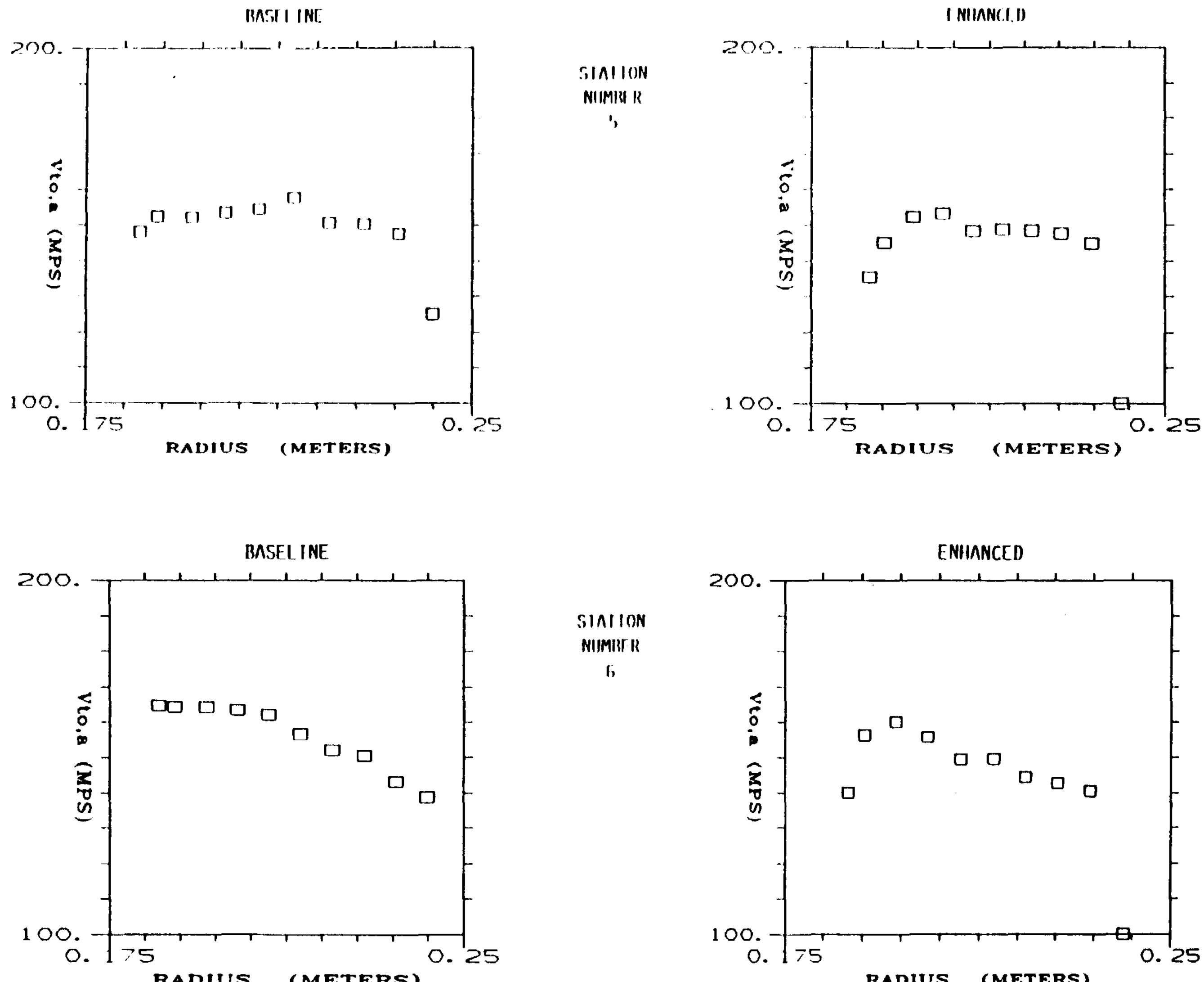

ABS TOTAL VELOCITY ST 5,6

FIGURE 25c.

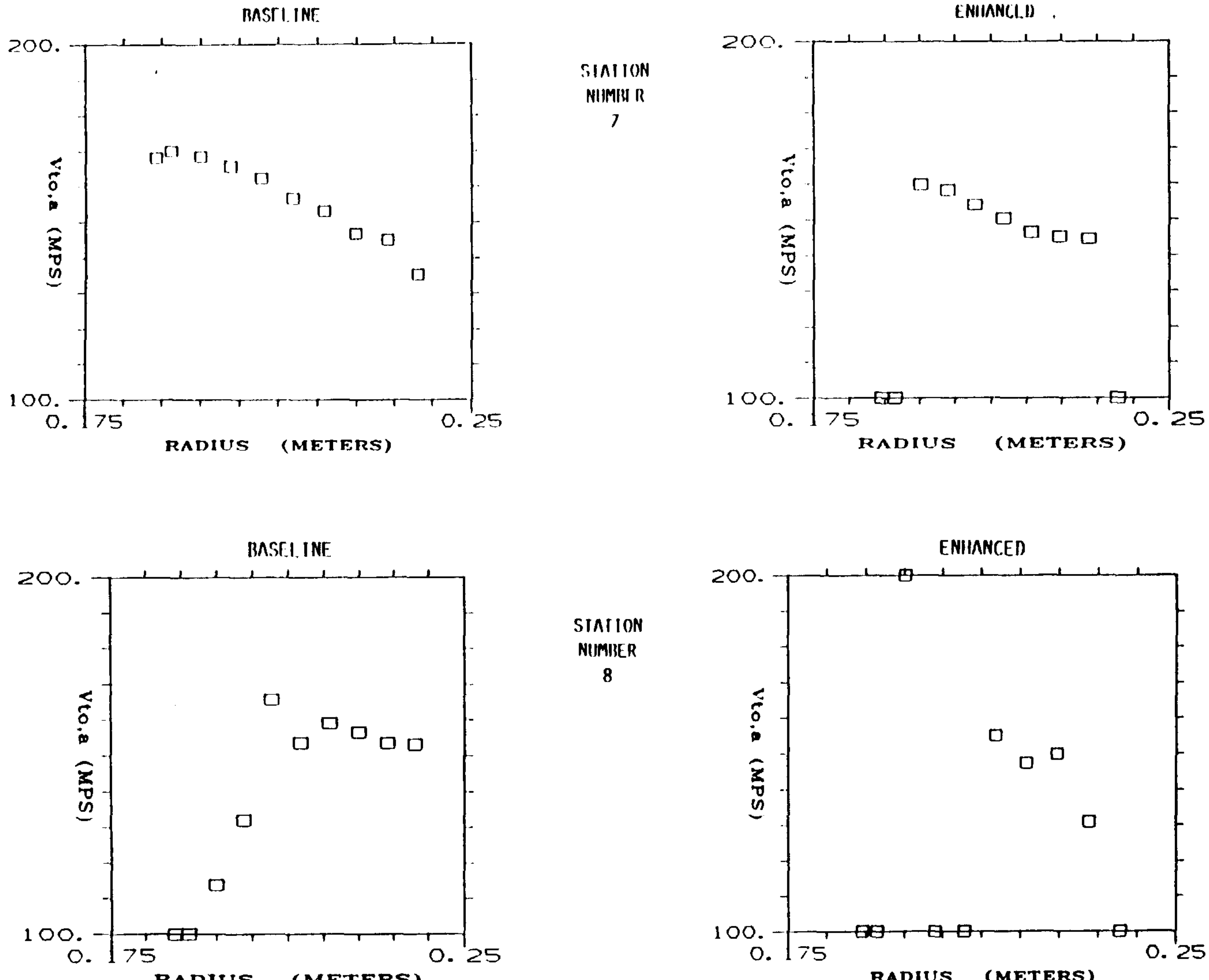

ABS TOTAL VELOCITY ST 7,8

FIGURE 25d.

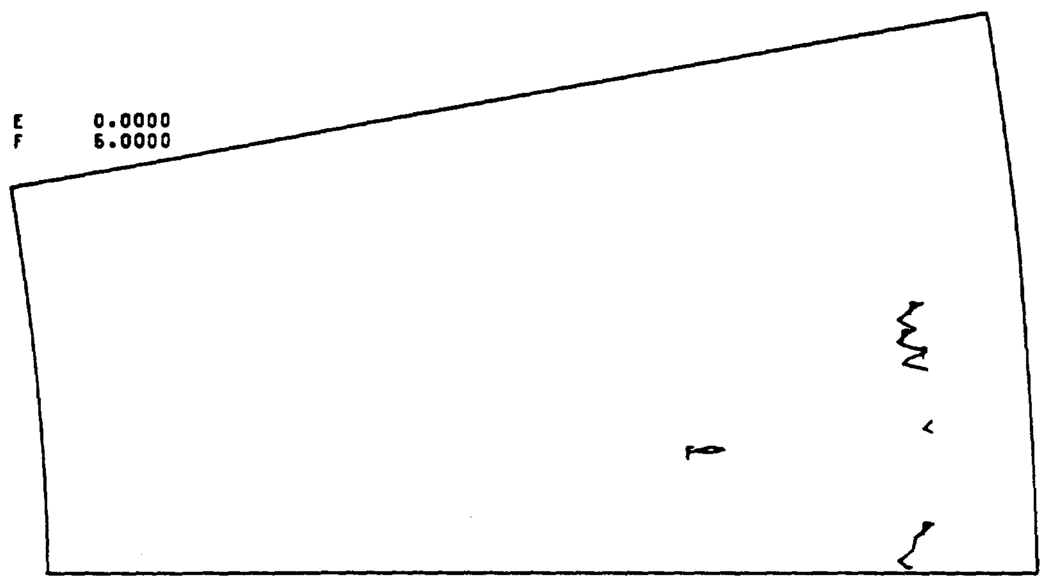

BASELINE

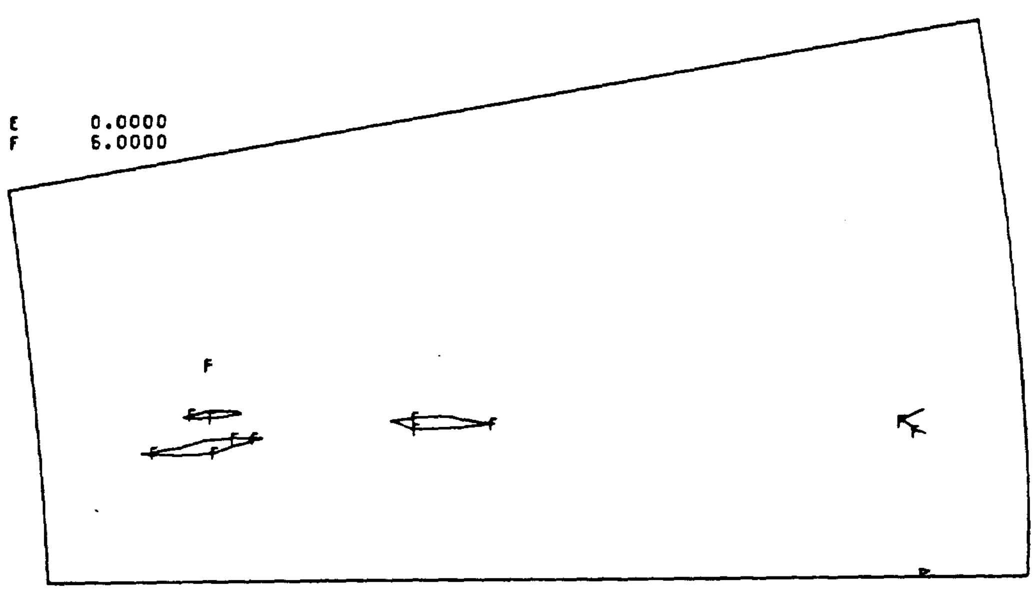

ENHANCED

(a) STATION 1.

FIGURE 26. - ABSOLUTE FLOW ANGLE, CROSS CHANNEL.

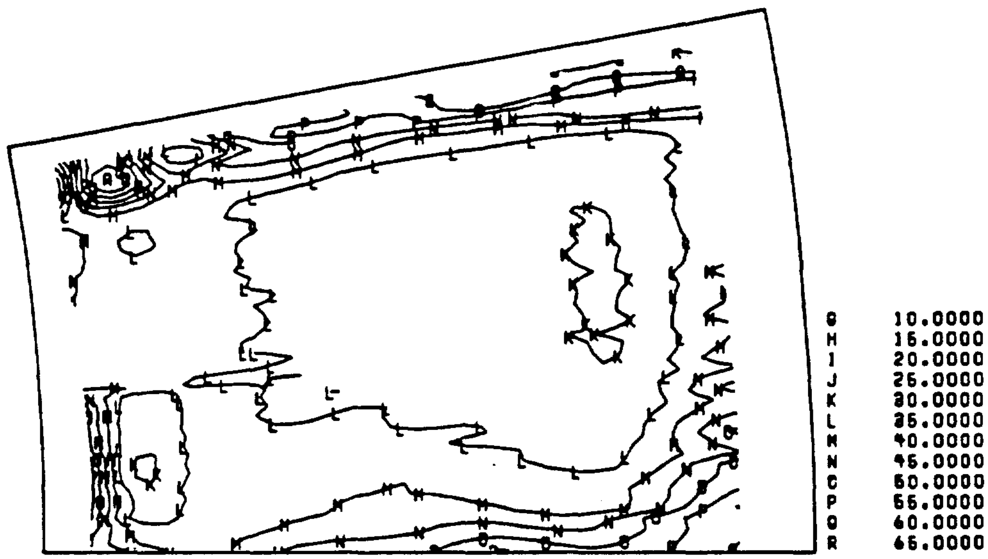

BASELINE

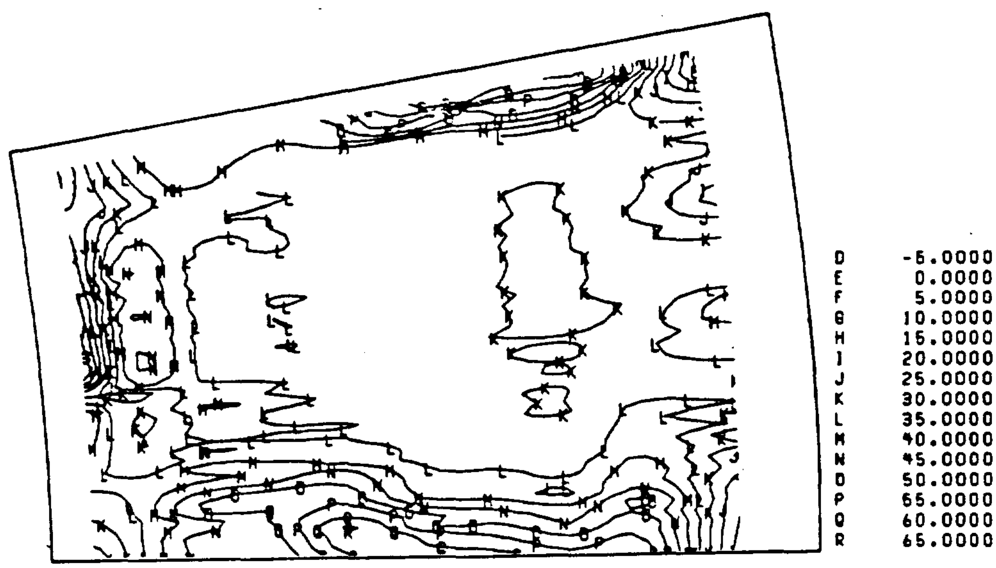

ENHANCED

(b) STATION 7.

FIGURE 26. - CONTINUED.

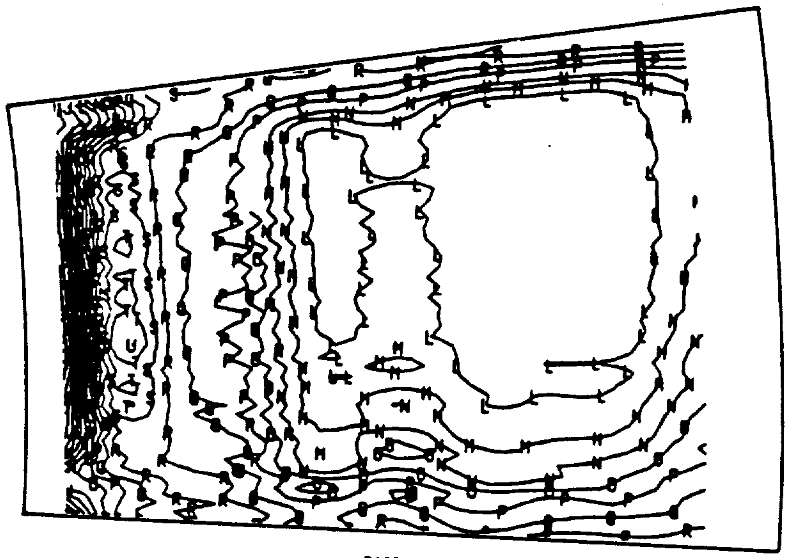

C	-10.0000
D	-5.0000
E	0.0000
F	5.0000
G	10.0000
H	15.0000
I	20.0000
J	25.0000
K	30.0000
L	35.0000
M	40.0000
N	45.0000
O	50.0000
P	55.0000
Q	60.0000
R	65.0000
S	70.0000
T	75.0000
U	80.0000

BASELINE

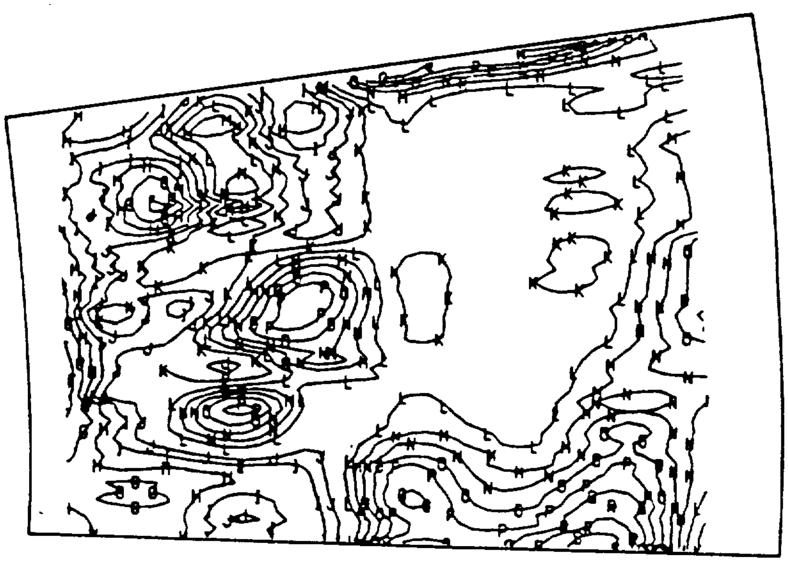

D	-5.0000
E	0.0000
F	5.0000
G	10.0000
H	15.0000
I	20.0000
J	25.0000
K	30.0000
L	35.0000
M	40.0000
N	45.0000
O	50.0000
P	55.0000
Q	60.0000
R	65.0000
S	70.0000

ENHANCED

(c) STATION 8.

FIGURE 26. - CONCLUDED.

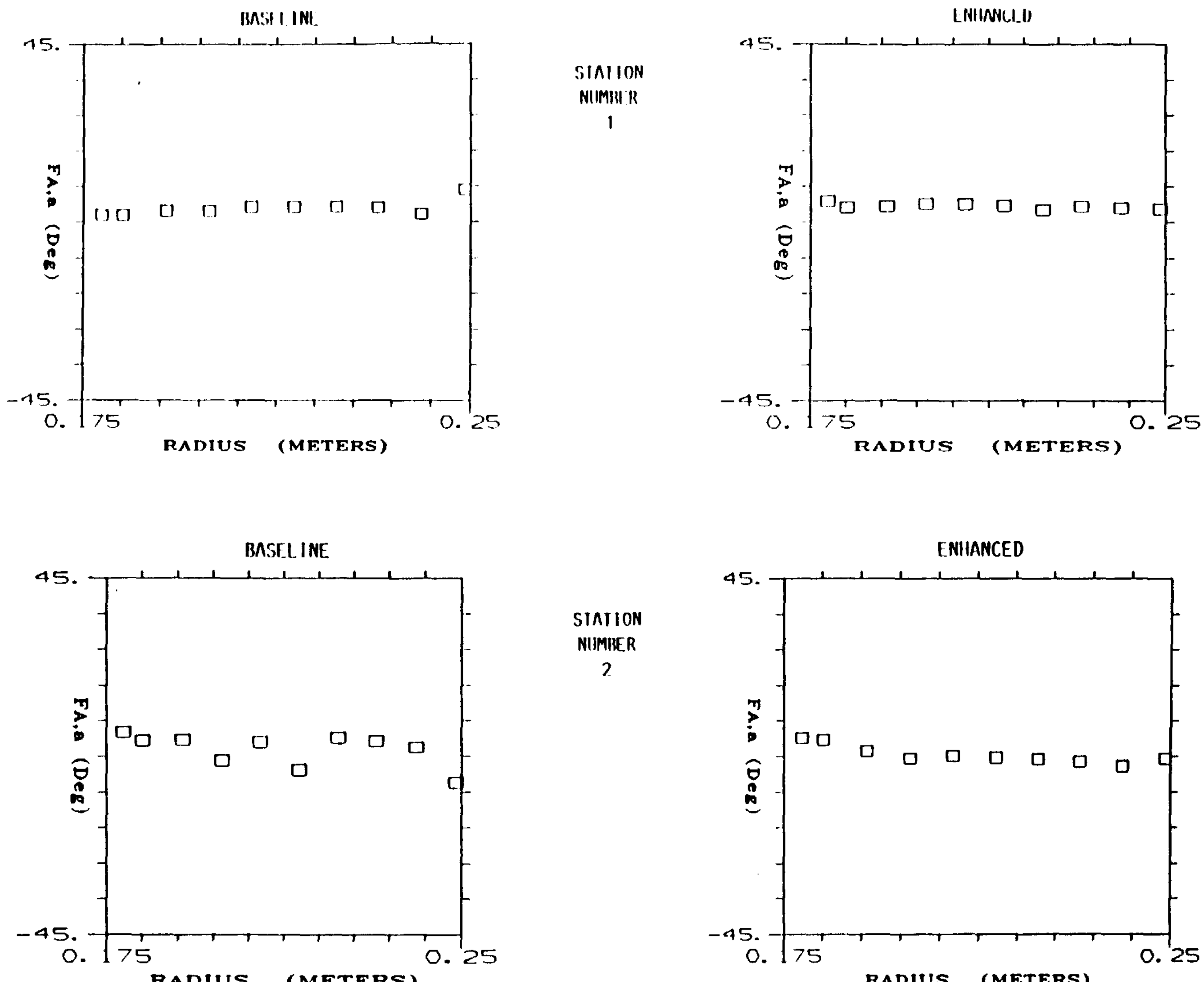

ABSOLUTE FLOW ANGLE

FIGURE 27a.

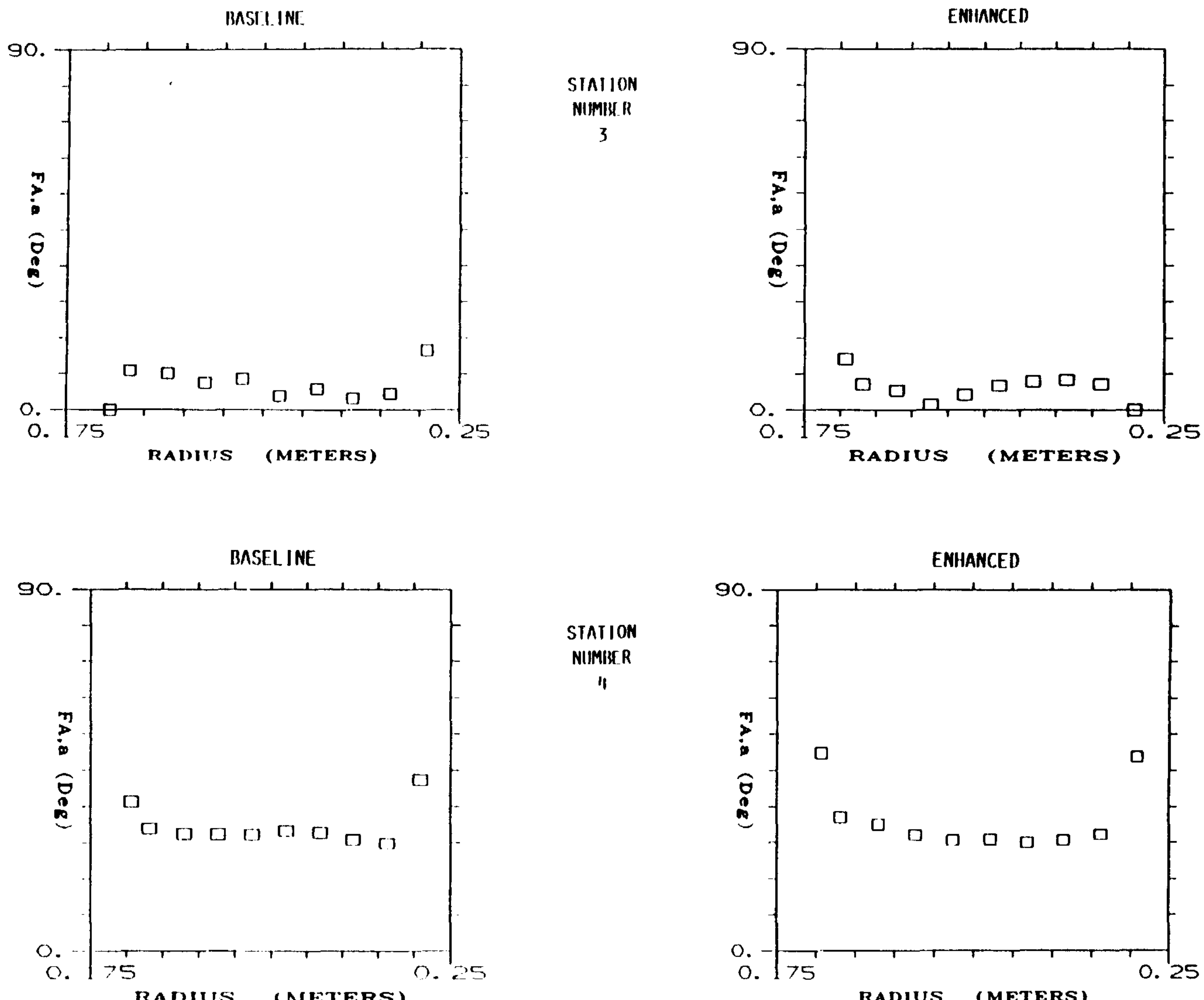

ABSOLUTE FLOW ANGLE ST 3,4

FIGURE 27b.

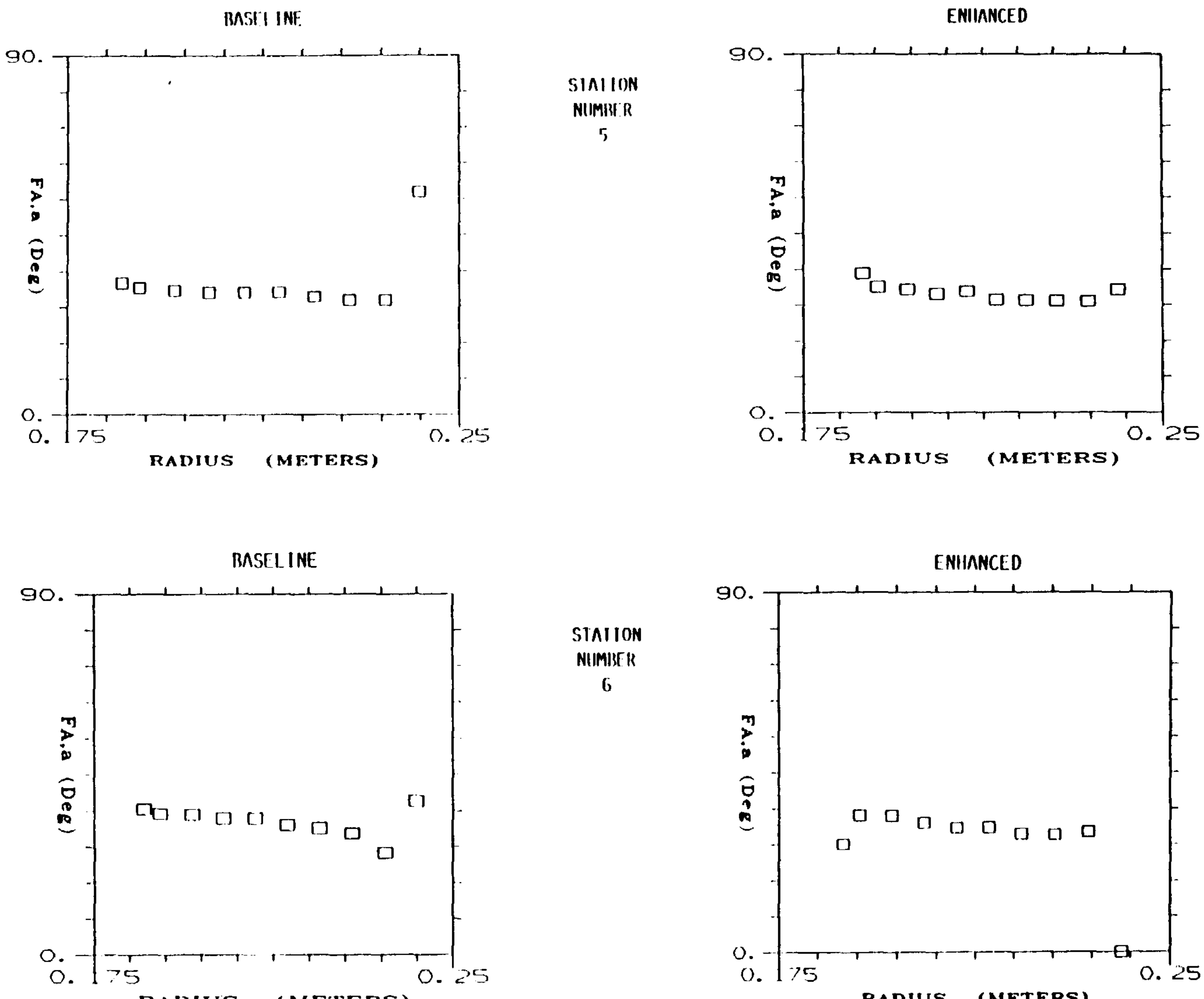

ABSOLUTE FLOW ANGLE ST 5,6

FIGURE 27c.

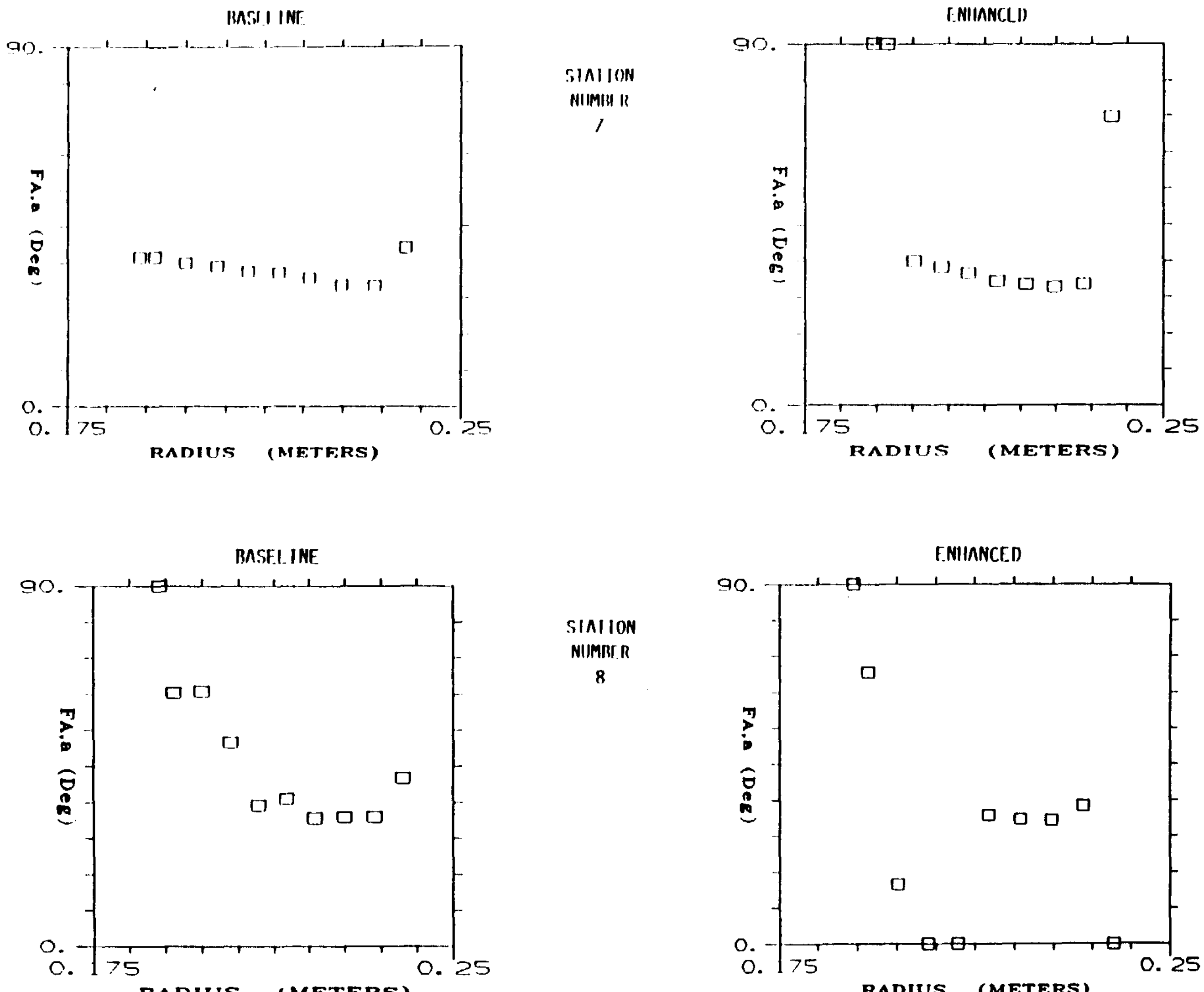

ABSOLUTE FLOW ANGLE ST 7,8

FIGURE 27d.

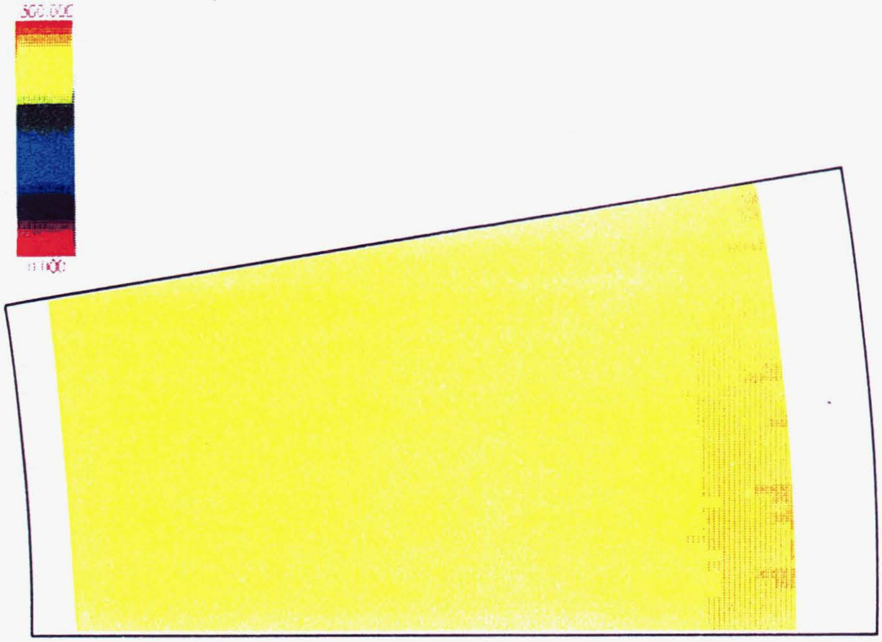

BASELINE

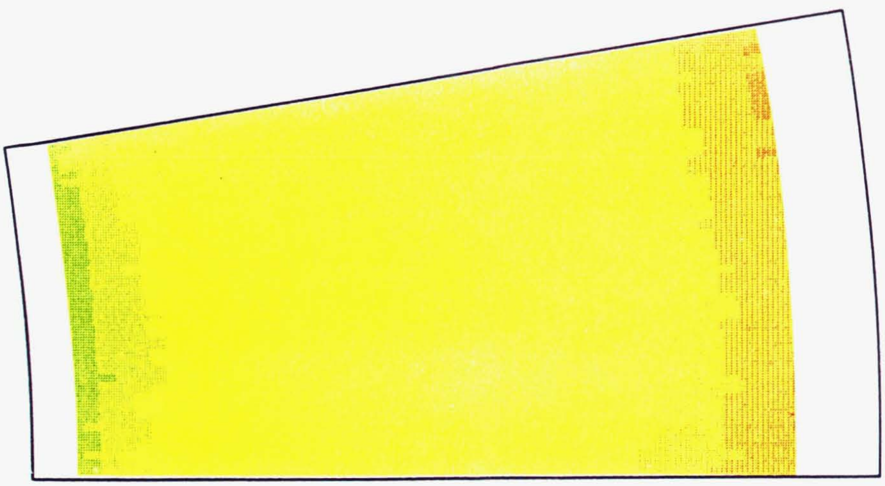

ENHANCED

(a) STATION 1.

FIGURE 28. - RELATIVE TOTAL VELOCITY, COLORFILL, MPS.

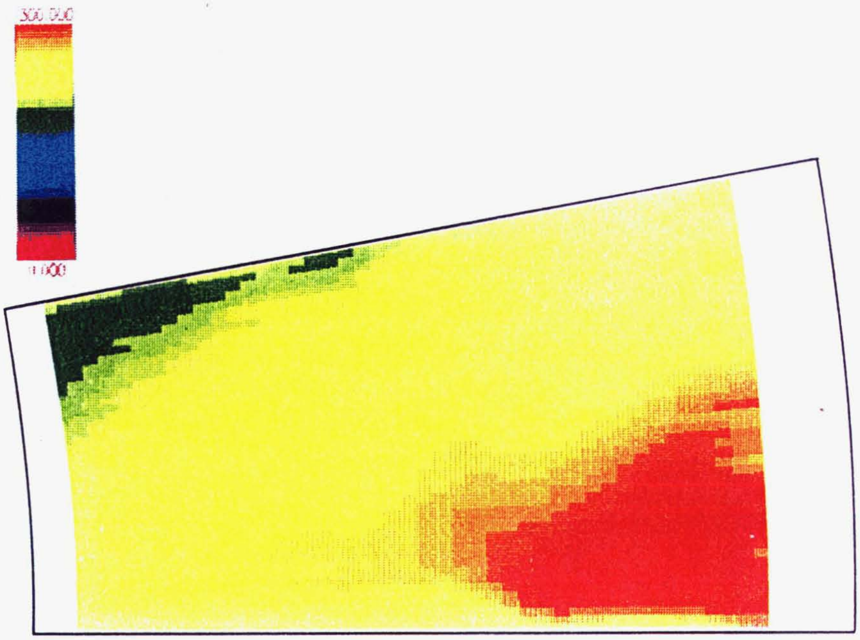

BASELINE

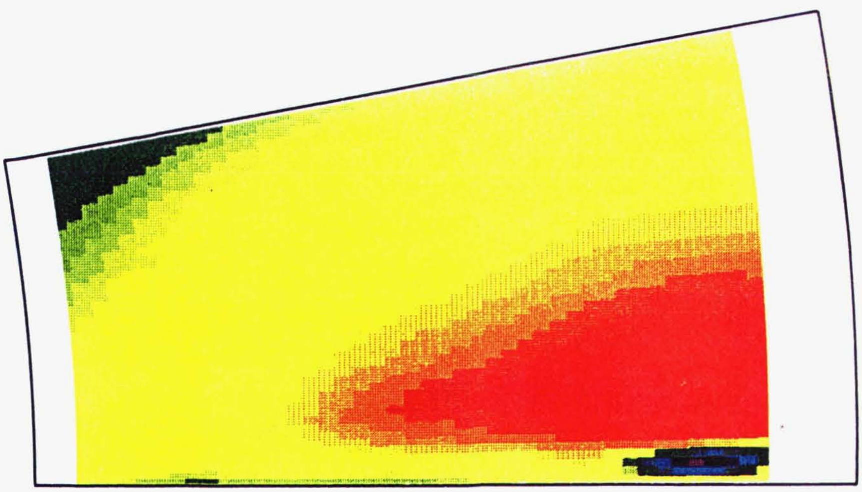

ENHANCED

(b) STATION 2.

FIGURE 28. - CONTINUED.

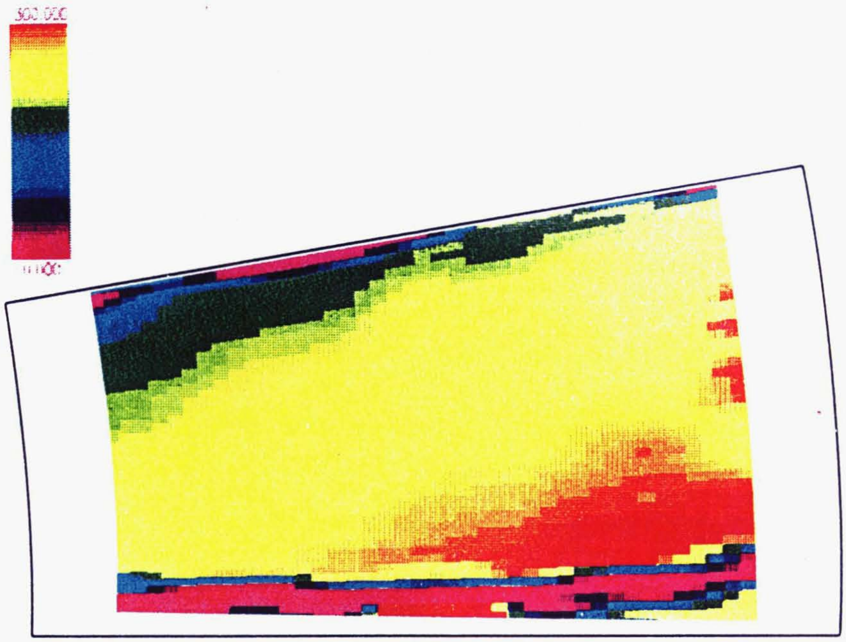

BASELINE

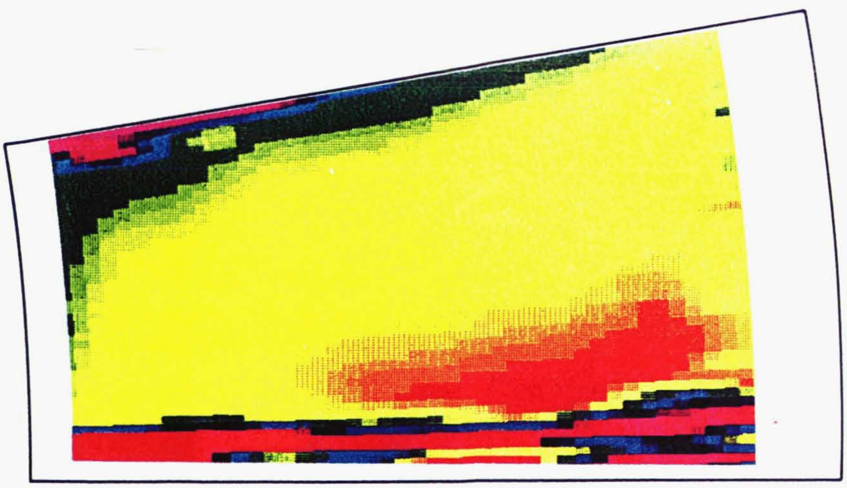

ENHANCED

(c) STATION 3.

FIGURE 28. - CONTINUED.

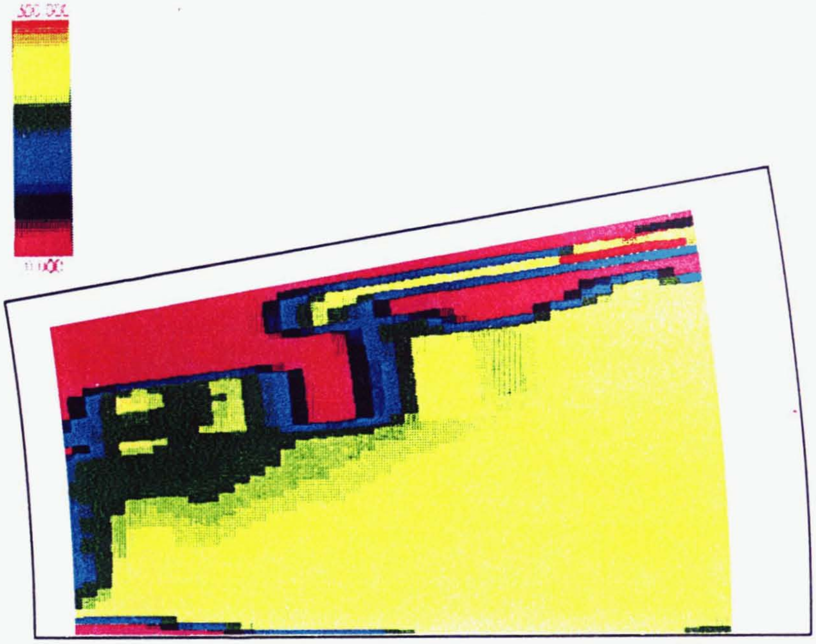

BASELINE

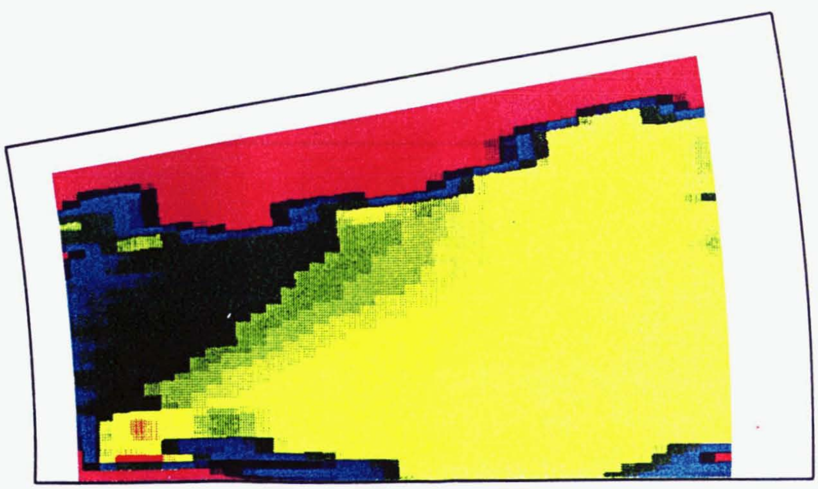

ENHANCED

(d) STATION 4.

FIGURE 28. - CONTINUED.

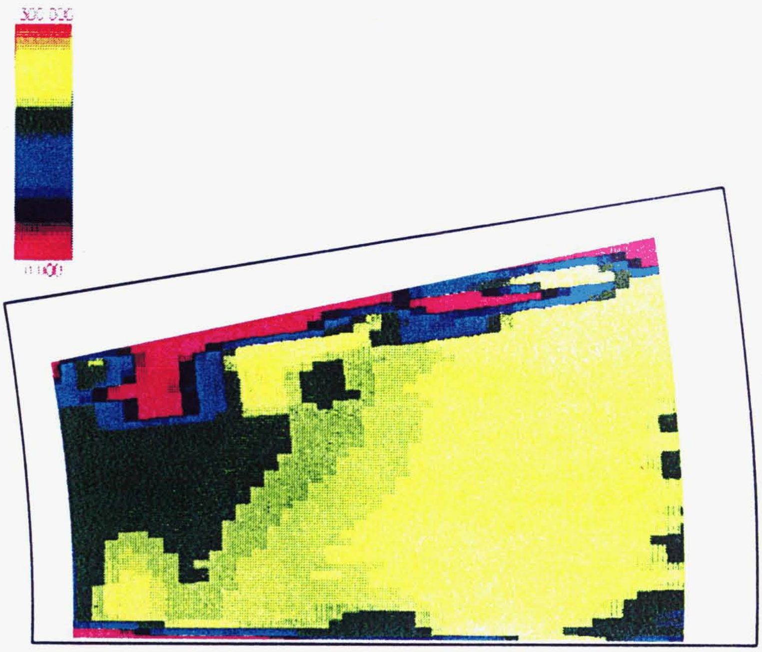

BASELINE

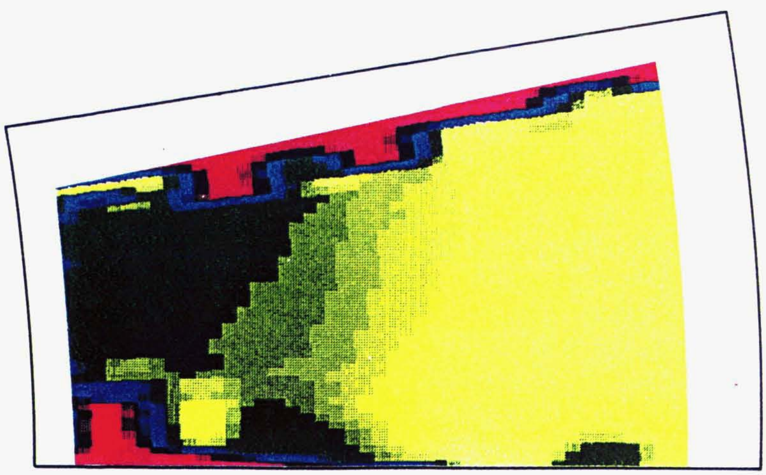

ENHANCED

(e) STATION 5.

FIGURE 28. - CONTINUED.

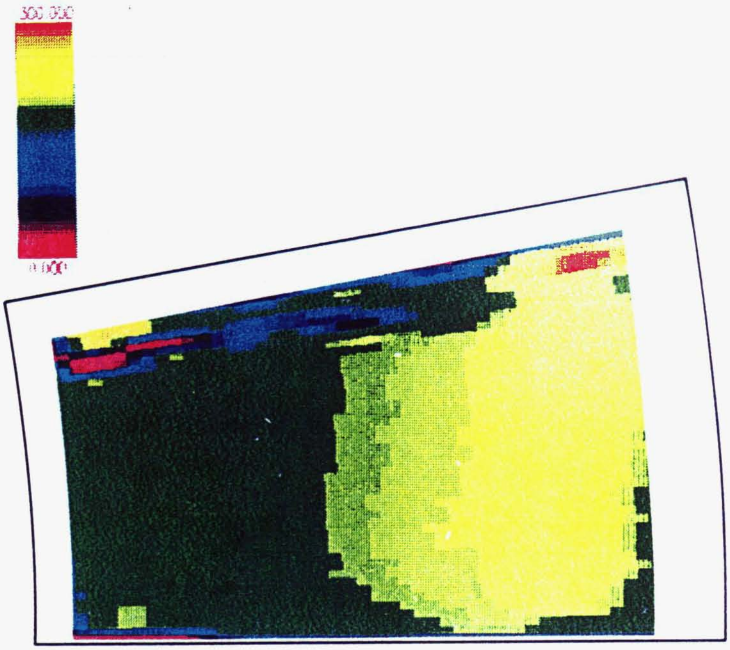

BASELINE

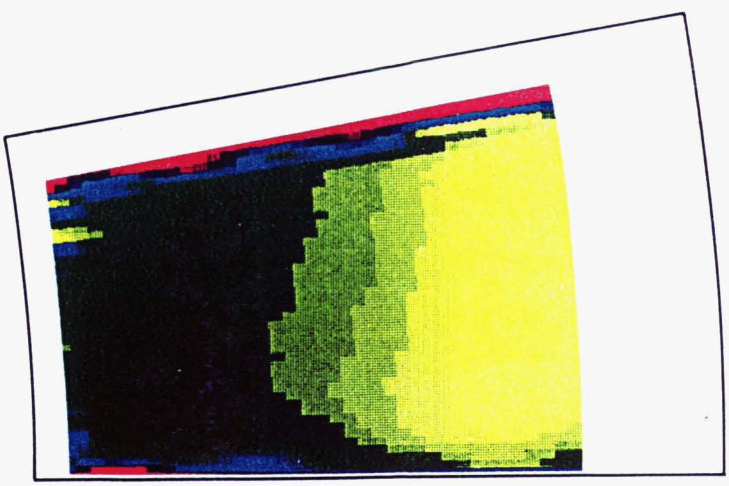

ENHANCED

(f) STATION 6.

FIGURE 28. - CONTINUED.

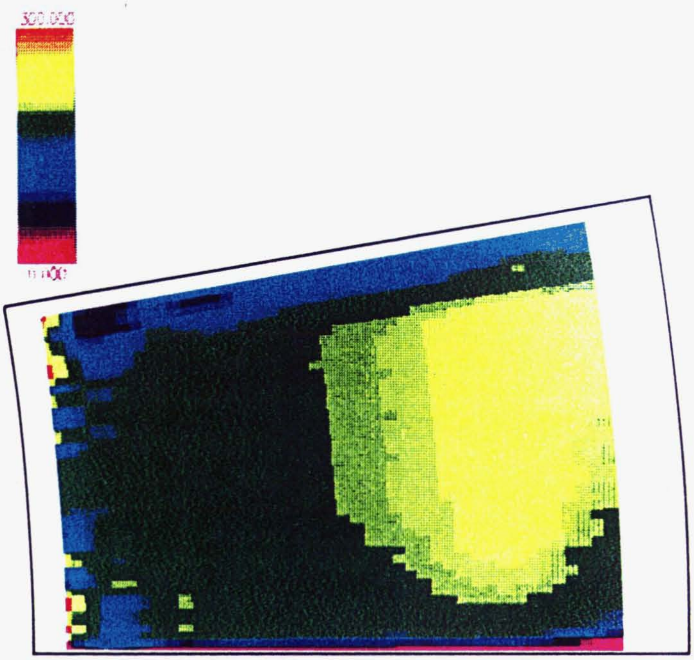

BASELINE

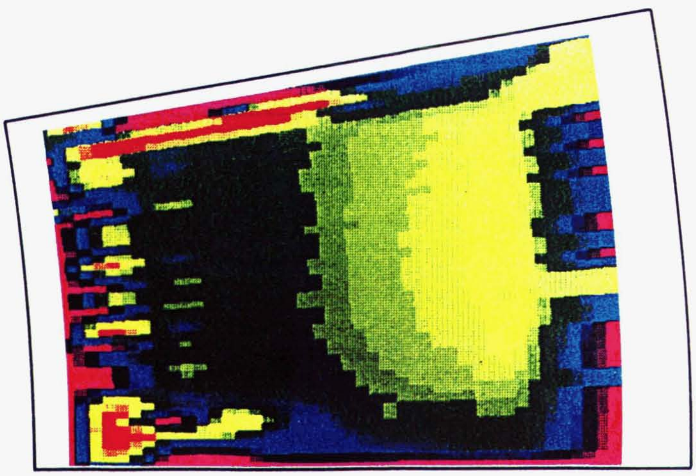

ENHANCED

(g) STATION 7.

FIGURE 28. - CONTINUED.

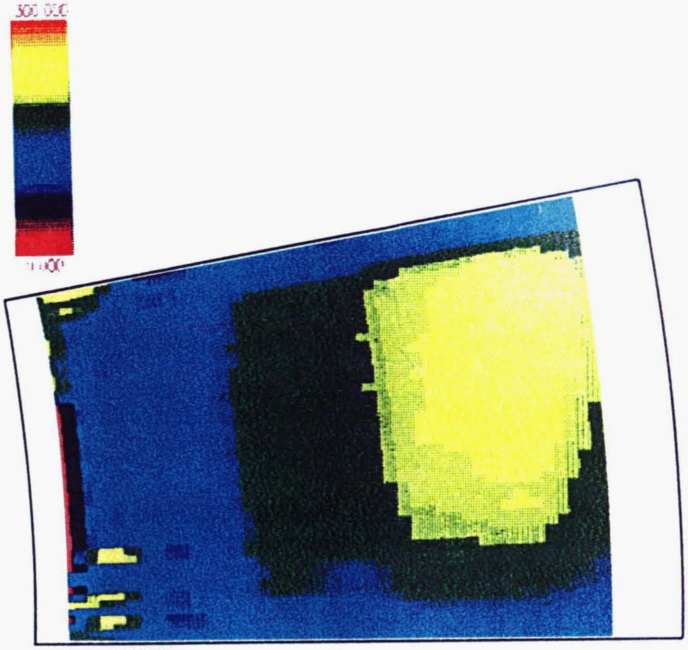

BASELINE

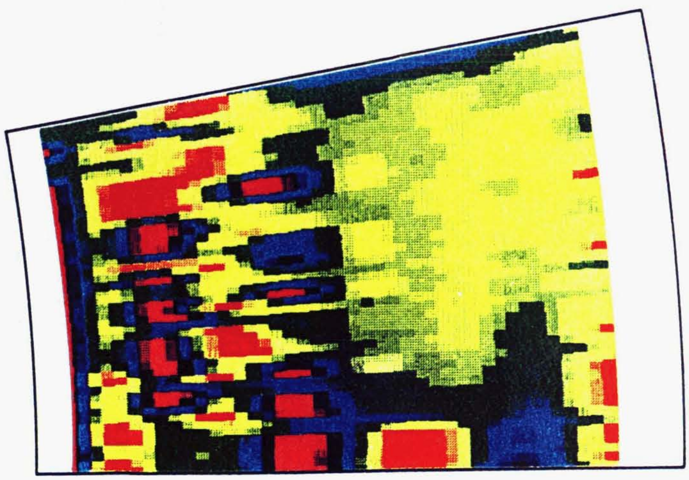

ENHANCED

(h) STATION 8.

FIGURE 28. - CONCLUDED.

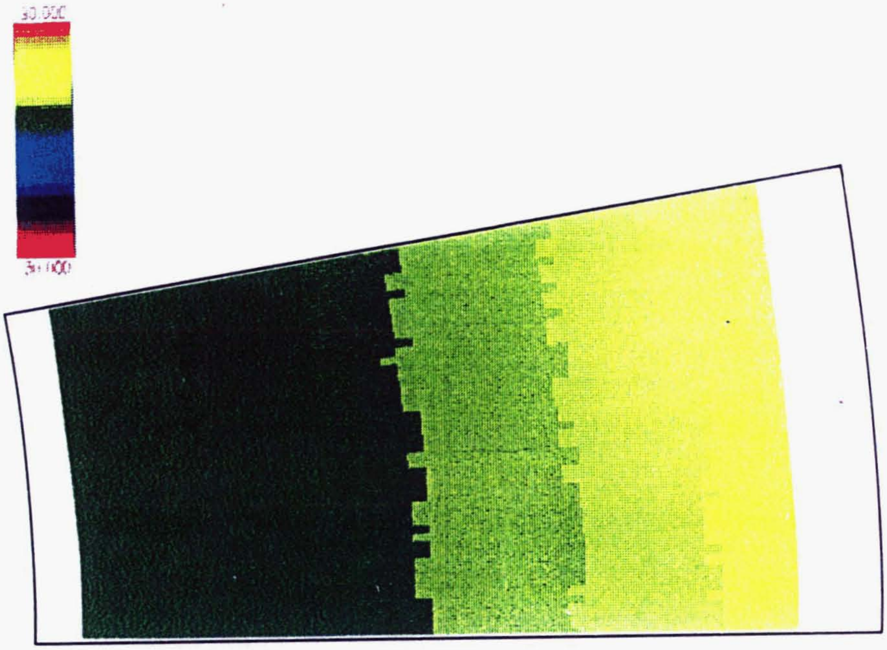

BASELINE

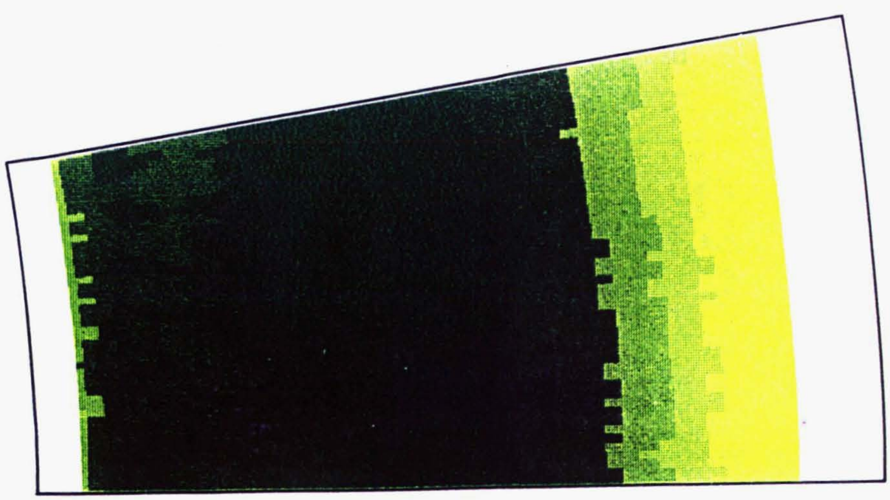

ENHANCED

(a) STATION 1.

FIGURE 29. - RELATIVE FLOW ANGLE, COLORFILL, DEG.

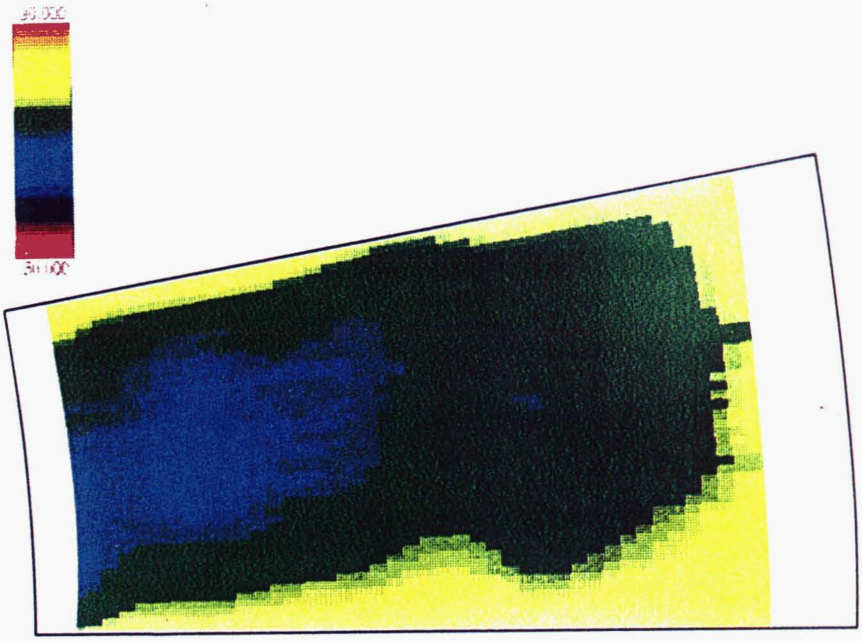

BASELINE

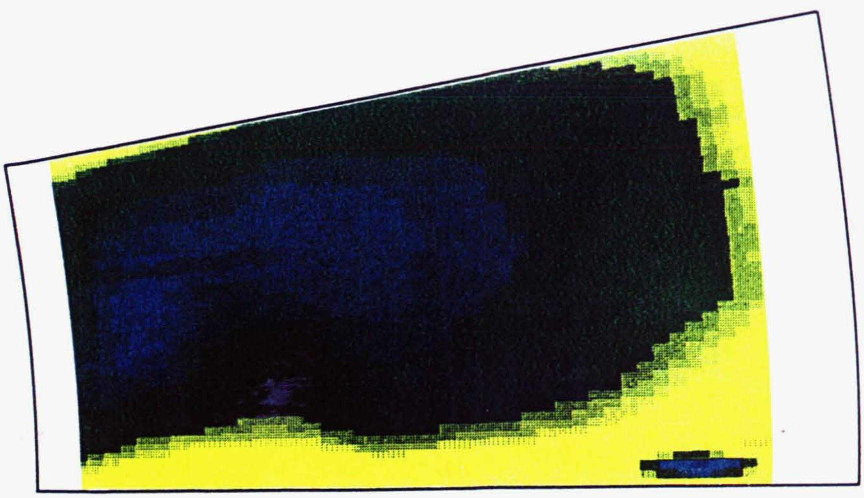

ENHANCED

(b) STATION 2.

FIGURE 29. - CONTINUED.

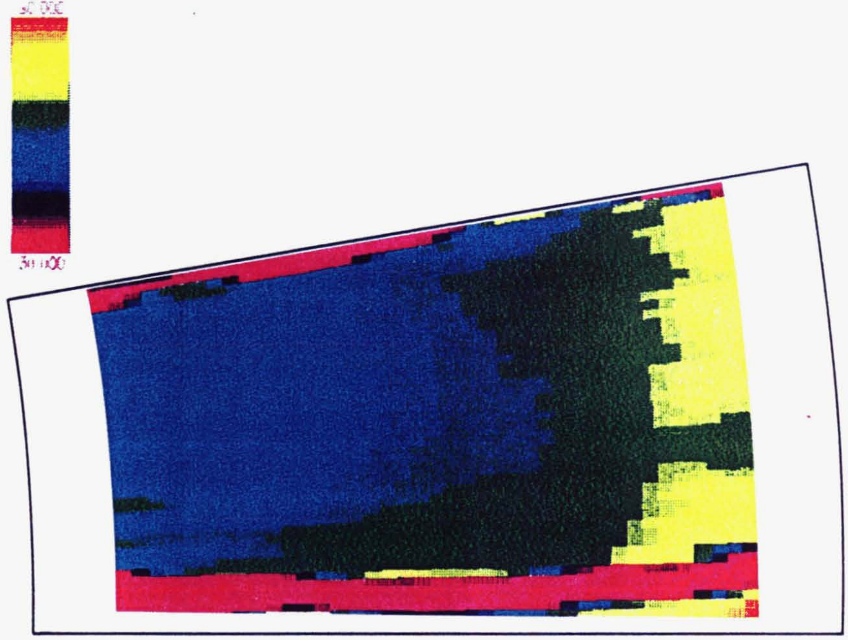

BASELINE

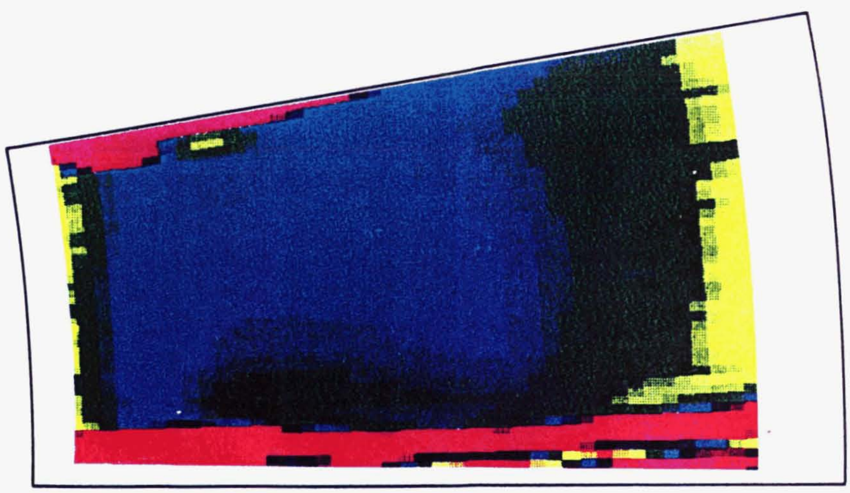

ENHANCED

(c) STATION 3.

FIGURE 29. - CONTINUED.

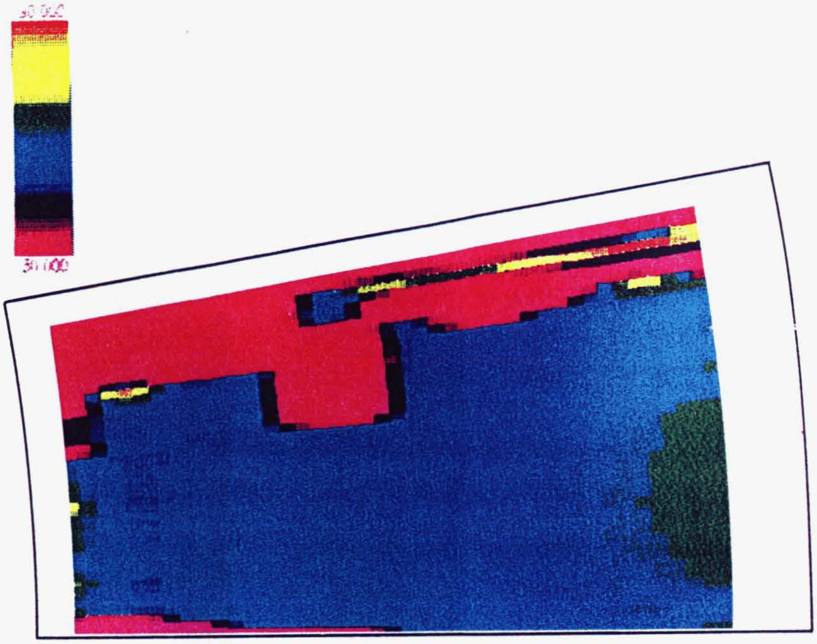

BASELINE

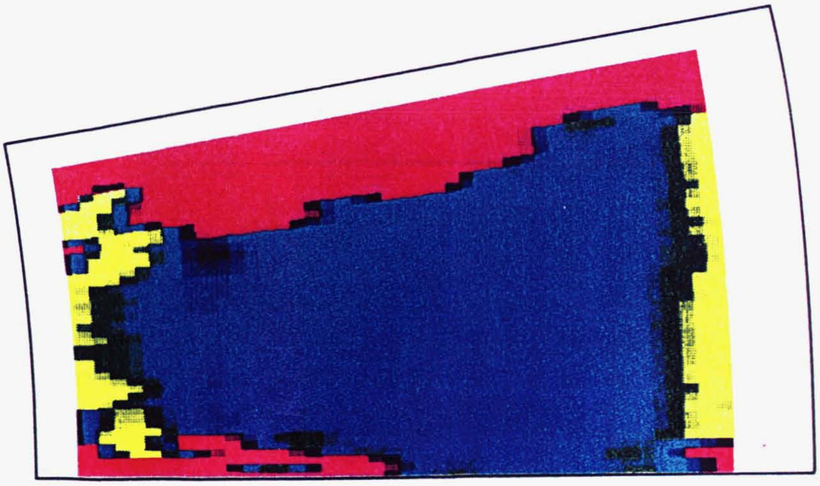

ENHANCED

(d) STATION 4.

FIGURE 29. - CONTINUED.

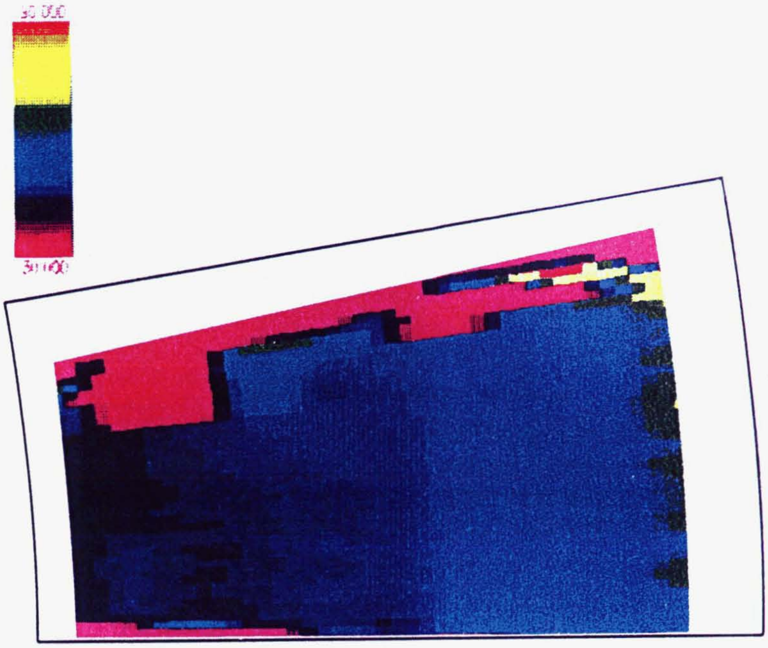

BASELINE

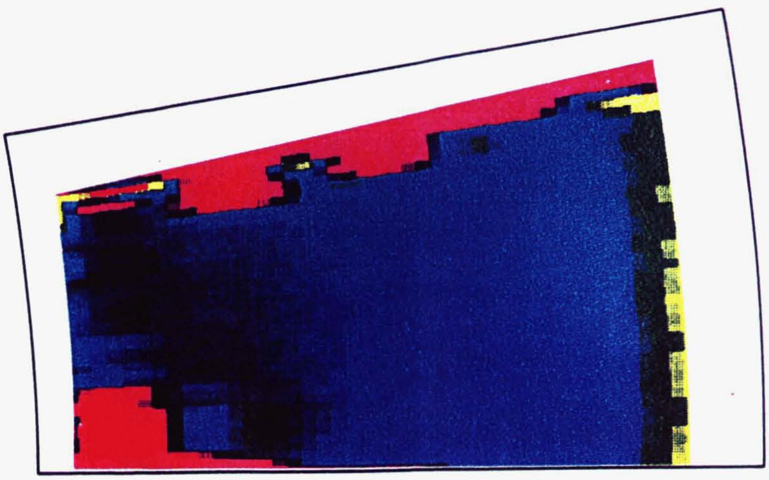

ENHANCED

(e) STATION 5.

FIGURE 29. - CONTINUED.

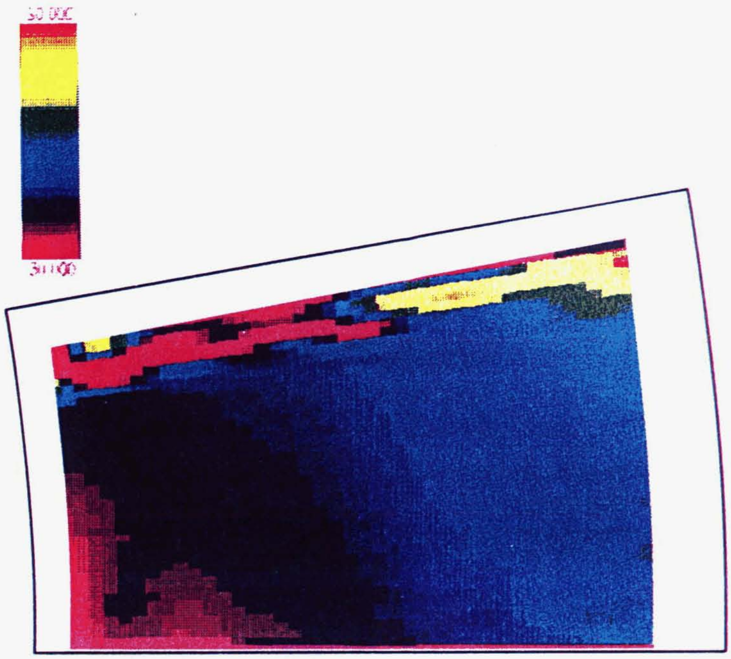

BASELINE

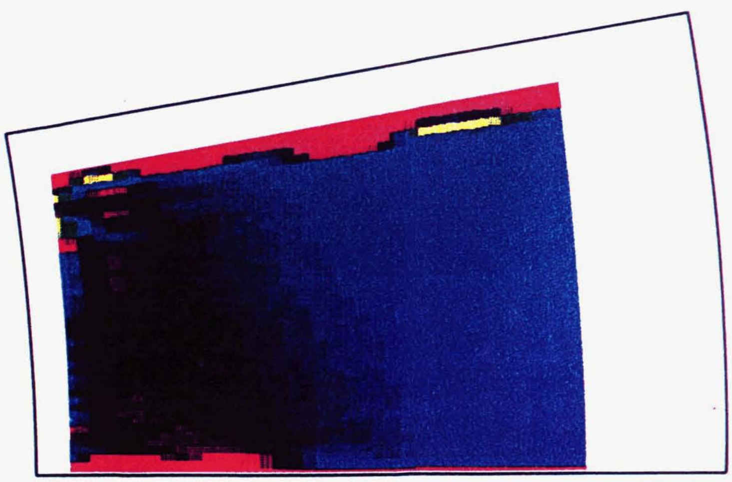

ENHANCED

(f) STATION 6.

FIGURE 29. - CONTINUED.

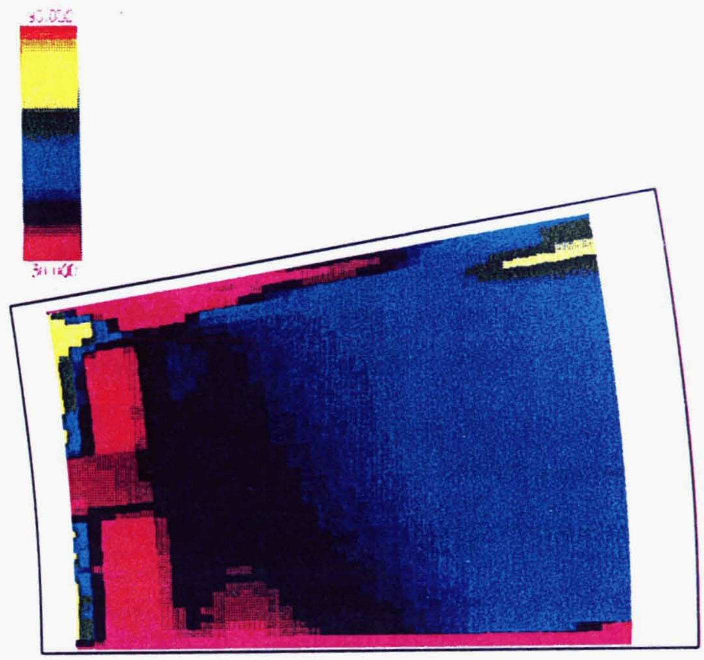

BASELINE

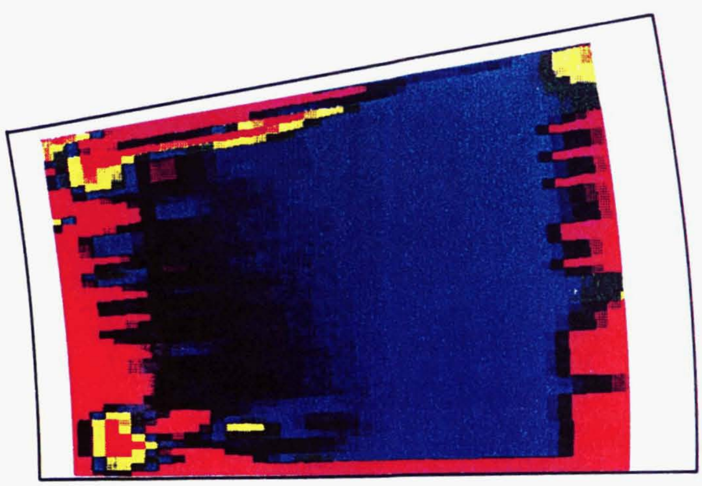

ENHANCED

(g) STATION 7.

FIGURE 29. - CONTINUED.

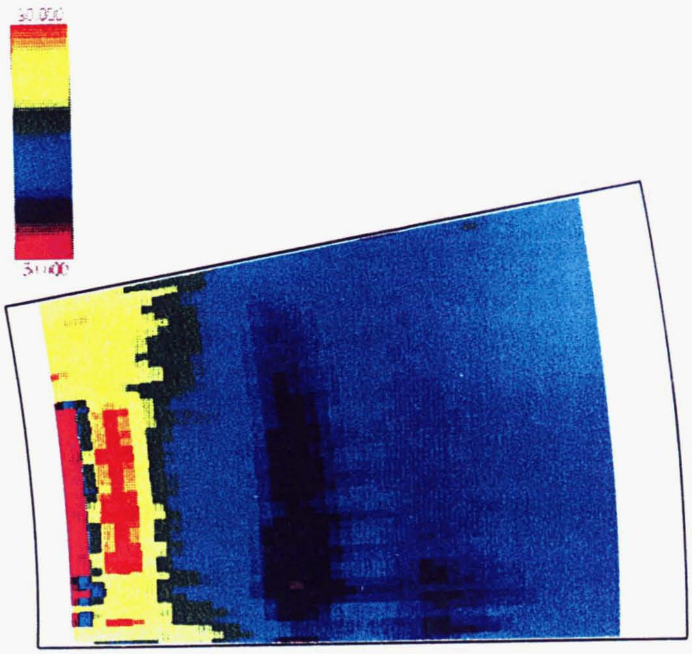

BASELINE

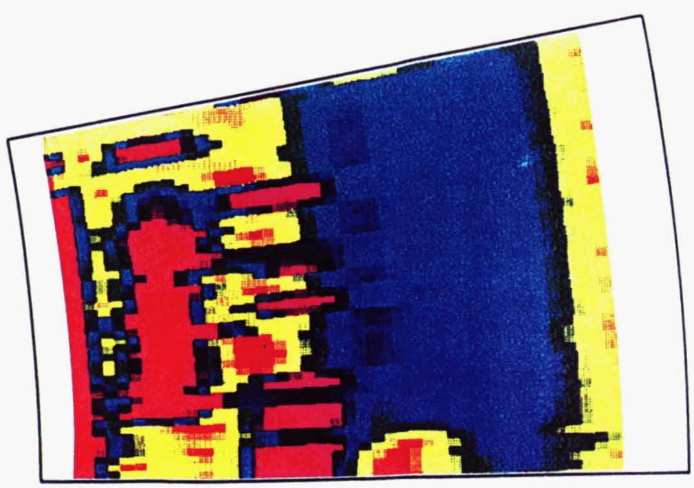

ENHANCED

(h) STATION 8.

FIGURE 29. - CONCLUDED.

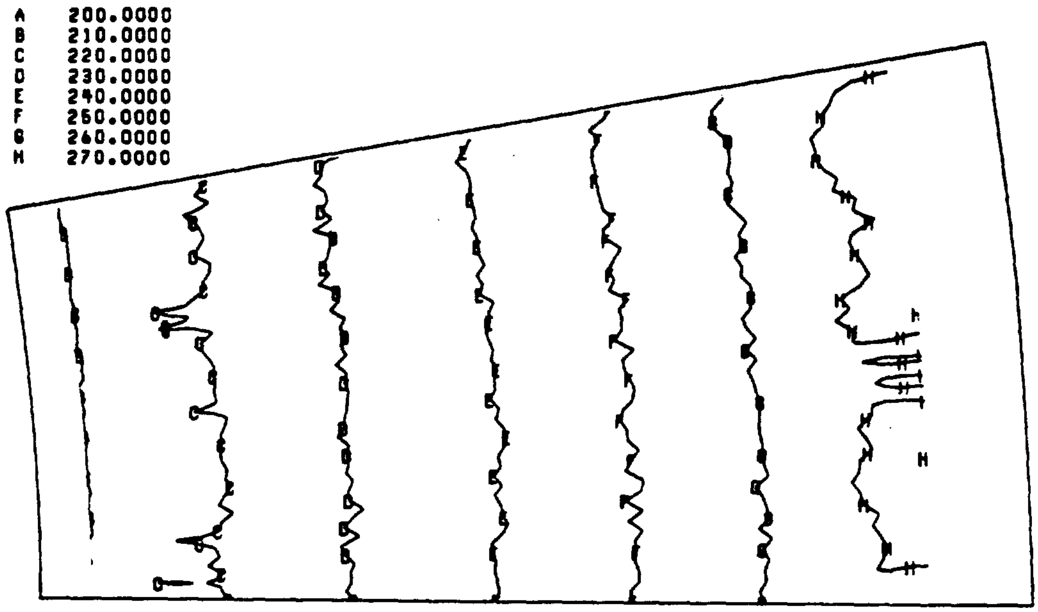

BASELINE

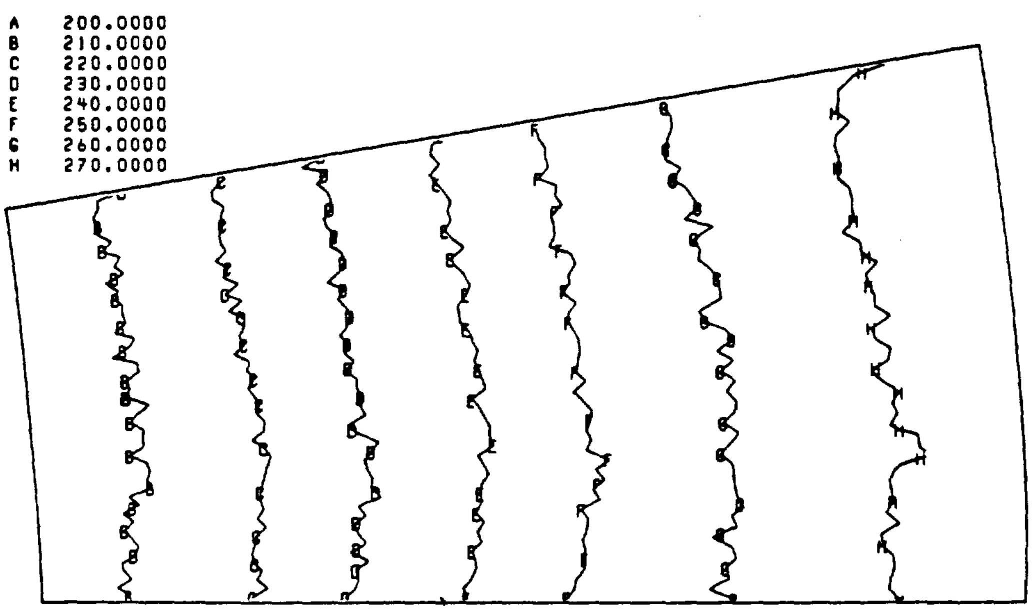

ENHANCED

(a) STATION 1.

FIGURE 30. - RELATIVE TOTAL VELOCITY, CROSS CHANNEL.

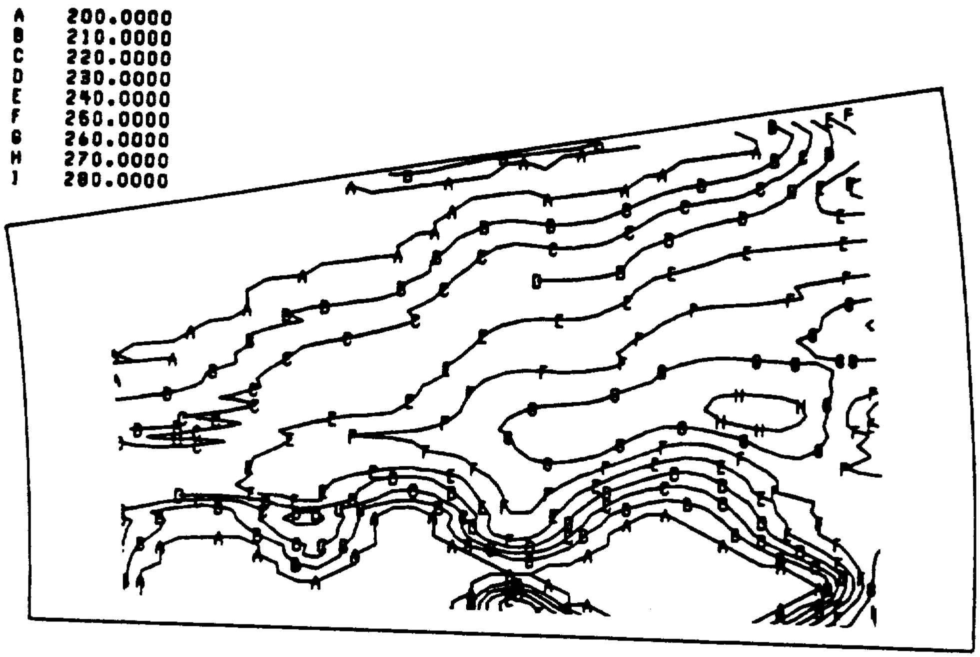

BASELINE

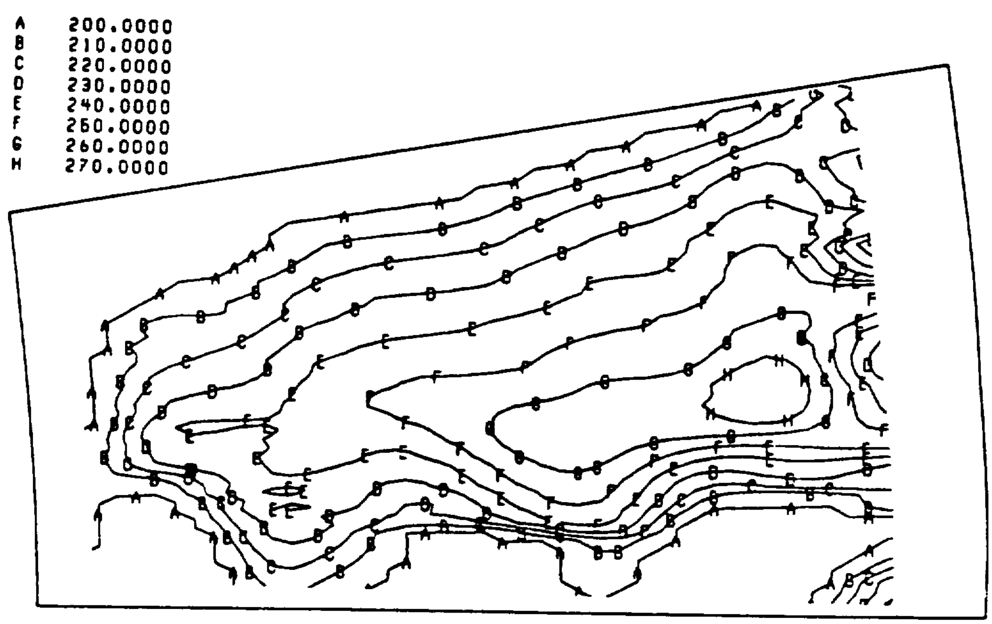

ENHANCED

(b) STATION 3.

FIGURE 30. - CONTINUED.

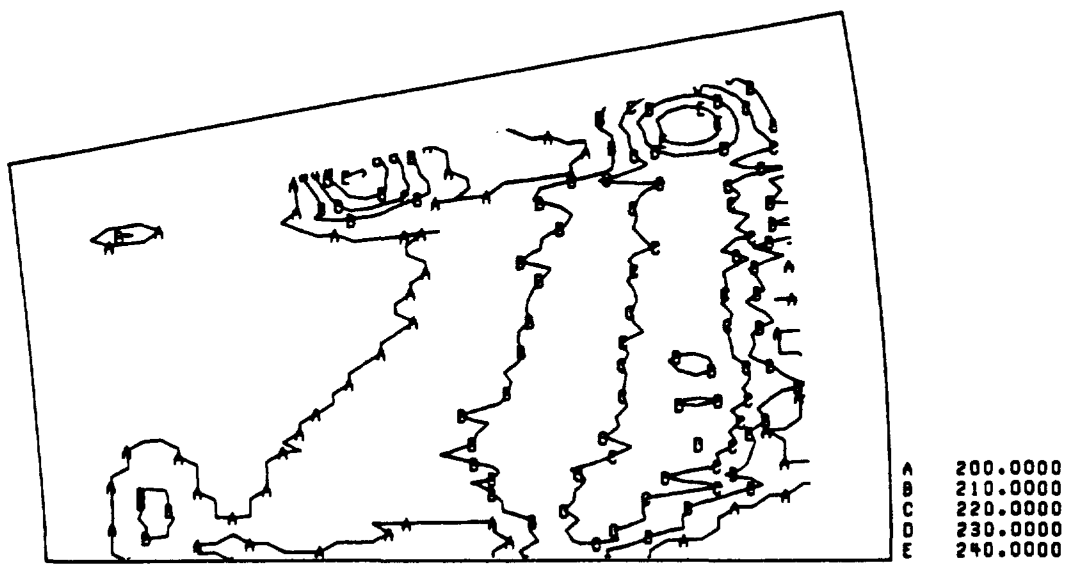

BASELINE

ENHANCED

(c) STATION 5.

FIGURE 30. - CONTINUED.

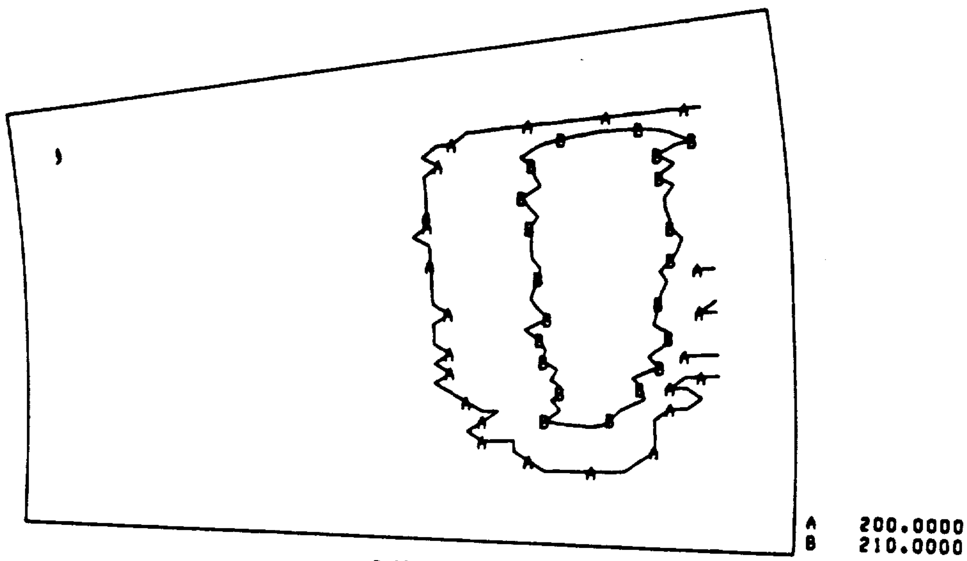

BASELINE

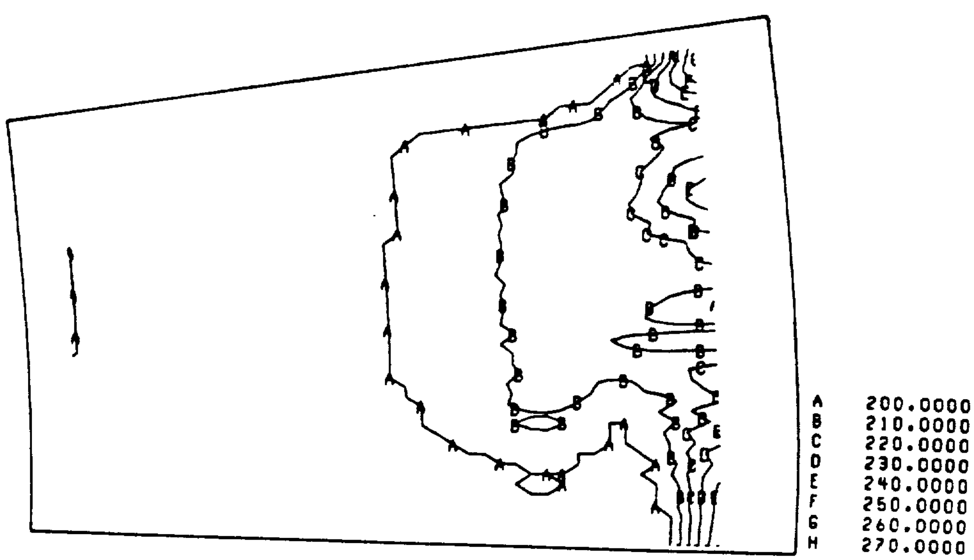

ENHANCED

(d) STATION 7.

FIGURE 30. - CONTINUED.

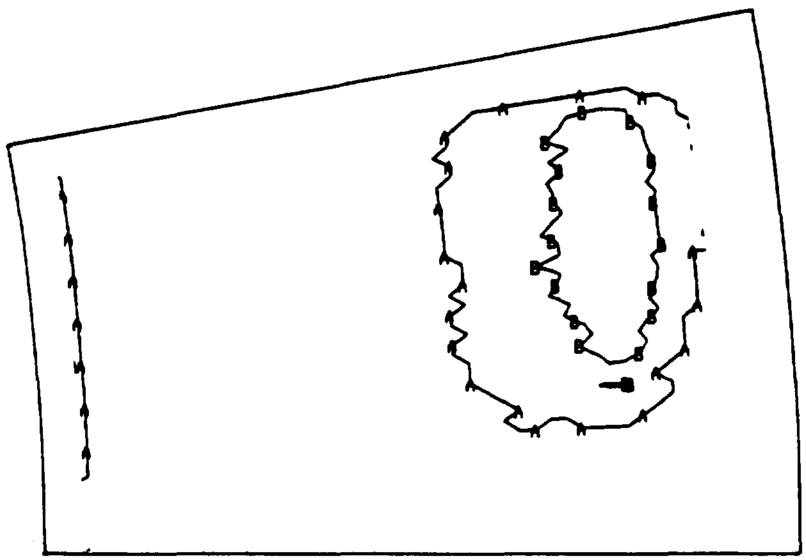

A	200.0000
B	210.0000
C	220.0000

BASELINE

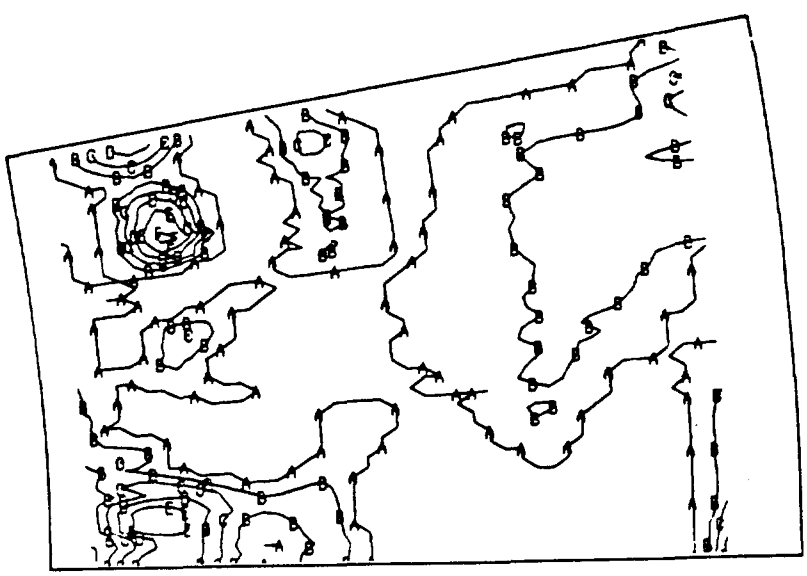

A	200.0000
B	210.0000
C	220.0000
D	230.0000
E	240.0000
F	250.0000

ENHANCED

(e) STATION 8.

FIGURE 30. - CONCLUDED.

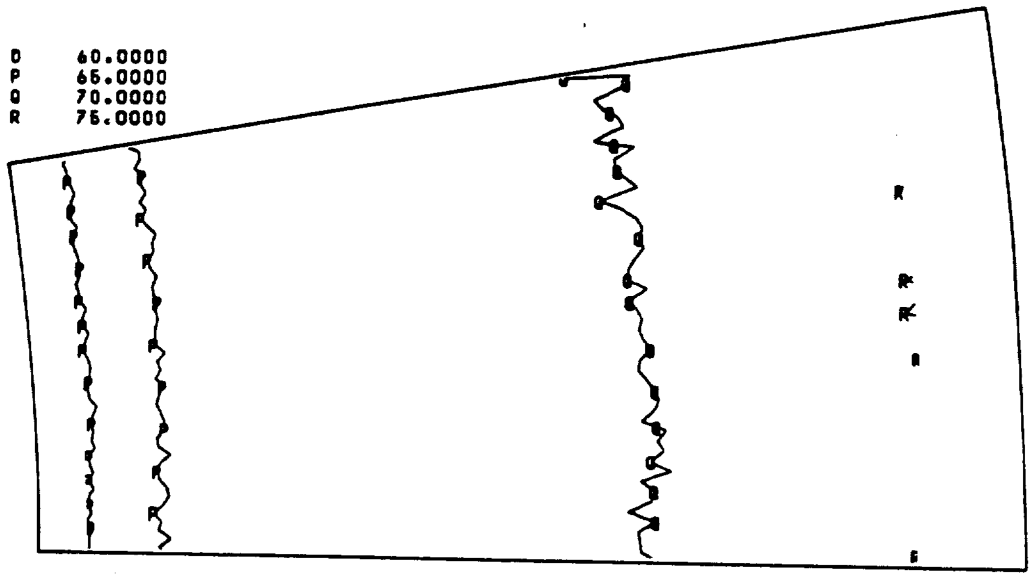

BASELINE

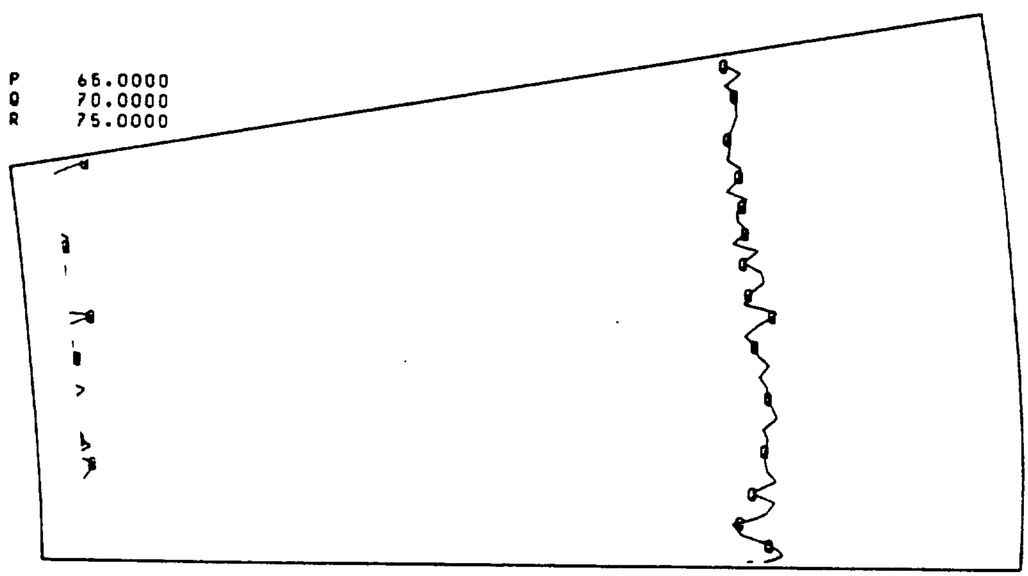

ENHANCED

(a) STATION 1.

FIGURE 31. - RELATIVE FLOW ANGLES, CROSS CHANNEL.

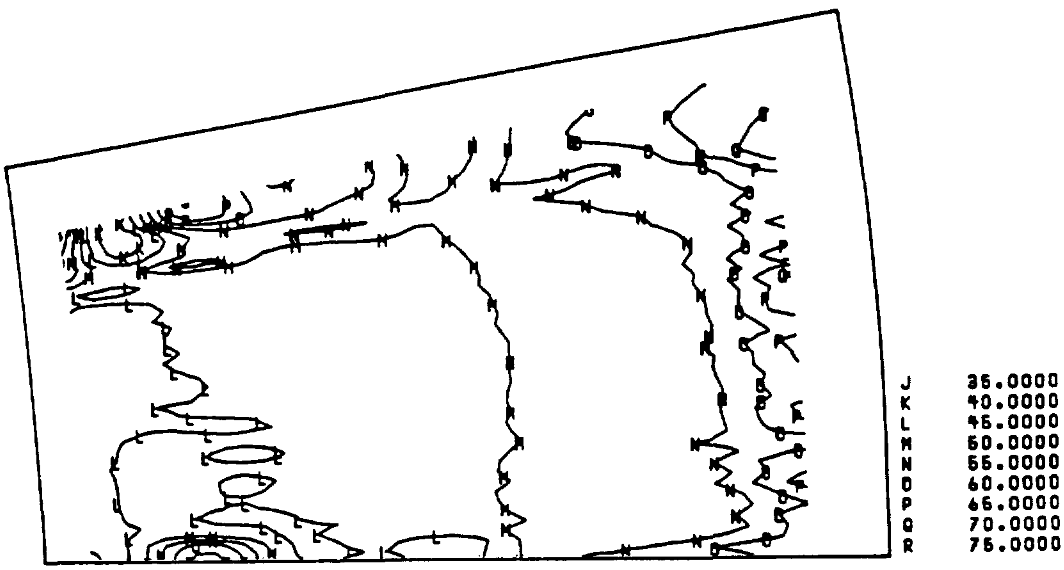

BASELINE

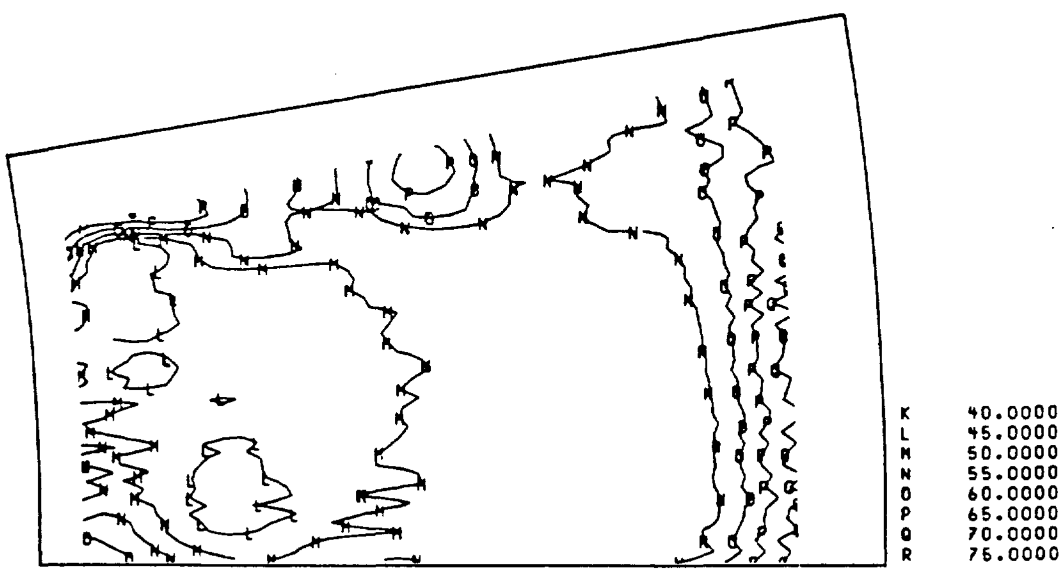

ENHANCED

(b) STATION 5.

FIGURE 31. - CONTINUED.

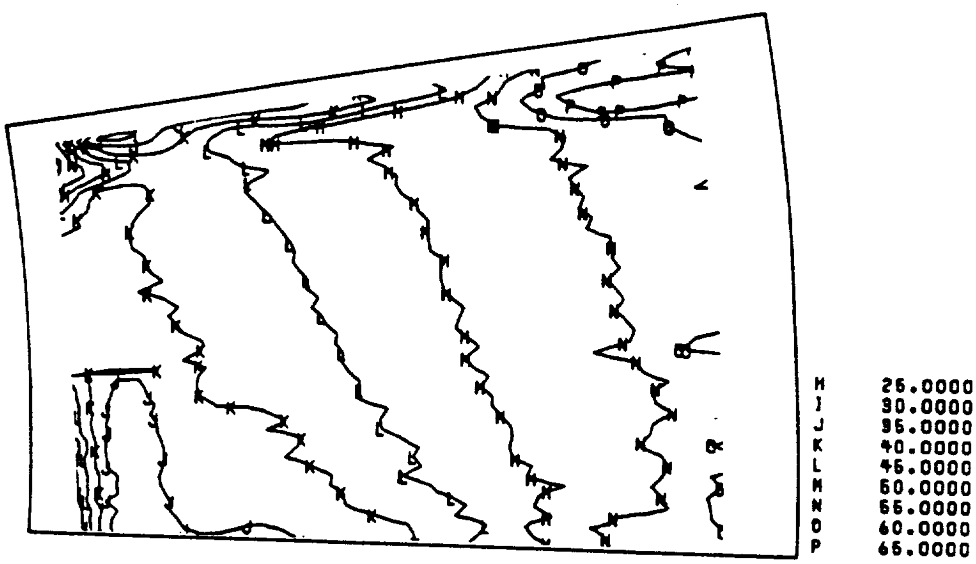

BASELINE

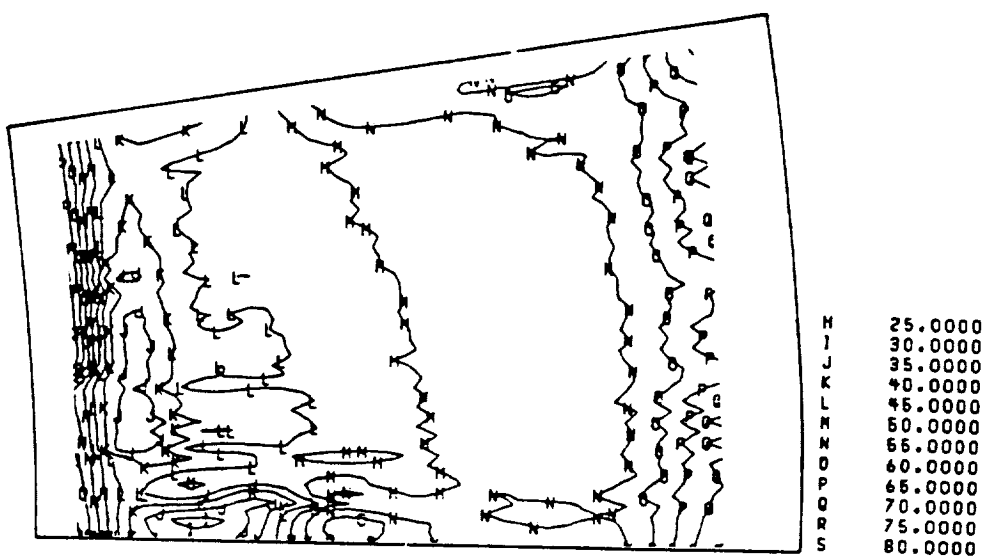

ENHANCED

(c) STATION 7.

FIGURE 31. - CONCLUDED.

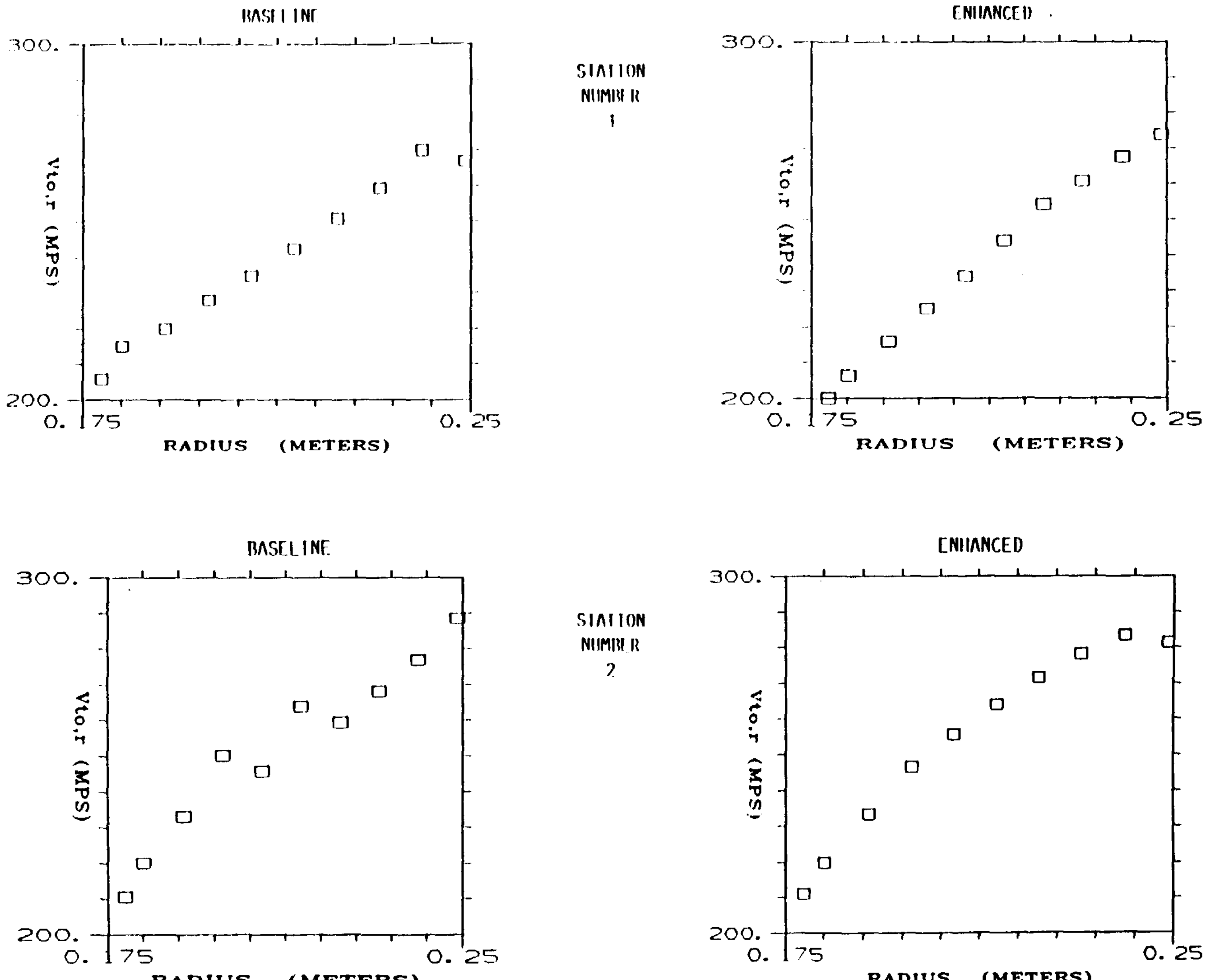

RELATIVE TOTAL VELOCITY ST 1,2

FIGURE 32a.

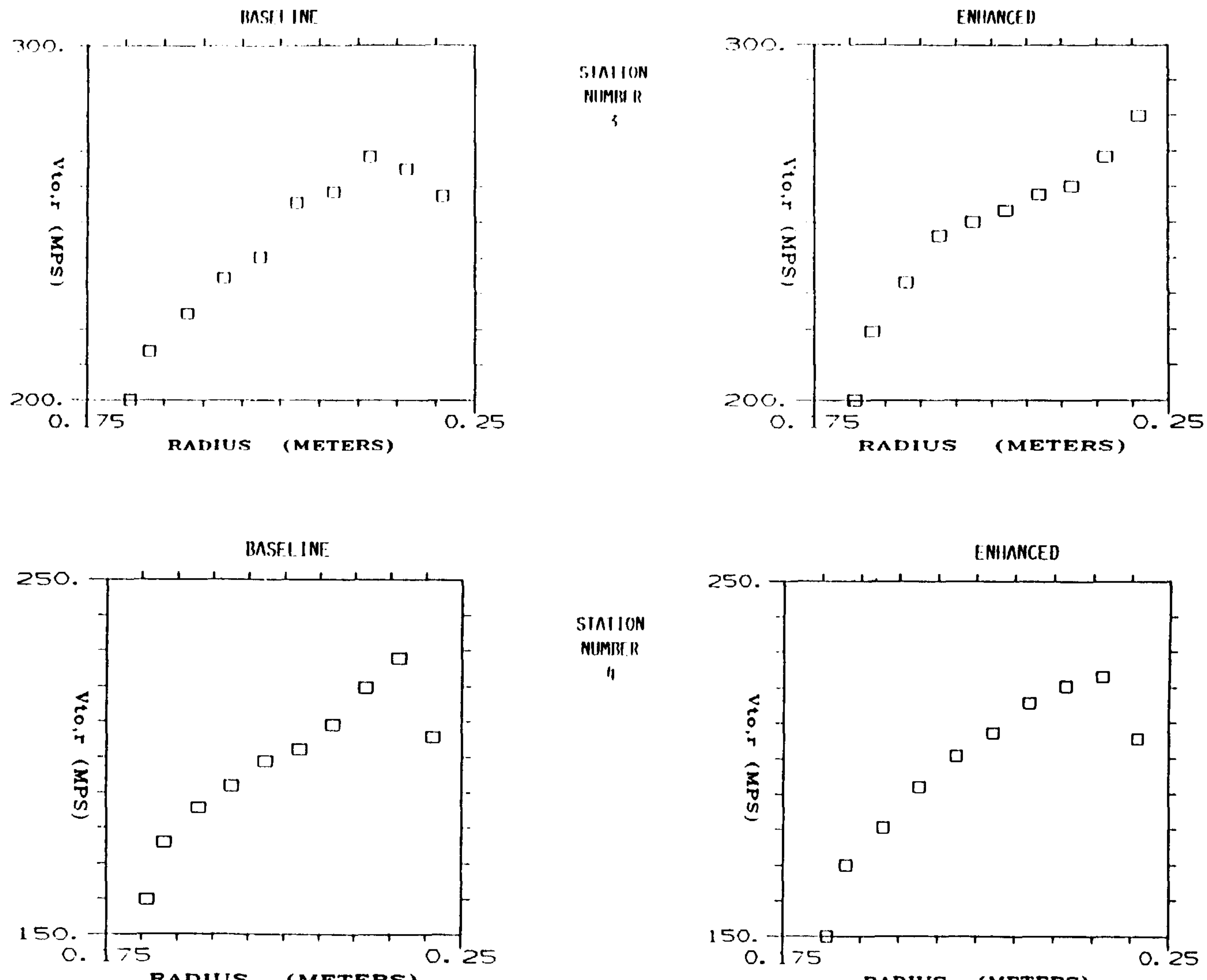

RELATIVE TOTAL VELOCITY ST 3,4

FIGURE 32b.

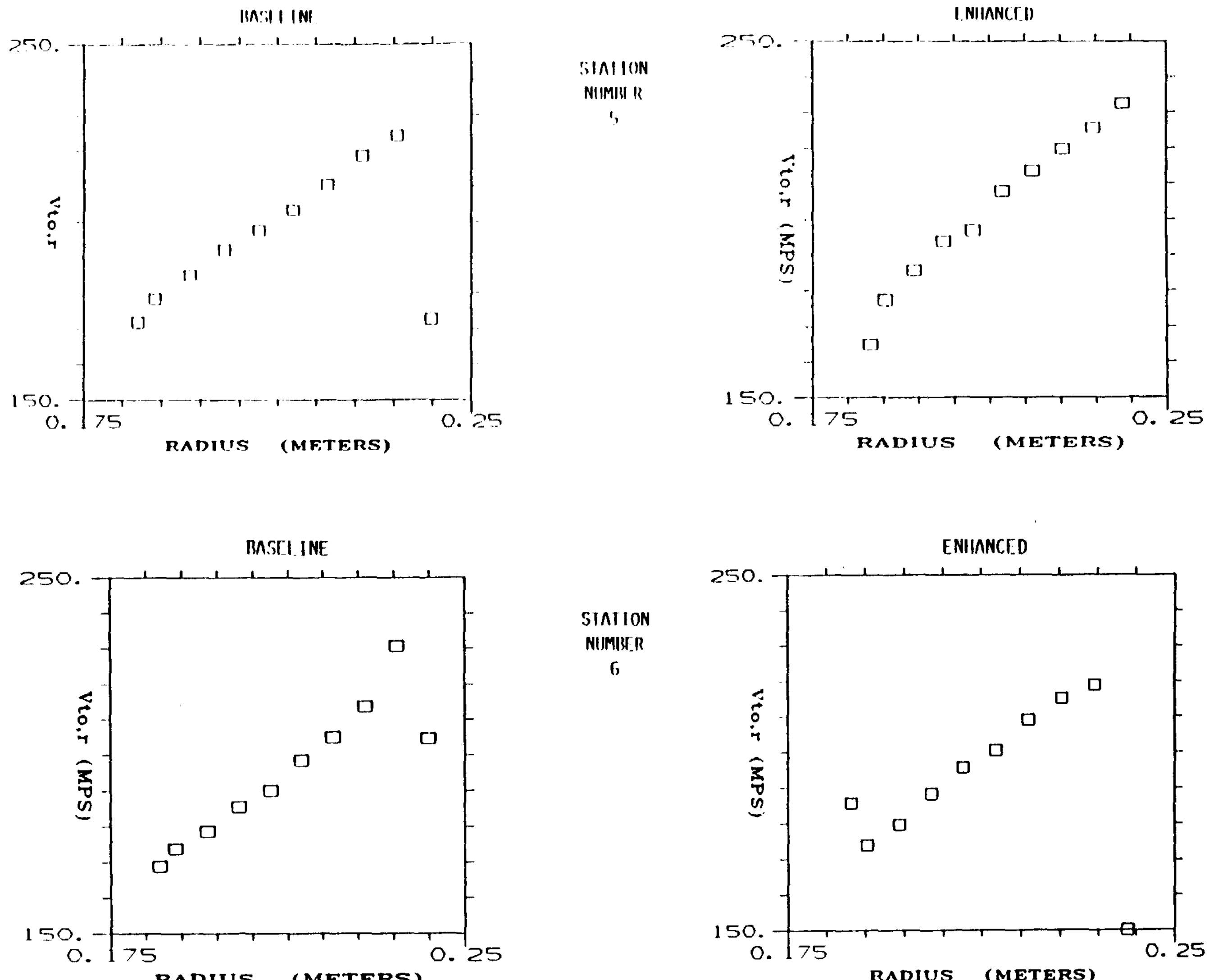

RELATIVE TOTAL VELOCITY ST 5,6

FIGURE 32c.

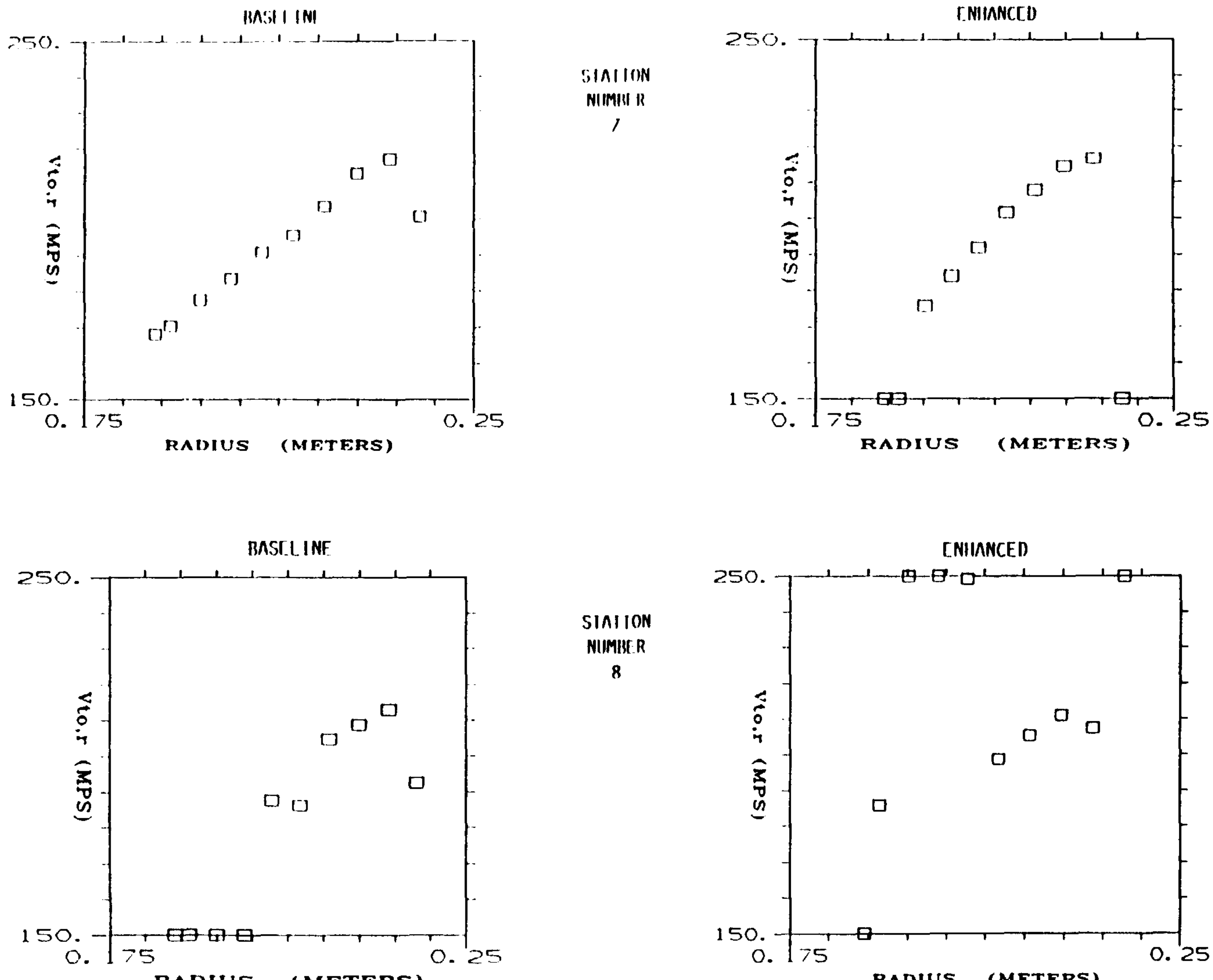

RELATIVE TOTAL VELOCITY ST 7,8

FIGURE 32d.

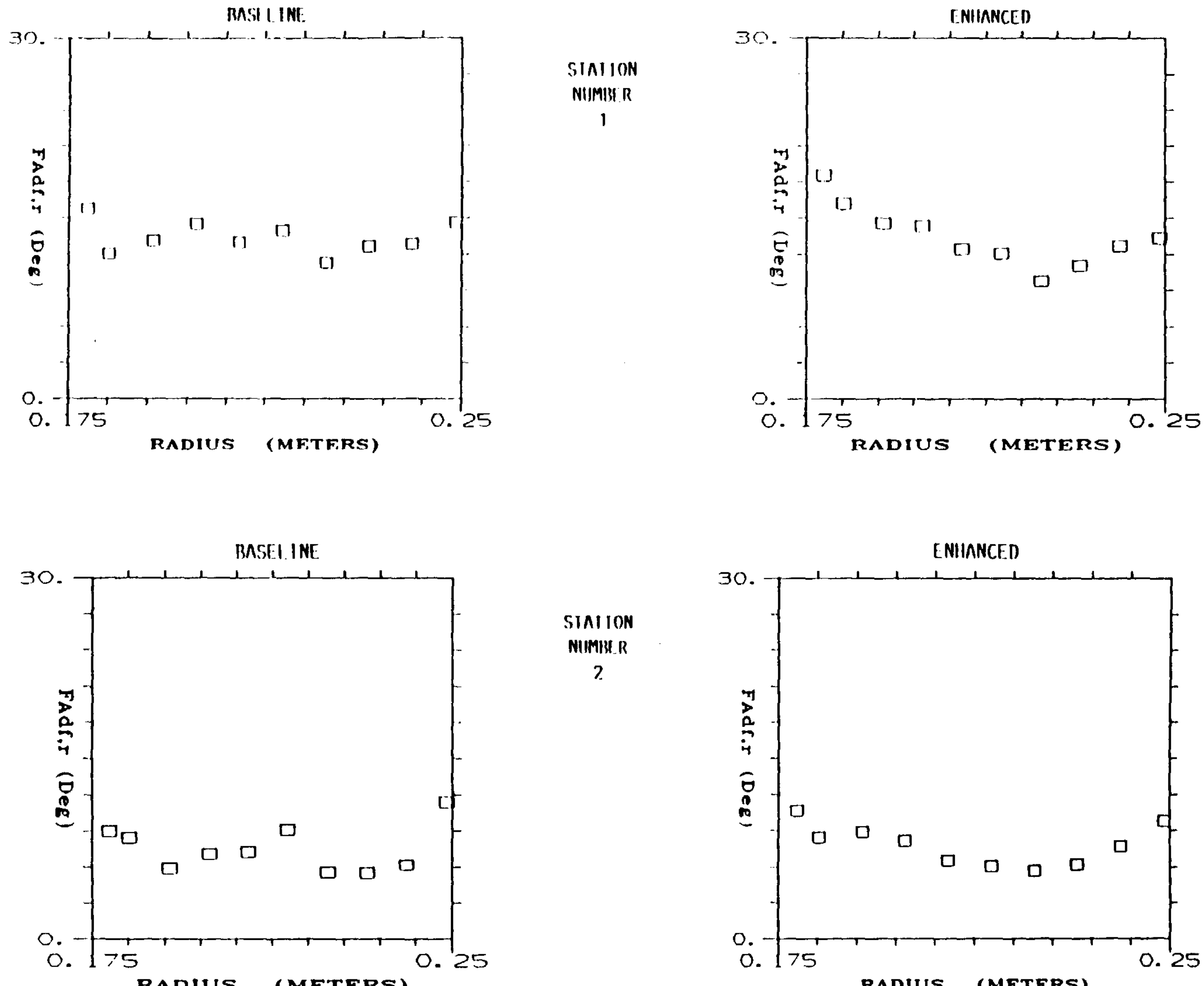

REL FLOW ANGLE DIFFERENCES ST 1,2

FIGURE 33a.

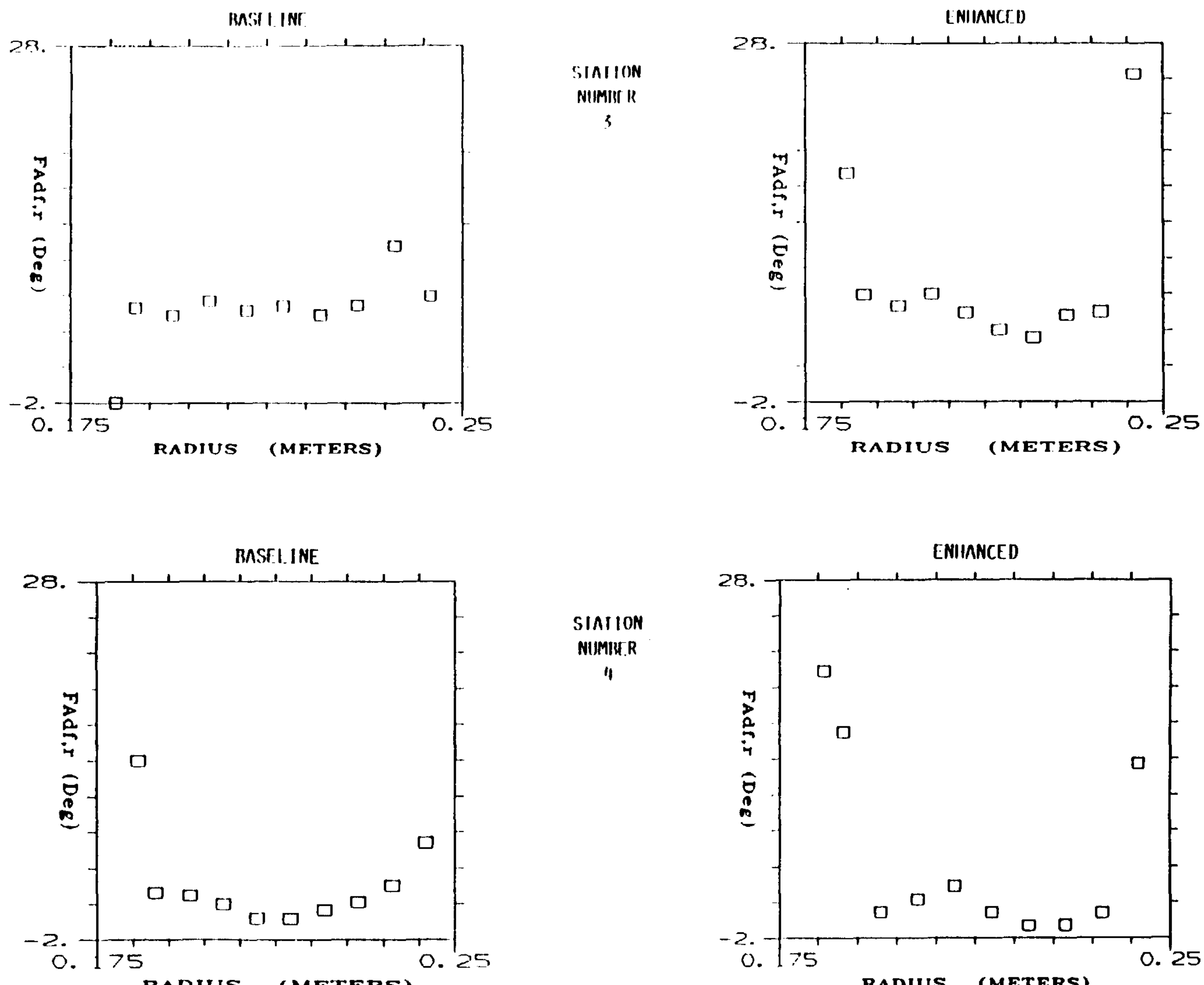

REL FLOW ANGLE DIFFERENCES ST 3,4

FIGURE 33b.

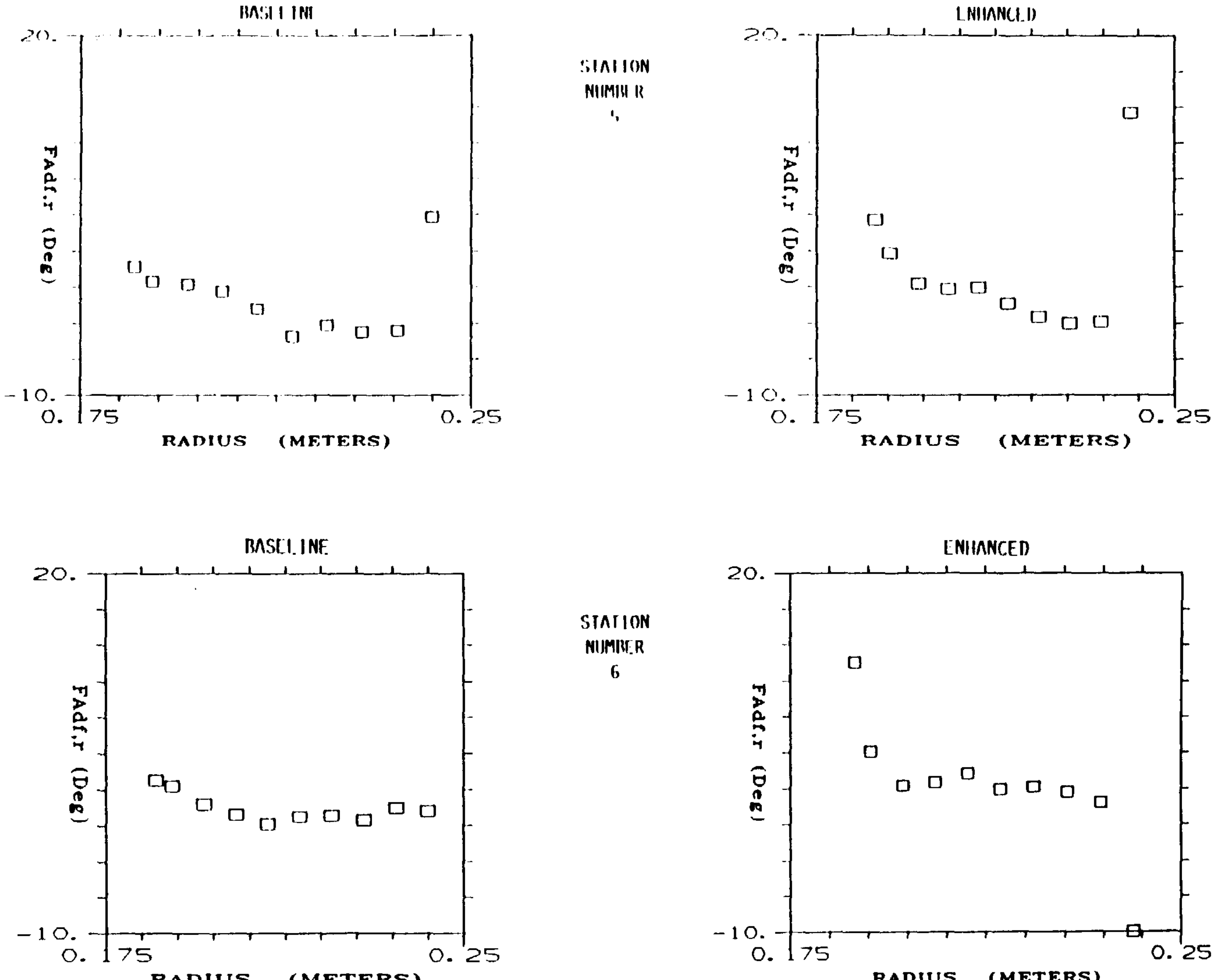

REL FLOW ANGLE DIF ST 5,6

FIGURE 33c.

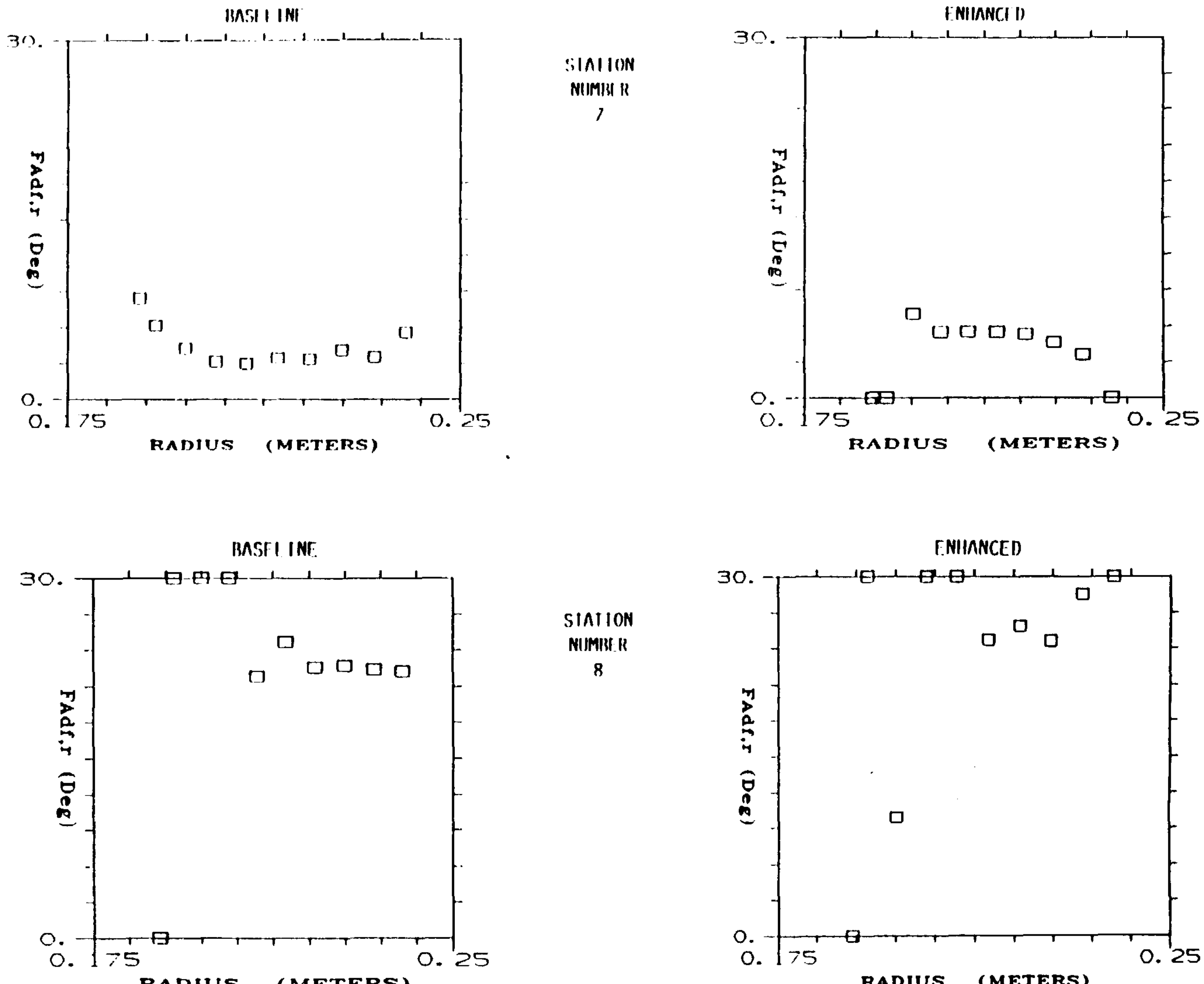

REL FLOW ANGLE DIF ST 7,8

FIGURE 33d.

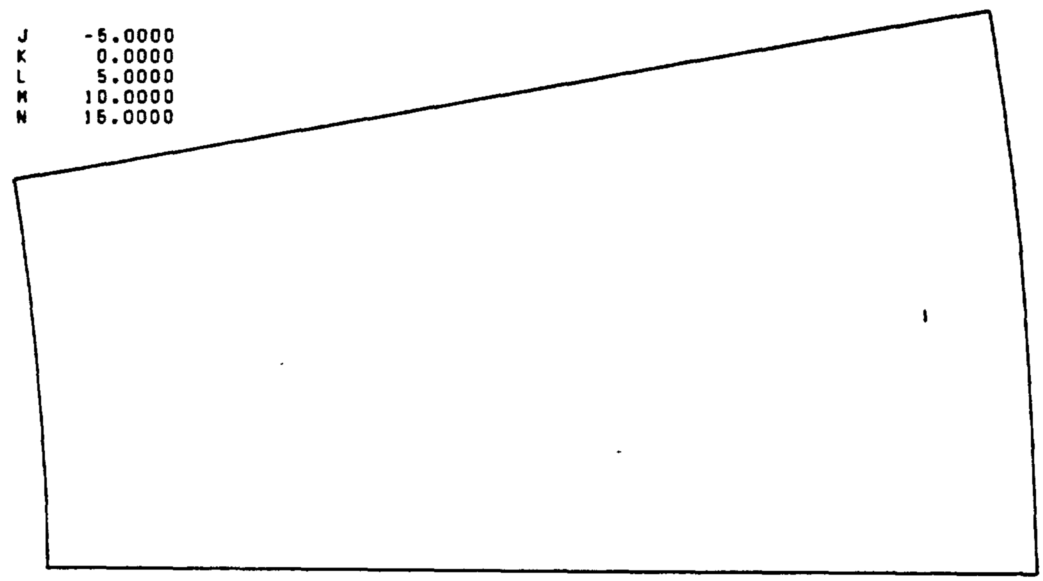

BASELINE

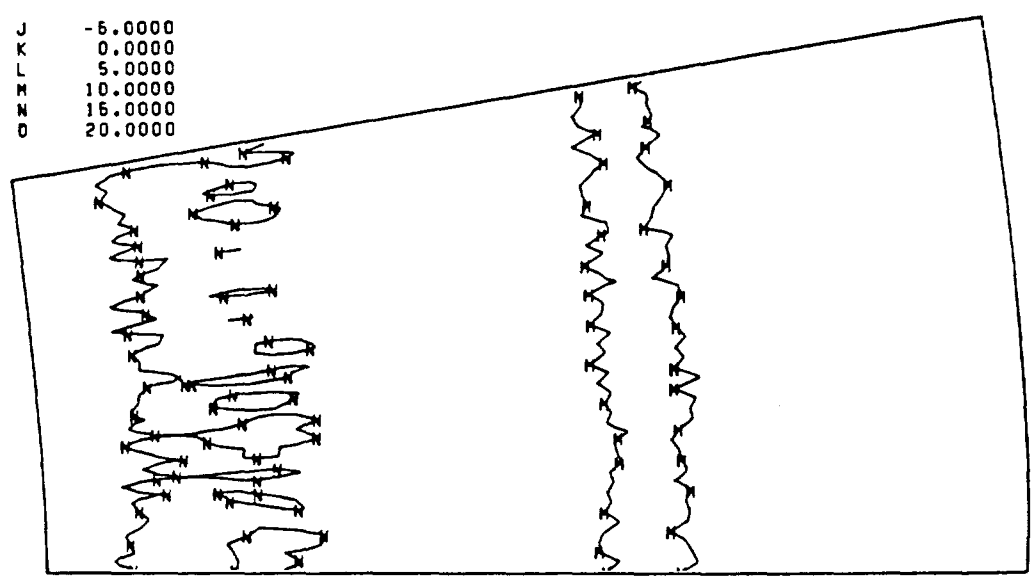

ENHANCED

(a) STATION 1.

FIGURE 34. - RELATIVE FLOW ANGLE/GRID DIFFERENCE, CROSS CHANNEL.

BASELINE

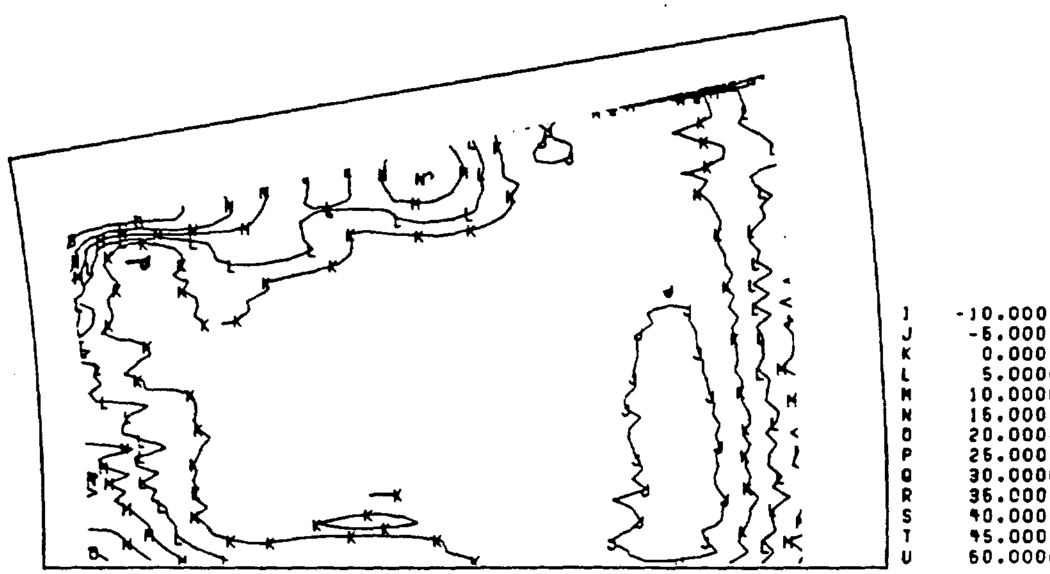

ENHANCED

(b) STATION 5.

FIGURE 34. - CONTINUED.

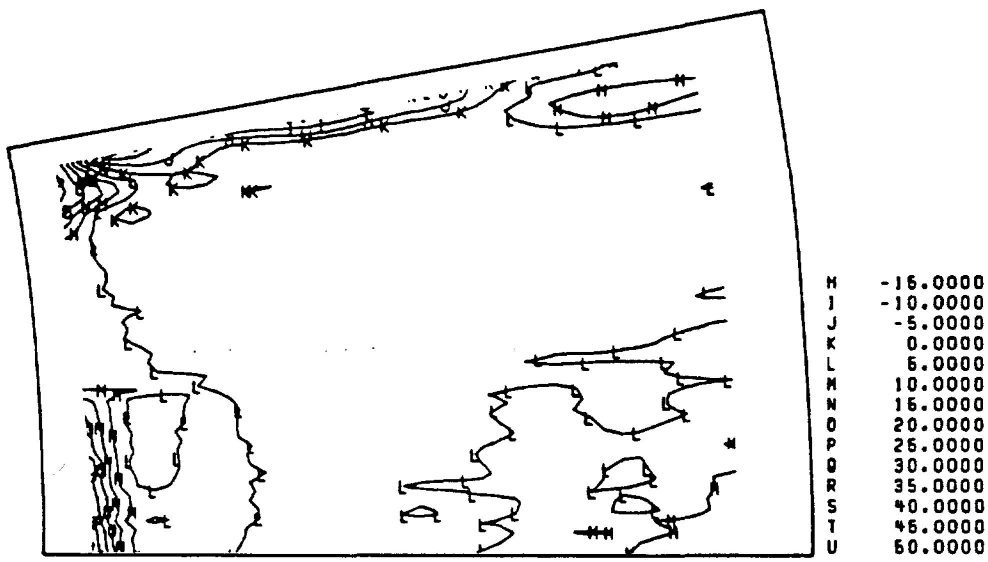

BASELINE

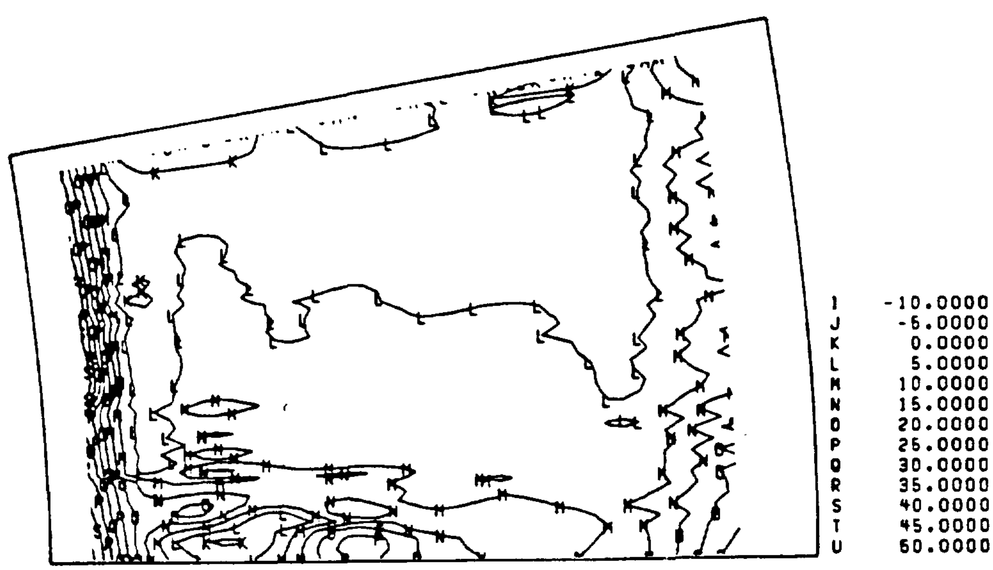

ENHANCED

(c) STATION 7.

FIGURE 34. - CONCLUDED.

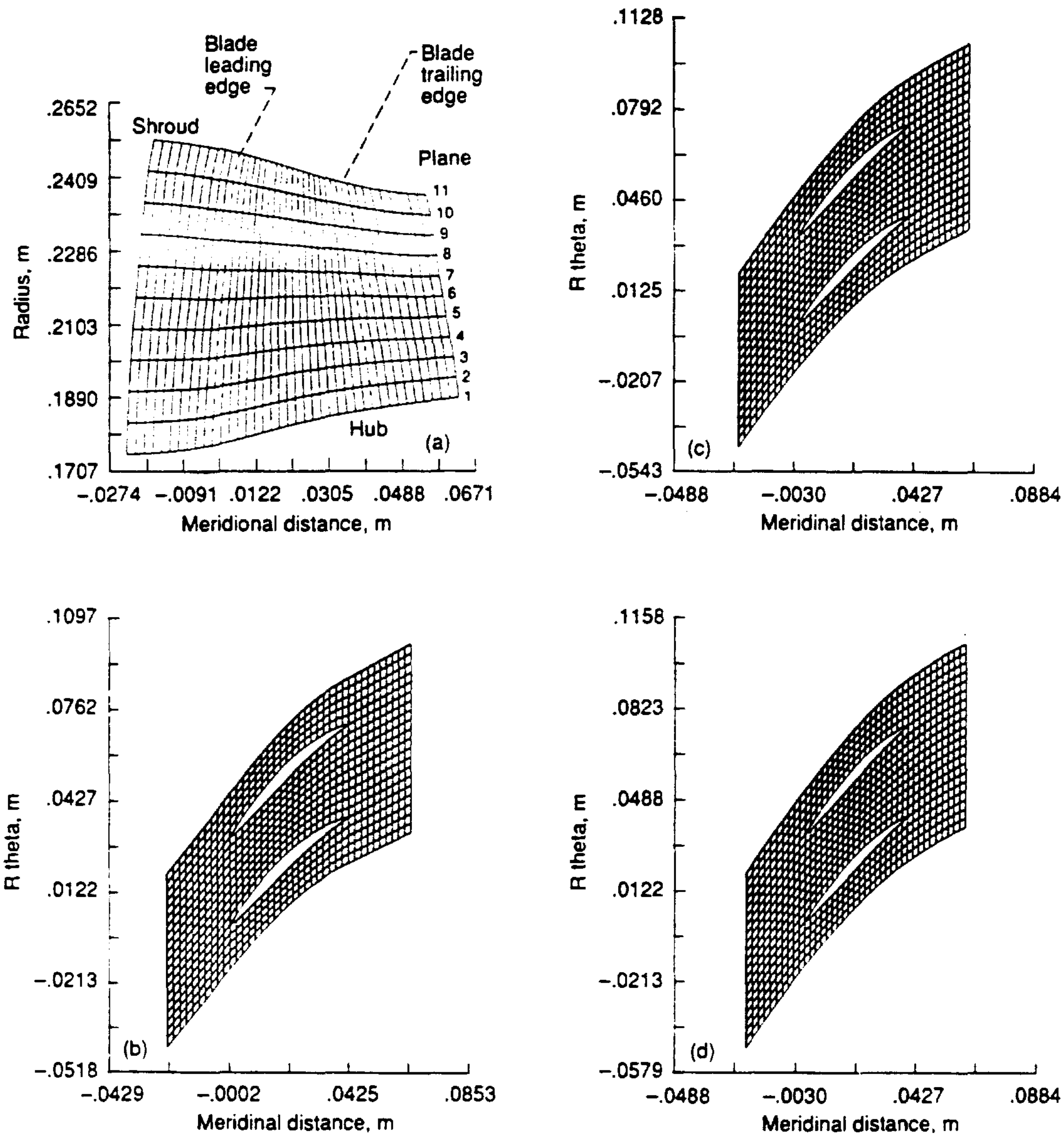
Blade leading edge
Blade trailing edge
Shroud
Plane
11
10
9
8
7
6
5
4
3
2
1
Hub
(a)
.2652
.2409
.2286
.2103
.1890
.1707
Radius, m
−.0274 −.0091 .0122 .0305 .0488 .0671
Meridional distance, m
.1128
.0792
.0460
.0125
−.0207
−.0543
R theta, m
(c)
−.0488 −.0030 .0427 .0884
Meridinal distance, m
.1097
.0762
.0427
.0122
−.0213
−.0518
R theta, m
(b)
−.0429 −.0002 .0425 .0853
Meridinal distance, m
.1158
.0823
.0488
.0122
−.0213
−.0579
R theta, m
(d)
−.0488 −.0030 .0427 .0884
Meridinal distance, m

Figure 35.

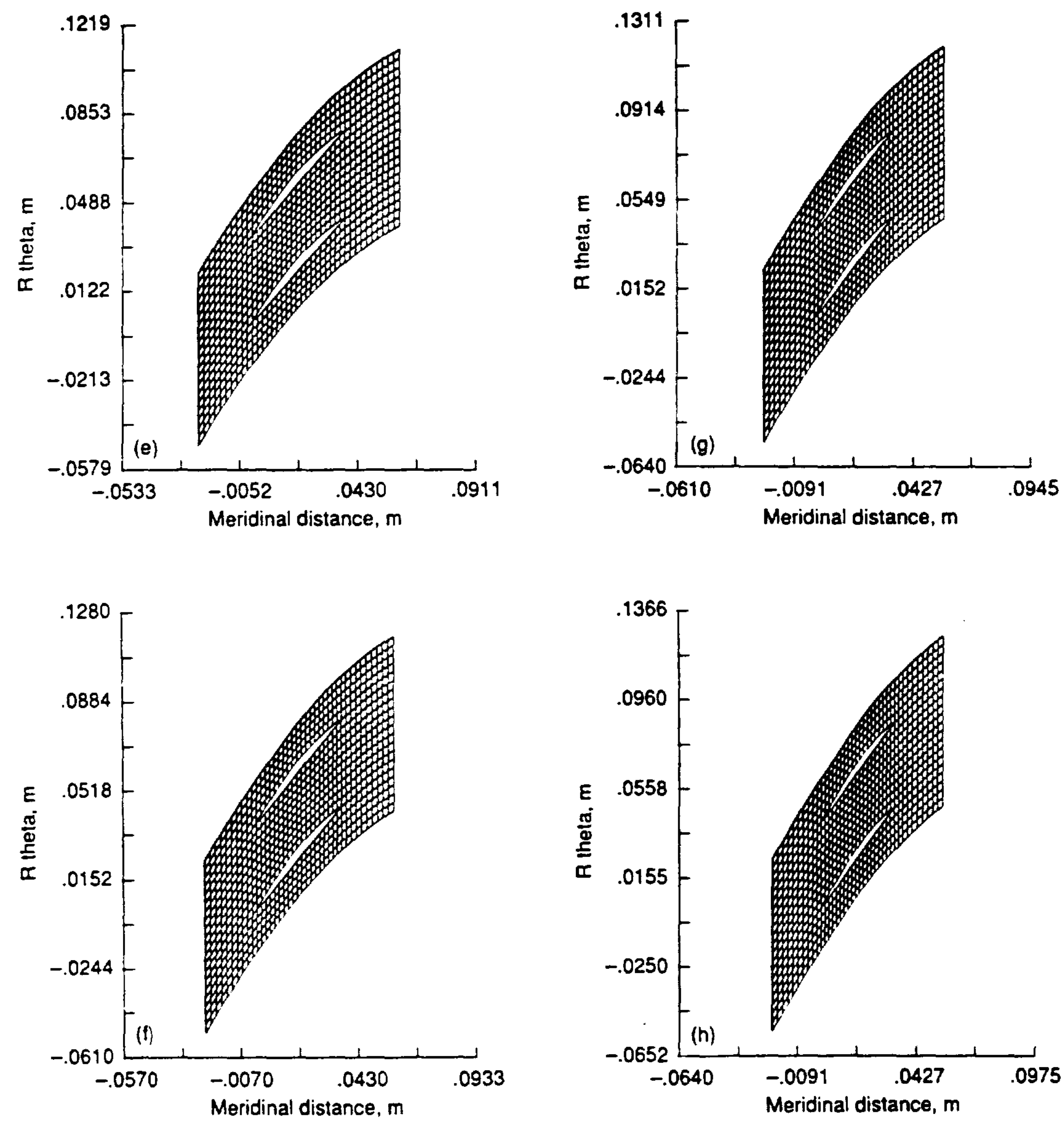

Figure 35.—Continued.

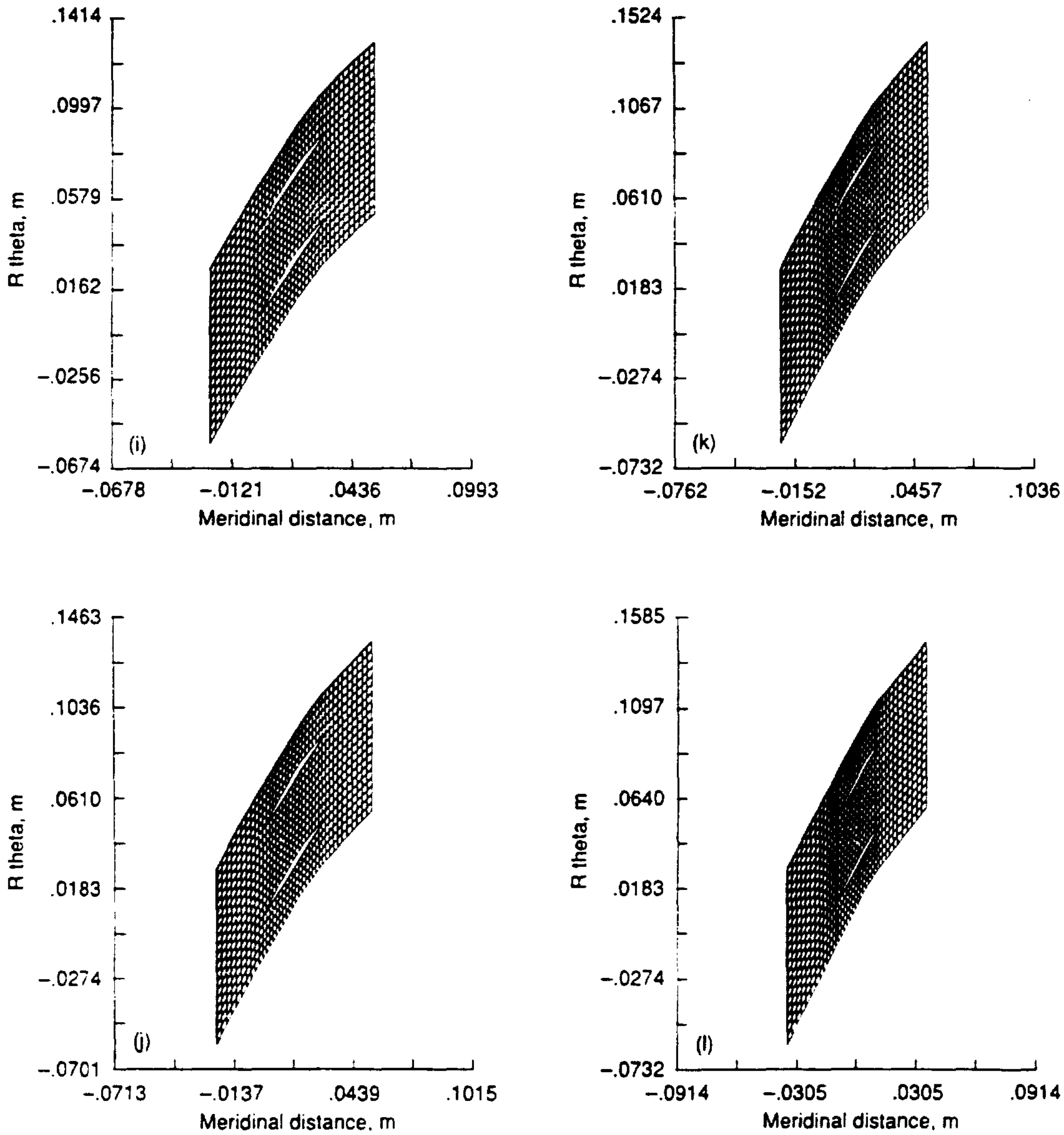

Figure 35.—Concluded.

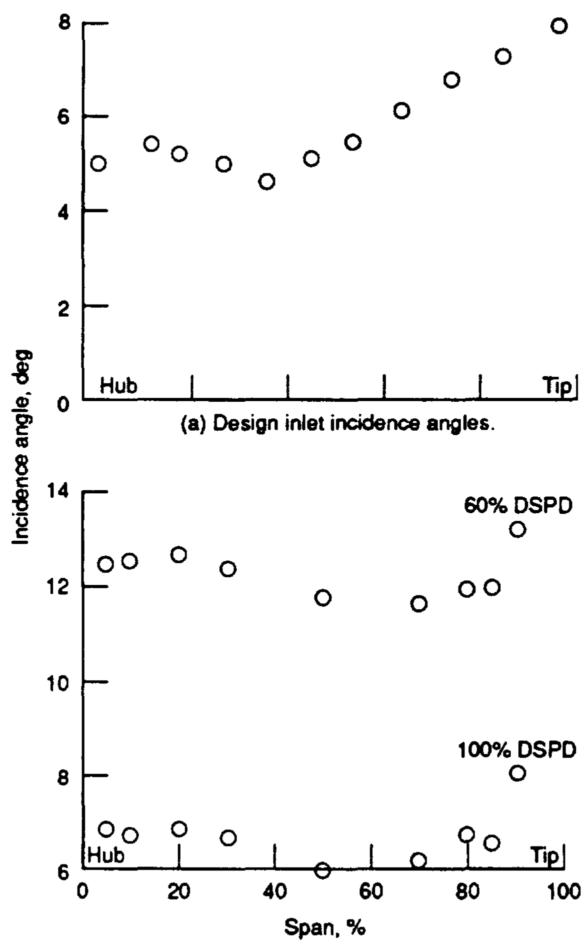

(a) Design inlet incidence angles.

(b) Peak efficiency incidence angles.

Figure 36.—Inlet incidence angle.

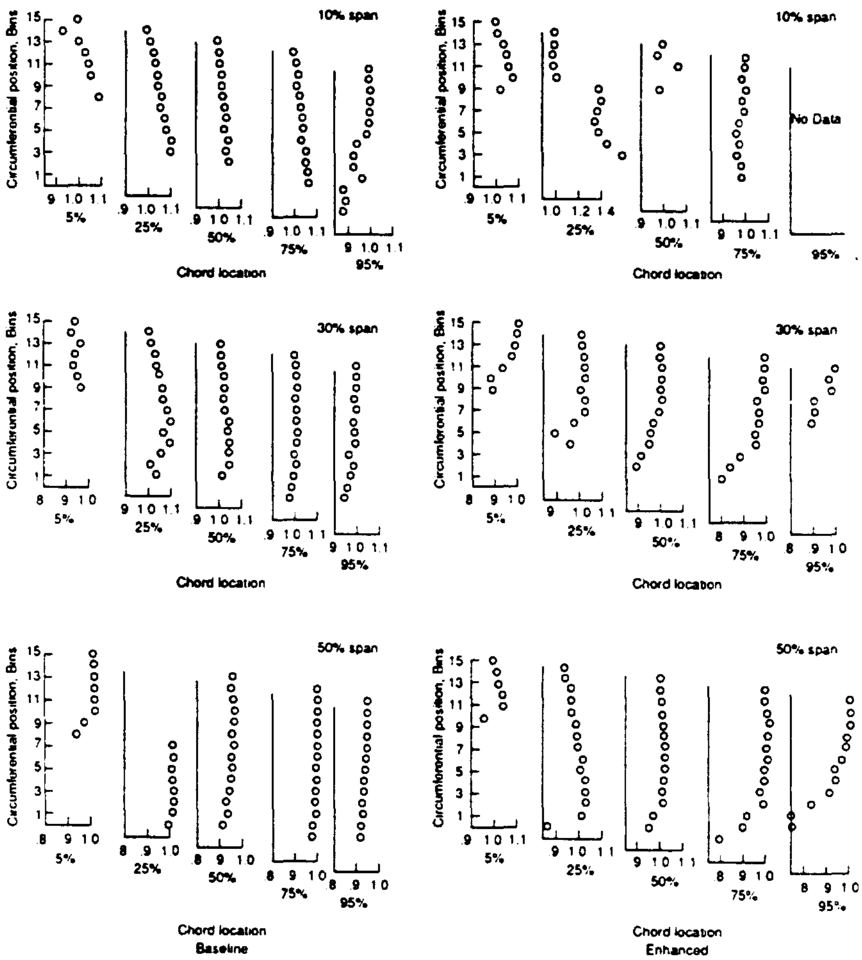

Figure 37 —Non-dimensionalized blade suction surface relative total velocity profiles, $V/V_{B_{in}:5}$

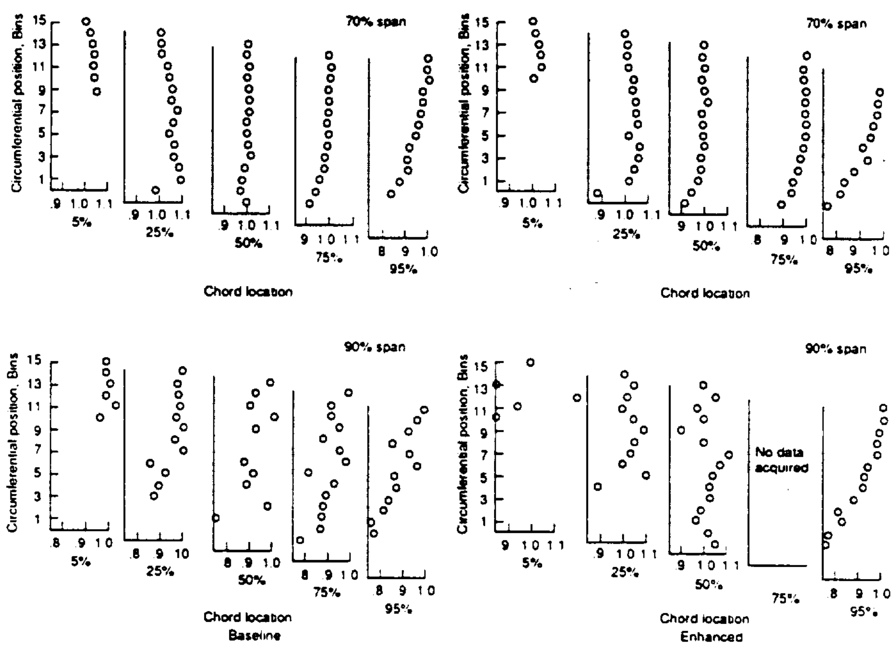

Figure 37 —Concluded.

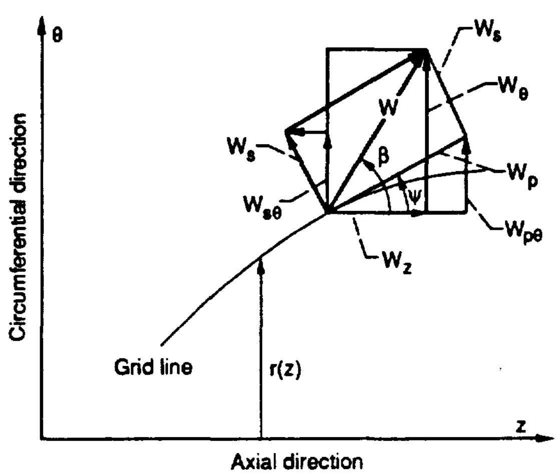

(a) Blade-to-blade view.

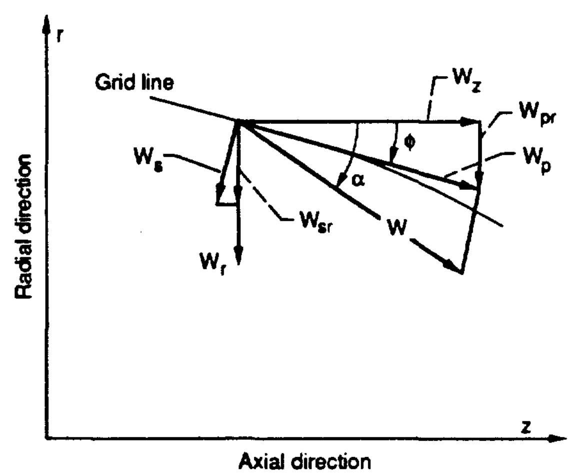

(b) Meridional view.

Figure 38.—Flow deviation calculation nomenclature.

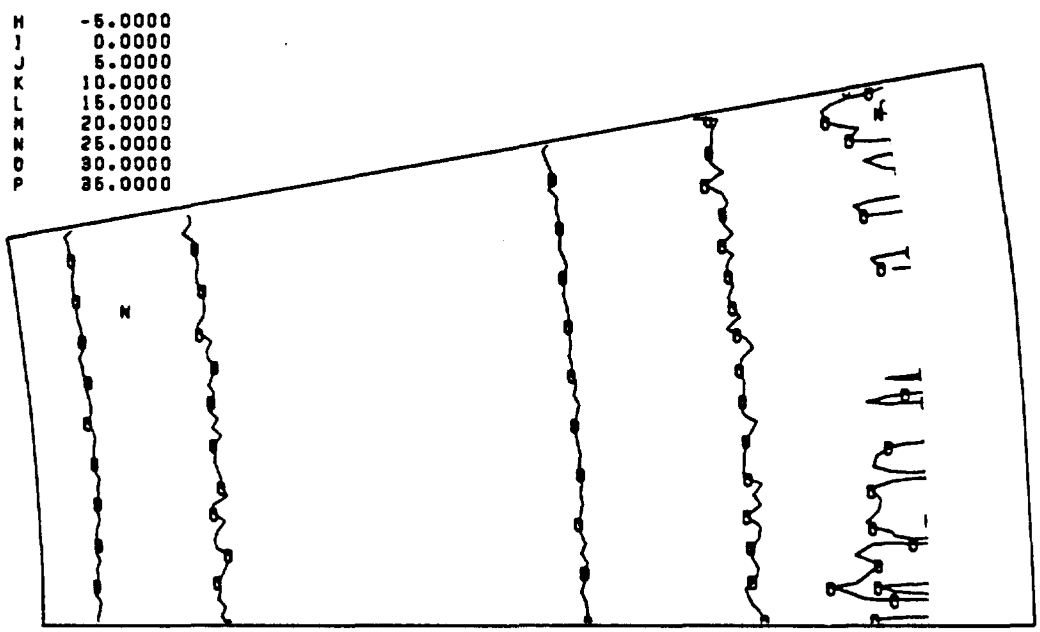

BASELINE

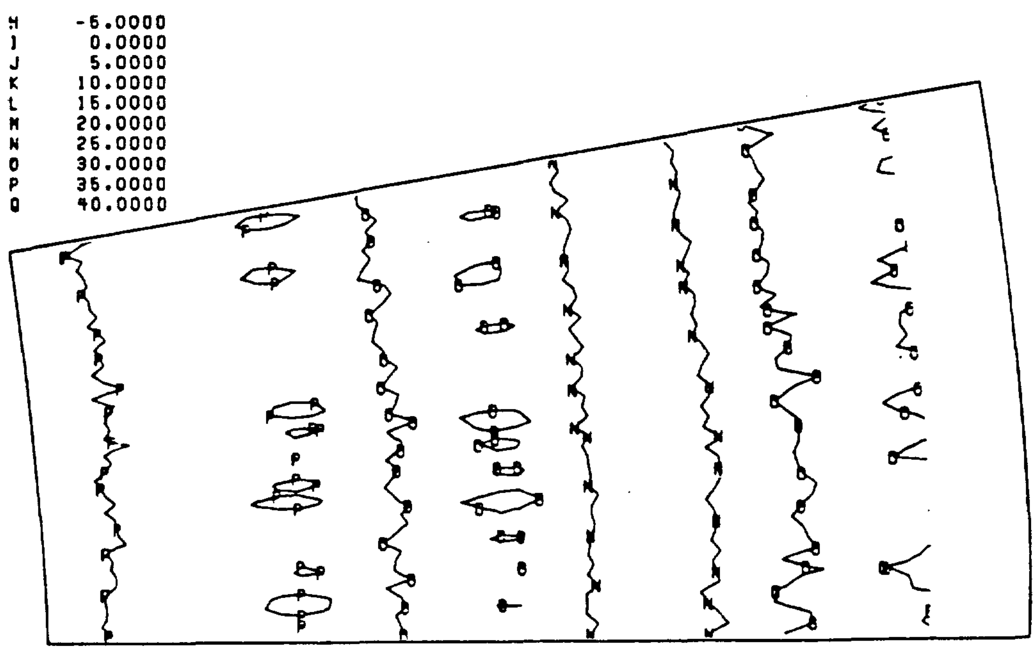

ENHANCED

(a) STATION 1.

FIGURE 39. - DEVIATION VELOCITIES, CROSS CHANNEL.

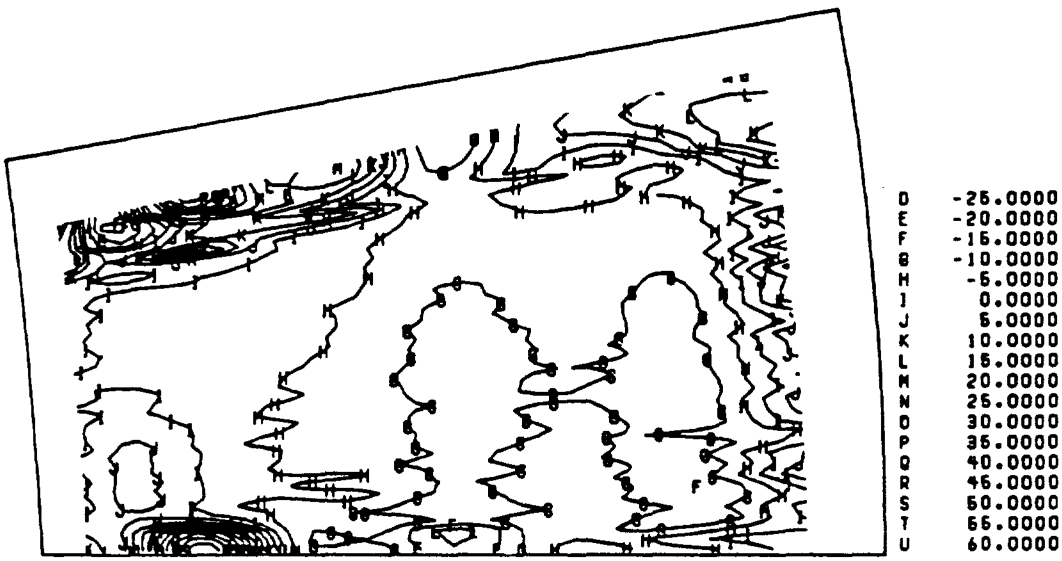

BASELINE

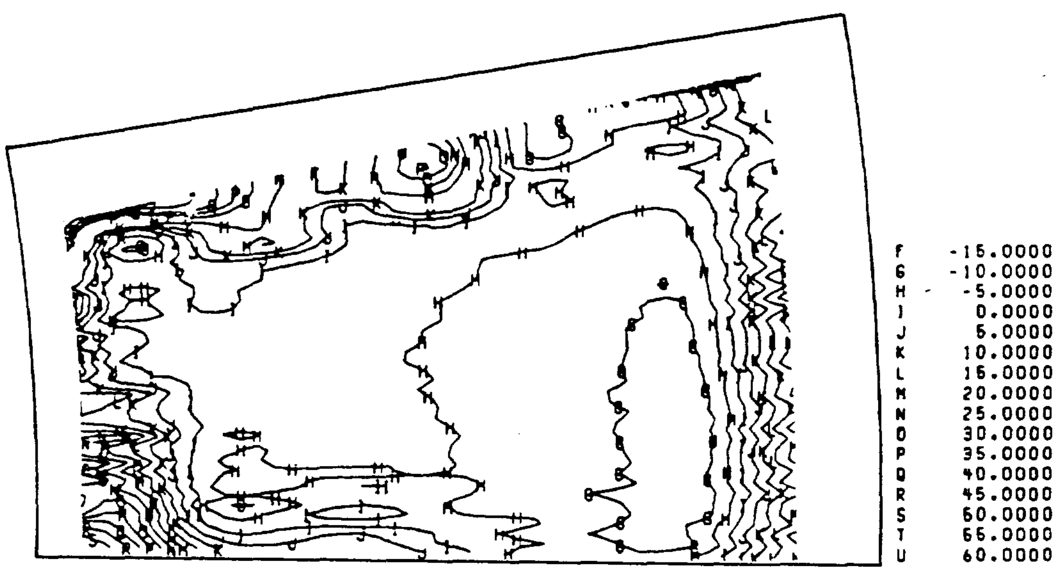

ENHANCED

(b) STATION 5.

FIGURE 39. - CONTINUED.

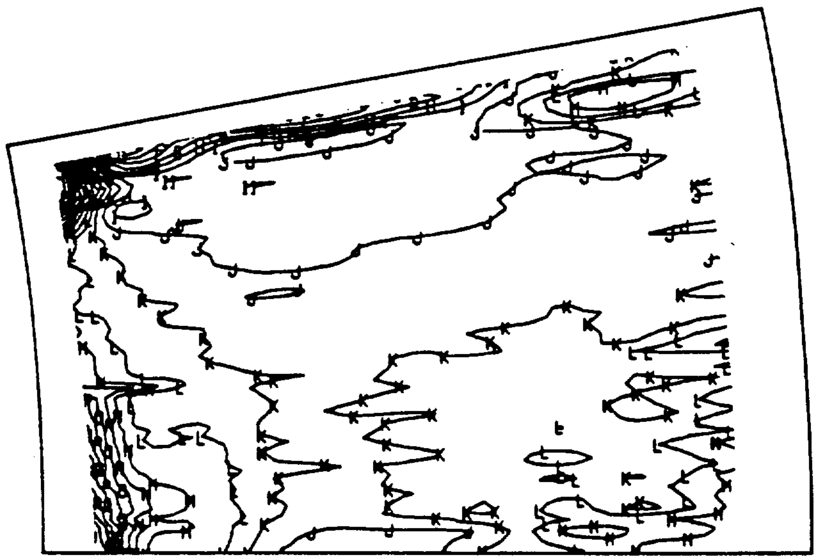

C	-30.0000
D	-25.0000
E	-20.0000
F	-15.0000
G	-10.0000
H	-5.0000
I	0.0000
J	5.0000
K	10.0000
L	15.0000
M	20.0000
N	25.0000
O	30.0000
P	35.0000
Q	40.0000
R	45.0000
S	50.0000
T	55.0000
U	60.0000

BASELINE

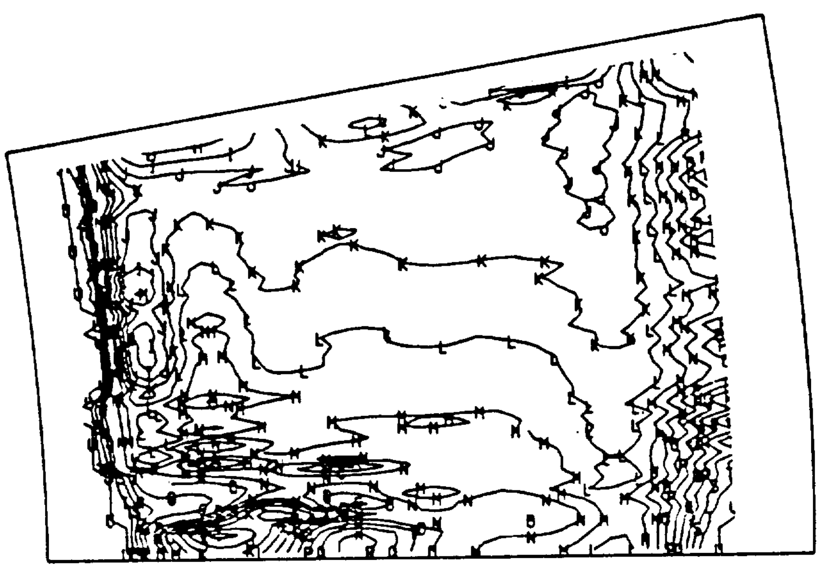

F	-15.0000
G	-10.0000
H	-5.0000
I	0.0000
J	5.0000
K	10.0000
L	15.0000
M	20.0000
N	25.0000
O	30.0000
P	35.0000
Q	40.0000
R	45.0000
S	50.0000
T	55.0000
U	60.0000

ENHANCED

(c) STATION 7.

FIGURE 39. - CONCLUDED.

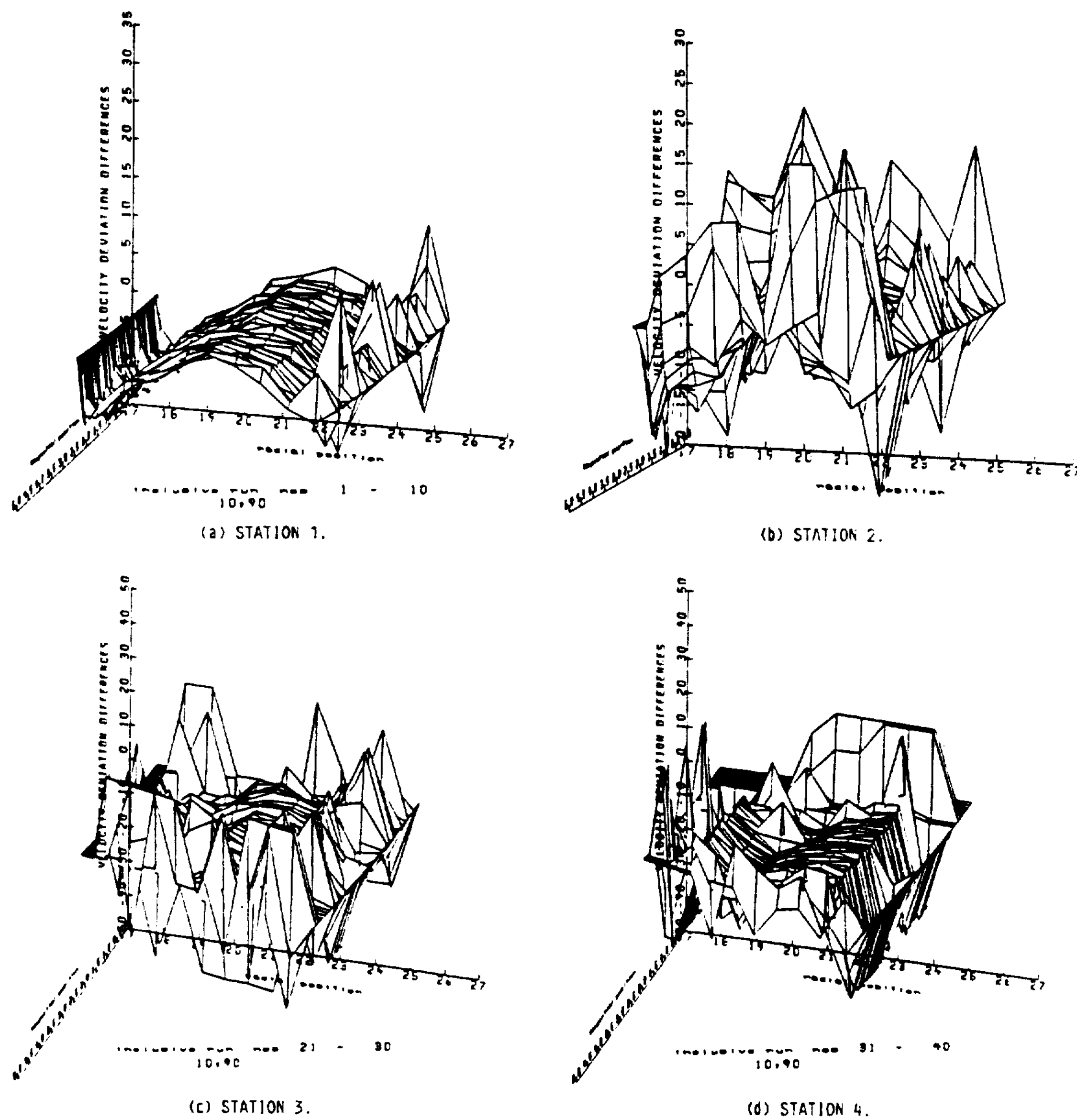

(a) STATION 1.

(b) STATION 2.

(c) STATION 3.

(d) STATION 4.

FIGURE 40. - VELOCITY DEVIATION DIFFERENCES, MPS.

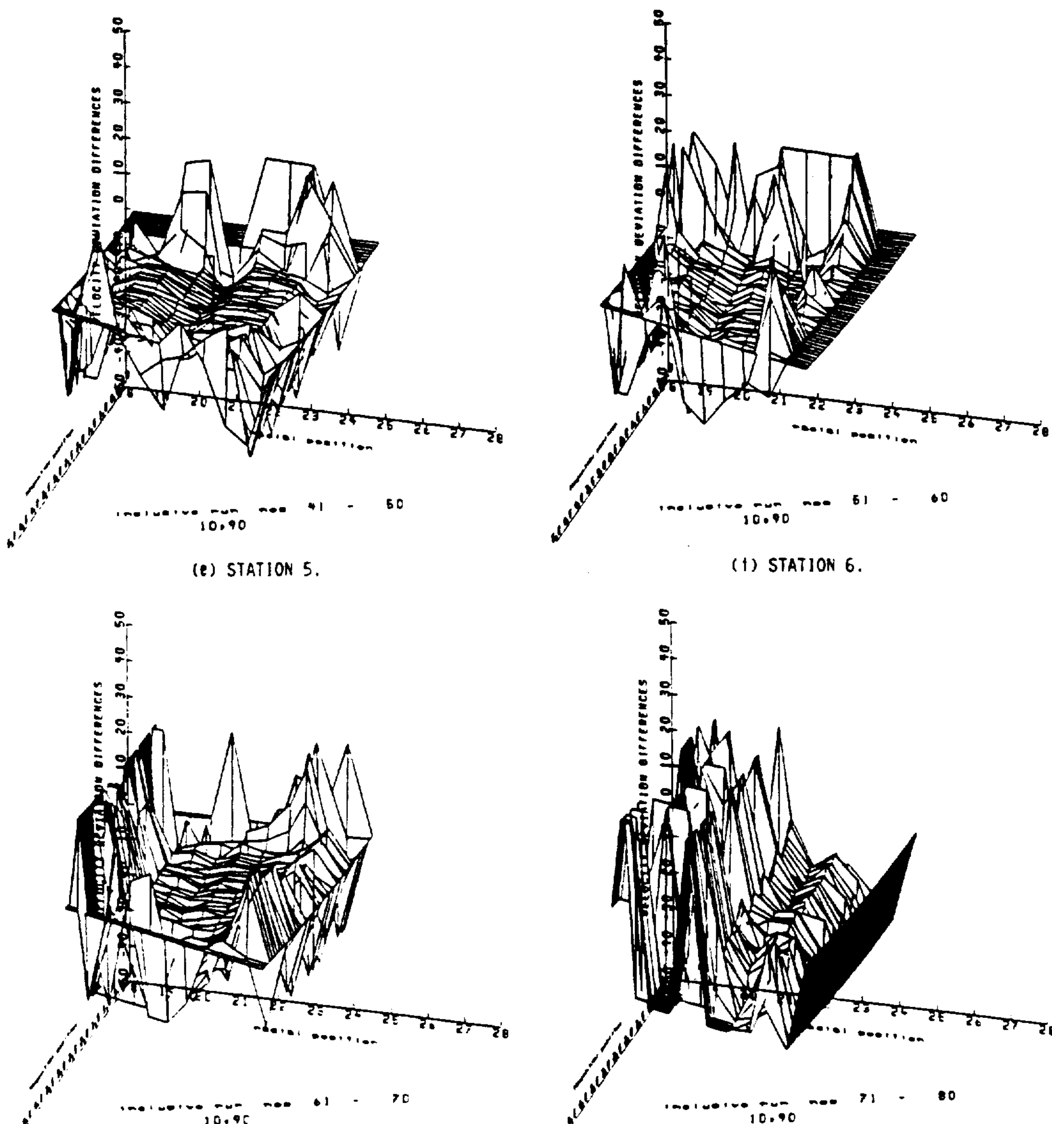

(e) STATION 5.

(f) STATION 6.

(g) STATION 7.

(h) STATION 8.

FIGURE 40. - CONCLUDED.

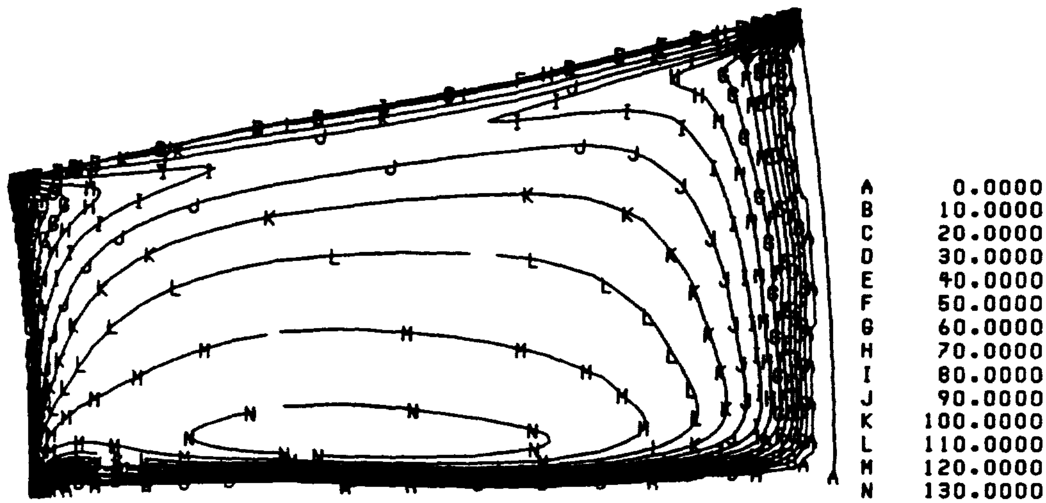

BASELINE

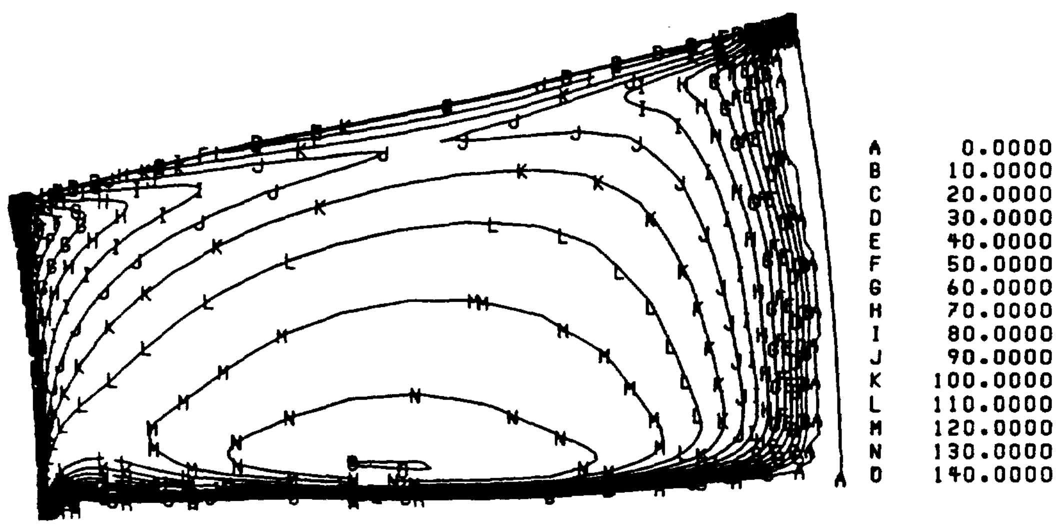

ENHANCED

(a) STATION 3.

FIGURE 41. - COMPUTED AXIAL VELOCITY, LINE PLOT.

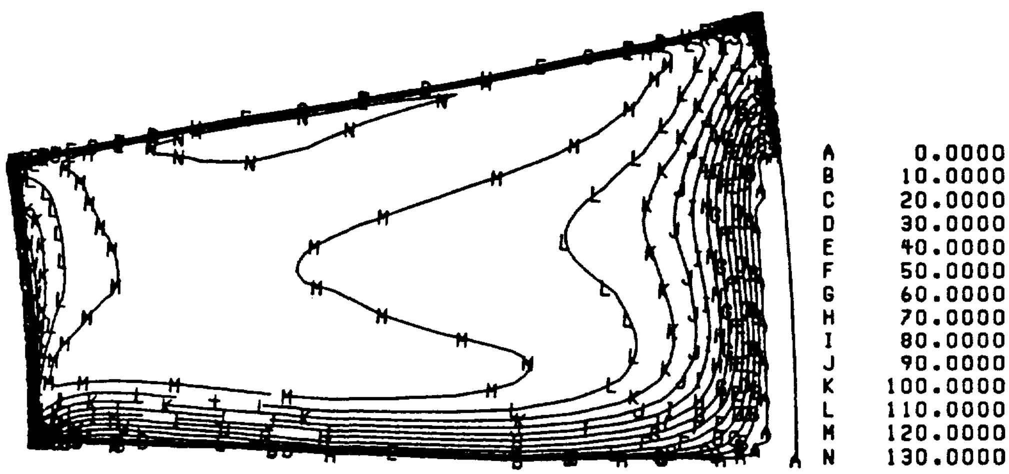

BASELINE

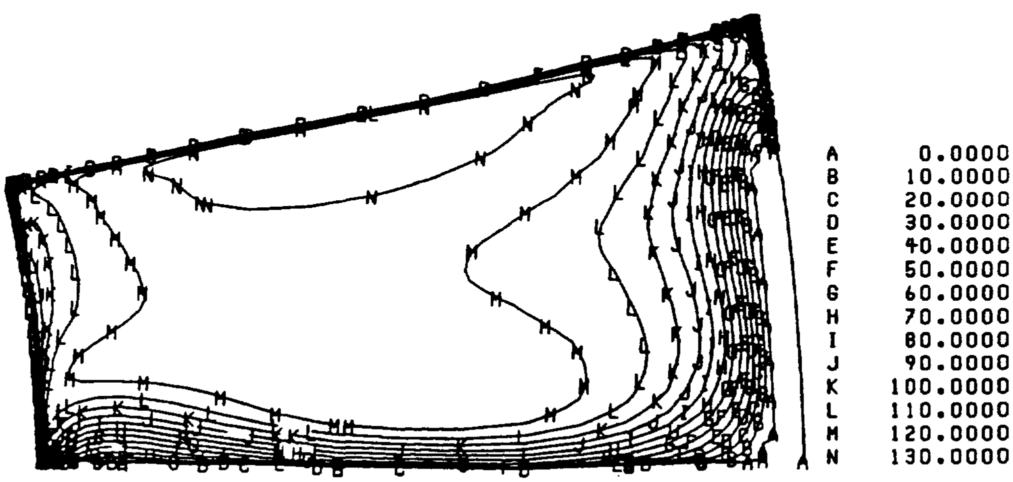

ENHANCED

(b) STATION 4.

FIGURE 41. - CONTINUED.

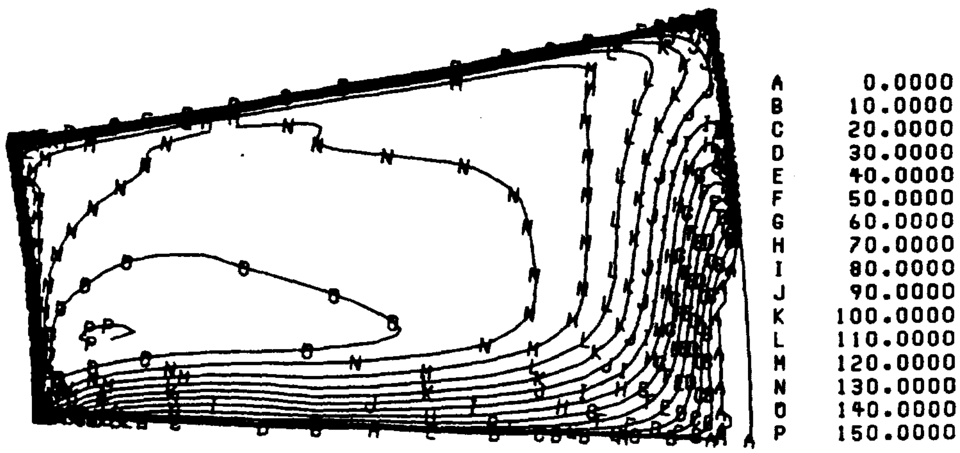

BASELINE

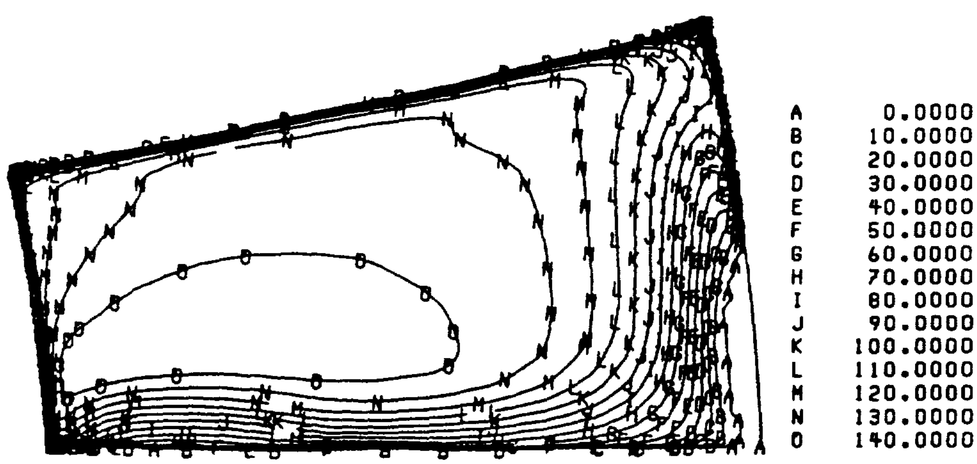

ENHANCED

(c) STATION 5.

FIGURE 41. - CONTINUED.

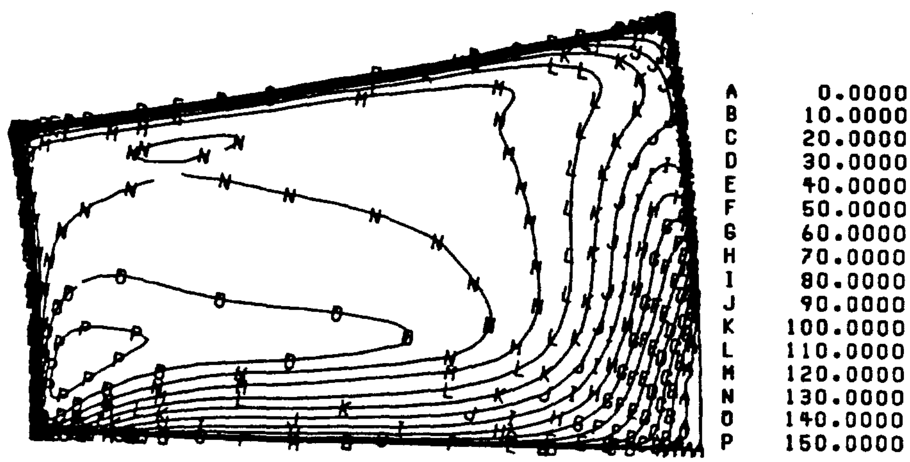

BASELINE

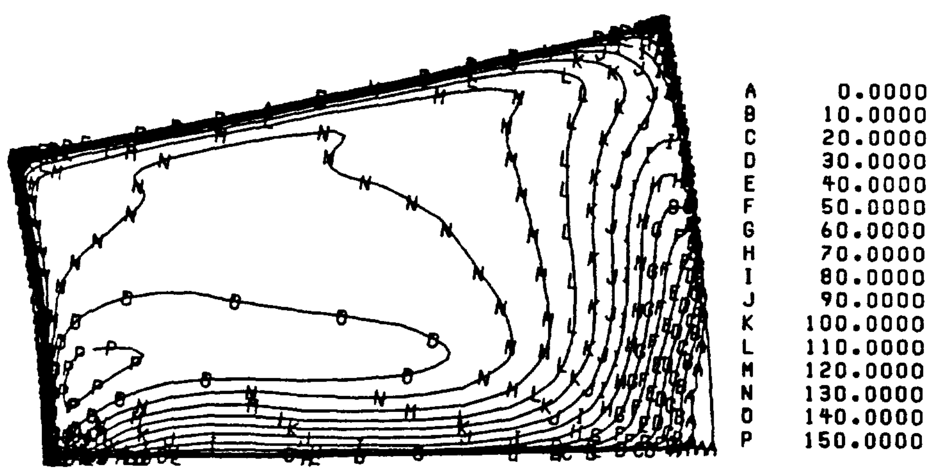

ENHANCED

(d) STATION 6.

FIGURE 41. - CONTINUED.

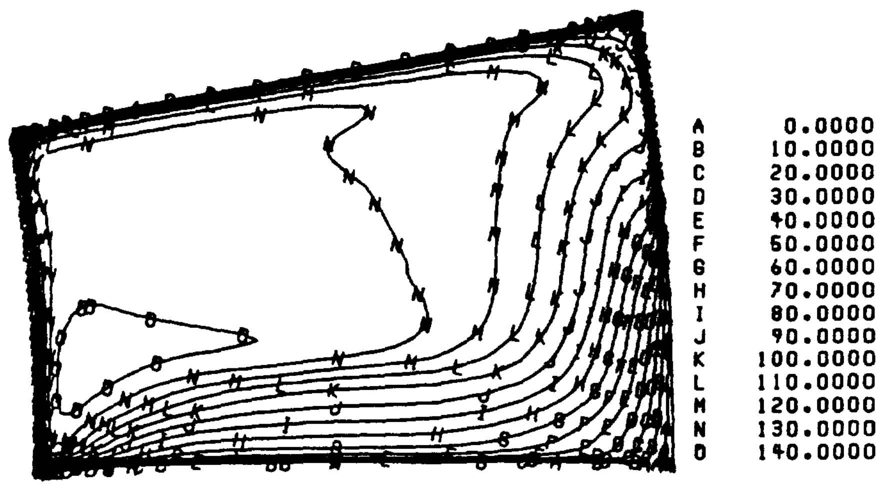

BASELINE

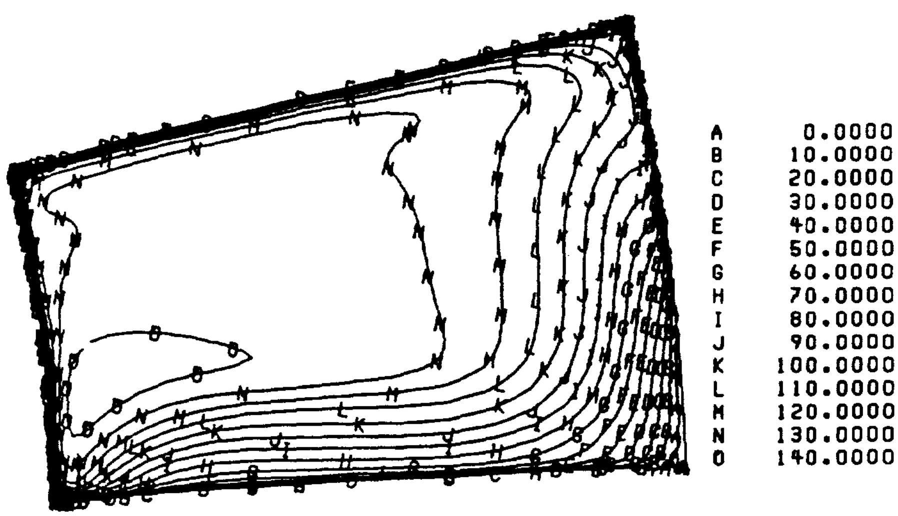

ENHANCED

(e) STATION 7.

FIGURE 41. - CONCLUDED.

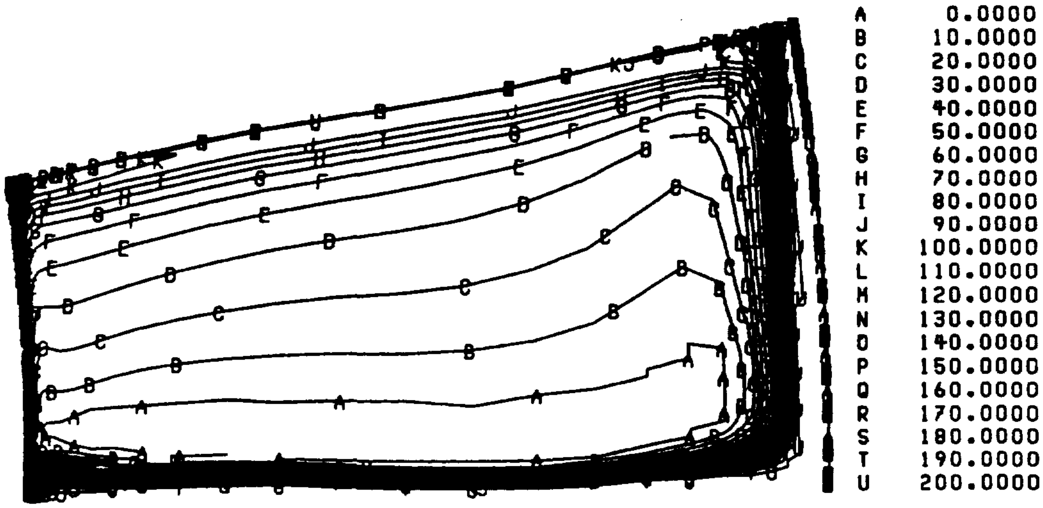

BASELINE

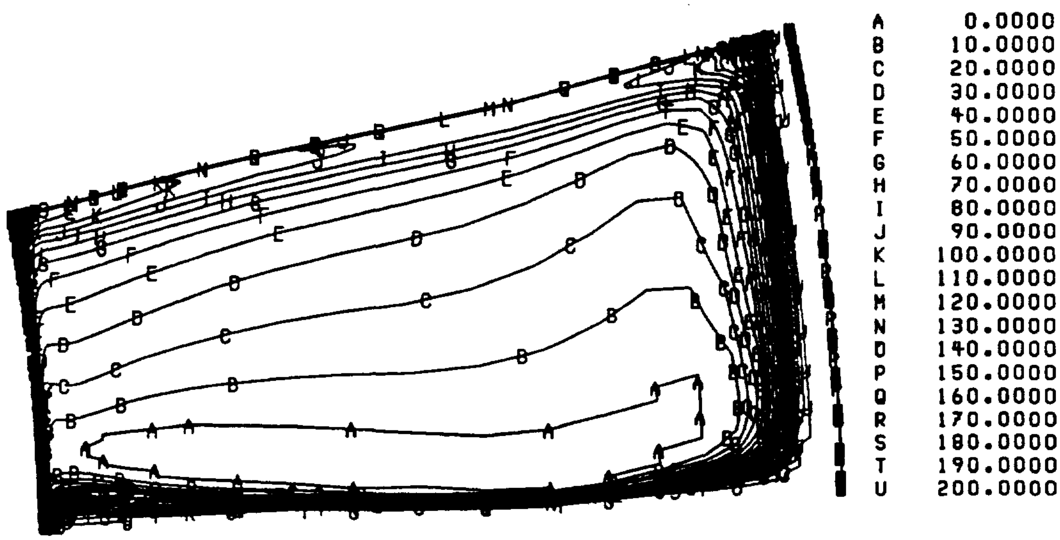

ENHANCED

(a) STATION 3.

FIGURE 42. - COMPUTED ABSOLUTE TANGENTIAL VELOCITY, LINE PLOTS.

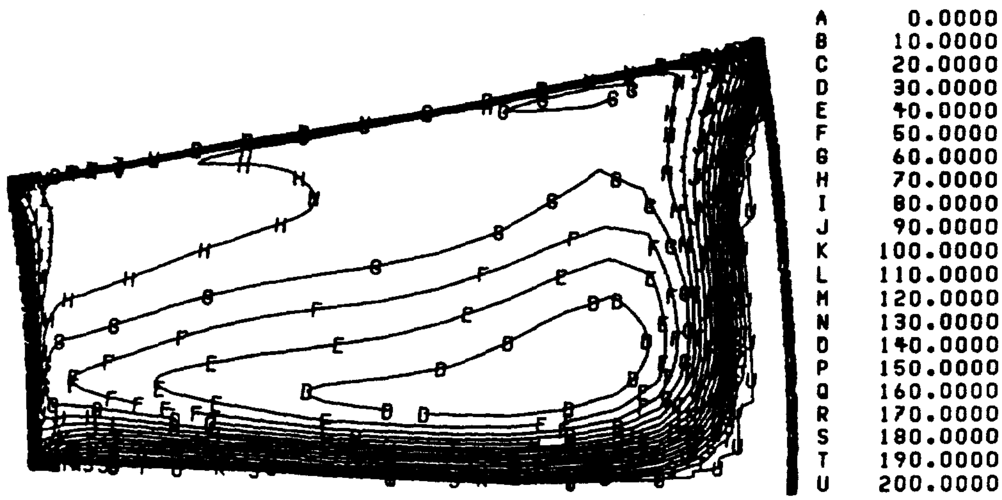

BASELINE

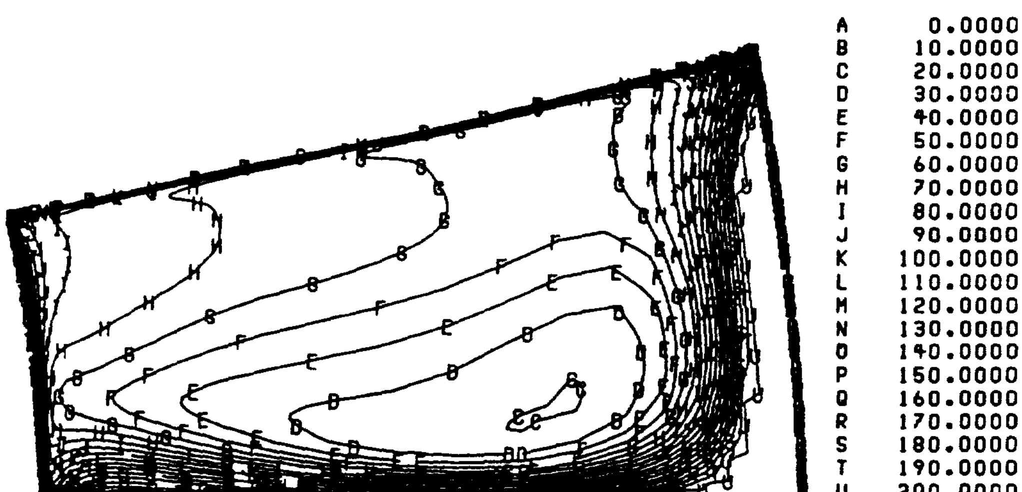

ENHANCED

(b) STATION 4.

FIGURE 42. - CONTINUED.

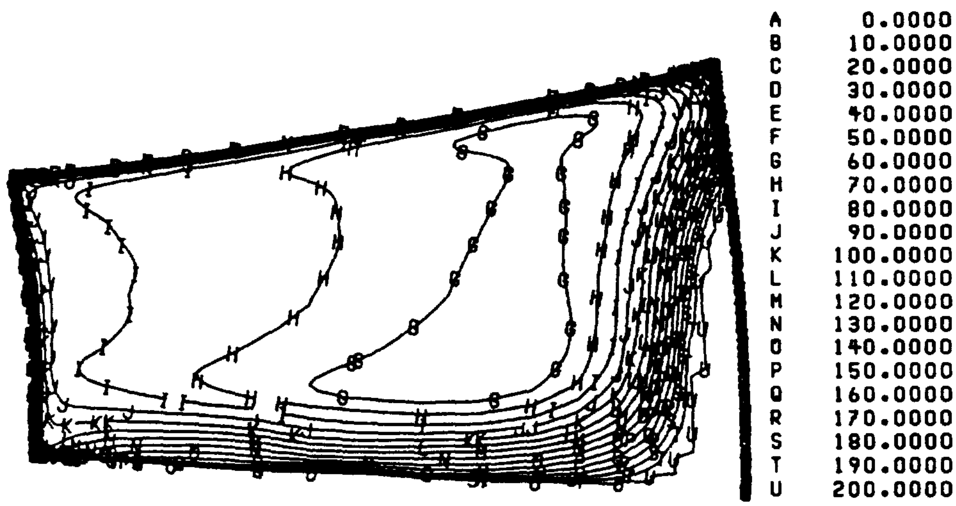

BASELINE

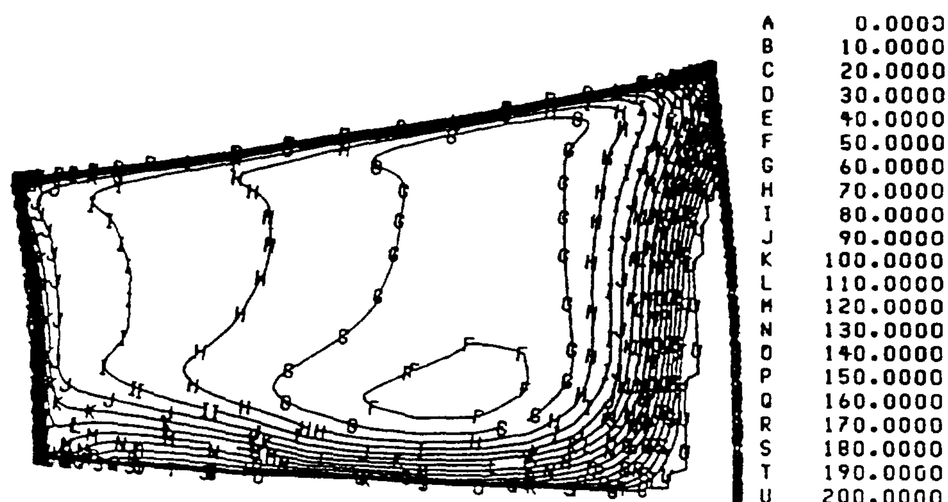

ENHANCED

(c) STATION 5.

FIGURE 42. - CONTINUED.

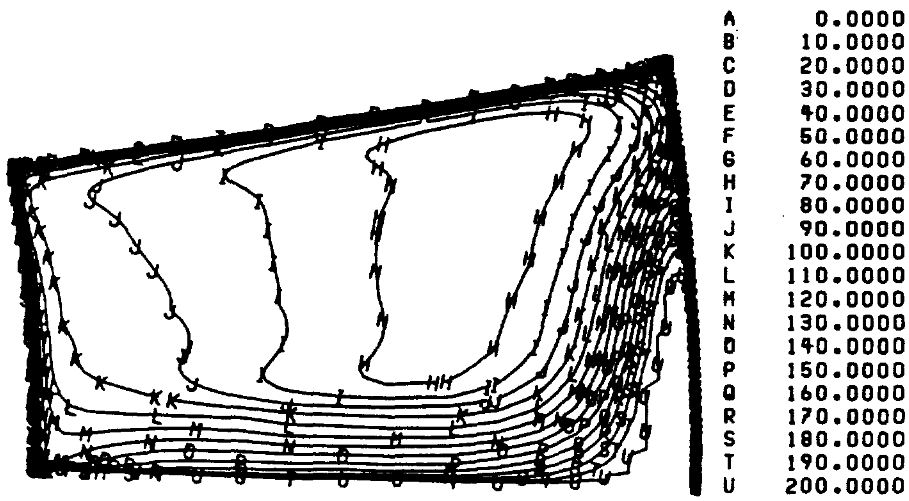

BASELINE

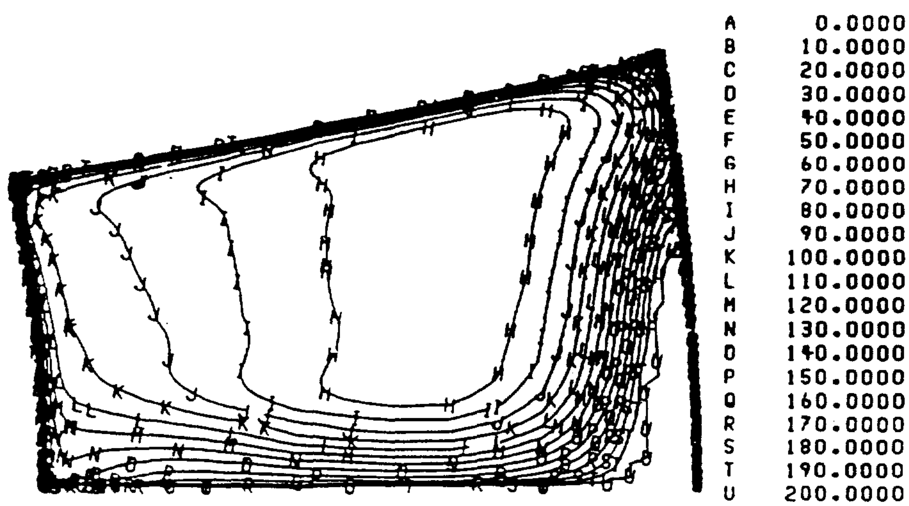

ENHANCED

(d) STATION 6.

FIGURE 42. - CONTINUED.

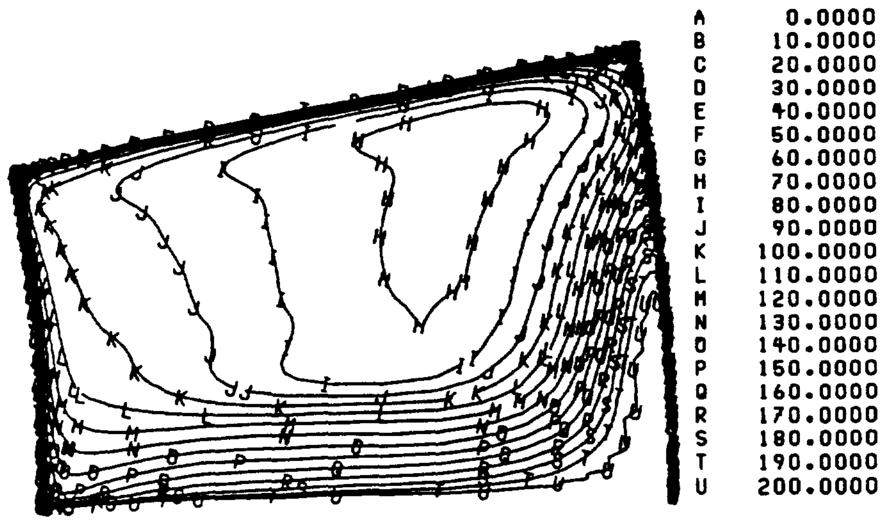

BASELINE

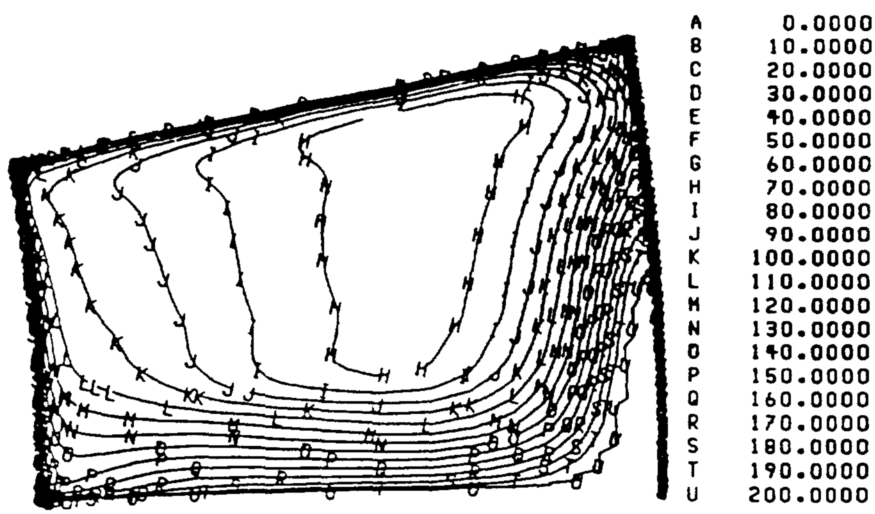

ENHANCED

(e) STATION 7.

FIGURE 42. - CONCLUDED.

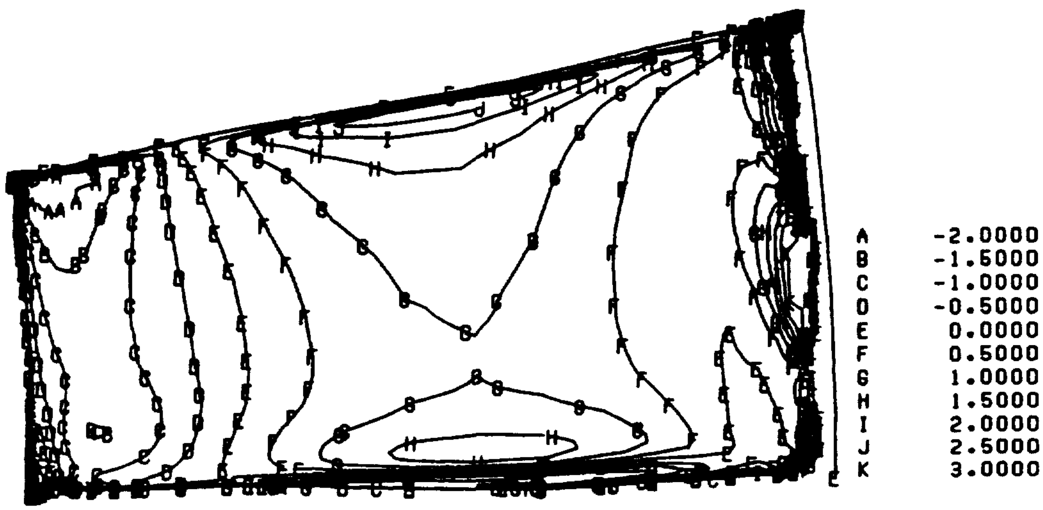

BASELINE

(a) STATION 2.

FIGURE 43. - DIFFERENCES BETWEEN COMPUTED TEST CASE RELATIVE FLOW ANGLE DIFFERENCES $\beta_{BASE} - \beta_{ENHANCED}$.

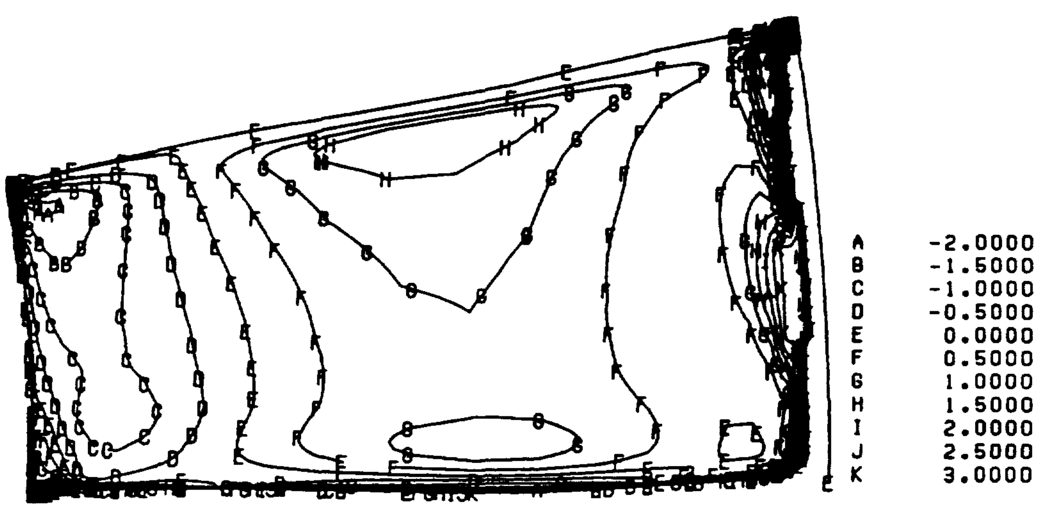

BASELINE

(b) STATION 3.

FIGURE 43. - CONTINUED.

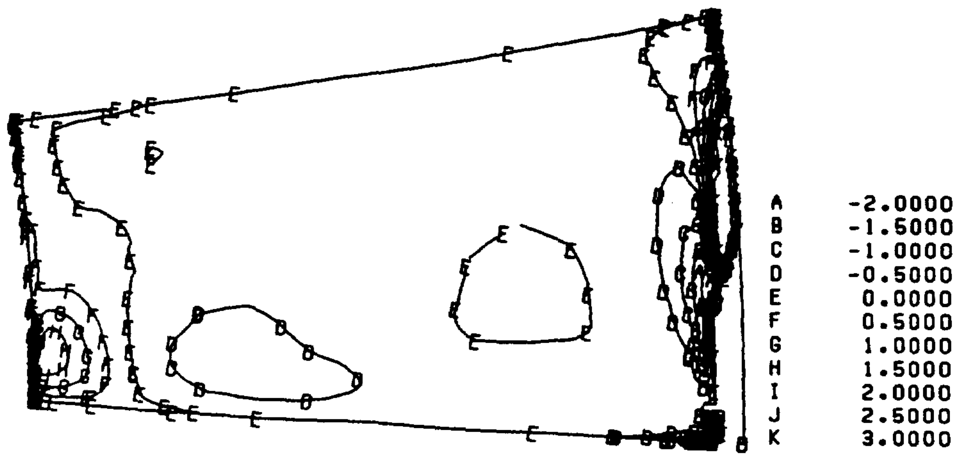

BASELINE

(c) STATION 5.

FIGURE 43. - CONTINUED.

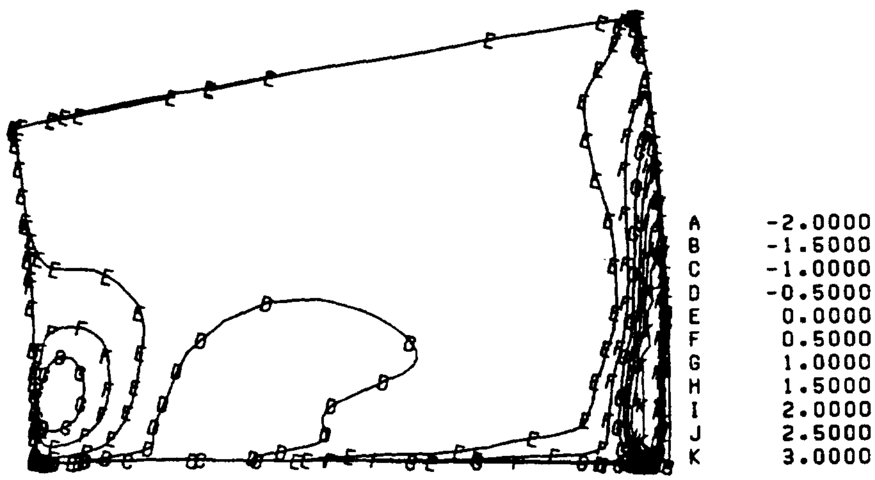

BASELINE

(d) STATION 7.

FIGURE 43. - CONTINUED.

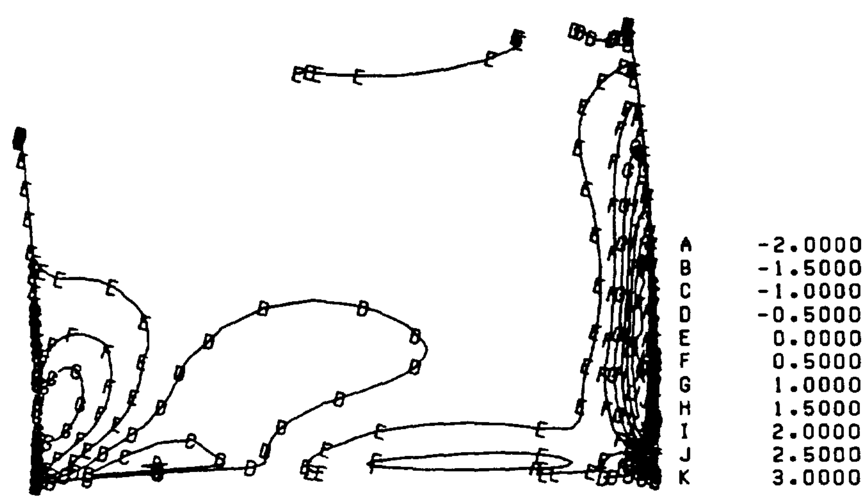

BASELINE

(e) STATION 8.

FIGURE 43. - CONCLUDED.

APPENDIX A

Appendix A contains tables of the acquired data and of calculated values of that data that has been used to develop the plots used in this report. Information provided is:

TABLE	DATA PROVIDED
A1	Axial Velocities
A2	Absolute Tangential Velocities
A3	Number of Axial Measurements
A4	Number of Tangential Measurements
A5	Calculated Axial Uncertainties
A6	Calculated Tangential Uncertainties

TABLE A1. -

(a) AXIAL VELOCITY (M/S)

BASELINE INLET, STATION 1

CP	VA1	VA2	VA3	VA4	VA5	VA6	VA7	VA8	VA9	VA10-AXIAL VEL
1	81.14	92.20	87.93	87.61	87.10	85.40	86.50	85.90	85.18	79.33
2	80.90	92.39	87.31	89.49	87.32	86.11	86.07	85.53	83.54	63.32
3	78.55	93.31	87.92	88.53	87.31	86.14	85.87	84.64	85.85	74.78
4	79.63	92.12	86.91	88.78	86.34	86.95	85.87	84.24	86.84	65.63
5	81.40	92.76	87.42	88.38	85.70	86.55	86.41	85.09	84.92	87.99
6	81.72	91.70	87.03	88.24	85.95	86.76	85.47	85.62	84.02	81.81
7	80.61	92.68	87.66	89.45	87.05	85.70	86.32	84.76	85.61	81.58
8	80.62	92.81	88.52	87.71	86.20	86.16	86.40	85.20	85.96	72.51
9	79.77	91.55	88.60	89.35	86.05	85.61	86.08	85.38	84.57	77.14
10	80.32	92.38	86.73	88.14	86.02	86.14	86.51	85.78	85.13	92.70
11	79.53	91.74	86.20	87.87	85.10	86.78	86.57	84.76	83.96	45.07
12	80.68	92.24	87.11	87.56	86.20	86.34	86.31	86.20	85.03	81.65
13	79.62	92.84	87.92	88.30	86.54	85.66	86.18	84.99	84.87	87.65
14	78.82	91.52	86.34	87.98	86.31	86.15	87.01	85.61	84.90	58.95
15	79.59	92.11	86.34	88.54	87.02	86.10	86.07	84.43	84.47	81.95
16	79.75	91.83	88.15	89.08	86.59	85.40	86.38	84.57	84.95	78.62
17	79.70	91.89	87.77	87.43	85.52	85.51	87.03	84.75	85.54	74.50
18	79.96	91.62	87.77	88.68	86.56	85.29	86.64	85.01	83.85	73.18
19	79.20	91.26	87.39	88.85	87.43	86.05	86.57	85.32	84.20	66.22
20	79.45	92.09	87.05	88.71	85.94	86.57	86.20	85.29	85.25	64.36
21	78.53	92.84	87.01	87.81	86.68	86.17	86.03	84.96	85.10	81.36
22	80.57	91.86	86.92	87.76	86.91	85.80	86.40	85.14	84.66	68.00
23	80.37	92.03	88.45	88.35	87.02	85.25	86.12	85.52	85.03	75.79
24	78.52	91.94	87.10	88.23	86.09	86.23	86.25	84.96	84.24	50.65
25	79.17	92.59	88.05	87.54	87.60	85.61	86.32	85.42	84.66	66.10
26	80.97	92.60	86.92	87.86	87.78	86.28	85.91	84.93	85.45	81.53
27	80.28	92.46	87.42	89.63	85.85	86.34	86.03	85.83	85.56	53.36
28	79.27	91.64	87.75	88.19	86.20	86.45	86.40	86.16	84.06	74.78
29	79.16	92.59	87.24	88.36	86.57	86.08	85.88	83.99	85.61	70.78
30	80.30	92.00	88.06	88.75	84.81	85.87	85.94	85.11	85.50	72.37
31	79.23	91.73	88.48	88.56	86.39	85.65	86.02	84.74	84.99	67.68
32	80.97	92.58	87.52	87.99	87.00	85.26	86.94	84.87	84.96	71.45
33	80.38	92.71	87.90	89.22	86.54	86.07	86.47	85.33	85.14	74.95
34	81.09	92.86	88.43	88.45	86.62	86.06	86.80	85.44	84.67	78.60
35	79.28	92.64	87.31	88.95	85.66	85.83	86.52	84.67	84.60	60.35
36	78.86	92.04	86.94	89.75	86.46	85.61	85.74	85.49	84.79	66.48
37	78.77	92.60	87.65	88.70	87.37	85.87	85.31	84.39	84.81	72.59
38	80.28	92.56	87.88	88.23	87.27	85.63	86.62	85.68	85.48	74.29
39	79.61	93.32	87.69	88.16	86.39	85.99	86.05	85.56	85.34	80.48
40	80.42	92.21	87.62	88.51	85.73	85.99	85.94	85.52	84.02	59.09
41	80.63	91.66	87.49	87.79	87.10	85.91	85.95	85.68	83.95	70.47
42	79.99	92.63	87.39	89.72	86.90	85.47	86.51	85.58	83.48	79.04
43	81.53	91.69	87.57	87.54	86.27	86.34	85.34	83.88	84.80	78.05
44	79.44	92.51	87.61	87.56	86.99	85.48	86.30	85.63	83.93	63.96
45	79.54	91.57	87.86	87.67	85.86	86.24	86.44	84.64	84.08	82.59
46	78.94	92.43	87.72	88.58	86.69	85.88	85.91	85.31	83.99	79.86
47	80.05	92.49	85.79	88.17	87.46	86.72	85.45	85.79	84.52	99.99
48	80.24	92.61	87.59	88.38	86.61	86.15	86.60	85.93	84.92	105.57
49	80.60	92.95	87.28	88.35	87.11	85.87	86.41	85.85	83.95	57.93
50	75.52	89.32	86.15	88.63	82.10	84.32	82.28	82.01	86.05	42.31

BASELINE INLET, STATION 2

CP	VA1	VA2	VA3	VA4	VA5	VA6	VA7	VA8	VA9	VA10-AXIAL VEL
1	71.38	61.87	59.09	51.02	47.44	58.05	38.23	32.81	36.64	55.29
2	83.78	67.06	65.43	59.46	53.05	49.82	54.77	40.80	32.20	33.18
3	91.24	76.68	72.06	67.77	60.14	51.40	66.96	53.56	39.38	55.84
4	102.38	84.49	80.35	70.84	69.87	54.74	75.30	67.83	47.51	49.54
5	106.39	92.50	86.39	79.94	73.32	61.93	86.18	77.07	58.86	37.64
6	109.41	96.68	92.37	85.32	79.69	71.33	93.44	84.72	67.54	49.10
7	110.52	100.19	103.29	86.81	84.80	74.60	100.67	94.05	73.93	62.94
8	112.29	104.66	103.41	98.23	89.98	81.36	105.97	96.37	80.33	55.88
9	113.20	108.33	107.06	105.31	92.70	87.03	111.06	103.68	85.61	74.80
10	114.39	110.09	109.62	103.90	98.16	90.13	109.29	104.98	88.07	37.92
11	113.23	109.55	114.62	109.40	100.70	92.73	112.38	105.99	92.33	93.76
12	112.69	110.36	112.68	111.14	104.23	96.00	118.93	110.95	95.33	63.02
13	111.25	110.84	108.88	108.16	107.08	99.55	120.17	116.39	93.78	66.74
14	109.88	110.66	119.74	118.42	108.08	103.53	118.38	114.72	98.19	73.43
15	108.76	114.01	114.35	115.86	110.10	103.79	120.38	113.61	104.46	81.58
16	109.56	110.64	119.97	119.98	110.74	104.50	115.10	115.53	107.71	101.55
17	107.06	107.71	120.70	117.33	111.50	106.80	116.99	118.09	110.49	63.82
18	107.07	109.15	124.77	113.35	111.84	108.92	121.82	119.20	105.50	105.48
19	105.62	108.89	122.06	119.06	113.79	108.58	123.03	118.58	112.70	84.22
20	105.06	108.81	121.17	119.95	116.37	109.44	120.18	118.70	110.40	97.38
21	103.86	108.66	118.11	124.98	115.03	111.34	120.24	119.83	113.19	73.99
22	102.57	108.33	125.22	119.21	115.22	109.67	121.03	116.21	112.08	84.19
23	102.22	106.50	116.56	114.17	114.34	112.01	117.27	119.00	112.92	76.84
24	100.96	107.38	120.28	116.75	113.79	110.86	115.94	117.75	112.27	58.52
25	100.58	106.99	120.90	121.98	114.79	111.08	117.79	117.84	114.46	88.47
26	99.97	103.79	114.97	115.22	113.28	112.13	114.93	112.54	112.05	88.59
27	99.56	102.37	115.60	112.30	112.07	111.89	115.63	116.21	111.11	85.80
28	96.66	103.07	112.51	119.48	111.17	111.09	116.28	114.71	111.03	82.76
29	96.57	103.55	111.23	112.99	110.91	110.16	113.20	111.77	110.02	71.59
30	95.41	101.30	114.42	112.84	110.48	109.84	111.03	112.34	111.27	99.67
31	93.33	100.21	109.10	109.38	110.15	110.33	109.53	109.50	108.07	72.58
32	87.54	91.92	110.09	108.29	104.26	105.44	105.31	99.02	96.88	88.01
33	91.58	95.65	108.13	103.60	108.02	109.06	108.77	108.29	108.45	125.04
34	89.59	94.35	106.24	110.94	107.86	107.92	107.67	108.19	107.84	76.15
35	88.71	93.06	105.38	109.92	107.01	107.89	106.31	103.36	104.81	83.56
36	85.86	89.37	100.29	102.67	104.37	104.84	106.44	104.54	106.23	69.54
37	84.09	89.79	103.96	101.02	103.65	104.31	103.39	105.26	102.73	66.61
38	82.24	88.16	100.10	103.79	102.24	104.07	102.41	102.10	100.99	79.18
39	79.91	88.88	97.26	99.52	100.28	103.41	101.86	97.05	101.54	55.92
40	77.45	81.30	92.58	93.09	98.94	101.32	97.63	97.62	100.09	86.44
41	74.05	80.98	92.79	93.59	96.87	100.12	96.42	97.87	96.94	71.96
42	72.55	80.15	89.87	92.66	93.77	98.12	94.00	95.06	96.55	72.21
43	68.40	77.15	85.09	89.08	91.67	95.95	90.54	91.17	90.81	73.14
44	63.88	72.94	84.07	85.01	87.94	94.35	88.88	88.73	90.95	68.39
45	57.17	67.69	80.98	81.10	84.70	92.28	85.82	85.66	86.79	66.33
46	51.05	65.27	66.54	73.18	80.62	88.39	81.56	82.60	84.63	72.59
47	44.43	57.83	61.69	65.21	75.47	85.45	72.81	75.26	80.90	69.93
48	43.42	47.98	53.37	52.28	67.53	80.43	64.29	70.75	74.10	57.76
49	48.77	47.75	50.03	49.59	59.49	75.30	51.94	59.20	65.64	65.53
50	60.36	56.62	54.42	40.80	49.43	67.29	40.72	43.32	51.85	42.64

BASELINE INLET, STATION 3

CP	VA1	VA2	VA3	VA4	VA5	VA6	VA7	VA8	VA9	VA10-AXIAL VEL
1		1731.37	32.81	7.97	27.06	0.00	30.22	0.00	15.00	0.00
2		29.65	29.82	8.14	0.00	0.00	28.07	0.00	31.71	43.72
3		27.65	74.59	53.69	71.75	56.98	47.23	24.17	37.11	16.13
4		0.00	0.00	19.31	32.15	1605.62	62.50	35.47	37.50	3.26
5		0.00	0.00	0.00	0.00	0.00	0.00	46.95	34.07	2.89
6		0.00	0.00	0.00	0.00	0.00	0.00	0.00	0.00	34.49
7		0.00	0.00	0.00	0.00	0.00	0.00	0.00	0.00	0.00
8		131.62	0.00	0.00	86.59	59.62	119.53	0.00	0.00	0.00
9		0.00	100.15	121.32	97.44	74.38	123.25	121.47	58.90	0.00
10		132.82	111.01	115.36	116.62	114.82	126.28	117.54	65.12	0.00
11		133.75	129.43	121.79	124.55	118.87	123.50	117.06	97.26	78.30
12		129.45	132.81	119.45	121.24	123.51	128.86	121.63	81.08	85.55
13		127.00	124.88	125.50	103.34	119.91	124.61	120.14	84.38	85.44
14		76.77	113.59	106.94	108.89	123.13	126.30	122.22	77.69	90.28
15		128.79	110.32	131.95	122.29	121.66	124.87	119.05	103.95	93.92
16		129.29	133.57	129.60	123.13	121.21	127.04	121.17	86.97	105.02
17		112.57	131.53	127.73	120.20	122.31	125.20	120.26	85.79	62.15
18		119.26	123.71	127.66	128.35	123.79	123.49	120.01	91.87	101.74
19		31.58	125.08	127.48	123.67	123.10	123.18	119.80	97.12	97.15
20		122.32	127.88	125.52	124.48	124.47	121.97	119.98	96.48	109.39
21		125.53	121.02	125.38	122.39	122.66	122.24	118.04	103.57	108.49
22		125.40	103.77	128.33	125.26	124.35	119.34	118.43	112.98	100.37
23		120.50	128.75	129.16	119.28	122.73	121.33	119.18	106.67	104.26
24		104.56	94.74	125.13	116.49	121.12	118.69	116.79	91.27	103.05
25		114.17	120.51	118.53	119.69	120.66	118.73	115.27	87.82	97.07
26		116.28	100.91	120.02	122.81	120.24	116.40	113.47	92.59	91.54
27		116.06	121.01	121.17	119.25	120.67	117.26	112.84	85.87	92.82
28		113.13	111.15	118.88	115.97	117.63	110.41	110.17	82.16	99.36
29		104.98	110.49	118.86	121.31	116.78	115.29	111.22	92.50	94.70
30		97.48	109.04	116.80	116.41	116.87	112.23	110.71	74.64	97.92
31		103.86	104.19	113.87	116.65	115.45	111.34	109.27	88.79	92.75
32		85.68	107.95	113.75	111.02	113.24	108.05	107.15	97.57	85.68
33		105.83	106.36	112.46	116.16	113.32	109.00	106.72	87.12	65.69
34		104.92	106.33	111.24	105.65	111.64	107.90	104.73	89.63	80.88
35		97.88	106.51	107.42	108.47	111.31	106.95	104.09	90.22	62.84
36		98.62	95.79	109.02	108.10	110.35	105.62	104.15	78.48	81.40
37		90.36	95.85	101.92	106.26	108.87	102.54	101.12	82.64	83.30
38		90.88	100.64	102.56	102.26	107.02	100.14	99.69	82.79	76.44
39		92.00	97.58	102.87	101.88	106.36	99.96	98.69	76.46	81.82
40		95.51	96.31	100.21	99.32	102.98	95.27	96.60	96.51	78.16
41		87.75	91.84	95.01	98.38	101.71	96.26	93.76	81.36	69.56
42		78.64	92.86	90.92	95.60	99.51	93.00	92.37	87.47	86.20
43		76.68	89.95	89.62	93.70	97.09	90.40	90.37	75.83	82.80
44		82.48	85.94	90.17	92.83	96.12	89.18	89.23	80.13	74.54
45		84.74	85.36	90.38	89.78	93.81	89.71	86.94	69.43	77.18
46		85.87	85.66	83.63	88.83	92.69	89.41	86.67	75.13	75.54
47		0.00	56.71	96.45	85.15	95.26	92.40	87.57	75.25	41.26
48		0.00	61.93	0.00	88.16	89.08	92.66	90.12	68.83	82.56
49		0.00	0.00	0.00	5.86	0.00	92.52	88.65	73.89	0.00
50		51.06	42.03	0.00	0.00	0.00	57.23	96.83	0.00	0.00

BASELINE INLET, STATION 4

CP	VA1	VA2	VA3	VA4	VA5	VA6	VA7	VA8	VA9	VA10-AXIAL VEL
1	0.00	0.00	0.00	0.00	0.00	117.40	134.38	117.44	99.86	52.32
2	0.00	0.00	0.00	122.46	134.23	113.05	133.56	129.63	128.72	70.46
3	0.00	0.00	122.36	118.66	132.61	133.08	130.10	129.41	119.39	117.22
4	81.64	130.60	138.43	125.25	131.85	125.92	128.99	122.53	115.08	131.88
5	101.51	130.79	134.98	136.05	132.19	126.85	129.74	125.12	125.80	107.32
6	76.66	125.35	126.88	129.62	125.60	115.56	114.50	119.71	111.61	98.30
7	94.59	127.83	132.49	134.15	131.06	128.06	123.47	123.49	120.25	94.25
8	52.49	125.53	131.16	133.34	129.41	125.61	123.68	127.87	117.15	100.53
9	44.75	122.99	129.59	132.41	128.97	125.64	121.31	123.32	117.65	101.09
10	63.63	122.89	128.89	130.31	126.62	123.05	121.16	122.24	115.93	96.02
11	63.68	121.35	128.16	127.87	125.44	123.13	118.66	119.00	114.01	102.92
12	73.45	119.02	124.92	128.18	124.62	121.19	118.77	118.01	112.77	112.99
13	64.70	118.16	125.21	126.47	123.87	121.37	118.37	117.48	112.23	97.55
14	66.83	116.86	124.05	124.13	122.64	121.27	117.67	116.72	112.30	88.40
15	52.28	116.47	122.17	122.67	123.62	120.97	115.32	116.83	110.91	100.75
16	68.96	115.13	121.96	121.66	122.72	118.91	114.95	113.98	110.39	108.01
17	50.69	115.32	119.14	122.41	121.82	118.56	114.20	112.82	110.05	94.55
18	76.18	113.26	118.82	120.82	121.77	117.96	115.31	113.42	109.09	86.09
19	25.62	111.37	117.68	120.38	121.39	116.02	114.97	111.78	108.45	88.17
20	56.41	111.04	117.95	119.61	120.38	116.81	113.85	111.17	107.40	93.95
21	75.95	111.88	116.88	119.34	120.47	117.46	113.04	111.57	107.01	82.49
22	66.77	109.93	116.90	118.26	120.40	117.95	113.11	110.55	107.70	86.66
23	79.51	109.94	116.94	119.10	120.16	117.57	113.63	111.28	106.73	90.75
24	70.64	110.67	116.19	117.92	120.19	116.86	113.33	110.74	106.60	79.14
25	75.80	111.03	115.87	118.50	120.95	117.31	113.46	112.77	107.59	80.16
26	87.48	111.84	114.97	118.45	119.31	117.89	114.14	111.75	107.73	100.96
27	22.46	112.17	115.35	118.01	97.24	117.84	116.33	112.91	109.50	93.08
28	53.10	110.79	114.94	117.63	0.00	118.44	115.34	113.14	111.03	97.87
29	35.06	111.16	114.22	117.38	110.45	119.06	114.64	113.44	111.68	100.57
30	90.20	111.48	114.23	117.92	0.00	119.18	116.14	113.01	113.23	90.74
31	33.45	110.03	113.33	116.82	40.58	119.37	116.51	114.83	111.58	106.05
32	28.17	113.31	113.63	116.58	0.00	119.46	116.33	115.21	115.49	106.13
33	71.82	110.91	114.13	115.71	0.00	120.43	116.95	115.63	114.75	101.19
34	47.83	72.91	111.51	118.86	0.00	121.21	119.56	115.56	115.15	98.61
35	10.33	12.15	116.45	95.50	0.00	121.26	116.28	118.55	115.29	100.62
36	62.53	45.56	0.00	58.68	0.00	122.42	105.24	115.82	115.35	111.66
37	0.00	65.85	46.17	47.92	0.00	119.07	115.50	114.68	115.12	112.09
38	0.00	57.49	47.19	67.51	0.00	122.59	0.00	110.78	114.80	111.10
39	0.00	34.38	32.02	58.99	0.00	121.05	139.65	18.09	55.35	96.96
40	0.00	0.00	29.80	23.01	132.95	105.45	0.00	10.28	55.33	0.00
41	0.00	0.00	0.00	0.00	120.05	0.00	0.00	0.00	58.72	0.00
42	0.00	0.00	0.00	0.00	124.91	127.45	0.00	0.00	0.00	0.00
43	0.00	0.00	0.00	0.00	122.75	113.09	96.82	67.19	10.59	18.82
44	0.00	0.00	0.00	0.00	97.90	40.54	77.13	44.65	12.38	28.94
45	0.00	0.00	0.00	0.00	0.00	0.00	0.00	0.00	68.37	42.56
46	0.00	0.00	0.00	0.00	0.00	0.00	0.00	0.00	0.00	0.00
47	0.00	0.00	0.00	0.00	0.00	0.00	0.00	0.00	0.00	0.00
48	0.00	0.00	0.00	0.00	0.00	0.00	0.00	0.00	0.00	0.00
49	0.00	0.00	0.00	0.00	0.00	0.00	0.00	0.00	0.00	0.00
50	0.00	0.00	0.00	0.00	0.00	0.00	0.00	0.00	0.00	0.00

BASELINE INLET, STATION 5

CP	VA1	VA2	VA3	VA4	VA5	VA6	VA7	VA8	VA9	VA10-AXIAL VEL
1	0.00	0.00	0.00	0.00	0.00	0.00	0.00	127.56	128.58	88.39
2	0.00	0.00	0.00	0.00	119.30	103.46	132.10	115.76	91.36	83.69
3	0.00	0.00	79.38	144.29	132.84	138.01	128.88	131.04	95.99	92.45
4	114.41	142.35	143.22	145.54	135.67	124.65	131.05	129.54	130.93	75.20
5	113.39	140.97	141.93	144.31	139.63	132.32	134.68	128.68	117.35	80.94
6	111.17	140.91	142.43	145.36	137.50	140.07	132.23	133.55	123.69	93.59
7	106.61	138.62	139.88	142.57	136.13	136.51	132.09	131.39	130.09	84.43
8	105.74	138.39	139.98	143.00	140.39	136.75	134.61	133.67	127.13	80.27
9	105.66	137.91	138.78	141.02	137.78	140.62	133.53	133.59	126.15	90.06
10	106.10	136.00	138.21	141.81	143.53	137.03	134.49	135.47	127.10	75.27
11	107.49	135.87	137.96	141.45	140.17	138.99	133.51	133.99	130.78	108.19
12	110.96	134.93	137.20	140.86	140.71	141.56	134.41	132.51	128.59	98.14
13	116.77	134.97	136.81	140.00	138.49	141.56	135.49	133.96	133.52	80.73
14	117.64	134.53	136.27	139.40	138.85	141.33	134.00	133.96	134.39	84.03
15	122.16	134.51	135.53	137.95	139.75	140.33	132.62	135.13	131.88	80.90
16	121.13	134.08	136.49	140.36	139.99	138.89	135.79	133.80	135.91	92.73
17	123.88	135.42	135.89	137.79	138.69	139.65	133.34	135.44	132.14	92.86
18	125.27	134.45	134.77	136.51	138.20	139.72	132.71	133.43	132.69	95.07
19	127.90	133.21	134.38	136.96	138.66	138.62	133.58	134.05	133.42	85.63
20	127.51	132.59	133.22	135.26	137.86	138.41	133.67	132.61	133.60	71.70
21	127.89	132.50	132.74	134.37	135.89	137.69	133.32	132.89	129.40	75.38
22	127.05	132.27	132.54	134.22	135.06	137.85	132.82	132.94	130.08	95.00
23	125.02	131.00	131.10	132.58	134.02	137.06	133.18	131.34	129.65	101.96
24	124.06	130.17	130.28	131.77	134.35	137.40	132.08	131.70	130.02	71.81
25	124.08	129.39	130.07	132.11	132.94	135.54	130.86	131.75	129.46	70.39
26	125.08	128.83	129.41	131.36	131.48	134.86	131.66	130.85	127.79	79.40
27	123.01	127.30	128.41	130.85	132.77	134.43	131.77	130.52	126.06	64.11
28	120.54	128.10	127.83	128.89	130.85	134.87	130.35	130.28	127.63	83.04
29	120.23	127.07	126.84	127.94	130.14	133.27	129.14	129.41	127.21	78.20
30	121.44	126.32	126.82	128.62	129.66	133.41	128.05	129.30	127.12	89.59
31	120.95	126.90	0.00	127.35	129.96	132.79	128.41	128.60	125.22	96.50
32	119.72	122.92	0.00	128.66	128.70	132.17	126.50	125.50	125.39	73.02
33	118.18	125.90	0.00	126.98	129.69	130.84	126.99	127.08	123.31	108.69
34	100.18	119.01	121.06	124.41	127.66	130.72	125.33	125.17	122.65	91.20
35	77.86	0.00	0.00	123.75	127.72	128.30	123.25	123.43	123.45	101.61
36	53.12	123.09	0.00	114.94	125.70	128.84	122.90	122.68	121.71	94.40
37	27.22	132.03	0.00	111.30	114.06	127.42	121.81	122.56	121.32	87.79
38	0.00	131.88	0.00	135.27	138.65	125.90	127.43	125.03	119.71	64.18
39	0.00	151.28	0.00	83.34	38.53	135.26	104.17	122.19	103.78	62.42
40	0.00	132.14	0.00	0.00	131.93	135.90	0.00	0.00	24.80	67.45
41	0.00	0.00	0.00	0.00	125.89	134.76	0.00	0.00	29.52	2.65
42	0.00	0.00	0.00	0.00	0.00	0.00	0.00	98.98	6.51	0.00
43	0.00	0.00	0.00	0.00	0.00	0.00	0.64	36.27	10.55	0.00
44	0.00	0.00	0.00	0.00	0.00	0.00	0.00	0.00	0.00	0.00
45	0.00	0.00	0.00	0.00	0.00	0.00	0.00	0.00	0.00	0.00
46	0.00	0.00	0.00	0.00	0.00	0.00	0.00	0.00	0.00	0.00
47	0.00	0.00	0.00	0.00	0.00	0.00	0.00	0.00	0.00	0.00
48	0.00	0.00	0.00	0.00	0.00	0.00	0.00	0.00	0.00	0.00
49	0.00	0.00	0.00	0.00	0.00	0.00	0.00	0.00	0.00	0.00
50	0.00	0.00	0.00	0.00	0.00	0.00	0.00	0.00	0.00	0.00

BASELINE INLET, STATION 6

CP	VA1	VA2	VA3	VA4	VA5	VA6	VA7	VA8	VA9	VA10-AXIAL VEL
1	0.00	0.00	0.00	0.00	0.00	0.00	0.00	0.00	0.00	0.00
2	0.00	0.00	0.00	144.71	140.49	131.89	132.19	130.45	114.44	79.75
3	127.49	150.49	152.25	146.34	134.91	132.44	132.29	136.99	107.35	80.35
4	126.27	148.55	151.83	147.18	140.53	138.89	133.44	136.83	104.32	93.81
5	126.24	146.68	150.85	148.23	142.64	137.33	137.32	138.41	93.77	99.07
6	130.00	145.50	149.21	146.77	142.77	135.31	135.79	137.52	105.77	91.41
7	127.76	144.04	147.84	146.92	142.39	141.87	136.18	137.51	112.38	87.11
8	130.69	143.74	147.71	147.24	143.43	140.67	136.13	138.18	126.01	86.49
9	132.35	142.72	146.90	146.22	144.13	141.11	137.30	137.65	130.61	104.72
10	131.11	143.94	146.86	145.30	146.34	138.06	136.08	137.15	124.23	98.23
11	132.01	142.01	145.74	145.00	139.46	139.09	136.02	138.63	132.77	85.32
12	136.25	141.03	143.45	144.32	144.31	140.37	134.86	135.35	134.22	81.71
13	137.12	141.70	143.68	144.18	141.20	139.88	135.46	136.05	138.17	88.05
14	136.91	141.11	141.97	143.02	142.10	138.08	136.06	136.77	136.22	98.42
15	138.73	138.91	141.75	142.33	139.47	138.18	134.81	135.26	141.73	97.91
16	137.20	141.12	140.48	139.64	139.70	137.99	133.50	136.04	134.44	99.01
17	134.21	139.16	142.14	138.09	138.69	137.26	133.15	136.09	129.30	88.58
18	137.58	138.02	139.24	140.27	138.15	136.30	132.57	133.15	133.27	85.85
19	136.19	139.12	137.48	138.61	137.18	135.49	132.51	132.75	128.57	105.52
20	135.39	136.69	137.39	138.24	136.70	135.07	130.73	132.29	129.77	101.86
21	135.81	136.59	136.93	137.50	135.84	135.54	130.50	132.76	132.02	101.11
22	134.39	136.19	135.07	135.93	135.98	134.72	129.88	131.31	130.24	108.13
23	133.32	135.84	136.46	134.66	133.94	132.12	129.80	131.48	127.62	105.83
24	133.65	134.26	133.70	134.88	133.27	132.98	129.88	131.43	129.96	105.36
25	132.54	134.18	134.48	135.32	134.21	132.21	129.43	129.83	129.23	108.80
26	130.56	133.49	133.36	132.57	132.58	131.93	129.33	130.71	125.44	105.14
27	129.60	130.45	133.06	132.51	132.39	129.80	127.33	128.72	129.01	90.83
28	129.79	131.75	132.74	131.49	131.39	130.67	127.98	129.35	124.32	117.03
29	129.27	128.13	132.56	132.18	131.41	129.32	126.81	127.61	129.98	107.07
30	127.68	130.74	130.62	131.33	129.92	129.59	127.14	128.19	128.96	101.20
31	126.95	125.19	130.36	129.81	131.19	129.35	127.30	127.73	124.08	104.77
32	126.49	125.18	129.70	130.32	128.25	126.76	127.54	126.48	123.32	110.58
33	124.24	121.52	128.14	128.26	128.06	127.99	126.64	125.32	125.07	106.87
34	124.38	117.26	126.61	128.60	127.41	126.77	125.60	126.55	120.56	101.46
35	124.38	121.79	129.53	126.72	126.18	126.40	124.80	126.05	120.30	108.91
36	89.32	134.23	126.65	124.09	126.42	123.78	123.75	123.19	120.64	104.44
37	85.66	73.96	111.69	118.46	121.34	125.41	121.76	120.29	116.70	100.48
38	48.54	0.00	103.41	117.56	118.94	117.22	114.10	111.32	105.49	95.71
39	78.96	0.00	124.44	115.00	115.04	42.60	109.31	109.79	104.98	83.25
40	0.00	0.00	0.00	0.00	98.55	0.00	106.91	93.41	99.60	74.60
41	0.00	129.08	0.00	125.78	122.82	129.33	83.00	105.93	96.76	46.73
42	0.00	110.32	179.56	122.89	121.36	87.86	39.42	15.47	125.82	33.45
43	0.00	78.90	149.80	135.56	150.94	94.66	12.46	31.58	68.50	1.97
44	137.09	129.75	131.81	121.36	131.78	98.36	38.07	53.14	74.39	4.34
45	0.00	0.00	0.00	0.00	0.00	95.65	49.34	78.03	53.80	27.14
46	0.00	0.00	0.00	0.00	0.00	0.00	0.00	0.00	0.00	0.00
47	0.00	0.00	0.00	0.00	0.00	0.00	0.00	0.00	0.00	0.00
48	0.00	0.00	0.00	0.00	0.00	0.00	0.00	0.00	0.00	0.00
49	0.00	0.00	0.00	0.00	0.00	0.00	0.00	0.00	0.00	0.00
50	0.00	0.00	0.00	0.00	0.00	0.00	0.00	0.00	0.00	0.00

BASELINE INLET, STATION 7

CP	VA1	VA2	VA3	VA4	VA5	VA6	VA7	VA8	VA9	VA10-AXIAL VEL
1	0.00	0.00	0.00	0.00	0.00	0.00	0.00	0.00	0.00	0.00
2	0.00	119.47	0.00	0.00	0.00	0.00	0.00	0.00	0.00	0.00
3	1.04	120.94	150.16	145.09	132.58	126.57	114.94	104.00	96.46	0.00
4	66.48	118.71	147.32	143.50	130.89	124.94	117.40	117.15	97.08	76.29
5	5.57	134.95	146.03	143.37	134.96	121.25	126.57	119.79	121.30	74.17
6	16.51	125.52	146.99	145.10	136.53	124.07	128.71	119.33	119.59	78.82
7	76.08	125.89	146.43	142.43	135.86	129.58	128.23	124.87	116.48	83.83
8	22.60	127.84	144.40	145.01	138.54	126.19	128.75	124.06	122.00	84.90
9	13.26	137.92	144.15	145.39	136.31	133.76	129.91	127.34	124.02	90.56
10	28.33	139.07	145.79	141.54	135.15	132.57	129.33	125.29	123.76	98.40
11	24.58	140.25	144.11	143.46	138.29	135.56	127.86	128.04	121.72	91.63
12	57.50	139.83	143.98	142.94	139.96	133.74	132.33	127.08	123.56	92.35
13	76.90	139.74	143.50	141.62	137.81	132.03	130.82	129.60	126.17	92.47
14	21.10	140.81	143.98	142.31	138.89	133.96	129.33	128.04	128.72	102.49
15	41.62	139.18	141.20	142.57	137.95	135.77	130.78	129.89	129.68	100.50
16	62.73	141.25	142.30	142.03	136.87	132.59	130.83	127.64	128.54	96.16
17	31.45	138.72	141.46	139.64	137.51	133.13	130.57	128.15	126.56	105.48
18	20.55	137.96	140.90	139.73	136.51	133.99	130.49	128.35	126.82	104.63
19	80.26	138.36	140.27	139.55	136.96	133.36	130.60	128.89	126.43	102.29
20	128.73	111.13	139.83	137.24	135.05	132.69	128.35	125.94	120.70	95.32
21	136.50	138.03	137.66	138.61	136.95	132.58	130.94	127.38	127.30	97.66
22	136.56	138.09	137.85	137.40	135.53	132.10	129.83	128.08	125.29	106.15
23	135.37	136.88	138.92	138.69	135.84	132.33	128.62	126.83	126.35	105.07
24	133.39	134.88	137.43	136.68	135.40	131.15	128.61	126.90	124.34	108.14
25	133.84	135.34	136.42	135.63	134.89	130.64	129.66	126.76	125.43	104.04
26	135.34	136.86	135.59	134.77	133.50	131.11	128.32	126.55	124.95	107.63
27	133.05	134.53	137.80	134.99	134.82	130.30	127.77	125.54	125.10	106.09
28	133.80	135.29	136.59	134.63	133.27	130.37	128.20	126.76	125.13	113.57
29	46.55	133.68	134.34	135.11	133.17	129.18	128.28	126.25	124.66	110.96
30	46.20	134.10	136.03	133.63	132.37	129.71	128.17	126.10	124.97	110.38
31	16.98	132.36	135.50	133.40	132.48	129.30	127.14	125.69	124.47	114.66
32	34.58	133.39	133.84	134.12	131.99	129.53	127.28	124.43	122.76	107.32
33	69.60	131.06	134.37	134.12	131.74	128.97	127.11	123.74	123.21	104.95
34	26.41	130.19	133.89	133.31	131.10	128.89	126.57	124.46	121.78	110.37
35	2.27	130.90	133.47	132.79	130.75	128.04	126.55	124.79	120.91	102.78
36	11.86	131.60	132.75	131.58	129.68	128.62	125.91	122.59	121.13	102.86
37	3.30	130.27	133.30	130.32	130.15	127.36	126.17	122.50	121.19	107.07
38	15.34	129.96	133.12	130.48	130.26	127.11	125.22	123.13	122.28	105.46
39	4.69	130.73	130.69	130.35	129.02	126.23	125.46	122.40	118.77	105.33
40	18.88	125.46	131.74	129.02	128.85	125.64	124.02	121.69	120.45	101.96
41	15.46	114.70	126.03	128.35	124.81	123.01	121.01	119.83	114.37	99.59
42	26.25	88.64	119.62	117.06	115.54	118.80	114.89	112.73	104.90	94.77
43	28.04	58.41	112.75	113.28	110.08	112.63	110.16	98.26	77.93	81.95
44	38.83	7.89	119.41	91.15	97.62	108.21	102.95	86.29	71.03	68.06
45	30.23	18.49	0.00	109.10	92.92	78.44	76.97	72.02	57.70	48.47
46	31.86	10.40	165.55	0.00	80.64	94.97	69.70	67.88	70.19	64.49
47	21.98	94.03	0.00	105.94	107.56	96.51	84.03	70.70	67.05	47.20
48	33.38	85.16	144.57	124.38	114.00	84.53	83.34	76.01	74.89	51.70
49	0.00	0.00	0.00	0.00	117.75	112.45	76.94	96.79	85.52	75.17
50	0.00	0.00	0.00	0.00	0.00	0.00	0.00	0.00	0.00	75.30

BASELINE INLET, STATION 8

CP	VA1	VA2	VA3	VA4	VA5	VA6	VA7	VA8	VA9	VA10-AXIAL VEL
1	34.77	128.64	39.87	44.48	112.69	63.10	84.24	58.69	63.03	65.64
2	11.71	38.26	42.29	50.29	80.45	66.26	93.46	80.05	72.23	66.93
3	33.29	26.97	40.68	22.67	77.80	79.53	97.14	95.69	79.53	71.70
4	18.31	31.71	24.96	65.37	92.55	77.89	104.00	88.60	91.31	76.60
5	0.00	15.06	37.66	44.72	121.44	66.95	100.32	95.73	94.67	76.06
6	90.39	38.16	34.24	55.84	95.80	86.15	117.71	117.87	102.65	82.93
7	59.20	23.98	34.08	69.85	123.45	106.13	120.21	120.52	102.64	84.13
8	0.00	65.11	48.11	79.73	132.83	108.47	125.43	116.04	107.07	89.01
9	25.23	67.07	51.87	62.42	136.42	95.09	122.38	127.25	108.64	93.26
10	60.85	30.63	38.36	60.82	131.34	95.04	130.29	121.49	115.46	88.32
11	0.00	26.47	36.31	70.95	132.07	97.82	134.04	125.84	116.37	97.73
12	0.00	33.82	46.52	72.91	136.14	123.00	128.29	122.12	122.84	88.71
13	0.00	9.44	42.31	79.59	140.13	112.41	134.05	126.16	122.81	94.79
14	0.00	20.99	32.03	68.07	142.27	103.16	134.27	130.94	124.93	102.43
15	0.00	36.24	41.11	75.76	138.80	111.40	130.70	129.42	124.53	101.61
16	0.00	24.03	45.06	72.45	137.38	123.69	133.68	131.17	129.02	105.28
17	0.00	43.03	40.62	74.55	141.86	127.02	134.28	134.37	128.34	99.23
18	0.00	25.25	44.08	61.24	121.48	104.22	133.76	128.25	117.39	103.73
19	0.00	17.33	31.23	80.64	140.79	115.35	136.55	132.65	125.88	102.76
20	0.00	17.71	48.75	73.39	136.00	113.65	136.95	131.46	129.54	104.74
21	0.00	25.83	41.74	75.62	135.39	130.19	137.10	131.90	129.68	110.77
22	0.00	26.96	39.75	81.55	138.36	121.42	136.34	131.95	131.13	110.75
23	0.00	49.05	42.95	74.49	139.48	123.48	134.58	129.71	130.55	112.33
24	0.00	18.83	44.66	63.83	139.83	115.98	135.33	131.52	131.57	116.55
25	0.00	43.29	50.44	83.29	135.33	122.94	134.91	132.40	129.47	113.82
26	0.00	21.82	38.22	82.03	136.73	120.34	133.82	134.77	130.19	115.89
27	0.00	9.78	49.53	66.82	138.45	123.47	135.76	133.09	129.18	110.67
28	0.00	28.87	43.44	70.54	136.68	118.49	134.62	132.23	128.52	114.96
29	0.00	38.23	44.64	64.21	135.01	116.05	133.06	131.95	128.26	113.85
30	0.00	22.04	41.90	70.93	134.97	117.73	132.78	132.04	129.20	113.76
31	0.00	49.37	39.58	55.32	133.51	123.24	133.98	130.96	128.84	115.78
32	0.00	21.05	41.81	76.78	136.59	122.16	133.52	131.66	128.50	116.74
33	0.00	37.61	41.25	82.88	133.23	117.80	131.64	131.81	128.50	115.45
34	0.00	49.81	40.60	65.05	132.88	123.26	131.49	128.38	127.99	117.84
35	31.88	25.15	50.46	74.89	133.42	116.41	132.64	129.16	127.47	115.26
36	16.34	42.09	42.96	69.27	133.28	112.90	131.65	130.39	126.58	115.39
37	30.71	30.48	36.22	70.32	132.37	124.96	130.91	129.24	126.31	114.52
38	2.47	19.72	38.84	71.68	131.43	121.64	130.89	128.54	125.14	116.10
39	11.69	15.54	44.81	68.68	131.80	116.91	130.82	128.67	126.74	111.86
40	29.10	26.32	41.33	61.52	131.97	114.86	130.24	127.12	124.48	113.27
41	31.79	22.43	40.70	67.37	130.70	117.54	129.62	127.96	125.44	110.10
42	35.78	24.71	40.37	63.91	129.52	114.19	128.06	127.97	122.31	110.63
43	31.33	31.50	34.37	63.15	126.64	102.49	126.80	125.61	123.12	109.78
44	21.53	26.20	33.36	61.45	121.18	92.47	124.28	123.71	118.58	100.89
45	31.85	8.47	34.12	56.89	101.55	86.68	115.58	117.13	108.65	98.32
46	29.75	16.72	30.80	58.58	84.29	72.89	98.52	103.29	95.08	89.11
47	36.10	27.57	29.74	48.08	68.54	70.60	81.76	81.43	80.74	76.88
48	30.70	21.74	21.26	40.93	68.37	64.92	71.01	61.75	65.83	60.20
49	37.53	30.63	65.84	46.51	61.09	45.79	66.16	44.87	54.98	57.72
50	40.59	31.71	6.72	13.22	94.19	63.27	84.05	62.42	62.70	52.56

ENHANCED INLET, STATION 1

CP	VA1	VA2	VA3	VA4	VA5	VA6	VA7	VA8	VA9	VA10-AXIAL VEL
1	65.70	76.09	80.45	87.03	90.10	94.02	95.44	90.02	82.96	73.72
2	62.68	78.97	81.06	86.00	90.73	94.08	94.19	93.89	83.60	75.76
3	67.32	76.30	80.38	86.57	90.65	94.39	95.92	91.61	83.71	75.47
4	66.36	76.74	80.50	84.81	90.37	92.37	96.56	89.25	82.51	74.29
5	65.85	77.11	82.05	84.44	90.26	94.12	94.69	88.49	83.99	75.12
6	69.02	76.20	80.41	87.58	91.68	93.46	93.91	91.82	82.06	78.77
7	65.57	74.05	82.03	86.03	89.01	93.31	95.57	92.01	85.13	76.69
8	64.47	74.54	82.40	85.57	91.10	92.39	94.87	90.26	81.71	76.34
9	63.61	76.09	80.01	86.40	90.77	93.49	95.01	92.10	84.28	74.61
10	68.04	75.19	79.93	87.17	89.32	94.24	93.94	90.89	83.77	74.53
11	61.15	76.83	80.90	88.29	90.46	91.89	94.47	91.14	83.43	75.20
12	63.70	72.60	79.63	85.43	89.47	93.30	93.13	91.67	81.46	76.13
13	60.46	73.29	81.70	85.85	88.53	93.03	93.06	91.42	83.32	74.67
14	67.66	73.62	79.71	85.91	88.80	92.12	93.62	90.52	84.22	68.07
15	60.93	73.09	80.04	86.03	88.42	90.67	92.48	92.37	84.29	73.50
16	63.01	75.81	78.89	84.77	90.17	92.58	94.94	92.26	82.35	69.75
17	65.02	73.72	78.64	85.82	90.33	92.04	94.41	92.04	82.95	78.48
18	64.99	75.84	81.22	84.35	89.54	91.57	95.50	92.24	82.35	75.98
19	69.94	75.53	80.82	86.42	89.20	92.37	94.02	90.70	83.25	74.31
20	69.57	76.64	79.22	86.62	91.12	91.84	96.22	92.38	82.45	74.99
21	64.85	74.62	79.61	85.37	88.88	92.11	94.37	90.72	84.44	75.31
22	61.80	73.92	80.68	87.69	88.63	94.27	95.85	90.78	83.76	79.16
23	67.06	75.32	78.81	86.39	89.39	90.97	94.64	90.13	82.88	75.81
24	68.63	71.87	80.64	85.08	87.97	91.81	95.88	91.24	82.16	71.15
25	67.28	75.19	81.53	87.12	89.46	93.48	93.90	92.67	84.61	73.75
26	64.25	73.95	81.31	84.95	90.11	94.83	94.99	89.88	83.45	74.38
27	64.72	74.76	81.23	85.68	88.57	92.67	94.39	90.75	82.27	76.90
28	65.13	73.70	79.71	87.92	89.82	93.05	94.45	92.80	83.40	75.74
29	67.90	72.81	81.76	87.47	89.58	94.37	95.54	92.25	84.43	75.16
30	64.68	77.49	80.69	87.41	89.19	93.44	93.20	90.48	81.83	77.64
31	61.11	70.96	81.98	87.97	89.93	93.56	94.04	91.23	84.52	73.62
32	68.14	74.13	81.79	86.95	90.01	94.07	95.69	89.71	82.29	75.08
33	63.43	76.99	80.23	86.94	90.42	91.94	94.04	91.19	83.66	79.53
34	66.88	73.86	82.09	87.46	90.94	93.00	95.97	90.84	81.46	78.07
35	69.62	74.76	80.37	86.43	90.34	92.93	93.11	90.45	84.62	77.90
36	68.38	74.94	82.04	87.83	91.65	94.16	93.26	91.77	82.64	76.46
37	66.13	73.85	80.22	87.00	89.74	94.90	95.30	89.49	83.13	73.78
38	68.09	74.40	80.46	86.79	88.17	92.90	95.27	91.21	83.18	76.43
39	65.34	76.47	82.88	86.75	89.23	92.89	95.87	91.45	82.60	75.74
40	64.82	72.99	81.77	88.23	91.88	93.22	95.80	90.24	83.95	73.11
41	62.14	74.80	81.85	86.23	91.82	92.95	94.16	90.54	83.80	74.05
42	67.64	74.56	80.54	86.07	90.92	92.90	93.54	90.93	82.18	75.37
43	69.38	76.58	80.45	87.31	90.99	92.69	94.03	91.19	83.73	78.15
44	67.17	74.93	81.09	86.45	89.93	93.92	96.42	91.72	84.50	76.78
45	66.85	76.14	80.79	86.58	90.47	92.67	93.57	92.08	82.60	73.80
46	66.25	76.98	81.37	86.70	89.86	94.64	94.59	92.37	82.88	76.52
47	64.27	75.74	81.71	87.36	90.15	94.45	95.04	91.24	83.31	77.35
48	70.81	77.60	82.82	84.40	92.27	93.39	94.65	92.13	85.03	74.03
49	64.09	75.03	79.58	87.96	91.37	94.30	94.30	91.20	83.73	76.51
50	60.30	67.18	77.75	85.55	89.70	93.94	96.36	90.84	81.82	72.91

ENHANCED INLET, STATION 2

CP	VA1	VA2	VA3	VA4	VA5	VA6	VA7	VA8	VA9	VA10-AXIAL VEL
1	49.43	47.26	50.47	54.55	58.70	63.89	68.05	69.15	63.59	55.35
2	56.94	43.83	44.75	56.24	42.43	44.86	46.50	51.94	54.00	47.74
3	66.23	50.00	48.07	54.02	50.56	49.55	47.67	33.94	33.68	40.39
4	71.88	59.79	55.31	55.68	65.19	64.97	63.00	44.38	21.67	16.65
5	79.02	66.64	59.58	64.03	74.92	74.34	72.43	60.92	36.27	18.77
6	82.88	76.85	66.60	71.32	83.77	82.98	80.80	69.59	47.37	32.35
7	91.38	82.61	72.76	78.00	94.13	92.78	90.06	81.59	58.02	35.95
8	95.87	87.31	77.32	81.95	100.81	98.40	94.54	89.39	66.64	45.38
9	99.68	92.92	82.80	89.05	105.30	103.94	101.03	93.56	74.68	48.49
10	100.79	98.82	88.58	90.78	110.34	109.28	106.59	96.95	80.87	59.65
11	102.42	103.35	91.19	95.02	113.69	114.24	113.06	102.42	85.87	72.39
12	89.01	106.35	97.87	99.02	116.16	115.04	112.20	107.41	90.71	69.07
13	105.10	110.17	99.92	101.40	120.08	119.58	117.25	111.58	94.07	79.32
14	104.18	108.93	101.45	105.00	121.47	120.06	116.86	110.83	97.66	86.66
15	103.82	110.03	103.67	108.28	121.82	121.22	118.77	113.42	101.22	84.02
16	103.19	110.89	105.47	107.92	121.87	121.21	118.72	115.40	101.67	87.81
17	101.01	109.70	110.52	108.85	122.64	122.95	121.38	118.21	101.79	86.19
18	101.24	111.40	107.32	111.99	123.75	124.26	122.86	118.10	108.09	95.68
19	101.77	112.74	111.80	112.27	125.56	125.14	122.84	120.07	107.73	88.73
20	99.47	112.52	106.39	112.17	124.01	124.80	123.69	119.39	108.01	92.59
21	98.24	111.50	110.01	114.41	123.78	123.68	121.70	119.32	111.16	96.38
22	99.93	110.69	111.97	112.26	123.24	124.13	123.14	119.30	109.42	99.70
23	97.93	106.75	111.28	112.47	123.60	123.78	122.07	118.28	110.03	94.05
24	95.37	108.67	111.58	114.39	123.82	123.61	121.52	117.73	110.10	95.94
25	95.45	106.82	110.27	116.23	122.38	123.47	122.68	119.15	110.06	93.53
26	93.38	108.50	108.77	115.04	120.88	122.46	122.15	118.23	109.14	90.35
27	92.06	106.75	110.70	114.75	121.24	121.61	120.14	118.70	108.59	94.80
28	91.92	105.63	102.64	116.35	119.36	121.13	121.02	118.80	106.41	92.41
29	91.42	103.81	111.24	112.49	118.33	119.85	119.54	116.76	106.42	92.25
30	90.25	103.45	108.02	113.56	117.25	119.35	119.63	115.26	106.58	86.13
31	89.79	101.83	108.91	112.64	117.73	118.83	118.11	114.01	107.25	91.60
32	83.63	90.78	91.09	109.44	116.92	117.61	116.50	113.53	103.71	84.77
33	87.81	102.35	107.76	111.05	117.19	117.51	116.02	112.54	103.51	88.52
34	86.89	99.83	105.45	109.97	115.07	116.02	115.20	110.09	102.32	92.26
35	86.54	96.31	104.14	109.69	112.66	114.16	113.92	111.34	102.89	74.60
36	83.48	94.78	104.26	109.04	112.95	113.24	111.80	109.37	102.51	76.18
37	84.02	94.40	103.22	108.61	111.69	112.84	112.26	108.52	99.08	75.77
38	82.67	93.25	100.14	107.67	109.99	111.03	110.36	107.24	98.08	72.78
39	80.15	88.30	98.47	106.74	108.87	109.90	109.27	105.72	97.62	67.94
40	78.98	89.97	97.12	103.30	106.65	108.31	108.32	103.73	96.02	74.97
41	77.09	87.32	95.60	102.38	105.77	107.18	106.95	104.09	93.53	74.15
42	74.03	84.14	92.27	99.69	102.44	104.93	105.79	102.06	94.11	75.08
43	73.49	83.62	89.32	98.52	100.25	101.49	101.19	99.63	91.26	68.50
44	72.01	79.78	86.39	94.66	98.51	101.00	101.94	98.83	89.95	70.93
45	70.31	76.03	84.29	92.62	95.43	98.04	99.12	96.12	87.79	68.72
46	65.06	72.08	79.54	90.14	93.44	95.93	96.90	93.24	86.70	60.62
47	62.70	68.29	76.56	87.48	91.21	92.94	93.23	90.72	83.75	67.41
48	55.57	61.63	70.86	81.16	85.60	87.99	89.01	86.18	79.61	58.83
49	51.52	52.91	63.63	75.42	79.05	81.20	82.03	82.42	74.26	58.00
50	46.17	46.00	56.59	67.76	73.27	76.20	77.95	76.77	70.17	65.83

ENHANCED INLET, STATION 3

CP	VA1	VA2	VA3	VA4	VA5	VA6	VA7	VA8	VA9	VA10-AXIAL VEL
1	0.00	0.00	0.00	0.00	0.00	0.00	0.00	0.00	0.00	18.86
2	0.00	0.00	0.00	0.00	0.00	0.00	0.00	0.00	2.82	10.52
3	0.00	4.29	0.00	7.20	7.21	91.71	0.26	0.00	0.00	1.40
4	0.00	0.00	0.00	3.01	119.03	2.52	0.56	2.53	0.00	0.00
5	0.00	0.00	0.00	0.00	0.00	0.00	0.00	8.07	2.12	27.74
6	0.00	0.00	0.00	0.00	0.00	0.00	0.00	0.00	0.00	25.57
7	0.00	0.00	0.00	0.00	0.00	0.00	0.00	0.00	0.00	0.00
8	0.00	0.00	0.00	0.00	77.61	89.16	88.70	0.00	0.00	0.00
9	60.43	119.93	85.41	78.84	87.30	100.01	124.24	110.18	43.48	0.00
10	48.63	130.45	107.46	105.77	121.06	128.03	133.56	99.40	35.55	81.08
11	69.16	128.77	113.99	99.20	127.17	126.93	131.76	113.59	68.13	148.01
12	71.06	122.96	119.98	116.42	120.97	130.94	135.33	117.06	78.89	53.46
13	60.15	122.04	115.98	114.83	124.37	130.53	134.86	117.82	109.70	82.13
14	68.50	121.42	127.18	115.30	127.45	133.84	134.13	116.58	113.78	46.92
15	81.87	121.26	120.68	112.41	127.13	134.10	135.70	117.13	109.73	60.30
16	93.21	119.57	123.74	118.25	126.66	133.24	136.23	116.91	109.69	61.97
17	75.58	123.96	126.74	122.46	130.07	133.74	135.74	119.87	112.70	25.91
18	49.08	122.38	128.23	122.47	128.16	133.26	133.68	122.91	111.56	57.16
19	72.76	119.36	125.85	122.86	130.83	133.40	133.29	121.07	116.99	48.44
20	48.92	115.00	124.70	123.71	129.07	132.15	131.30	119.16	114.56	38.15
21	64.53	119.17	122.68	124.02	128.06	132.68	130.87	117.85	114.01	25.58
22	60.82	118.03	127.75	121.47	127.75	130.06	129.30	117.40	113.72	91.36
23	53.57	112.98	124.56	124.65	129.67	128.84	127.87	119.53	114.92	32.07
24	53.89	110.08	124.69	123.11	128.57	129.33	127.42	116.43	116.50	29.29
25	69.99	113.92	122.85	122.71	125.68	127.64	126.36	115.47	113.58	18.17
26	74.59	108.85	120.87	121.42	126.08	124.54	125.54	113.04	111.72	72.80
27	66.82	110.18	119.72	121.24	125.49	123.12	124.47	113.06	110.08	37.08
28	56.54	109.51	116.47	122.33	123.49	122.64	121.64	113.26	110.87	47.58
29	73.98	106.92	118.78	119.28	124.02	122.52	121.38	112.31	110.07	51.54
30	65.94	103.52	116.68	120.03	122.23	121.85	120.35	111.99	107.58	44.63
31	56.11	101.90	115.76	115.91	120.35	121.21	118.52	110.26	110.05	107.92
32	58.69	102.54	111.34	117.61	120.52	119.41	118.11	109.09	109.35	45.82
33	51.56	100.65	111.14	114.73	118.93	116.97	115.26	107.80	105.24	35.38
34	50.45	98.10	108.91	113.57	118.83	116.75	114.19	104.45	106.68	48.38
35	47.92	99.28	107.82	113.88	116.58	114.48	113.21	105.87	105.71	48.41
36	64.79	92.04	105.51	111.45	113.67	113.64	110.69	104.45	104.78	43.90
37	50.49	90.19	105.28	109.88	112.27	112.09	109.90	104.33	102.32	121.56
38	53.73	90.23	103.05	108.49	110.78	109.18	107.98	102.37	100.35	59.00
39	39.31	89.72	99.43	104.51	111.15	106.87	106.65	100.07	98.94	65.81
40	51.67	85.61	97.16	104.14	107.71	107.44	104.21	99.68	97.57	39.53
41	50.12	85.98	94.58	102.22	104.83	104.05	103.11	97.22	96.56	72.94
42	56.11	83.74	93.00	96.87	103.45	102.65	101.38	95.07	93.39	49.04
43	54.43	80.72	91.01	98.67	102.13	100.22	98.56	93.83	91.85	62.00
44	60.15	77.79	88.66	94.95	99.94	97.67	96.38	91.70	90.14	77.16
45	33.17	72.16	85.54	94.04	95.42	94.66	95.26	87.91	88.59	45.95
46	34.57	0.00	83.41	91.28	93.74	92.64	93.61	87.76	85.09	75.93
47	42.47	0.00	81.10	90.98	92.14	91.88	91.81	86.49	85.24	40.24
48	0.00	0.00	83.51	90.50	90.13	90.48	92.79	84.78	84.13	25.65
49	0.00	0.00	0.00	0.00	91.70	90.89	93.94	86.64	85.66	46.28
50	0.00	0.00	0.00	0.00	0.00	93.58	95.53	88.66	85.55	60.33

ENHANCED INLET, STATION 4

CP	VA1	VA2	VA3	VA4	VA5	VA6	VA7	VA8	VA9	VA10-AXIAL VEL
1	0.00	0.00	0.00	0.00	0.00	96.51	124.52	106.39	45.50	0.00
2	0.00	0.00	0.00	52.45	151.55	133.38	134.51	135.97	68.25	93.27
3	0.00	0.00	132.63	49.77	0.00	136.31	136.26	132.07	85.48	0.00
4	0.00	157.74	131.06	0.00	109.67	134.42	135.89	140.04	102.31	0.00
5	0.00	121.79	113.37	120.22	109.57	135.01	136.45	133.48	91.09	34.95
6	0.00	38.37	127.16	95.88	123.24	129.62	128.59	121.89	105.32	19.95
7	21.43	40.25	131.20	98.19	119.41	132.28	129.84	133.42	119.34	38.76
8	0.00	74.13	127.48	122.63	128.35	129.61	130.07	131.93	123.20	4.65
9	32.46	99.26	129.86	125.87	116.38	128.78	129.24	130.05	113.31	14.71
10	0.00	86.75	132.85	116.75	122.28	129.65	129.15	124.69	125.09	56.78
11	32.90	74.05	131.52	122.28	127.37	125.44	125.07	127.09	119.82	33.85
12	35.64	55.28	127.71	122.57	121.99	124.95	125.30	126.86	120.44	27.19
13	40.25	41.31	132.33	125.22	121.06	124.78	125.24	125.43	121.02	14.52
14	34.18	43.21	126.34	122.05	121.62	123.46	124.15	123.40	119.77	30.10
15	51.97	66.67	126.05	123.27	124.18	123.24	123.02	123.23	119.79	25.45
16	53.08	65.59	125.68	122.18	121.72	121.23	122.23	122.79	120.07	40.91
17	43.38	67.08	123.89	118.18	121.99	122.49	121.30	121.16	116.65	34.64
18	42.58	64.34	123.17	119.95	120.10	120.94	121.23	121.29	114.16	34.72
19	73.85	81.07	122.34	119.57	120.26	119.94	120.15	119.87	117.39	21.10
20	40.87	69.79	118.90	117.18	119.17	120.74	120.81	118.29	114.23	46.52
21	47.45	55.77	118.72	117.58	118.76	119.74	120.35	119.38	115.92	46.49
22	44.59	93.17	117.05	117.81	118.36	118.82	119.51	118.86	115.75	43.30
23	55.57	65.65	117.44	118.91	118.09	119.61	119.80	119.23	113.95	56.10
24	29.58	67.28	117.09	117.64	115.11	119.81	120.90	118.06	112.88	67.34
25	52.54	74.13	116.31	117.89	114.97	119.16	121.77	119.94	113.66	58.19
26	42.38	56.24	115.98	116.57	119.17	119.56	120.85	119.70	116.30	66.48
27	21.37	72.19	115.68	119.47	116.74	120.11	119.92	121.17	117.21	54.46
28	51.52	70.77	116.33	117.95	118.58	118.90	120.59	120.91	117.07	53.08
29	54.30	22.93	116.26	117.91	118.35	118.99	123.15	122.60	119.44	76.09
30	14.53	42.12	115.52	117.54	118.19	120.35	121.87	121.72	119.61	36.33
31	0.00	12.97	114.74	115.95	119.65	120.31	121.30	123.35	120.28	43.68
32	23.29	36.60	114.81	104.49	119.41	120.71	122.13	122.64	120.93	54.54
33	0.00	44.52	112.84	100.82	120.39	118.99	124.82	123.05	122.06	59.37
34	40.61	59.26	100.63	0.00	119.68	115.13	124.18	123.92	123.64	44.93
35	21.06	35.36	92.87	0.00	119.79	106.77	123.24	123.46	123.67	60.26
36	35.26	68.35	0.00	0.00	115.23	132.55	121.60	123.88	124.64	34.25
37	33.10	50.36	0.00	0.00	0.00	0.00	113.53	123.36	122.67	55.36
38	27.42	52.68	0.00	0.00	0.00	0.00	0.00	123.77	123.48	34.19
39	34.28	30.68	0.00	0.00	0.00	0.00	0.00	117.50	122.07	60.99
40	39.41	31.57	0.00	0.00	0.00	0.00	131.05	115.57	121.06	64.02
41	57.48	22.08	11.15	0.00	123.81	0.00	126.81	122.23	121.77	0.00
42	0.00	20.76	22.93	0.00	0.00	0.00	126.78	121.25	119.57	0.00
43	0.00	0.00	0.00	0.00	0.00	0.00	0.00	138.29	100.73	0.00
44	0.00	0.00	0.00	0.00	0.00	0.00	0.00	0.00	0.00	0.00
45	0.00	0.00	0.00	0.00	0.00	0.00	0.00	0.00	0.00	0.00
46	0.00	0.00	0.00	0.00	0.00	0.00	0.00	0.00	0.00	0.00
47	0.00	0.00	0.00	0.00	0.00	0.00	0.00	0.00	0.00	0.00
48	0.00	0.00	0.00	0.00	0.00	0.00	0.00	0.00	0.00	0.00
49	0.00	0.00	0.00	0.00	0.00	0.00	0.00	0.00	0.00	0.00
50	0.00	0.00	0.00	0.00	0.00	0.00	0.00	0.00	0.00	0.00

ENHANCED INLET, STATION 5

CP	VA1	VA2	VA3	VA4	VA5	VA6	VA7	VA8	VA9	VA10-AXIAL VEL
1	0.00	0.00	0.00	0.00	0.00	0.00	128.28	124.70	93.19	73.29
2	0.00	0.00	0.00	0.00	84.27	122.95	125.24	129.36	100.22	75.99
3	0.00	0.00	118.54	113.47	95.16	125.87	133.30	134.77	97.10	54.40
4	92.60	0.00	113.88	123.43	117.60	132.28	129.61	135.02	110.89	80.35
5	90.03	127.01	129.37	128.16	110.92	134.55	132.89	132.20	123.61	72.91
6	78.54	0.00	137.22	137.04	115.05	136.30	135.86	135.97	122.94	74.73
7	82.44	112.68	134.74	133.12	130.51	134.65	136.65	138.02	126.85	97.08
8	79.38	128.56	140.71	138.02	125.21	134.16	133.13	132.73	125.68	78.28
9	77.74	118.32	136.61	140.49	136.90	137.00	134.05	135.04	126.23	91.36
10	86.19	130.23	137.90	141.16	135.73	135.71	135.72	136.12	131.83	68.62
11	79.68	112.09	141.45	138.38	130.31	135.89	136.25	135.90	131.78	76.04
12	77.51	129.16	138.43	140.26	131.59	135.23	134.93	136.10	133.53	81.40
13	82.98	131.36	136.96	140.16	133.20	133.91	134.79	137.77	132.88	63.20
14	69.40	97.77	136.74	138.21	133.22	134.25	135.16	135.56	135.10	82.92
15	89.03	119.00	134.21	139.07	132.50	134.76	134.98	135.35	131.86	89.24
16	84.67	118.16	134.43	138.92	132.02	134.16	134.57	136.87	134.41	73.52
17	101.97	116.76	133.34	137.42	131.76	133.61	134.95	136.59	131.58	75.67
18	99.32	117.60	134.01	136.40	132.81	134.29	133.49	133.04	131.34	78.88
19	97.61	114.42	132.88	135.94	130.66	132.61	132.47	134.40	131.05	64.12
20	108.91	122.35	131.75	135.25	131.33	133.18	133.82	134.20	130.98	75.84
21	103.30	130.88	131.36	133.86	131.72	133.53	133.71	133.04	129.32	75.94
22	102.56	121.65	130.63	133.91	132.62	132.83	132.40	133.17	131.11	78.13
23	104.73	124.74	131.04	133.70	130.09	132.81	131.76	132.87	129.62	71.21
24	95.81	119.92	130.21	133.26	127.95	132.21	131.47	131.83	129.82	94.42
25	110.86	123.52	130.44	132.80	127.90	130.93	130.64	130.23	127.99	61.32
26	109.41	121.62	129.65	132.51	128.38	130.65	131.07	130.57	127.24	86.69
27	114.67	124.42	130.11	131.43	129.29	130.70	129.89	130.03	126.15	71.64
28	123.61	133.00	128.34	130.90	127.12	129.36	129.16	129.41	124.64	99.91
29	61.10	122.90	127.43	130.74	126.75	128.68	128.62	128.72	124.27	82.00
30	70.12	119.18	126.71	130.66	125.10	128.23	128.02	127.80	123.71	84.56
31	83.35	120.87	127.07	128.37	126.09	127.83	126.60	125.96	121.78	78.02
32	119.52	119.50	125.07	128.35	125.68	126.23	125.39	126.59	121.85	81.21
33	140.52	119.22	125.64	126.04	124.62	126.02	125.57	126.11	121.65	93.97
34	107.96	118.53	122.71	113.97	123.16	123.74	124.34	124.56	120.03	93.63
35	71.49	116.21	123.39	106.25	122.69	120.96	124.59	123.08	118.02	95.80
36	17.07	123.90	122.40	0.00	122.62	110.57	123.47	122.51	115.82	93.37
37	20.42	112.33	121.27	0.00	120.09	99.52	122.66	121.23	117.52	81.86
38	19.53	0.00	109.37	0.00	118.66	0.00	122.24	120.65	113.57	104.31
39	74.90	17.48	70.87	120.76	106.11	0.00	115.28	118.61	116.26	102.38
40	37.13	23.33	20.28	0.00	13.21	78.57	126.94	120.99	117.39	96.20
41	0.00	23.66	0.00	0.00	0.00	0.00	126.95	126.87	113.77	11.69
42	0.00	0.00	0.00	0.00	0.00	0.00	0.00	0.00	86.51	49.37
43	0.00	0.00	0.00	0.00	0.00	0.00	0.00	0.00	119.00	14.69
44	0.00	0.00	0.00	0.00	0.00	0.00	0.00	0.00	0.00	0.00
45	0.00	0.00	0.00	0.00	0.00	0.00	0.00	0.00	0.00	0.00
46	0.00	0.00	0.00	0.00	0.00	0.00	0.00	0.00	0.00	0.00
47	0.00	0.00	0.00	0.00	0.00	0.00	0.00	0.00	0.00	0.00
48	0.00	0.00	0.00	0.00	0.00	0.00	0.00	0.00	0.00	0.00
49	0.00	0.00	0.00	0.00	0.00	0.00	0.00	0.00	0.00	0.00
50	0.00	0.00	0.00	0.00	0.00	0.00	0.00	0.00	0.00	0.00

ENHANCED INLET, STATION 6

CP	VA1	VA2	VA3	VA4	VA5	VA6	VA7	VA8	VA9	VA10-AXIAL VEL
1	0.00	0.00	0.00	0.00	0.00	0.00	0.00	0.00	0.00	
2	0.00	0.00	0.00	92.86	95.40	89.21	105.47	116.62	102.72	
3	96.82	0.00	131.53	115.23	110.23	119.08	119.02	125.67	107.97	
4	94.99	112.89	138.73	122.23	106.79	119.32	123.62	126.56	118.02	
5	98.17	130.79	140.59	127.64	121.21	132.97	130.93	128.89	126.08	
6	90.21	123.82	139.64	129.33	128.05	130.00	131.76	129.66	124.54	
7	107.61	132.60	141.19	136.19	129.54	135.23	132.45	131.58	121.25	
8	108.84	125.37	142.77	136.98	125.63	132.56	132.32	132.72	126.13	
9	99.48	129.48	140.15	135.93	134.94	132.53	130.59	130.38	126.81	
10	107.67	130.75	139.90	137.40	131.93	134.67	132.45	130.41	127.71	
11	106.12	131.57	140.61	135.21	135.82	135.70	131.73	130.20	133.49	
12	113.39	132.43	139.70	138.76	134.46	134.86	130.13	129.69	127.72	
13	122.17	131.35	139.29	138.06	135.38	133.57	132.00	129.21	128.25	
14	104.42	133.05	137.55	137.71	134.09	132.25	130.98	130.06	128.02	
15	114.60	132.62	137.99	137.95	132.61	131.82	129.47	130.15	127.64	
16	120.05	133.33	137.11	137.49	132.51	133.03	129.44	126.95	125.69	
17	123.31	134.81	135.60	135.88	132.26	131.57	129.27	128.37	126.62	
18	124.30	133.40	135.14	136.50	131.58	130.80	128.84	126.85	125.55	
19	128.81	133.20	134.83	135.96	131.87	130.91	128.28	126.19	125.77	
20	126.78	133.07	134.61	135.53	131.73	130.71	128.56	126.08	126.35	
21	116.07	131.36	132.66	134.83	130.93	129.81	127.54	126.37	122.16	
22	130.80	131.88	131.86	133.93	129.88	128.68	127.63	125.37	123.39	
23	121.12	132.33	132.36	133.33	128.34	129.10	126.08	124.74	124.12	
24	126.28	130.66	131.56	131.71	128.62	127.27	126.53	123.98	120.72	
25	124.54	128.92	132.25	131.38	127.90	127.80	125.38	124.24	121.38	
26	101.81	129.21	130.66	130.05	127.50	127.63	125.63	123.86	119.79	
27	104.94	129.09	128.86	130.03	127.77	127.42	124.60	123.82	121.15	
28	105.71	128.41	128.58	129.03	126.99	126.94	124.50	123.75	121.44	
29	108.86	126.14	127.72	127.92	125.93	126.37	123.36	122.46	119.67	
30	80.47	126.16	126.58	128.56	126.78	126.15	124.48	121.49	117.79	
31	118.84	126.45	127.33	126.87	125.56	125.95	122.89	120.82	119.90	
32	118.01	126.04	126.17	127.40	124.86	126.04	122.68	121.31	119.12	
33	114.65	125.90	126.44	126.19	124.58	125.70	121.69	120.09	118.87	
34	116.34	124.32	126.61	126.46	125.12	124.54	121.50	120.23	118.59	
35	32.60	123.99	126.08	126.84	125.05	124.53	121.04	119.61	116.38	
36	61.29	124.82	124.88	124.61	124.25	124.15	121.32	118.74	115.29	
37	45.91	123.75	124.09	122.57	122.24	124.66	120.38	119.14	115.74	
38	0.00	120.93	123.65	123.09	122.23	123.63	120.50	117.14	113.10	
39	45.69	121.58	121.68	121.94	122.23	122.18	115.92	116.17	113.90	
40	49.36	111.74	119.85	111.78	109.78	108.69	100.71	109.44	111.07	
41	0.00	46.63	98.73	10.81	111.89	92.87	85.45	90.25	105.99	
42	0.00	0.56	111.55	77.23	134.98	83.35	35.10	43.79	89.61	
43	0.00	0.00	0.00	0.00	0.00	0.00	0.00	0.00	0.00	
44	0.00	0.00	0.00	0.00	0.00	0.00	0.00	0.00	0.00	
45	0.00	0.00	0.00	0.00	0.00	0.00	0.00	0.00	0.00	
46	0.00	0.00	0.00	0.00	0.00	0.00	0.00	0.00	0.00	
47	0.00	0.00	0.00	0.00	0.00	0.00	0.00	0.00	0.00	
48	0.00	0.00	0.00	0.00	0.00	0.00	0.00	0.00	0.00	
49	0.00	0.00	0.00	0.00	0.00	0.00	0.00	0.00	0.00	
50	0.00	0.00	0.00	0.00	0.00	0.00	0.00	0.00	0.00	

ENHANCED INLET, STATION 7

CP	VA1	VA2	VA3	VA4	VA5	VA6	VA7	VA8	VA9	VA10-AXIAL VEL
1	0.00	0.00	0.00	0.00	0.00	0.00	0.00	0.00	0.00	0.00
2	0.00	15.70	0.00	0.00	0.00	0.00	0.00	0.00	0.00	0.00
3	0.00	168.94	27.69	41.08	51.84	73.08	86.49	93.81	88.76	0.00
4	0.00	16.01	121.76	89.91	58.19	93.19	90.78	98.02	88.35	113.97
5	0.00	15.49	132.77	115.52	87.24	91.39	97.93	100.35	97.06	0.00
6	0.00	13.67	57.08	138.28	75.75	106.35	101.57	111.36	88.34	49.23
7	0.00	14.78	0.00	69.80	86.14	124.42	115.64	125.13	100.08	82.81
8	0.00	13.37	0.00	72.86	92.38	121.24	118.98	115.23	111.13	78.70
9	0.00	15.88	139.43	120.83	100.66	120.68	116.25	121.78	109.43	73.59
10	0.00	117.38	141.97	115.35	88.85	122.41	120.98	121.94	109.55	90.23
11	0.00	177.88	98.95	112.73	124.70	126.13	123.99	124.88	116.12	64.68
12	0.00	0.00	137.65	128.78	118.01	127.81	124.89	125.91	116.60	92.27
13	0.00	0.00	121.36	126.52	129.36	126.90	127.51	125.65	115.52	67.63
14	0.00	0.00	146.24	138.83	129.20	129.17	126.04	124.99	120.96	89.31
15	0.00	0.00	130.91	129.69	126.22	127.08	125.93	126.76	114.76	67.63
16	0.00	137.93	136.42	135.89	132.94	130.12	127.30	127.51	121.04	87.58
17	0.00	0.00	133.79	133.08	130.03	128.87	127.48	126.84	122.95	42.25
18	85.41	0.00	112.28	120.63	126.65	129.85	126.69	126.21	125.42	110.36
19	0.00	251.41	129.56	130.68	129.38	129.52	127.09	126.49	123.31	88.49
20	0.00	240.86	130.94	129.08	124.97	128.27	126.42	125.64	121.58	70.86
21	0.00	123.20	132.40	133.03	131.24	129.97	127.04	127.03	122.98	83.52
22	0.00	0.00	133.18	132.91	130.20	129.44	126.18	125.93	123.20	78.62
23	0.00	0.00	134.04	132.48	128.54	129.57	126.61	128.68	124.77	82.99
24	0.00	113.68	132.88	130.69	126.19	128.69	127.18	126.82	126.41	83.96
25	0.00	0.00	129.43	130.63	129.45	129.05	126.70	126.29	125.05	85.01
26	0.00	0.00	132.39	130.68	126.68	128.76	125.92	126.34	122.72	105.18
27	0.00	121.25	126.83	128.24	127.28	128.68	126.18	126.42	122.79	92.76
28	0.00	117.40	127.70	128.48	126.90	128.64	126.52	127.36	121.53	94.04
29	0.00	109.77	129.31	127.88	124.21	128.59	125.36	124.89	121.44	87.08
30	0.00	0.00	132.07	130.38	126.38	127.48	125.23	126.83	123.15	73.57
31	0.00	129.15	127.09	127.46	125.52	127.54	125.70	125.47	122.42	91.65
32	0.00	117.57	130.66	129.17	125.37	127.55	125.47	125.20	121.84	77.35
33	0.00	123.14	129.00	128.74	126.15	127.37	125.11	125.58	124.51	48.50
34	0.00	109.37	129.95	128.84	125.46	126.27	125.36	123.19	123.05	104.59
35	0.00	0.00	125.48	125.80	123.80	125.69	124.60	123.49	119.22	83.53
36	18.68	0.00	124.61	125.15	123.44	127.00	124.29	123.59	120.24	64.43
37	61.17	128.80	123.37	125.09	124.46	125.58	123.73	123.37	119.87	94.13
38	0.00	0.00	126.73	126.60	124.17	125.79	122.53	122.61	117.32	59.42
39	0.00	110.68	126.67	126.60	124.21	126.07	122.79	122.21	118.76	78.23
40	0.00	122.46	125.02	124.53	121.76	125.16	122.87	121.09	118.80	99.04
41	0.00	15.59	125.23	124.49	121.47	125.87	121.87	121.80	119.22	86.80
42	10.85	21.92	124.39	125.94	125.12	124.41	121.56	119.32	118.82	92.60
43	0.00	9.93	114.94	119.68	122.04	123.63	118.30	109.43	117.03	94.93
44	0.00	10.47	0.34	9.14	11.52	118.36	107.86	99.51	110.32	87.80
45	5.41	10.06	0.58	1.85	3.13	73.40	92.63	83.26	100.02	81.99
46	7.31	13.91	10.46	0.00	4.38	0.41	90.78	73.24	89.94	5.34
47	4.67	23.01	2.88	0.00	17.04	12.79	55.80	80.51	75.78	9.43
48	16.83	23.76	8.05	4.02	0.00	65.61	61.29	65.78	76.29	17.71
49	0.00	0.00	0.00	0.00	49.31	64.01	62.13	77.89	76.30	57.15
50	0.00	0.00	0.00	0.00	0.00	0.00	0.00	0.00	0.00	0.00

ENHANCED INLET, STATION 8

CP	VA1	VA2	VA3	VA4	VA5	VA6	VA7	VA8	VA9	VA10-AXIAL VEL
1	0.00	274.76	39.97	47.04	45.80	36.17	20.20	54.63	41.50	26.65
2	4.14	277.59	42.51	42.55	0.00	47.65	33.31	65.58	29.60	89.58
3	0.00	43.75	41.48	42.96	63.85	35.72	37.64	69.69	74.52	34.84
4	0.00	79.60	38.75	42.42	4.48	52.55	30.59	80.99	47.59	1.20
5	0.00	175.44	35.23	42.34	16.07	44.66	35.29	89.20	64.78	250.76
6	0.00	277.53	36.61	42.27	14.00	106.93	2.08	92.31	49.90	17.40
7	0.00	194.49	31.01	47.14	29.62	72.00	36.07	99.87	49.60	87.10
8	0.00	213.77	29.61	37.08	28.06	77.25	79.14	105.49	84.00	13.05
9	0.00	76.28	11.11	44.88	11.74	83.29	105.95	113.81	75.47	102.02
10	0.00	158.58	209.00	19.05	1.66	96.40	101.33	117.85	86.19	29.79
11	0.00	213.45	274.35	35.82	2.79	102.06	113.47	123.59	91.47	31.48
12	0.00	104.55	252.95	0.00	18.11	118.42	117.14	122.70	85.72	75.57
13	0.00	139.37	274.17	39.01	47.60	125.35	121.49	125.50	87.46	5.45
14	0.00	277.53	239.60	62.73	28.25	124.03	123.78	127.27	107.92	31.86
15	0.00	105.66	252.61	56.78	30.84	126.96	125.77	128.70	88.73	5.26
16	0.00	62.69	252.77	57.46	36.75	127.21	124.16	127.78	92.50	21.30
17	0.00	48.50	230.71	32.89	33.23	130.19	125.60	129.32	93.02	9.11
18	0.00	60.61	231.17	102.61	13.97	124.53	117.30	126.48	92.31	7.12
19	0.00	96.27	273.29	39.68	40.05	131.07	131.28	130.06	96.56	29.45
20	0.00	49.58	247.91	39.01	35.37	125.98	128.22	128.99	101.51	49.34
21	0.00	79.55	269.21	0.00	30.51	129.41	129.64	128.41	101.50	8.99
22	0.00	95.94	259.83	22.59	48.86	132.38	131.40	129.02	109.03	28.00
23	0.00	139.85	274.06	61.66	23.53	132.16	130.91	128.22	98.94	7.20
24	0.00	106.62	272.50	30.67	31.02	130.37	130.27	128.74	102.44	27.89
25	0.00	8.67	274.31	5.71	26.31	131.09	126.10	128.36	107.77	14.34
26	0.00	56.20	240.32	124.13	18.53	128.35	125.90	129.66	103.97	13.03
27	0.00	56.98	276.79	40.37	36.20	129.97	124.75	129.58	114.32	22.28
28	0.00	87.87	232.89	9.68	26.36	128.82	126.69	128.10	106.39	32.31
29	0.00	74.99	253.45	139.41	41.19	131.63	125.24	128.38	113.41	28.42
30	0.00	12.15	274.00	159.62	30.67	129.63	125.07	127.75	105.61	7.72
31	0.00	113.73	263.61	271.76	32.26	128.06	125.48	128.30	113.16	23.04
32	0.00	16.49	257.34	19.85	21.51	128.43	124.05	127.69	106.33	55.48
33	0.00	119.07	260.92	133.11	25.79	127.83	123.99	128.31	106.06	8.66
34	0.00	56.84	273.59	130.07	33.07	126.56	125.15	127.46	115.30	0.38
35	0.00	104.19	271.00	53.32	48.86	130.22	124.71	126.91	113.66	11.54
36	0.00	76.71	261.25	146.59	47.96	130.44	123.86	126.58	108.83	20.48
37	0.00	49.09	251.24	81.35	44.82	127.45	124.17	127.10	116.67	32.33
38	0.00	61.40	262.46	133.11	23.47	125.38	123.37	126.04	107.61	30.66
39	0.00	79.99	212.29	89.48	21.51	126.22	123.51	125.86	107.53	8.57
40	0.00	56.92	211.31	9.31	19.00	126.07	121.83	125.45	112.09	5.86
41	0.00	63.12	33.71	43.16	36.66	125.59	122.78	125.07	109.93	30.63
42	1.53	73.49	32.13	26.72	45.32	125.16	122.25	124.51	105.77	43.27
43	1.71	30.59	25.88	40.06	42.52	125.66	121.93	124.50	104.65	13.39
44	1.91	64.62	261.20	115.53	34.10	124.44	120.15	124.98	100.73	23.16
45	0.00	22.45	272.03	112.77	35.81	123.20	119.68	122.35	104.36	8.51
46	0.00	17.71	256.83	84.76	30.08	120.73	117.12	118.70	104.63	33.20
47	17.91	26.75	18.93	31.08	31.45	111.94	108.51	109.48	102.07	1.02
48	18.30	26.36	31.23	39.35	29.56	95.45	94.28	93.99	91.72	22.13
49	14.63	21.07	37.89	37.94	26.80	70.45	68.53	70.34	81.83	29.40
50	8.91	39.73	38.92	44.02	36.02	45.36	19.68	51.76	50.59	43.52

TABLE A2. -

(b) ABSOLUTE TANGENTIAL VELOCITY (M/S)

BASELINE INLET, STATION 1

CP	VT1	VT2	VT3	VT4	VT5	VT6	VT7	VT8	VT9	VT10- ABS TAN
1	4.64	3.66	4.70	4.13	4.82	4.75	6.25	6.36	4.06	5.73
2	4.50	2.96	4.09	4.29	6.00	5.09	5.87	5.97	5.00	9.00
3	4.79	3.12	4.08	4.71	5.70	5.19	6.42	6.37	4.99	9.18
4	4.09	3.10	3.89	4.59	5.35	5.16	6.44	6.35	2.59	8.51
5	5.66	3.54	3.73	4.43	5.67	4.74	6.41	6.65	5.22	8.85
6	4.44	3.35	3.86	3.99	5.26	5.02	6.16	6.13	5.41	8.08
7	3.81	3.13	4.02	4.34	4.96	4.64	6.31	6.73	5.67	-0.44
8	4.39	3.32	3.76	4.59	5.77	5.69	6.92	5.86	4.36	2.43
9	4.23	4.20	4.59	4.35	5.69	5.85	5.67	6.69	4.90	8.16
10	7.03	3.93	3.86	4.35	5.84	5.73	6.98	6.75	4.83	6.96
11	3.37	3.89	4.39	4.84	6.05	5.28	5.83	6.05	3.19	1.35
12	4.22	3.06	3.88	4.09	5.16	5.29	6.87	6.12	1.66	8.22
13	3.54	3.90	4.58	4.38	5.63	5.59	6.89	7.01	4.21	8.38
14	3.78	4.03	4.30	4.65	5.38	4.84	6.15	6.96	1.96	-0.39
15	4.83	3.32	3.94	4.17	6.87	5.40	6.19	6.15	5.15	8.00
16	3.59	3.37	5.03	4.90	5.47	5.34	6.79	6.27	5.03	-0.38
17	3.39	3.49	4.49	3.75	5.78	5.53	6.25	6.15	2.82	5.61
18	3.39	3.55	4.41	4.51	6.16	5.94	6.03	6.18	3.65	8.29
19	3.52	2.70	4.39	4.08	5.84	5.99	5.60	6.38	3.74	3.84
20	3.90	3.65	4.16	4.33	5.52	5.38	5.82	6.73	4.40	9.51
21	4.04	3.17	4.29	4.27	5.40	5.95	6.39	5.97	5.46	7.52
22	3.65	3.54	4.51	4.51	5.17	5.21	6.79	5.99	3.99	9.98
23	4.10	2.88	4.05	4.78	5.35	5.51	6.31	5.58	3.59	8.44
24	5.03	3.15	3.97	4.74	5.49	5.44	6.07	6.50	4.81	-7.07
25	2.53	2.89	4.34	4.29	5.89	5.78	5.97	5.54	2.95	9.54
26	4.53	3.21	3.89	4.65	5.75	5.67	6.93	6.59	3.85	1.22
27	3.43	2.73	4.13	4.39	5.89	5.32	5.38	6.15	1.96	6.84
28	5.89	3.40	4.29	4.81	5.41	5.48	6.10	5.63	3.12	5.72
29	3.48	3.73	3.90	4.41	5.50	5.06	6.13	6.10	2.40	-0.42
30	5.13	3.90	4.11	4.62	5.79	5.08	5.99	6.54	4.87	6.61
31	4.23	3.26	4.27	4.45	5.88	5.26	6.68	6.37	4.75	5.06
32	4.34	3.24	4.26	4.80	6.25	5.61	5.51	5.35	4.49	5.09
33	4.89	2.96	3.69	4.25	5.56	4.68	6.03	5.82	4.34	6.89
34	5.24	4.07	4.33	4.93	5.05	5.49	5.59	5.17	3.73	6.90
35	3.99	2.68	3.20	4.83	5.01	4.48	6.23	6.22	1.54	6.16
36	3.89	3.79	3.00	3.93	5.18	5.59	6.61	5.88	5.87	-0.53
37	4.61	3.27	4.18	4.33	6.11	4.97	5.01	6.38	4.83	5.27
38	3.35	2.95	4.31	3.50	5.90	4.76	5.60	5.94	5.13	6.32
39	2.81	3.72	4.64	4.35	4.93	5.34	6.50	4.90	2.32	7.90
40	4.89	3.52	4.97	4.51	5.31	4.54	5.65	5.48	3.18	4.99
41	4.01	3.12	3.58	4.46	6.42	4.95	5.55	6.17	2.72	6.15
42	4.24	3.91	4.07	4.03	5.43	4.85	5.62	5.68	0.36	7.31
43	4.24	3.76	4.50	4.55	5.54	5.05	5.15	5.52	2.36	6.39
44	5.61	3.36	4.36	3.29	5.88	4.64	5.60	6.34	0.89	5.09
45	4.33	3.38	4.19	4.75	4.93	5.61	5.39	5.83	2.75	5.87
46	4.40	2.77	3.98	4.75	5.77	4.66	5.27	5.02	2.57	5.27
47	3.52	3.39	4.40	3.85	5.08	4.26	5.83	4.89	4.83	5.80
48	2.31	3.04	4.31	4.66	5.67	5.06	5.47	4.99	4.32	-0.25
49	3.89	2.87	4.75	4.86	5.51	5.80	6.94	6.68	4.71	8.93
50	5.77	5.31	3.85	7.56	7.34	7.37	6.11	5.69	9.07	18.71

BASELINE INLET, STATION 2

CP	VT1	VT2	VT3	VT4	VT5	VT6	VT7	VT8	VT9	VT10- ABS TAN
1	-40.00	-30.85	-13.34	-3.44	13.94	38.54	6.83	18.60	25.72	-21.50
2	-41.93	-39.29	-20.07	-15.35	-0.50	25.31	-17.74	-3.61	9.29	-20.10
3	-38.17	-41.31	-26.69	-11.12	-14.48	7.82	-26.39	-19.25	-19.83	-16.18
4	-33.27	-42.03	-31.52	-28.26	-20.98	-7.00	-37.02	-31.32	-27.46	-26.42
5	-28.36	-41.49	-33.17	-31.48	-24.55	-16.22	-38.17	-37.20	-22.17	-19.83
6	-23.93	-39.05	-32.81	-32.58	-29.58	-21.24	-38.70	-42.25	-29.48	-23.44
7	-19.86	-35.75	-31.85	-34.53	-29.05	-26.76	-40.67	-43.18	-40.72	-7.49
8	-16.67	-31.50	-33.42	-34.43	-29.07	-28.55	-36.36	-40.58	-41.12	-15.64
9	-13.09	-27.76	-29.51	-19.40	-28.14	-29.60	-34.06	-38.02	-34.86	-10.88
10	-9.91	-24.58	-27.73	-32.33	-26.55	-31.03	-30.08	-36.49	-32.94	-12.00
11	-7.68	-21.25	-26.34	-32.44	-24.75	-29.63	-28.25	-34.57	-38.73	-11.96
12	-6.10	-18.67	-22.87	-28.81	-22.60	-30.26	-23.86	-28.55	-35.13	-42.10
13	-4.09	-15.20	-20.63	-28.39	-20.97	-28.58	-20.81	-26.57	-40.11	-29.76
14	-2.84	-13.93	-17.38	-23.46	-18.51	-27.71	-18.68	-23.85	-35.25	-12.22
15	-0.34	-10.05	-14.49	-18.19	-15.54	-25.95	-14.54	-19.66	-24.09	-15.13
16	0.96	-7.57	-11.77	-18.01	-14.02	-25.30	-12.75	-16.99	-22.82	-42.34
17	2.43	-4.56	-9.17	-20.54	-10.41	-22.58	-10.17	-14.94	-20.67	-9.90
18	3.21	-3.45	-6.03	-14.18	-8.90	-19.72	-8.14	-12.17	-24.83	-13.73
19	4.86	-4.04	-3.54	-9.90	-6.54	-17.87	-4.07	-7.44	-13.43	22.86
20	5.71	-0.54	-0.81	-9.27	-4.02	-16.14	-1.71	-5.76	-16.30	7.68
21	6.58	2.77	0.91	-4.01	-1.41	-15.47	-0.41	-3.07	-8.26	-6.98
22	7.60	3.39	2.90	-2.79	0.87	-12.18	3.70	-0.48	-9.95	3.23
23	8.49	4.36	4.90	-0.57	3.83	-11.33	4.12	1.54	-4.93	-14.33
24	9.74	5.69	8.06	1.73	5.59	-9.82	7.49	6.24	0.54	10.60
25	10.68	7.38	8.83	-2.30	7.09	-6.86	9.51	7.73	4.45	-10.27
26	11.65	7.99	11.32	4.86	9.53	-6.19	10.55	9.30	-2.23	-24.27
27	12.42	10.36	12.56	5.55	11.02	-2.76	12.59	10.93	3.41	10.56
28	13.15	10.84	13.70	20.17	14.31	-0.94	14.36	14.35	8.65	-17.82
29	14.75	13.22	15.78	3.63	15.74	1.64	18.68	13.45	6.55	13.61
30	16.01	13.14	16.48	8.69	17.98	1.29	18.60	18.25	16.01	5.60
31	16.91	14.51	17.55	7.06	19.26	4.83	21.07	17.86	17.17	30.28
32	17.68	16.99	19.28	16.47	20.88	6.79	25.49	25.15	26.98	11.98
33	19.37	16.30	19.86	5.93	22.16	8.67	22.70	22.75	20.82	13.40
34	20.92	17.02	22.22	20.27	24.11	10.89	25.52	24.49	18.31	25.58
35	21.96	18.82	23.36	21.12	27.04	12.50	26.99	24.50	24.41	18.26
36	22.97	19.12	24.85	19.11	28.14	13.76	28.81	27.21	22.53	14.63
37	23.02	20.34	25.14	16.00	29.75	16.35	28.39	28.72	23.38	32.24
38	23.51	21.51	26.71	13.63	30.81	17.19	29.97	30.53	23.82	34.92
39	25.25	21.71	27.42	16.58	32.17	20.25	33.12	30.74	28.21	31.70
40	24.77	24.24	29.32	6.24	33.42	21.00	34.21	34.10	25.27	15.57
41	24.50	25.19	29.99	26.92	34.09	22.67	36.52	33.77	26.33	2.46
42	24.85	24.17	31.89	34.98	36.43	24.81	37.26	36.42	31.45	29.97
43	25.43	26.69	32.41	16.14	37.14	26.58	39.03	37.59	26.29	0.92
44	25.58	26.29	33.31	26.27	38.23	27.08	41.30	40.17	37.48	32.45
45	23.73	24.13	33.89	35.13	39.70	29.17	43.24	41.67	37.82	25.23
46	18.87	25.68	33.32	31.60	41.63	32.46	44.70	43.90	37.96	33.02
47	12.63	19.56	31.36	32.04	41.61	34.98	46.01	45.72	42.49	0.02
48	-2.25	10.15	27.76	27.67	43.04	37.45	47.86	50.11	42.83	54.60
49	-22.28	-1.06	16.70	14.25	39.46	39.42	47.38	51.16	50.25	29.66
50	-34.42	-20.53	0.76	5.90	31.81	41.20	37.38	45.85	42.88	-3.41

BASELINE INLET, STATION 3

CP	VT1	VT2	VT3	VT4	VT5	VT6	VT7	VT8	VT9	VT10- ABS TAN
1		*******	14.49	-6.30	6.23	0.00	-20.85	0.00	0.00	0.00
2		0.00	4.82	44.69	0.00	0.00	2.11	0.00	11.42	1.75
3		-20.38	162.52	-6.52	112.24	31.17	19.98	-0.79	23.59	-1.25
4		0.00	0.00	121.12	187.61	26.88	189.19	185.30	39.73	-3.59
5		0.00	0.00	0.00	0.00	0.00	0.00	158.04	184.44	14.17
6		0.00	0.00	0.00	0.00	0.00	0.00	0.00	0.00	-28.43
7		0.00	0.00	0.00	0.00	0.00	0.00	0.00	0.00	0.00
8		-19.98	0.00	0.00	-11.58	69.25	-31.18	0.00	0.00	0.00
9		0.00	-33.25	-25.42	-31.49	20.96	-28.41	-32.63	37.20	0.00
10		-9.96	-26.49	-24.93	-28.61	-27.00	-29.66	-30.39	-20.87	0.00
11		-6.52	-19.49	-17.04	-26.54	-28.38	-24.93	-30.25	-28.01	26.97
12		-3.97	-14.52	-21.33	-24.06	-27.20	-20.63	-27.03	-28.07	-31.79
13		0.55	-11.46	-22.65	-20.85	-23.70	-18.87	-26.59	-31.69	-24.69
14		-3.91	-7.97	-19.50	-18.48	-20.92	-17.15	-23.38	-26.60	-32.59
15		4.05	-3.39	-12.31	-13.59	-18.68	-12.86	-18.30	-20.94	3.66
16		6.65	2.82	-4.12	-12.74	-17.16	-8.04	-15.55	-20.98	-106.43
17		7.07	4.69	-8.51	-4.61	-13.37	-6.96	-10.87	-18.06	-24.89
18		9.85	4.64	-1.80	-0.42	-11.05	-5.52	-11.06	-15.39	-7.80
19		3.70	10.51	3.98	-2.87	-7.77	-3.25	-5.33	-11.38	18.99
20		14.62	11.16	2.37	5.11	-4.66	0.81	-3.81	-6.20	41.31
21		15.86	11.34	5.89	1.22	-2.46	3.50	-2.90	-4.77	52.67
22		17.68	16.09	7.12	6.57	0.11	6.48	1.66	-3.03	56.00
23		17.98	17.51	7.98	10.19	1.45	5.12	3.16	0.75	46.91
24		17.85	18.22	15.04	13.04	4.86	8.02	5.71	1.94	34.24
25		19.54	19.23	13.99	16.00	7.28	10.81	5.78	6.23	25.58
26		21.38	21.97	17.08	19.87	7.94	13.13	9.89	8.19	-0.50
27		23.60	25.31	18.40	18.84	11.08	17.18	11.02	10.54	-19.07
28		24.60	26.19	27.93	23.03	12.90	19.25	13.98	11.51	-12.72
29		26.12	27.55	19.15	24.55	14.52	20.71	15.50	14.38	-15.19
30		25.97	27.40	24.71	26.73	16.61	20.67	18.93	15.40	-45.09
31		28.66	30.55	24.81	28.81	18.72	25.15	18.94	18.27	20.29
32		28.83	32.76	27.36	27.96	19.35	23.94	21.26	21.74	-9.19
33		31.09	33.04	31.02	34.34	22.11	27.12	23.47	22.91	55.82
34		33.12	35.20	29.21	33.72	25.18	28.94	26.38	23.72	-99.93
35		33.76	37.30	35.73	34.21	26.32	28.76	27.78	26.91	14.99
36		34.81	38.97	34.09	39.19	27.89	32.37	28.65	25.91	-12.98
37		38.30	41.09	39.77	43.00	30.53	37.03	33.34	28.27	29.18
38		40.51	44.15	38.97	42.26	32.59	37.36	33.74	31.84	-79.44
39		43.59	46.33	38.29	47.98	35.01	40.40	34.85	31.76	41.60
40		47.27	50.21	44.37	46.69	36.75	43.36	39.95	37.83	46.10
41		51.73	51.16	50.49	52.95	38.56	47.14	43.10	38.52	23.28
42		56.55	55.00	53.73	52.10	42.79	51.12	45.65	46.12	-2.48
43		61.91	59.98	52.51	62.62	45.44	56.44	49.80	46.28	23.31
44		67.20	63.64	59.39	60.51	48.73	61.43	55.44	51.98	-52.00
45		66.50	62.10	62.17	66.75	53.44	67.32	62.67	55.34	40.43
46		76.29	66.67	70.43	64.74	58.08	73.20	68.02	63.43	37.77
47		0.00	56.79	59.22	71.58	64.23	77.86	75.11	69.95	39.09
48		0.00	61.89	0.00	0.00	63.86	78.65	77.57	74.27	39.54
49		0.00	0.00	0.00	0.00	0.00	80.73	77.97	67.78	0.00
50		-15.67	8.54	0.00	0.00	0.00	24.54	68.13	0.00	0.00

BASELINE INLET, STATION 4

CP	VT1	VT2	VT3	VT4	VT5	VT6	VT7	VT8	VT9	VT10- ABS TAN
1	0.00	0.00	0.00	0.00	0.00	54.90	27.92	44.19	91.46	111.08
2	0.00	0.00	0.00	36.38	49.39	38.75	24.53	21.76	52.19	102.46
3	0.00	0.00	32.81	42.24	49.59	34.86	24.33	24.08	45.88	87.47
4	-71.34	33.02	34.64	33.84	43.97	32.60	25.41	25.18	28.15	89.79
5	31.84	33.35	34.93	32.71	40.92	35.71	28.20	26.51	41.17	66.92
6	27.28	34.11	30.67	34.67	45.72	38.86	30.91	29.66	51.40	79.36
7	35.58	37.15	33.30	30.60	32.83	34.97	30.26	25.81	34.46	39.02
8	51.45	40.11	34.79	33.35	34.01	34.62	33.43	24.43	34.85	50.44
9	73.93	37.92	37.14	37.01	35.99	35.01	33.91	28.84	32.93	40.96
10	86.99	41.21	37.16	37.15	36.49	35.84	33.13	28.07	32.90	47.78
11	89.43	41.15	39.86	38.38	38.04	37.72	35.21	29.23	34.43	45.08
12	89.67	42.28	40.19	41.19	41.02	40.85	37.38	30.76	34.24	52.01
13	70.17	42.12	44.65	42.94	41.46	40.04	39.03	35.96	33.21	43.74
14	44.47	44.29	47.03	45.07	43.99	42.97	40.36	37.02	37.49	39.52
15	82.96	47.68	47.65	46.76	49.47	45.24	44.11	37.24	32.87	42.41
16	60.25	48.13	48.63	49.17	51.77	47.78	44.82	40.77	36.21	49.34
17	64.05	48.12	51.48	50.98	54.51	48.21	46.92	42.47	40.76	55.88
18	62.37	48.75	52.84	53.33	56.35	51.56	49.09	42.80	38.95	51.01
19	65.12	52.34	54.26	55.60	58.27	53.54	52.14	46.81	40.19	57.86
20	51.23	54.46	55.91	59.27	60.16	55.11	53.78	50.04	44.65	64.67
21	50.56	54.79	59.20	58.53	62.01	58.64	56.50	50.68	46.77	62.84
22	47.30	57.08	59.85	61.10	63.77	60.50	58.07	55.17	47.12	63.11
23	54.09	58.49	62.07	62.48	65.67	62.28	61.32	54.85	50.48	62.68
24	57.36	59.62	63.75	64.45	65.81	65.57	63.99	58.91	52.53	71.52
25	57.24	65.30	64.40	66.15	67.00	67.77	64.49	59.13	54.47	73.38
26	55.28	64.50	67.07	67.29	66.73	70.52	68.37	63.09	58.59	67.70
27	0.00	67.27	69.38	69.94	67.02	70.68	68.48	64.39	58.85	77.44
28	0.00	72.79	70.36	72.15	0.00	71.86	68.93	65.85	58.82	75.91
29	-28.82	72.24	70.93	70.97	0.00	73.59	71.56	66.85	62.24	72.33
30	0.00	73.19	70.56	73.74	0.00	74.34	72.34	69.18	63.96	68.38
31	43.33	74.44	71.88	73.92	0.00	75.08	71.96	68.31	66.25	73.13
32	0.00	72.36	72.13	73.68	0.00	74.85	72.69	70.14	66.61	72.93
33	0.00	72.39	70.97	76.47	0.00	76.46	73.43	69.92	66.76	70.60
34	0.00	55.94	68.15	74.36	0.00	75.47	73.33	70.20	67.67	74.61
35	0.00	65.67	70.37	70.83	0.00	78.10	72.66	69.80	64.73	68.53
36	0.00	0.00	0.00	0.00	0.00	79.00	70.14	70.49	65.46	74.31
37	0.00	0.00	0.00	0.00	0.00	80.66	80.33	72.28	64.53	73.39
38	0.00	0.00	0.00	0.00	0.00	66.65	0.00	66.67	60.74	75.41
39	0.00	0.00	0.00	0.00	0.00	84.31	0.00	0.00	46.59	61.31
40	0.00	0.00	0.00	0.00	66.94	0.00	0.00	0.00	44.33	0.00
41	0.00	0.00	0.00	0.00	51.91	0.00	0.00	0.00	0.00	0.00
42	0.00	0.00	0.00	0.00	57.36	0.00	0.00	0.00	0.00	0.00
43	0.00	0.00	0.00	0.00	56.76	41.84	56.23	-3.59	-34.29	7.25
44	0.00	0.00	0.00	0.00	60.76	23.08	0.32	-23.72	-234.04	-9.82
45	0.00	0.00	0.00	0.00	0.00	0.00	0.00	0.00	244.36	119.93
46	0.00	0.00	0.00	0.00	0.00	0.00	0.00	0.00	0.00	0.00
47	0.00	0.00	0.00	0.00	0.00	0.00	0.00	0.00	0.00	0.00
48	0.00	0.00	0.00	0.00	0.00	0.00	0.00	0.00	0.00	0.00
49	0.00	0.00	0.00	0.00	0.00	0.00	0.00	0.00	0.00	0.00
50	0.00	0.00	0.00	0.00	0.00	0.00	0.00	0.00	0.00	0.00

BASELINE INLET, STATION 5

CP	VT1	VT2	VT3	VT4	VT5	VT6	VT7	VT8	VT9	VT10- ABS TAN
1	0.00	0.00	0.00	0.00	0.00	0.00	0.00	80.70	114.71	0.00
2	0.00	0.00	0.00	0.00	92.29	113.65	66.43	81.06	91.73	140.87
3	0.00	0.00	20.98	81.98	86.00	108.27	69.52	75.13	121.05	92.38
4	97.56	66.42	69.65	73.68	76.86	96.48	67.44	71.25	97.49	159.32
5	96.80	66.38	69.93	74.31	83.33	89.90	73.63	65.66	95.79	107.74
6	111.09	65.35	69.34	74.18	75.26	84.22	66.53	70.03	95.39	107.58
7	111.18	65.67	68.66	72.46	72.02	80.91	66.36	69.62	87.51	111.41
8	106.89	65.14	68.45	72.58	74.09	78.20	67.61	70.41	66.27	52.66
9	113.41	65.74	69.68	74.45	71.46	76.70	71.39	67.55	84.93	65.01
10	107.89	67.12	70.86	75.48	74.30	79.53	68.37	69.01	73.22	95.49
11	105.29	66.74	70.19	74.48	74.24	75.72	71.32	69.60	77.22	94.00
12	98.57	66.63	70.31	74.84	72.92	75.80	71.79	71.15	66.25	112.43
13	104.00	68.36	72.70	77.95	73.27	77.98	72.97	67.70	72.66	97.36
14	97.34	69.33	72.34	76.19	74.37	78.31	71.94	70.34	70.78	72.34
15	91.24	70.38	73.06	76.57	74.49	77.15	73.21	70.77	72.52	83.49
16	91.27	73.02	74.54	76.87	77.07	75.13	73.34	71.70	67.06	86.93
17	89.13	74.22	75.77	78.14	75.79	78.70	73.15	72.66	73.69	67.66
18	84.13	73.99	75.03	76.88	76.82	78.66	74.15	71.05	68.70	77.11
19	85.52	74.98	76.09	78.03	78.41	78.80	75.09	72.18	66.28	79.57
20	82.67	76.25	77.38	79.35	77.84	79.41	73.95	70.28	67.61	98.35
21	84.31	77.99	78.33	79.49	77.56	80.13	75.12	71.97	68.43	84.24
22	81.69	78.44	78.24	78.87	78.23	80.62	74.91	70.50	69.99	100.55
23	80.99	77.91	77.86	78.63	78.52	80.35	74.97	72.68	72.89	67.22
24	82.19	77.85	77.73	78.43	79.12	80.03	74.46	72.31	70.05	67.48
25	80.80	80.48	78.91	78.16	78.78	80.66	74.53	72.20	70.94	103.33
26	81.16	79.64	78.84	78.86	80.42	81.45	74.71	72.12	70.81	73.33
27	80.99	80.84	79.12	78.20	79.75	79.77	75.09	72.04	68.73	71.37
28	81.21	81.46	79.82	79.00	78.55	80.07	74.58	71.07	68.77	84.41
29	79.52	79.35	79.00	79.49	78.05	80.00	74.25	72.91	62.42	53.94
30	80.25	82.60	79.87	77.95	77.13	80.21	75.17	70.85	69.56	104.87
31	78.26	79.72	78.86	78.82	77.36	81.30	71.73	70.59	71.72	58.69
32	79.99	78.54	78.05	78.35	77.10	80.05	72.48	71.54	65.84	70.67
33	78.87	81.29	79.19	77.93	77.16	79.20	73.92	69.24	68.35	69.53
34	76.47	76.98	76.74	77.27	77.16	77.71	74.80	70.46	66.01	74.29
35	71.47	0.00	43.16	75.58	76.90	79.68	74.66	69.84	62.50	77.29
36	86.92	63.61	68.67	74.22	67.71	78.26	72.17	69.92	64.35	76.48
37	93.41	79.72	67.34	56.44	39.11	77.51	69.49	69.17	68.86	56.56
38	0.00	83.20	73.79	65.19	57.78	79.81	0.00	63.32	62.50	60.87
39	0.00	71.59	75.20	71.65	-21.97	76.03	83.76	78.27	-44.58	46.68
40	0.00	88.16	44.08	0.00	0.00	76.90	0.00	0.00	0.00	-2.83
41	0.00	0.00	0.00	0.00	0.00	81.51	0.00	0.00	10.59	61.85
42	0.00	0.00	0.00	0.00	0.00	0.00	0.00	67.96	-20.53	0.00
43	0.00	0.00	0.00	0.00	0.00	0.00	-39.87	61.55	26.51	0.00
44	0.00	0.00	0.00	0.00	0.00	0.00	0.00	0.00	0.00	0.00
45	0.00	0.00	0.00	0.00	0.00	0.00	0.00	0.00	0.00	0.00
46	0.00	0.00	0.00	0.00	0.00	0.00	0.00	0.00	0.00	0.00
47	0.00	0.00	0.00	0.00	0.00	0.00	0.00	0.00	0.00	0.00
48	0.00	0.00	0.00	0.00	0.00	0.00	0.00	0.00	0.00	0.00
49	0.00	0.00	0.00	0.00	0.00	0.00	0.00	0.00	0.00	0.00
50	0.00	0.00	0.00	0.00	0.00	0.00	0.00	0.00	0.00	0.00

BASELINE INLET, STATION 6

CP	VT1	VT2	VT3	VT4	VT5	VT6	VT7	VT8	VT9	VT10- ABS TAN
1	0.00	0.00	0.00	0.00	0.00	0.00	0.00	0.00	0.00	0.00
2	0.00	0.00	0.00	105.03	112.36	110.86	101.79	99.26	93.29	123.46
3	137.64	94.47	97.92	105.91	114.73	110.18	95.37	97.64	140.37	104.56
4	131.87	93.07	97.65	102.00	112.97	106.24	95.77	93.72	77.62	110.25
5	123.25	91.88	96.66	101.09	104.89	98.86	91.76	87.57	55.22	111.35
6	119.65	90.03	96.62	101.33	108.21	95.23	88.77	87.93	69.70	104.31
7	124.84	93.07	96.85	98.67	101.44	94.62	88.36	83.49	60.93	93.64
8	126.09	89.93	96.19	98.09	103.36	96.59	85.95	83.12	57.20	119.88
9	117.94	92.40	95.95	98.65	99.42	88.85	85.63	84.12	49.52	92.42
10	118.32	94.31	96.10	97.23	97.05	91.50	87.15	82.63	53.18	93.50
11	115.08	93.03	95.93	98.33	97.73	87.55	83.99	81.66	46.42	104.91
12	112.52	94.55	96.16	96.30	96.45	88.44	82.50	80.99	64.48	85.82
13	109.87	94.47	94.99	96.56	96.11	86.16	81.83	78.79	78.41	96.65
14	110.67	95.88	95.36	95.16	95.75	85.71	82.43	79.06	61.68	102.33
15	109.10	96.88	95.64	95.97	93.15	84.02	80.91	78.68	71.99	84.01
16	107.90	96.94	95.24	94.70	92.09	87.43	82.35	77.41	58.09	107.05
17	104.81	95.99	95.34	94.21	93.22	85.12	80.68	77.59	74.88	95.68
18	104.54	94.42	95.09	93.26	93.09	84.48	80.54	76.78	64.42	93.58
19	103.68	97.83	93.74	93.11	92.67	84.64	82.10	76.94	61.60	90.81
20	101.99	96.97	94.65	93.60	89.93	85.46	81.06	77.88	54.90	94.04
21	101.69	97.92	95.60	93.86	90.68	84.86	81.05	74.69	65.88	96.40
22	100.62	95.87	93.54	93.05	91.15	84.61	80.95	76.68	67.79	85.22
23	101.29	96.70	93.78	92.65	91.25	84.38	80.04	75.90	36.23	93.27
24	98.97	96.16	92.87	94.06	89.49	84.18	80.75	76.84	57.36	96.62
25	97.59	94.80	94.06	91.58	90.81	83.96	79.69	76.04	61.61	86.14
26	97.49	95.60	93.02	91.97	89.66	82.40	80.18	75.95	50.52	81.81
27	91.08	86.89	90.32	90.32	87.86	81.03	80.53	75.18	55.29	81.48
28	97.22	95.05	93.63	90.56	88.31	82.52	80.08	75.62	73.19	88.14
29	95.92	95.99	91.20	89.65	88.64	82.47	80.27	75.88	52.99	85.73
30	93.96	90.39	92.24	89.18	87.89	83.17	79.50	75.59	63.11	82.06
31	94.84	94.16	92.34	86.86	88.01	81.92	79.26	75.20	64.35	81.84
32	96.99	91.67	91.75	87.85	87.23	80.79	79.96	75.04	52.60	81.41
33	76.50	89.17	93.14	89.65	86.48	81.59	78.51	76.45	64.40	78.06
34	93.07	92.65	89.12	89.79	86.66	80.31	78.86	74.04	64.08	88.92
35	77.52	86.55	86.14	84.73	86.48	81.31	79.18	75.38	62.00	78.35
36	30.11	86.57	86.87	88.17	84.52	80.44	80.10	74.65	40.31	84.58
37	62.58	4.78	81.46	89.29	87.08	96.19	81.45	76.66	55.17	82.97
38	17.05	0.00	92.36	88.32	100.77	32.43	89.95	86.03	43.52	88.60
39	-51.66	0.00	100.60	100.55	94.93	133.09	99.99	93.35	53.31	84.68
40	0.00	0.00	0.00	0.00	69.82	0.00	91.44	96.45	54.85	95.79
41	0.00	99.46	0.00	112.29	0.00	121.02	84.46	99.42	29.61	84.75
42	0.00	4.15	106.50	98.51	113.55	118.57	59.15	43.29	-15.03	-6.30
43	0.00	22.34	72.71	121.29	132.46	50.40	51.48	55.41	-17.78	-21.52
44	132.20	-37.96	51.71	95.82	140.30	62.26	142.55	110.04	-23.44	-17.86
45	0.00	0.00	0.00	0.00	0.00	157.85	158.90	148.96	-9.01	23.98
46	0.00	0.00	0.00	0.00	0.00	0.00	0.00	0.00	0.00	0.00
47	0.00	0.00	0.00	0.00	0.00	0.00	0.00	0.00	0.00	0.00
48	0.00	0.00	0.00	0.00	0.00	0.00	0.00	0.00	0.00	0.00
49	0.00	0.00	0.00	0.00	0.00	0.00	0.00	0.00	0.00	0.00
50	0.00	0.00	0.00	0.00	0.00	0.00	0.00	0.00	0.00	0.00

BASELINE INLET, STATION 7

CP	VT1	VT2	VT3	VT4	VT5	VT6	VT7	VT8	VT9	VT10- ABS TAN
1	0.00	0.00	0.00	0.00	0.00	0.00	0.00	0.00	0.00	0.00
2	0.00	112.90	0.00	0.00	0.00	0.00	0.00	0.00	0.00	0.00
3	128.37	112.06	110.85	120.08	125.41	126.22	125.77	103.07	109.28	0.00
4	-131.68	109.86	107.42	115.08	123.89	119.67	114.94	102.49	109.34	125.19
5	-123.18	108.23	107.13	110.48	117.17	114.84	108.92	95.09	102.31	125.94
6	115.85	107.08	105.78	107.49	115.08	111.95	105.16	97.37	100.21	116.43
7	-126.90	107.83	104.05	110.12	112.07	108.36	99.57	96.95	98.20	113.79
8	-121.27	105.87	104.76	105.22	110.35	105.46	97.56	90.23	96.74	107.17
9	-123.94	105.67	104.17	105.34	107.88	101.46	95.51	88.01	89.74	114.30
10	123.86	105.24	103.11	102.65	105.95	101.10	93.51	83.72	87.54	95.64
11	115.86	105.16	103.52	103.88	102.78	99.92	92.59	83.37	84.57	97.38
12	115.09	105.29	101.58	104.20	102.49	97.18	88.24	82.97	82.34	114.52
13	112.24	104.53	102.49	100.93	100.95	95.11	90.76	77.50	82.68	99.78
14	-121.16	104.96	102.11	102.23	101.00	92.33	89.45	78.73	82.88	97.10
15	113.82	104.46	101.45	100.66	97.56	93.28	85.28	78.90	79.91	88.35
16	112.02	104.48	101.92	98.63	95.66	91.60	85.12	79.20	77.48	100.40
17	115.25	104.38	101.07	98.26	95.28	89.54	82.68	77.77	78.91	99.50
18	115.18	104.31	100.51	97.70	95.66	89.53	84.51	78.61	76.91	84.77
19	108.75	103.78	100.70	97.73	93.37	87.49	81.28	76.92	74.50	95.49
20	106.44	103.25	97.36	95.60	93.10	87.14	82.38	74.94	70.15	81.25
21	102.46	103.60	98.30	96.75	92.58	86.22	82.25	75.41	73.46	80.37
22	102.45	103.59	100.52	97.81	92.37	86.35	81.36	73.92	75.18	87.33
23	101.86	103.00	99.63	96.75	92.19	86.31	80.46	76.14	71.50	95.80
24	101.74	102.88	98.80	95.16	90.75	85.76	81.86	74.67	72.34	90.27
25	101.78	102.91	98.84	95.09	90.32	86.28	81.22	73.90	72.83	86.44
26	101.56	102.69	98.18	95.04	89.92	85.80	80.31	74.20	71.96	86.88
27	100.62	101.74	97.97	94.92	89.90	85.35	79.88	73.97	70.37	91.99
28	99.89	101.01	97.05	94.28	89.50	85.02	79.13	75.63	72.29	88.94
29	106.80	100.96	96.78	96.00	89.16	83.33	81.01	73.85	71.98	84.60
30	107.35	101.29	97.67	93.30	89.75	83.63	81.43	73.33	71.64	83.15
31	-111.01	100.95	97.09	93.37	88.59	84.08	79.11	73.86	72.07	88.45
32	106.91	100.78	97.23	92.75	89.19	83.06	79.22	72.76	71.08	83.79
33	102.97	100.15	96.51	93.56	88.17	83.79	78.19	73.62	71.26	84.11
34	106.57	99.93	96.18	92.59	88.35	84.06	79.60	72.70	71.23	85.78
35	109.46	99.48	96.16	92.12	87.64	83.39	79.29	72.58	72.48	77.45
36	-109.72	99.58	94.70	92.69	86.49	82.08	78.66	73.53	72.33	81.90
37	108.50	98.62	96.08	91.95	87.11	81.75	78.30	72.88	72.25	80.31
38	106.95	101.02	94.58	90.24	87.21	81.34	78.39	73.29	73.05	82.79
39	-108.17	99.47	97.85	89.64	85.58	82.47	78.41	71.25	71.35	76.87
40	-108.48	101.84	97.14	91.17	87.77	81.36	78.10	73.55	71.40	78.07
41	-110.36	104.95	99.72	96.08	89.85	81.60	78.93	78.69	76.86	77.94
42	-39.79	104.48	106.33	103.06	96.21	91.36	89.71	85.82	84.04	90.28
43	-50.24	104.19	115.09	103.65	101.01	92.46	88.36	84.64	92.21	90.97
44	21.64	113.50	106.17	112.51	104.13	92.91	86.31	82.09	69.00	94.71
45	-6.80	121.07	0.00	84.89	114.46	114.42	128.56	107.34	63.88	92.72
46	-39.16	123.53	105.62	0.00	155.16	130.42	156.51	142.03	126.90	122.54
47	-133.51	141.57	0.00	133.07	146.71	177.34	167.34	124.88	136.57	121.15
48	-127.93	124.95	122.84	143.05	148.14	151.44	163.65	137.40	123.14	132.82
49	0.00	0.00	0.00	0.00	144.13	145.07	151.00	144.94	124.63	140.84
50	0.00	0.00	0.00	0.00	0.00	0.00	0.00	0.00	0.00	132.89

BASELINE INLET, STATION 8

CP	VT1	VT2	VT3	VT4	VT5	VT6	VT7	VT8	VT9	VT10- ABS TAN
1	9.93	30.33	87.78	122.43	138.43	146.11	152.15	152.24	145.74	164.17
2	26.28	65.04	106.23	130.05	135.99	144.87	144.88	156.76	141.49	152.45
3	17.52	70.28	92.97	125.69	139.28	145.08	143.10	149.96	148.58	148.10
4	147.06	-48.67	114.43	119.97	125.62	134.61	133.40	137.33	132.72	149.91
5	0.00	63.40	111.30	120.88	123.57	132.21	131.19	133.75	134.23	142.91
6	-12.94	122.68	113.36	118.81	124.09	128.50	122.53	126.92	130.09	142.97
7	21.29	-89.74	114.78	116.26	117.87	127.71	115.10	116.42	124.63	140.18
8	0.00	87.37	107.72	112.56	121.19	118.28	115.31	114.57	117.61	131.97
9	0.00	94.72	110.15	113.78	114.30	122.52	114.59	110.98	114.73	128.54
10	-22.63	112.13	110.57	112.77	115.92	114.82	108.78	105.88	108.68	129.22
11	0.00	83.15	110.05	110.43	112.34	112.59	101.22	101.21	102.41	129.72
12	0.00	86.45	107.93	110.52	111.37	104.01	101.90	97.37	102.25	116.80
13	0.00	-102.43	106.91	108.95	107.10	104.97	99.25	93.30	97.80	119.71
14	0.00	112.78	107.89	109.30	108.03	104.20	97.99	94.24	97.28	121.13
15	0.00	99.96	106.37	109.30	104.13	102.27	94.88	90.56	92.22	115.63
16	0.00	105.84	104.63	106.91	105.90	99.38	93.42	91.21	92.15	111.25
17	0.00	92.48	105.79	107.28	102.44	98.83	91.71	89.76	86.99	112.83
18	0.00	81.64	98.34	99.48	93.61	95.95	89.27	90.23	87.17	113.96
19	0.00	85.58	106.37	105.69	98.79	95.97	91.33	87.67	86.05	110.66
20	0.00	90.11	104.13	103.52	98.18	95.66	89.72	86.97	85.35	108.35
21	0.00	104.33	104.32	102.65	98.41	97.08	86.55	84.45	83.09	107.59
22	0.00	98.95	104.98	103.99	95.65	93.47	87.61	85.88	86.68	106.92
23	0.00	98.61	103.74	103.07	96.64	92.22	86.94	83.31	84.42	101.60
24	0.00	92.44	103.80	103.05	96.15	90.68	85.27	82.22	79.79	107.47
25	0.00	86.39	102.00	102.43	95.56	91.98	84.21	83.40	82.30	102.45
26	0.00	93.00	102.99	102.44	94.48	91.36	86.04	83.19	80.83	104.02
27	0.00	94.59	101.48	101.31	95.27	90.26	84.91	82.62	78.18	99.74
28	0.00	91.72	102.50	102.24	94.68	91.38	85.80	82.60	78.98	98.05
29	0.00	99.42	101.59	101.21	92.31	87.97	85.74	79.93	80.19	97.04
30	0.00	82.49	101.82	99.59	93.45	89.56	84.46	82.52	79.08	92.23
31	0.00	95.67	101.62	99.93	92.29	89.14	84.81	81.66	78.80	95.77
32	0.00	100.37	100.76	100.12	91.24	88.28	84.18	80.42	78.77	95.64
33	0.00	99.92	101.60	99.20	91.94	87.61	83.11	81.65	77.75	96.52
34	0.00	95.87	100.88	99.00	92.68	88.44	82.95	80.58	79.32	95.38
35	60.70	90.78	100.08	99.10	90.61	87.70	83.69	80.25	78.50	92.81
36	-19.49	85.70	100.95	99.57	90.27	87.81	82.80	80.98	78.86	96.18
37	19.79	86.98	100.39	97.67	90.32	85.72	83.69	79.81	76.96	92.39
38	-10.83	97.07	100.13	97.91	90.42	87.26	83.28	81.30	77.23	92.38
39	24.51	84.89	100.34	96.85	88.54	86.02	84.33	80.15	77.24	92.77
40	16.72	93.81	100.20	96.25	89.31	85.83	83.04	81.07	78.46	90.46
41	4.13	79.44	100.05	97.79	88.55	85.21	82.36	79.46	76.87	93.31
42	-12.46	84.07	100.24	97.00	87.38	84.51	81.81	80.50	78.28	93.83
43	-6.25	84.31	104.09	98.39	89.10	85.12	82.74	79.85	79.16	93.74
44	21.39	82.95	108.52	102.83	93.97	88.99	84.44	81.46	83.47	102.05
45	23.37	66.40	117.43	112.19	101.89	93.88	93.93	91.14	89.90	104.84
46	26.29	7.69	120.56	118.60	113.89	108.20	108.48	108.13	105.68	119.80
47	24.03	14.27	105.72	124.38	117.25	119.57	120.75	123.83	123.76	131.17
48	27.28	32.45	86.93	118.43	140.23	131.42	136.24	134.87	136.34	149.21
49	17.32	-57.85	125.10	138.38	126.45	145.01	156.24	152.12	151.28	161.58
50	19.70	-120.28	128.56	135.50	116.42	151.99	169.99	146.24	152.06	161.21

ORIGINAL PAGE IS
OF POOR QUALITY

ENHANCED INLET, STATION 1

CP	VT1	VT2	VT3	VT4	VT5	VT6	VT7	VT8	VT9	VT10- ABS TAN
1	4.92	4.66	5.44	4.58	5.44	5.00	4.35	6.03	4.53	7.49
2	4.23	4.40	6.94	5.85	5.35	5.22	4.55	5.85	4.61	5.61
3	5.77	5.33	5.41	5.79	6.41	5.89	5.42	6.46	7.16	2.73
4	6.41	3.66	5.38	5.46	4.33	6.66	5.30	5.38	5.58	5.58
5	8.62	4.59	4.53	5.74	6.68	6.36	5.99	5.59	6.02	6.64
6	2.97	5.98	5.39	5.32	6.39	6.01	5.50	6.97	4.83	5.46
7	5.27	5.27	5.57	6.59	6.04	6.83	4.43	5.65	5.38	5.71
8	4.21	3.37	6.31	5.34	6.58	6.08	5.75	6.32	5.83	6.41
9	5.07	3.85	7.02	5.45	6.32	7.34	5.48	6.74	5.11	7.37
10	5.59	4.94	5.29	6.48	6.45	6.28	5.44	6.82	5.80	5.95
11	7.48	4.98	6.03	7.14	6.20	6.83	6.77	6.63	6.69	2.94
12	3.49	4.75	4.44	6.91	7.64	6.24	6.37	6.73	5.06	5.63
13	7.61	3.48	6.53	5.77	7.19	6.33	7.37	6.51	5.65	6.06
14	3.56	5.21	6.37	6.51	7.24	7.08	6.30	6.13	5.34	6.71
15	6.07	5.91	6.73	6.52	6.49	6.38	7.13	5.46	5.57	8.76
16	2.86	6.74	7.07	5.71	6.93	5.59	6.27	6.79	5.87	6.36
17	5.70	5.06	7.07	6.87	8.01	8.12	5.86	7.53	5.62	6.97
18	4.74	4.40	6.19	6.89	8.43	6.74	5.89	6.52	5.92	6.50
19	4.18	5.66	5.74	5.62	6.85	7.49	5.77	6.58	6.41	3.60
20	6.27	5.69	7.92	5.31	6.12	8.13	6.70	7.30	6.66	6.16
21	6.79	6.27	6.66	6.53	6.62	6.42	5.27	6.18	5.62	6.21
22	5.63	4.40	6.42	7.31	6.48	5.29	6.13	6.73	5.29	5.03
23	4.78	5.09	6.62	5.95	7.51	6.47	6.46	5.17	5.81	6.13
24	5.86	5.29	6.64	4.84	6.23	6.64	4.40	6.90	5.94	4.99
25	6.28	4.82	5.77	7.08	7.19	6.87	5.12	6.50	5.35	4.29
26	5.88	4.62	7.12	4.62	6.53	7.75	6.19	6.45	4.98	4.64
27	7.14	4.92	6.22	4.09	7.27	6.39	6.01	6.34	6.33	8.84
28	4.56	5.17	6.61	5.33	7.15	6.11	5.56	5.66	4.11	6.83
29	5.84	5.84	5.06	5.41	6.60	6.68	5.12	5.03	4.63	7.35
30	7.56	4.53	5.47	5.25	5.40	5.60	5.08	6.16	4.81	4.40
31	6.53	4.78	5.45	6.51	5.80	6.08	6.19	6.37	5.01	5.20
32	3.12	5.35	6.93	6.19	6.28	5.52	5.80	5.81	5.34	5.95
33	4.86	4.83	5.62	5.79	6.95	5.51	5.22	5.99	5.82	5.22
34	3.99	4.81	4.58	5.22	6.53	8.25	4.83	5.40	3.58	6.02
35	6.96	4.65	5.76	5.61	6.66	6.67	5.55	4.22	3.87	4.34
36	4.81	5.52	5.04	4.36	6.27	6.65	6.64	5.14	4.33	3.66
37	4.70	3.33	5.36	5.79	5.84	5.59	3.45	6.47	4.51	3.92
38	4.98	4.61	4.25	4.95	7.13	5.81	3.77	4.93	4.51	5.31
39	5.31	4.40	4.90	6.11	5.81	5.47	5.45	5.90	4.40	3.84
40	5.51	5.79	4.08	5.44	6.24	5.09	5.19	4.96	3.90	3.26
41	3.11	5.11	5.70	5.58	6.28	6.52	4.89	4.74	4.06	1.70
42	4.67	5.86	4.45	4.68	5.84	5.99	4.05	3.95	3.18	4.91
43	3.63	2.66	3.15	4.92	6.16	6.18	4.93	4.82	4.08	2.67
44	4.74	4.83	6.04	5.24	6.04	5.28	3.27	4.71	4.96	2.65
45	3.68	3.76	4.14	5.84	5.59	5.04	4.33	4.25	4.67	6.40
46	3.39	4.29	5.00	5.73	4.08	5.27	5.22	4.21	3.53	3.61
47	4.94	3.38	4.39	4.72	5.80	6.35	5.98	4.58	4.51	3.79
48	4.29	4.95	3.80	4.90	6.16	4.76	4.24	5.08	4.43	5.88
49	6.00	4.16	5.82	4.15	5.37	5.62	2.99	4.26	4.88	6.14
50	9.64	6.44	6.72	5.17	6.42	6.28	3.95	5.63	4.36	16.31

ENHANCED INLET, STATION 2

CP	VT1	VT2	VT3	VT4	VT5	VT6	VT7	VT8	VT9	VT10- ABS TAN
1	-11.27	6.33	24.78	32.19	42.39	41.05	38.68	43.71	44.19	36.01
2	-21.35	-7.07	14.60	21.09	29.20	31.92	34.20	45.05	50.38	41.79
3	-29.48	-18.40	0.05	-3.42	6.70	9.37	11.78	28.66	226.57	44.15
4	-29.92	-27.27	-7.69	-16.26	-17.09	-9.81	-2.74	5.58	227.65	99.76
5	-29.42	-30.02	-11.82	-25.70	-24.23	-20.06	-15.76	-19.32	-0.16	46.35
6	-28.16	-32.53	-18.11	-29.33	-32.86	-29.14	-25.14	-27.34	-24.67	-14.02
7	-23.44	-30.72	-20.28	-34.01	-34.09	-34.35	-34.07	-34.06	-29.54	-36.24
8	-20.51	-29.76	-20.48	-34.00	-32.82	-33.30	-33.22	-36.65	-41.53	-35.44
9	-17.07	-29.09	-20.13	-35.16	-36.41	-34.97	-33.06	-39.30	-42.74	-38.35
10	-13.71	-23.99	-14.70	-33.74	-36.67	-35.59	-34.01	-40.64	-39.05	-44.27
11	-28.76	-22.25	-17.28	-31.96	-33.73	-34.41	-34.56	-39.85	-42.80	-42.87
12	-20.99	-20.53	-21.30	-30.14	-32.39	-32.45	-32.01	-36.88	-43.08	-41.60
13	-7.98	-14.84	-20.83	-28.41	-27.83	-30.05	-31.78	-36.11	-40.32	-33.52
14	-13.05	-13.94	-17.42	-27.54	-26.17	-27.26	-27.90	-33.83	-38.61	-35.44
15	-4.56	-10.84	-16.06	-24.65	-22.62	-24.41	-25.78	-30.11	-34.33	-33.34
16	-2.73	-8.18	-14.45	-21.06	-19.74	-21.27	-22.44	-29.02	-32.27	-29.79
17	0.05	-5.46	-11.58	-19.57	-17.13	-18.80	-20.17	-23.43	-29.27	-23.04
18	0.04	-3.90	-11.30	-16.50	-14.51	-16.35	-17.92	-21.67	-24.11	-20.82
19	1.94	-0.98	-10.58	-15.73	-13.80	-14.36	-14.69	-18.90	-22.41	-20.92
20	3.14	1.06	-6.19	-13.59	-10.89	-11.89	-12.71	-15.15	-18.18	-11.45
21	4.71	2.90	-4.65	-9.76	-8.91	-10.23	-11.38	-13.94	-13.82	-7.10
22	4.74	5.10	-2.52	-8.34	-6.75	-8.00	-9.13	-11.90	-13.73	-5.81
23	7.36	5.06	-0.98	-7.09	-3.94	-5.19	-6.35	-7.99	-7.42	-6.01
24	8.39	8.41	1.35	-4.69	-1.27	-2.77	-4.21	-5.49	-7.27	-2.02
25	7.54	7.75	2.53	-1.17	0.18	-0.77	-1.71	-2.83	-4.68	-0.97
26	9.02	10.47	4.71	0.18	2.17	1.04	-0.11	-1.36	-1.02	2.58
27	11.27	11.52	4.93	1.85	4.12	2.52	0.90	0.52	2.82	1.68
28	10.77	13.60	7.21	2.39	6.30	4.78	3.17	2.93	5.42	8.61
29	11.63	12.84	10.08	6.32	6.69	5.79	4.78	5.47	8.68	8.40
30	12.51	13.99	9.51	6.48	7.96	8.12	8.16	6.43	8.55	9.94
31	13.30	15.35	10.25	7.83	10.44	9.52	8.45	7.68	11.41	12.83
32	14.30	17.71	17.95	10.88	13.39	11.74	9.92	10.39	13.12	11.63
33	14.14	16.96	14.97	11.33	13.50	11.58	9.51	11.44	13.49	19.46
34	15.92	18.43	14.17	13.97	14.67	13.59	12.31	11.87	15.58	19.62
35	16.88	20.19	15.23	15.25	16.97	16.09	14.96	15.22	16.06	16.50
36	17.98	20.63	20.07	17.24	18.46	16.85	15.01	17.56	19.32	18.53
37	16.69	22.50	19.46	16.44	18.43	17.33	15.95	18.25	17.54	21.35
38	19.20	21.14	19.48	19.78	21.58	20.21	18.52	18.92	20.23	16.96
39	18.84	22.61	20.36	19.92	22.97	22.63	21.93	20.87	23.60	18.83
40	18.96	23.94	18.96	23.48	22.04	22.14	21.90	22.26	22.81	23.68
41	19.15	24.08	24.55	25.78	24.23	24.51	24.41	22.17	24.81	27.66
42	18.99	24.63	25.12	26.34	26.57	25.71	24.41	24.31	26.13	24.62
43	20.11	24.74	24.41	27.04	28.99	28.25	27.08	26.65	28.20	24.44
44	19.44	26.25	26.20	26.82	30.37	29.65	28.43	28.32	29.58	29.79
45	19.82	26.33	26.56	30.09	31.68	30.47	28.73	30.97	31.56	30.02
46	19.76	26.61	26.98	31.29	33.96	32.09	29.66	30.26	32.46	33.25
47	19.89	27.56	31.57	31.78	34.66	33.68	32.16	31.78	33.75	27.40
48	18.31	26.99	31.14	33.66	35.65	34.43	32.62	33.33	36.21	35.08
49	13.67	24.95	30.35	33.13	38.67	36.51	33.74	35.76	38.29	35.02
50	4.28	18.13	30.39	34.51	40.18	39.21	37.54	39.02	39.45	35.83

ENHANCED INLET, STATION 3

CP	VT1	VT2	VT3	VT4	VT5	VT6	VT7	VT8	VT9	VT10- ABS TAN
1	0.00	0.00	0.00	0.00	0.00	0.00	0.00	0.00	0.00	75.26
2	0.00	0.00	0.00	0.00	0.00	0.00	0.00	0.00	0.00	12.78
3	0.00	189.41	0.00	0.00	0.00	-6.95	32.94	0.00	0.00	0.00
4	0.00	0.00	0.00	-197.87	42.70	-218.20	-231.64	143.21	0.00	0.00
5	0.00	0.00	0.00	0.00	0.00	0.00	0.00	-14.45	123.25	-7.61
6	0.00	0.00	0.00	0.00	0.00	0.00	0.00	0.00	0.00	-13.71
7	0.00	0.00	0.00	0.00	0.00	0.00	0.00	0.00	0.00	0.00
8	0.00	0.00	0.00	0.00	41.68	81.34	-8.86	0.00	0.00	0.00
9	-8.59	-13.04	164.26	-4.55	53.10	39.52	-20.14	45.26	212.11	0.00
10	-14.34	-21.69	18.27	10.03	-3.98	-2.06	-28.60	-24.63	164.55	115.83
11	-6.41	-17.56	-2.92	-9.08	-22.12	-27.17	-26.31	-30.23	75.06	55.53
12	-7.36	-18.41	-20.88	-12.74	-25.93	-24.22	-23.23	-26.52	-6.56	-64.21
13	2.19	-15.27	-23.22	-16.74	-27.56	-19.61	-18.45	-23.71	-15.96	51.36
14	1.52	-9.34	-19.34	-20.58	-25.55	-16.67	-13.94	-20.73	-15.96	80.73
15	-0.36	-6.98	-19.56	-23.28	-21.87	-12.22	-8.92	-16.21	-19.32	-0.84
16	9.68	-4.17	-15.43	-19.44	-17.17	-9.70	-7.01	-12.36	-17.01	4.05
17	5.58	-1.54	-13.09	-15.71	-12.15	-3.95	-2.88	-9.88	-13.00	2.37
18	8.33	2.82	-7.04	-12.80	-11.32	-2.78	-1.63	-5.92	-9.02	0.43
19	8.04	3.88	-8.52	-10.62	-9.47	2.40	2.34	-3.47	-3.29	-1.27
20	12.45	3.91	-5.28	-9.58	-8.05	3.86	5.51	1.53	-3.04	73.50
21	8.96	9.97	-1.66	-7.92	-2.50	6.39	7.52	3.60	0.36	30.35
22	10.43	6.99	1.54	-4.41	-0.87	7.00	10.77	8.34	4.64	31.67
23	12.78	6.37	5.67	-2.03	0.90	10.92	11.68	8.04	6.61	70.93
24	13.58	14.31	6.81	-1.12	3.81	13.21	13.69	11.74	9.51	69.46
25	15.69	12.83	10.36	2.90	8.26	13.69	15.75	15.23	12.90	-15.34
26	13.15	10.46	11.74	5.45	8.98	16.97	16.87	16.61	13.73	38.14
27	17.13	16.07	16.58	7.22	11.25	17.21	19.21	18.58	18.05	42.97
28	15.74	15.77	19.58	7.59	13.60	19.00	19.80	19.15	17.72	57.03
29	16.54	17.96	16.39	11.20	14.85	21.78	22.41	22.78	19.61	1.80
30	18.17	19.90	19.19	15.40	17.39	23.73	23.77	22.53	20.82	0.86
31	15.64	19.10	22.19	13.55	19.83	24.44	26.24	25.29	21.63	-11.76
32	20.37	17.58	22.76	14.52	20.80	27.22	28.32	26.38	25.09	64.79
33	16.24	21.86	25.46	19.92	22.63	28.50	29.06	29.47	25.25	80.43
34	22.35	19.66	26.46	22.27	25.44	30.84	28.95	28.70	26.92	-0.01
35	22.26	21.71	28.81	21.09	27.26	32.43	31.74	30.74	30.11	155.16
36	24.80	24.96	27.69	23.74	29.62	33.55	33.33	31.88	30.48	7.04
37	22.39	27.00	33.81	26.36	31.45	35.00	35.34	32.25	30.85	106.26
38	25.05	29.75	31.25	28.45	33.10	38.33	36.74	35.16	31.86	34.31
39	22.85	31.03	36.96	30.20	36.37	40.49	38.45	36.54	34.79	17.98
40	26.61	32.03	37.37	33.73	37.60	42.27	41.91	39.77	37.95	107.11
41	29.76	34.08	41.79	34.68	42.03	45.44	43.02	42.30	38.11	67.18
42	33.24	37.92	45.95	37.31	44.81	48.94	45.77	44.06	39.68	42.03
43	29.07	41.48	45.49	39.17	47.17	50.62	48.58	48.96	43.33	68.43
44	39.97	47.28	55.76	46.69	52.64	56.19	53.08	51.85	46.83	85.00
45	36.09	56.26	55.17	45.96	55.49	60.51	56.81	55.33	49.60	35.99
46	33.77	0.00	60.17	46.79	61.79	65.27	63.21	59.73	56.33	6.51
47	-20.66	0.00	72.63	51.95	67.79	71.96	69.15	63.86	61.01	69.21
48	0.00	0.00	58.27	52.99	72.15	78.73	74.71	72.56	64.73	53.83
49	0.00	0.00	0.00	0.00	65.47	78.69	79.01	76.73	74.39	30.25
50	0.00	0.00	0.00	0.00	0.00	83.06	73.20	74.73	70.06	17.61

ENHANCED INLET, STATION 4

CP	VT1	VT2	VT3	VT4	VT5	VT6	VT7	VT8	VT9	VT10- ABS TAN
1	0.00	0.00	0.00	0.00	0.00	47.24	35.97	63.68	162.59	0.00
2	0.00	0.00	0.00	80.94	62.38	31.81	35.13	46.28	136.66	88.20
3	0.00	0.00	0.00	120.43	0.00	28.96	28.12	34.85	99.35	0.00
4	0.00	-45.25	70.37	0.00	39.35	27.80	30.05	36.49	95.99	0.00
5	0.00	-31.51	53.28	55.06	28.31	26.91	29.79	32.17	61.32	64.38
6	0.00	-41.65	0.00	56.39	32.11	28.75	31.20	38.16	76.96	16.47
7	44.53	-35.07	37.21	37.15	25.96	28.30	30.74	34.01	42.50	41.85
8	0.00	-31.10	45.18	40.03	32.74	30.68	33.20	34.52	51.93	31.23
9	41.32	-28.73	43.76	42.28	29.07	32.44	34.20	34.32	48.60	28.19
10	0.00	-30.34	46.28	41.44	31.34	34.11	35.46	34.87	38.96	25.72
11	-7.86	37.69	43.65	39.37	34.06	35.77	36.27	35.90	40.70	30.95
12	41.38	35.57	46.26	39.52	34.64	36.58	38.61	39.86	42.36	39.78
13	54.46	32.35	48.35	42.04	34.23	36.84	39.16	41.10	43.75	35.47
14	86.31	28.82	49.02	42.84	37.33	39.75	40.52	39.79	41.67	30.56
15	41.28	36.08	51.52	44.80	40.43	42.12	42.42	42.92	43.08	39.04
16	-19.32	41.68	57.13	46.69	43.20	44.49	44.63	45.59	44.38	35.55
17	59.74	45.32	57.54	48.14	43.60	45.50	45.56	45.14	43.51	37.48
18	50.47	40.45	58.89	49.05	46.56	47.84	48.25	48.86	47.24	40.53
19	68.46	38.66	62.10	53.38	47.34	50.17	51.25	49.73	51.20	51.23
20	52.83	41.20	62.47	54.95	50.84	51.08	52.44	52.66	53.76	54.93
21	68.49	46.34	64.55	56.46	52.88	53.64	53.48	53.95	53.74	41.05
22	35.95	49.20	65.62	57.34	55.07	56.62	56.07	57.48	55.72	36.75
23	42.15	51.97	68.91	61.15	57.97	58.88	58.90	58.24	57.50	57.74
24	38.14	51.06	71.80	62.42	59.10	60.31	60.72	60.41	58.92	68.74
25	60.91	48.75	71.42	65.43	60.06	62.73	61.92	62.69	63.08	65.52
26	51.14	53.05	73.91	66.38	62.79	63.93	64.34	64.19	65.85	73.87
27	45.48	55.42	75.06	67.80	65.23	65.30	64.70	64.24	65.44	78.92
28	62.47	55.45	78.42	68.68	65.15	65.61	66.68	68.21	67.15	60.67
29	30.34	60.37	78.75	70.96	67.77	67.08	65.57	68.43	67.83	55.60
30	49.93	59.22	79.42	72.52	69.56	68.76	66.37	68.52	68.80	25.72
31	0.00	53.00	80.23	71.68	70.41	69.95	67.48	68.05	69.77	96.56
32	50.73	62.97	81.13	71.34	70.95	69.45	67.36	69.46	67.51	63.94
33	0.00	71.02	80.82	65.65	71.08	70.49	67.49	69.66	70.14	51.09
34	0.00	50.76	77.62	0.00	72.60	67.46	68.22	69.00	69.55	73.38
35	26.10	32.44	82.98	0.00	72.16	62.15	67.71	68.64	69.74	64.67
36	20.34	39.10	0.00	0.00	69.43	0.00	66.20	68.22	68.90	65.11
37	-5.48	35.18	0.00	0.00	0.00	0.00	62.86	69.71	68.55	64.39
38	13.48	13.47	0.00	0.00	0.00	0.00	0.00	64.65	68.26	68.37
39	-2.04	42.09	0.00	0.00	0.00	0.00	0.00	65.59	67.32	54.81
40	0.00	70.04	0.00	0.00	0.00	0.00	0.00	59.43	67.75	42.62
41	0.00	48.83	0.00	0.00	0.00	0.00	0.00	41.92	64.71	0.00
42	0.00	0.00	0.00	0.00	0.00	0.00	0.00	0.00	72.98	0.00
43	0.00	0.00	0.00	0.00	0.00	0.00	0.00	0.00	0.00	0.00
44	0.00	0.00	0.00	0.00	0.00	0.00	0.00	0.00	0.00	0.00
45	0.00	0.00	0.00	0.00	0.00	0.00	0.00	0.00	0.00	0.00
46	0.00	0.00	0.00	0.00	0.00	0.00	0.00	0.00	0.00	0.00
47	0.00	0.00	0.00	0.00	0.00	0.00	0.00	0.00	0.00	0.00
48	0.00	0.00	0.00	0.00	0.00	0.00	0.00	0.00	0.00	0.00
49	0.00	0.00	0.00	0.00	0.00	0.00	0.00	0.00	0.00	0.00
50	0.00	0.00	0.00	0.00	0.00	0.00	0.00	0.00	0.00	0.00

ENHANCED INLET, STATION 5

CP	VT1	VT2	VT3	VT4	VT5	VT6	VT7	VT8	VT9	VT10- ABS TAN
1	0.00	0.00	0.00	0.00	0.00	0.00	74.70	79.90	106.00	31.62
2	0.00	0.00	0.00	0.00	106.82	72.49	69.00	74.87	113.75	39.50
3	0.00	0.00	0.00	107.18	99.39	68.89	65.13	71.70	112.24	44.75
4	32.06	0.00	95.36	89.20	94.41	62.56	62.97	67.06	91.68	50.84
5	73.25	0.00	79.66	86.23	83.15	65.81	60.32	66.60	86.14	37.36
6	92.04	0.00	77.85	85.62	87.76	65.40	61.49	64.37	88.06	39.41
7	126.94	0.00	73.55	79.94	77.23	64.67	62.82	67.40	83.34	43.57
8	96.82	0.00	72.15	82.61	74.31	62.89	62.86	64.63	79.30	28.84
9	7.99	0.00	74.64	78.08	73.12	63.60	62.60	66.64	76.85	25.09
10	0.00	0.00	73.39	75.04	74.52	64.54	63.23	61.24	72.81	37.85
11	90.48	53.98	70.05	74.87	71.09	64.92	63.76	64.05	71.75	19.13
12	132.66	0.00	71.59	74.73	69.67	65.40	63.95	64.91	71.91	45.21
13	11.02	49.86	71.85	74.40	70.19	66.08	64.31	64.16	70.91	34.13
14	89.94	47.35	71.37	75.02	71.85	66.46	67.26	66.71	71.64	35.20
15	123.52	56.44	71.06	74.46	73.50	67.50	68.16	64.28	70.35	49.90
16	101.04	68.05	73.35	74.88	72.76	67.92	67.23	66.38	68.80	32.60
17	50.85	71.38	75.34	75.58	72.89	69.29	67.92	66.65	69.27	40.95
18	69.30	62.73	73.76	75.81	72.51	69.72	67.84	68.43	69.26	41.00
19	82.92	52.75	75.32	75.25	73.60	70.11	68.78	67.23	67.74	36.43
20	75.22	68.83	75.94	75.67	74.68	70.08	69.44	67.39	68.40	32.41
21	77.34	68.59	75.89	75.49	74.25	71.79	69.00	68.52	68.64	45.41
22	62.32	73.41	77.30	76.15	74.32	71.26	70.49	68.40	66.11	30.62
23	63.45	76.52	76.63	77.11	73.67	71.16	70.44	68.77	67.37	28.79
24	69.69	75.66	76.73	75.71	74.85	72.21	70.01	67.57	67.81	46.79
25	77.91	76.14	78.43	76.40	75.23	70.87	70.42	69.52	68.01	36.70
26	61.42	74.87	77.19	76.50	76.13	71.23	71.31	68.12	66.25	40.97
27	90.34	79.56	78.08	76.11	75.91	71.03	70.32	68.27	68.55	44.38
28	65.71	79.41	78.71	76.92	75.32	70.45	71.32	69.38	68.51	27.98
29	74.61	81.72	77.42	76.26	75.17	69.74	70.40	68.73	68.92	33.85
30	70.31	81.35	78.77	75.12	74.92	70.39	70.09	69.22	67.83	39.27
31	54.14	81.15	78.65	75.29	74.60	71.62	70.43	67.86	66.96	33.81
32	77.02	84.82	78.24	74.85	74.41	70.35	70.06	68.92	67.31	39.98
33	50.42	79.61	78.04	73.25	74.50	69.42	70.25	66.93	66.39	34.08
34	50.90	79.25	76.86	66.60	76.03	69.14	70.08	67.70	65.50	32.43
35	58.79	80.14	77.81	48.07	76.90	68.07	69.88	67.12	63.89	42.59
36	75.19	76.72	77.91	0.00	75.92	60.52	69.14	68.11	63.06	32.80
37	19.99	77.44	75.92	0.00	75.27	46.96	68.72	65.83	66.74	45.19
38	-9.57	0.00	67.64	0.00	72.11	0.00	69.21	65.39	61.03	37.42
39	-9.38	-22.86	-16.69	0.00	47.39	0.00	72.32	62.79	78.45	31.18
40	3.86	-29.37	-9.67	0.00	72.06	0.00	71.71	69.42	79.97	46.81
41	0.00	0.00	0.00	0.00	0.00	0.00	74.21	69.65	61.24	43.34
42	0.00	0.00	0.00	0.00	0.00	0.00	0.00	0.00	83.46	31.71
43	0.00	0.00	0.00	0.00	0.00	0.00	0.00	0.00	78.23	0.00
44	0.00	0.00	0.00	0.00	0.00	0.00	0.00	0.00	0.00	0.00
45	0.00	0.00	0.00	0.00	0.00	0.00	0.00	0.00	0.00	0.00
46	0.00	0.00	0.00	0.00	0.00	0.00	0.00	0.00	0.00	0.00
47	0.00	0.00	0.00	0.00	0.00	0.00	0.00	0.00	0.00	0.00
48	0.00	0.00	0.00	0.00	0.00	0.00	0.00	0.00	0.00	0.00
49	0.00	0.00	0.00	0.00	0.00	0.00	0.00	0.00	0.00	0.00
50	0.00	0.00	0.00	0.00	0.00	0.00	0.00	0.00	0.00	0.00

ENHANCED INLET, STATION 6

CP	VT1	VT2	VT3	VT4	VT5	VT6	VT7	VT8	VT9	VT10- ABS TAN
1	0.00	0.00	0.00	0.00	0.00	0.00	0.00	0.00	0.00	
2	0.00	0.00	0.00	158.70	115.77	95.96	94.49	89.39	111.27	
3	25.37	0.00	110.21	171.22	106.50	92.12	86.19	85.24	104.44	
4	104.75	71.22	95.43	124.45	95.92	91.07	82.53	85.71	98.82	
5	75.52	88.98	96.85	118.87	100.27	80.96	79.84	80.03	97.31	
6	114.80	87.09	105.02	107.00	94.04	82.63	76.05	78.04	92.14	
7	139.39	93.66	96.14	94.21	89.70	79.47	76.15	75.95	86.55	
8	117.17	89.30	96.00	95.69	87.10	78.97	73.90	75.08	86.94	
9	4.32	87.88	96.66	90.45	82.99	76.16	73.57	73.69	83.74	
10	108.09	85.61	92.62	92.11	82.29	79.21	72.73	73.83	83.25	
11	77.95	88.36	96.54	90.72	80.97	77.33	72.43	73.32	79.81	
12	61.06	83.23	92.71	87.50	79.97	75.61	71.84	71.60	80.50	
13	114.55	88.10	90.68	88.19	80.81	76.21	72.06	71.91	76.09	
14	15.46	87.38	92.28	85.08	79.53	76.72	72.09	72.22	76.74	
15	105.57	85.73	90.69	84.63	78.61	76.21	71.99	72.10	75.66	
16	44.94	88.40	90.17	85.11	80.01	77.24	72.13	70.91	74.23	
17	75.58	86.37	90.22	84.72	78.53	78.23	72.26	70.93	72.76	
18	71.57	89.43	89.15	86.00	78.03	78.58	71.49	70.47	71.92	
19	57.63	89.37	90.33	84.71	78.31	76.64	71.87	70.72	71.81	
20	45.54	87.74	89.83	84.35	77.58	77.54	71.61	71.99	71.98	
21	97.96	90.74	90.59	83.36	77.92	75.94	71.74	70.01	71.19	
22	77.32	91.46	92.03	83.71	78.57	77.37	71.72	69.76	70.34	
23	70.51	90.17	90.88	83.90	77.99	77.42	71.12	70.43	71.24	
24	40.01	91.29	89.88	82.85	78.29	77.26	71.66	69.57	69.79	
25	64.00	88.22	90.02	83.55	77.28	77.63	71.55	70.03	70.58	
26	59.08	89.60	90.26	84.34	77.70	77.71	71.10	69.53	70.62	
27	53.88	90.51	90.43	83.97	78.28	77.62	71.92	69.98	68.97	
28	70.38	92.22	90.45	83.11	77.34	78.22	72.19	69.87	68.48	
29	74.10	92.29	90.84	84.34	78.45	77.35	72.19	69.75	71.06	
30	62.81	95.13	90.16	84.75	78.43	76.52	72.13	70.57	71.27	
31	61.38	92.66	90.38	82.46	78.01	78.11	71.80	68.93	70.49	
32	38.33	91.88	89.40	84.38	78.34	77.90	71.18	70.12	68.95	
33	0.00	93.07	90.69	83.70	78.71	77.62	71.66	69.12	70.18	
34	12.49	62.11	90.82	85.10	79.05	77.64	71.55	69.92	68.60	
35	-9.93	27.74	89.99	83.03	78.34	77.22	71.87	69.79	71.23	
36	6.05	82.34	89.17	83.92	77.06	77.23	71.84	69.49	70.07	
37	24.28	89.14	91.22	84.34	77.97	77.58	71.03	69.20	70.67	
38	0.00	91.82	89.16	84.25	79.11	76.16	71.79	69.54	70.60	
39	-21.90	92.01	88.08	86.33	78.32	77.46	74.70	70.21	67.60	
40	-24.24	98.34	89.93	82.87	85.38	89.01	89.52	75.22	70.44	
41	0.00	107.77	80.17	202.45	130.32	218.83	88.81	81.59	79.89	
42	0.00	96.93	0.00	201.46	67.68	214.45	19.18	-31.90	100.61	
43	0.00	0.00	0.00	0.00	0.00	0.00	0.00	0.00	0.00	
44	0.00	0.00	0.00	0.00	0.00	0.00	0.00	0.00	0.00	
45	0.00	0.00	0.00	0.00	0.00	0.00	0.00	0.00	0.00	
46	0.00	0.00	0.00	0.00	0.00	0.00	0.00	0.00	0.00	
47	0.00	0.00	0.00	0.00	0.00	0.00	0.00	0.00	0.00	
48	0.00	0.00	0.00	0.00	0.00	0.00	0.00	0.00	0.00	
49	0.00	0.00	0.00	0.00	0.00	0.00	0.00	0.00	0.00	
50	0.00	0.00	0.00	0.00	0.00	0.00	0.00	0.00	0.00	

ENHANCED INLET, STATION 7

CP	VT1	VT2	VT3	VT4	VT5	VT6	VT7	VT8	VT9	VT10- ABS TAN
1	0.00	0.00	0.00	0.00	0.00	0.00	0.00	0.00	0.00	0.00
2	0.00	-74.97	0.00	0.00	0.00	0.00	0.00	0.00	0.00	0.00
3	0.00	86.15	141.51	131.99	119.22	119.67	119.29	110.58	123.41	0.00
4	0.00	-92.31	124.21	132.66	131.79	115.51	108.93	99.64	119.57	0.00
5	0.00	-69.06	106.71	142.52	172.39	116.52	104.67	98.25	113.80	0.00
6	0.00	-105.50	-123.29	-9.89	116.51	106.33	94.29	94.35	110.60	0.00
7	0.00	-95.16	0.00	-17.82	112.39	101.85	89.05	88.71	103.90	0.00
8	0.00	-85.43	0.00	-19.30	115.83	92.83	86.43	87.68	101.42	0.00
9	0.00	-102.00	104.53	110.86	112.63	91.90	85.11	85.00	99.19	0.00
10	0.00	86.91	104.47	103.31	96.46	87.27	81.70	82.18	94.09	0.00
11	0.00	94.15	102.23	101.92	98.49	84.31	78.09	78.90	89.46	42.44
12	0.00	0.00	101.42	99.77	96.06	84.26	79.25	79.09	89.53	0.00
13	0.00	0.00	100.23	97.27	92.46	81.97	77.19	75.78	88.07	0.00
14	0.00	0.00	98.55	94.46	88.76	82.17	76.81	77.68	87.16	0.00
15	0.00	0.00	96.77	93.80	89.31	81.91	75.58	73.70	82.96	0.00
16	0.00	90.18	97.45	93.40	87.88	80.46	75.93	74.51	80.22	0.00
17	0.00	0.00	95.93	92.59	87.75	79.38	75.06	73.67	80.48	0.00
18	84.69	0.00	96.24	92.21	86.04	79.60	74.96	73.97	76.88	50.38
19	0.00	90.77	95.80	91.06	84.85	78.42	75.07	73.00	76.41	0.00
20	0.00	68.55	95.20	91.56	86.47	77.59	74.29	72.87	77.20	54.49
21	0.00	92.41	94.54	90.19	84.39	78.67	74.24	71.94	80.03	67.43
22	0.00	0.00	95.23	90.16	83.70	78.40	74.19	73.29	75.81	50.38
23	0.00	0.00	95.65	90.84	84.63	78.25	72.99	73.92	76.00	81.36
24	0.00	-100.32	94.92	90.26	84.22	78.44	74.25	71.38	75.83	0.00
25	0.00	0.00	93.73	89.44	83.69	77.14	73.58	71.42	72.79	0.00
26	0.00	0.00	93.59	89.84	84.66	78.58	73.60	70.79	75.48	44.49
27	0.00	92.91	93.74	89.25	83.31	78.21	74.43	71.98	75.97	0.00
28	0.00	87.55	93.63	89.16	83.27	78.25	73.71	71.11	74.90	0.00
29	0.00	-101.30	92.16	88.72	83.86	78.01	73.71	69.64	75.46	0.00
30	0.00	0.00	92.91	88.84	83.39	77.60	74.04	70.97	75.84	52.42
31	0.00	96.33	92.61	88.41	82.81	77.91	73.66	71.73	74.13	0.00
32	0.00	92.53	92.12	87.89	82.30	77.52	73.26	71.50	74.63	51.47
33	0.00	90.83	92.67	88.36	82.67	77.93	73.82	71.43	73.96	0.00
34	0.00	91.24	91.92	88.23	83.14	78.06	73.41	70.17	73.26	0.00
35	0.00	0.00	93.37	88.71	82.64	77.36	74.35	71.43	74.28	25.83
36	-60.40	0.00	91.71	87.92	82.71	77.49	73.45	71.34	74.83	0.00
37	38.29	86.91	93.01	88.31	82.16	77.07	73.37	70.43	73.95	0.00
38	0.00	0.00	93.41	89.04	83.27	77.25	73.67	71.56	72.63	81.36
39	0.00	74.32	92.64	88.07	82.12	77.16	74.46	71.23	75.24	0.00
40	0.00	71.13	94.09	89.31	83.15	77.23	74.10	70.79	71.94	0.00
41	0.00	-67.67	93.10	88.20	81.94	78.28	74.36	71.12	73.10	55.56
42	24.70	52.64	93.73	88.87	82.57	76.80	75.91	72.46	73.87	48.36
43	0.00	-40.64	96.92	91.47	84.31	77.68	79.39	80.63	75.82	52.42
44	0.00	-30.25	-202.18	-149.63	-95.27	84.00	90.63	95.50	78.39	-18.13
45	19.38	-41.20	-201.99	-207.86	-210.05	101.62	103.17	107.91	93.15	12.74
46	17.54	0.00	0.00	-80.26	-215.10	-212.57	108.01	92.12	102.77	2.13
47	15.87	-106.89	0.00	0.00	0.00	0.00	196.25	159.73	166.92	11.34
48	19.38	-76.92	0.00	0.00	0.00	157.82	165.82	167.12	167.72	-23.16
49	0.00	0.00	0.00	0.00	0.00	136.53	155.84	151.40	151.92	0.00
50	0.00	0.00	0.00	0.00	0.00	0.00	0.00	0.00	0.00	0.00

ENHANCED INLET, STATION 8

CP	VT1	VT2	VT3	VT4	VT5	VT6	VT7	VT8	VT9	VT10- ABS TAN
1	0.00	43.75	33.78	33.58	0.00	112.26	-131.52	127.13	137.14	46.36
2	0.00	33.55	34.00	24.38	0.00	75.05	-159.88	133.77	169.20	-48.27
3	0.00	15.12	33.68	40.67	0.00	80.77	-128.68	79.28	137.56	-83.02
4	0.00	39.49	33.55	33.28	0.00	103.29	-123.81	124.11	129.97	52.69
5	0.00	22.96	27.31	38.82	0.00	119.82	-133.65	111.85	154.07	-94.36
6	0.00	9.49	29.86	27.21	0.00	119.47	-120.43	111.06	137.06	74.28
7	0.00	26.71	28.17	2.88	-74.71	112.03	113.28	106.76	126.76	61.66
8	0.00	63.74	36.36	-102.30	0.00	119.85	104.15	103.84	123.62	-70.87
9	0.00	23.93	36.37	-110.02	0.00	115.28	100.67	91.76	111.84	-60.67
10	0.00	33.95	0.00	99.11	0.00	104.44	94.53	95.07	104.88	-65.28
11	0.00	41.12	0.00	-103.91	0.00	102.01	91.70	88.60	110.16	-59.00
12	0.00	40.83	0.00	0.00	-50.18	96.54	89.56	87.61	112.77	-54.74
13	0.00	42.63	113.59	-96.13	0.00	91.67	84.27	84.95	104.02	-85.59
14	0.00	12.49	0.00	-90.88	0.00	89.52	82.90	84.23	101.34	50.19
15	0.00	28.80	0.00	92.66	97.71	88.11	81.59	84.12	104.87	57.60
16	0.00	22.21	0.00	-91.74	-12.97	87.25	79.07	79.20	88.54	-40.49
17	0.00	35.73	0.00	-89.63	-29.84	84.79	79.27	81.59	81.81	-58.62
18	0.00	17.01	0.00	-87.90	33.45	85.94	77.65	77.86	85.37	61.23
19	0.00	40.64	0.00	-88.08	33.45	82.23	80.82	78.56	85.67	-79.64
20	0.00	34.24	84.47	-87.46	82.47	83.06	80.37	76.79	83.25	54.54
21	0.00	6.91	0.00	0.00	49.39	83.79	80.95	77.29	76.45	66.61
22	0.00	33.26	0.00	-86.06	-82.12	80.76	79.85	78.09	79.71	-66.06
23	0.00	58.89	0.00	-85.80	0.00	81.55	78.60	74.88	72.51	74.97
24	0.00	42.21	0.00	83.31	0.00	80.67	78.85	76.21	77.12	67.64
25	0.00	21.35	72.54	-83.88	-22.30	82.52	76.24	77.20	74.20	-45.80
26	0.00	38.84	0.00	84.14	39.01	80.65	75.94	75.72	69.89	-47.33
27	0.00	49.96	0.00	-83.82	95.08	79.79	76.38	73.55	74.38	74.79
28	0.00	32.89	42.78	-83.92	0.00	79.77	76.44	75.74	68.84	-72.36
29	0.00	30.46	94.57	81.57	0.00	79.89	75.86	75.48	69.16	52.64
30	0.00	34.95	0.00	84.78	0.00	80.27	75.37	75.88	63.96	68.60
31	0.00	24.50	0.00	83.29	-17.04	80.00	75.29	76.01	69.35	46.91
32	0.00	64.12	0.00	81.34	-49.13	80.00	76.27	74.70	70.12	46.58
33	0.00	38.28	0.00	82.46	22.70	79.53	74.88	75.82	67.30	-65.44
34	0.00	23.14	0.00	82.00	17.34	79.59	75.05	74.41	65.52	-67.68
35	0.00	34.36	89.45	-81.14	26.79	80.29	75.69	74.55	66.79	73.30
36	0.00	30.67	8.55	81.95	0.00	80.83	75.46	74.38	68.99	-58.04
37	0.00	29.05	3.06	81.29	0.00	80.82	75.89	74.14	68.49	59.78
38	0.00	30.18	-25.46	80.31	0.00	79.35	75.70	75.41	65.80	57.26
39	0.00	31.50	-26.14	-80.64	26.36	79.45	75.15	76.96	66.49	77.40
40	0.00	15.09	-24.53	-81.52	25.77	79.25	75.78	75.66	67.18	57.96
41	0.00	32.02	22.52	-80.16	16.18	80.53	75.63	75.26	69.66	53.42
42	20.09	27.60	21.31	-81.83	60.18	79.78	75.75	75.75	66.40	-64.29
43	19.46	25.15	21.59	-81.13	8.03	79.09	75.10	75.94	76.80	48.25
44	19.36	22.68	79.61	81.65	13.19	79.69	75.83	75.96	76.35	47.40
45	0.00	35.16	82.02	81.60	-5.58	79.09	75.26	77.58	73.01	55.70
46	0.00	25.80	0.00	83.88	12.48	78.21	76.98	80.22	75.63	43.60
47	24.01	23.86	-57.83	-93.81	12.52	83.55	83.10	89.93	75.92	-56.27
48	22.65	18.74	39.59	-103.69	17.26	97.81	97.24	105.83	87.80	79.42
49	27.00	30.23	35.18	-110.38	-1.77	113.38	112.58	122.15	101.31	62.31
50	23.49	-13.84	37.35	-26.34	0.00	129.40	123.15	137.94	134.73	61.26

TABLE A3. -

(C) NUMBER OF AXIAL MEASUREMENTS

BASELINE INLET, STATION 1

CP	MA1	MA2	MA3	MA4	MA5	MA6	MA7	MA8	MA9	MA10-AXIAL MEAS
1	99	249	172	149	200	315	217	219	165	13
2	119	263	176	145	193	310	207	192	152	7
3	98	260	200	138	182	358	209	186	118	15
4	101	303	184	158	197	300	229	207	128	8
5	106	268	185	142	165	334	196	220	139	6
6	108	284	187	142	190	363	204	215	133	9
7	105	274	174	129	190	335	213	218	139	6
8	93	295	191	120	200	321	223	216	124	7
9	87	267	180	134	182	311	199	218	131	8
10	112	257	175	155	190	342	176	206	150	4
11	106	283	184	147	188	358	198	202	134	6
12	121	298	158	150	201	343	197	210	129	7
13	119	257	171	134	207	328	208	213	123	12
14	95	279	171	123	225	317	220	217	158	9
15	103	269	186	142	203	336	215	216	148	11
16	112	267	166	128	189	319	189	229	146	8
17	110	275	183	146	187	336	226	244	130	12
18	104	293	174	158	190	344	185	197	119	8
19	84	290	191	114	210	325	224	211	126	8
20	108	287	197	129	210	297	214	245	109	13
21	110	282	182	144	205	333	203	233	136	10
22	104	267	185	139	196	326	229	250	134	11
23	121	299	182	143	202	323	209	212	139	9
24	117	255	181	157	175	345	249	231	145	6
25	100	248	190	140	210	357	210	216	143	9
26	101	259	152	128	179	326	185	214	130	7
27	102	293	191	140	195	352	214	243	137	10
28	120	285	203	161	200	315	216	223	132	12
29	117	261	181	130	215	333	193	225	123	6
30	104	299	201	151	204	343	210	251	131	9
31	111	254	187	147	185	329	196	232	163	7
32	115	275	163	122	230	323	211	232	133	10
33	98	287	215	136	175	310	197	212	130	6
34	113	288	187	141	213	305	189	209	127	13
35	126	287	171	126	208	336	208	222	130	7
36	118	275	186	135	198	361	190	205	134	14
37	112	273	175	149	191	346	219	214	133	9
38	105	291	174	129	216	342	202	236	149	13
39	108	283	197	140	219	344	209	208	112	6
40	117	298	180	137	224	360	243	189	129	6
41	137	257	189	128	173	349	180	231	122	6
42	115	280	193	133	212	362	204	225	125	5
43	92	246	183	137	223	315	216	232	135	14
44	98	272	191	131	192	342	221	195	145	12
45	107	293	201	156	188	349	207	220	141	8
46	98	293	185	159	182	327	207	237	131	11
47	117	308	192	141	197	339	196	217	130	7
48	105	238	197	152	202	332	202	202	141	4
49	105	288	182	131	197	328	212	215	132	6
50	184	436	296	209	340	552	398	311	188	4

BASELINE INLET, STATION 2

CP	MA1	MA2	MA3	MA4	MA5	MA6	MA7	MA8	MA9	MA10-AXIAL MEAS
1	200	37	11	11	146	174	91	104	170	43
2	210	41	9	13	142	157	78	70	112	24
3	231	44	14	16	151	125	86	92	98	11
4	228	42	17	13	94	100	106	100	90	9
5	244	55	13	10	120	138	96	95	89	8
6	214	38	10	9	120	110	99	89	101	10
7	233	66	7	12	111	96	96	92	89	14
8	258	49	15	11	92	135	103	114	90	12
9	236	41	9	10	108	145	84	96	89	11
10	238	44	5	13	116	150	87	95	92	6
11	237	43	15	14	97	157	93	81	107	10
12	217	42	10	11	122	140	83	101	106	12
13	288	49	15	8	95	136	86	84	90	16
14	265	59	8	11	113	153	76	77	80	10
15	260	46	13	7	105	137	93	78	79	7
16	258	44	11	8	83	147	87	89	64	7
17	271	54	10	12	100	158	92	78	85	8
18	333	47	7	16	108	149	68	72	88	6
19	304	57	10	7	112	168	91	104	75	8
20	287	56	17	8	78	142	86	82	84	9
21	285	60	7	12	101	132	82	97	78	12
22	292	48	8	9	107	127	84	81	85	11
23	316	60	7	19	96	134	95	87	85	12
24	297	43	10	9	91	136	84	68	83	5
25	320	52	10	8	99	142	82	73	73	7
26	291	46	12	12	114	132	93	85	71	11
27	325	48	15	16	96	141	77	103	101	6
28	340	67	9	11	87	160	74	100	75	11
29	350	41	7	19	113	156	89	87	94	9
30	326	57	16	15	98	143	90	89	84	4
31	290	47	15	11	109	142	93	83	86	11
32	522	100	22	13	197	245	196	194	158	7
33	329	47	10	16	99	149	101	87	73	7
34	315	54	14	10	137	149	97	108	104	7
35	352	50	16	10	112	167	108	98	80	16
36	356	61	12	12	121	150	100	90	109	11
37	334	63	14	10	112	155	89	117	89	8
38	333	59	12	9	135	173	96	84	97	9
39	347	65	11	7	109	167	88	93	99	10
40	358	57	10	9	103	165	118	92	92	11
41	367	57	19	11	117	157	123	113	98	9
42	370	70	14	17	150	172	100	115	102	9
43	319	73	17	16	132	178	101	120	119	14
44	336	62	14	12	149	194	114	100	123	11
45	392	51	12	15	151	185	123	112	139	11
46	365	40	26	18	151	190	117	114	130	10
47	330	42	24	15	176	181	138	114	136	16
48	262	44	23	12	199	209	143	117	119	4
49	243	37	15	22	147	189	132	142	144	16
50	191	35	18	19	184	185	116	150	154	22

ORIGINAL PAGE IS
OF POOR QUALITY

BASELINE INLET, STATION 3

CP	MA1	MA2	MA3	MA4	MA5	MA6	MA7	MA8	MA9	MA10-AXIAL MEAS
1		19	56	1	3	0	9	0	1	0
2		22	41	1	0	0	20	0	112	6
3		14	1	4	1	3	22	7	433	10
4		0	0	4	5	12	5	7	101	4
5		0	0	0	0	0	0	3	10	1
6		0	0	0	0	0	0	0	0	2
7		0	0	0	0	0	0	0	0	0
8		1	0	0	12	37	19	0	0	0
9		0	11	15	22	16	32	31	13	0
10		5	14	21	15	38	54	62	15	0
11		7	10	18	13	54	44	58	22	2
12		3	15	20	15	80	59	68	36	3
13		3	13	15	21	123	64	63	34	2
14		2	16	18	21	108	59	73	19	2
15		4	10	19	15	111	61	65	17	6
16		2	12	11	11	88	56	83	17	3
17		8	6	16	19	89	62	73	34	2
18		3	12	13	14	97	64	64	13	2
19		3	17	14	18	89	67	54	19	4
20		7	11	11	14	95	72	58	34	7
21		3	24	15	24	97	59	62	15	2
22		2	10	20	16	86	46	59	16	8
23		9	8	14	15	102	60	66	23	3
24		5	7	20	12	89	75	57	25	7
25		11	16	19	12	93	58	54	27	2
26		2	12	14	12	114	71	71	15	2
27		5	12	19	16	100	55	81	27	8
28		9	12	28	27	161	127	115	42	6
29		6	13	24	19	117	78	68	15	4
30		7	13	20	20	121	65	62	23	6
31		6	18	22	17	122	72	78	19	1
32		8	16	26	18	90	60	75	19	7
33		7	17	25	15	106	65	76	25	4
34		10	17	21	22	116	65	91	19	3
35		10	18	11	21	134	74	79	27	2
36		8	20	23	19	126	74	88	22	7
37		12	15	18	20	122	74	99	21	5
38		15	15	21	26	119	67	83	20	5
39		8	13	20	28	116	92	84	24	5
40		12	13	23	21	153	79	102	17	4
41		9	19	29	24	133	77	93	25	4
42		12	21	21	26	127	74	91	27	5
43		11	24	30	32	116	86	96	37	2
44		10	16	23	19	107	90	91	33	5
45		9	9	25	24	108	103	111	36	6
46		2	12	6	14	44	88	99	34	4
47		0	3	1	9	24	71	101	25	3
48		0	2	0	2	11	42	50	25	3
49		0	0	0	1	0	9	16	6	0
50		15	12	0	0	0	2	6	0	0

BASELINE INLET, STATION 4

CP	MA1	MA2	MA3	MA4	MA5	MA6	MA7	MA8	MA9	MA10-AXIAL MEAS
1	0	0	0	0	0	10	7	26	35	3
2	0	0	0	7	129	29	22	30	33	9
3	0	0	9	16	206	27	15	44	36	7
4	4	18	15	20	259	45	26	55	65	9
5	6	39	28	17	397	56	30	43	52	11
6	10	49	70	72	853	137	53	119	110	18
7	4	30	41	41	542	85	31	66	59	16
8	5	42	50	57	583	87	38	72	62	14
9	9	39	45	63	589	125	38	67	96	17
10	8	31	69	67	628	127	36	84	89	22
11	10	46	65	82	655	86	39	75	94	18
12	7	55	66	76	696	123	47	104	83	21
13	9	69	79	103	720	118	56	70	117	25
14	10	67	83	84	709	127	52	89	112	15
15	11	75	92	102	748	131	50	81	103	20
16	11	69	102	119	668	131	54	93	136	11
17	8	74	136	114	648	153	65	95	137	19
18	13	80	152	122	597	165	54	107	130	16
19	4	106	131	132	557	158	63	95	129	16
20	12	85	161	153	512	172	46	95	136	27
21	10	103	154	121	467	215	59	97	154	28
22	15	101	178	143	411	188	56	137	150	24
23	13	127	170	140	387	196	77	98	153	23
24	11	119	168	137	341	198	44	121	181	37
25	8	131	175	152	221	167	68	129	174	24
26	3	120	159	118	43	183	61	122	149	14
27	6	98	146	135	5	167	78	135	170	19
28	2	135	127	105	0	140	67	127	174	11
29	6	118	113	79	1	142	49	120	186	16
30	4	109	101	90	0	115	48	126	191	36
31	4	78	61	71	1	117	27	127	190	25
32	2	50	50	65	0	100	28	113	201	25
33	4	13	35	50	0	94	23	102	198	30
34	5	4	10	14	0	72	23	82	171	22
35	1	5	1	4	0	70	20	65	147	25
36	1	2	0	2	0	31	10	57	131	29
37	0	3	2	6	0	14	2	14	83	24
38	0	18	25	25	0	1	0	1	49	11
39	0	3	14	30	0	1	1	1	87	3
40	0	0	1	1	2	4	0	1	136	0
41	0	0	0	0	4	0	0	0	19	0
42	0	0	0	0	12	1	0	0	0	0
43	0	0	0	0	11	1	3	3	8	5
44	0	0	0	0	14	11	5	8	69	8
45	0	0	0	0	0	0	0	0	3	10
46	0	0	0	0	0	0	0	0	0	0
47	0	0	0	0	0	0	0	0	0	0
48	0	0	0	0	0	0	0	0	0	0
49	0	0	0	0	0	0	0	0	0	0
50	0	0	0	0	0	0	0	0	0	0

BASELINE INLET, STATION 5

CP	MA1	MA2	MA3	MA4	MA5	MA6	MA7	MA8	MA9	MA10-AXIAL MEAS
1	0	0	0	0	0	0	0	32	19	6
2	0	0	0	0	27	27	35	39	28	8
3	0	0	113	17	15	11	43	40	28	5
4	106	80	118	21	22	27	47	35	13	12
5	158	98	160	33	19	48	58	48	23	11
6	143	109	179	46	32	40	47	56	15	13
7	137	109	185	44	52	51	64	56	17	9
8	137	118	182	63	58	53	66	66	21	16
9	146	103	178	53	73	56	76	70	27	11
10	113	105	152	82	60	48	66	71	25	14
11	106	112	166	84	88	84	79	61	24	16
12	101	113	148	83	99	75	85	67	29	18
13	100	125	151	86	85	106	69	89	31	27
14	98	116	122	95	99	96	83	84	29	24
15	121	117	128	105	102	83	87	78	38	21
16	83	133	109	101	118	93	74	79	38	20
17	89	125	104	121	114	111	74	82	40	21
18	85	114	97	124	119	98	89	75	37	19
19	97	125	75	141	133	89	117	85	38	27
20	84	107	61	114	129	104	101	83	31	23
21	85	97	67	134	144	99	132	99	36	28
22	81	80	63	132	125	111	109	98	33	29
23	91	58	66	118	126	131	107	112	52	13
24	73	62	49	125	109	117	116	105	36	37
25	70	50	27	125	128	129	106	103	41	30
26	69	39	30	123	119	109	133	123	64	36
27	58	37	28	85	119	119	119	117	38	22
28	48	23	24	91	113	122	111	123	50	36
29	47	22	7	96	73	87	93	103	51	13
30	44	25	1	82	95	71	76	101	54	30
31	41	21	0	88	66	79	63	99	51	16
32	37	13	0	64	68	74	65	103	44	25
33	28	12	0	79	65	56	53	68	53	25
34	29	4	1	66	52	50	44	64	42	21
35	26	0	0	41	27	68	43	61	35	22
36	17	2	0	13	11	42	30	38	25	43
37	3	6	0	5	10	40	6	19	18	25
38	0	7	0	4	1	21	9	9	6	24
39	0	1	0	2	1	7	3	1	4	28
40	0	3	0	0	2	4	0	0	7	16
41	0	0	0	0	1	3	0	0	4	4
42	0	0	0	0	0	0	0	9	35	0
43	0	0	0	0	0	0	1	23	167	0
44	0	0	0	0	0	0	0	0	0	0
45	0	0	0	0	0	0	0	0	0	0
46	0	0	0	0	0	0	0	0	0	0
47	0	0	0	0	0	0	0	0	0	0
48	0	0	0	0	0	0	0	0	0	0
49	0	0	0	0	0	0	0	0	0	0
50	0	0	0	0	0	0	0	0	0	0

BASELINE INLET, STATION 6

CP	MA1	MA2	MA3	MA4	MA5	MA6	MA7	MA8	MA9	MA10-AXIAL MEAS
1	0	0	0	0	0	0	0	0	0	0
2	0	0	0	47	15	40	69	81	10	20
3	41	59	74	49	29	51	81	82	19	37
4	57	92	74	73	48	49	95	106	21	32
5	60	73	80	65	36	46	94	78	24	37
6	61	100	91	75	37	69	104	111	16	23
7	65	90	98	75	62	57	115	103	18	41
8	65	107	84	60	50	73	126	121	21	17
9	70	88	94	94	66	84	127	116	21	12
10	66	114	102	66	50	56	129	133	24	31
11	61	111	106	101	66	73	123	107	21	46
12	62	102	90	90	81	81	119	118	12	40
13	73	92	98	71	74	86	142	115	14	34
14	86	116	93	68	72	84	121	121	16	29
15	95	93	113	110	74	99	133	125	18	24
16	101	85	103	80	85	94	135	129	14	34
17	82	125	89	97	76	82	123	124	12	46
18	125	130	118	85	90	93	157	130	13	41
19	100	118	105	100	81	120	168	118	13	38
20	119	123	113	103	105	100	144	142	11	27
21	143	98	104	116	84	82	159	148	22	29
22	108	100	117	113	87	112	181	135	12	25
23	141	88	110	113	97	111	156	141	18	39
24	132	74	95	107	94	108	185	146	15	36
25	120	84	81	101	104	110	178	152	18	28
26	123	74	82	78	101	100	170	167	19	40
27	187	103	129	169	168	158	313	261	20	57
28	99	54	65	92	94	86	177	186	11	22
29	76	55	55	79	104	89	164	179	12	23
30	76	37	51	76	97	76	199	167	27	43
31	57	28	44	59	79	62	175	187	14	44
32	42	34	34	49	85	58	160	182	18	39
33	38	21	16	40	63	58	162	147	19	42
34	24	16	19	36	61	31	149	164	14	59
35	26	7	15	26	58	17	116	115	27	60
36	14	1	8	22	46	15	112	112	18	88
37	23	2	11	20	55	9	99	118	37	124
38	14	0	1	20	38	3	84	104	40	140
39	3	0	2	8	16	2	27	46	26	108
40	0	0	0	0	6	0	8	24	7	64
41	0	1	0	2	1	2	5	3	2	36
42	0	2	1	2	2	6	17	13	3	19
43	0	2	4	5	1	9	38	23	11	41
44	1	3	6	2	1	13	25	22	13	45
45	0	0	0	0	0	15	20	39	15	21
46	0	0	0	0	0	0	0	0	0	0
47	0	0	0	0	0	0	0	0	0	0
48	0	0	0	0	0	0	0	0	0	0
49	0	0	0	0	0	0	0	0	0	0
50	0	0	0	0	0	0	0	0	0	0

BASELINE INLET, STATION 7

CP	MA1	MA2	MA3	MA4	MA5	MA6	MA7	MA8	MA9	MA10-AXIAL MEAS
1	0	0	0	0	0	0	0	0	0	0
2	0	20	0	0	0	0	0	0	0	0
3	9	34	8	16	43	24	47	52	52	0
4	1	37	20	19	37	44	64	45	49	42
5	1	42	26	32	50	51	47	78	40	34
6	5	43	36	28	59	53	59	74	52	49
7	3	79	42	54	81	72	55	75	72	61
8	3	63	49	48	84	80	76	71	60	40
9	2	88	38	42	83	72	92	80	69	55
10	4	88	37	55	95	77	78	99	80	41
11	4	104	43	58	106	96	99	80	81	44
12	8	120	48	56	103	109	83	101	92	63
13	2	121	36	74	128	100	104	97	82	49
14	3	127	35	78	118	110	106	111	77	47
15	8	147	47	60	120	112	112	92	91	59
16	6	140	46	64	137	128	104	92	103	44
17	4	134	51	74	125	110	125	125	112	55
18	6	137	52	61	127	114	106	106	112	39
19	4	152	41	72	115	145	109	123	114	49
20	2	316	75	109	235	194	231	200	191	78
21	2	132	50	81	130	122	106	117	97	67
22	9	118	41	70	143	135	134	125	105	43
23	4	129	54	95	148	137	136	116	130	52
24	7	132	48	66	132	142	127	115	111	45
25	2	157	51	71	148	156	133	120	124	57
26	6	162	51	64	156	129	145	142	120	44
27	10	134	40	62	133	159	142	126	123	43
28	9	149	53	75	148	137	137	147	135	46
29	4	152	46	81	139	138	154	124	143	62
30	8	153	47	65	151	121	145	146	128	40
31	5	155	59	83	143	152	142	152	158	56
32	8	143	46	69	148	150	174	119	139	45
33	4	165	50	78	155	150	165	123	136	64
34	4	153	60	86	139	154	157	159	142	60
35	13	139	60	81	130	185	165	131	148	63
36	16	144	60	73	142	189	164	123	149	63
37	19	142	55	70	184	159	171	155	162	73
38	13	152	47	68	157	183	151	131	142	73
39	8	136	44	75	152	190	193	139	170	81
40	39	157	40	73	163	164	170	133	185	98
41	26	192	41	58	135	122	153	153	220	104
42	43	86	18	45	113	91	95	112	187	136
43	199	35	13	26	52	58	59	60	122	146
44	219	25	5	7	18	18	30	44	26	66
45	306	53	0	1	13	10	15	24	15	33
46	244	43	1	0	7	10	23	37	42	25
47	171	14	0	7	20	20	13	42	33	28
48	76	25	2	3	9	27	15	22	40	27
49	0	0	0	0	15	16	17	46	32	36
50	0	0	0	0	0	0	0	0	0	37

BASELINE INLET, STATION 8

CP	MA1	MA2	MA3	MA4	MA5	MA6	MA7	MA8	MA9	MA10-AXIAL MEAS
1	27	1	11	13	7	10	27	29	41	128
2	6	6	17	16	13	23	41	34	52	107
3	3	7	19	15	8	23	34	42	52	134
4	1	9	28	37	19	16	66	53	57	84
5	0	6	38	37	12	19	60	44	67	112
6	1	6	51	53	41	27	68	41	47	107
7	1	7	30	59	22	32	62	42	60	116
8	0	6	32	41	25	32	61	68	55	131
9	2	10	51	61	32	27	75	58	64	94
10	1	15	53	66	46	35	87	79	101	116
11	0	17	55	106	51	58	70	91	94	88
12	0	14	69	71	67	45	78	92	55	90
13	0	16	85	119	51	50	78	79	66	107
14	0	21	70	104	51	70	106	66	63	103
15	0	14	116	105	59	62	128	92	82	84
16	0	21	73	119	72	67	98	91	79	89
17	0	25	95	103	75	77	86	97	95	102
18	0	17	170	204	178	133	173	166	151	153
19	0	26	97	129	80	98	99	106	89	96
20	0	22	77	125	96	86	132	94	93	93
21	0	27	92	102	91	77	118	117	101	77
22	0	20	82	116	83	85	93	103	101	57
23	0	28	105	118	84	79	106	101	96	101
24	0	30	93	117	79	76	119	119	92	79
25	0	22	96	148	117	98	121	115	84	59
26	0	20	86	100	79	92	132	108	80	86
27	0	26	130	127	96	97	103	124	98	85
28	0	33	90	158	81	82	140	103	107	71
29	0	20	114	135	100	98	111	111	107	99
30	0	36	103	134	75	105	128	121	108	93
31	0	32	107	120	105	64	124	141	96	77
32	0	22	104	144	107	84	129	102	104	73
33	0	33	97	107	97	96	129	119	99	91
34	0	31	105	124	84	90	134	128	118	83
35	1	24	143	98	92	90	117	112	105	96
36	4	32	109	149	113	93	131	148	94	86
37	5	38	96	125	104	81	145	117	114	88
38	8	33	105	128	103	96	129	138	121	105
39	6	21	141	147	127	117	140	141	137	112
40	11	40	165	164	120	111	154	138	126	120
41	9	21	195	209	140	148	155	135	125	129
42	8	58	366	230	179	143	181	133	116	166
43	15	81	584	409	228	225	194	208	200	174
44	75	159	737	550	334	373	264	261	225	222
45	176	113	517	496	402	452	300	293	311	293
46	264	130	197	291	352	411	303	301	382	455
47	215	96	36	89	142	192	182	235	302	367
48	118	75	9	36	31	72	84	143	192	263
49	84	6	4	15	18	38	43	66	95	182
50	62	3	9	7	6	12	37	31	65	157

ORIGINAL PAGE IS
OF POOR QUALITY

ENHANCED INLET, STATION 1

CP	MA1	MA2	MA3	MA4	MA5	MA6	MA7	MA8	MA9	MA10-AXIAL MEAS
1	51	51	50	58	59	65	53	70	56	35
2	43	45	54	64	53	67	67	61	65	30
3	33	45	60	62	62	57	75	67	51	24
4	29	63	60	68	49	65	76	75	50	28
5	56	57	74	61	56	65	72	65	67	34
6	55	62	67	70	45	53	63	81	76	25
7	54	55	52	68	64	66	58	62	64	24
8	33	53	60	73	60	66	56	80	66	33
9	59	60	59	64	43	71	71	68	69	40
10	51	61	65	67	66	75	69	74	69	24
11	39	60	66	76	48	64	79	63	65	32
12	51	62	58	69	57	58	65	63	54	41
13	54	59	59	49	67	70	55	66	56	36
14	39	53	65	68	67	52	63	67	70	27
15	50	49	64	78	59	60	69	73	51	30
16	54	56	56	58	53	64	61	73	61	25
17	54	61	73	65	48	75	61	71	58	34
18	45	49	55	57	46	75	62	86	62	35
19	46	61	80	67	71	70	67	58	77	26
20	34	46	50	72	53	64	75	77	64	28
21	56	69	68	56	61	73	66	63	59	25
22	46	53	65	64	55	77	63	65	62	38
23	43	52	54	77	58	59	66	83	61	28
24	45	55	56	88	50	57	66	64	49	22
25	39	56	60	61	56	49	71	58	52	27
26	49	59	63	58	52	73	66	81	57	23
27	59	59	52	46	59	61	65	68	57	24
28	46	53	65	49	55	62	71	84	60	30
29	43	49	63	64	64	70	46	57	59	31
30	53	57	62	65	57	72	70	74	69	30
31	44	57	67	52	46	71	58	67	51	27
32	32	52	56	70	51	58	72	62	59	26
33	56	56	53	49	62	60	59	78	47	28
34	40	64	65	74	63	62	59	67	62	37
35	63	50	58	68	46	71	45	54	76	29
36	35	66	69	68	52	71	55	67	56	30
37	52	55	49	58	62	80	72	64	58	39
38	46	74	68	54	46	66	75	61	62	27
39	48	53	59	62	60	64	61	60	64	22
40	52	56	56	74	49	76	68	66	53	28
41	42	57	58	66	43	73	59	69	70	25
42	46	57	59	86	65	61	82	65	48	32
43	44	58	70	63	62	51	74	73	64	30
44	49	61	55	67	57	60	64	64	54	22
45	41	59	51	63	56	56	83	61	70	31
46	40	70	54	66	58	53	68	72	51	19
47	48	65	69	75	58	67	62	63	54	19
48	44	54	63	72	50	62	63	69	56	24
49	35	51	60	70	56	66	70	76	62	33
50	99	104	87	100	74	105	94	115	123	53

ENHANCED INLET, STATION 2

CP	MA1	MA2	MA3	MA4	MA5	MA6	MA7	MA8	MA9	MA10-AXIAL MEAS
1	42	68	110	95	103	60	110	84	104	22
2	33	49	83	88	107	81	126	100	136	20
3	42	63	56	55	61	62	69	89	102	23
4	42	64	58	67	57	50	52	44	44	8
5	53	57	74	57	74	49	44	42	56	11
6	51	64	71	63	58	45	57	60	62	9
7	50	71	67	65	59	43	46	58	86	16
8	46	59	73	63	66	56	42	85	58	22
9	53	64	68	57	56	55	50	75	78	12
10	48	49	60	65	70	56	51	57	85	13
11	53	56	85	48	65	55	57	64	63	16
12	74	47	57	55	74	48	47	51	64	12
13	53	43	63	49	52	49	54	61	46	10
14	67	56	47	50	71	58	51	56	66	22
15	43	50	73	52	50	57	60	69	60	18
16	59	54	60	60	49	59	61	56	50	11
17	53	70	55	57	66	45	44	44	61	18
18	62	57	63	51	56	43	54	70	55	8
19	64	49	57	60	52	42	55	51	46	13
20	55	46	51	45	55	44	50	49	56	11
21	52	52	62	48	49	54	51	50	44	13
22	44	58	65	47	49	47	54	53	47	10
23	60	56	62	48	56	55	43	49	44	8
24	56	51	67	34	41	58	56	69	45	5
25	63	59	49	50	40	73	43	51	46	14
26	54	52	54	52	55	50	37	58	51	9
27	59	55	59	46	48	75	53	48	64	11
28	70	52	55	48	50	57	58	61	49	9
29	65	58	63	51	60	49	61	48	51	11
30	52	54	46	44	57	73	49	65	59	11
31	70	52	57	56	58	68	60	47	50	7
32	103	113	122	82	91	107	88	90	78	13
33	72	55	54	51	50	56	58	54	65	11
34	75	56	55	44	66	57	50	62	54	8
35	65	75	64	56	64	58	56	49	51	11
36	78	74	70	43	58	71	53	55	67	11
37	71	56	73	51	72	45	61	71	53	12
38	82	77	62	62	61	66	65	64	59	8
39	61	72	64	60	65	89	66	62	56	23
40	77	84	66	54	60	63	67	72	69	18
41	67	81	68	62	58	77	64	77	68	14
42	89	72	89	74	58	83	65	69	50	12
43	90	87	64	67	63	67	69	52	65	20
44	93	85	87	76	77	69	70	70	70	8
45	93	90	70	89	91	68	86	80	70	13
46	84	90	107	94	78	66	72	88	57	12
47	110	94	108	96	82	48	87	81	92	14
48	93	101	123	101	98	96	78	77	73	15
49	113	101	153	119	114	67	80	83	91	14
50	85	94	132	139	89	101	103	111	95	16

ENHANCED INLET, STATION 3

CP	MA1	MA2	MA3	MA4	MA5	MA6	MA7	MA8	MA9	MA10-AXIAL MEAS
1	0	0	0	0	0	0	0	0	0	8
2	0	0	0	0	0	0	0	0	1	3
3	0	2	0	1	24	1	1	0	0	1
4	0	0	0	47	161	92	35	35	0	0
5	0	0	0	0	0	0	0	813	27	50
6	0	0	0	0	0	0	0	0	0	17
7	0	0	0	0	0	0	0	0	0	0
8	0	0	0	0	14	3	7	0	0	0
9	7	1	6	10	17	14	26	2	18	0
10	5	2	5	8	29	24	65	11	11	3
11	11	2	5	11	29	20	76	31	26	3
12	11	6	5	13	36	36	76	28	44	5
13	17	3	10	33	43	39	113	23	27	6
14	31	8	16	29	35	35	107	33	45	6
15	16	11	17	26	49	44	111	25	43	6
16	10	13	22	19	33	56	124	31	58	3
17	34	11	27	27	38	53	113	35	49	1
18	22	11	17	18	54	40	116	23	62	4
19	28	12	20	27	60	69	108	19	60	8
20	15	4	17	28	45	54	124	30	40	7
21	24	7	20	24	61	50	107	28	44	4
22	42	10	17	33	57	58	107	26	41	5
23	34	10	16	31	51	51	109	22	52	4
24	27	9	22	27	51	59	126	30	60	5
25	27	6	20	31	52	51	120	29	59	3
26	28	8	20	29	64	58	123	27	42	5
27	32	4	22	32	49	66	129	27	59	4
28	19	13	36	49	109	84	198	43	94	11
29	15	7	21	35	59	67	155	25	51	9
30	20	8	29	29	65	73	144	24	64	10
31	29	11	21	28	59	70	137	35	54	2
32	28	10	19	28	67	73	149	30	58	7
33	48	10	22	37	69	76	166	31	72	3
34	29	10	30	25	61	63	170	24	74	5
35	29	9	30	37	72	55	164	36	77	4
36	22	13	34	43	65	58	148	30	63	2
37	28	11	35	41	76	76	180	36	61	3
38	30	11	34	45	73	70	175	28	88	5
39	15	11	34	41	74	82	208	28	70	8
40	20	12	32	35	80	88	159	35	65	6
41	12	5	29	33	96	78	209	29	97	11
42	20	10	36	38	91	91	191	36	82	4
43	6	8	41	52	95	83	197	45	89	9
44	11	2	42	54	90	100	226	40	72	11
45	20	1	43	54	90	99	220	35	99	8
46	12	0	55	60	93	92	233	47	107	8
47	3	0	46	53	95	80	235	52	89	7
48	0	0	9	14	34	66	206	44	103	9
49	0	0	0	0	3	27	155	50	102	8
50	0	0	0	0	0	1	18	16	31	7

ENHANCED INLET, STATION 4

CP	MA1	MA2	MA3	MA4	MA5	MA6	MA7	MA8	MA9	MA10-AXIAL MEAS
1	0	0	0	0	0	19	17	7	16	0
2	0	0	0	1	1	20	34	36	50	1
3	0	0	3	1	0	38	55	30	47	0
4	0	2	1	0	3	48	60	35	47	0
5	0	1	11	2	9	54	57	43	26	3
6	0	3	12	3	13	114	118	84	78	3
7	1	7	10	5	11	77	80	59	23	2
8	0	5	27	11	13	80	63	57	47	1
9	2	6	40	6	17	88	66	66	61	2
10	0	8	54	16	25	86	88	61	66	3
11	4	9	49	11	18	86	75	69	49	7
12	2	11	64	14	35	101	72	69	69	7
13	1	11	63	17	28	93	78	63	40	5
14	5	11	52	23	23	101	89	85	57	10
15	5	14	68	32	37	100	79	75	62	9
16	4	14	82	31	36	104	78	77	64	2
17	7	7	97	42	48	109	77	69	72	6
18	4	13	103	29	34	117	101	75	60	6
19	2	20	100	39	31	128	112	76	77	7
20	5	19	122	35	52	114	112	100	71	8
21	5	17	129	31	29	124	118	93	80	7
22	4	10	143	41	51	111	118	95	95	8
23	5	12	157	36	26	108	113	105	84	11
24	3	10	149	39	27	117	113	99	87	7
25	2	17	165	32	38	135	111	104	83	6
26	4	19	199	38	35	115	114	112	98	11
27	1	14	192	45	39	106	117	114	90	4
28	3	16	179	35	33	97	107	117	99	5
29	2	7	184	29	42	90	100	113	91	2
30	1	18	157	19	49	90	95	114	93	6
31	0	7	169	19	47	76	76	118	103	6
32	3	10	128	8	34	88	71	100	86	5
33	0	8	103	2	42	71	72	86	119	9
34	2	12	40	0	44	49	56	86	114	4
35	1	8	4	0	34	7	55	63	123	3
36	1	15	0	0	12	1	39	62	102	3
37	3	18	0	0	0	0	26	68	76	6
38	10	23	0	0	0	0	0	40	65	1
39	52	41	0	0	0	0	0	11	63	4
40	85	778	0	0	0	0	4	2	30	2
41	28	299	7	0	3	0	34	33	25	0
42	0	30	1	0	0	0	5	10	24	0
43	0	0	0	0	0	0	0	1	8	0
44	0	0	0	0	0	0	0	0	0	0
45	0	0	0	0	0	0	0	0	0	0
46	0	0	0	0	0	0	0	0	0	0
47	0	0	0	0	0	0	0	0	0	0
48	0	0	0	0	0	0	0	0	0	0
49	0	0	0	0	0	0	0	0	0	0
50	0	0	0	0	0	0	0	0	0	0

ENHANCED INLET, STATION 5

CP	MA1	MA2	MA3	MA4	MA5	MA6	MA7	MA8	MA9	MA10-AXIAL MEAS
1	0	0	0	0	0	0	29	46	48	10
2	0	0	0	0	16	69	30	24	49	11
3	0	0	2	47	22	81	32	42	53	8
4	19	0	1	56	19	88	67	56	41	16
5	22	1	2	54	26	119	52	67	26	20
6	15	0	12	65	27	106	52	49	37	12
7	20	1	12	78	28	118	42	53	56	18
8	17	3	31	59	30	137	48	54	41	18
9	31	2	19	81	30	158	67	52	41	13
10	28	3	38	73	37	164	45	56	55	19
11	19	5	39	84	45	176	61	51	58	24
12	31	6	52	91	45	176	86	78	46	28
13	14	5	42	84	38	162	65	67	59	15
14	25	4	50	108	42	180	55	42	64	21
15	21	6	43	116	56	189	100	57	58	15
16	16	5	47	128	39	166	85	67	72	25
17	17	11	52	123	51	203	81	80	59	23
18	18	7	62	118	55	216	81	72	65	25
19	6	7	53	127	45	219	88	68	71	20
20	8	3	59	107	62	260	80	74	70	15
21	14	6	66	100	77	256	81	84	62	18
22	10	10	67	106	62	221	88	93	61	18
23	11	8	60	104	74	228	83	86	86	15
24	9	7	62	81	62	208	98	88	77	14
25	10	4	62	69	68	233	112	107	81	11
26	9	9	72	78	80	193	114	108	90	12
27	5	5	66	73	69	173	103	107	92	13
28	3	2	76	73	86	139	120	104	113	9
29	3	10	58	83	71	161	114	115	105	5
30	5	5	71	76	74	144	92	99	113	12
31	2	5	57	76	76	159	109	93	130	6
32	2	5	80	80	71	116	94	102	92	10
33	1	3	62	72	71	118	93	113	129	11
34	1	5	67	40	61	136	82	100	94	6
35	5	4	67	14	71	98	73	88	93	15
36	27	1	54	0	73	51	82	70	87	16
37	111	2	40	0	75	5	72	55	78	12
38	331	0	16	0	26	0	55	71	44	16
39	342	1	3	1	6	0	35	44	4	16
40	10	12	8	0	1	6	47	76	28	9
41	0	6	0	0	0	0	6	8	21	1
42	0	0	0	0	0	0	0	0	6	5
43	0	0	0	0	0	0	0	0	2	9
44	0	0	0	0	0	0	0	0	0	0
45	0	0	0	0	0	0	0	0	0	0
46	0	0	0	0	0	0	0	0	0	0
47	0	0	0	0	0	0	0	0	0	0
48	0	0	0	0	0	0	0	0	0	0
49	0	0	0	0	0	0	0	0	0	0
50	0	0	0	0	0	0	0	0	0	0

ENHANCED INLET, STATION 6

CP	MA1	MA2	MA3	MA4	MA5	MA6	MA7	MA8	MA9	MA10-AXIAL MEAS
1	0	0	0	0	0	0	0	0	0	
2	0	0	0	8	20	41	68	118	60	
3	24	0	15	21	20	31	86	85	51	
4	15	10	24	23	31	40	110	118	64	
5	18	24	30	32	42	37	102	110	49	
6	19	25	48	26	48	58	106	105	53	
7	30	40	60	43	49	52	116	113	60	
8	25	34	73	55	66	59	104	104	44	
9	22	49	83	53	69	62	106	115	49	
10	25	47	84	59	73	73	135	123	54	
11	17	55	92	72	75	57	119	117	58	
12	12	56	98	82	69	60	127	115	55	
13	21	57	107	77	70	69	125	120	49	
14	28	66	96	83	76	65	134	126	63	
15	32	64	105	85	79	71	135	136	73	
16	17	68	100	91	92	81	139	129	53	
17	16	60	97	87	91	76	135	121	57	
18	19	74	120	91	112	75	115	126	57	
19	14	87	149	112	103	73	137	163	58	
20	14	79	138	103	98	101	141	154	59	
21	23	77	124	107	92	87	158	162	79	
22	16	72	140	130	99	80	136	156	60	
23	20	79	144	95	102	91	142	158	75	
24	11	77	145	114	102	91	163	180	74	
25	13	66	107	116	120	92	166	155	73	
26	15	61	95	101	97	96	173	202	70	
27	17	83	179	154	225	164	262	248	116	
28	8	50	99	81	113	95	167	181	104	
29	9	37	79	81	124	81	189	180	79	
30	7	42	84	76	116	97	181	181	75	
31	2	35	79	55	98	100	198	166	75	
32	5	42	65	43	83	81	206	180	70	
33	1	23	48	38	65	69	177	200	86	
34	2	26	38	24	68	76	169	179	88	
35	2	22	27	13	46	75	185	174	84	
36	2	11	30	17	62	66	154	156	87	
37	3	19	23	12	41	71	167	134	93	
38	0	22	22	11	40	58	162	103	84	
39	6	15	24	9	41	81	171	99	66	
40	4	27	20	15	66	105	211	121	64	
41	0	15	20	90	20	32	104	76	47	
42	0	2	1	13	2	1	15	10	27	
43	0	0	0	0	0	0	0	0	0	
44	0	0	0	0	0	0	0	0	0	
45	0	0	0	0	0	0	0	0	0	
46	0	0	0	0	0	0	0	0	0	
47	0	0	0	0	0	0	0	0	0	
48	0	0	0	0	0	0	0	0	0	
49	0	0	0	0	0	0	0	0	0	
50	0	0	0	0	0	0	0	0	0	

ENHANCED INLET, STATION 7

CP	MA1	MA2	MA3	MA4	MA5	MA6	MA7	MA8	MA9	MA10-AXIAL MEAS
1	0	0	0	0	0	0	0	0	0	0
2	0	1	0	0	0	0	0	0	0	0
3	0	2	1	3	2	15	78	91	80	0
4	0	5	1	6	2	26	115	68	73	1
5	0	20	1	10	1	30	92	61	64	0
6	0	92	1	4	4	33	114	50	85	4
7	0	160	0	9	4	25	72	44	90	3
8	0	75	0	10	6	20	91	53	61	1
9	0	50	3	12	9	47	77	51	68	4
10	0	1	3	17	6	49	83	57	53	2
11	0	2	5	7	6	48	100	47	65	6
12	0	0	3	27	16	50	96	64	52	10
13	0	0	6	25	12	64	85	62	57	5
14	0	0	4	23	11	71	94	51	54	6
15	0	0	10	27	23	76	87	57	67	3
16	0	1	4	31	10	82	85	51	50	4
17	0	0	11	55	17	70	95	52	56	5
18	1	0	5	15	15	74	100	54	58	4
19	0	1	9	23	22	71	107	56	54	7
20	0	1	10	50	44	130	162	92	95	7
21	0	1	5	44	19	88	91	55	57	8
22	0	0	8	19	17	71	99	61	59	7
23	0	0	8	20	21	80	102	45	56	7
24	0	1	7	23	26	85	110	65	47	8
25	0	0	8	20	26	90	128	59	53	10
26	0	0	6	22	33	94	110	43	49	4
27	0	5	10	24	24	79	101	68	57	9
28	0	1	12	22	30	78	117	65	50	11
29	0	1	8	21	28	99	110	66	55	8
30	0	0	11	21	31	99	99	68	52	6
31	0	2	11	27	46	106	111	68	66	9
32	0	1	11	33	28	93	123	58	58	7
33	0	1	15	22	33	90	115	64	67	6
34	0	1	14	26	36	104	122	56	57	4
35	0	0	12	27	50	102	136	70	61	5
36	1	0	13	18	32	107	138	82	71	5
37	1	1	11	36	31	111	133	65	62	6
38	0	0	12	29	43	92	167	75	58	8
39	0	2	11	26	41	92	152	79	59	10
40	0	1	18	26	40	68	127	56	68	8
41	0	15	26	23	30	65	138	68	78	10
42	2	11	14	33	24	40	153	81	101	9
43	0	125	25	58	17	34	170	94	104	10
44	0	2380	2576	90	127	29	252	125	107	13
45	70	1433	4066	41	6967	34	169	111	124	15
46	777	6	160	0	302	20	33	27	66	50
47	956	14	10	0	2	3	9	26	23	98
48	259	25	16	2	0	3	42	56	45	2
49	0	0	0	0	1	1	48	56	87	1
50	0	0	0	0	0	0	0	0	0	0

ENHANCED INLET, STATION 8

CP	MA1	MA2	MA3	MA4	MA5	MA6	MA7	MA8	MA9	MA10-AXIAL MEAS
1	0	1	340	114	4	19	138	178	17	7
2	1	4	545	176	0	6	106	183	8	6
3	0	1	503	192	3	5	102	177	4	4
4	0	3	349	134	6	8	88	184	8	6
5	0	3	205	120	6	6	48	210	8	1
6	0	2	225	145	6	9	60	181	7	2
7	0	3	261	103	8	6	38	163	10	4
8	0	4	271	70	7	11	31	180	22	6
9	0	3	150	23	7	16	48	137	15	4
10	0	5	37	5	8	14	58	144	21	5
11	0	4	24	1	9	19	56	117	20	6
12	0	5	27	0	7	23	44	143	18	7
13	0	2	21	1	9	22	70	136	16	4
14	0	2	29	1	15	24	64	127	9	7
15	0	3	27	2	18	27	59	146	23	6
16	0	3	28	2	14	33	96	112	22	8
17	0	7	29	3	21	31	73	142	16	13
18	0	4	38	3	18	59	157	234	30	6
19	0	4	20	2	25	36	86	144	24	16
20	0	5	23	1	31	37	88	126	20	6
21	0	7	17	0	14	33	88	157	26	9
22	0	9	23	2	25	44	76	140	9	8
23	0	6	26	2	23	30	90	136	20	10
24	0	10	27	2	31	35	81	140	21	13
25	0	5	23	3	25	29	89	151	20	11
26	0	5	27	1	22	41	76	165	20	9
27	0	6	21	2	27	37	86	167	13	12
28	0	15	29	2	35	36	75	183	15	14
29	0	9	30	2	38	48	90	181	12	14
30	0	13	22	3	42	46	68	150	12	13
31	0	12	25	1	37	30	76	177	16	8
32	0	7	21	2	34	42	92	162	21	10
33	0	10	21	1	38	40	88	146	19	8
34	0	12	23	1	35	42	94	176	14	5
35	0	8	27	7	37	31	103	176	16	17
36	0	10	27	3	36	45	76	190	18	15
37	0	10	25	2	17	43	101	180	13	15
38	0	10	25	2	57	46	93	162	20	11
39	0	14	28	2	25	52	110	179	29	15
40	0	11	30	13	33	58	104	153	22	20
41	0	14	266	32	62	55	105	177	16	15
42	145	19	473	33	74	58	111	195	24	10
43	407	14	148	1	83	57	115	205	22	23
44	16	30	25	1	147	88	118	194	21	16
45	0	31	31	2	219	102	176	215	25	38
46	0	71	32	19	544	165	211	229	22	44
47	17	30	113	45	928	293	304	324	26	20
48	245	38	588	354	881	458	392	336	32	31
49	520	49	731	618	215	276	304	321	38	71
50	133	22	546	141	23	66	180	191	28	45

TABLE A4. -

(d) NUMBER OF TANGENTIAL MEASUREMENTS

BASELINE INLET, STATION 1

CP	MT1	MT2	MT3	MT4	MT5	MT6	MT7	MT8	MT9	MT10-TANG MEAS
1	75	259	203	279	225	321	233	197	232	40
2	61	253	159	280	226	343	247	196	226	46
3	67	259	164	293	196	316	232	226	236	41
4	54	244	170	307	212	319	245	215	231	46
5	66	268	178	293	202	336	218	203	243	42
6	62	251	170	276	211	326	227	195	242	46
7	53	255	184	297	212	319	227	227	223	44
8	48	255	184	304	204	320	224	208	234	51
9	58	251	181	317	208	324	219	205	227	45
10	72	258	198	291	202	339	241	213	261	42
11	56	242	188	286	226	336	207	212	269	50
12	59	268	171	288	212	326	234	210	259	47
13	61	264	187	292	205	337	263	245	250	37
14	77	248	177	277	211	294	228	230	241	40
15	78	239	177	279	241	362	217	223	244	55
16	60	256	206	317	213	328	228	205	256	42
17	56	265	192	284	212	323	223	214	277	49
18	81	250	185	274	202	319	213	193	232	48
19	61	252	160	292	229	309	248	218	238	34
20	61	264	194	318	221	322	183	217	236	41
21	58	248	176	273	237	337	217	224	278	42
22	64	264	175	275	204	341	246	206	258	60
23	59	247	181	319	219	314	224	191	244	56
24	63	244	173	282	207	334	225	218	247	46
25	58	259	181	321	196	335	236	233	241	57
26	66	252	181	320	231	322	222	217	265	39
27	61	252	181	303	213	325	219	223	247	48
28	64	260	183	302	213	356	210	212	259	41
29	60	266	183	305	217	286	215	214	263	44
30	47	279	197	298	223	311	228	192	256	47
31	59	258	179	312	191	325	239	248	265	43
32	64	249	180	320	220	319	199	205	236	52
33	67	228	180	269	223	335	220	211	219	49
34	50	249	180	318	225	332	230	218	231	62
35	51	266	196	287	198	312	233	234	231	53
36	59	248	188	289	218	344	212	211	226	43
37	65	272	185	286	237	318	221	198	231	43
38	72	229	197	285	209	332	232	217	248	43
39	61	263	177	301	221	332	230	198	261	46
40	56	241	168	283	198	309	217	201	234	40
41	59	248	165	278	246	321	228	189	241	38
42	52	263	180	291	201	315	220	214	242	46
43	66	268	189	309	231	333	220	214	257	36
44	68	270	177	291	212	358	236	207	229	41
45	52	267	171	278	194	333	226	221	259	47
46	77	250	208	305	235	323	236	200	219	39
47	77	255	187	262	231	330	251	219	239	51
48	64	257	191	278	198	349	210	202	224	40
49	61	259	175	256	216	332	221	215	265	49
50	98	436	285	550	337	537	329	352	490	77

BASELINE INLET, STATION 2

CP	MT1	MT2	MT3	MT4	MT5	MT6	MT7	MT8	MT9	MT10-TANG MEAS
1	246	70	127	14	178	131	81	75	141	99
2	263	58	140	15	170	131	81	84	157	89
3	264	76	135	15	209	117	88	82	105	25
4	293	61	132	12	192	136	86	80	88	11
5	284	63	106	14	200	162	91	97	90	14
6	331	62	127	11	227	187	104	67	74	7
7	353	68	129	14	199	159	69	77	74	13
8	302	89	127	13	224	155	98	87	78	14
9	378	78	118	10	227	163	94	70	65	10
10	367	76	111	12	202	176	99	86	85	10
11	351	86	132	13	256	154	86	87	60	9
12	359	70	116	13	219	169	90	94	74	3
13	374	81	139	8	254	178	112	100	87	8
14	370	82	144	12	267	171	105	98	73	5
15	380	88	108	11	281	180	117	86	81	9
16	367	91	115	12	237	164	123	109	98	11
17	366	90	123	19	213	163	109	106	76	7
18	350	81	135	14	216	162	116	112	93	13
19	356	75	133	12	245	177	96	130	110	11
20	383	105	140	14	259	178	113	112	89	13
21	369	95	147	17	236	170	109	143	111	13
22	383	87	117	16	228	166	124	108	106	13
23	405	97	125	17	221	141	108	115	98	11
24	382	110	114	17	269	149	109	116	92	15
25	386	91	126	20	278	156	138	125	109	20
26	359	93	139	17	241	129	121	107	107	9
27	343	93	111	13	246	141	140	127	116	18
28	373	90	156	16	242	169	115	122	132	12
29	405	87	133	19	246	139	129	142	132	13
30	335	82	99	22	268	144	119	113	115	6
31	365	92	113	22	268	152	123	123	128	13
32	604	141	215	18	413	206	195	212	221	12
33	336	101	128	17	260	155	135	126	119	9
34	338	85	124	11	247	159	118	128	121	21
35	325	93	116	17	256	165	129	144	125	18
36	351	87	150	7	302	162	145	131	103	11
37	363	84	126	18	263	147	118	130	117	13
38	357	103	129	17	294	173	135	127	129	14
39	332	86	112	25	247	137	128	119	128	7
40	316	84	124	16	297	170	139	134	123	20
41	344	87	131	13	243	140	129	148	118	12
42	281	84	125	11	250	144	127	118	114	16
43	298	76	127	13	266	159	127	110	133	12
44	278	77	124	16	295	149	125	132	136	6
45	251	85	147	12	261	151	120	113	142	15
46	239	84	125	13	241	133	109	113	140	12
47	214	75	123	13	243	161	119	133	112	18
48	203	64	143	16	268	136	110	108	125	15
49	234	53	133	10	277	170	97	126	137	22
50	240	79	133	18	204	146	82	88	160	46

BASELINE INLET, STATION 3

CP	MT1	MT2	MT3	MT4	MT5	MT6	MT7	MT8	MT9	MT10-TANG MEAS
1		1	46	8	4	0	11	1	0	29
2		0	26	3	4	0	26	40	12	341
3		1	2	2	3	5	23	18	51	241
4		0	8	2	3	33	5	3	17	78
5		0	0	0	0	0	0	4	6	149
6		0	0	0	0	0	0	0	0	15
7		0	0	0	0	0	0	0	0	0
8		38	0	0	10	54	31	0	0	0
9		42	39	22	9	62	51	34	23	0
10		50	48	29	20	59	51	62	22	478
11		30	59	31	15	109	82	71	28	41
12		38	44	31	17	166	66	71	56	39
13		48	38	23	29	190	58	65	51	34
14		34	46	30	14	191	71	74	70	16
15		56	47	35	19	180	56	69	74	4
16		53	54	36	16	197	59	63	59	6
17		45	51	51	22	208	65	58	72	26
18		53	34	41	18	181	75	73	54	187
19		44	67	26	15	152	67	71	68	733
20		41	68	38	23	161	70	78	83	1600
21		50	56	42	24	149	64	67	64	2144
22		40	52	36	17	156	89	79	83	1748
23		47	64	35	22	172	68	64	75	1421
24		52	57	39	18	165	75	78	77	973
25		43	70	38	12	163	82	57	84	700
26		36	51	40	27	176	47	63	56	373
27		54	57	48	18	142	82	81	73	181
28		74	84	56	27	256	125	130	122	150
29		42	59	44	19	144	85	78	73	38
30		39	52	39	23	147	77	67	74	6
31		49	48	48	23	155	84	73	80	2
32		47	53	46	19	142	81	97	90	4
33		49	42	42	20	144	78	69	101	1
34		59	61	52	27	139	91	88	89	6
35		40	68	46	31	126	77	76	76	5
36		43	69	47	26	130	84	92	80	6
37		26	40	42	23	142	74	100	95	2
38		45	42	50	33	158	109	88	87	3
39		38	49	36	22	153	75	81	91	7
40		34	44	44	31	154	77	87	75	6
41		38	43	39	23	137	83	83	103	3
42		33	40	36	30	147	78	97	88	9
43		18	41	34	24	122	101	98	98	7
44		29	40	31	20	125	98	100	91	3
45		16	26	23	16	83	93	97	87	9
46		8	11	20	16	87	74	86	98	13
47		5	8	11	7	63	61	72	85	5
48		0	2	2	0	23	42	43	60	1
49		0	0	1	0	15	19	21	10	4
50		1	11	1	0	2	1	3	3	2

BASELINE INLET, STATION 4

CP	MT1	MT2	MT3	MT4	MT5	MT6	MT7	MT8	MT9	MT10-TANG MEAS
1	0	0	0	0	0	16	21	20	21	11
2	0	0	0	8	110	27	40	20	13	15
3	0	0	14	9	209	46	56	33	14	24
4	4	61	41	24	271	56	52	48	21	19
5	1	68	56	43	398	84	67	45	34	36
6	3	133	139	104	786	176	134	122	70	32
7	1	69	92	70	494	148	73	75	52	18
8	3	70	92	72	552	169	94	76	61	20
9	5	78	101	94	563	198	89	54	74	36
10	5	71	108	92	638	170	64	83	62	28
11	2	87	112	120	565	208	93	93	90	35
12	3	90	108	112	615	204	79	72	92	28
13	9	80	126	107	579	212	98	86	83	28
14	7	74	118	138	664	198	105	82	87	41
15	10	84	122	109	708	196	101	96	97	33
16	10	88	134	133	756	197	100	86	93	39
17	11	86	117	116	677	227	96	91	107	36
18	7	90	117	122	592	229	82	83	116	36
19	9	72	162	160	571	231	89	111	131	30
20	9	68	148	130	550	225	95	120	109	29
21	6	71	138	137	591	177	103	111	100	27
22	13	75	139	147	581	206	98	98	102	35
23	8	67	132	116	630	196	96	97	111	32
24	4	61	104	109	563	221	98	112	114	52
25	5	56	121	122	376	230	106	115	106	45
26	2	47	98	99	68	238	98	106	94	37
27	0	47	77	91	9	249	108	101	129	48
28	0	54	91	108	1	234	117	116	130	66
29	1	59	84	90	0	215	118	99	131	41
30	0	59	73	87	0	185	104	95	147	34
31	1	61	71	102	0	177	108	115	132	49
32	0	51	71	74	0	163	103	78	106	39
33	0	29	30	49	0	144	78	76	145	54
34	0	9	6	14	0	142	71	79	113	64
35	0	1	1	5	0	72	64	61	95	57
36	0	0	1	0	0	33	20	55	71	54
37	0	0	0	0	0	13	2	16	65	27
38	0	0	0	0	0	6	0	2	16	20
39	0	0	0	0	0	1	0	0	5	12
40	0	0	0	0	1	0	0	0	1	1
41	0	0	0	0	1	1	0	0	0	0
42	0	0	0	0	13	0	0	0	0	0
43	0	0	0	0	32	1	9	13	6	19
44	0	0	0	2	17	24	75	49	17	26
45	0	0	0	0	0	0	0	0	11	14
46	0	0	0	0	0	0	0	0	0	0
47	0	0	0	0	0	0	0	0	0	0
48	0	0	0	0	0	0	0	0	0	0
49	0	0	0	0	0	0	0	0	0	0
50	0	0	0	0	0	0	0	0	0	0

BASELINE INLET, STATION 5

CP	MT1	MT2	MT3	MT4	MT5	MT6	MT7	MT8	MT9	MT10-TANG MEAS
1	0	0	0	0	0	0	0	28	9	0
2	0	0	0	0	14	18	29	58	15	2
3	0	0	79	31	16	33	48	35	12	1
4	77	76	85	32	32	23	60	59	12	1
5	97	105	115	44	43	32	79	60	16	6
6	94	104	123	47	49	44	43	65	18	4
7	88	103	140	51	55	51	75	72	13	5
8	103	88	155	74	60	84	58	75	6	3
9	103	117	148	65	88	64	76	93	19	7
10	83	100	173	82	86	77	85	82	11	3
11	73	111	151	90	99	96	81	86	16	6
12	87	116	181	93	101	70	93	76	17	7
13	74	114	171	90	101	84	94	80	15	10
14	68	121	160	113	111	94	102	80	21	7
15	91	103	151	87	120	120	101	88	13	5
16	105	128	129	121	105	105	100	69	18	12
17	114	102	138	115	107	102	127	87	14	13
18	117	109	147	144	140	99	101	95	20	6
19	128	121	141	115	111	102	85	89	16	7
20	126	99	122	110	131	95	103	100	21	12
21	141	99	118	106	111	119	87	108	16	8
22	136	102	112	126	121	110	111	108	17	11
23	106	100	105	121	104	106	116	123	20	9
24	143	93	81	119	108	115	130	109	25	7
25	100	80	80	102	106	112	128	98	24	9
26	122	72	81	100	79	104	120	115	24	12
27	92	57	58	95	89	87	109	118	22	4
28	94	58	47	84	80	89	103	112	28	12
29	78	43	11	89	80	80	95	115	29	6
30	91	46	1	69	63	79	60	110	28	7
31	72	41	0	78	60	73	77	109	26	13
32	65	31	0	76	60	70	62	63	40	13
33	72	39	0	60	70	58	55	90	24	13
34	51	14	0	54	57	51	44	62	15	15
35	18	9	0	47	40	44	42	52	14	18
36	8	2	0	16	14	41	27	37	19	14
37	3	1	0	10	11	41	12	23	11	25
38	0	3	0	5	7	15	0	5	2	21
39	0	2	0	1	1	8	3	1	1	18
40	0	2	0	0	0	2	1	0	0	2
41	0	1	0	0	0	1	1	1	2	1
42	0	0	0	0	1	0	5	2	17	0
43	0	2	1	1	2	0	10	13	40	5
44	0	0	0	0	0	0	0	0	0	0
45	0	0	0	0	0	0	0	0	0	0
46	0	0	0	0	0	0	0	0	0	0
47	0	0	0	0	0	0	0	0	0	0
48	0	0	0	0	0	0	0	0	0	0
49	0	0	0	0	0	0	0	0	0	0
50	0	0	0	0	0	0	0	0	0	0

BASELINE INLET, STATION 6

CP	MT1	MT2	MT3	MT4	MT5	MT6	MT7	MT8	MT9	MT10-TANG MEAS
1	0	0	0	0	0	0	0	0	0	0
2	0	0	0	56	49	45	89	93	11	27
3	63	92	176	78	38	60	119	124	1	27
4	53	89	195	65	53	63	138	126	10	32
5	49	118	211	70	62	61	129	120	9	15
6	67	140	195	97	68	60	139	132	8	30
7	62	139	188	94	67	82	148	136	15	37
8	66	154	202	99	69	51	143	119	14	13
9	73	153	202	98	77	84	160	144	10	35
10	92	163	212	112	97	100	144	125	12	32
11	100	157	216	111	91	97	153	134	12	36
12	99	157	205	101	91	100	167	138	22	16
13	107	160	208	101	105	90	158	146	9	21
14	118	152	215	80	103	92	126	172	23	20
15	118	134	251	112	106	96	169	142	16	46
16	119	144	224	99	99	105	179	140	26	27
17	122	130	203	102	100	89	136	162	25	24
18	138	135	230	110	103	113	155	169	21	33
19	159	131	226	106	85	123	140	197	9	18
20	132	146	227	118	97	95	165	154	24	44
21	143	114	244	98	119	115	167	139	21	28
22	112	120	196	123	105	104	188	171	7	25
23	120	117	189	111	105	125	183	187	23	20
24	105	103	195	99	96	90	195	182	21	26
25	122	87	152	91	111	102	193	199	14	27
26	118	59	164	89	95	100	173	205	25	50
27	135	117	201	117	136	144	270	281	29	53
28	65	70	95	64	84	76	170	174	11	44
29	54	54	102	43	88	70	174	192	32	29
30	43	43	80	53	59	58	155	186	17	56
31	36	27	57	38	66	47	138	188	14	47
32	28	37	46	35	56	48	132	207	27	55
33	31	26	40	28	40	21	121	155	35	29
34	12	25	26	18	41	23	91	144	29	56
35	7	12	27	14	29	18	111	106	28	98
36	20	9	14	10	32	12	115	95	76	115
37	12	4	17	13	26	5	108	92	71	168
38	8	5	12	11	14	3	80	57	78	139
39	2	1	6	6	12	2	24	28	24	122
40	1	1	3	8	4	3	6	16	14	79
41	1	1	1	3	0	7	5	1	8	44
42	1	2	3	3	2	2	9	18	58	32
43	1	4	3	2	2	17	44	32	91	41
44	1	11	12	4	1	17	10	60	82	41
45	0	0	0	0	0	7	45	36	26	41
46	0	0	0	0	0	0	0	0	0	0
47	0	0	0	0	0	0	0	0	0	0
48	0	0	0	0	0	0	0	0	0	0
49	0	0	0	0	0	0	0	0	0	0
50	0	0	0	0	0	0	0	0	0	0

BASELINE INLET, STATION 7

CP	MT1	MT2	MT3	MT4	MT5	MT6	MT7	MT8	MT9	MT10-TANG MEAS
1	0	0	0	0	0	0	0	0	0	0
2	0	59	0	0	0	0	0	0	0	0
3	60	110	56	25	74	54	40	17	39	0
4	66	124	67	32	67	49	77	17	50	34
5	91	165	85	35	83	62	77	19	48	34
6	88	213	89	37	87	69	65	21	44	41
7	110	266	99	37	93	96	80	40	66	40
8	117	260	101	40	116	96	83	45	58	36
9	152	244	97	44	146	99	83	47	86	40
10	159	277	89	50	125	112	92	53	83	53
11	165	267	97	51	120	121	104	40	80	56
12	194	275	99	47	142	100	92	96	95	32
13	181	276	101	39	147	131	125	60	101	48
14	205	281	105	42	163	143	103	70	112	47
15	194	318	99	45	152	146	128	63	93	42
16	211	269	112	54	148	121	124	38	114	49
17	193	305	95	47	165	145	132	60	96	35
18	190	281	101	52	150	157	137	61	106	66
19	232	291	98	47	158	138	132	54	116	56
20	378	439	157	67	239	236	194	98	196	83
21	249	283	108	39	172	151	151	74	112	49
22	229	260	101	59	177	164	117	60	126	36
23	249	262	122	50	165	152	148	72	117	47
24	227	256	97	43	189	166	122	66	130	43
25	238	281	93	44	184	164	153	76	124	36
26	220	269	103	43	165	154	170	73	116	43
27	243	301	102	48	184	157	148	74	143	39
28	192	296	102	55	196	188	167	71	133	38
29	197	243	112	54	164	181	154	78	121	60
30	173	250	96	48	182	165	160	72	126	50
31	185	226	105	49	196	168	196	93	147	46
32	148	200	97	50	178	160	164	85	134	70
33	142	177	93	51	174	189	160	71	131	47
34	103	155	74	32	196	183	154	78	129	62
35	93	129	88	33	167	161	170	67	147	55
36	87	115	62	36	138	126	175	83	153	71
37	73	98	71	31	126	147	169	83	151	67
38	79	77	61	32	93	110	136	94	131	77
39	48	63	46	18	88	100	153	80	211	75
40	30	60	62	33	74	77	111	65	219	82
41	27	42	45	33	51	66	86	66	235	112
42	39	20	23	24	40	53	81	46	222	116
43	9	12	16	13	25	40	39	26	100	155
44	27	10	7	4	13	12	19	12	56	77
45	58	8	3	1	3	14	14	10	24	30
46	26	6	2	3	18	13	14	8	27	28
47	10	13	6	6	29	10	20	8	34	23
48	36	17	12	6	18	21	15	13	30	26
49	0	0	0	0	42	29	21	9	30	26
50	0	0	0	0	0	0	0	0	0	32

BASELINE INLET, STATION 8

CP	MT1	MT2	MT3	MT4	MT5	MT6	MT7	MT8	MT9	MT10-TANG MEAS
1	9	4	10	17	20	13	21	30	23	71
2	10	6	11	14	14	18	30	37	32	67
3	3	4	16	26	15	31	41	46	50	79
4	1	1	16	33	17	35	26	39	45	66
5	0	12	27	33	21	29	40	48	62	71
6	2	4	47	53	18	35	56	48	55	86
7	2	10	58	59	49	53	58	74	70	93
8	2	14	69	69	38	57	54	75	65	95
9	0	6	81	88	55	49	70	75	57	94
10	1	10	112	73	54	63	77	91	64	95
11	0	27	98	104	53	76	66	86	76	77
12	0	49	117	94	64	100	84	83	114	98
13	0	36	128	120	87	98	105	89	93	83
14	0	30	129	144	100	102	107	92	93	94
15	0	36	115	138	102	113	103	106	78	80
16	0	19	130	151	115	103	111	112	83	105
17	0	42	128	114	84	112	132	116	107	70
18	0	63	189	198	183	179	158	180	161	144
19	0	34	126	108	122	127	107	116	92	94
20	0	58	102	111	107	129	122	99	112	72
21	0	49	108	119	126	112	114	132	92	100
22	1	51	130	135	120	122	127	112	111	67
23	0	51	117	130	133	162	136	110	90	82
24	0	36	127	119	116	125	115	96	109	104
25	1	38	133	141	102	135	123	133	116	71
26	1	51	119	148	122	135	142	140	116	103
27	1	57	121	116	107	141	143	135	118	101
28	0	38	131	138	131	141	111	131	122	90
29	0	42	129	129	128	147	153	126	109	98
30	1	38	123	144	132	132	124	109	114	68
31	1	42	143	155	112	137	142	111	107	114
32	3	28	129	145	121	138	146	148	94	96
33	2	41	129	138	137	157	145	143	104	98
34	0	35	139	155	127	139	128	163	97	109
35	2	35	133	128	135	150	153	130	122	83
36	3	42	131	153	115	165	150	150	104	118
37	7	46	136	145	126	157	155	156	123	127
38	7	40	123	157	139	167	130	133	103	124
39	13	42	137	152	143	156	170	126	128	130
40	16	41	141	149	157	176	169	161	123	141
41	17	49	176	158	190	199	132	153	157	153
42	23	62	229	192	163	179	179	183	167	195
43	20	80	328	268	228	250	249	195	206	222
44	45	96	364	261	333	296	277	261	306	276
45	204	65	241	267	358	349	327	336	364	356
46	294	79	88	149	245	287	345	355	434	445
47	273	60	31	51	101	181	181	258	329	413
48	119	22	6	18	27	70	69	85	179	256
49	36	4	3	11	18	30	28	62	79	159
50	9	2	3	16	7	10	15	29	66	98

ENHANCED INLET, STATION 1

CP	MT1	MT2	MT3	MT4	MT5	MT6	MT7	MT8	MT9	MT10-TANG MEAS
1	46	48	62	66	57	70	61	83	60	24
2	48	61	56	78	58	58	68	94	68	19
3	49	71	65	59	64	64	64	76	63	27
4	41	46	62	65	65	68	49	104	56	34
5	46	54	57	69	57	63	67	89	65	28
6	44	68	69	60	72	71	66	91	54	37
7	62	62	58	68	71	70	62	92	51	27
8	56	50	66	57	69	65	66	100	60	28
9	50	66	58	69	74	65	75	81	66	34
10	64	54	52	58	63	55	73	99	72	31
11	46	68	61	76	57	80	69	103	59	24
12	59	58	47	58	73	64	66	88	64	37
13	54	57	75	66	68	61	70	88	62	34
14	62	57	50	73	67	65	73	84	68	30
15	60	67	56	63	57	66	80	85	66	25
16	50	64	77	62	78	64	67	89	69	20
17	55	63	53	62	80	60	61	88	53	24
18	56	58	64	63	75	68	58	88	68	20
19	54	64	53	56	62	68	69	90	70	26
20	35	51	71	59	57	68	59	89	67	31
21	69	68	65	57	51	62	67	92	60	30
22	55	62	68	78	69	58	71	81	64	29
23	69	63	59	72	72	62	61	74	65	35
24	49	61	71	69	58	67	59	89	70	28
25	58	68	56	54	68	67	68	107	63	22
26	47	57	61	82	71	71	55	79	68	33
27	47	64	67	57	68	74	66	91	67	28
28	58	63	61	58	76	65	59	102	61	37
29	49	60	68	63	64	71	51	77	63	27
30	54	63	67	71	58	64	65	82	59	29
31	62	71	67	73	59	71	79	99	73	37
32	58	72	80	59	64	67	66	82	57	27
33	57	59	67	61	60	60	63	101	67	20
34	52	64	65	59	78	70	67	87	54	31
35	61	74	71	74	61	69	71	90	60	24
36	42	66	51	65	51	69	67	80	73	22
37	50	60	55	78	63	60	64	80	67	29
38	56	61	65	81	56	66	56	93	56	24
39	62	71	72	66	69	65	80	91	57	32
40	48	53	66	63	69	63	65	94	56	32
41	48	60	68	54	64	69	63	79	55	32
42	47	53	58	76	60	69	70	102	62	19
43	57	49	56	72	56	67	61	81	57	27
44	52	63	67	68	67	74	68	80	58	21
45	51	55	69	84	72	67	55	99	67	22
46	41	56	53	59	67	70	68	83	69	32
47	54	59	64	61	77	66	83	85	68	30
48	59	70	66	62	67	72	74	77	57	27
49	61	67	56	67	60	58	53	80	63	32
50	97	117	92	75	102	82	110	124	100	52

ENHANCED INLET, STATION 2

CP	MT1	MT2	MT3	MT4	MT5	MT6	MT7	MT8	MT9	MT10-TANG MEAS
1	99	106	93	59	64	111	56	50	48	17
2	100	103	112	42	50	93	47	51	54	16
3	77	111	126	46	52	113	35	40	284	19
4	115	110	111	62	54	85	52	44	258	23
5	99	99	96	90	63	86	51	61	40	16
6	78	85	85	73	55	84	52	66	36	22
7	100	97	91	88	57	67	49	60	57	24
8	88	99	94	67	73	98	54	67	44	16
9	72	95	65	80	64	87	60	65	68	24
10	82	80	95	65	59	102	60	58	46	27
11	120	95	73	73	63	72	66	63	56	25
12	95	93	73	70	56	65	70	76	66	14
13	78	95	75	59	61	101	70	65	59	20
14	74	84	79	55	73	67	71	63	60	11
15	81	97	83	52	72	74	95	64	44	16
16	75	107	76	77	63	76	68	67	49	16
17	77	86	95	49	60	79	66	63	61	18
18	71	118	87	55	68	70	61	74	42	20
19	96	117	92	56	66	80	69	78	34	15
20	111	103	97	63	62	80	65	74	53	8
21	79	109	92	52	66	81	77	65	54	18
22	92	110	89	60	59	84	65	63	43	10
23	97	120	94	71	78	74	60	67	54	15
24	86	132	94	70	80	82	72	48	51	15
25	84	112	89	59	64	93	71	73	52	13
26	97	106	98	76	60	92	66	74	42	16
27	101	134	74	72	57	85	62	64	57	15
28	89	118	104	53	69	77	62	71	53	9
29	86	103	93	78	82	80	62	70	52	17
30	86	106	106	63	59	99	60	68	54	10
31	82	122	91	53	62	70	64	54	62	13
32	141	164	166	100	99	195	100	100	88	19
33	82	111	77	70	70	113	58	47	56	13
34	83	124	88	61	73	108	77	58	54	9
35	83	89	86	68	65	87	52	70	64	16
36	75	100	90	72	73	92	76	70	68	21
37	82	117	89	62	62	118	80	67	57	12
38	78	107	70	59	60	92	57	61	54	16
39	76	92	108	80	63	108	66	67	58	15
40	88	125	94	62	62	87	64	56	57	15
41	79	123	97	69	58	97	67	72	66	17
42	70	115	98	66	60	111	67	64	62	9
43	73	99	97	61	77	119	44	77	63	15
44	94	101	88	58	71	111	69	60	48	18
45	81	133	106	62	57	98	58	63	51	8
46	79	104	87	65	70	116	68	70	51	18
47	83	103	83	52	76	97	64	59	54	13
48	81	115	93	61	70	119	54	61	55	17
49	74	121	107	69	60	89	50	69	45	16
50	82	135	104	53	72	94	58	63	66	19

ORIGINAL PAGE IS
OF POOR QUALITY

ENHANCED INLET, STATION 3

CP	MT1	MT2	MT3	MT4	MT5	MT6	MT7	MT8	MT9	MT10-TANG MEAS
1	0	0	0	0	0	0	0	0	0	5
2	0	0	0	0	0	0	0	0	0	1
3	3	128	0	0	0	1	3	0	0	0
4	0	0	0	289	12	54	16	5	12	1
5	0	0	0	0	0	0	0	28	121	152
6	0	0	0	0	0	0	0	0	0	58
7	0	0	0	0	0	0	0	0	0	0
8	0	0	0	0	3	5	3	0	0	0
9	5	2	2	1	5	4	9	7	12	0
10	14	2	3	8	10	15	18	11	13	1
11	22	10	4	8	25	21	37	30	23	2
12	19	10	15	6	43	34	39	74	19	1
13	24	14	17	19	29	26	63	81	40	1
14	20	13	23	12	51	39	51	96	60	3
15	25	15	23	16	48	53	50	79	83	1
16	24	14	19	11	63	41	75	72	64	4
17	26	12	21	28	58	61	62	79	61	2
18	26	8	21	22	71	64	74	77	70	4
19	26	16	27	17	63	65	76	76	69	3
20	18	16	35	31	67	71	65	93	64	1
21	31	12	34	29	83	73	72	87	76	2
22	25	13	35	26	81	72	85	79	68	4
23	32	12	38	16	99	65	89	94	64	2
24	31	18	34	27	95	76	80	79	75	2
25	20	21	31	28	75	72	82	77	81	2
26	36	10	24	22	99	71	92	89	79	3
27	29	16	32	32	106	81	89	76	89	5
28	46	20	66	46	133	130	141	110	136	4
29	32	18	42	28	102	85	77	95	94	1
30	31	8	44	29	101	85	84	82	90	2
31	37	10	24	34	99	84	82	98	80	1
32	32	12	40	38	113	98	84	83	92	1
33	43	13	42	39	108	93	74	92	78	1
34	44	9	37	26	116	84	86	74	79	3
35	35	10	46	27	94	87	91	85	83	1
36	26	12	35	23	122	84	76	102	104	4
37	27	14	32	26	105	81	87	71	103	3
38	35	14	36	24	104	109	77	87	92	7
39	37	11	31	30	118	82	79	86	85	1
40	39	11	26	27	100	87	75	75	78	3
41	21	13	37	15	100	102	88	88	93	3
42	30	9	20	13	84	103	80	64	81	4
43	31	10	27	16	103	98	73	90	97	5
44	31	14	34	13	106	88	87	79	105	7
45	12	14	38	11	76	84	73	94	97	4
46	20	14	25	7	87	95	80	80	84	6
47	2	1	11	12	78	92	107	79	95	4
48	1	0	5	2	52	100	74	63	87	3
49	0	0	0	1	4	34	82	65	90	6
50	0	0	0	0	0	2	15	25	20	6

ENHANCED INLET, STATION 4

CP	MT1	MT2	MT3	MT4	MT5	MT6	MT7	MT8	MT9	MT10-TANG MEAS
1	0	0	0	0	0	16	24	19	20	1
2	0	0	0	1	2	23	52	22	23	3
3	0	0	0	2	3	42	42	27	33	1
4	0	6	3	3	8	68	63	61	28	2
5	0	38	2	6	12	66	72	66	32	7
6	1	563	0	15	43	119	130	88	72	1
7	2	690	8	20	41	72	80	61	32	3
8	4	721	21	40	51	83	77	57	44	5
9	1	460	20	52	47	91	82	84	45	10
10	3	85	34	75	69	93	75	80	61	6
11	1	13	44	70	64	93	77	63	57	8
12	3	10	52	108	74	99	86	67	58	7
13	7	7	57	105	88	103	89	77	56	6
14	2	24	59	132	116	119	103	81	75	5
15	10	18	72	117	81	95	104	94	77	11
16	4	17	67	131	95	81	113	80	74	11
17	10	12	81	139	121	117	103	88	82	4
18	13	16	87	151	117	116	104	92	72	7
19	13	19	110	147	112	108	101	84	82	7
20	10	25	111	142	101	105	110	91	97	8
21	9	28	139	137	128	104	111	92	78	5
22	12	17	130	136	128	101	108	87	81	6
23	8	27	141	160	130	117	87	108	79	3
24	10	21	164	144	121	117	100	70	77	14
25	7	23	184	164	139	134	112	108	83	7
26	10	29	161	147	120	135	113	82	99	7
27	7	30	184	146	115	87	112	100	97	6
28	9	29	159	128	101	103	115	108	86	6
29	7	21	145	142	120	81	97	114	99	3
30	8	23	173	117	125	93	96	117	87	10
31	7	13	177	84	122	93	75	118	120	6
32	12	11	146	42	124	82	87	128	106	9
33	5	7	105	3	119	76	58	95	125	8
34	0	30	26	1	123	41	66	95	144	13
35	4	21	2	0	109	6	64	72	116	6
36	4	10	0	0	48	0	52	69	108	12
37	3	4	0	0	8	0	21	60	92	13
38	13	9	0	0	0	0	3	40	61	5
39	2	9	0	0	0	0	0	18	51	10
40	0	3	0	0	0	0	0	3	42	4
41	0	2	0	0	0	0	0	1	32	2
42	0	0	0	0	0	0	0	0	20	0
43	0	0	0	0	0	0	0	0	0	0
44	0	0	0	0	0	0	1	0	0	0
45	0	0	0	0	0	0	0	0	21	35
46	0	0	0	0	0	0	0	0	0	0
47	0	0	0	0	0	0	0	0	0	0
48	0	0	0	0	0	0	0	0	0	0
49	0	0	0	0	0	0	0	0	0	0
50	0	0	0	0	0	0	0	0	0	0

ENHANCED INLET, STATION 5

CP	MT1	MT2	MT3	MT4	MT5	MT6	MT7	MT8	MT9	MT10-TANG MEAS
1	0	0	0	0	0	0	18	29	26	25
2	0	0	0	0	17	39	43	32	36	44
3	0	0	0	9	15	45	33	44	37	10
4	1	0	2	30	26	63	68	41	47	41
5	4	0	2	32	14	57	52	61	44	23
6	2	0	9	41	12	74	59	53	60	55
7	5	0	18	40	25	77	69	49	42	34
8	4	0	21	57	32	80	58	70	40	41
9	3	0	22	77	22	88	89	57	68	32
10	0	0	23	78	37	101	71	65	61	39
11	2	1	25	95	45	91	58	79	57	47
12	1	0	43	125	39	101	64	67	74	36
13	2	4	40	132	55	95	81	75	55	45
14	3	1	46	145	56	88	99	95	73	37
15	2	3	54	144	39	98	94	71	73	37
16	2	2	48	159	44	93	102	93	60	52
17	3	3	45	144	50	94	101	88	85	59
18	5	4	61	160	56	106	105	86	74	52
19	6	4	71	158	44	101	113	86	84	48
20	7	7	74	150	44	114	113	110	100	57
21	9	7	67	139	58	119	105	92	82	61
22	10	5	74	140	59	117	100	104	89	69
23	8	8	92	117	67	114	120	92	92	61
24	10	13	94	118	61	115	101	104	76	69
25	14	4	89	103	56	107	100	118	109	76
26	7	5	97	106	54	101	103	99	97	74
27	12	10	86	112	63	87	147	106	117	73
28	17	14	107	89	57	76	130	129	125	57
29	5	8	100	81	57	48	116	112	123	80
30	15	7	104	75	40	55	100	126	119	80
31	11	6	120	92	52	54	112	103	113	75
32	9	7	87	80	43	52	91	138	116	84
33	12	7	110	85	41	46	83	109	102	94
34	10	7	101	30	37	42	71	105	95	99
35	21	7	108	6	40	33	60	84	74	119
36	14	10	108	0	50	16	51	59	59	107
37	23	4	72	1	33	2	43	53	46	184
38	39	0	25	0	17	0	46	45	25	192
39	188	2	41	0	7	0	18	31	13	183
40	6	2	607	0	4	0	63	94	14	204
41	0	0	76	0	0	0	10	23	8	38
42	0	0	0	0	0	0	0	0	8	4
43	0	0	0	0	0	0	0	0	4	0
44	0	0	0	0	0	0	0	0	0	0
45	0	0	0	0	0	0	0	0	0	0
46	0	0	0	0	0	0	0	0	0	0
47	0	0	0	0	0	0	0	0	0	0
48	0	0	0	0	0	0	0	0	0	0
49	0	0	0	0	0	0	0	0	0	0
50	0	0	0	0	0	0	0	0	0	0

ENHANCED INLET, STATION 6

CP	MT1	MT2	MT3	MT4	MT5	MT6	MT7	MT8	MT9	MT10-TANG MEAS
1	0	0	0	0	0	0	0	0	0	
2	0	0	0	9	12	15	63	95	56	
3	4	3	1	4	15	14	84	102	46	
4	10	6	2	6	12	23	101	110	58	
5	10	5	10	5	26	28	111	128	49	
6	8	11	11	7	22	39	123	137	60	
7	3	7	12	9	37	51	140	116	59	
8	7	13	11	17	36	57	140	140	40	
9	3	20	22	15	52	49	158	131	59	
10	6	10	38	27	67	85	160	174	67	
11	7	23	28	31	74	68	154	139	62	
12	4	16	46	38	90	76	168	142	72	
13	8	21	49	49	101	74	167	155	68	
14	9	18	56	59	94	83	180	149	60	
15	8	30	58	52	121	87	181	150	89	
16	9	28	40	66	119	83	200	158	62	
17	15	21	62	50	119	84	167	165	83	
18	9	27	52	60	110	83	184	154	76	
19	18	29	52	51	117	93	171	145	94	
20	11	22	61	65	121	103	186	156	76	
21	10	22	55	61	122	89	207	204	74	
22	13	30	76	66	147	94	190	183	94	
23	15	24	68	63	125	100	196	160	76	
24	12	32	56	67	125	92	215	187	79	
25	13	23	61	59	125	95	179	172	88	
26	12	27	57	62	136	91	218	180	88	
27	11	36	96	92	210	149	296	292	133	
28	11	28	59	68	126	104	209	213	84	
29	5	31	74	56	130	98	217	214	91	
30	8	37	61	64	134	113	225	181	108	
31	8	32	47	62	123	89	229	208	106	
32	4	25	45	40	104	79	201	235	97	
33	0	21	40	47	96	80	162	194	114	
34	8	26	30	20	98	79	160	218	91	
35	6	38	18	23	73	65	134	186	92	
36	4	11	18	23	67	70	125	174	94	
37	6	12	14	11	61	58	117	128	104	
38	15	12	18	14	56	53	119	104	74	
39	271	14	13	9	45	65	126	71	62	
40	142	9	14	7	33	47	125	90	54	
41	0	6	6	733	17	458	50	69	27	
42	0	1	0	18	1	8	11	52	14	
43	0	0	0	0	0	0	0	9	0	
44	0	0	0	0	0	0	0	0	0	
45	0	0	0	0	0	0	0	0	0	
46	0	0	0	0	0	0	0	0	0	
47	0	0	0	0	0	0	0	0	0	
48	0	0	0	0	0	0	0	0	0	
49	0	0	0	0	0	0	0	0	0	
50	0	0	0	0	0	0	0	0	0	

ENHANCED INLET, STATION 7

CP	MT1	MT2	MT3	MT4	MT5	MT6	MT7	MT8	MT9	MT10-TANG MEAS
1	0	0	0	0	0	0	0	0	0	0
2	0	17	0	0	0	0	0	0	0	0
3	2	19	14	0	3	12	39	45	56	0
4	4	15	11	1	1	15	49	43	60	0
5	1	29	9	2	2	16	56	72	66	0
6	4	19	12	3	7	29	70	81	61	0
7	2	25	23	3	11	35	80	91	63	0
8	5	39	28	5	16	36	104	77	80	0
9	4	31	36	4	12	59	98	92	54	0
10	7	39	55	9	19	76	110	117	44	0
11	6	38	68	9	27	78	115	111	59	1
12	5	39	73	11	36	99	118	109	57	0
13	11	63	83	10	38	125	131	104	61	0
14	11	53	112	13	58	130	122	116	83	0
15	8	55	112	13	63	154	113	118	62	0
16	11	39	127	24	43	129	116	95	67	0
17	8	51	110	19	54	131	112	111	60	0
18	14	46	126	22	51	147	121	111	64	1
19	14	37	125	26	59	138	157	120	58	0
20	7	94	209	34	106	219	198	195	114	1
21	12	43	122	16	58	153	123	134	63	1
22	13	37	107	21	70	140	128	116	61	1
23	22	55	111	27	80	153	141	139	71	1
24	22	49	140	29	77	161	143	138	58	0
25	14	40	141	23	77	160	146	133	74	0
26	23	43	121	29	62	170	149	135	88	2
27	11	43	145	35	76	174	127	115	69	0
28	20	48	138	27	80	149	157	128	79	0
29	15	44	136	27	84	175	146	120	83	0
30	12	44	159	25	71	162	141	123	85	1
31	22	62	157	27	87	180	159	137	75	0
32	18	51	163	32	91	165	147	138	59	2
33	11	64	156	22	101	192	142	125	84	0
34	18	39	145	23	94	205	162	138	75	0
35	19	45	133	23	94	182	163	138	69	1
36	16	39	142	24	86	170	169	156	92	0
37	13	35	141	37	96	199	169	143	97	0
38	19	33	119	26	92	189	160	121	86	1
39	21	29	133	33	91	211	195	147	73	0
40	25	32	137	30	83	191	164	122	82	0
41	27	39	119	30	78	155	163	118	73	2
42	30	88	135	35	80	149	208	109	75	1
43	18	134	134	46	80	164	359	82	79	1
44	7	70	516	61	99	180	455	82	83	1
45	12	9	532	311	902	106	337	68	40	8
46	199	0	0	2	89	36	34	40	32	257
47	817	2	0	0	0	0	1	16	12	142
48	697	10	0	0	0	1	5	24	49	3
49	0	0	0	0	0	2	18	29	48	0
50	0	0	0	0	0	0	0	0	0	0

ENHANCED INLET, STATION 8

CP	MT1	MT2	MT3	MT4	MT5	MT6	MT7	MT8	MT9	MT10-TANG MEAS
1	2	5	224	7	0	4	13	23	14	10
2	0	14	244	12	0	3	12	15	12	2
3	0	12	215	28	0	3	16	34	10	8
4	0	12	282	17	0	6	14	17	12	8
5	0	14	366	37	0	5	21	20	8	2
6	0	22	347	29	0	2	19	39	11	6
7	0	21	313	17	1	5	24	29	12	8
8	1	20	112	3	0	5	38	40	11	10
9	0	13	24	2	0	8	40	51	15	8
10	0	21	0	7	0	19	61	80	12	11
11	0	16	0	11	0	21	76	70	21	18
12	0	20	0	19	1	28	89	70	18	10
13	0	27	1	13	0	31	96	86	20	16
14	0	23	0	15	0	34	122	91	24	6
15	0	22	0	18	1	44	143	96	8	16
16	0	28	0	18	1	56	140	94	16	17
17	0	35	0	28	1	69	161	77	13	18
18	0	22	0	45	1	105	232	159	35	24
19	0	30	0	38	1	71	136	103	24	26
20	0	27	1	34	1	54	177	100	17	24
21	0	31	0	36	3	74	175	107	21	20
22	0	28	0	38	1	68	157	113	18	20
23	0	29	0	36	0	74	187	96	27	15
24	0	28	0	42	0	74	173	103	29	25
25	0	28	1	42	1	70	185	94	25	31
26	0	28	0	50	2	80	173	126	24	23
27	0	30	0	42	1	74	169	107	28	16
28	0	28	2	49	0	80	170	124	36	29
29	0	29	1	44	1	69	169	104	26	29
30	0	38	0	41	0	79	174	120	16	19
31	0	41	0	43	1	73	169	105	38	20
32	0	29	0	50	1	77	177	122	45	20
33	0	32	0	60	2	68	190	108	29	14
34	0	34	0	65	2	89	155	116	24	23
35	0	15	1	37	2	90	190	107	27	32
36	0	31	2	38	0	75	184	117	40	25
37	18	40	3	47	0	86	197	106	43	24
38	48	46	18	45	0	78	193	148	39	30
39	21	36	91	47	2	101	206	127	35	19
40	8	40	501	42	4	98	213	125	33	34
41	62	49	1817	51	4	109	233	137	36	31
42	1484	53	555	63	4	89	219	144	38	27
43	60	70	6	94	8	110	219	133	33	46
44	9	155	1	113	18	113	235	126	31	22
45	0	343	1	120	21	121	264	149	38	44
46	0	497	0	156	36	145	293	172	47	47
47	18	289	3	190	81	256	334	188	43	33
48	172	165	41	97	57	188	332	171	49	25
49	240	122	88	15	14	93	184	120	50	57
50	34	25	81	2	0	22	44	45	21	65

TABLE A5. -

(e) CALCULATED AXIAL UNCERTAINTY (PERCENT)

BASELINE INLET, STATION 1

CP	EA1	EA2	EA3	EA4	EA5	EA6	EA7	EA8	EA9	EA10-% AXIAL ERROR
1	1.60	0.72	0.98	1.13	0.84	0.52	0.77	0.75	1.13	3.93
2	1.33	0.68	0.95	1.18	0.87	0.54	0.80	0.85	1.06	9.19
3	1.57	0.70	0.85	1.23	0.92	0.47	0.79	0.88	1.40	3.23
4	1.54	0.59	0.91	1.08	0.85	0.56	0.72	0.78	1.31	7.25
5	1.50	0.67	0.91	1.19	1.00	0.50	0.85	0.74	1.18	13.31
6	1.48	0.62	0.89	1.19	0.87	0.46	0.81	0.76	1.22	6.45
7	1.50	0.65	0.97	1.34	0.88	0.50	0.78	0.75	1.19	12.26
8	1.70	0.61	0.89	1.41	0.83	0.52	0.75	0.76	1.34	8.93
9	1.80	0.66	0.95	1.28	0.91	0.53	0.83	0.75	1.25	7.38
10	1.40	0.70	0.95	1.09	0.87	0.49	0.95	0.80	1.10	28.77
11	1.47	0.63	0.90	1.15	0.87	0.47	0.84	0.80	1.21	15.23
12	1.30	0.60	1.06	1.12	0.83	0.49	0.85	0.79	1.27	9.61
13	1.31	0.70	0.99	1.27	0.81	0.51	0.80	0.77	1.33	4.57
14	1.62	0.63	0.97	1.38	0.74	0.53	0.76	0.76	1.04	6.60
15	1.51	0.66	0.89	1.20	0.83	0.50	0.77	0.75	1.10	4.69
16	1.39	0.67	1.02	1.34	0.88	0.52	0.88	0.71	1.12	7.49
17	1.42	0.65	0.92	1.15	0.88	0.49	0.74	0.67	1.27	3.78
18	1.50	0.60	0.97	1.08	0.88	0.48	0.90	0.83	1.36	7.18
19	1.85	0.61	0.88	1.50	0.80	0.51	0.75	0.78	1.29	7.23
20	1.44	0.62	0.85	1.33	0.79	0.56	0.78	0.67	1.51	3.77
21	1.40	0.64	0.92	1.17	0.82	0.50	0.82	0.70	1.21	5.40
22	1.52	0.67	0.90	1.21	0.85	0.51	0.73	0.65	1.22	4.41
23	1.30	0.59	0.93	1.18	0.83	0.51	0.79	0.77	1.18	6.02
24	1.31	0.70	0.92	1.08	0.95	0.48	0.67	0.71	1.12	13.91
25	1.55	0.72	0.89	1.20	0.80	0.46	0.79	0.76	1.14	6.03
26	1.57	0.69	1.10	1.33	0.95	0.51	0.90	0.76	1.27	9.60
27	1.54	0.61	0.88	1.23	0.85	0.47	0.78	0.68	1.21	6.45
28	1.29	0.62	0.83	1.05	0.83	0.53	0.77	0.74	1.23	3.78
29	1.32	0.69	0.93	1.31	0.78	0.50	0.86	0.72	1.34	11.53
30	1.51	0.59	0.84	1.13	0.80	0.48	0.79	0.65	1.26	5.92
31	1.40	0.70	0.91	1.16	0.90	0.50	0.85	0.70	1.01	8.94
32	1.38	0.65	1.03	1.39	0.73	0.51	0.79	0.70	1.23	5.03
33	1.61	0.62	0.78	1.26	0.95	0.54	0.85	0.77	1.26	11.64
34	1.40	0.62	0.91	1.20	0.78	0.55	0.89	0.78	1.29	3.89
35	1.23	0.62	0.98	1.36	0.79	0.49	0.80	0.73	1.26	9.47
36	1.31	0.65	0.90	1.28	0.84	0.46	0.87	0.80	1.22	3.39
37	1.38	0.66	0.96	1.14	0.88	0.48	0.75	0.76	1.23	5.92
38	1.50	0.61	0.97	1.32	0.78	0.48	0.83	0.70	1.11	3.71
39	1.44	0.64	0.86	1.21	0.76	0.48	0.79	0.79	1.47	12.12
40	1.34	0.60	0.94	1.24	0.74	0.46	0.68	0.87	1.26	12.38
41	1.15	0.69	0.89	1.32	0.97	0.48	0.92	0.71	1.33	11.53
42	1.36	0.64	0.87	1.30	0.79	0.46	0.82	0.73	1.29	16.06
43	1.74	0.72	0.92	1.23	0.74	0.53	0.76	0.69	1.21	3.45
44	1.59	0.66	0.88	1.29	0.87	0.48	0.75	0.84	1.12	4.09
45	1.45	0.60	0.84	1.08	0.88	0.48	0.81	0.74	1.15	7.90
46	1.58	0.61	0.91	1.07	0.92	0.51	0.80	0.69	1.24	4.55
47	1.34	0.58	0.86	1.20	0.86	0.50	0.84	0.76	1.25	13.05
48	1.50	0.75	0.86	1.12	0.83	0.50	0.83	0.82	1.16	34.79
49	1.50	0.62	0.92	1.30	0.85	0.51	0.79	0.77	1.23	12.55
50	0.79	0.40	0.56	0.81	0.47	0.29	0.40	0.51	0.88	25.63

BASELINE INLET, STATION 2

CP	EA1	EA2	EA3	EA4	EA5	EA6	EA7	EA8	EA9	EA10-% AXIAL ERROR
1	0.69	3.48	11.82	10.34	0.66	0.65	0.86	0.65	0.42	2.12
2	0.77	3.42	15.60	9.83	0.74	0.63	1.38	1.15	0.56	3.50
3	0.77	3.63	9.85	8.55	0.77	0.82	1.51	1.13	0.79	8.60
4	0.87	4.18	8.63	11.60	1.43	1.09	1.38	1.31	1.03	11.75
5	0.85	3.46	12.15	17.13	1.17	0.88	1.73	1.56	1.29	15.57
6	0.99	5.26	18.23	20.36	1.27	1.26	1.82	1.85	1.31	10.17
7	0.92	3.10	28.72	15.27	1.46	1.51	2.02	1.97	1.63	6.71
8	0.84	4.35	12.56	18.79	1.88	1.16	1.99	1.62	1.75	8.00
9	0.93	5.39	23.20	21.93	1.65	1.16	2.55	2.07	1.88	9.20
10	0.93	5.08	48.17	16.61	1.63	1.16	2.42	2.12	1.87	24.23
11	0.93	5.16	13.90	16.17	2.01	1.14	2.33	2.54	1.69	12.35
12	1.01	5.31	21.97	21.06	1.65	1.32	2.76	2.11	1.76	8.18
13	0.75	4.55	13.21	28.74	2.19	1.41	2.69	2.69	2.04	6.11
14	0.81	3.76	29.04	22.31	1.86	1.30	3.02	2.89	2.40	10.36
15	0.81	4.97	15.76	35.21	2.05	1.46	2.50	2.83	2.59	14.73
16	0.82	5.04	20.05	31.56	2.61	1.37	2.55	2.52	3.31	16.70
17	0.77	3.97	23.51	20.14	2.19	1.30	2.45	2.94	2.54	12.88
18	0.63	4.63	34.45	13.89	2.03	1.41	3.48	3.21	2.35	15.09
19	0.68	3.80	23.77	35.95	2.00	1.25	2.61	2.19	2.95	13.38
20	0.71	3.85	12.61	31.35	2.95	1.48	2.69	2.81	2.57	13.76
21	0.71	3.58	32.62	21.19	2.25	1.62	2.83	2.37	2.84	8.80
22	0.68	4.47	30.37	27.35	2.13	1.66	2.78	2.78	2.58	10.00
23	0.63	3.50	32.20	11.33	2.36	1.60	2.38	2.65	2.60	9.02
24	0.66	4.95	23.43	26.70	2.49	1.57	2.66	3.36	2.65	20.98
25	0.61	4.06	23.55	31.72	2.31	1.50	2.77	3.13	3.08	15.13
26	0.67	4.46	17.75	19.41	1.98	1.63	2.38	2.57	3.10	10.46
27	0.60	4.20	14.02	13.56	2.33	1.53	2.91	2.17	2.15	13.83
28	0.55	3.01	24.34	21.81	2.56	1.34	3.05	2.20	2.90	9.86
29	0.54	4.98	30.77	11.17	1.96	1.36	2.45	2.49	2.29	11.33
30	0.57	3.48	13.08	14.49	2.26	1.48	2.38	2.45	2.59	28.38
31	0.63	4.18	13.23	20.16	2.03	1.49	2.27	2.56	2.46	9.05
32	0.33	1.78	8.56	16.63	1.06	0.83	1.03	0.98	1.19	15.10
33	0.54	3.98	21.11	12.50	2.20	1.41	2.08	2.41	2.91	21.39
34	0.55	3.41	13.72	22.37	1.58	1.39	2.14	1.92	2.03	14.65
35	0.49	3.63	12.06	22.15	1.93	1.25	1.90	2.02	2.57	7.33
36	0.47	2.84	15.60	17.11	1.74	1.34	2.05	2.24	1.90	8.89
37	0.49	2.76	13.44	20.45	1.87	1.30	2.24	1.73	2.26	12.80
38	0.48	2.89	15.58	23.54	1.53	1.16	2.06	2.36	2.03	11.76
39	0.45	2.65	16.46	29.53	1.87	1.19	2.23	2.00	2.00	9.95
40	0.42	2.75	18.27	21.31	1.95	1.18	1.60	2.05	2.13	10.23
41	0.39	2.74	8.54	16.99	1.68	1.23	1.51	1.66	1.93	11.34
42	0.38	2.20	11.75	10.26	1.27	1.10	1.81	1.59	1.85	11.35
43	0.42	2.02	9.04	10.68	1.42	1.04	1.73	1.45	1.49	7.28
44	0.37	2.25	11.09	14.12	1.21	0.94	1.51	1.70	1.44	8.83
45	0.28	2.55	13.03	10.22	1.15	0.96	1.35	1.47	1.21	8.75
46	0.27	3.13	4.85	7.55	1.10	0.90	1.35	1.39	1.27	10.31
47	0.27	2.65	5.07	6.43	0.89	0.91	1.02	1.27	1.16	6.30
48	0.33	2.12	4.99	9.17	0.70	0.75	0.87	1.16	1.21	28.63
49	0.39	2.57	7.53	4.70	0.84	0.77	0.77	0.81	0.89	6.04
50	0.62	3.33	6.43	4.91	0.56	0.71	0.70	0.57	0.65	3.70

BASELINE INLET, STATION 3

CP	EA1	EA2	EA3	EA4	EA5	EA6	EA7	EA8	EA9	EA10-% AXIAL ERROR
1		6.97	1.80	0.00	33.20	0.00	13.89	0.00	0.00	0.00
2		5.68	2.68	0.00	0.00	0.00	4.48	0.00	0.66	20.91
3		9.48	0.00	28.26	0.00	55.62	4.86	7.84	0.20	13.69
4		0.00	0.00	25.72	21.66	284.94	32.14	16.81	0.84	53.80
5		0.00	0.00	0.00	0.00	0.00	0.00	59.30	10.89	0.00
6		0.00	0.00	0.00	0.00	0.00	0.00	0.00	0.00	67.88
7		0.00	0.00	0.00	0.00	0.00	0.00	0.00	0.00	0.00
8		0.00	0.00	0.00	13.15	3.13	11.62	0.00	0.00	0.00
9		0.00	14.51	15.61	7.76	9.40	7.09	7.59	10.11	0.00
10		48.17	12.40	10.25	14.21	5.87	4.33	3.62	8.82	0.00
11		31.91	21.33	12.71	17.49	4.24	5.17	3.85	8.62	109.28
12		65.37	14.13	11.18	14.86	2.94	4.05	3.42	4.29	51.85
13		63.84	14.71	16.21	8.92	1.87	3.59	3.65	4.71	120.57
14		95.45	11.06	11.10	9.42	2.18	3.97	3.21	8.17	128.52
15		56.28	18.58	13.12	15.11	2.09	3.82	3.53	12.46	16.25
16		156.81	16.72	23.30	20.42	2.63	4.27	2.82	10.39	63.00
17		21.53	36.21	15.62	11.55	2.63	3.75	3.19	4.85	86.72
18		58.89	15.50	19.38	17.15	2.43	3.59	3.63	14.72	148.08
19		60.18	11.13	18.02	12.52	2.64	3.43	4.31	18.42	33.60
20		29.37	18.48	22.65	16.68	2.51	3.18	4.02	5.51	15.27
21		63.74	8.14	16.53	9.25	2.41	3.90	3.71	14.38	159.96
22		152.27	17.89	12.29	14.78	2.76	4.90	3.92	14.67	11.81
23		19.37	28.54	18.31	14.99	2.29	3.81	3.53	9.26	62.49
24		37.89	24.74	12.04	18.11	2.60	2.99	4.01	7.29	14.05
25		16.32	11.89	11.97	18.67	2.48	3.87	4.18	6.41	140.00
26		139.13	13.19	17.10	19.24	2.02	3.11	3.14	13.01	130.63
27		42.52	15.39	12.28	14.18	2.30	4.08	2.74	6.29	10.76
28		18.15	14.26	8.29	7.98	1.39	1.67	1.89	3.83	17.08
29		28.11	13.49	9.59	11.91	1.91	2.83	3.23	13.07	32.86
30		23.64	13.34	11.31	10.91	1.85	3.28	3.54	6.63	16.84
31		27.88	9.26	10.05	12.73	1.81	2.96	2.77	9.80	0.00
32		17.10	10.89	8.53	11.50	2.40	3.45	2.84	10.79	11.97
33		25.64	9.80	8.79	14.86	2.04	3.20	2.79	7.11	29.69
34		16.02	9.81	10.31	8.87	1.84	3.17	2.30	9.94	49.89
35		14.99	9.47	19.81	9.78	1.59	2.78	2.63	6.70	87.58
36		19.31	8.09	9.28	10.75	1.67	2.75	2.37	7.36	11.82
37		11.60	10.95	11.11	10.11	1.71	2.69	2.05	8.13	20.30
38		9.05	11.40	9.59	7.43	1.72	2.89	2.41	8.79	19.85
39		18.29	12.39	10.08	6.94	1.75	2.12	2.36	6.61	20.16
40		12.23	12.31	8.62	9.08	1.28	2.36	1.92	12.18	29.64
41		14.63	8.24	6.45	7.78	1.46	2.46	2.05	6.77	29.44
42		10.67	7.42	8.65	7.03	1.50	2.48	2.07	6.63	20.66
43		11.91	6.55	5.92	5.73	1.60	2.09	1.93	4.23	116.33
44		13.38	9.48	7.89	9.48	1.71	1.98	2.02	5.03	19.83
45		14.42	17.61	7.31	7.24	1.66	1.76	1.63	4.06	15.35
46		107.32	12.26	29.45	12.53	4.08	2.05	1.83	4.65	29.47
47		0.00	65.30	0.00	20.93	7.95	2.62	1.82	6.50	49.88
48		0.00	134.99	0.00	123.82	17.39	4.43	3.78	6.03	50.56
49		0.00	0.00	0.00	0.00	0.00	20.05	12.42	31.16	0.00
50		8.04	11.80	0.00	0.00	0.00	111.98	40.12	0.00	0.00

BASELINE INLET, STATION 4

CP	EA1	EA2	EA3	EA4	EA5	EA6	EA7	EA8	EA9	EA10-% AXIAL ERROR
1	0.00	0.00	0.00	0.00	0.00	24.80	41.43	9.34	6.05	45.14
2	0.00	0.00	0.00	39.97	1.97	7.84	12.39	8.76	7.94	14.48
3	0.00	0.00	30.67	15.80	1.22	10.01	17.90	5.89	6.73	26.63
4	46.49	15.38	19.79	13.11	0.96	5.59	9.89	4.46	3.55	25.57
5	34.47	6.89	9.89	16.85	0.63	4.45	8.64	5.84	4.89	16.37
6	13.62	5.24	3.61	3.65	0.27	1.67	4.30	1.98	2.05	9.27
7	54.26	8.85	6.57	6.68	0.45	2.97	7.98	3.72	4.10	9.57
8	20.64	6.17	5.27	4.75	0.42	2.85	6.53	3.50	3.81	11.91
9	9.32	6.51	5.80	4.28	0.41	1.98	6.41	3.67	2.43	9.81
10	14.72	8.26	3.74	3.96	0.38	1.91	6.76	2.88	2.60	7.31
11	11.25	5.44	3.95	3.17	0.36	2.84	6.12	3.15	2.41	9.59
12	20.80	4.45	3.80	3.44	0.34	1.95	5.09	2.25	2.71	9.27
13	13.45	3.51	3.19	2.50	0.32	2.03	4.23	3.34	1.91	6.49
14	11.81	3.58	3.00	3.02	0.33	1.89	4.53	2.62	2.00	9.43
15	8.63	3.19	2.67	2.45	0.31	1.84	4.63	2.88	2.14	8.54
16	11.23	3.44	2.38	2.09	0.34	1.81	4.28	2.46	1.62	16.38
17	11.66	3.21	1.75	2.20	0.35	1.54	3.54	2.39	1.61	8.49
18	10.51	2.91	1.57	2.03	0.38	1.43	4.30	2.12	1.68	8.85
19	20.86	2.15	1.80	1.86	0.40	1.47	3.69	2.37	1.69	9.06
20	8.55	2.70	1.47	1.60	0.43	1.36	5.05	2.37	1.59	5.64
21	13.48	2.23	1.53	2.03	0.48	1.09	3.89	2.33	1.40	4.78
22	8.07	2.24	1.32	1.69	0.54	1.26	4.10	1.62	1.45	6.21
23	11.00	1.78	1.38	1.75	0.57	1.20	3.01	2.30	1.41	6.73
24	11.51	1.91	1.39	1.77	0.65	1.19	5.30	1.84	1.19	3.56
25	17.79	1.75	1.33	1.60	1.02	1.42	3.41	1.75	1.25	5.83
26	70.86	1.92	1.46	2.08	5.17	1.30	3.83	1.85	1.47	12.04
27	10.97	2.37	1.60	1.81	44.73	1.43	3.06	1.69	1.31	8.43
28	104.46	1.70	1.84	2.33	0.00	1.72	3.53	1.80	1.29	14.94
29	12.69	1.96	2.06	3.10	0.00	1.70	4.79	1.91	1.22	10.31
30	51.60	2.13	2.31	2.73	0.00	2.10	5.00	1.81	1.20	4.04
31	22.68	2.96	3.82	3.44	0.00	2.07	8.92	1.82	1.20	7.14
32	55.43	4.78	4.71	3.76	0.00	2.42	8.59	2.07	1.17	7.14
33	40.79	19.14	6.85	4.88	0.00	2.61	10.76	2.31	1.18	5.47
34	19.04	50.81	25.57	18.65	0.00	3.42	10.99	2.88	1.37	7.57
35	0.00	8.76	0.00	62.76	0.00	3.53	12.34	3.75	1.60	6.76
36	0.00	89.95	0.00	94.68	0.00	8.13	23.06	4.21	1.80	6.18
37	0.00	65.00	91.14	17.68	0.00	18.10	240.35	17.61	2.83	8.02
38	0.00	6.68	3.81	5.49	0.00	0.00	0.00	0.00	4.81	17.03
39	0.00	33.93	4.86	3.97	0.00	0.00	0.00	0.00	1.35	17.92
40	0.00	0.00	0.00	0.00	248.86	65.76	0.00	0.00	0.86	0.00
41	0.00	0.00	0.00	0.00	75.40	0.00	0.00	0.00	6.40	0.00
42	0.00	0.00	0.00	0.00	21.34	0.00	0.00	0.00	0.00	0.00
43	0.00	0.00	0.00	0.00	23.06	0.00	82.86	65.63	8.66	31.56
44	0.00	0.00	0.00	0.00	13.95	9.82	35.66	11.94	0.58	15.63
45	0.00	0.00	0.00	0.00	0.00	0.00	0.00	0.00	71.95	11.05
46	0.00	0.00	0.00	0.00	0.00	0.00	0.00	0.00	0.00	0.00
47	0.00	0.00	0.00	0.00	0.00	0.00	0.00	0.00	0.00	0.00
48	0.00	0.00	0.00	0.00	0.00	0.00	0.00	0.00	0.00	0.00
49	0.00	0.00	0.00	0.00	0.00	0.00	0.00	0.00	0.00	0.00
50	0.00	0.00	0.00	0.00	0.00	0.00	0.00	0.00	0.00	0.00

BASELINE INLET, STATION 5

CP	EA1	EA2	EA3	EA4	EA5	EA6	EA7	EA8	EA9	EA10-% AXIAL ERROR
1	0.00	0.00	0.00	0.00	0.00	0.00	0.00	8.28	14.17	20.31
2	0.00	0.00	0.00	0.00	8.95	8.17	7.75	6.15	6.70	16.79
3	0.00	0.00	18.08	18.08	18.47	27.90	6.13	6.74	7.13	29.14
4	2.22	3.56	5.84	14.54	12.67	9.69	5.69	7.63	21.21	9.91
5	1.47	2.87	4.42	9.02	15.18	5.60	4.73	5.47	10.39	11.81
6	1.61	2.58	3.73	6.46	8.61	7.19	5.74	4.86	17.29	10.79
7	1.61	2.54	3.72	6.63	5.24	5.41	4.19	4.78	15.90	13.97
8	1.60	2.34	3.12	4.57	4.85	5.21	4.13	4.12	12.41	7.76
9	1.50	2.68	3.61	5.43	3.78	5.06	3.56	3.87	9.45	12.72
10	1.95	2.59	2.98	3.48	4.79	5.77	4.13	3.87	10.23	8.25
11	2.10	2.43	2.84	3.39	3.19	3.32	3.42	4.47	10.98	10.01
12	2.27	2.39	2.82	3.42	2.84	3.79	3.20	4.02	8.90	8.02
13	2.41	2.16	2.62	3.28	3.26	2.68	3.99	3.04	8.66	4.02
14	2.47	2.32	2.61	2.95	2.81	2.96	3.27	3.23	9.31	4.92
15	2.06	2.30	2.46	2.64	2.74	3.40	3.09	3.51	6.97	5.77
16	3.00	2.02	2.36	2.80	2.38	3.00	3.72	3.43	7.17	6.68
17	2.85	2.17	2.23	2.29	2.44	2.53	3.66	3.35	6.64	6.50
18	3.01	2.36	2.29	2.22	2.33	2.86	3.02	3.61	7.19	7.35
19	2.69	2.14	2.04	1.95	2.09	3.13	2.31	3.20	7.03	4.18
20	3.10	2.49	2.44	2.39	2.14	2.67	2.68	3.24	8.64	4.77
21	3.08	2.74	2.32	2.02	1.89	2.80	2.04	2.73	7.21	3.66
22	3.20	3.32	2.53	2.05	2.17	2.50	2.46	2.76	7.91	4.11
23	2.81	4.58	3.03	2.26	2.14	2.09	2.52	2.38	4.96	11.71
24	3.48	4.26	2.83	2.12	2.48	2.36	2.30	2.55	7.25	3.27
25	3.63	5.27	3.03	2.13	2.09	2.10	2.50	2.60	6.34	3.54
26	3.71	6.75	3.26	2.15	2.22	2.49	2.00	2.16	3.97	3.58
27	4.35	7.04	4.30	3.11	2.24	2.27	2.24	2.26	6.66	4.80
28	5.21	11.53	4.61	2.86	2.33	2.21	2.38	2.15	5.07	3.69
29	5.30	11.97	4.42	2.69	3.58	3.09	2.81	2.56	4.94	9.37
30	5.73	10.44	4.87	3.17	2.74	3.79	3.42	2.60	4.68	4.06
31	6.13	12.54	4.78	2.93	3.96	3.39	4.15	2.64	4.88	8.96
32	6.75	20.05	6.77	4.07	3.80	3.60	3.96	2.48	5.65	4.28
33	8.90	22.37	5.77	3.25	4.01	4.72	4.89	3.80	4.62	5.87
34	7.31	72.68	7.75	3.82	4.93	5.29	5.84	3.98	5.86	6.39
35	6.41	0.00	6.22	6.22	9.50	3.81	5.88	4.12	7.07	6.62
36	7.08	201.26	43.54	19.28	24.01	6.22	8.51	6.65	9.77	3.22
37	31.55	50.13	52.62	55.61	23.85	6.55	48.87	13.65	13.90	4.80
38	0.00	42.12	59.53	90.00	0.00	12.63	31.11	31.24	43.71	4.29
39	0.00	0.00	113.03	169.55	0.00	45.06	105.72	0.00	57.45	3.47
40	0.00	118.26	118.26	0.00	257.76	90.56	0.00	0.00	14.20	7.11
41	0.00	0.00	0.00	0.00	0.00	134.96	0.00	0.00	52.57	48.88
42	0.00	0.00	0.00	0.00	0.00	0.00	0.00	24.96	1.33	0.00
43	0.00	0.00	0.00	0.00	0.00	0.00	0.00	3.50	0.36	0.00
44	0.00	0.00	0.00	0.00	0.00	0.00	0.00	0.00	0.00	0.00
45	0.00	0.00	0.00	0.00	0.00	0.00	0.00	0.00	0.00	0.00
46	0.00	0.00	0.00	0.00	0.00	0.00	0.00	0.00	0.00	0.00
47	0.00	0.00	0.00	0.00	0.00	0.00	0.00	0.00	0.00	0.00
48	0.00	0.00	0.00	0.00	0.00	0.00	0.00	0.00	0.00	0.00
49	0.00	0.00	0.00	0.00	0.00	0.00	0.00	0.00	0.00	0.00
50	0.00	0.00	0.00	0.00	0.00	0.00	0.00	0.00	0.00	0.00

BASELINE INLET, STATION 6

CP	EA1	EA2	EA3	EA4	EA5	EA6	EA7	EA8	EA9	EA10-% AXIAL ERROR
1	0.00	0.00	0.00	0.00	0.00	0.00	0.00	0.00	0.00	0.00
2	0.00	0.00	0.00	6.09	18.98	5.92	3.59	3.01	19.64	7.17
3	6.13	4.80	3.94	5.90	9.26	4.66	3.07	3.13	9.48	4.00
4	4.36	3.04	3.93	3.89	5.73	5.13	2.64	2.42	8.73	5.42
5	4.14	3.78	3.62	4.43	7.86	5.43	2.75	3.34	6.88	4.96
6	4.19	2.72	3.15	3.78	7.65	3.53	2.46	2.33	11.86	7.27
7	3.87	3.01	2.90	3.78	4.45	4.50	2.23	2.51	10.96	3.95
8	3.96	2.51	3.37	4.80	5.55	3.45	2.04	2.15	10.69	9.15
9	3.69	3.05	3.00	2.96	4.20	3.01	2.04	2.23	11.14	17.62
10	3.88	2.35	2.77	4.27	5.67	4.46	1.99	1.93	9.10	5.90
11	4.26	2.38	2.65	2.74	4.07	3.43	2.09	2.44	11.34	3.43
12	4.32	2.58	3.06	3.05	3.42	3.10	2.14	2.16	19.92	3.80
13	3.67	2.89	2.82	3.94	3.68	2.90	1.80	2.23	17.64	4.80
14	3.11	2.26	2.93	4.08	3.80	2.94	2.13	2.13	15.44	6.29
15	2.84	2.78	2.42	2.46	3.63	2.50	1.92	2.04	13.82	7.56
16	2.64	3.11	2.63	3.35	3.16	2.62	1.87	1.98	17.33	5.40
17	3.20	2.07	3.07	2.71	3.52	3.00	2.05	2.07	19.04	3.58
18	2.14	1.97	2.28	3.17	2.95	2.62	1.60	1.92	18.35	3.89
19	2.65	2.19	2.52	2.64	3.25	2.01	1.49	2.12	17.70	5.20
20	2.22	2.06	2.34	2.56	2.50	2.40	1.72	1.75	20.94	7.02
21	1.85	2.59	2.53	2.26	3.10	2.96	1.55	1.69	10.68	6.49
22	2.42	2.53	2.23	2.29	3.00	2.15	1.35	1.83	19.26	8.05
23	1.84	2.89	2.39	2.27	2.64	2.12	1.57	1.75	12.64	5.08
24	1.97	3.39	2.71	2.39	2.71	2.19	1.32	1.69	15.67	5.47
25	2.15	2.99	3.18	2.55	2.47	2.14	1.37	1.60	12.62	7.27
26	2.07	3.37	3.12	3.28	2.51	2.35	1.43	1.47	11.72	4.94
27	1.34	2.36	1.98	1.48	1.50	1.46	0.76	0.92	11.47	2.97
28	2.55	4.60	3.96	2.72	2.67	2.71	1.36	1.30	19.82	9.91
29	3.32	4.39	4.66	3.23	2.42	2.59	1.46	1.34	19.38	8.64
30	3.28	6.71	4.95	3.33	2.56	3.07	1.20	1.44	8.43	4.42
31	4.38	8.50	5.72	4.30	3.21	3.78	1.37	1.28	15.88	4.48
32	5.92	6.98	7.45	5.26	2.90	3.95	1.51	1.30	12.09	5.34
33	6.42	11.33	16.69	6.35	3.94	3.99	1.48	1.60	11.59	4.79
34	10.40	14.53	13.74	7.09	4.05	7.51	1.59	1.45	15.42	3.20
35	9.58	37.91	18.08	9.72	4.22	13.99	2.03	2.06	7.85	3.40
36	13.07	0.00	35.35	11.29	5.43	15.58	2.08	2.07	11.91	2.17
37	7.53	143.87	21.82	11.89	4.27	28.24	2.32	1.92	5.34	1.47
38	7.80	0.00	0.00	11.80	6.20	110.97	2.55	2.00	4.40	1.23
39	69.45	0.00	243.14	32.13	14.52	57.94	7.72	4.48	7.13	1.39
40	0.00	0.00	0.00	0.00	38.54	0.00	28.61	7.47	26.48	2.14
41	0.00	0.00	0.00	245.98	0.00	228.91	38.59	97.88	183.95	2.45
42	0.00	214.94	0.00	240.35	237.34	29.74	4.48	2.14	123.24	4.01
43	0.00	151.41	97.56	66.28	0.00	21.84	1.50	2.53	12.73	1.08
44	0.00	128.96	51.51	237.34	0.00	14.45	3.01	4.38	11.39	0.93
45	0.00	0.00	0.00	0.00	0.00	10.91	4.71	3.59	7.94	3.20
46	0.00	0.00	0.00	0.00	0.00	0.00	0.00	0.00	0.00	0.00
47	0.00	0.00	0.00	0.00	0.00	0.00	0.00	0.00	0.00	0.00
48	0.00	0.00	0.00	0.00	0.00	0.00	0.00	0.00	0.00	0.00
49	0.00	0.00	0.00	0.00	0.00	0.00	0.00	0.00	0.00	0.00
50	0.00	0.00	0.00	0.00	0.00	0.00	0.00	0.00	0.00	0.00

BASELINE INLET, STATION 7

CP	EA1	EA2	EA3	EA4	EA5	EA6	EA7	EA8	EA9	EA10-% AXIAL ERROR
1	0.00	0.00	0.00	0.00	0.00	0.00	0.00	0.00	0.00	0.00
2	0.00	11.84	0.00	0.00	0.00	0.00	0.00	0.00	0.00	0.00
3	3.92	6.90	40.70	18.34	5.84	10.07	4.62	3.72	3.41	0.00
4	0.00	6.21	14.39	14.32	6.71	5.40	3.48	4.90	3.65	3.24
5	0.00	6.23	10.90	8.37	5.13	4.52	5.12	2.88	5.74	3.89
6	3.09	5.65	7.88	9.66	4.40	4.46	4.16	3.02	4.33	2.89
7	84.59	3.02	6.63	4.91	3.19	3.43	4.45	3.13	3.02	2.48
8	32.22	3.88	5.60	5.62	3.14	2.99	3.23	3.29	3.82	3.90
9	46.77	2.98	7.31	6.42	3.13	3.56	2.70	3.00	3.39	3.00
10	11.32	3.01	7.60	4.81	2.69	3.27	3.17	2.39	2.91	4.50
11	9.34	2.57	6.37	4.62	2.46	2.69	2.47	3.03	2.83	3.87
12	15.52	2.22	5.71	4.77	2.58	2.34	3.05	2.38	2.53	2.67
13	130.16	2.20	7.69	3.59	2.04	2.52	2.41	2.53	2.91	3.50
14	30.76	2.11	7.94	3.43	2.23	2.32	2.32	2.17	3.16	4.09
15	11.41	1.80	5.71	4.45	2.18	2.31	2.23	2.68	2.70	3.19
16	20.54	1.92	5.88	4.16	1.89	1.98	2.41	2.63	2.36	4.07
17	13.82	1.97	5.27	3.54	2.08	2.31	1.98	1.93	2.13	3.58
18	4.06	1.92	5.15	4.29	2.04	2.24	2.35	2.29	2.14	5.10
19	45.75	1.73	6.50	3.64	2.30	1.76	2.29	1.97	2.10	3.91
20	231.71	0.66	3.55	2.38	1.09	1.30	1.06	1.18	1.18	2.26
21	49.23	1.99	5.23	3.22	2.00	2.08	2.36	2.05	2.49	2.72
22	10.29	2.23	6.39	3.68	1.79	1.87	1.84	1.93	2.26	4.68
23	4.96	2.02	4.89	2.75	1.73	1.84	1.80	2.06	1.83	3.79
24	0.89	1.95	5.44	3.88	1.94	1.76	1.92	2.08	2.12	4.55
25	226.15	1.64	5.08	3.59	1.72	1.60	1.85	1.99	1.91	3.44
26	0.51	1.61	5.05	3.95	1.61	1.94	1.68	1.68	1.96	4.64
27	3.18	1.91	6.55	4.08	1.92	1.56	1.71	1.88	1.92	4.66
28	6.67	1.73	4.90	3.37	1.70	1.82	1.78	1.62	1.74	4.69
29	24.07	1.68	5.55	3.14	1.81	1.79	1.58	1.92	1.63	3.38
30	12.73	1.67	5.50	3.85	1.65	2.05	1.68	1.62	1.84	5.27
31	12.95	1.63	4.36	3.02	1.75	1.62	1.70	1.55	1.47	3.87
32	9.79	1.78	5.53	3.65	1.68	1.65	1.39	1.97	1.66	4.53
33	39.19	1.51	5.11	3.23	1.60	1.64	1.47	1.90	1.70	3.06
34	11.05	1.62	4.24	2.92	1.78	1.60	1.53	1.47	1.61	3.47
35	2.19	1.79	4.23	3.08	1.91	1.32	1.46	1.80	1.52	3.08
36	2.83	1.74	4.20	3.39	1.73	1.30	1.46	1.88	1.52	3.08
37	1.25	1.75	4.60	3.49	1.33	1.53	1.40	1.48	1.39	2.75
38	2.64	1.63	5.38	3.60	1.56	1.32	1.58	1.77	1.61	2.70
39	5.02	1.83	5.64	3.27	1.59	1.26	1.23	1.66	1.30	2.42
40	1.39	1.52	6.25	3.32	1.49	1.46	1.38	1.72	1.21	1.93
41	1.92	1.12	5.82	4.13	1.74	1.92	1.50	1.46	0.96	1.78
42	1.32	1.93	12.92	4.82	1.93	2.48	2.31	1.87	1.03	1.28
43	0.31	3.14	16.97	8.10	4.01	3.71	3.56	3.07	1.15	1.01
44	0.35	0.32	56.33	28.39	10.56	11.89	6.56	3.67	5.18	1.85
45	0.21	0.54	0.00	0.00	14.06	15.55	9.99	5.49	7.43	2.58
46	0.30	0.28	0.00	0.00	24.51	18.98	5.71	3.15	2.93	4.58
47	0.38	13.34	0.00	32.97	10.30	9.15	12.46	2.96	3.52	2.82
48	1.11	6.55	273.21	116.58	25.15	5.82	10.64	6.19	3.33	3.20
49	0.00	0.00	0.00	0.00	15.23	13.75	8.67	3.77	4.85	3.67
50	0.00	0.00	0.00	0.00	0.00	0.00	0.00	0.00	0.00	3.60

BASELINE INLET, STATION 8

CP	EA1	EA2	EA3	EA4	EA5	EA6	EA7	EA8	EA9	EA10-% AXIAL ERROR
1	2.82	0.00	6.21	7.17	36.31	12.87	6.26	4.13	3.04	1.00
2	4.57	18.41	4.41	6.49	12.96	5.70	4.49	4.67	2.74	1.22
3	32.51	15.60	3.84	3.13	21.49	6.84	5.65	4.47	3.01	1.04
4	0.00	10.97	1.40	3.47	9.74	9.73	3.08	3.27	3.15	1.78
5	0.00	16.90	1.67	2.37	21.34	7.00	3.27	4.27	2.77	1.32
6	0.00	18.39	1.07	2.14	4.46	6.29	3.37	5.63	4.31	1.51
7	0.00	18.51	1.96	2.36	10.87	6.53	3.78	5.62	3.36	1.41
8	0.00	24.63	2.69	3.81	10.29	6.67	4.01	3.32	3.83	1.32
9	49.29	14.15	1.74	2.05	8.26	6.95	3.16	4.28	3.33	1.93
10	0.00	5.98	1.18	1.84	5.44	5.33	2.90	2.99	2.23	1.48
11	0.00	5.27	1.06	1.30	4.89	3.29	3.73	2.69	2.42	2.16
12	0.00	6.64	1.12	2.03	3.86	5.36	3.18	2.58	4.39	1.92
13	0.00	6.65	0.81	1.29	5.19	4.40	3.32	3.11	3.65	1.72
14	0.00	4.36	0.74	1.28	5.27	2.87	2.45	3.86	3.89	1.93
15	0.00	6.74	0.56	1.40	4.46	3.51	1.97	2.73	2.97	2.35
16	0.00	4.38	1.02	1.18	3.63	3.60	2.64	2.80	3.19	2.30
17	0.00	4.06	0.69	1.41	3.60	3.21	3.02	2.69	2.64	1.89
18	0.00	5.24	0.42	0.58	1.31	1.51	1.49	1.49	1.51	1.31
19	0.00	3.35	0.50	1.21	3.35	2.28	2.67	2.43	2.76	2.08
20	0.00	4.11	1.05	1.14	2.71	2.57	2.01	2.72	2.72	2.19
21	0.00	3.23	0.73	1.44	2.84	3.30	2.25	2.19	2.50	2.80
22	0.00	4.29	0.79	1.36	3.18	2.78	2.83	2.49	2.53	3.79
23	0.00	3.81	0.66	1.22	3.17	3.05	2.45	2.49	2.65	2.16
24	0.00	2.73	0.78	1.06	3.37	2.97	2.20	2.14	2.79	2.87
25	0.00	4.57	0.87	1.09	2.21	2.43	2.15	2.23	3.01	3.76
26	0.00	4.17	0.72	1.59	3.30	2.53	1.96	2.42	3.18	2.62
27	0.00	3.41	0.62	1.02	2.76	2.46	2.55	2.07	2.57	2.53
28	0.00	2.54	0.79	0.87	3.22	2.81	1.86	2.49	2.34	3.15
29	0.00	4.74	0.64	0.93	2.58	2.29	2.32	2.31	2.34	2.23
30	0.00	2.16	0.66	1.03	3.43	2.17	2.01	2.12	2.33	2.38
31	0.00	3.32	0.59	0.90	2.43	3.76	2.09	1.79	2.62	2.93
32	0.00	4.09	0.65	1.03	2.44	2.83	2.00	2.51	2.41	3.11
33	0.00	2.77	0.69	1.50	2.62	2.37	1.97	2.15	2.53	2.47
34	0.00	3.45	0.62	1.02	3.02	2.65	1.90	1.93	2.11	2.76
35	0.00	3.80	0.58	1.49	2.77	2.50	2.19	2.24	2.37	2.33
36	10.64	3.03	0.64	0.90	2.26	2.35	1.94	1.70	2.63	2.61
37	15.00	2.17	0.61	1.09	2.43	3.01	1.75	2.14	2.16	2.53
38	3.23	2.39	0.59	1.08	2.44	2.45	1.96	1.79	2.01	2.15
39	4.57	4.39	0.51	0.91	1.99	1.93	1.81	1.76	1.79	1.94
40	5.42	1.95	0.40	0.73	2.11	2.00	1.63	1.77	1.92	1.83
41	7.32	4.37	0.33	0.63	1.79	1.52	1.62	1.83	1.95	1.66
42	9.36	1.40	0.17	0.54	1.39	1.54	1.37	1.85	2.05	1.29
43	4.22	0.99	0.09	0.30	1.07	0.87	1.26	1.16	1.19	1.22
44	0.63	0.50	0.07	0.22	0.69	0.47	0.91	0.91	1.02	0.88
45	0.36	0.67	0.10	0.22	0.48	0.37	0.74	0.77	0.67	0.65
46	0.22	0.73	0.22	0.39	0.46	0.34	0.63	0.66	0.48	0.38
47	0.33	1.12	1.40	1.08	0.94	0.71	0.87	0.67	0.52	0.40
48	0.53	1.21	3.29	2.24	4.34	1.76	1.66	0.84	0.66	0.44
49	0.90	25.75	35.31	6.43	7.07	2.37	3.09	1.37	1.13	0.62
50	1.33	85.14	1.09	4.26	36.41	10.65	4.51	4.07	1.89	0.66

ENHANCED INLET, STATION 1

CP	EA1	EA2	EA3	EA4	EA5	EA6	EA7	EA8	EA9	EA10-% AXIAL ERROR
1	2.60	3.03	3.27	3.01	3.09	2.88	3.68	2.59	2.99	4.28
2	2.96	3.57	3.04	2.69	3.48	2.80	2.82	3.11	2.57	5.14
3	4.17	3.45	2.71	2.80	2.96	3.30	2.54	2.76	3.32	6.43
4	4.70	2.46	2.71	2.48	3.75	2.83	2.53	2.40	3.34	5.41
5	2.37	2.74	2.22	2.77	3.27	2.89	2.63	2.75	2.51	4.49
6	2.53	2.49	2.41	2.48	4.15	3.52	2.99	2.27	2.16	6.43
7	2.45	2.73	3.20	2.51	2.81	2.82	3.36	2.99	2.66	6.53
8	3.99	2.85	2.78	2.33	3.08	2.79	3.45	2.26	2.48	4.70
9	2.16	2.57	2.74	2.70	4.31	2.63	2.68	2.73	2.44	3.78
10	2.70	2.49	2.47	2.58	2.74	2.51	2.73	2.47	2.43	6.35
11	3.19	2.59	2.46	2.31	3.83	2.86	2.38	2.92	2.57	4.78
12	2.52	2.37	2.78	2.46	3.18	3.21	2.87	2.94	3.05	3.76
13	2.26	2.51	2.80	3.52	2.67	2.65	3.45	2.79	3.01	4.21
14	3.53	2.82	2.46	2.51	2.68	3.53	2.98	2.72	2.41	5.15
15	2.46	3.03	2.53	2.19	3.04	3.01	2.68	2.55	3.34	4.99
16	2.36	2.74	2.85	2.93	3.45	2.88	3.14	2.55	2.70	5.70
17	2.43	2.44	2.16	2.64	3.83	2.45	3.13	2.61	2.89	4.69
18	2.93	3.14	2.99	2.96	3.96	2.43	3.11	2.15	2.66	4.41
19	3.08	2.50	2.02	2.56	2.54	2.63	2.81	3.16	2.16	5.83
20	4.18	3.39	3.22	2.39	3.49	2.86	2.55	2.40	2.58	5.46
21	2.34	2.17	2.35	3.06	2.95	2.52	2.86	2.90	2.89	6.15
22	2.72	2.83	2.49	2.74	3.27	2.44	3.05	2.82	2.70	4.22
23	3.16	2.94	2.96	2.23	3.12	3.07	2.87	2.17	2.72	5.51
24	3.09	2.65	2.92	1.91	3.58	3.21	2.91	2.88	3.39	6.63
25	3.51	2.72	2.75	2.86	3.24	3.80	2.65	3.23	3.29	5.57
26	2.65	2.54	2.61	2.93	3.52	2.59	2.88	2.22	2.96	6.62
27	2.19	2.56	3.17	3.74	3.04	3.03	2.91	2.69	2.92	6.55
28	2.87	2.82	2.46	3.60	3.31	2.99	2.66	2.21	2.78	5.14
29	3.20	3.02	2.62	2.74	2.83	2.69	4.25	3.27	2.89	4.93
30	2.47	2.75	2.63	2.69	3.17	2.59	2.67	2.46	2.37	5.26
31	2.82	2.52	2.45	3.39	3.98	2.63	3.30	2.75	3.35	5.56
32	4.36	2.89	2.96	2.47	3.59	3.23	2.66	2.92	2.82	5.89
33	2.29	2.78	3.07	3.56	2.95	3.06	3.22	2.34	3.60	5.78
34	3.40	2.33	2.53	2.35	2.92	2.99	3.29	2.73	2.63	4.28
35	2.21	3.04	2.81	2.52	4.00	2.61	4.24	3.38	2.23	5.47
36	3.99	2.29	2.38	2.57	3.58	2.64	3.46	2.76	2.98	5.18
37	2.57	2.72	3.32	3.01	2.93	2.37	2.65	2.82	2.89	3.83
38	3.00	2.01	2.37	3.22	3.90	2.81	2.53	3.02	2.69	5.77
39	2.76	2.93	2.84	2.80	3.01	2.89	3.17	3.08	2.58	7.05
40	2.52	2.64	2.96	2.37	3.81	2.45	2.82	2.76	3.20	5.32
41	3.00	2.66	2.86	2.59	4.36	2.54	3.22	2.65	2.40	6.05
42	2.98	2.65	2.76	1.99	2.83	3.04	2.27	2.82	3.46	4.79
43	3.20	2.67	2.30	2.77	2.97	3.62	2.54	2.52	2.62	5.30
44	2.77	2.48	2.99	2.56	3.20	3.12	3.02	2.89	3.16	7.15
45	3.31	2.61	3.21	2.75	3.28	3.30	2.24	3.05	2.36	4.84
46	3.37	2.20	3.05	2.61	3.14	3.56	2.79	2.59	3.29	8.28
47	2.71	2.35	2.37	2.31	3.15	2.81	3.10	2.92	3.12	8.37
48	3.26	2.91	2.66	2.33	3.75	3.00	3.01	2.69	3.07	6.30
49	3.74	2.99	2.68	2.50	3.31	2.85	2.70	2.42	2.70	4.71
50	1.21	1.29	1.79	1.68	2.45	1.78	2.04	1.57	1.33	2.73

ENHANCED INLET, STATION 2

CP	EA1	EA2	EA3	EA4	EA5	EA6	EA7	EA8	EA9	EA10-% AXIAL ERROR
1	2.38	1.41	0.92	1.16	1.15	1.20	1.25	1.65	1.23	4.67
2	3.47	1.83	1.09	1.29	0.82	0.78	0.75	1.05	0.80	4.59
3	3.16	1.61	1.75	2.00	1.70	1.55	1.42	0.81	0.70	3.63
4	3.42	1.90	1.94	1.69	2.32	2.39	2.47	2.12	1.31	7.91
5	2.95	2.38	1.62	2.29	2.04	2.53	3.35	2.95	1.39	5.69
6	3.22	2.44	1.88	2.30	2.92	2.89	2.87	2.33	1.57	8.65
7	3.62	2.36	2.18	2.44	3.22	3.55	3.97	2.82	1.36	5.12
8	4.17	3.01	2.12	2.64	3.08	3.66	4.56	2.10	2.32	4.06
9	3.73	2.95	2.44	3.18	3.80	3.93	4.08	2.50	1.91	8.21
10	4.20	4.11	2.97	2.84	3.18	3.62	4.22	3.40	1.90	8.92
11	3.83	3.76	2.15	4.05	3.53	3.75	4.00	3.20	2.73	8.10
12	2.39	4.62	3.46	3.67	3.16	3.81	4.83	4.21	2.82	10.99
13	3.93	5.24	3.18	4.23	4.67	4.52	4.38	3.66	4.09	16.74
14	3.09	3.96	4.36	4.29	3.45	3.94	4.63	3.96	2.94	7.10
15	4.83	4.49	2.85	4.25	4.92	4.42	3.99	3.29	3.38	8.48
16	3.47	4.18	3.54	3.66	5.03	4.42	3.93	4.12	4.07	15.98
17	3.78	3.18	4.05	3.89	3.75	4.48	5.58	5.37	3.34	8.70
18	3.24	3.98	3.42	4.48	4.46	4.53	4.59	3.37	3.93	25.64
19	3.16	4.69	3.95	3.81	4.88	4.69	4.51	4.71	4.69	13.05
20	3.59	5.00	4.21	5.10	4.55	4.77	5.00	4.87	3.86	16.88
21	3.74	4.37	3.56	4.87	5.11	4.96	4.82	4.77	5.06	14.21
22	4.55	3.88	3.46	4.88	5.08	4.83	4.60	4.50	4.66	21.08
23	3.24	3.88	3.60	4.79	4.46	5.02	5.75	4.83	5.00	25.19
24	3.38	4.34	3.34	6.94	6.12	5.11	4.38	3.41	4.90	48.01
25	3.01	3.68	4.54	4.75	6.20	5.98	5.77	4.67	4.79	12.84
26	3.43	4.25	4.06	4.51	4.44	5.38	6.79	4.08	4.28	21.33
27	3.09	3.95	3.78	5.10	5.11	4.83	4.58	4.95	3.37	17.30
28	2.61	4.14	3.76	4.95	4.83	4.49	4.21	3.90	4.35	21.82
29	2.79	3.64	3.54	4.50	3.98	3.97	3.95	4.86	4.18	16.82
30	3.44	3.90	4.74	5.28	4.15	4.51	4.93	3.55	3.62	15.67
31	2.55	3.99	3.85	4.10	4.10	4.03	3.97	4.85	4.29	28.32
32	1.61	1.62	1.49	2.70	2.57	2.62	2.66	2.52	2.64	12.46
33	2.42	3.79	4.02	4.44	4.74	4.36	4.04	4.17	3.16	16.12
34	2.30	3.63	3.86	5.12	3.52	4.01	4.66	3.55	3.79	24.70
35	2.64	2.60	3.26	3.99	3.55	3.81	4.11	4.54	4.04	13.54
36	2.13	2.59	2.99	5.19	3.93	4.09	4.26	3.98	3.04	13.83
37	2.35	3.43	2.83	4.35	3.13	3.39	3.71	3.06	3.74	12.00
38	2.00	2.45	3.24	3.53	3.64	3.53	3.42	3.35	3.33	19.49
39	2.61	2.49	3.09	3.62	3.38	3.36	3.34	3.41	3.49	5.37
40	2.04	2.17	2.95	3.90	3.59	3.41	3.26	2.88	2.77	7.57
41	2.28	2.18	2.82	3.36	3.68	3.52	3.37	2.70	2.73	10.17
42	1.65	2.37	2.08	2.73	3.57	3.42	3.28	2.96	3.77	11.90
43	1.62	1.94	2.80	2.99	3.21	3.08	2.96	3.83	2.79	6.11
44	1.53	1.90	1.99	2.53	2.58	2.75	2.93	2.82	2.55	19.00
45	1.50	1.71	2.41	2.09	2.10	2.21	2.32	2.40	2.49	10.14
46	1.54	1.62	1.48	1.93	2.41	2.56	2.71	2.12	3.05	9.77
47	1.13	1.47	1.41	1.83	2.24	2.20	2.16	2.24	1.81	9.28
48	1.19	1.23	1.15	1.62	1.75	1.99	2.30	2.24	2.17	7.37
49	0.91	1.06	0.83	1.27	1.39	1.67	2.07	1.99	1.63	8.11
50	1.09	0.99	0.86	0.98	1.65	1.58	1.52	1.39	1.48	7.42

ENHANCED INLET, STATION 3

CP	EA1	EA2	EA3	EA4	EA5	EA6	EA7	EA8	EA9	EA10-% AXIAL ERROR
1	0.00	0.00	0.00	0.00	0.00	0.00	0.00	0.00	0.00	5.26
2	0.00	0.00	0.00	0.00	0.00	0.00	0.00	0.00	0.00	27.06
3	0.00	159.86	0.00	0.00	3.34	0.00	0.00	0.00	0.00	0.00
4	0.00	0.00	0.00	0.76	1.47	0.36	0.44	0.44	0.00	0.00
5	0.00	0.00	0.00	0.00	0.00	0.00	0.00	0.06	0.49	1.30
6	0.00	0.00	0.00	0.00	0.00	0.00	0.00	0.00	0.00	3.43
7	0.00	0.00	0.00	0.00	0.00	0.00	0.00	0.00	0.00	0.00
8	0.00	0.00	0.00	0.00	11.05	91.46	29.33	0.00	0.00	0.00
9	18.60	0.00	36.37	16.79	10.16	15.51	9.84	223.54	5.99	0.00
10	22.81	185.70	53.92	28.30	8.14	11.06	4.12	19.71	8.27	62.16
11	12.24	183.10	56.80	18.83	8.51	13.18	3.47	7.50	5.66	125.05
12	12.59	20.31	59.48	18.51	6.53	7.19	3.57	8.60	3.63	18.92
13	6.01	71.03	25.53	7.01	5.64	6.62	2.38	10.64	8.40	27.46
14	3.52	13.63	16.83	8.01	7.08	7.57	2.51	7.24	5.09	14.74
15	8.78	10.99	14.96	8.72	5.02	6.04	2.45	9.71	5.14	18.51
16	18.39	9.96	11.71	12.67	7.47	4.72	2.20	7.77	3.80	41.37
17	3.62	11.31	9.69	9.17	6.69	5.01	2.41	7.03	4.63	0.00
18	3.94	11.12	15.96	13.90	4.61	6.62	2.31	11.16	3.60	25.76
19	4.25	11.29	13.18	9.21	4.25	3.85	2.48	13.44	3.93	10.81
20	5.96	38.61	15.53	8.94	5.56	4.87	2.13	8.22	5.87	9.85
21	4.35	16.18	12.88	10.50	4.10	5.29	2.46	8.74	5.25	13.20
22	2.32	12.39	15.94	7.44	4.37	4.47	2.43	9.42	5.70	38.05
23	2.70	11.79	16.59	8.14	4.95	5.04	2.36	11.41	4.48	14.87
24	3.32	13.60	11.87	9.26	4.92	4.37	2.03	8.06	3.93	11.81
25	4.19	18.92	12.94	8.03	4.72	5.00	2.12	8.29	3.90	23.73
26	4.36	12.04	12.74	8.51	3.86	4.29	2.06	8.74	5.41	29.29
27	3.36	37.22	11.43	7.69	5.00	3.73	1.94	8.75	3.79	16.33
28	5.02	9.12	6.68	5.04	2.23	2.92	1.23	5.43	2.37	7.97
29	8.66	14.67	11.91	6.91	4.12	3.66	1.58	9.43	4.39	10.52
30	5.42	11.64	8.36	8.43	3.70	3.34	1.68	9.81	3.40	8.18
31	3.19	9.36	11.62	8.44	4.01	3.47	1.75	6.54	4.15	189.66
32	3.46	10.82	12.43	8.56	3.54	3.28	1.60	7.59	3.84	11.93
33	1.85	10.69	10.64	6.30	3.40	3.09	1.40	7.26	2.96	24.51
34	2.96	10.54	7.56	9.30	3.84	3.72	1.35	9.17	2.92	17.72
35	2.87	12.57	7.49	6.26	3.20	4.18	1.39	6.11	2.76	23.86
36	4.96	8.27	6.44	5.27	3.45	3.94	1.51	7.28	3.37	66.73
37	3.07	9.06	6.25	5.45	2.93	2.96	1.23	6.03	3.40	100.81
38	3.03	9.06	6.30	4.90	3.01	3.14	1.24	7.67	2.30	22.86
39	5.21	9.06	6.09	5.20	2.98	2.65	1.03	7.51	2.87	15.59
40	4.41	9.11	6.34	6.09	2.67	2.46	1.33	5.95	3.06	12.56
41	7.83	23.94	6.84	6.35	2.17	2.69	1.00	7.05	2.01	12.53
42	4.69	10.24	5.39	5.22	2.26	2.28	1.07	5.52	2.31	22.05
43	20.00	12.15	4.61	3.83	2.14	2.44	1.01	4.34	2.09	13.52
44	10.63	123.42	4.40	3.53	2.21	1.97	0.87	4.80	2.56	13.44
45	3.65	0.00	4.15	3.50	2.12	1.94	0.88	5.29	1.82	10.51
46	5.73	0.00	3.15	3.04	2.02	2.05	0.82	3.91	1.62	18.26
47	42.51	0.00	3.70	3.49	1.95	2.35	0.80	3.48	1.96	10.38
48	0.00	0.00	21.34	13.69	5.35	2.81	0.92	4.06	1.67	5.54
49	0.00	0.00	0.00	0.00	78.96	7.03	1.25	3.65	1.72	10.54
50	0.00	0.00	0.00	0.00	0.00	0.00	11.49	12.17	5.87	15.83

ENHANCED INLET, STATION 4

CP	EA1	EA2	EA3	EA4	EA5	EA6	EA7	EA8	EA9	EA10-% AXIAL ERROR
1	0.00	0.00	0.00	0.00	0.00	10.67	14.26	36.69	7.53	0.00
2	0.00	0.00	0.00	0.00	0.00	13.97	7.84	7.82	3.11	0.00
3	0.00	0.00	131.40	0.00	0.00	7.23	4.92	9.21	3.84	0.00
4	0.00	77.83	0.00	0.00	111.21	5.51	4.43	8.24	4.47	0.00
5	0.00	0.00	23.21	240.18	27.59	4.93	4.72	6.36	7.49	20.17
6	0.00	67.24	22.91	95.99	20.69	2.23	2.12	2.97	2.77	24.63
7	0.00	22.87	29.38	48.98	23.98	3.37	3.15	4.62	10.85	24.68
8	0.00	20.03	9.94	24.44	21.54	3.18	4.05	4.73	5.18	0.00
9	50.54	13.59	6.74	50.18	14.64	2.88	3.84	4.02	3.71	67.15
10	0.00	9.66	5.08	15.52	10.26	2.96	2.85	4.18	3.76	30.25
11	15.49	10.87	5.54	24.37	15.10	2.87	3.24	3.76	4.81	8.52
12	54.34	10.15	4.11	18.79	7.24	2.44	3.43	3.77	3.47	9.83
13	0.00	11.40	4.33	15.60	9.05	2.64	3.13	4.08	5.99	20.91
14	14.69	11.23	5.04	10.85	11.17	2.41	2.70	2.97	4.16	5.44
15	18.64	7.57	3.83	7.82	6.98	2.43	3.04	3.37	3.84	7.11
16	25.32	7.58	3.17	8.01	7.05	2.29	3.06	3.28	3.73	22.45
17	11.28	13.96	2.64	5.63	5.26	2.20	3.07	3.61	3.23	10.81
18	22.16	8.05	2.47	8.42	7.40	2.03	2.34	3.33	3.79	10.77
19	121.69	5.81	2.54	6.13	8.15	1.84	2.10	3.25	3.06	11.21
20	15.62	5.71	2.02	6.70	4.76	2.08	2.11	2.44	3.23	5.74
21	17.78	6.16	1.91	7.73	8.65	1.90	2.00	2.65	2.92	7.15
22	22.71	10.19	1.70	5.75	4.84	2.10	1.99	2.59	2.45	5.89
23	19.92	8.39	1.55	6.62	9.67	2.17	2.08	2.35	2.74	4.15
24	19.35	10.02	1.64	6.05	9.07	2.01	2.10	2.47	2.63	9.94
25	82.34	6.12	1.47	7.51	6.37	1.74	2.15	2.39	2.78	9.64
26	22.07	5.59	1.21	6.15	7.19	2.04	2.08	2.21	2.40	5.61
27	0.00	7.58	1.26	5.32	6.32	2.22	2.02	2.20	2.64	18.49
28	35.85	6.62	1.36	6.76	7.61	2.41	2.21	2.14	2.39	12.39
29	81.70	25.53	1.32	8.31	5.94	2.60	2.41	2.25	2.67	62.75
30	0.00	6.21	1.54	12.79	5.07	2.63	2.51	2.22	2.61	10.53
31	0.00	28.74	1.42	12.62	5.36	3.11	3.13	2.17	2.37	9.08
32	17.91	13.23	1.89	29.94	7.46	2.70	3.42	2.55	2.85	12.58
33	0.00	16.38	2.31	202.09	6.05	3.29	3.45	2.98	2.07	5.91
34	57.32	8.57	5.42	0.00	5.74	4.63	4.46	3.00	2.19	16.81
35	0.00	19.48	65.64	0.00	7.48	35.41	4.51	4.08	2.03	34.01
36	0.00	6.78	0.00	0.00	21.60	0.00	6.25	4.16	2.47	20.11
37	19.54	6.00	0.00	0.00	0.00	0.00	8.69	3.78	3.26	9.27
38	7.83	4.66	0.00	0.00	0.00	0.00	0.00	6.47	3.82	0.00
39	1.36	2.48	0.00	0.00	0.00	0.00	0.00	24.25	3.90	20.37
40	0.87	0.11	0.00	0.00	0.00	0.00	87.00	237.83	8.15	39.76
41	3.36	0.28	3.68	0.00	123.07	0.00	7.32	7.68	10.09	0.00
42	0.00	3.83	0.00	0.00	0.00	0.00	63.12	26.89	10.39	0.00
43	0.00	0.00	0.00	0.00	0.00	0.00	0.00	0.00	28.73	0.00
44	0.00	0.00	0.00	0.00	0.00	0.00	0.00	0.00	0.00	0.00
45	0.00	0.00	0.00	0.00	0.00	0.00	0.00	0.00	0.00	0.00
46	0.00	0.00	0.00	0.00	0.00	0.00	0.00	0.00	0.00	0.00
47	0.00	0.00	0.00	0.00	0.00	0.00	0.00	0.00	0.00	0.00
48	0.00	0.00	0.00	0.00	0.00	0.00	0.00	0.00	0.00	0.00
49	0.00	0.00	0.00	0.00	0.00	0.00	0.00	0.00	0.00	0.00
50	0.00	0.00	0.00	0.00	0.00	0.00	0.00	0.00	0.00	0.00

ENHANCED INLET, STATION 5

CP	EA1	EA2	EA3	EA4	EA5	EA6	EA7	EA8	EA9	EA10-% AXIAL ERROR
1	0.00	0.00	0.00	0.00	0.00	0.00	9.41	5.40	3.68	5.16
2	0.00	0.00	0.00	0.00	11.82	3.57	8.86	11.31	3.88	5.80
3	0.00	0.00	235.95	4.77	9.45	3.11	8.79	6.50	3.47	10.85
4	10.33	0.00	0.00	4.37	13.49	3.01	4.02	4.80	5.22	5.35
5	8.78	0.00	263.91	4.71	9.14	2.25	5.32	3.95	9.50	3.85
6	11.66	0.00	25.40	4.18	9.12	2.57	5.44	5.49	6.46	5.60
7	9.16	0.00	24.91	3.38	9.89	2.27	6.81	5.17	4.40	5.53
8	10.34	73.70	9.53	4.65	8.83	1.95	5.79	4.88	5.98	4.58
9	5.15	166.67	15.44	3.44	9.63	1.72	4.15	5.16	6.02	5.31
10	6.33	74.61	7.58	3.84	7.60	1.64	6.30	4.83	4.68	4.12
11	9.19	34.34	7.55	3.27	5.91	1.53	4.64	5.28	4.44	3.35
12	5.49	28.18	5.51	3.05	5.97	1.53	3.24	3.50	5.69	2.94
13	12.70	39.85	6.79	3.31	7.25	1.64	4.30	4.11	4.40	5.45
14	6.04	37.15	5.67	2.52	6.48	1.48	5.12	6.52	4.12	3.83
15	9.34	26.58	6.49	2.36	4.83	1.42	2.79	4.72	4.44	5.41
16	11.75	36.08	5.94	2.14	7.00	1.61	3.28	4.08	3.65	3.11
17	12.88	12.12	5.32	2.20	5.28	1.31	3.45	3.43	4.36	3.35
18	11.91	20.44	4.47	2.28	4.93	1.23	3.42	3.70	3.95	3.24
19	40.05	19.93	5.20	2.11	5.94	1.20	3.12	3.96	3.61	3.86
20	31.70	71.93	4.63	2.49	4.33	1.01	3.47	3.64	3.65	5.10
21	16.23	29.19	4.12	2.64	3.50	1.03	3.42	3.19	4.08	4.52
22	23.14	14.66	4.03	2.49	4.37	1.19	3.12	2.89	4.21	4.57
23	21.26	17.41	4.52	2.53	3.59	1.15	3.29	3.11	2.91	5.16
24	24.44	20.89	4.35	3.26	4.22	1.26	2.78	3.02	3.25	5.56
25	25.11	42.00	4.36	3.82	3.85	1.11	2.40	2.46	3.06	7.45
26	27.72	17.38	3.72	3.37	3.28	1.34	2.37	2.44	2.72	4.93
27	58.66	38.06	4.08	3.57	3.83	1.50	2.61	2.45	2.63	5.63
28	125.09	191.13	3.49	3.55	3.02	1.85	2.22	2.51	2.12	7.21
29	63.65	14.85	4.56	3.12	3.65	1.59	2.33	2.26	2.27	10.23
30	36.20	36.53	3.69	3.41	3.46	1.77	2.89	2.61	2.11	4.98
31	169.54	37.02	4.63	3.35	3.39	1.60	2.40	2.73	1.80	8.39
32	243.06	36.67	3.23	3.18	3.62	2.16	2.77	2.51	2.54	4.80
33	0.00	70.65	4.20	3.47	3.59	2.12	2.80	2.26	1.82	5.51
34	0.00	36.32	3.79	5.68	4.14	1.81	3.15	2.52	2.45	6.56
35	36.62	40.01	3.82	16.12	3.54	2.47	3.55	2.82	2.44	5.79
36	1.55	0.00	4.72	0.00	3.44	4.37	3.13	3.51	2.57	5.97
37	0.38	163.16	6.35	0.00	3.28	49.26	3.55	4.39	2.91	5.10
38	0.11	0.00	14.88	0.00	9.72	0.00	4.65	3.41	5.06	6.79
39	0.43	0.00	69.67	0.00	43.15	0.00	6.98	5.33	74.53	6.63
40	8.20	15.60	5.64	0.00	0.00	31.38	5.67	3.20	8.36	6.68
41	0.00	35.27	0.00	0.00	0.00	0.00	52.18	34.81	11.02	0.00
42	0.00	0.00	0.00	0.00	0.00	0.00	0.00	0.00	32.75	23.71
43	0.00	0.00	0.00	0.00	0.00	0.00	0.00	0.00	229.06	17.78
44	0.00	0.00	0.00	0.00	0.00	0.00	0.00	0.00	0.00	0.00
45	0.00	0.00	0.00	0.00	0.00	0.00	0.00	0.00	0.00	0.00
46	0.00	0.00	0.00	0.00	0.00	0.00	0.00	0.00	0.00	0.00
47	0.00	0.00	0.00	0.00	0.00	0.00	0.00	0.00	0.00	0.00
48	0.00	0.00	0.00	0.00	0.00	0.00	0.00	0.00	0.00	0.00
49	0.00	0.00	0.00	0.00	0.00	0.00	0.00	0.00	0.00	0.00
50	0.00	0.00	0.00	0.00	0.00	0.00	0.00	0.00	0.00	0.00

ENHANCED INLET, STATION 6

CP	EA1	EA2	EA3	EA4	EA5	EA6	EA7	EA8	EA9	EA10-% AXIAL ERROR
1	0.00	0.00	0.00	0.00	0.00	0.00	0.00	0.00	0.00	
2	0.00	0.00	0.00	26.62	10.06	4.44	2.99	1.91	3.17	
3	7.39	0.00	18.18	11.56	11.54	7.84	2.69	2.89	3.96	
4	11.33	25.20	11.83	11.15	7.02	6.07	2.18	2.08	3.48	
5	10.02	11.19	9.38	8.13	5.87	7.32	2.50	2.29	4.88	
6	8.51	10.16	5.83	10.18	5.42	4.50	2.42	2.42	4.47	
7	6.12	6.75	4.67	6.44	5.36	5.22	2.22	2.28	3.85	
8	7.56	7.52	3.89	5.05	3.86	4.51	2.48	2.51	5.47	
9	8.52	5.36	3.34	5.21	3.96	4.29	2.40	2.21	4.95	
10	7.52	5.65	3.30	4.72	3.66	3.70	1.90	2.07	4.52	
11	11.44	4.85	3.01	3.81	3.67	4.78	2.15	2.17	4.42	
12	17.18	4.79	2.81	3.43	3.95	4.51	1.99	2.20	4.45	
13	10.31	4.67	2.57	3.64	3.92	3.89	2.06	2.10	5.03	
14	6.80	4.05	2.82	3.36	3.57	4.09	1.90	2.02	3.90	
15	6.28	4.16	2.59	3.29	3.38	3.73	1.86	1.87	3.35	
16	13.24	3.94	2.70	3.06	2.85	3.30	1.81	1.92	4.56	
17	14.20	4.55	2.76	3.16	2.89	3.48	1.86	2.07	4.27	
18	12.17	3.62	2.23	3.04	2.34	3.50	2.18	1.97	4.24	
19	17.03	3.04	1.78	2.45	2.54	3.60	1.82	1.51	4.17	
20	16.85	3.36	1.92	2.66	2.67	2.60	1.77	1.60	4.12	
21	9.05	3.41	2.11	2.55	2.82	3.00	1.57	1.52	2.97	
22	15.10	3.68	1.85	2.06	2.60	3.23	1.82	1.57	3.96	
23	11.28	3.34	1.80	2.84	2.50	2.85	1.72	1.54	3.18	
24	21.07	3.39	1.78	2.34	2.50	2.81	1.50	1.34	3.13	
25	17.56	3.92	2.44	2.29	2.11	2.79	1.46	1.56	3.19	
26	12.50	4.26	2.71	2.61	2.61	2.67	1.41	1.20	3.28	
27	11.47	3.11	1.41	1.69	1.12	1.53	0.92	0.97	2.00	
28	22.82	5.22	2.56	3.23	2.24	2.68	1.44	1.33	2.24	
29	21.19	6.95	3.20	3.20	2.01	3.13	1.26	1.33	2.90	
30	20.44	6.11	2.98	3.43	2.18	2.61	1.33	1.31	3.01	
31	8.68	7.37	3.19	4.68	2.54	2.53	1.20	1.42	3.06	
32	44.58	6.11	3.86	6.02	3.01	3.13	1.15	1.31	3.26	
33	0.00	11.25	5.27	6.75	3.89	3.66	1.33	1.17	2.65	
34	9.61	9.78	6.67	11.03	3.73	3.29	1.39	1.31	2.59	
35	154.63	11.55	9.34	21.21	5.51	3.33	1.27	1.34	2.65	
36	99.53	25.08	8.33	15.63	4.06	3.78	1.53	1.48	2.54	
37	59.74	13.45	11.05	22.36	6.04	3.53	1.39	1.73	2.40	
38	0.00	11.32	11.52	24.70	6.20	4.28	1.44	2.23	2.58	
39	21.19	16.88	10.37	30.59	6.04	3.03	1.31	2.30	3.32	
40	36.91	8.50	12.31	16.02	3.38	2.08	0.91	1.75	3.32	
41	0.00	7.31	10.16	0.39	11.77	5.94	1.58	2.30	4.28	
42	0.00	2.82	0.00	12.92	273.02	0.00	5.82	10.13	6.26	
43	0.00	0.00	0.00	0.00	0.00	0.00	0.00	0.00	0.00	
44	0.00	0.00	0.00	0.00	0.00	0.00	0.00	0.00	0.00	
45	0.00	0.00	0.00	0.00	0.00	0.00	0.00	0.00	0.00	
46	0.00	0.00	0.00	0.00	0.00	0.00	0.00	0.00	0.00	
47	0.00	0.00	0.00	0.00	0.00	0.00	0.00	0.00	0.00	
48	0.00	0.00	0.00	0.00	0.00	0.00	0.00	0.00	0.00	
49	0.00	0.00	0.00	0.00	0.00	0.00	0.00	0.00	0.00	
50	0.00	0.00	0.00	0.00	0.00	0.00	0.00	0.00	0.00	

ENHANCED INLET, STATION 7

CP	EA1	EA2	EA3	EA4	EA5	EA6	EA7	EA8	EA9	EA10-% AXIAL ERROR
1	0.00	0.00	0.00	0.00	0.00	0.00	0.00	0.00	0.00	0.00
2	0.00	0.00	0.00	0.00	0.00	0.00	0.00	0.00	0.00	0.00
3	0.00	332.19	0.00	63.67	95.51	9.87	2.15	1.91	2.02	0.00
4	0.00	9.63	0.00	71.56	107.34	7.16	1.53	2.71	2.22	0.00
5	0.00	1.89	0.00	0.00	0.00	6.04	2.08	3.12	2.82	0.00
6	0.00	0.38	0.00	38.29	47.86	6.44	1.74	4.28	1.92	37.77
7	0.00	0.23	0.00	54.90	54.90	10.11	3.18	5.54	2.08	25.39
8	0.00	0.44	0.00	35.39	35.39	12.46	2.59	4.20	3.45	0.00
9	0.00	0.79	135.59	52.06	24.22	5.14	2.99	4.64	3.04	31.69
10	0.00	0.00	138.12	68.87	34.25	5.00	2.89	4.16	3.93	38.42
11	0.00	349.52	47.62	48.15	48.58	5.27	2.46	5.20	3.41	22.76
12	0.00	0.00	133.91	33.64	14.83	5.12	2.58	3.83	4.29	10.21
13	0.00	0.00	47.07	30.35	21.99	3.93	2.98	3.95	3.88	26.87
14	0.00	0.00	95.06	43.01	24.08	3.61	2.66	4.79	4.30	22.81
15	0.00	0.00	26.85	15.60	10.71	3.29	2.88	4.35	3.28	40.47
16	0.00	0.00	88.55	44.89	27.42	3.11	2.98	4.90	4.67	31.66
17	0.00	0.00	24.84	19.12	15.42	3.65	2.67	4.78	4.24	34.60
18	0.00	0.00	54.38	26.42	17.09	3.48	2.52	4.58	4.18	37.07
19	0.00	0.00	31.51	17.31	11.50	3.62	2.36	4.42	4.42	17.72
20	0.00	0.00	26.86	9.50	5.55	1.94	1.53	2.65	2.46	17.90
21	0.00	0.00	64.45	24.43	13.90	2.89	2.78	4.53	4.16	14.56
22	0.00	0.00	37.05	22.37	15.46	3.62	2.53	4.03	4.04	17.58
23	0.00	0.00	37.29	18.95	11.97	3.17	2.47	5.62	4.31	17.57
24	0.00	0.00	43.12	16.62	9.49	2.96	2.29	3.81	5.22	14.55
25	0.00	0.00	35.99	15.92	9.74	2.81	1.94	4.19	4.58	10.20
26	0.00	0.00	51.57	14.29	7.51	2.68	2.27	5.79	4.85	35.34
27	0.00	59.06	26.01	14.97	10.37	3.19	2.48	3.62	4.17	12.12
28	0.00	0.00	21.63	12.09	8.27	3.23	2.13	3.83	4.71	8.81
29	0.00	0.00	35.98	14.74	8.67	2.55	2.26	3.69	4.27	14.54
30	0.00	0.00	24.53	12.31	7.97	2.53	2.51	3.63	4.59	22.28
31	0.00	251.83	23.59	8.86	5.34	2.36	2.25	3.59	3.59	12.09
32	0.00	0.00	24.27	13.13	8.76	2.69	2.01	4.23	4.06	17.61
33	0.00	0.00	16.70	10.36	7.48	2.77	2.15	3.84	3.60	24.97
34	0.00	0.00	18.76	10.16	6.82	2.38	2.02	4.31	4.18	35.16
35	0.00	0.00	21.25	8.02	4.84	2.42	1.79	3.43	3.78	24.28
36	0.00	0.00	19.42	10.97	7.54	2.33	1.76	2.92	3.27	27.64
37	0.00	0.00	22.88	11.79	7.85	2.23	1.82	3.71	3.74	23.31
38	0.00	0.00	21.46	9.10	5.65	2.68	1.43	3.17	3.91	16.43
39	0.00	216.38	23.51	9.65	5.93	2.68	1.58	3.00	3.89	10.43
40	0.00	0.00	13.06	8.16	5.95	3.65	1.89	4.23	3.38	15.01
41	0.00	2.57	8.76	8.31	7.92	3.84	1.73	3.48	2.95	10.18
42	19.20	4.02	17.93	13.04	10.19	6.26	1.55	2.85	2.25	12.11
43	0.00	0.18	8.31	10.81	14.47	7.35	1.35	2.23	2.15	10.28
44	0.00	0.02	0.02	0.05	0.57	8.27	0.83	1.50	1.96	6.95
45	0.13	0.03	0.01	0.01	0.01	4.25	1.05	1.37	1.51	5.92
46	0.02	5.58	0.60	0.38	0.26	0.83	5.46	5.15	2.54	4.43
47	0.02	4.12	8.87	13.09	34.18	12.85	12.28	5.56	5.84	2.16
48	0.12	2.21	7.63	7.63	0.00	60.30	2.72	1.97	2.94	182.84
49	0.00	0.00	0.00	0.00	0.00	0.00	2.42	2.45	1.53	0.00
50	0.00	0.00	0.00	0.00	0.00	0.00	0.00	0.00	0.00	0.00

ENHANCED INLET, STATION 8

CP	EA1	EA2	EA3	EA4	EA5	EA6	EA7	EA8	EA9	EA10-% AXIAL ERROR
1	0.00	0.00	0.39	1.27	26.11	4.68	0.41	0.62	7.02	15.13
2	0.00	120.46	0.39	0.69	0.00	22.78	0.74	0.72	16.04	59.31
3	0.00	0.00	0.39	0.62	47.23	27.89	0.85	0.79	41.22	62.86
4	0.00	173.45	0.37	0.98	25.35	16.45	0.77	0.88	15.14	26.07
5	0.00	132.04	0.40	1.13	23.92	22.29	1.70	0.84	15.85	0.00
6	0.00	380.63	0.45	0.88	29.02	25.23	0.46	1.02	17.82	89.10
7	0.00	130.79	0.34	1.35	14.77	28.33	2.00	1.22	11.56	41.05
8	0.00	96.59	0.32	1.95	18.33	15.12	5.18	1.17	6.47	30.83
9	0.00	175.66	0.15	9.65	18.85	10.86	4.45	1.65	8.55	104.22
10	0.00	64.57	11.57	57.82	16.05	14.33	3.52	1.63	6.84	46.00
11	0.00	96.50	23.77	0.00	13.14	11.03	4.08	2.10	7.69	37.37
12	0.00	73.71	19.38	0.00	18.46	10.25	5.37	1.71	7.93	42.56
13	0.00	283.81	27.31	0.00	13.84	11.61	3.49	1.84	9.05	46.83
14	0.00	380.63	17.05	0.00	6.80	10.29	3.89	2.00	18.78	14.51
15	0.00	157.57	19.36	112.49	5.42	9.36	4.29	1.76	6.31	24.79
16	0.00	185.00	18.65	113.84	7.72	7.67	2.58	2.27	6.98	24.72
17	0.00	65.86	16.42	179.37	4.77	8.36	3.46	1.81	9.54	13.65
18	0.00	107.96	12.45	232.58	5.21	4.17	1.49	1.07	5.05	24.22
19	0.00	96.19	28.66	78.62	4.03	7.25	2.93	1.80	6.35	13.33
20	0.00	90.64	22.45	0.00	2.97	6.78	2.88	2.04	8.44	15.75
21	0.00	57.86	33.52	0.00	7.53	7.81	2.88	1.63	6.08	16.13
22	0.00	42.50	23.53	44.76	4.41	5.99	3.39	1.84	18.98	26.39
23	0.00	53.43	21.84	122.17	4.05	8.77	2.77	1.88	8.24	16.20
24	0.00	36.13	20.88	60.77	2.85	7.41	3.13	1.83	7.90	8.94
25	0.00	106.15	24.84	161.91	3.67	9.00	2.84	1.69	8.93	17.86
26	0.00	88.32	18.42	0.00	4.30	6.23	3.33	1.56	8.63	20.56
27	0.00	73.48	27.57	79.99	3.55	6.99	2.91	1.55	15.27	10.45
28	0.00	25.08	16.57	19.18	2.39	7.12	3.39	1.39	11.33	16.31
29	0.00	46.63	17.41	276.22	2.49	5.46	2.78	1.41	16.14	8.61
30	0.00	41.38	26.00	145.59	1.98	5.61	3.70	1.70	15.00	11.33
31	0.00	28.70	21.88	0.00	2.34	8.50	3.32	1.44	11.53	15.26
32	0.00	74.71	25.64	39.33	2.42	6.09	2.69	1.57	8.18	10.35
33	0.00	34.06	25.99	0.00	2.12	6.36	2.83	1.75	9.13	21.69
34	0.00	37.41	24.78	0.00	2.52	6.00	2.66	1.44	13.70	33.67
35	0.00	45.87	20.77	51.04	2.84	8.36	2.42	1.44	11.58	8.10
36	0.00	41.43	20.02	140.16	2.90	5.77	3.27	1.33	9.73	13.53
37	0.00	46.64	20.86	161.18	6.52	5.90	2.45	1.41	15.60	7.49
38	0.00	44.29	21.79	263.73	1.46	5.43	2.65	1.55	8.92	10.93
39	0.00	28.78	15.67	177.29	3.62	4.83	2.24	1.40	5.96	9.96
40	0.00	41.01	14.52	17.57	2.51	4.29	2.34	1.63	8.32	7.93
41	0.00	31.07	0.35	5.92	1.43	4.50	2.33	1.41	11.19	7.64
42	0.02	20.63	0.37	4.95	1.32	4.26	2.20	1.27	6.90	25.91
43	0.01	35.61	0.35	0.00	1.13	4.35	2.12	1.21	7.79	6.21
44	0.25	11.45	21.68	0.00	0.58	2.79	2.03	1.28	7.78	7.58
45	0.00	12.73	18.07	223.42	0.40	2.39	1.35	1.13	6.63	3.50
46	0.00	3.90	16.51	9.33	0.15	1.43	1.10	1.03	7.79	2.47
47	2.24	13.15	0.34	3.27	0.08	0.74	0.71	0.67	6.11	8.50
48	0.15	11.19	0.35	0.31	0.08	0.40	0.48	0.55	4.68	4.04
49	0.05	7.51	0.33	0.15	0.38	0.50	0.45	0.44	3.55	1.43
50	0.13	20.10	0.38	0.93	4.28	1.47	0.25	0.55	4.03	2.32

TABLE A6. -

(f) CALCULATED TANGENTIAL UNCERTAINTIES (PERCENT)

BASELINE INLET, STATION 1

CP	ET1	ET2	ET3	ET4	ET5	ET6	ET7	ET8	ET9	ET10-% TANG ERROR
1	0.12	0.03	0.04	0.03	0.04	0.03	0.06	0.06	0.04	0.28
2	0.15	0.02	0.05	0.03	0.05	0.03	0.05	0.06	0.04	0.39
3	0.14	0.02	0.05	0.03	0.06	0.03	0.06	0.05	0.04	0.44
4	0.15	0.03	0.04	0.03	0.05	0.03	0.06	0.06	0.02	0.37
5	0.17	0.03	0.04	0.03	0.05	0.03	0.06	0.06	0.04	0.42
6	0.14	0.03	0.04	0.03	0.05	0.03	0.06	0.06	0.04	0.35
7	0.14	0.02	0.04	0.03	0.05	0.03	0.06	0.06	0.05	0.02
8	0.18	0.03	0.04	0.03	0.06	0.03	0.06	0.05	0.04	0.09
9	0.14	0.03	0.05	0.03	0.05	0.03	0.06	0.06	0.04	0.36
10	0.19	0.03	0.04	0.03	0.06	0.03	0.06	0.06	0.04	0.33
11	0.12	0.03	0.05	0.03	0.05	0.03	0.06	0.06	0.02	0.05
12	0.14	0.02	0.04	0.03	0.05	0.03	0.06	0.06	0.02	0.35
13	0.11	0.03	0.05	0.03	0.05	0.03	0.05	0.06	0.03	0.45
14	0.10	0.03	0.05	0.03	0.05	0.03	0.06	0.06	0.02	0.02
15	0.12	0.03	0.04	0.03	0.06	0.03	0.06	0.05	0.04	0.29
16	0.12	0.03	0.05	0.03	0.05	0.03	0.06	0.06	0.04	0.02
17	0.12	0.03	0.05	0.03	0.05	0.03	0.06	0.06	0.02	0.23
18	0.08	0.03	0.05	0.03	0.06	0.04	0.06	0.06	0.03	0.34
19	0.11	0.02	0.05	0.03	0.05	0.04	0.05	0.06	0.03	0.23
20	0.13	0.03	0.04	0.03	0.05	0.03	0.07	0.06	0.04	0.46
21	0.14	0.03	0.05	0.03	0.04	0.03	0.06	0.05	0.04	0.36
22	0.11	0.03	0.05	0.03	0.05	0.03	0.06	0.06	0.03	1.29
23	0.14	0.02	0.04	0.03	0.05	0.03	0.06	0.06	0.03	0.30
24	0.16	0.03	0.04	0.03	0.05	0.03	0.06	0.06	0.04	0.30
25	0.09	0.02	0.05	0.03	0.06	0.03	0.05	0.05	0.03	0.33
26	0.14	0.03	0.04	0.03	0.05	0.03	0.07	0.06	0.03	0.06
27	0.11	0.02	0.04	0.03	0.05	0.03	0.05	0.05	0.02	0.28
28	0.18	0.03	0.05	0.03	0.05	0.03	0.06	0.05	0.03	0.28
29	0.11	0.03	0.04	0.03	0.05	0.03	0.06	0.06	0.02	0.02
30	0.22	0.03	0.04	0.03	0.05	0.03	0.06	0.07	0.04	0.28
31	0.14	0.03	0.05	0.03	0.06	0.03	0.06	0.05	0.04	0.23
32	0.13	0.03	0.05	0.03	0.06	0.03	0.06	0.05	0.04	0.19
33	0.14	0.03	0.04	0.03	0.05	0.03	0.06	0.05	0.04	0.28
34	0.21	0.03	0.05	0.03	0.04	0.03	0.05	0.05	0.03	1.20
35	0.15	0.02	0.03	0.03	0.05	0.03	0.06	0.05	0.02	0.23
36	0.13	0.03	0.03	0.03	0.05	0.03	0.07	0.05	0.05	0.02
37	0.14	0.02	0.04	0.03	0.05	0.03	0.05	0.06	0.04	0.24
38	0.09	0.03	0.04	0.02	0.06	0.03	0.05	0.05	0.04	0.29
39	0.09	0.03	0.05	0.03	0.04	0.03	0.06	0.05	0.02	0.34
40	0.17	0.03	0.06	0.03	0.05	0.03	0.06	0.05	0.03	0.25
41	0.13	0.03	0.04	0.03	0.05	0.03	0.05	0.06	0.02	0.32
42	0.16	0.03	0.04	0.03	0.05	0.03	0.06	0.05	0.01	0.31
43	0.13	0.03	0.05	0.03	0.05	0.03	0.05	0.05	0.02	0.35
44	0.16	0.03	0.05	0.02	0.05	0.03	0.05	0.06	0.01	0.25
45	0.16	0.03	0.05	0.03	0.05	0.03	0.05	0.05	0.02	0.25
46	0.11	0.02	0.04	0.03	0.05	0.03	0.05	0.05	0.03	0.27
47	0.09	0.03	0.05	0.03	0.04	0.03	0.05	0.04	0.04	0.22
48	0.07	0.02	0.04	0.03	0.06	0.03	0.06	0.05	0.04	0.01
49	0.13	0.02	0.05	0.04	0.05	0.03	0.07	0.06	0.04	0.36
50	0.12	0.02	0.03	0.03	0.04	0.03	0.04	0.03	0.04	1.00

BASELINE INLET, STATION 2

CP	ET1	ET2	ET3	ET4	ET5	ET6	ET7	ET8	ET9	ET10-% TANG ERROR
1	0.32	0.75	0.22	2.85	0.11	0.58	0.17	0.49	0.51	1.08
2	0.32	1.16	0.29	3.41	0.06	0.38	0.44	0.08	0.32	1.22
3	0.29	0.93	0.40	2.96	0.19	0.13	0.60	0.46	0.62	2.29
4	0.23	1.14	0.48	6.44	0.28	0.10	0.85	0.77	0.88	8.45
5	0.20	1.08	0.63	5.51	0.31	0.20	0.83	0.75	0.78	5.27
6	0.14	1.01	0.52	7.14	0.32	0.22	0.74	1.24	1.12	15.63
7	0.11	0.82	0.49	5.84	0.36	0.33	1.17	1.10	1.33	4.45
8	0.11	0.52	0.53	6.29	0.33	0.36	0.74	0.91	1.25	4.79
9	0.07	0.49	0.50	5.59	0.32	0.36	0.73	1.07	1.43	7.05
10	0.06	0.42	0.50	6.62	0.34	0.35	0.61	0.83	1.00	7.22
11	0.05	0.30	0.40	5.87	0.26	0.38	0.65	0.78	1.28	8.50
12	0.04	0.30	0.40	5.35	0.29	0.35	0.53	0.59	1.22	82.57
13	0.03	0.18	0.30	9.74	0.24	0.32	0.38	0.52	1.09	14.23
14	0.03	0.15	0.24	5.15	0.21	0.32	0.36	0.48	1.24	22.33
15	0.02	0.08	0.28	4.56	0.18	0.28	0.26	0.45	0.93	9.07
16	0.02	0.08	0.21	4.45	0.20	0.30	0.22	0.31	0.71	11.20
17	0.03	0.12	0.16	2.84	0.19	0.27	0.20	0.28	0.96	12.21
18	0.02	0.16	0.10	3.21	0.17	0.24	0.16	0.22	0.78	5.11
19	0.03	0.16	0.07	3.67	0.13	0.20	0.12	0.12	0.53	4.96
20	0.03	0.17	0.04	2.83	0.11	0.18	0.07	0.11	0.74	3.58
21	0.04	0.25	0.03	1.98	0.10	0.18	0.06	0.05	0.50	4.40
22	0.04	0.29	0.06	2.18	0.08	0.14	0.07	0.02	0.54	3.69
23	0.04	0.27	0.08	2.01	0.06	0.16	0.09	0.04	0.59	6.57
24	0.05	0.27	0.14	2.08	0.04	0.13	0.14	0.11	0.65	3.28
25	0.06	0.36	0.14	1.84	0.03	0.09	0.14	0.12	0.51	2.53
26	0.06	0.36	0.16	2.22	0.01	0.10	0.17	0.17	0.51	10.85
27	0.07	0.40	0.22	3.17	0.02	0.04	0.18	0.17	0.47	2.52
28	0.07	0.43	0.17	3.77	0.04	0.01	0.24	0.23	0.41	6.36
29	0.07	0.50	0.23	2.05	0.05	0.02	0.28	0.18	0.40	3.66
30	0.09	0.52	0.33	1.87	0.06	0.02	0.30	0.31	0.56	12.04
31	0.09	0.49	0.30	1.79	0.07	0.06	0.33	0.28	0.49	4.97
32	0.06	0.34	0.18	2.87	0.06	0.06	0.25	0.23	0.34	3.82
33	0.11	0.47	0.30	2.22	0.10	0.11	0.33	0.35	0.58	5.90
34	0.12	0.58	0.35	5.70	0.12	0.13	0.42	0.37	0.54	2.79
35	0.13	0.56	0.39	3.53	0.13	0.15	0.41	0.33	0.58	2.88
36	0.13	0.60	0.32	8.99	0.12	0.17	0.39	0.40	0.72	4.44
37	0.12	0.65	0.39	2.79	0.15	0.22	0.47	0.43	0.62	5.19
38	0.13	0.55	0.41	2.77	0.15	0.20	0.43	0.47	0.55	5.10
39	0.15	0.67	0.48	1.99	0.19	0.29	0.50	0.50	0.60	9.73
40	0.15	0.73	0.46	2.39	0.16	0.24	0.48	0.49	0.60	2.37
41	0.14	0.72	0.45	5.24	0.21	0.32	0.55	0.44	0.65	4.11
42	0.17	0.72	0.50	7.86	0.22	0.34	0.57	0.60	0.74	4.32
43	0.17	0.86	0.50	3.88	0.21	0.33	0.60	0.66	0.55	4.22
44	0.18	0.83	0.53	4.10	0.20	0.36	0.64	0.59	0.67	11.70
45	0.19	0.69	0.45	6.73	0.24	0.38	0.70	0.72	0.64	4.21
46	0.15	0.73	0.52	5.63	0.28	0.48	0.80	0.76	0.65	5.43
47	0.12	0.64	0.50	5.59	0.28	0.43	0.75	0.67	0.92	2.48
48	0.03	0.44	0.38	3.94	0.27	0.54	0.85	0.91	0.81	7.50
49	0.19	0.15	0.25	4.71	0.24	0.46	0.95	0.79	0.82	2.87
50	0.29	0.42	0.04	2.14	0.26	0.56	0.89	1.02	0.61	2.31

BASELINE INLET, STATION 3

CP	ET1	ET2	ET3	ET4	ET5	ET6	ET7	ET8	ET9	ET10-% TANG ERROR
1		0.00	0.92	2.91	2.50	0.00	4.58	0.00	0.80	0.00
2		0.00	0.57	42.60	0.00	0.00	0.03	0.00	3.17	0.20
3		0.00	282.43	21.73	102.68	15.21	1.40	4.24	0.94	0.31
4		0.00	0.00	231.40	179.06	2.83	89.55	203.67	4.90	1.21
5		0.00	0.00	0.00	0.00	0.00	0.00	113.54	73.41	0.51
6		0.00	0.00	0.00	0.00	0.00	0.00	0.00	0.00	4.51
7		0.00	0.00	0.00	0.00	0.00	0.00	0.00	0.00	0.00
8		1.67	0.00	0.00	4.54	2.54	2.71	0.00	0.00	0.00
9		0.00	2.67	3.55	9.69	1.15	1.53	3.10	3.10	0.00
10		0.87	1.87	2.54	4.69	1.70	1.59	1.47	2.51	0.00
11		1.26	1.30	1.90	6.49	0.79	0.86	1.26	2.64	1.91
12		0.83	1.68	2.16	5.24	0.49	0.96	1.19	1.77	3.13
13		0.45	1.32	3.15	2.77	0.39	1.02	1.30	1.67	3.47
14		0.66	1.31	2.05	5.81	0.36	0.79	1.05	1.37	4.84
15		0.43	1.12	1.45	3.57	0.37	0.85	1.00	1.20	2.40
16		0.19	0.83	0.96	4.38	0.33	0.65	1.05	1.56	41.74
17		0.16	0.86	0.88	2.45	0.29	0.55	1.04	1.15	4.96
18		0.07	0.63	0.83	2.67	0.32	0.43	0.78	1.53	0.47
19		0.09	0.51	0.82	3.68	0.38	0.42	0.69	1.13	0.08
20		0.20	0.49	0.73	1.72	0.34	0.28	0.59	0.78	0.05
21		0.20	0.66	0.52	2.12	0.36	0.23	0.70	1.12	0.05
22		0.33	0.73	0.40	2.37	0.34	0.09	0.59	0.76	0.06
23		0.31	0.54	0.39	1.60	0.29	0.16	0.65	0.82	0.07
24		0.33	0.67	0.46	1.91	0.31	0.07	0.46	0.76	0.08
25		0.44	0.49	0.47	3.54	0.31	0.03	0.74	0.64	0.09
26		0.61	0.82	0.48	1.32	0.28	0.13	0.61	1.09	0.19
27		0.49	0.74	0.41	1.95	0.38	0.17	0.51	0.77	0.56
28		0.41	0.48	0.62	1.38	0.18	0.16	0.25	0.37	0.63
29		0.79	0.77	0.48	2.02	0.39	0.25	0.46	0.77	2.61
30		0.88	0.89	0.77	1.70	0.38	0.28	0.61	0.76	17.68
31		0.78	1.08	0.63	1.81	0.37	0.36	0.54	0.69	39.78
32		0.89	1.01	0.76	2.29	0.42	0.36	0.44	0.60	6.01
33		0.87	1.33	0.99	2.59	0.43	0.45	0.66	0.54	0.00
34		0.81	0.92	0.74	1.86	0.47	0.42	0.56	0.63	39.19
35		1.24	0.87	1.11	1.62	0.51	0.50	0.66	0.82	7.35
36		1.20	0.92	1.02	2.24	0.51	0.55	0.56	0.76	5.09
37		2.33	1.73	1.42	2.85	0.51	0.75	0.58	0.65	57.22
38		1.42	1.74	1.16	1.91	0.47	0.52	0.68	0.75	77.88
39		1.85	1.56	1.59	3.41	0.51	0.83	0.77	0.74	13.60
40		2.27	1.91	1.56	2.33	0.52	0.90	0.81	0.99	18.08
41		2.29	2.01	2.09	3.69	0.60	0.92	0.92	0.72	22.82
42		2.99	2.33	2.49	2.75	0.61	1.09	0.82	0.97	3.83
43		6.22	2.50	2.58	4.24	0.77	0.95	0.89	0.89	7.62
44		4.13	2.74	3.27	5.16	0.79	1.08	0.97	1.06	50.98
45		7.54	4.04	4.67	7.27	1.31	1.26	1.15	1.18	9.93
46		18.64	10.55	6.25	7.04	1.34	1.75	1.41	1.19	6.20
47		0.00	12.55	9.60	20.71	2.04	2.27	1.90	1.51	19.16
48		0.00	91.13	0.00	0.00	5.61	3.35	3.35	2.32	0.00
49		0.00	0.00	0.00	0.00	0.00	7.87	7.32	14.40	0.00
50		0.00	1.76	0.00	0.00	0.00	0.00	87.83	0.00	0.00

BASELINE INLET, STATION 4

CP	ET1	ET2	ET3	ET4	ET5	ET6	ET7	ET8	ET9	ET10-% TANG ERROR
1	0.00	0.00	0.00	0.00	0.00	5.83	1.82	3.42	8.12	20.53
2	0.00	0.00	0.00	7.18	1.09	2.18	0.74	1.10	6.70	13.11
3	0.00	0.00	5.12	7.80	0.57	1.01	0.89	0.78	5.35	6.87
4	46.78	0.70	1.33	1.95	0.40	0.77	1.01	0.60	1.77	8.86
5	0.00	0.64	0.94	1.32	0.26	0.58	0.77	0.69	1.79	3.63
6	26.83	0.34	0.30	0.50	0.14	0.32	0.37	0.34	1.35	4.80
7	0.00	0.74	0.52	0.69	0.20	0.32	0.74	0.40	0.92	4.81
8	50.60	0.82	0.55	0.72	0.18	0.27	0.60	0.35	1.20	5.04
9	36.36	0.69	0.54	0.59	0.18	0.24	0.65	0.66	0.91	2.71
10	42.78	0.85	0.50	0.61	0.16	0.29	0.94	0.41	1.14	3.87
11	175.92	0.69	0.53	0.48	0.19	0.25	0.64	0.39	0.73	2.92
12	88.20	0.70	0.56	0.56	0.18	0.29	0.82	0.56	0.71	4.02
13	17.26	0.78	0.54	0.62	0.19	0.27	0.67	0.58	0.79	3.71
14	14.58	0.91	0.62	0.50	0.17	0.32	0.64	0.64	0.81	2.29
15	18.13	0.88	0.61	0.67	0.17	0.35	0.74	0.55	0.65	2.99
16	13.17	0.85	0.57	0.58	0.16	0.37	0.76	0.70	0.73	2.70
17	12.60	0.87	0.71	0.70	0.19	0.33	0.84	0.70	0.68	3.21
18	20.45	0.85	0.73	0.70	0.22	0.35	1.05	0.78	0.60	3.04
19	16.01	1.17	0.54	0.55	0.23	0.37	1.02	0.66	0.54	4.02
20	12.60	1.30	0.61	0.74	0.25	0.39	0.98	0.66	0.73	4.51
21	19.89	1.25	0.71	0.69	0.24	0.54	0.95	0.73	0.77	4.79
22	7.75	1.25	0.71	0.68	0.25	0.48	1.03	0.91	0.82	3.61
23	15.20	1.44	0.78	0.89	0.23	0.52	1.12	0.91	0.80	3.96
24	37.61	1.62	1.03	0.98	0.26	0.49	1.14	0.86	0.81	2.73
25	28.15	1.97	0.89	0.90	0.40	0.49	1.06	0.84	0.90	3.14
26	108.75	2.32	1.16	1.14	2.24	0.50	1.23	0.99	1.11	3.57
27	0.00	2.43	1.55	1.29	18.49	0.48	1.11	1.06	0.79	3.09
28	0.00	2.32	1.33	1.13	0.00	0.52	1.03	0.94	0.78	2.20
29	0.00	2.10	1.45	1.33	0.00	0.58	1.06	1.12	0.82	3.39
30	0.00	2.13	1.67	1.44	0.00	0.68	1.22	1.22	0.78	3.95
31	0.00	2.11	1.76	1.23	0.00	0.72	1.17	0.99	0.87	2.93
32	0.00	2.43	1.76	1.69	0.00	0.78	1.24	1.52	1.09	3.59
33	0.00	4.35	4.31	2.68	0.00	0.90	1.69	1.56	0.82	2.58
34	0.00	12.14	29.52	9.64	0.00	0.90	1.86	1.51	1.04	2.24
35	0.00	0.00	0.00	30.60	0.00	1.86	2.06	1.93	1.20	2.38
36	0.00	0.00	0.00	0.00	0.00	4.18	6.14	2.18	1.65	2.67
37	0.00	0.00	0.00	0.00	0.00	11.48	137.76	7.98	1.79	5.33
38	0.00	0.00	0.00	0.00	0.00	21.93	0.00	111.85	6.64	7.14
39	0.00	0.00	0.00	0.00	0.00	0.00	0.00	0.00	20.49	10.15
40	0.00	0.00	0.00	0.00	0.00	0.00	0.00	0.00	0.00	0.00
41	0.00	0.00	0.00	0.00	0.00	0.00	0.00	0.00	0.00	0.00
42	0.00	0.00	0.00	0.00	11.14	0.00	0.00	0.00	0.00	0.00
43	0.00	0.00	0.00	0.00	4.26	0.00	11.09	2.15	13.83	3.68
44	0.00	0.00	0.00	0.00	8.48	1.66	0.49	1.16	28.85	4.13
45	0.00	0.00	0.00	0.00	0.00	0.00	0.00	0.00	46.80	16.63
46	0.00	0.00	0.00	0.00	0.00	0.00	0.00	0.00	0.00	0.00
47	0.00	0.00	0.00	0.00	0.00	0.00	0.00	0.00	0.00	0.00
48	0.00	0.00	0.00	0.00	0.00	0.00	0.00	0.00	0.00	0.00
49	0.00	0.00	0.00	0.00	0.00	0.00	0.00	0.00	0.00	0.00
50	0.00	0.00	0.00	0.00	0.00	0.00	0.00	0.00	0.00	0.00

BASELINE INLET, STATION 5

CP	ET1	ET2	ET3	ET4	ET5	ET6	ET7	ET8	ET9	ET10-% TANG ERROR
1	0.00	0.00	0.00	0.00	0.00	0.00	0.00	5.15	21.54	0.00
2	0.00	0.00	0.00	0.00	12.90	12.36	4.20	2.52	10.79	213.81
3	0.00	0.00	4.75	4.75	9.97	6.04	2.71	3.80	17.90	0.00
4	2.35	1.57	2.31	4.09	4.43	7.94	2.08	2.13	13.86	0.00
5	1.84	1.13	1.68	2.99	3.57	5.13	1.69	1.91	10.47	41.34
6	2.20	1.12	1.64	2.79	2.81	3.45	2.92	1.89	9.28	73.43
7	2.36	1.14	1.59	2.51	2.39	2.85	1.62	1.69	11.48	57.54
8	1.93	1.33	1.50	1.71	2.24	1.65	2.15	1.64	18.51	61.80
9	2.06	1.00	1.37	2.02	1.46	2.12	1.70	1.26	7.55	22.35
10	2.44	1.21	1.39	1.62	1.55	1.83	1.44	1.46	11.27	88.11
11	2.70	1.08	1.24	1.45	1.34	1.39	1.59	1.41	8.29	36.82
12	2.09	1.03	1.20	1.41	1.29	1.91	1.38	1.64	6.74	34.84
13	2.62	1.08	1.27	1.53	1.30	1.64	1.40	1.47	8.29	20.55
14	2.65	1.03	1.11	1.19	1.20	1.47	1.27	1.53	5.50	24.07
15	1.83	1.24	1.38	1.55	1.11	1.14	1.31	1.40	9.50	45.78
16	1.59	1.03	1.07	1.12	1.32	1.25	1.32	1.83	6.41	15.03
17	1.42	1.32	1.26	1.20	1.27	1.36	1.03	1.46	8.98	11.41
18	1.30	1.23	1.07	0.94	0.98	1.40	1.32	1.30	5.59	31.61
19	1.21	1.12	1.16	1.20	1.27	1.37	1.59	1.42	7.13	25.87
20	1.19	1.41	1.34	1.28	1.06	1.48	1.29	1.22	5.26	16.50
21	1.08	1.44	1.38	1.33	1.26	1.20	1.55	1.16	7.37	26.48
22	1.08	1.41	1.24	1.11	1.16	1.30	1.21	1.14	7.09	19.29
23	1.38	1.43	1.28	1.15	1.36	1.35	1.16	1.03	5.94	18.97
24	1.04	1.53	1.33	1.17	1.32	1.24	1.03	1.16	4.59	22.92
25	1.46	1.85	1.58	1.36	1.34	1.28	1.04	1.29	4.89	25.55
26	1.20	2.04	1.67	1.40	1.85	1.39	1.12	1.10	4.89	13.46
27	1.59	2.63	1.90	1.46	1.62	1.63	1.24	1.07	5.15	54.51
28	1.57	2.60	2.05	1.67	1.78	1.60	1.31	1.11	4.04	14.72
29	1.86	3.43	2.19	1.59	1.77	1.78	1.41	1.11	3.55	25.45
30	1.60	3.35	2.55	2.02	2.24	1.80	2.31	1.12	4.09	32.69
31	1.98	3.62	2.43	1.80	2.36	1.98	1.69	1.13	4.55	10.76
32	2.26	4.77	2.68	1.83	2.35	2.03	2.16	2.01	2.83	11.66
33	2.00	3.90	2.95	2.33	2.01	2.43	2.49	1.35	4.73	11.57
34	2.80	10.79	4.27	2.57	2.48	2.74	3.19	2.01	7.63	9.73
35	7.79	0.00	2.43	2.89	3.57	3.27	3.35	2.37	7.78	10.40
36	23.61	113.80	20.51	8.85	9.16	3.45	4.90	3.34	5.73	10.88
37	90.35	0.00	9.95	10.95	6.46	3.42	10.97	5.31	10.71	6.41
38	0.00	75.67	46.05	28.28	16.40	10.15	0.00	27.64	109.45	8.01
39	0.00	126.99	84.66	0.00	0.00	19.12	76.25	0.00	0.00	8.71
40	0.00	161.01	161.01	0.00	0.00	135.47	0.00	0.00	0.00	148.79
41	0.00	0.00	0.00	0.00	0.00	0.00	0.00	0.00	17.60	0.00
42	0.00	0.00	0.00	0.00	0.00	0.00	0.00	122.24	6.12	0.00
43	0.00	0.00	0.00	0.00	0.00	0.00	8.64	9.30	2.78	0.00
44	0.00	0.00	0.00	0.00	0.00	0.00	0.00	0.00	0.00	0.00
45	0.00	0.00	0.00	0.00	0.00	0.00	0.00	0.00	0.00	0.00
46	0.00	0.00	0.00	0.00	0.00	0.00	0.00	0.00	0.00	0.00
47	0.00	0.00	0.00	0.00	0.00	0.00	0.00	0.00	0.00	0.00
48	0.00	0.00	0.00	0.00	0.00	0.00	0.00	0.00	0.00	0.00
49	0.00	0.00	0.00	0.00	0.00	0.00	0.00	0.00	0.00	0.00
50	0.00	0.00	0.00	0.00	0.00	0.00	0.00	0.00	0.00	0.00

BASELINE INLET, STATION 6

CP	ET1	ET2	ET3	ET4	ET5	ET6	ET7	ET8	ET9	ET10-% TANG ERROR
1	0.00	0.00	0.00	0.00	0.00	0.00	0.00	0.00	0.00	0.00
2	0.00	0.00	0.00	3.67	4.53	5.30	2.35	2.21	19.26	9.27
3	4.29	2.15	1.08	2.62	5.98	3.94	1.65	1.64	0.00	7.86
4	4.94	2.19	0.97	3.07	4.21	3.65	1.43	1.55	17.84	6.78
5	5.06	1.64	0.89	2.80	3.31	3.54	1.47	1.53	14.43	15.65
6	3.50	1.36	0.96	2.01	3.11	3.48	1.32	1.40	20.62	6.95
7	3.95	1.41	1.00	2.02	2.96	2.55	1.23	1.29	8.12	4.93
8	3.75	1.23	0.93	1.91	2.93	4.11	1.24	1.47	8.68	19.50
9	3.17	1.27	0.92	1.94	2.53	2.36	1.10	1.23	12.21	5.17
10	2.51	1.21	0.88	1.66	1.95	2.03	1.25	1.39	10.21	5.78
11	2.27	1.24	0.86	1.69	2.09	2.01	1.13	1.29	9.24	5.66
12	2.24	1.26	0.91	1.84	2.06	1.97	1.02	1.24	5.43	11.25
13	2.01	1.23	0.89	1.84	1.78	2.14	1.07	1.14	20.77	9.41
14	1.84	1.32	0.86	2.30	1.81	2.08	1.36	0.97	5.05	10.50
15	1.81	1.51	0.74	1.64	1.71	1.96	0.99	1.17	8.82	3.53
16	1.77	1.41	0.82	1.84	1.81	1.86	0.95	1.17	4.34	8.09
17	1.68	1.55	0.91	1.78	1.82	2.14	1.23	1.01	5.63	8.13
18	1.50	1.47	0.80	1.62	1.76	1.67	1.07	0.96	5.81	5.59
19	1.28	1.56	0.80	1.68	2.13	1.54	1.22	0.82	16.55	10.61
20	1.51	1.38	0.81	1.52	1.81	2.01	1.01	1.07	4.38	4.16
21	1.40	1.79	0.76	1.84	1.48	1.64	1.00	1.14	5.93	7.04
22	1.76	1.67	0.93	1.45	1.69	1.82	0.89	0.95	23.86	7.02
23	1.65	1.72	0.96	1.59	1.69	1.51	0.90	0.86	3.38	9.61
24	1.85	1.94	0.93	1.83	1.82	2.09	0.85	0.89	5.22	7.62
25	1.57	2.26	1.20	1.93	1.59	1.84	0.85	0.81	9.30	6.56
26	1.62	3.34	1.10	1.99	1.84	1.84	0.96	0.78	3.94	3.17
27	1.32	1.56	0.87	1.48	1.25	1.26	0.61	0.56	3.80	2.97
28	2.94	2.79	1.94	2.77	2.06	2.42	0.97	0.92	15.51	3.93
29	3.54	3.68	1.76	4.08	1.97	2.63	0.95	0.83	3.67	6.07
30	4.31	4.36	2.27	3.29	2.92	3.19	1.06	0.86	7.03	2.85
31	5.23	7.37	3.22	4.47	2.61	3.87	1.19	0.84	9.62	3.38
32	6.93	5.17	3.98	4.91	3.08	3.70	1.25	0.76	3.72	2.89
33	4.91	7.26	4.67	6.26	4.29	8.94	1.34	1.04	3.81	5.54
34	16.32	7.80	6.97	10.04	4.20	8.02	1.79	1.09	4.22	3.08
35	24.86	15.29	6.47	12.29	6.04	10.43	1.48	1.50	4.23	1.56
36	3.01	21.82	13.06	18.18	5.27	16.40	1.44	1.65	1.26	1.41
37	10.97	6.06	9.95	13.98	6.81	52.65	1.55	1.75	1.63	0.96
38	4.64	0.00	16.40	16.47	15.16	42.51	2.31	3.19	1.30	1.22
39	102.18	0.00	39.31	35.92	16.88	266.86	8.68	7.14	4.16	1.32
40	0.00	0.00	0.00	0.00	45.51	0.00	37.37	13.14	8.13	2.26
41	0.00	0.00	0.00	109.81	0.00	43.48	42.82	0.00	9.49	3.68
42	0.00	21.29	104.04	96.33	222.07	247.10	14.80	5.05	1.65	1.94
43	0.00	17.68	71.03	237.21	259.05	7.14	2.33	3.58	0.97	1.96
44	0.00	12.40	9.18	62.46	0.00	8.53	31.17	3.72	1.18	1.82
45	0.00	0.00	0.00	0.00	0.00	54.37	7.06	8.51	3.12	1.50
46	0.00	0.00	0.00	0.00	0.00	0.00	0.00	0.00	0.00	0.00
47	0.00	0.00	0.00	0.00	0.00	0.00	0.00	0.00	0.00	0.00
48	0.00	0.00	0.00	0.00	0.00	0.00	0.00	0.00	0.00	0.00
49	0.00	0.00	0.00	0.00	0.00	0.00	0.00	0.00	0.00	0.00
50	0.00	0.00	0.00	0.00	0.00	0.00	0.00	0.00	0.00	0.00

BASELINE INLET, STATION 7

CP	ET1	ET2	ET3	ET4	ET5	ET6	ET7	ET8	ET9	ET10-% TANG ERROR
1	0.00	0.00	0.00	0.00	0.00	0.00	0.00	0.00	0.00	0.00
2	0.00	3.87	0.00	0.00	0.00	0.00	0.00	0.00	0.00	0.00
3	4.14	2.04	3.96	9.79	3.44	4.83	6.45	13.12	5.73	0.00
4	3.69	1.78	3.22	7.21	3.75	5.06	3.05	13.16	4.49	7.70
5	2.57	1.32	2.54	6.35	2.85	3.83	2.91	10.96	4.46	7.74
6	2.56	1.01	2.40	5.86	2.68	3.35	3.33	10.11	4.77	5.94
7	2.07	0.81	2.13	5.99	2.44	2.32	2.57	5.24	3.88	5.98
8	1.91	0.81	2.10	5.31	1.92	2.26	2.40	4.35	3.49	6.29
9	1.52	0.87	2.17	4.84	1.50	2.10	2.35	4.08	2.19	6.03
10	1.50	0.76	2.34	4.16	1.72	1.85	2.08	3.45	2.22	3.85
11	1.34	0.79	2.16	4.13	1.74	1.70	1.82	4.58	2.23	3.68
12	1.17	0.77	2.08	4.49	1.47	2.00	1.97	3.21	1.85	7.59
13	1.24	0.76	2.05	5.23	1.40	1.49	1.49	2.83	1.75	4.41
14	1.09	0.75	1.97	4.92	1.26	1.33	1.78	2.45	1.58	4.42
15	1.14	0.66	2.07	4.53	1.30	1.32	1.37	2.74	1.85	4.53
16	1.05	0.78	1.84	3.71	1.32	1.56	1.41	4.60	1.46	4.35
17	1.15	0.69	2.15	4.24	1.18	1.28	1.29	2.83	1.76	6.12
18	1.16	0.75	2.01	3.81	1.30	1.17	1.27	2.81	1.56	2.77
19	0.94	0.72	2.08	4.22	1.20	1.31	1.27	3.15	1.39	3.64
20	0.59	0.47	1.26	2.90	0.79	0.75	0.87	1.67	0.78	2.07
21	0.88	0.74	1.84	5.02	1.09	1.18	1.13	2.23	1.42	3.54
22	0.95	0.80	2.01	3.37	1.06	1.08	1.44	2.71	1.29	5.26
23	0.86	0.79	1.65	3.93	1.14	1.17	1.12	2.31	1.33	4.37
24	0.95	0.81	2.06	4.48	0.98	1.06	1.39	2.48	1.21	4.54
25	0.90	0.73	2.15	4.38	1.00	1.08	1.10	2.13	1.28	5.21
26	0.97	0.77	1.93	4.47	1.11	1.15	0.97	2.23	1.35	4.38
27	0.87	0.68	1.94	4.01	1.00	1.12	1.12	2.19	1.08	5.09
28	1.10	0.69	1.92	3.48	0.93	0.93	0.98	2.33	1.18	5.09
29	1.06	0.83	1.75	3.61	1.11	0.95	1.09	2.08	1.29	3.06
30	1.21	0.81	2.06	3.94	1.00	1.04	1.05	2.24	1.24	3.62
31	1.12	0.90	1.87	3.87	0.92	1.03	0.83	1.74	1.07	4.18
32	1.40	1.02	2.02	3.77	1.02	1.07	1.00	1.88	1.16	2.57
33	1.45	1.14	2.10	3.72	1.03	0.91	1.01	2.27	1.18	3.87
34	2.00	1.30	2.62	5.84	0.92	0.94	1.07	2.04	1.20	2.99
35	2.23	1.56	2.21	5.63	1.07	1.07	0.96	2.38	1.07	3.06
36	2.40	1.75	3.07	5.20	1.28	1.35	0.93	1.94	1.03	2.47
37	2.88	2.04	2.72	5.97	1.41	1.15	0.96	1.92	1.04	2.58
38	2.65	2.65	3.11	5.69	1.92	1.53	1.19	1.71	1.21	2.30
39	4.31	3.22	4.29	10.21	1.99	1.71	1.06	1.95	0.73	2.21
40	7.03	3.45	3.14	5.57	2.44	2.21	1.46	2.47	0.71	2.03
41	7.98	5.17	4.45	5.85	3.61	2.59	1.89	2.58	0.70	1.47
42	2.13	11.02	9.35	8.72	4.96	3.60	2.28	4.03	0.79	1.62
43	11.59	18.80	14.48	16.13	8.54	4.84	4.70	7.03	1.88	1.21
44	2.71	24.61	30.30	75.32	17.52	17.22	9.53	15.02	2.58	2.54
45	0.87	33.85	0.00	0.00	115.07	17.66	19.80	23.26	5.88	6.51
46	3.01	48.24	154.31	0.00	18.17	21.84	23.97	38.85	9.39	9.24
47	28.37	23.50	0.00	49.37	10.35	39.34	17.21	34.22	8.02	11.11
48	6.74	15.57	20.75	53.38	17.50	15.13	23.33	22.51	8.25	10.72
49	0.00	0.00	0.00	0.00	7.00	10.43	14.76	35.40	8.39	11.48
50	0.00	0.00	0.00	0.00	0.00	0.00	0.00	0.00	0.00	8.68

BASELINE INLET, STATION 8

CP	ET1	ET2	ET3	ET4	ET5	ET6	ET7	ET8	ET9	ET10-% TANG ERROR
1	2.42	19.79	19.57	14.80	14.08	23.54	14.70	10.15	12.79	4.53
2	5.70	25.46	21.22	19.35	20.22	16.48	9.65	8.41	8.81	4.46
3	17.12	45.85	12.42	9.54	19.23	9.21	6.91	6.44	5.86	3.67
4	0.00	0.00	15.00	7.14	15.18	7.55	10.31	6.98	5.83	4.45
5	0.00	10.64	8.35	7.20	11.94	8.98	6.50	5.50	4.25	3.94
6	25.28	80.04	4.83	4.34	14.11	7.21	4.30	5.22	4.65	3.25
7	41.60	18.58	3.92	3.81	4.75	4.71	3.90	3.04	3.49	2.94
8	0.00	12.22	3.13	3.13	6.33	4.05	4.20	2.95	3.55	2.71
9	0.00	37.08	2.73	2.46	4.09	4.89	3.21	2.86	3.96	2.67
10	0.00	23.14	1.96	2.97	4.23	3.55	2.77	2.24	3.33	2.65
11	0.00	5.92	2.23	2.01	4.18	2.88	3.01	2.27	2.64	3.30
12	0.00	3.32	1.85	2.24	3.42	2.02	2.37	2.27	1.73	2.33
13	0.00	5.41	1.67	1.73	2.39	2.08	1.84	2.02	2.05	2.82
14	0.00	7.23	1.66	1.45	2.10	1.99	1.77	1.97	2.04	2.52
15	0.00	5.28	1.85	1.51	1.98	1.76	1.79	1.64	2.31	2.83
16	0.00	10.90	1.61	1.35	1.79	1.87	1.63	1.56	2.17	2.07
17	0.00	4.15	1.65	1.79	2.37	1.71	1.34	1.49	1.57	3.16
18	0.00	2.45	1.04	0.96	0.99	1.04	1.09	0.96	1.04	1.54
19	0.00	4.79	1.67	1.86	1.57	1.47	1.65	1.45	1.83	2.30
20	0.00	2.94	2.05	1.77	1.78	1.44	1.42	1.69	1.47	2.95
21	0.00	3.99	1.93	1.64	1.52	1.68	1.47	1.23	1.76	2.10
22	0.00	3.64	1.61	1.47	1.55	1.49	1.33	1.47	1.51	3.13
23	0.00	3.63	1.77	1.51	1.41	1.10	1.24	1.46	1.83	2.42
24	0.00	4.88	1.64	1.65	1.61	1.41	1.43	1.65	1.41	2.01
25	0.00	4.34	1.54	1.39	1.82	1.32	1.32	1.21	1.37	2.83
26	0.00	3.43	1.72	1.32	1.50	1.31	1.17	1.14	1.35	1.97
27	0.00	3.13	1.69	1.66	1.73	1.24	1.15	1.18	1.28	1.93
28	0.00	4.60	1.57	1.41	1.40	1.26	1.49	1.21	1.25	2.13
29	0.00	4.46	1.58	1.50	1.40	1.16	1.08	1.22	1.42	1.93
30	0.00	4.15	1.66	1.32	1.37	1.32	1.32	1.46	1.34	2.66
31	0.00	4.30	1.42	1.23	1.60	1.26	1.15	1.41	1.42	1.64
32	0.00	6.88	1.56	1.32	1.46	1.24	1.11	1.05	1.64	1.94
33	0.00	4.65	1.57	1.37	1.30	1.08	1.11	1.10	1.46	1.92
34	0.00	5.20	1.45	1.22	1.42	1.23	1.25	0.95	1.60	1.71
35	118.58	4.93	1.52	1.48	1.30	1.13	1.06	1.19	1.24	2.19
36	19.04	3.86	1.54	1.24	1.52	1.03	1.07	1.04	1.48	1.59
37	6.44	3.59	1.47	1.29	1.39	1.06	1.04	0.99	1.21	1.42
38	3.53	4.63	1.62	1.19	1.26	1.01	1.24	1.18	1.46	1.45
39	3.99	3.82	1.47	1.22	1.20	1.07	0.95	1.22	1.16	1.39
40	2.18	4.37	1.42	1.23	1.10	0.95	0.94	0.97	1.23	1.25
41	0.50	3.06	1.13	1.18	0.90	0.83	1.21	1.00	0.94	1.19
42	1.65	2.55	0.87	0.97	1.04	0.92	0.88	0.85	0.90	0.93
43	1.54	1.99	0.62	0.70	0.75	0.66	0.64	0.79	0.74	0.82
44	1.04	1.62	0.58	0.75	0.54	0.58	0.59	0.60	0.52	0.72
45	0.25	1.96	0.96	0.80	0.54	0.52	0.55	0.52	0.47	0.57
46	0.18	0.92	2.70	1.52	0.89	0.73	0.60	0.58	0.46	0.52
47	0.19	1.41	6.86	4.72	2.26	1.28	1.28	0.92	0.72	0.61
48	0.51	4.66	34.27	13.48	10.43	3.66	3.87	3.07	1.47	1.13
49	1.11	37.74	126.28	26.77	14.38	9.52	11.18	4.78	3.75	1.97
50	4.81	235.42	124.62	17.47	37.51	32.66	23.46	10.09	4.52	3.21

ENHANCED INLET, STATION 1

CP	ET1	ET2	ET3	ET4	ET5	ET6	ET7	ET8	ET9	ET10-% TANG ERROR
1	0.22	0.24	0.18	0.14	0.19	0.14	0.15	0.15	0.15	0.65
2	0.18	0.18	0.25	0.15	0.19	0.18	0.14	0.13	0.14	0.62
3	0.24	0.17	0.17	0.20	0.20	0.18	0.17	0.17	0.23	0.21
4	0.32	0.23	0.18	0.17	0.13	0.20	0.22	0.10	0.20	0.34
5	0.38	0.21	0.16	0.17	0.24	0.20	0.18	0.13	0.19	0.49
6	0.14	0.19	0.16	0.18	0.18	0.17	0.17	0.15	0.18	0.30
7	0.17	0.19	0.19	0.19	0.17	0.20	0.15	0.12	0.22	0.44
8	0.15	0.20	0.19	0.19	0.19	0.19	0.18	0.13	0.20	0.47
9	0.21	0.15	0.24	0.16	0.17	0.23	0.15	0.17	0.16	0.45
10	0.18	0.22	0.21	0.22	0.21	0.23	0.15	0.14	0.16	0.40
11	0.33	0.17	0.20	0.19	0.22	0.17	0.20	0.13	0.23	0.26
12	0.12	0.20	0.19	0.24	0.21	0.20	0.20	0.15	0.16	0.31
13	0.28	0.17	0.17	0.17	0.21	0.21	0.21	0.15	0.19	0.37
14	0.12	0.21	0.26	0.18	0.22	0.22	0.18	0.15	0.16	0.46
15	0.20	0.19	0.24	0.21	0.23	0.19	0.18	0.13	0.17	0.73
16	0.12	0.22	0.18	0.18	0.18	0.18	0.19	0.15	0.17	0.67
17	0.21	0.19	0.27	0.22	0.20	0.27	0.20	0.17	0.22	0.61
18	0.17	0.19	0.20	0.22	0.23	0.20	0.21	0.15	0.18	0.68
19	0.16	0.20	0.22	0.20	0.22	0.22	0.17	0.15	0.19	0.29
20	0.37	0.25	0.22	0.18	0.22	0.24	0.23	0.17	0.20	0.41
21	0.20	0.20	0.21	0.23	0.26	0.21	0.16	0.14	0.19	0.43
22	0.21	0.17	0.19	0.19	0.19	0.18	0.18	0.17	0.17	0.36
23	0.14	0.19	0.23	0.16	0.21	0.21	0.22	0.14	0.18	0.36
24	0.24	0.20	0.19	0.14	0.22	0.20	0.15	0.16	0.17	0.37
25	0.22	0.16	0.21	0.26	0.21	0.21	0.15	0.12	0.17	0.41
26	0.25	0.20	0.24	0.11	0.19	0.22	0.23	0.16	0.15	0.29
27	0.31	0.18	0.19	0.15	0.22	0.17	0.19	0.14	0.19	0.65
28	0.16	0.19	0.22	0.18	0.19	0.19	0.19	0.11	0.14	0.38
29	0.24	0.22	0.15	0.17	0.21	0.19	0.21	0.13	0.15	0.57
30	0.28	0.17	0.16	0.15	0.19	0.18	0.16	0.15	0.17	0.31
31	0.21	0.16	0.16	0.18	0.20	0.17	0.16	0.13	0.14	0.29
32	0.11	0.17	0.17	0.21	0.20	0.17	0.18	0.14	0.19	0.46
33	0.17	0.19	0.17	0.19	0.23	0.18	0.17	0.12	0.18	0.55
34	0.16	0.18	0.14	0.18	0.17	0.24	0.15	0.12	0.14	0.40
35	0.23	0.15	0.16	0.15	0.22	0.19	0.16	0.09	0.13	0.38
36	0.23	0.19	0.20	0.14	0.25	0.19	0.20	0.13	0.12	0.35
37	0.19	0.16	0.20	0.15	0.19	0.19	0.11	0.16	0.14	0.28
38	0.18	0.18	0.13	0.12	0.26	0.18	0.14	0.11	0.16	0.46
39	0.17	0.15	0.14	0.18	0.17	0.17	0.14	0.13	0.16	0.25
40	0.23	0.24	0.12	0.17	0.18	0.16	0.16	0.11	0.14	0.21
41	0.13	0.20	0.17	0.21	0.20	0.19	0.16	0.12	0.15	0.11
42	0.20	0.25	0.16	0.12	0.20	0.17	0.12	0.08	0.10	0.55
43	0.13	0.20	0.11	0.14	0.22	0.19	0.16	0.12	0.15	0.21
44	0.18	0.18	0.18	0.15	0.18	0.14	0.10	0.12	0.17	0.26
45	0.15	0.19	0.12	0.14	0.16	0.15	0.16	0.09	0.14	0.61
46	0.17	0.19	0.19	0.19	0.12	0.15	0.16	0.10	0.10	0.23
47	0.18	0.16	0.14	0.16	0.15	0.19	0.15	0.11	0.13	0.26
48	0.15	0.16	0.12	0.16	0.19	0.13	0.12	0.13	0.16	0.45
49	0.20	0.15	0.21	0.13	0.18	0.19	0.12	0.11	0.16	0.40
50	0.20	0.12	0.15	0.14	0.13	0.15	0.07	0.09	0.09	0.64

ENHANCED INLET, STATION 2

CP	ET1	ET2	ET3	ET4	ET5	ET6	ET7	ET8	ET9	ET10-% TANG ERROR
1	0.24	0.27	0.53	1.09	1.34	1.37	1.41	1.78	1.88	4.20
2	0.44	0.31	0.26	1.02	1.18	1.33	1.49	1.80	1.90	4.94
3	0.78	0.43	0.05	0.19	0.27	0.44	0.69	1.47	1.60	4.97
4	0.53	0.58	0.15	0.57	0.67	0.39	0.11	0.26	1.77	9.41
5	0.60	0.70	0.26	0.59	0.80	0.72	0.63	0.64	0.05	5.50
6	0.74	0.78	0.44	0.84	1.24	1.11	0.99	0.85	1.42	2.68
7	0.48	0.73	0.46	0.80	1.23	1.32	1.42	1.15	1.06	3.74
8	0.48	0.70	0.45	1.05	0.92	1.06	1.25	1.12	1.94	6.12
9	0.49	0.72	0.63	0.91	1.17	1.15	1.12	1.24	1.28	3.89
10	0.35	0.61	0.32	1.08	1.28	1.22	1.15	1.43	1.74	3.77
11	0.49	0.59	0.48	0.91	1.10	1.08	1.06	1.29	1.56	3.98
12	0.45	0.45	0.59	0.90	1.20	1.05	0.93	0.99	1.33	8.16
13	0.22	0.46	0.57	1.01	0.94	0.93	0.92	1.14	1.40	4.48
14	0.37	0.34	0.46	1.06	0.74	0.77	0.80	1.09	1.31	9.67
15	0.13	0.39	0.40	1.01	0.65	0.59	0.55	0.96	1.61	5.86
16	0.09	0.31	0.40	0.57	0.65	0.66	0.67	0.89	1.35	5.41
17	0.05	0.13	0.26	0.87	0.60	0.61	0.62	0.76	0.98	3.86
18	0.05	0.23	0.27	0.65	0.45	0.52	0.60	0.60	1.18	3.34
19	0.05	0.22	0.24	0.61	0.44	0.44	0.43	0.50	1.37	4.74
20	0.06	0.26	0.14	0.47	0.38	0.39	0.40	0.42	0.70	6.21
21	0.12	0.24	0.12	0.44	0.29	0.30	0.31	0.44	0.53	2.57
22	0.11	0.25	0.08	0.33	0.26	0.27	0.28	0.38	0.66	5.36
23	0.15	0.22	0.05	0.24	0.12	0.16	0.21	0.25	0.29	3.01
24	0.20	0.21	0.05	0.18	0.07	0.09	0.12	0.23	0.30	2.65
25	0.18	0.26	0.07	0.15	0.08	0.06	0.05	0.89	0.19	3.08
26	0.19	0.31	0.10	0.09	0.11	0.06	0.01	0.06	0.07	2.12
27	0.22	0.24	0.14	0.10	0.17	0.10	0.03	0.02	0.10	2.39
28	0.24	0.30	0.14	0.17	0.19	0.15	0.10	0.09	0.21	4.59
29	0.27	0.35	0.22	0.17	0.17	0.16	0.16	0.16	0.34	1.99
30	0.29	0.35	0.18	0.22	0.28	0.28	0.28	0.19	0.32	3.90
31	0.33	0.31	0.23	0.31	0.34	0.31	0.27	0.29	0.37	2.77
32	0.20	0.24	0.22	0.22	0.27	0.24	0.20	0.21	0.30	2.24
33	0.35	0.37	0.39	0.33	0.39	0.36	0.33	0.50	0.49	3.26
34	0.39	0.34	0.32	0.46	0.41	0.36	0.32	0.42	0.58	4.91
35	0.41	0.46	0.35	0.45	0.53	0.55	0.59	0.44	0.51	2.30
36	0.48	0.48	0.45	0.48	0.51	0.45	0.40	0.51	0.57	2.99
37	0.41	0.43	0.44	0.53	0.60	0.49	0.40	0.55	0.62	3.75
38	0.50	0.45	0.56	0.67	0.73	0.69	0.66	0.63	0.76	2.33
39	0.50	0.49	0.38	0.50	0.74	0.70	0.68	0.63	0.83	2.64
40	0.43	0.42	0.40	0.76	0.72	0.71	0.70	0.81	0.81	3.09
41	0.49	0.43	0.51	0.75	0.84	0.79	0.74	0.62	0.76	3.31
42	0.55	0.47	0.51	0.80	0.89	0.81	0.74	0.77	0.85	5.52
43	0.55	0.55	0.50	0.89	0.76	0.94	1.26	0.70	0.91	3.16
44	0.42	0.57	0.60	0.93	0.86	0.85	0.84	0.96	1.26	3.80
45	0.49	0.42	0.50	0.97	1.12	1.07	1.01	1.00	1.26	7.40
46	0.50	0.55	0.62	0.97	0.98	0.93	0.89	0.87	1.30	4.13
47	0.48	0.58	0.76	1.23	0.92	0.97	1.02	1.10	1.27	4.16
48	0.46	0.50	0.67	1.11	1.03	1.12	1.23	1.11	1.34	4.10
49	0.37	0.45	0.57	0.96	1.30	1.34	1.38	1.05	1.74	4.13
50	0.11	0.31	0.59	1.31	1.13	1.21	1.32	1.26	1.21	4.14

ENHANCED INLET, STATION 3

CP	ET1	ET2	ET3	ET4	ET5	ET6	ET7	ET8	ET9	ET10-% TANG ERROR
1	0.00	0.00	0.00	0.00	0.00	0.00	0.00	0.00	0.00	37.35
2	0.00	0.00	0.00	0.00	0.00	0.00	0.00	0.00	0.00	0.00
3	0.00	2.98	0.00	0.00	0.00	0.00	32.78	0.00	0.00	0.00
4	0.00	0.00	0.00	1.36	6.80	8.18	30.75	71.57	0.00	0.00
5	0.00	0.00	0.00	0.00	0.00	0.00	0.00	1.09	2.05	0.50
6	0.00	0.00	0.00	0.00	0.00	0.00	0.00	0.00	0.00	1.33
7	0.00	0.00	0.00	0.00	0.00	0.00	0.00	0.00	0.00	0.00
8	0.00	0.00	0.00	0.00	35.08	38.88	11.90	0.00	0.00	0.00
9	4.30	27.66	321.77	0.00	23.76	23.88	6.09	13.80	38.32	0.00
10	2.73	44.96	35.40	4.22	2.25	0.93	3.90	5.62	27.24	0.00
11	1.17	5.66	27.63	6.66	2.25	3.14	1.71	2.36	6.61	100.87
12	1.47	5.83	5.05	11.73	1.44	1.77	1.49	0.84	1.04	0.00
13	1.05	3.30	4.52	2.79	2.30	1.92	0.75	0.70	1.08	0.00
14	1.36	2.80	2.82	5.60	1.20	1.15	0.76	0.52	0.70	79.20
15	0.92	2.03	2.82	4.24	1.13	0.67	0.57	0.52	0.58	0.00
16	1.42	1.95	3.22	6.08	0.70	0.75	0.39	0.46	0.69	1.26
17	1.06	2.20	2.64	1.71	0.59	0.30	0.26	0.36	0.59	2.94
18	1.20	3.68	2.20	2.02	0.46	0.25	0.27	0.27	0.40	1.05
19	1.18	1.24	1.61	2.55	0.46	0.10	0.20	0.21	0.25	2.96
20	2.37	1.24	1.19	1.20	0.39	0.07	0.06	0.06	0.27	0.00
21	0.98	2.17	1.10	1.20	0.18	0.07	0.20	0.01	0.14	58.99
22	1.39	1.77	0.99	1.07	0.14	0.08	0.20	0.11	0.11	19.01
23	1.12	1.95	0.82	1.89	0.08	0.20	0.20	0.08	0.13	139.82
24	1.21	1.70	0.96	0.84	0.04	0.23	0.27	0.20	0.16	137.07
25	2.33	1.32	1.10	0.65	0.11	0.26	0.30	0.29	0.23	32.00
26	0.98	2.77	1.37	0.89	0.09	0.36	0.29	0.29	0.26	35.65
27	1.54	2.11	1.18	0.54	0.13	0.32	0.35	0.39	0.32	20.87
28	0.83	1.65	0.60	0.32	0.14	0.22	0.22	0.28	0.20	36.96
29	1.32	2.06	0.84	0.73	0.21	0.41	0.48	0.40	0.34	0.00
30	1.47	5.20	0.87	0.89	0.26	0.46	0.47	0.46	0.38	1.39
31	1.07	3.98	1.86	0.67	0.31	0.48	0.54	0.44	0.45	0.00
32	1.54	3.07	1.11	0.63	0.29	0.47	0.58	0.55	0.47	0.00
33	0.92	3.43	1.15	0.85	0.34	0.52	0.68	0.56	0.56	0.00
34	1.16	4.55	1.38	1.49	0.37	0.64	0.58	0.69	0.59	1.70
35	1.49	4.45	1.17	1.35	0.49	0.65	0.61	0.64	0.64	0.00
36	2.32	4.21	1.53	1.82	0.42	0.71	0.78	0.56	0.52	3.67
37	2.05	3.89	2.00	1.79	0.52	0.77	0.72	0.82	0.53	102.16
38	1.64	4.29	1.65	2.12	0.56	0.63	0.86	0.73	0.62	12.53
39	1.43	5.69	2.26	1.78	0.55	0.90	0.88	0.78	0.74	0.00
40	1.52	5.88	2.79	2.27	0.68	0.89	1.02	0.98	0.89	105.88
41	3.46	5.29	2.14	4.31	0.77	0.82	0.89	0.89	0.75	64.73
42	2.49	8.56	4.46	5.44	0.98	0.88	1.05	1.29	0.91	26.92
43	2.14	8.45	3.28	4.61	0.85	0.96	1.24	1.03	0.83	33.18
44	2.83	6.88	3.15	6.92	0.93	1.20	1.14	1.25	0.84	23.23
45	7.93	8.23	2.77	8.11	1.38	1.37	1.46	1.12	0.97	22.96
46	4.06	0.00	4.68	13.41	1.35	1.31	1.50	1.43	1.28	13.19
47	41.37	0.00	13.01	8.46	1.66	1.50	1.23	1.56	1.23	45.27
48	0.00	0.00	23.45	99.30	2.68	1.51	1.93	2.25	1.43	53.01
49	0.00	0.00	0.00	0.00	39.35	4.52	1.84	2.30	1.60	13.84
50	0.00	0.00	0.00	0.00	0.00	158.64	9.93	5.97	7.07	12.56

ENHANCED INLET, STATION 4

CP	ET1	ET2	ET3	ET4	ET5	ET6	ET7	ET8	ET9	ET10-% TANG ERROR
1	0.00	0.00	0.00	0.00	0.00	6.27	3.10	6.04	15.62	0.00
2	0.00	0.00	0.00	0.00	102.45	2.88	1.26	3.41	11.35	96.16
3	0.00	0.00	0.00	236.97	0.00	1.40	1.34	1.95	5.79	0.00
4	0.00	23.27	57.92	0.00	8.95	0.82	0.89	0.87	6.58	0.00
5	0.00	2.55	85.26	20.99	3.71	0.82	0.76	0.69	4.10	19.19
6	0.00	0.23	0.00	7.75	1.11	0.48	0.42	0.70	2.05	0.00
7	62.13	0.17	7.23	3.70	0.87	0.79	0.70	0.81	3.41	60.74
8	0.00	0.16	3.22	1.93	1.78	0.74	0.78	0.89	2.49	22.36
9	0.00	0.25	3.22	1.56	1.55	0.71	0.76	0.64	2.35	10.36
10	0.00	1.05	2.02	1.06	1.51	0.73	0.86	0.70	1.66	16.21
11	0.00	4.94	1.44	1.07	1.70	0.77	0.86	0.85	1.84	11.10
12	29.85	6.41	1.33	0.69	1.39	0.73	0.81	0.92	1.82	14.29
13	15.80	9.44	1.27	0.76	1.51	0.71	0.80	0.83	1.93	17.69
14	54.97	2.11	1.27	0.62	1.18	0.66	0.71	0.80	1.30	21.94
15	9.59	3.42	1.11	0.73	1.38	0.88	0.74	0.74	1.28	9.32
16	50.45	4.29	1.36	0.68	1.43	1.10	0.72	0.94	1.36	9.36
17	9.55	6.77	1.14	0.66	1.13	0.77	0.80	0.84	1.19	33.53
18	7.60	4.43	1.09	0.62	1.19	0.82	0.85	0.88	1.45	14.56
19	7.88	3.37	0.92	0.70	1.27	0.92	0.93	0.99	1.30	16.33
20	9.35	2.80	0.92	0.74	1.39	0.97	0.87	0.98	1.10	14.64
21	11.88	2.93	0.77	0.79	1.15	1.03	0.88	0.99	1.42	24.92
22	7.64	4.90	0.84	0.81	1.16	1.11	0.96	1.13	1.39	17.74
23	12.86	3.38	0.82	0.74	1.15	1.00	1.25	0.92	1.47	71.82
24	9.67	4.34	0.74	0.84	1.20	1.02	1.12	1.48	1.54	7.48
25	16.27	3.70	0.65	0.77	1.10	0.93	1.02	1.00	1.48	19.27
26	9.33	3.27	0.78	0.87	1.24	0.94	1.05	1.35	1.26	21.33
27	15.49	3.23	0.69	0.90	1.32	1.50	1.07	1.11	1.28	29.25
28	11.25	3.35	0.84	1.04	1.50	1.27	1.08	1.10	1.50	23.49
29	16.31	5.63	0.93	0.97	1.27	1.67	1.25	1.04	1.29	69.65
30	12.73	4.87	0.79	1.20	1.26	1.48	1.28	1.02	1.50	10.47
31	0.00	8.20	0.78	1.66	1.27	1.50	1.67	1.00	1.07	35.49
32	7.46	11.29	0.96	3.36	1.27	1.70	1.44	0.95	1.19	13.99
33	0.00	22.04	1.33	63.32	1.31	1.87	2.16	1.28	1.03	13.82
34	0.00	3.00	5.26	0.00	1.27	3.35	1.92	1.26	0.90	8.81
35	29.77	2.83	147.20	0.00	1.44	24.73	1.97	1.65	1.11	24.61
36	31.63	6.89	0.00	0.00	2.74	0.00	2.37	1.71	1.18	9.31
37	72.59	20.21	0.00	0.00	0.00	0.00	5.74	2.02	1.40	8.17
38	9.94	2.18	0.00	0.00	0.00	0.00	0.00	2.82	2.20	35.64
39	146.17	9.70	0.00	0.00	0.00	0.00	0.00	6.52	2.53	11.08
40	0.00	66.27	0.00	0.00	0.00	0.00	0.00	51.00	3.15	35.15
41	0.00	92.40	0.00	0.00	0.00	0.00	0.00	0.00	4.15	0.00
42	0.00	0.00	0.00	0.00	0.00	0.00	0.00	0.00	7.72	0.00
43	0.00	0.00	0.00	0.00	0.00	0.00	0.00	0.00	0.00	0.00
44	0.00	0.00	0.00	0.00	0.00	0.00	0.00	0.00	0.00	0.00
45	0.00	0.00	0.00	0.00	0.00	0.00	0.00	0.00	0.00	0.00
46	0.00	0.00	0.00	0.00	0.00	0.00	0.00	0.00	0.00	0.00
47	0.00	0.00	0.00	0.00	0.00	0.00	0.00	0.00	0.00	0.00
48	0.00	0.00	0.00	0.00	0.00	0.00	0.00	0.00	0.00	0.00
49	0.00	0.00	0.00	0.00	0.00	0.00	0.00	0.00	0.00	0.00
50	0.00	0.00	0.00	0.00	0.00	0.00	0.00	0.00	0.00	0.00

ENHANCED INLET, STATION 5

CP	ET1	ET2	ET3	ET4	ET5	ET6	ET7	ET8	ET9	ET10-% TANG ERROR
1	0.00	0.00	0.00	0.00	0.00	0.00	7.75	5.22	8.84	2.63
2	0.00	0.00	0.00	0.00	12.86	3.92	2.95	4.38	6.78	1.84
3	0.00	0.00	0.00	27.13	13.57	3.23	3.63	3.00	6.50	9.93
4	0.00	0.00	179.56	6.26	7.12	2.09	1.68	2.99	4.23	2.54
5	41.13	0.00	147.03	5.67	12.01	2.43	2.10	1.98	4.29	3.39
6	125.62	0.00	17.84	4.38	15.00	1.85	1.88	2.19	3.20	1.46
7	48.98	0.00	7.91	4.19	5.94	1.76	1.64	2.50	4.38	2.64
8	53.41	0.00	6.56	3.02	4.43	1.65	1.96	1.67	4.39	1.44
9	56.46	0.00	6.50	2.11	6.38	1.52	1.26	2.12	2.50	1.62
10	0.00	0.00	6.08	2.00	3.76	1.34	1.60	1.69	2.67	1.99
11	123.79	0.00	5.29	1.63	2.94	1.50	1.99	1.45	2.83	0.83
12	0.00	0.00	3.10	1.23	3.33	1.36	1.81	1.75	2.17	2.58
13	134.46	21.72	3.36	1.16	2.36	1.46	1.43	1.53	2.91	1.55
14	70.80	0.00	2.89	1.06	2.38	1.59	1.22	1.26	2.20	1.95
15	168.89	42.03	2.44	1.06	3.52	1.44	1.31	1.63	2.16	2.77
16	136.41	88.01	2.85	0.97	3.08	1.53	1.19	1.28	2.59	1.28
17	49.57	53.55	3.14	1.07	2.71	1.54	1.21	1.36	1.82	1.43
18	26.30	27.03	2.25	0.97	2.40	1.37	1.17	1.44	2.10	1.61
19	25.77	22.93	1.97	0.98	3.12	1.45	1.10	1.41	1.81	1.55
20	20.05	17.76	1.91	1.03	3.17	1.28	1.11	1.10	1.54	1.18
21	16.08	17.59	2.11	1.11	2.38	1.26	1.19	1.35	1.87	1.53
22	11.82	26.38	1.95	1.11	2.34	1.27	1.28	1.19	1.67	0.93
23	15.11	17.53	1.55	1.35	2.04	1.30	1.06	1.35	1.64	0.98
24	13.14	10.72	1.52	1.32	2.29	1.31	1.26	1.17	2.00	1.40
25	10.64	33.69	1.64	1.53	2.51	1.38	1.28	1.07	1.40	1.01
26	16.88	26.99	1.48	1.49	2.63	1.47	1.26	1.25	1.54	1.15
27	13.76	14.68	1.69	1.39	2.25	1.71	0.86	1.17	1.31	1.26
28	7.14	10.42	1.37	1.79	2.47	1.94	1.00	0.97	1.22	1.02
29	28.42	18.90	1.44	1.95	2.46	3.06	1.10	1.11	1.25	0.91
30	9.18	21.50	1.41	2.08	3.52	2.69	1.27	0.99	1.27	1.04
31	9.31	24.91	1.22	1.69	2.68	2.78	1.14	1.20	1.32	0.95
32	15.87	22.55	1.68	1.94	3.24	2.84	1.40	0.90	1.29	1.01
33	7.74	20.98	1.32	1.79	3.41	3.18	1.54	1.11	1.46	0.80
34	10.03	20.88	1.42	4.70	3.87	3.47	1.81	1.17	1.55	0.72
35	5.13	21.18	1.34	19.85	3.62	4.38	2.13	1.46	1.94	0.80
36	10.82	14.10	1.35	0.00	2.85	8.31	2.49	2.12	2.42	0.69
37	3.00	34.67	1.98	0.00	4.31	97.23	2.95	2.28	3.23	0.58
38	2.51	0.00	5.20	0.00	8.34	0.00	2.77	2.68	5.56	0.48
39	0.48	126.93	0.98	0.00	14.21	0.00	7.56	3.76	14.04	0.44
40	19.52	138.68	0.05	0.00	47.52	0.00	2.08	1.35	13.21	0.55
41	0.00	0.00	0.00	0.00	0.00	0.00	14.20	5.71	19.14	2.34
42	0.00	0.00	0.00	0.00	0.00	0.00	0.00	0.00	25.06	21.12
43	0.00	0.00	0.00	0.00	0.00	0.00	0.00	0.00	56.13	0.00
44	0.00	0.00	0.00	0.00	0.00	0.00	0.00	0.00	0.00	0.00
45	0.00	0.00	0.00	0.00	0.00	0.00	0.00	0.00	0.00	0.00
46	0.00	0.00	0.00	0.00	0.00	0.00	0.00	0.00	0.00	0.00
47	0.00	0.00	0.00	0.00	0.00	0.00	0.00	0.00	0.00	0.00
48	0.00	0.00	0.00	0.00	0.00	0.00	0.00	0.00	0.00	0.00
49	0.00	0.00	0.00	0.00	0.00	0.00	0.00	0.00	0.00	0.00
50	0.00	0.00	0.00	0.00	0.00	0.00	0.00	0.00	0.00	0.00

ENHANCED INLET, STATION 6

CP	ET1	ET2	ET3	ET4	ET5	ET6	ET7	ET8	ET9	ET10-% TANG ERROR
1	0.00	0.00	0.00	0.00	0.00	0.00	0.00	0.00	0.00	
2	0.00	0.00	0.00	39.81	20.80	12.35	3.16	2.02	4.18	
3	47.29	0.00	0.00	114.54	14.98	13.20	2.17	1.81	4.79	
4	21.14	28.06	191.09	49.95	17.15	7.76	1.74	1.68	3.64	
5	16.54	43.87	21.55	59.64	7.43	5.70	1.54	1.36	4.26	
6	28.10	18.98	21.03	35.79	8.37	4.20	1.33	1.24	3.32	
7	119.31	30.80	17.50	23.63	4.67	3.07	1.17	1.43	3.17	
8	32.50	15.96	19.22	12.00	4.66	2.71	1.14	1.18	4.74	
9	53.42	9.74	8.80	12.97	3.05	3.06	1.00	1.23	3.09	
10	39.25	20.95	4.81	6.98	2.34	1.84	0.98	0.93	2.72	
11	24.23	8.38	6.77	5.97	2.09	2.23	1.02	1.16	2.83	
12	42.21	11.91	3.99	4.68	1.69	1.96	0.92	1.11	2.46	
13	28.48	9.24	3.63	3.65	1.53	2.03	0.93	1.02	2.47	
14	15.62	10.89	3.24	2.92	1.61	1.82	0.86	1.06	2.81	
15	26.43	6.01	3.08	3.30	1.23	1.73	0.86	1.05	1.88	
16	15.41	6.66	4.45	2.59	1.28	1.84	0.77	0.98	2.64	
17	10.82	9.07	2.87	3.44	1.25	1.84	0.93	0.94	1.95	
18	18.08	7.12	3.36	2.90	1.36	1.87	0.84	1.00	2.10	
19	7.41	6.48	3.41	3.37	1.27	1.63	0.90	1.07	1.70	
20	11.84	8.74	2.90	2.62	1.22	1.48	0.83	1.01	2.10	
21	20.19	9.03	3.24	2.77	1.21	1.69	0.74	0.75	2.13	
22	12.53	6.39	2.39	2.55	1.02	1.63	0.81	0.84	1.67	
23	10.30	8.16	2.64	2.69	1.19	1.53	0.78	0.96	2.08	
24	10.43	5.96	3.15	2.48	1.19	1.66	0.71	0.82	1.96	
25	11.10	8.37	2.91	2.87	1.18	1.62	0.86	0.89	1.78	
26	11.48	7.13	3.11	2.75	1.09	1.69	0.70	0.85	1.78	
27	12.23	5.08	1.87	1.83	0.71	1.03	0.52	0.52	1.15	
28	13.68	6.94	3.02	2.45	1.17	1.48	0.74	0.72	1.81	
29	34.32	6.23	2.42	3.05	1.15	1.56	0.71	0.71	1.73	
30	19.02	5.19	2.91	2.68	1.12	1.34	0.69	0.85	1.46	
31	19.12	6.05	3.81	2.69	1.21	1.73	0.67	0.73	1.48	
32	43.81	7.95	3.93	4.29	1.44	1.94	0.76	0.65	1.58	
33	0.00	9.74	4.48	3.61	1.57	1.91	0.95	0.78	1.36	
34	19.03	5.27	5.95	8.99	1.54	1.94	0.96	0.70	1.68	
35	31.22	1.93	10.07	7.57	2.05	2.33	1.15	0.82	1.71	
36	55.25	18.06	9.97	7.66	2.19	2.17	1.23	0.87	1.65	
37	25.51	17.49	13.55	16.93	2.45	2.62	1.30	1.18	1.50	
38	0.00	17.97	9.97	13.01	2.71	2.83	1.29	1.46	2.10	
39	0.54	15.06	14.14	21.66	3.35	2.34	1.27	2.17	2.40	
40	0.92	24.31	13.36	27.72	4.99	3.72	1.50	1.80	2.65	
41	0.00	42.90	32.11	0.52	17.09	0.95	3.72	2.53	6.48	
42	0.00	0.00	0.00	23.78	0.00	59.17	5.40	1.16	15.94	
43	0.00	0.00	0.00	0.00	0.00	0.00	0.00	0.00	0.00	
44	0.00	0.00	0.00	0.00	0.00	0.00	0.00	0.00	0.00	
45	0.00	0.00	0.00	0.00	0.00	0.00	0.00	0.00	0.00	
46	0.00	0.00	0.00	0.00	0.00	0.00	0.00	0.00	0.00	
47	0.00	0.00	0.00	0.00	0.00	0.00	0.00	0.00	0.00	
48	0.00	0.00	0.00	0.00	0.00	0.00	0.00	0.00	0.00	
49	0.00	0.00	0.00	0.00	0.00	0.00	0.00	0.00	0.00	
50	0.00	0.00	0.00	0.00	0.00	0.00	0.00	0.00	0.00	

ENHANCED INLET, STATION 7

CP	ET1	ET2	ET3	ET4	ET5	ET6	ET7	ET8	ET9	ET10-X TANG ERROR
1	0.00	0.00	0.00	0.00	0.00	0.00	0.00	0.00	0.00	0.00
2	0.00	9.31	0.00	0.00	0.00	0.00	0.00	0.00	0.00	0.00
3	0.00	10.24	21.89	39.42	121.23	22.29	6.46	5.24	4.68	0.00
4	0.00	13.12	25.66	23.52	0.00	17.02	4.69	4.98	4.24	0.00
5	0.00	4.90	27.80	86.64	351.43	16.01	3.94	2.92	3.69	0.00
6	0.00	11.68	22.02	28.57	39.78	7.75	2.83	2.51	3.87	0.00
7	0.00	7.90	0.00	7.48	23.12	6.18	2.34	2.13	3.56	0.00
8	0.00	4.42	0.00	5.78	15.90	5.49	1.74	2.48	2.73	0.00
9	0.00	6.77	6.07	9.84	21.15	3.27	1.83	2.03	4.00	0.00
10	0.00	4.73	3.87	5.72	11.08	2.40	1.56	1.55	4.69	0.00
11	0.00	5.36	2.95	4.36	7.92	2.27	1.43	1.58	3.34	0.00
12	0.00	0.00	2.75	3.74	5.73	1.79	1.42	1.61	3.46	0.00
13	0.00	0.00	2.40	3.29	5.25	1.38	1.25	1.62	3.18	0.00
14	0.00	0.00	1.77	2.28	3.28	1.33	1.33	1.49	2.31	0.00
15	0.00	0.00	1.73	2.20	3.03	1.11	1.41	1.40	2.96	0.00
16	0.00	4.94	1.55	2.27	4.41	1.31	1.38	1.75	2.67	0.00
17	0.00	0.00	1.75	2.32	3.49	1.28	1.42	1.49	3.00	0.00
18	13.78	0.00	1.53	2.13	3.62	1.14	1.31	1.49	2.70	0.00
19	0.00	5.46	1.54	2.04	3.09	1.20	1.01	1.36	2.96	0.00
20	0.00	1.61	0.92	1.19	1.73	0.74	0.79	0.83	1.49	0.00
21	0.00	4.56	1.56	2.07	3.13	1.08	1.28	1.21	2.84	0.00
22	0.00	0.00	1.78	2.09	2.56	1.18	1.23	1.41	2.80	0.00
23	0.00	0.00	1.73	1.95	2.26	1.07	1.10	1.19	2.39	0.00
24	0.00	3.94	1.37	1.71	2.34	1.02	1.10	1.16	2.95	0.00
25	0.00	0.00	1.34	1.69	2.32	1.01	1.07	1.21	2.21	0.00
26	0.00	0.00	1.56	2.02	2.93	0.97	1.05	1.18	1.91	90.07
27	0.00	4.58	1.31	1.66	2.34	0.94	1.24	1.40	2.47	0.00
28	0.00	3.82	1.37	1.68	2.22	1.10	1.00	1.25	2.12	0.00
29	0.00	4.43	1.37	1.66	2.13	0.93	1.07	1.31	2.03	0.00
30	0.00	0.00	1.18	1.59	2.51	1.00	1.11	1.30	1.99	0.00
31	0.00	3.19	1.19	1.49	2.03	0.90	0.98	1.18	2.21	0.00
32	0.00	3.79	1.14	1.43	1.93	0.98	1.06	1.16	2.85	98.95
33	0.00	2.91	1.20	1.41	1.74	0.85	1.10	1.28	1.97	0.00
34	0.00	4.94	1.28	1.52	1.89	0.80	0.96	1.14	2.19	0.00
35	0.00	0.00	1.41	1.60	1.87	0.89	0.96	1.16	2.42	0.00
36	7.96	0.00	1.30	1.59	2.05	0.96	0.92	1.03	1.81	0.00
37	6.95	5.31	1.33	1.53	1.82	0.81	0.92	1.11	1.70	0.00
38	0.00	0.00	1.58	1.73	1.93	0.85	0.97	1.32	1.88	0.00
39	0.00	5.59	1.40	1.61	1.92	0.77	0.81	1.09	2.29	0.00
40	0.00	4.87	1.38	1.67	2.14	0.84	0.95	1.30	1.96	0.00
41	0.00	3.50	1.57	1.84	2.24	1.06	0.96	1.35	2.24	104.67
42	1.75	1.22	1.40	1.70	2.20	1.08	0.77	1.48	2.20	0.00
43	0.00	0.62	1.45	1.75	2.25	0.99	0.46	2.15	2.13	0.00
44	0.00	1.02	0.77	0.96	1.94	0.97	0.41	2.49	2.08	0.00
45	3.59	10.22	0.74	0.56	0.45	1.95	0.63	3.34	5.14	13.05
46	0.18	0.00	0.00	4.89	4.89	12.07	6.76	4.88	7.05	0.15
47	0.04	212.38	0.00	0.00	0.00	0.00	0.00	21.70	31.37	0.38
48	0.06	16.93	0.00	0.00	0.00	0.00	84.27	14.79	7.17	61.28
49	0.00	0.00	0.00	0.00	0.00	278.45	18.65	11.11	6.65	0.00
50	0.00	0.00	0.00	0.00	0.00	0.00	0.00	0.00	0.00	0.00

ENHANCED INLET, STATION 8

CP	ET1	ET2	ET3	ET4	ET5	ET6	ET7	ET8	ET9	ET10-% TANG ERROR
1	0.00	23.49	0.32	11.09	0.00	65.17	21.86	11.51	19.78	10.39
2	0.00	5.03	0.29	4.21	0.00	61.24	28.99	19.03	28.76	50.71
3	0.00	3.46	0.33	2.94	0.00	65.69	17.11	4.78	27.93	14.18
4	0.00	7.03	0.25	4.00	0.00	37.67	19.00	15.45	21.89	12.02
5	0.00	3.64	0.16	2.47	0.00	53.92	13.33	11.72	39.53	69.33
6	0.00	1.56	0.18	1.89	0.00	175.25	13.35	5.82	25.26	17.99
7	0.00	2.63	0.19	0.85	0.00	50.25	9.82	7.59	21.33	12.07
8	0.00	6.29	0.65	101.34	0.00	53.94	5.49	5.30	22.70	10.61
9	0.00	4.18	3.15	217.98	0.00	30.83	5.04	3.65	14.49	12.04
10	0.00	3.23	0.00	32.73	0.00	11.26	3.07	2.40	17.58	9.30
11	0.00	5.21	0.00	21.17	0.00	9.92	2.39	2.56	10.28	5.72
12	0.00	4.03	0.00	0.00	0.00	6.86	1.99	2.53	12.23	10.14
13	0.00	3.58	0.00	16.28	0.00	5.91	1.73	1.99	10.20	7.50
14	0.00	1.56	0.00	13.17	0.00	5.27	1.34	1.86	8.13	18.77
15	0.00	2.67	0.00	11.01	0.00	4.01	1.12	1.75	26.47	6.42
16	0.00	2.22	0.00	10.90	0.00	3.12	1.11	1.70	10.94	6.43
17	0.00	2.26	0.00	6.66	0.00	2.44	0.97	2.14	12.69	5.72
18	0.00	1.86	0.00	3.95	0.00	1.61	0.66	0.97	4.73	3.99
19	0.00	3.00	0.00	4.70	0.00	2.31	1.13	1.53	6.93	4.31
20	0.00	3.03	0.00	5.24	0.00	3.09	0.86	1.54	9.76	3.90
21	0.00	1.50	0.00	0.00	48.94	2.25	0.85	1.44	7.33	5.23
22	0.00	2.84	0.00	4.60	0.00	2.37	0.95	1.38	8.87	5.21
23	0.00	4.34	0.00	4.85	0.00	2.20	0.80	1.56	5.29	7.57
24	0.00	3.41	0.00	4.02	0.00	2.17	0.86	1.48	5.19	4.06
25	0.00	2.17	0.00	4.05	0.00	2.35	0.81	1.65	5.86	3.12
26	0.00	3.19	0.00	3.40	77.30	2.01	0.86	1.19	5.80	4.16
27	0.00	3.56	0.00	4.04	0.00	2.15	0.89	1.37	5.21	6.87
28	0.00	2.82	85.23	3.46	0.00	1.99	0.88	1.21	3.81	3.78
29	0.00	2.55	0.00	3.76	0.00	2.31	0.88	1.45	5.31	3.36
30	0.00	2.63	0.00	4.19	0.00	2.03	0.85	1.25	8.44	5.70
31	0.00	2.63	0.00	3.92	0.00	2.19	0.88	1.45	3.63	5.05
32	0.00	4.69	0.00	3.29	0.00	2.07	0.85	1.21	3.06	5.05
33	0.00	2.66	0.00	2.82	44.98	2.34	0.78	1.40	4.65	7.16
34	0.00	1.76	0.00	2.58	34.36	1.78	0.95	1.27	5.51	4.42
35	0.00	4.78	0.00	4.46	53.09	1.77	0.78	1.39	4.97	3.51
36	0.00	2.35	17.04	4.38	0.00	2.15	0.81	1.26	3.44	3.82
37	0.00	2.71	3.05	3.50	0.00	1.87	0.76	1.40	3.14	3.96
38	0.00	2.32	2.98	3.61	0.00	2.03	0.77	1.00	3.39	3.32
39	0.00	2.73	0.58	3.47	52.23	1.56	0.72	1.20	3.81	6.07
40	0.00	2.66	0.10	3.94	17.02	1.61	0.70	1.20	4.08	2.95
41	0.00	2.14	0.03	3.18	10.69	1.46	0.64	1.08	3.85	3.17
42	0.03	1.94	0.08	2.66	39.75	1.78	0.68	1.04	3.50	3.72
43	0.66	1.49	8.60	1.74	7.75	1.42	0.68	1.12	4.56	2.11
44	4.84	0.56	0.00	1.45	2.57	1.40	0.64	1.19	4.82	4.41
45	0.00	0.27	0.00	1.37	2.27	1.30	0.56	1.03	3.79	2.22
46	0.00	0.16	0.00	1.09	1.14	1.07	0.52	0.92	3.14	2.06
47	2.83	0.29	57.61	1.00	0.59	0.64	0.49	0.94	3.43	3.00
48	0.27	0.61	1.97	2.14	0.82	1.02	0.58	1.22	3.46	4.53
49	0.22	1.00	0.81	15.92	3.44	2.39	1.21	2.02	3.90	1.78
50	1.42	2.02	0.93	52.18	0.00	12.02	5.61	6.24	12.56	2.25

Report Documentation Page

NASA
National Aeronautics and Space Administration

1. Report No. NASA TM -104356 AVSCOM TR 90 - C - 012	2. Government Accession No.	3. Recipient's Catalog No.

4. Title and Subtitle Effects of Inlet Distortion on the Development of Secondary Flows in a Subsonic Axial Inlet Compressor Rotor	5. Report Date April 1991
	6. Performing Organization Code
7. Author(s) Albert K. Owen	8. Performing Organization Report No. E - 5583
	10. Work Unit No. 505 - 62 - 52 1L161102AH45
9. Performing Organization Name and Address NASA Lewis Research Center Cleveland, Ohio 44135 - 3191 and Propulsion Directorate U.S. Army Aviation Systems Command Cleveland, Ohio 44135 - 3191	11. Contract or Grant No.
	13. Type of Report and Period Covered Technical Memorandum
12. Sponsoring Agency Name and Address National Aeronautics and Space Administration Washington, D.C. 20546 - 0001 and U.S. Army Aviation Systems Command St. Louis, Mo. 63120 - 1798	14. Sponsoring Agency Code

15. Supplementary Notes

Report was submitted as a thesis in partial fulfillment of the requirements of Doctor of Philosophy in Engineering Sciences to the University of Toledo, Toledo, Ohio. Responsible person, Albert K. Owen, (216) 433-5895.

16. Abstract

Detailed flow measurements were taken inside an isolated axial compressor rotor operating subsonically near peak efficiency. Laser Anemometer measurements were made with two inlet velocity profiles. One profile consisted of an unmodified baseline flow, and the second profile was distorted by placing axisymmetric screens on the hub and shroud well upstream of the rotor. A primary flow is defined in the rotor and deviations from this primary flow for each inlet flow condition are identified. A comparison between the two flow deviations is made to assess the development of a passage vortex due to the distortion of the inlet flow. A comparison of experimental results with computational predictions from a Navier-Stokes solver showed good agreement between predicted and measured flows. Measured results indicate that a distorted inlet profile has minimal effect on the development of the flow in the rotor passage and the resulting passage vortex.

17. Key Words (Suggested by Author(s)) Inlet distortion Secondary flows Laser anemometer Axial compressor	18. Distribution Statement Unclassified - Unlimited Subject Category 07

19. Security Classif. (of the report)	20. Security Classif. (of this page)	21. No. of pages	22. Price*
Unclassified	Unclassified	340	A15

NASA FORM 1626 OCT 86

*For sale by the National Technical Information Service, Springfield, Virginia 22161